

Identification and functional characterization of binding partners and substrates of viral macrodomains with a focus on Chikungunya virus

Von der Fakultät für Mathematik, Informatik und Naturwissenschaften der RWTH Aachen University zur Erlangung des akademischen Grades einer Doktorin der Naturwissenschaften genehmigte Dissertation

vorgelegt von

Sarah Krieg

Master of Science

aus

Köln

Berichter: Univ.-Prof. Dr. rer. nat. Bernhard Lüscher
Univ.-Prof. Dr. rer. nat. Michael Huber

Tag der mündlichen Prüfung: 07. Juli 2022

Diese Dissertation ist auf den Internetseiten der Universitätsbibliothek verfügbar.

Parts of this thesis were pre-published as part of the following co-authored articles:

Eckei L*, **Krieg S***, Bütepage M, Lehmann A, Gross A, Lippok B, Grimm AR, Kümmerer BM, Rossetti G, Lüscher B, Verheugd P (2017) The conserved macrodomains of the non-structural proteins of Chikungunya virus and other pathogenic positive strand RNA viruses function as mono-ADP-ribosylhydrolases. Scientific Reports 7:41746. doi:10.1038/srep41746

**these authors contributed equally to this work*

Krieg S, Pott F, Eckei L, Verheirstraeten M, Bütepage M, Lippok B, Goffinet C, Lüscher B, Verheugd P (2020) Mono-ADP-ribosylation by ARTD10 restricts Chikungunya virus replication by interfering with the proteolytic activity of nsP2. bioRxiv:2020.2001.2007.896977. doi:10.1101/2020.01.07.896977

Work performed by others as well as contributions of collaborators as far as presented in this thesis have been indicated at the appropriate locations.

Additional articles of which I am the main author or a co-author and additional scientific contributions are listed separately in section 6.6.

Abstract

Positive single stranded RNA ((+)ssRNA) viruses pose a major health threat due to their high mutation rates and adaptability. To counteract arising resistances against existing treatments and vaccines, novel therapeutic targets are urgently needed. A subset of (+)ssRNA viruses encodes for so-called macrodomains (macros). These comprise a conserved protein fold that is highly associated with ADP-ribosylation. ADP-ribosylation is a post-translational modification (PTM) of proteins. Recently, it was also found as a modification of DNA and RNA. Intracellularly ADP-ribosylation is mainly mediated by the ADP-ribosyltransferase Diphtheria toxin-like (ARTD aka PARP) family. These enzymes mediate the transfer of ADP-ribose (ADPr) from their co-factor NAD⁺ to the substrate. ADP-ribosylation comes in two variants: mono-ADP-ribosylation (MARylation) which is the transfer of a single ADPr moiety and poly-ADP-ribosylation (PARylation) which constitutes the iterative addition of ADPr units resulting in polymers. The majority of ARTDs mediate MARylation and a subset, including ARTD10, is interferon(IFN)-inducible proposing a role in innate immunity.

In this work, the isolated, viral macros of four alphaviruses, two ortho-hepeviruses and one alphacoronavirus were characterized as efficient MAR-hydrolases on several protein substrates *in vitro*. Meanwhile, their activity towards PARylation was shown to be inefficient. A more detailed characterization focused on the macro of Chikungunya virus (CHIKV), a (re)emerging alphavirus that has already infected millions of people worldwide. CHIKV causes an acute flu-like disease that progresses to a chronic arthralgia in about 30% of the patients. The MAR-hydrolase activity was also confirmed for the macro within the full-length non-structural (ns) protein 3 (nsP3) and catalytically important amino acids were identified. Further the MAR-hydrolase activity was demonstrated in cells.

In the following, the mechanistical relevance for the MAR-hydrolase activity of the CHIKV macro and for MARylation mediated by the IFN-responsive ARTDs was investigated in more detail. An RNA replicon-based system was established where Gaussia luciferase was used as a measure for viral replication. Using this setup, ARTD10 was identified as a restriction factor for CHIKV dependent on its catalytic activity and the MAR-interaction of the viral macro was discovered to be crucial for replication. These effects of MARylation on replication were at least in part attributed to a defect in processing of the viral ns polyprotein, which is mediated by the viral protease within nsP2. NsP2 was further identified as a substrate for ARTD10 *in vitro* and in cells. Its MARylation inhibited protease activity *in vitro*, while reversal of the modification by the CHIKV macro rescued this effect.

Lastly, complementary approaches were used to identify potential host factors that are regulated by (de-)MARylation. Therefore, the BioID system and classical pulldown experiments were performed with nsP3, nsP3-macro and ARTD10 to identify potential common interactors and substrates by mass spectrometry analysis. Additionally, the influence of IFN and catalytic activity was assessed for the interactome of ARTD10. Initial verification could confirm novel and known interactors of nsP3 and Ras GTPase-activating protein-binding protein 1 (G3BP1) was identified as a new, substrate of (de-)MARylation *in vitro* with potential relevance in CHIKV infection.

Zusammenfassung

Einzelsträngige RNA Viren mit positiver Polarität ((+)ssRNA) stellen, aufgrund ihrer hohen Mutationsraten und Anpassungsfähigkeit, eine substanzielle gesundheitliche Bedrohung dar. Daher werde fortwährend neue therapeutische Angriffspunkte gesucht um Resistenzen entgegenzuwirken. Ein Teil dieser (+)ssRNA Viren kodiert für sogenannte Makrodomänen (Makros). Diese sind charakterisiert durch eine konservierte Domänenarchitektur, die stark mit ADP-Ribosylierung assoziiert ist. ADP-Ribosylierung umfasst eine posttranslationale Proteinmodifikation, die aus einer einzelnen ADP-Ribose (ADPr) Einheit oder aus einem ADPr-Polymer bestehen kann. Diese Varianten werden jeweils als Mono- und Poly-ADP-Ribosylierung (alias MARYlierung und PARYlierung) bezeichnet. Neben Proteinen wurden kürzlich auch DNA und RNA als Substrate für ADP-Ribosylierung identifiziert. Intrazellulär ist hauptsächlich die Familie der Diphtheriatoxin-verwandten ADP-Ribosyltransferasen (ARTDs alias PARPs) für diese Modifikationen verantwortlich. Die meisten ARTDs katalysieren MARYlierung und von diesen sind einige, z.B. ARTD10, Interferon(IFN)-induzierbar. Dies impliziert eine Rolle in der angeborenen Immunantwort.

Im Zuge dieser Arbeit, wurden die viralen Makros von vier Alphaviren, zwei Ortho-Hepeviren und einem Alphacoronavirus *in vitro* als effiziente Hydrolasen für MARYlierung von verschiedenen Proteinen identifiziert. Dagegen konnte gezeigt werden, dass die Aktivität gegenüber PARYlierung ineffizient ist. Im Weiteren wurde eine detailliertere Charakterisierung der Makro von Chikungunya Virus (CHIKV) durchgeführt. CHIKV ist ein Alphavirus, der sich ausbreitet und weltweit bereits Millionen Menschen infiziert hat. Neben einer akuten, Grippe-ähnlichen Phase, entwickelt sich eine Erkrankung in ca. 30% der Fälle zu einer chronischen Arthralgie. In der CHIKV Makro wurden katalytisch relevante Aminosäuren identifiziert. Die MAR-Hydrolaseaktivität konnte sowohl für das Volllänge Nichtstrukturprotein 3 (nsP3), welches die Makro enthält, als auch in Zellen bestätigt werden.

Im Weiteren wurde die mechanistische Relevanz der MAR-Hydrolaseaktivität der CHIKV Makro sowie die der MARYlierung durch IFN-induzierbare ARTDs detaillierter untersucht. Dazu wurde ein RNA Replicon-basiertes System genutzt, in dem Gaussia Luciferase als Maßstab für CHIKV-Replikation verwendet wurde. Mit diesem System konnte ARTD10, abhängig von seiner katalytischen Aktivität, als Restriktionsfaktor für CHIKV identifiziert werden. Außerdem konnte gezeigt werden, dass die Interaktion der viralen Makro mit MARYlierung essentiell für die Replikation ist. Diese Effekte konnten, zumindest partiell, auf Defekte in der proteolytischen Spaltung des Nichtstrukturpolyproteins zurückgeführt werden. Die virale Protease binnen nsP2 ist für diese essentielle Proteolyse verantwortlich. NsP2 wurde als Substrate von ARTD10-vermittelte MARYlierung *in vitro* und in Zellen identifiziert. Diese MARYlierung inhibiert die Proteaseaktivität *in vitro*, während Hydrolyse durch die CHIKV Makro diesen Effekt aufheben kann.

Darüber hinaus wurden Experimente durchgeführt um Wirtsfaktoren zu identifizieren, die durch MARYlierung reguliert werden. Hierfür wurden das BioID-System sowie klassische Pulldown-Assays mit nsP3, der isolierten Makro und ARTD10 durchgeführt, um gemeinsame Interaktoren mittels Massenspektrometrie zu identifizieren. Für ARTD10 wurde außerdem der Einfluss von IFN und katalytischer Aktivität auf das Interaktom untersucht. Es wurden sowohl neue als auch bekannte Interaktoren von nsP3 bestätigt und G3BP1 (Ras GTPase-activating protein-binding protein 1) wurde als Substrat von (De-)MARYlierung *in vitro* identifiziert, mit potenzieller Relevanz für CHIKV Infektionen.

Table of Contents

ABSTRACT.....	III
ZUSAMMENFASSUNG.....	IV
TABLE OF CONTENTS.....	V
1 INTRODUCTION	8
1.1 Viruses – “organisms at the edge of life”	8
1.1.1 Classification of viruses	8
1.1.2 Viral evolution as a major health threat	12
1.1.3 Antiviral intervention strategies – concepts and drawbacks	13
1.2 ADP-ribosylation.....	14
1.2.1 Eukaryotic writers of poly-ADP-ribosylation	16
1.2.1.1 The DNA damage regulators ARTD1 and ARTD2	17
1.2.1.2 The tankyrases – ARTD5 and ARTD6	19
1.2.2 Eukaryotic writers of mono-ADP-ribosylation	19
1.2.2.1 The ecto-ARTC family	20
1.2.2.2 The mono-ARTDs	20
1.1.1.1.1 The role of mono-ARTDs in the cellular DNA damage response	21
1.1.1.1.2 Regulation of signaling and transcription by mono-ARTDs	22
1.1.1.1.3 ARTD-mediated mono-ADP-ribosylation in RNA biology.....	24
1.1.1.1.4 ARTD10	27
1.2.3 ARTDs in immunity – a focus on mono-ADP-ribosylation	30
1.2.4 Readers and Erasers of ADP-ribosylation.....	35
1.2.4.1 Macrodomains as modulators of ADP-ribosylation.....	37
1.2.5 ADP-ribosylation of nucleic acids	40
1.2.6 Non-eukaryotic ADP-ribosylation – a conserved modification	41
1.2.6.1 Viral macrodomains.....	41
1.3 Chikungunya virus – an emerging virus	43
1.3.1 Chikungunya fever: symptoms, vaccines and therapy	45
1.3.2 The life cycle of CHIKV.....	47
1.3.3 Functions of the CHIKV non-structural proteins	50
1.4 Aims of this work	56
2 RESULTS AND DISCUSSION	57
2.1 The viral macrodomains of Chikungunya virus and other pathogenic (+)ssRNA viruses are (protein) mono-ADP-ribosyl-hydrolases.....	57
2.1.1 Viral macrodomains exhibit hydrolase activity towards protein mono-ADP-ribosylation <i>in vitro</i>	57
2.1.2 Viral macrodomains are ineffective hydrolases of protein poly-ADP-ribosylation <i>in vitro</i>	61
2.1.3 Identification of catalytically essential amino acids of the CHIKV macrodomain by mutational analysis.....	65
2.1.4 The full-length CHIKV nsP3 protein possesses similar hydrolase properties to the isolated macrodomain <i>in vitro</i>	68
2.1.5 The Chikungunya virus macrodomain can hydrolyze ARDT10-mediated mono-ADP-ribosylation in cells	70

2.2	Mono-ADP-ribosylation restricts Chikungunya virus replication by inhibiting the auto-proteolytic activity of nsP2	73
2.2.1	The interferon-induced ARTD10 and ARTD12 restrict viral replication of CHIKV	73
2.2.2	Mono-ADP-ribosylation affects CHIKV polyprotein processing	81
2.2.3	CHIKV nsP2 is a substrate of mono-ADP-ribosylation <i>in vitro</i> and in cells	96
2.2.4	Mono-ADP-ribosylation inhibits the proteolytic activity of nsP2 reversibly	101
2.2.5	Investigation of the CHIKV Y114V macrodomain mutant	105
2.2.6	CHIKV nsP1 and nsP3 are substrates for mono-ADP-ribosylation <i>in vitro</i>	107
2.3	Identification of common cellular interactors and substrates of ARTD10 and the CHIKV nsP3 macrodomain	110
2.3.1	Identification of cellular interactors of the CHIKV nsP3 macrodomain by MS analysis.....	110
2.3.2	Identification of ARTD10 interactors dependent on interferon and catalytic activity.....	115
2.3.3	Identification of common, cellular interactors of ARTD10 and nsP3	121
3	CONCLUSION AND FUTURE PERSPECTIVES	128
4	MATERIAL AND METHODS	137
4.1	Material	137
4.1.1	Kits.....	137
4.1.2	Synthetic oligonucleotides.....	138
4.1.3	Plasmids	143
4.1.4	Antibodies	152
4.1.5	Inhibitors.....	154
4.1.6	Bacterial strains.....	154
4.1.7	Eukaryotic cell lines.....	155
4.2	Experimental Procedures	156
4.2.1	Work with nucleic acids	156
4.2.1.1	Restriction digestion of DNA	156
4.2.1.2	Agarose gel electrophoresis	156
4.2.1.3	Gel purification of DNA from an agarose gel.....	156
4.2.1.4	Polymerase chain reaction (PCR).....	156
4.2.1.5	Gateway cloning	157
4.2.1.6	Blunt end cloning.....	157
4.2.1.7	Ligation of DNA fragments	157
4.2.1.8	Site-directed mutagenesis.....	157
4.2.1.9	Plasmid preparation from bacterial cultures.....	158
4.2.1.10	Sequencing of DNA.....	158
4.2.1.11	<i>In vitro</i> transcription of m ⁷ G-capped replicon RNA	158
4.2.2	Work with prokaryotic cells	159
4.2.2.1	Cultivation of bacterial cells	159
4.2.2.2	Heat shock transformation.....	159
4.2.3	Work with eukaryotic cells.....	160
4.2.3.1	Cultivation of eukaryotic cells	160
4.2.3.2	Cryoconservation of eukaryotic cells.....	160
4.2.3.3	Cell seeding.....	160
4.2.3.4	Calcium phosphate transfection of plasmid DNA.....	161
4.2.3.5	Transfection of <i>in vitro</i> transcribed replicon RNA	162
4.2.3.6	Transfection of siRNA	162
4.2.3.7	Viral replication assay.....	162
4.2.3.8	Flow cytometry analysis	163
4.2.4	Protein chemical methods	164
4.2.4.1	Purification of glutathione S transferase (GST)-tagged fusion proteins from bacteria	164
4.2.4.2	Purification of hexahistidine-(His)-tagged fusion proteins from bacteria	165
4.2.4.3	Sodium dodecyl sulfate polyacrylamide gel electrophoresis (SDS-PAGE).....	165

4.2.4.4	Coomassie Blue (CB) staining	165
4.2.4.5	Circular dichroism (CD) analysis	166
4.2.4.6	Preparation of protein lysates from eukaryotic cells	166
4.2.4.7	(Co-)immunoprecipitation	167
4.2.4.8	Semidry Western blot	167
4.2.4.9	Tank Western blot	168
4.2.4.10	Immunodetection of proteins and modifications	168
4.2.4.11	<i>In vitro</i> ADP-ribosylation assay with recombinant proteins	169
4.2.4.12	<i>In vitro</i> ADP-ribosylation assay with immunoprecipitated HA-ARTD10	169
4.2.4.13	Hydrolase assay with recombinant proteins	170
4.2.4.14	Hydrolase assay with immunoprecipitated HA-ARTD1	170
4.2.4.15	Thin Layer Chromatography (TLC) of released products from hydrolase assays	170
4.2.4.16	Sequencing PAGE of released products from hydrolase assays	171
4.2.4.17	<i>In vitro</i> protease assay with nsP2	171
4.2.4.18	ADP-ribosylation assay with subsequent <i>in vitro</i> protease assay	171
4.2.4.19	BioID Assay	172
4.2.4.20	Tandem-Affinity Purification	173
4.2.4.21	GFP-Trap of GFP-ARTD10 for mass spectrometry analysis	174
4.2.4.22	Mass spectrometry analysis	175
4.2.5	Microscopic methods	176
4.2.5.1	Fixation and immunofluorescence (IF) staining of adherent cells	176
4.2.5.2	Fluorescence laser-scanning confocal microscopy of fixed cells	176
5	REFERENCES	CLXXVIII
6	APPENDIX	CCVI
6.1	Supplementary Figures	CCVI
6.2	Abbreviations	CCVIII
6.3	List of figures	CCXIV
6.4	List of tables	CCXVI
6.5	Curriculum Vitae	CCXVII
6.6	Scientific Contributions	CCXVIII
6.6.1	Publications in scientific journals	CCXVIII
6.6.2	Presentations at scientific meetings	CCXIX
6.7	Eidesstattliche Erklärung	CCXX
6.8	Danksagung	CCXXI

1 Introduction

1.1 Viruses – “organisms at the edge of life”

In 1798 Edward Jenner introduced the first successful vaccine. He used material from cowpox pustules to confer protection against the much more hazardous smallpox virus without even knowing yet that viruses existed and what they were. In 1980 the World Health Organization (WHO) officially declared smallpox globally eradicated with the last natural case in Somalia in 1977 (WHO 2007). Since then, versatile vaccinations have been developed for a multitude of different pathogens and alongside smallpox diverse other diseases, like polio, are about to be eliminated globally or at least locally due to world-wide eradication initiatives (Aylward et al. 2000; Dowdle 1998; WHO 2019).

Even though modern medicine keeps developing with new strategies for vaccines and therapeutics, so do the pathogens through constant evolution and thus infectious diseases remain one of the major health issues of the 21st century. Among the top ten causes of death worldwide, the WHO still state three diseases caused by infection, namely lower respiratory infections, diarrheal diseases and tuberculosis (WHO 2018b). In addition to investigation of the causes of death, the WHO annually publishes the Research and Development Blueprint report, that includes a priority list for diseases that are likely to cause an epidemic and are in urgent need of development of a vaccine or therapeutics. Strikingly, this list exclusively featured viruses in the five years since its initiation. Likewise, the pathogens that were considered for the list by experts mainly consisted of viral infectants (WHO 2015, 2017, 2018a).

The first virus was described in 1882, when Dimitri Ivanovsky discovered that the agent causing tobacco mosaic disease was so small, that it withstood filtration (Ivanovsky 1882). His research was based on the findings of Adolf Mayer who identified the infectious nature of the disease befalling tobacco plants (Mayer 1886). Later, Martinus Beijerinck independently extended Ivanovsky’s research by demonstrating that the infectant could replicate inside living plant cells and termed it “contagium vivum fluidum” – a contagious, living fluid (Beijerinck 1898). The identification of Tobacco mosaic virus (TMV) was promptly followed by the discoveries of animal and human viruses, quickly cementing the concept of a filterable, disease causing agent that is replicating in living cells and not visible in light microscopy (Lustig et al. 1992). The controversial discussion, whether viruses are liquid or particulate, however was only settled with the first plaque assay and the first electron microscopy images of TMV (d’Herelle 1917; Kausche 1939). Since its discovery, TMV remained a model for the progression of knowledge on viruses and even benefitted research on the genetic code in general (Lustig et al. 1992).

1.1.1 Classification of viruses

As viruses are metabolically inert, intracellular parasites that rely on their host cells for replication and propagation, they were termed “organisms at the edge of life” (Rybicki 1990). The purpose of a virus is to deliver its genome to the host cell, where it is expressed and amplified to establish new infectious and fully assembled virions. In turn this starts new rounds of infection and thus guarantees the persistence of the virus. Viruses can infect mammals, plants, archaea, and bacteria. Since 1966 the universal classification of viruses into taxa is regulated in a centralized way by the International Committee on Taxonomy of Viruses

regardless of their host (ICTV; formerly International Committee on Nomenclature of Viruses (ICNV)) (Adams et al. 2017). This has resulted in the classical five rank structure for virus taxonomy, comprising order, family, subfamily (used rarely), genus and species, that has been used since 1991 and persisted until 2017 (Francki et al. 2012; International Committee on Taxonomy of Viruses Executive 2020). It was based on features such as the phenotype, e.g. the disease caused by the virus, genomic properties, sequence and other molecular traits if eligible. However, it did not consider all evolutionary relationships between viruses, resulting in disjointed taxa (International Committee on Taxonomy of Viruses Executive 2020). Classification of viruses is complicated due to the large evolutionary distances of their relationships that are of polyphyletic origins. The connections between viruses are not strictly hierarchical and there is intermingling of basic features of different origins when the whole genome is considered and this is where a classical phylogeny-based system for classification, like it is applied to other organisms, fails (Rybicki 1990; International Committee on Taxonomy of Viruses Executive 2020). To expand on the grouping of closely related viruses only, the ICTV extended the original five to 15 taxonomic ranks to allow consideration of basal evolutionary links between distantly related viruses recently. These ranks include eight primary and seven secondary ranks. The primary ranks include the classical order, family, genus and species and additionally feature realm, kingdom, phylum and class (International Committee on Taxonomy of Viruses Executive 2020).

Due to the difficulties in systematics of virus grouping, alternative classification systems have been established that complement the ICTV taxonomy and are widely used as well (Xu et al. 2011). For instance, the Holmes classification simply divides virus into three groups depending on the host type: Phaginae (attacks bacteria), Phytophaginae (attacks plants), and Zoophaginae (attacks animals) (Steinhaus 1949; Xu et al. 2011). Because viruses rely on their host for replication, co-evolutionary relationships are widespread and therefore viruses attacking the same host are proposed to be more similar and thus relevant for classification (Xu et al. 2011).

Other systems focus more on the chemical and physical properties of the virus. Herein, they are commonly classified by two means: their morphology or their chemical composition and mode of replication. An infectious and fully assembled viral particle outside of the host cell is called a virion. The simplest virions comprise a nucleic acid, carrying the genetic information, and a protein coat, the capsid. This entity is called the nucleocapsid, with the capsid enclosing and protecting the genome from chemical and physical damage and from nucleases. The viral genome generally codes for non-structural proteins (nsPs), which often possess enzymatic functions and modulate the host cell and viral replication, and structural proteins. The viral structural proteins form the capsid and they are frequently arranged in symmetrical icosahedral (also called spherical) or helical shapes (**Figure 1**). These structures self-assemble without energy usage from repetitions of usually only one or a few distinct structural proteins called capsomeres or protomers for the icosahedral and helical nucleocapsids, respectively. If the virion exclusively comprises the nucleocapsid it is also referred to as a “naked virus” (**Figure 1**). However, many viruses are additionally enveloped by a lipid bilayer, that is usually derived from the host cell membrane during budding of the virus and forms another protective layer. These envelopes are frequently interspersed with glycosylated viral envelope proteins that often form spikes on the outside and facilitate entry into the cell by interaction with cellular receptors, while the capsid proteins perform this task in naked viruses (Gelderblom 1996; Ryu 2017). Additionally, some enveloped viruses possess matrix (M) proteins on the inside of the lipid bilayer that support virus assembly by interaction with the envelope, the transmembrane glycoprotein and the nucleocapsid (**Figure 1**) (Matsumoto

1982; Gelderblom 1996; Ryu 2017). In the case of herpesviruses, the matrix proteins are called tegument which consists of multiple different proteins. Besides virion assembly they are likewise involved in the initiation of infection and the regulation of the host immune response and metabolism. Furthermore, the tegument proteins control viral gene expression and the transport of incoming virions to the nucleus, where they are unpacked and they support the packaging of the viral genome (Zhou et al. 1994; Mocarski et al. 2007; Kalejta 2008).

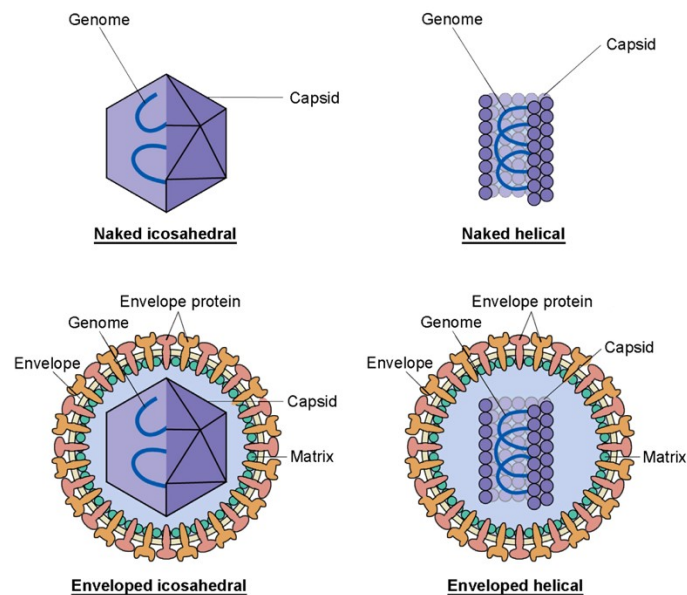


Figure 1: Classical virion morphologies.

Schematic representation of naked and enveloped icosahedral and naked and enveloped helical symmetries of virions. Parts of the nucleocapsid are uncovered to depict the genome and three different structural proteins are shown: the capsid proteins, the glycoproteins in the envelope, and the M proteins at the viroplasmic site of the membrane (adapted from (Ryu 2017)).

In addition to the two classical symmetries, larger viruses often build more complex structures. For instance, their architecture can consist of both helical and icosahedral elements, which is also referred to as binal symmetry. For instance, the T2, T4 and T6 (T-Even) bacteriophages of *Escherichia coli* (*E. coli*) comprise an icosahedral head and a helical tail to increase flexibility and allow injection through the bacterial cell wall (**Figure 2**) (Waterson 1965). One of the largest and most complex viral families are the Poxviridae with the Vaccinia virus (VV) as the best studied member that is also frequently used for vaccine production. They do neither possess icosahedral nor helical symmetries, but the virion assembles from over 100 different structural proteins into a multilayered particle entailing several independent structural elements, that is nearly visible under the light microscope (**Figure 2**). The genome of VV and a subset of virion enzymes, e.g. the DNA-dependent RNA polymerase (DdRp), are enclosed within the dumbbell-shaped core, surrounded by a membrane studded with spike glycoproteins also termed the palisades. This core is further ensheathed by two envelopes of lipid bilayers that contain once more different envelope proteins. Interestingly, the viroplasm and the core are not completely compacted, however, they exhibit regions of high compaction or low density and two lateral bodies that are connected to the core as well as the inner membrane. The functions of many of these features are not fully understood (Harrison et al. 2004; Cyrklaff et al. 2005; Grünwald et al. 2006).

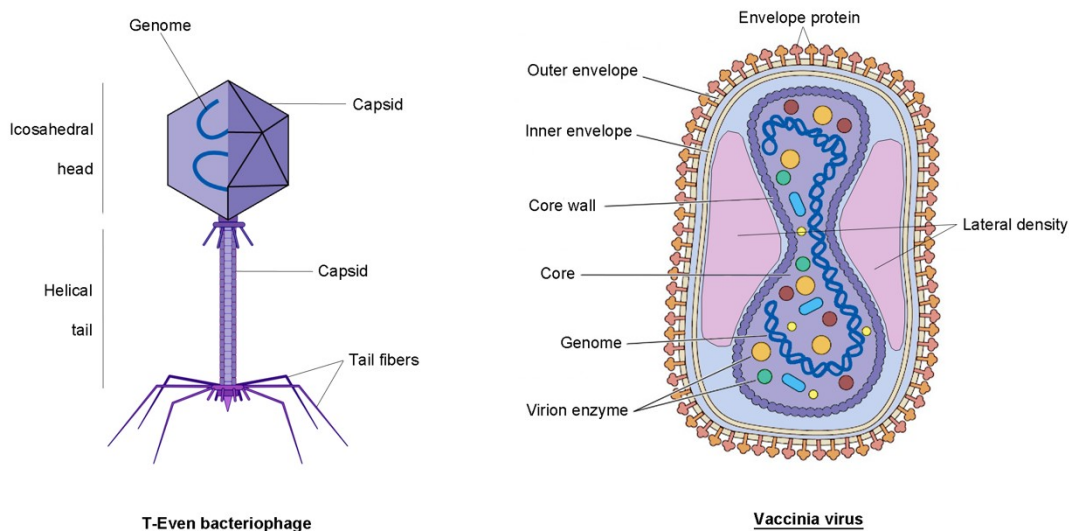


Figure 2: Exemplary virion morphologies of complex viruses.

Schematic representation of two complex virions. The T-Even bacteriophage consists of an icosahedral head and a helical tail, that is flexible and injectable to facilitate entry through the bacterial wall with the help of the tail fibers. Parts of the nucleocapsid are uncovered to depict the genome. (adapted from BioRender and (Ryu 2017)). The Vaccinia virus is a model Poxvirus, that possesses a dumbbell-shaped core, that contains the viral genome and virion enzymes. The core is surrounded by a core wall, a membrane studded with spikes, and two further membrane envelopes with envelope glycoproteins. The space between the outer envelopes and the core harbors two lateral densities (adapted from (Harrison et al. 2004)).

A critical step in every viral lifecycle is the production of mRNA to allow translation of viral proteins by the host machinery. The achievement of this objective, however, is largely conditioned by the structure of the genetic material. The genome composition and organization of viruses is as diverse as the morphology of the virions. The viral genome can consist of DNA or RNA and can be single stranded (ss) or double stranded (ds), positive sense ((+), identical to mRNA) or negative sense ((-), complementary to mRNA), linear or circular, monopartite or segmented and range from 2 kb to 2500 kb in size (O'Carroll et al. 2016). The Baltimore classification, one of the most frequently used, groups viruses based on their genome type and the consequential mode of replication and therein defines 7 classes: Class I: dsDNA viruses, class II: ssDNA viruses, class III: dsRNA, class IV: (+)ssRNA viruses, that rely on generation of a negative strand RNA, class V: (-)ssRNA viruses, class VI: (+)ssRNA(RT) viruses, that reverse transcribe a DNA intermediate, and class VII: dsDNA(RT) viruses, that replicated their genome through a ssRNA intermediate that is in turn reverse transcribed into DNA again (**Figure 3**)(Baltimore 1971; Hull et al. 1989; Krupovic et al. 2018). Since the update of the ICTV taxonomy classes, the introduction of the realm rank accommodates the Baltimore classification at a basal level, integrating two frequently used systems (Gorbalenya 2018; International Committee on Taxonomy of Viruses Executive 2020).

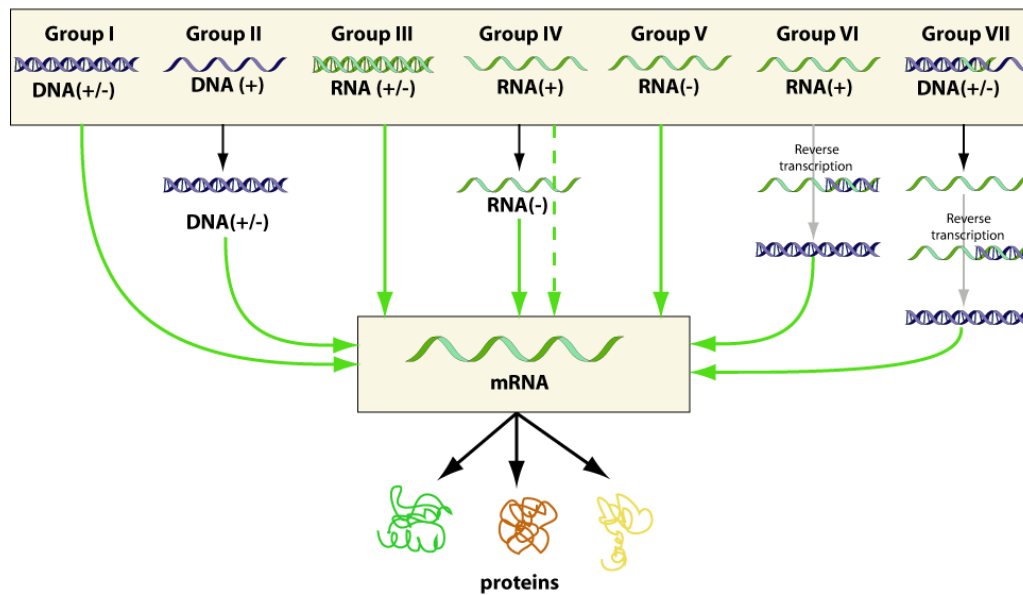


Figure 3: Baltimore classification of viruses.

Classification of viruses based on the structure of the genome and the mode of replication centered around the generation of mRNA (ViralZone, <https://viralzone.expasy.org/254>).

1.1.2 Viral evolution as a major health threat

What makes virus control and treatment so difficult, is their high adaptability to new environments and host species, which is the result of high evolutionary rates due to large population sizes, brief generation times, high mutation rates and limited proof-reading activity. Consequently, this leads to antigenic variances, increased virulence and arising drug resistances resulting in (re-)emergence of viral diseases and sudden outbreaks (Hicks et al. 2014; Peck et al. 2018; Hanada et al. 2004; Holmes 2009). RNA viruses often have higher mutations rates than DNA viruses due to the lack of proof-reading activity of RNA-dependent RNA polymerases (RdRp) and ss genomes mutate more frequently than ds genomes for so far unknown reasons (Peck et al. 2018). This is in line with the fact, that especially diseases caused by ssRNA viruses pose a major health threat and are hard to control (WHO 2018a; Heaton 2019). However, most mutations are harmful or even lethal to viruses and thus eliminated by natural selection. In general, only few mutations are selectively neutral or beneficial and will be fixed as a substitution. Higher mutation rates increase the probability of beneficial substitutions but it is not the only determinant (Peck et al. 2018). Within the kingdom of *Orthornavirae*, that comprises RNA viruses that dependent on RdRp for replication, the basal replication error is rather constant, but still the substitution rates differ greatly by up to 5 orders in magnitude ranging from 1×10^{-7} to 6×10^{-2} . For comparison non-viral life forms possess substitution rate from 10^{-9} to 10^{-8} (Hanada et al. 2004). Apart from the mutation rate caused by errors during replication, replication frequency and generation times have been described as the major factors for differences in the evolution speed amongst RNA viruses, which are influenced by cell tropism, transmission routes and infection modes (Hanada et al. 2004; Hicks et al. 2014). Increased replication rates lead to quicker accumulation of replication errors and mutations and faster fixation of substitutions that ultimately result in evolved viruses. Therefore, high mutation rates and replication frequencies of RNA viruses contribute to their genetic diversity and thus tremendous adaptability and epidemiological and zoonotic fitness (Holmes 2009).

One of the most recent and far-reaching examples demonstrating the epidemiological potential of these fast-evolving RNA viruses is the COVID-19 pandemic, caused by Severe Acute Respiratory Syndrome Coronavirus 2 (SARS-CoV-2). Since its zoonotic origin on an animal market in Wuhan City (Hubei, China) in December 2019, it has spread to 27 countries with over 70,000 confirmed infections on February 17th 2020 (Dong et al. 2020) and to 99 countries with nearly 200,000 cases by March 10th 2020 (Dawood et al. 2020; Johns Hopkins University 2021). Accordingly, within only 11 weeks after its initial detection the virus spread to half of the countries worldwide and was thus declared a global pandemic by the WHO (Dawood et al. 2020; WHO 2020e). Until August 3rd 2021, there were over 180 million diagnosed COVID-19 infections around the world leading to nearly 4 million fatalities resulting in a yet unprecedented global health threat (Johns Hopkins University 2021). SARS-CoV-2 is a positive-sense, single stranded RNA ((+)ssRNA) virus with an intrinsic proofreading mechanism that primarily infects lung epithelial cells mainly via the droplet and aerosol transmission route and leads to an acute infection (Hui et al. 2020; Jayaweera et al. 2020; Wang et al. 2021). In line with the criteria that increase the substitution rate of an RNA virus described above, SARS-CoV-2 exhibits a mild evolution rate compared to other RNA viruses but overall it still evolves with a rate of 7×10^{-4} and thus exhibits high genomic diversity (Rambaut et al. 2020; Wang et al. 2021). This pandemic exemplifies the difficulty in anticipating and controlling outbreaks of rapidly evolving RNA viruses and why the unique evolution properties and consequences thereof need to be studied to develop intervention strategies against emerging RNA viruses.

1.1.3 Antiviral intervention strategies – concepts and drawbacks

Classical intervention strategies rely largely on vaccination and hence humoral or cellular recognition of antigens. But, as described previously, high evolutionary rates of especially RNA viruses lead to variability in the exposed structural proteins, which are the primary antigens of viruses. This results in escape of the immune system rendering vaccination inefficient (Holmes 2009). Therefore, additional antiviral strategies are needed for therapeutic intervention. In particular, inhibitors of virally encoded enzymes with conserved functions are thought to be relevant targets (Heaton 2019; Guo et al. 2020). For instance, viral proteases are considered druggable targets, for instance those of Human Immunodeficiency virus 1 (HIV-1), Hepatitis C virus (HCV), Dengue virus and Coronaviruses (CoV). A common viral strategy is to translate progenitor polyproteins that subsequently need to be auto-catalytically cleaved into the functional protein subunits by a viral protease. This is true for the non-structural as well as the structural components. Generally, viral proteases have evolved from eukaryotic prototypes with well-studied catalytic mechanisms, but they developed unique properties and distinct substrate specificities. Best studied are probably the aspartic protease of HIV-1 and the chymotrypsin-like serine protease of HCV, given that both specimens are targeted by several FDA approved protease inhibitors. Despite their crucial role for viral replication and high conservation, drug resistant viral strains arise frequently (Anderson et al. 2009a; Kurt Yilmaz et al. 2016). Other drug targets are the viral polymerases. No matter if the virus relies on a DNA polymerase (DNA pol), DdRp, RdRp or reverse transcriptase (RT), they are all essential for amplification of the viral genome and thus crucial. Furthermore, they share common structural features involving two conserved aspartic acid residues that bind a pair of bivalent metal ions. Several viral polymerase inhibitors are in clinical use, e.g. directed against the DNA pol of Herpesviruses, the RdRp of HCV or the RT of HIV-1. Commonly, polymerase inhibitors can be subdivided into nucleoside and non-nucleoside inhibitors. The former bind to the active site of the polymerase, are incorporated into the growing RNA chain and

subsequently lead to chain termination and lethal mutagenesis. The non-nucleoside inhibitors are multifaceted, including active site and covalent inhibitors. Still nearly all polymerase inhibitors likewise gave rise to resistant viral variants (Tsai et al. 2006; De Clercq 2019).

As mandatory intracellular pathogens, viruses are strictly reliant on their host cell for their propagation and have therefore co-evolved to hijack the host machinery for their own purposes and evade the antiviral response. As virus evolution exclusively conveys resistance through alteration of its own genome, a different approach would be to target the host. On the one hand, this includes interferon (IFN) treatment to boost the immune response, chloroquine to block the release of the virus into the cell or corticosteroids to suppress the immune response (Trofatter 1987; Plantone et al. 2018; Guo et al. 2020; WHO 2020d). However, these systemic treatments can have severe adverse effects (Bayas et al. 2000; Santaella et al. 2007; Sulkowski et al. 2011; Plantone et al. 2018). Furthermore, immunostimulating agents are often restricted to a narrow time window for effectiveness before the infection is established and otherwise rather increase the cytokine storm that is often responsible for the severity of the disease (Barry et al. 2000; Monath 2008; Channappanavar et al. 2017). Immunosuppressives on the other hand, merely alleviates symptoms but do not help with clearing the infection and show long term adverse effects (WHO 2020d). Advances in the fields of bioactive compounds, immunotherapy, precision medicine and RNA interference (RNAi) are being developed and are thought to revolutionize antiviral therapy (Heaton 2019).

As drug resistance due to evolution of the target remains a common drawback of all strategies, the combination of targets provides a promising approach to raise the (genetic) barrier for evasion. One innovative strategy is to even further increase the high mutation rates of viruses to a level that is toxic. To achieve this combinatory effect, established antiviral treatment is combined with a mutagen targeting the fidelity of the viral polymerase with nucleoside analogues (Gerrish et al. 2003; Pariente et al. 2001). A similar example is the combination of a nucleoside-inhibitor with interferon α treatment (Tsai et al. 2006). Even so there is a constant increase in the number of treatment options, so far none of these strategies provided long-lasting predominance over the tremendous evolutionary evasion capacity of viruses. Therefore, new targets and combinatorial treatments need to be evaluated and established.

1.2 ADP-ribosylation

Upon viral infection, the host cell has to react quickly and initiate an immune response. The fastest way to adapt to new conditions and environmental challenges are affecting preexisting macromolecules, for instance by post-translational modifications (PTMs) of proteins. PTMs are frequent with over 500 known variants and control the function of proteins (Keenan et al. 2021). Therefore, PTMs play an essential role in antiviral signaling. Through co-evolution with their host, the fast-evolving viruses have developed numerous strategies to circumvent or even hijack the cellular response including mechanisms to counteract PTMs transferred by the host machinery. For instance, some viral genomes encode non-structural proteins that can directly regulate PTMs of host or viral factors (Bailey-Elkin et al. 2017; Chang et al. 2016; Chen et al. 2018; Crow et al. 2016; Luscher et al. 2018). This places the regulation of PTMs at the frontline of the biological arms race between viruses and their hosts. In addition to prominent examples like phosphorylation and ubiquitination, recent studies have suggested adenosine diphosphate-ribosylation (ADP-ribosylation) at the interface of host-virus interaction. Thus, enzymes controlling ADP-ribosylation are potential targets for antiviral therapies (Atasheva et al. 2012; Atasheva et al. 2014; Butepage et al. 2015; Todorova et al. 2015; Zhang et al. 2015).

ADP-ribosylation is an ancient, fully reversible posttranslational modification, that describes the addition of ADP-ribose (ADPr) from the cofactor nicotinamide adenine dinucleotide (NAD⁺) onto a substrate while releasing nicotinamide (Nam). ADP-ribosylation exists in two forms: mono-ADP-ribosylation (MARylation) that is limited to the covalent attachment of a single, monomeric ADPr moiety to the substrate, and poly-ADP-ribosylation (PARylation) that extends the initial ADPr subunit into a long, potentially branched poly-ADP-ribose (PAR) polymer through ribose–ribose *O*-glycosidic bonds (**Figure 4**)(Luscher et al. 2018).

When PAR was first detected in hen nuclear extracts in 1963, it was misidentified as a potential polymer of adenosine (poly(A)) (Chambon et al. 1963). This assumption was modified a few years later when the molecule was correctly characterized as a polymer of ADPr resembling RNA (Chambon et al. 1966; Nishizuka et al. 1967; Sugimura et al. 1967). Importantly, it was demonstrated that PAR chains are covalently attached to chromatin associated proteins (Nishizuka et al. 1968; Otake et al. 1969). In parallel, Diphtheria toxin was found to MARylate and thus inactivate the eukaryotic elongation factor 2 (Honjo et al. 1968; Gill et al. 1969). This established both versions of ADP-ribosylation, PAR- and MARylation, as PTMs.

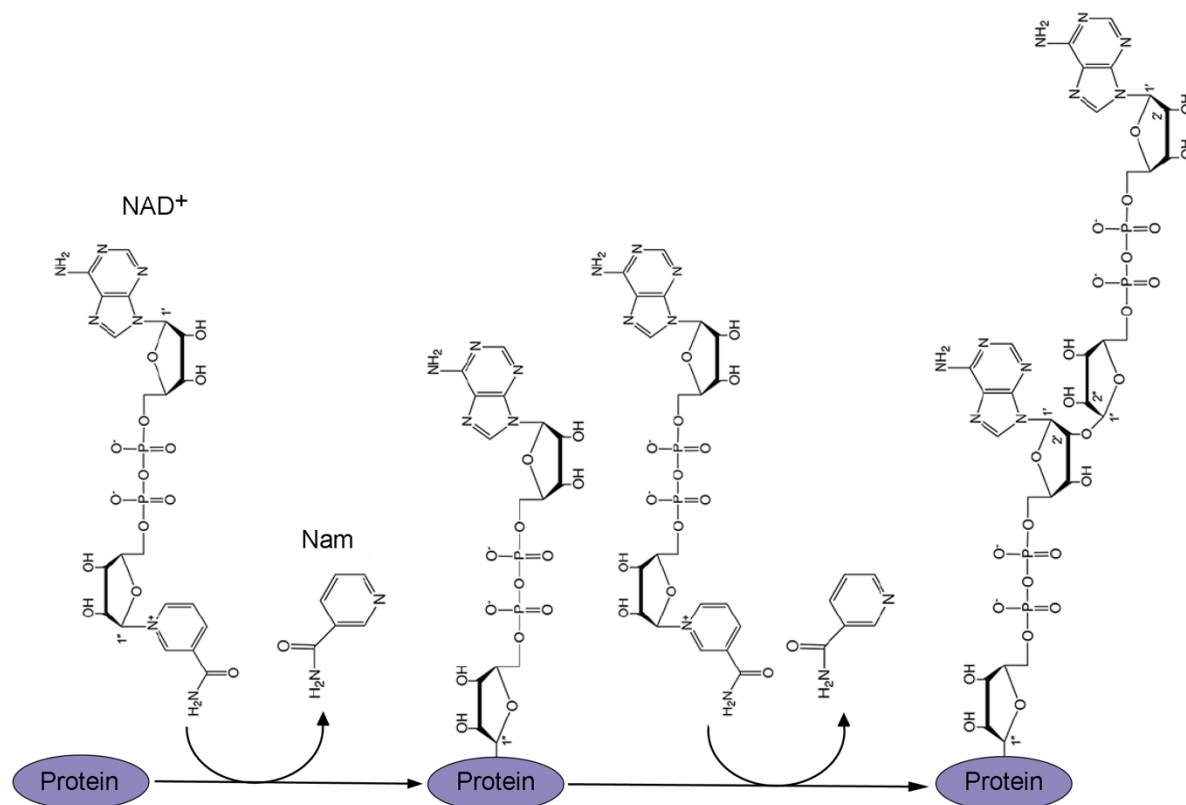


Figure 4: Mono- and poly-ADP-ribosylation of proteins.

The reactions of protein MARylation and subsequent PARylation are shown. Further, the structures of NAD⁺ and the reaction products, namely Nam and ADPr subunits, are depicted. The acceptor amino acid is linked to the C1'' carbon of NAD⁺ through nucleophilic attack and Nam is released. Subsequently, the ADPr chain is extended by an additional nucleophilic attack of the C2'' hydroxyl group of the adenine ribose of the protein linked ADPr on the C1'' carbon of another NAD⁺ molecule (modified from Luscher et al. 2018).

ADP-ribosylation of proteins is mediated by ADP-ribosyltransferases (ARTs). In eukaryotes, the two best studied families are the ART Diphtheria toxin-likes (ARTDs, aka PARPs) and the Cholera toxin-like ecto-enzymes (ARTCs).

Since its discovery in the 1960s, further investigation has attributed versatile functions in multiple cellular processes to ADP-ribosylation and its substrate spectrum of multiple amino acid side chains of diverse proteins has even extended to DNA and RNA (Luscher et al. 2018;

Weixler et al. 2021). An excerpt of the impact of ADP-ribosylation and its modulators will be outlined in the following chapters.

1.2.1 Eukaryotic writers of poly-ADP-ribosylation

According to the current state of research, the only enzymes capable of PARylating substrates are members of the eukaryotic family of ARTDs (Luscher et al. 2018). These poly-ARTDs (pARTDs) comprise ARTD1, ARTD2 (PARP2), ARTD5 (PARP5, tankyrase 1 (TANK1)) and ARTD6 (PARP6, tankyrase 2 (TANK2)) (Luscher et al. 2018)(**Figure 5**). ARTD1, the founding member of the mammalian ARTs, dominated the research for many years. It was initially isolated from rat liver nuclei (Shimizu et al. 1967; Yamada et al. 1971) and subsequently its cDNA was cloned (Alkhatib et al. 1987; Kurosaki et al. 1987; Uchida et al. 1987). Extensive studies were performed on its structure, catalytic activity, substrate spectrum and mechanistic functions (Kurosaki et al. 1987; Pieper et al. 1999; Shall et al. 2000; Eisemann et al. 2020). However, it took about 10 more years, until additional members of the ARTD family were discovered and nearly 20 years until all 16 current members were identified via sequence similarities of the catalytic ART domain (Smith 2001; Amé et al. 2004; Otto et al. 2005)(**Figure 5**). The nomenclature of the ARTD family has long been discussed in the field and it was recently decided to use the according PARP names for the enzymes, however as this thesis was written previously, it will stick to the ARTD nomenclature and only introduce the equivalent PARP names (Lüscher et al. 2021).

In the initial *in silico* screens, comparison to the characteristic catalytic triad of ARTD1, consisting of histidine, tyrosine and the catalytic glutamate (H-Y-E), already suggested that not all 17 family members are able to actually catalyze PARylation due to substitutions of the glutamate (Amé et al. 2004; Otto et al. 2005). Indeed, subsequent studies suggest that most ARTD family members are MARYlating enzymes (**Figure 5**)(Luscher et al. 2018).

All ARTDs share the conserved catalytic ART domain with and H-Y-E motif or a variant thereof. Apart from that, these transferases contain multiple domains, usually N-terminal of the ART domain, that modulate activity, substrate specificity, interaction, and subcellular localization (**Figure 5**). Furthermore, they are regulated through expression, co-factors and PTMs. This allows the manifold and diverse functions carried out by this family of enzymes (Luscher et al. 2018).

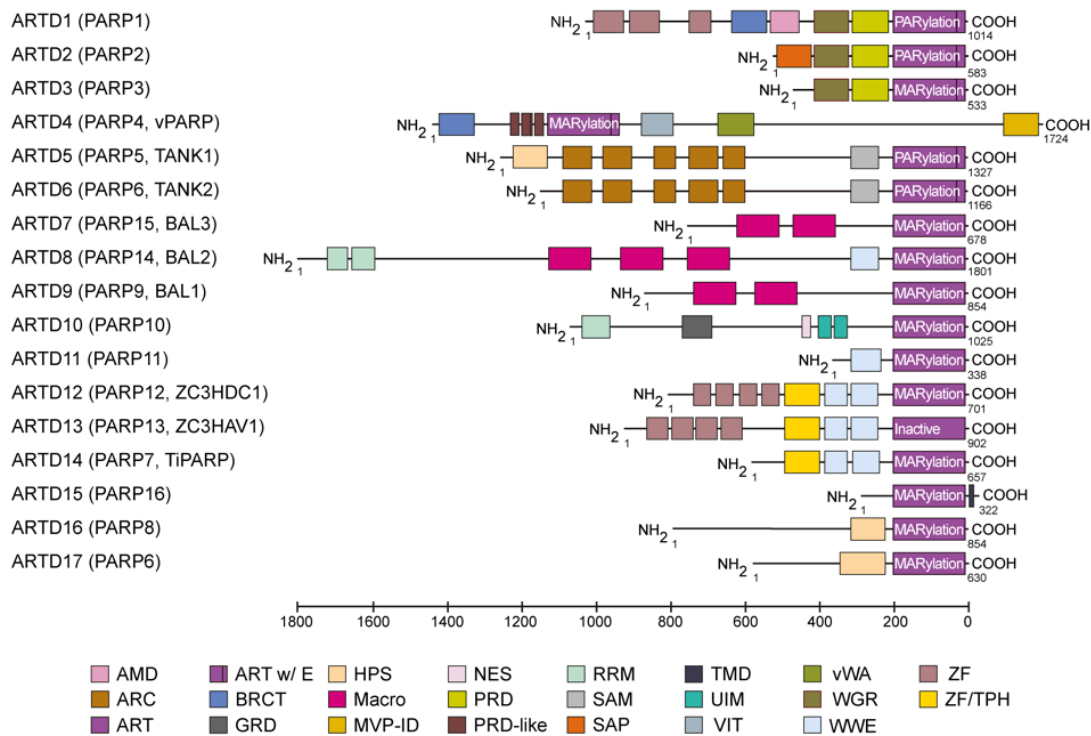


Figure 5: Schematic representation of the 17 human ARTD family members.

Depicted are the human ARTD enzymes with their various domains, that were grouped together due to their ART domains with sequence homology to the Diphtheria toxin. In addition to the ARTD nomenclature, other frequently used names are shown. “PARylation”, “MARylation” and “Inactive” refer to the catalytic activity and therein the form of ADP-ribosylation that the enzyme can transfer. NH₂ and COOH mark the N-terminus or the C-terminus of the protein, respectively. The scale and the annotated numbers next to the ARTDs indicate the length of the amino acid sequence. The following domains are depicted: AMD, automodification domain; ARC, ankyrin repeat cluster, for protein–protein interactions; ART, ADP-ribosyltransferase domain; ART w/E, ART domain with a catalytic glutamate; BRCT, BRCA1 carboxy-terminal domain, associated with DNA damage repair and cell cycle checkpoint proteins; GRD, glycine-rich domain; HPS, histidine–proline–serine region; Macro, macrodomain, some possess ADP-ribose-1'-phosphatase, some ADP-ribosylhydrolase activity, and some interact with MARylated or PARylated substrates; MVP-ID, major vault particle interaction domain; NES, nuclear export sequence; PRD, PARP regulatory domain, autoinhibitory domain of ARTD1 involved in branching activity; PRD-like, similar to PRD but function elusive; RRM, RNA-recognition motif; SAM, sterile α motif, for homo- or heterodimerization; SAP, SAF/ acinus/PIAS-DNA-binding domain; TMD, transmembrane domain; UIM, ubiquitin interaction motif; VIT, vault protein inter- α -trypsin domain, potentially for protein–protein interactions; vWA, von Willebrand type A domain, potentially for protein–protein interactions; WGR, domain with conserved central motif (W-G-R); WWE, domain with three conserved residues (W-W-E), mediates protein–protein interactions, some interact with iso-ADP-ribose; ZF, zinc finger domain; ZF/TPH, Ti-PARP (ARTD14) homologous zinc finger domain (modified from Luscher et al. 2018).

1.2.1.1 The DNA damage regulators ARTD1 and ARTD2

With a head start of 10–20 years of research, ARTD1 is by far the best-studied member of the ARTD family, especially its role in DNA damage repair. In the unchallenged state, ARTD1 activity is downregulated. Upon genotoxic stress, the N-terminal Zinc finger (ZF) domains bind to single or double strand breaks in the DNA (SSBs and DSBs, respectively), which leads to allosteric activation of ARTD1. This unleashes the full PARylation capacity of ARTD1 and leads to massive auto- as well as substrate modification (Langelier et al. 2012; Dawicki-McKenna et al. 2015). As a result, ARTD1-mediated PARylation acts as a recruitment platform for multiple components of DNA damage repair complexes and chromatin remodelers (Ahel et al. 2009; Thompson 2012). Additionally, ARTD1 PARylates core histones and DNA replication and transcription factors which consequently dissociate and facilitate DNA decondensation (Strickfaden et al. 2016; Shall et al. 2000; Oei et al. 1998; Tallis et al. 2014). This second role

for DNA damage-induced PARylation prevents utilization of corrupted genetic information and ensures accessibility of broken strand(s) to repair complexes. Comparably, ARTD2 is also activated upon DNA damage where it cooperates with ARTD1. Although ARTD2 is less active and less abundant than ARTD1, its functions are partially redundant and can compensate for ARTD1 deficiency, but both enzymes additionally show unique functions (Ménissier de Murcia et al. 2003; Schreiber et al. 2006). While single knockouts (KO) are more sensitive to DNA damage, a double KO of *Artd1* and *Artd2* is lethal in mice (Amé et al. 1999; Schreiber et al. 2002; Ménissier de Murcia et al. 2003). Taken together, ARTD1 and ARTD2 play roles in base excision repair (BER), chromatin remodeling and shutdown of transcription upon DNA damage. Furthermore, involvement of ARTD1/2 is suggested in different forms of DNA damage repair and there seems to be a role for basal, DNA-damage independent activity of ARTD1 in gene regulation of distinct promoters. However, these functions are poorly understood so far (Luscher et al. 2018).

The fact that ARTD1 and ARTD2 activity are essential for BER is harnessed for cancer treatment. Combinatory treatment of HR-impaired cancers with PARP inhibitors (PARPi), that inhibit ARTD1, ARTD2 and other family members (Wahlberg et al. 2012a), leads to increased genomic instability of the cancers cells and ultimately cell death. This is called synthetic lethality (Farmer et al. 2005; Nickoloff et al. 2017). The most prominent examples for this are tumors that display homozygous breast cancer (BRCA) genes 1 or 2 deletions, that are frequently treated with PARPi in the clinic (Zimmer et al. 2018).

The amount of ARTD1 activation, which correlates with the severity of the insult, can further decide the cell fate by modulation between survival, apoptosis, and necrosis. During DNA damage repair, the activated ARTD1 continuously auto-modifies. Subsequently, the PAR chains are degraded by PAR glycohydrolase (PARG) and ADP-ribosyl hydrolase 3 (ARH3) within minutes and ARTD1 is recovered to its original state. When the damage inflicted on the DNA was moderate and detachable, ARTD1 remains inactive, the NAD⁺ pools can be regenerated and the cell survives. If the damage was more substantial and cannot be repaired, the ARTD1 PARylation cycle gets reactivated. The initial ARTD1 response already decreases the NAD⁺ pools by around 20% and further activation would result in complete exhaustion of the cellular energy resources and cell death (Henning et al. 2018). In this case free PAR chains are released from the nucleus into the cytoplasm where they locate to mitochondria and mediate the protease-dependent AIF-MIF-mediated form of necroptosis termed parthanatos (Wang et al. 2016b; Henning et al. 2018; Kiselevsky 2020). Lastly, massive DNA damage hyperactivates ARTD1, which depletes NAD⁺, inhibits glycolysis, the Krebs cycle, and the mitochondrial electron transport chain and results in necrosis. The timely caspase-cleavage of ARTD1 can thus be regarded as a switch between apoptosis and necrosis (Los et al. 2002; Virág et al. 2013; Henning et al. 2018).

Accordingly, fine-tuning of ARTD1 activity is crucial to maintain cellular homeostasis and to prevent or induce cell death. In addition to PTMs, interactors are described to regulate ARTD1 activity. Conventionally, ARTD1 modifies mainly acidic residues, like glutamates and aspartates, or lysines and is its own best substrate. Upon binding to its cofactor histone PARylation factor 1 (HPF1) however, the sites of modification are completely shifted towards serine-ADP-ribosylation. In addition, auto-PARylation is reduced and in turn, substrate modification is enhanced. Serine-ADP-ribosylation obligatorily requires HPF1 association but it was found to be widespread in the DNA damage response (Bonfiglio et al. 2017; Fontana et al. 2017).

1.2.1.2 The tankyrases – ARTD5 and ARTD6

The tankyrases are two closely related homologs, that display distinct as well as partially overlapping functions (Hsiao et al. 2008). The spectrum of molecular functions of the tankyrases is broad, which is promoted by the variety of subcellular localizations ranging from the nucleus to the cytoplasm. Therein, they can be found in e.g. centrosomes and stress granules dependent on the cellular state (Smith et al. 1999; Leung et al. 2011). The recruitment of tankyrases to different parts of the cell is regulated by their interaction partners (Azarm et al. 2020; Hsiao et al. 2008).

Similar to the other pARTDs, the tankyrases play a role in the maintenance of the genomic integrity of the cell (Azarm et al. 2020). ARTD5 is a positive regulator of telomere length and required for the dissociation of sister chromosomes during mitosis by PARylation of TTAGGG repeat binding factor 1 (TRF1) (Smith et al. 2000; Cook et al. 2002; Hsiao et al. 2008).

In addition to telomere maintenance, ARTD5 exhibits another essential function during mitosis: its PARylation activity is crucial for the correct assembly of the mitotic spindle poles, where PARylation by ARTD5 potentially recruits spindle pole proteins to allow the assembly (Chang et al. 2005; Hsiao et al. 2008; Chang et al. 2009).

As the previously described nuclear functions are only desirable leading up to and during mitosis, the activity of the tankyrases at the telomeres must be restricted (Azarm et al. 2020). This is controlled by cell cycle-dependent ubiquitination. During interphase, RNF146-mediated K48-linked ubiquitination leads to proteasomal degradation while during G2/M, ARTD5/6 are stabilized by RNF8-mediated K63-linked ubiquitination (Callow et al. 2011; Zhang et al. 2011; Tripathi et al. 2016).

Apart from the regulation of its own abundance, many functions of the tankyrases are tightly linked to RNF146-mediated ubiquitination and proteasomal degradation (Callow et al. 2011; Zhang et al. 2011; Luscher et al. 2018; Bhardwaj et al. 2017; Nie et al. 2020). This connection has first been described for axin (representing the homology axin1 and axin2). Axin is the scaffold for a complex that restricts canonical Wnt/ β -catenin signaling. Axin is PARylated by ARTD5, which leads to RNF146-mediated ubiquitination and proteasomal degradation. This leads to nuclear translocation of β -catenin and target gene expression. Therefore, ARTD5 is a positive regulator of Wnt/ β -catenin signaling dependent on its catalytic activity and RNF146 (Callow et al. 2011; Zhang et al. 2011). Recent proteome studies elucidated that this type of protein level regulation by the Tankyrase-RNF146-proteasome axis is a highly abundant mechanism (Bhardwaj et al. 2017; Nie et al. 2020). Among the proteins regulated by the PAR-mediated ubiquitination are members of pathways like Notch, PTEN and HIPPO signaling, microRNA (miRNA) processing, and intracellular trafficking like glucose transport through GLUT4 (Hsiao et al. 2008; Li et al. 2015b; Bhardwaj et al. 2017; Grimaldi et al. 2019; Nie et al. 2020). This involvement in multiple signaling pathways, implicates the tankyrases in crucial maintenance mechanisms as well as multiple diseases (Hsiao et al. 2008; Li et al. 2015b; McGurk et al. 2018; Zimmerlin et al. 2020).

1.2.2 Eukaryotic writers of mono-ADP-ribosylation

Even though the known enzymes transferring mono- versus poly-ADP-ribosylation are much more abundant (16 vs. 4 in humans, respectively), the pARTDs described above are overall studied in more detail. This might in part be due to the fact, that the research on the ARTD1 has a head start of up to 20 years and that accordingly the tools to investigate PARylation are much more advanced (Butepage et al. 2018a; Luscher et al. 2018). However, in recent years

the improved techniques to visualize MAR and the increased research interest have elucidated on more and more functions, some of which will be introduced in the following. In general, as mentioned before, mainly enzymes stemming from two classes have been described to be able to transfer MARYlation: ARTCs and the ARTDs (Luscher et al. 2018). In the latter, this thesis will focus on the ARTDs

1.2.2.1 The ecto-ARTC family

The family of the Cholera-toxin-like ARTs, that are also referred to as ecto-enzymes/-ARTs or ARTCs, comprises 5 members in mammals: ARTC1-5 (aka ART1-5). However, in mice, *Artc2* is encoded by two genes, *Artc2.1* and *Artc2.2*, while it is a pseudogene in humans due to premature stop codons, resulting in six or four ARTCs, respectively (Haag et al. 1994; Glowacki et al. 2002; Haag et al. 1990). These enzymes are grouped together on the grounds of similarity to the Cholera toxins ART domain (Glowacki et al. 2002; Luscher et al. 2018). Furthermore, all ARTCs are extracellular enzymes as they are either anchored in the plasma membrane or secreted. The active ecto-ARTs, including ARTC1/*Artc1*, *Artc2.1*, *Artc2.2* and ARTC5/*Artc5*, share the characteristic arginine-serine-glutamate (R-S-E) catalytic triade as opposed to the H-Y-E triade of the ARTDs and modify arginines. ARTC3 and ARTC4 on the other hand, do not contain an intact R-S-E motif and are thus proposed to be inactive and unable to bind NAD⁺ (Di Girolamo et al. 2019; Glowacki et al. 2002). Overall, the ARTCs are less well studied than their Diphtheria toxin-like relatives. The ecto-ARTs show distinct expression patterns, hinting at tissue-specific roles for their arginine modification in the organism. Therein, they are predominantly expressed in skeletal muscle, heart, testis, and immune cells, including T-cells and B-cells (Glowacki et al. 2001; Glowacki et al. 2002). They are known to modify transmembrane and extracellular substrates like integrins, receptors and potentially cytokines and are described to modulate the immune response and skeletal muscle development (Di Girolamo et al. 2019; Menzel et al. 2021).

1.2.2.2 The mono-ARTDs

Looking at the 17 members of the human ARTD family, 12 of them are restricted to MARYlation. Although more abundant than their PARYlating counterparts, they are generally less well studied (Butepage et al. 2015; Luscher et al. 2018). The mono-ARTDs, except for ARTD3 and ARTD4 (PARP3 and PARP4, respectively), possess variants of the characteristic H-Y-E triade in their catalytic domains. Specifically, the catalytic E is replaced by an isoleucine (I), leucine (L), tyrosine (Y) or threonine (T) (**Figure 5**)(Vyas et al. 2014; Luscher et al. 2018). Usually, the E is responsible for the hydrolysis of NAD⁺ and the nucleophilic attack on the ADPr. Since most of the mono-ARTDs lack this residue though, the acceptor site on the substrate overtakes this function. This is called substrate-assisted catalysis. After accepting the ADPr, the site is blocked, limiting the mono-ARTDs to MARYlation as opposed to the iterative cycles of nucleophilic attacks and transfers performed by pARTDs (Kleine et al. 2008; Luscher et al. 2018). Conversely, ARTD3 and ARTD4, that both contain the intact H-Y-E motif, are unable to transfer ADPr polymers on their own which suggests that the catalytic triade is not the sole determinant of PARYlating versus MARYlating activity. Additionally, in ARTD9 (PARP9) and ARTD13 (PARP13), the H is substituted by either glutamine (Q) or tyrosine (Y), respectively. This H is involved in binding of the NAD⁺ (Kleine et al. 2008; Aguiar et al. 2005). Therefore, ARTD13 is incapable of binding NAD⁺ which renders it inactive (Karlberg et al. 2015; Kleine et al. 2008). ARTD9 was long suggested to be inactive as well until a recent study discovered

MARylation activity exclusively in complex with the E3 ubiquitin ligase DTX3L (Yang et al. 2017). Controversially, a recent study rather suggests that DTX3L possesses the MARylation activity within the complex and not ARTD9 (Chatrin et al. 2020).

The intracellular mono-ARTDs and the MARylation they mediate are implicated in a multitude of cellular mechanisms in health and disease within different compartments in the cell. For instance they regulate DNA damage repair, transcription and mitosis in the nucleus as well as stress responses, signal transduction, translation and mRNA metabolism at the ER, in the cytosol or in cytosolic membraneless compartments like stress granules (Butepage et al. 2015; Luscher et al. 2018). As mentioned previously (**chapter 1.2.1.1**), these various functions, substrate specificities and subcellular localizations are conveyed by a multitude of additional domains apart from the conserved, catalytic ART domain (**Figure 5**) (Butepage et al. 2015; Luscher et al. 2018). In the following chapters, an excerpt of the molecular roles of ARTD-mediated MARylation will be outlined to give a broad and general overview of its relevance in health as well as disease.

1.1.1.1.1 The role of mono-ARTDs in the cellular DNA damage response

Albeit the fact, that PARylation mediated by ARTD1 and to a lesser extent ARTD2 are best studied in the context of DNA damage, some mono-ARTDs and MARylation also have functions in the response to genotoxic stress. The domain structure of ARTD3 resembles those of ARTD1 and ARTD2 and it also localizes to the nucleus (**Figure 5**) (Rouleau et al. 2007; Boehler et al. 2011). Even though less well studied than the PARylating counterparts, this MAR transferase is similarly implicated in the cellular response to DNA damage (Beck et al. 2014; Boehler et al. 2011; Vyas et al. 2014). In contrast however, it is rather associated with non-homologous end joining (NHEJ) of single and double strand breaks (Beck et al. 2014; Boehler et al. 2011; Vyas et al. 2014).

Additionally, more MAR transferases localize to the nucleus and play a role in the cellular response to DNA damage. The loss of ARTD8 (PAPR14) as well as ARTD10 (PARP10) led to increased sensitivity to genotoxic stress implicating these enzymes in the response to DNA damage (Nicolae et al. 2015; Nicolae et al. 2014). Both enzymes interact with proliferating cell nuclear antigen (PCNA), a co-factor of the DNA polymerase and the master regulator of the replication fork (Nicolae et al. 2015; Nicolae et al. 2014; Moldovan et al. 2007). The genomic instability resulting from ARTD10 deficiency or inhibition has been described to critically impair and decelerate development and to drive hypersensitivity to DNA damage, especially in tumor cells (Shahrour et al. 2016; Venkannagari et al. 2016; Schleicher et al. 2018). ARTD8 deficiency hampers diffusion of Rad51 foci and efficient HR upon replication stress (Nicolae et al. 2015). Additionally, ARTD9/DTX3L have been loosely implicated in DSB repair dependent on ARTD1. Proposedly PARylation recruits ARTD9 and DTX3L resulting in mono-ubiquitination of H4 and recruitment of checkpoint proteins (Yan et al. 2009; Yan et al. 2013). The exact role of the ARTD9/DTX3L complex is not understood, however they can mediate chemoresistance of cancers (Yan et al. 2009; Yan et al. 2013; Camicia et al. 2013).

ARTD9 in complex with DTX3L is described to also influence ubiquitination, in this case by direct modification of ubiquitin, proposedly at the C-terminal glycine 76 (G76) (Yang et al. 2017). As this position is required for ubiquitin conjugation to substrates, it reduces the cellular pool of ubiquitin, that is available for conjugation. The ARTD9/DTX3L-mediated MARylation of ubiquitin correlates with the NAD⁺ levels (Yang et al. 2017). Under low NAD⁺ concentration, the activity of the E1/E2/ARTD9/DTX3L complex shifts from MARylation to ubiquitination (Yang et al. 2017). This suggests a switch for ARTD9/DTX3L activity under

certain conditions regulated by NAD⁺ availability. A comprehensible situation where this might be relevant is for instance DNA damage, where ARTD1 activation reduces the cellular NAD⁺ pool drastically and ARTD9/DTX3L activity is essential for efficient DNA damage repair (Yan et al. 2013; Henning et al. 2018). Additionally, it might be interesting in the context of viral infections, as they are described to dysregulate the cellular NAD⁺ metabolome (Heer et al. 2020).

1.1.1.1.2 Regulation of signaling and transcription by mono-ARTDs

Remaining in the nuclear compartment, the ARTDs have functions besides DNA damage repair. For instance, ARTD3, that localizes exclusively to the nucleus, was linked to mitosis, the cell cycle and proliferation as well as differentiation and transcriptional regulation, especially in cancers (Rodriguez-Vargas et al. 2019). ARTD3 promotes proliferation and ARTD3 deficiency or inhibition leads to synthetic lethality in several cancers including BRCA1-deficient breast cancers and glioblastoma (Quan et al. 2015; Beck et al. 2019).

In addition to ARTD3, more mono-ARTDs are associated with tumorigenesis or cancer progression due to their roles in central signaling pathways. The B aggressive lymphoma (BAL) family proteins, including ARTD7-9, that are also called PARP15/BAL3, PARP14/BAL2 and PARP9/BAL1, respectively, share several characteristic features and alterations in their expression are associated with several cancers (**Figure 5**) (Aguiar et al. 2000; Aguiar et al. 2005; Juszczynski et al. 2006; Yan et al. 2013; Lin et al. 2013; lansante et al. 2015; Morandi et al. 2017). These three ARTDs are the only mammalian proteins, that contain a C-terminal PARP domain and multiple N-terminal macrodomains, an ADPr-associated fold that will be further discussed later on (**Figure 8**, chapter 1.2.4). Their tumor modulating functions have mostly been attributed to their capacity to regulate transcription in macrodomain- and/or MAR-dependent ways to regulate central signaling and ensure survival (Aguiar et al. 2005; Camicia et al. 2013; Cho et al. 2009; Goenka et al. 2006; Iwata et al. 2016). For instance, in diffuse large B-cell lymphoma, ARTD9 promotes proliferation and chemoresistance by repressing interferon response factor 1 (IRF1) expression in response to IFN- γ by binding to signal transducer and transcription activator 1 (STAT1) in a MAR-dependent manner (Camicia et al. 2013). In metastatic prostate cancer cells this might be supported by ARTD8 function promoting tumor cell migration (Bachmann et al. 2014). In addition to regulating STAT1 activity, ARTD8 was identified as a co-activator of STAT6 subsequent to interleukin 4 (IL-4) stimulation (Cho et al. 2009; Goenka et al. 2006; Huang et al. 2020; Mehrotra et al. 2011). Besides STAT signaling, in hepatocellular carcinoma (HCC) and multiple melanoma elevated levels of ARTD8 promoted survival by regulation of the pro-apoptotic kinase JNK1 (Barbarulo et al. 2013; lansante et al. 2015). Therein, ARTD8 is described to directly bind and thus inhibit JNK1 and in turn promote the pro-survival signaling mediated by JNK2 (Barbarulo et al. 2013). Finally, a recent study discovered that loss of ARTD8 decreases NF- κ B signaling in pancreatic cancer cells, while, inversely, inhibition of nuclear factor κ B (NF- κ B) signaling abolishes the carcinogenic effect of ARTD8 overexpression (Yao et al. 2019).

Overall exact mechanisms are often unknown, largely due to the lack of relevant substrates. Taken together, ARTD8 and to a lesser extent ARTD9 are known to control a multitude of signaling pathways, that modulate the fate of cells, especially immune cells, through transcriptional regulation in response to cytokine stimuli. Both MAR transferases are therefore generally considered pro-survival genes. This is not only relevant in the negative context of degenerate cancer tissues but also essential under physiological conditions and for instance promotes an immune response in host-pathogen conflicts. These desirable effects of

ARTD8 and ARTD9 functions will be discussed in more detail in the chapter about the role of ARTDs in innate immunity (chapter 1.2.3). The third BAL family member, ARTD7, is less well studied than the other macro-ARTDs. While its ability to influence transcription was only demonstrated in an artificial setup (Aguiar et al. 2005), alterations in the expression or sequences have been implicated in cancers (Lin et al. 2013; Guerrero-Preston et al. 2014; Lee et al. 2016; Morandi et al. 2017).

One of the best studied regulators of transcription within the ARTD family is probably ARTD14 (aka PARP7) which itself is induced by multiple transcription factors and generally functions as a downstream feedback regulator (Diani-Moore et al. 2010; Bindsbøll et al. 2016; Zhang et al. 2020). Stimulus-dependent signaling is crucial for the adaptation to environmental changes, however the efficient termination of this signaling is just as important to maintain homeostasis and prevent diseases like cancer. Therefore, negative feedback loops are usually essential components of signaling cascades (Ivashkiv et al. 2011; Komori 2018; Hill et al. 2013; Pando et al. 2000). Accordingly, ARTD14 has been described as a therapeutic target for instance in ovarian, colon and breast cancer (Goode et al. 2010; Cheng et al. 2019; Hutin et al. 2018; Zhang et al. 2020).

On a mechanistic level, ARTD14 expression is induced by the environmental toxin 2,3,7,8-tetrachlorodibenzo-p-dioxin (TCDD) downstream of the ligand-activated transcription factor aryl hydrocarbon receptor (AHR) and is therefore also termed TCDD-inducible PARP (TiPARP) (Diani-Moore et al. 2010). AHR represses hepatic gluconeogenesis (Diani-Moore et al. 2010). ARTD14 is a negative feedback regulator of AHR signaling (MacPherson et al. 2013). In the nucleus, ARTD14 directly binds to and MARYlates AHR, which leads to its degradation and abolishes AHR-mediated signaling (MacPherson et al. 2013; Ahmed et al. 2015; Gomez et al. 2018). Of note is, that to date ARTD14 is the only family member described to modify cysteines (Rodriguez et al. 2021; Gomez et al. 2018).

Apart from AHR, ARTD14 was also described to regulate other transcription factors, namely liver X receptors (LXR), androgen receptor (AR), hypoxia-inducible factor 1 (HIF-1), c-Myc and estrogen receptor dependent on its catalytic activity (Bindsbøll et al. 2016; Zhang et al. 2020; Yang et al. 2021). Further, dependent on its ADP-ribosyltransferase activity, ARTD14 leads to the formation of nuclear membraneless condensates, that are important for the regulation of the transcription factors (Zhang et al. 2020). This proposes a general mode of action, where ARTD14 suppresses (tumorigenic) transcription factors dependent on ADP-ribosylation, ubiquitination and subsequent degradation as part of a negative feedback inhibition (Zhang et al. 2020).

When talking about gene expression, it is of note, that several mono-ARTDs have been described to modify histones *in vitro*, suggesting a direct role in chromatin organization and transcription. This includes ARTD3, ARTD10 and ARTD14 that modify core histones and ARTD8 that MARYlated isolated and whole histones on a microarray (Rulten et al. 2011; Grundy et al. 2016; Forst et al. 2013; García-Saura et al. 2021; MacPherson et al. 2013; Feijs et al. 2013b). However, none of these modifications were ever confirmed in cells.

Under basal condition, ARTD12 (PARP12) is associated with an organelle involved in the secretory pathway: it localizes to the Golgi and the trans-Golgi network (TGN) in the absence of a stress signals (Vyas et al. 2013; Catara et al. 2017; Grimaldi et al. 2019). In the TGN it associates with an MARYlates Golgin-97, a protein involved in transport of distinct proteins from the Golgi to the plasma membrane and subsequent exocytosis (Grimaldi et al. 2020).

This MARYlation is required for trafficking of cargo, for instance E-cadherin, and loss of the modification leads to accumulation in the TGN (Grimaldi et al. 2020). In addition to its catalytic domain, ARTD12 possess five Zinc fingers and two WWE domains (**Figure 5**)(Luscher et al. 2018). Therein, the first WWE domain can bind to PAR, which is essential for ARTD12 relocation during stress conditions (Catara et al. 2017). Upon oxidative stress, ARTD12 leaves the Golgi and instead localizes to cytoplasmic stress granules (SGs) (Catara et al. 2017). This recruitment to SGs is governed by free PAR chains derived from ARTD1 activation in the nucleus and therefore displays a possibility for crosstalk between nuclear stress and cytoplasmic adaption (Catara et al. 2017). ARTD12 removal from the TGN is accompanied by fragmentation of the Golgi and blockade of transport, however the causality was not investigated. Nonetheless it is comprehensible, that ARTD12 plays a role in this since Golgin-97, that is regulated by ARTD12, is involved in transport as well as organization of the organelle structure (Catara et al. 2017; Grimaldi et al. 2019; Grimaldi et al. 2020). Moreover, ARTD12 overexpression has been previously described to disrupt Golgi structure (Vyas et al. 2013). Further, alleviation of the stress condition allows relocation of ARTD12 to the Golgi and restoration of Golgi and transport functions (Catara et al. 2017; Grimaldi et al. 2019). Comparable to ARTD15, ARTD12 might thus be involved in stalling and storing of the secretory pathway machinery during the cellular stress response. In addition to SGs, ARTD12 can also reside in granules containing p62 and ubiquitin, comparable to ARTD10 (Welsby et al. 2014). In HCC, ARTD12 has been described to regulate the stability of four and a half LIM domains protein 2 (FHL2) (Shao et al. 2018). FHL2 promotes β -catenin signaling and decreases the levels of E-cadherin supporting epithelial-to-mesenchymal transition (EMT) and metastasis downstream of TGF- β 1 (Cai et al. 2018). ARTD12 mediates the ubiquitination and degradation of FHL2 (Shao et al. 2018). Further, ARTD12 loss increases secretion of TGF- β 1 and expression of N-cadherin in HCC, both of which are hallmarks and drivers of EMT (Shao et al. 2018; Prieto-García et al. 2017; Loh et al. 2019). ARTD12 loss increases EMT and metastasis in HCC, attributing tumor suppressor functions to ARTD12 dependent on a mechanism that remains to be revealed (Shao et al. 2018).

1.1.1.1.3 ARTD-mediated mono-ADP-ribosylation in RNA biology

Subsequent to transcription, RNA can be regulated by multiple mechanism. Several of the mono-ARTDs have been linked to RNA biology in the cytoplasm, spanning from translation and silencing to degradation (Kim et al. 2020; Leung et al. 2012; Bock et al. 2015). The fact, that four mono-ARTDs contain RNA binding motifs already suggests functions in RNA biology: ARTD12 and ARTD14 contain CCCH zinc finger domains and ARTD8 and ARTD10 possess potential RNA recognition motifs (RRMs). Additionally, the inactive ARTD13 likewise carries CCCH zinc finger domains (**Figure 5 and 6**)(Luscher et al. 2018; Bock et al. 2015). Comparable to other functions of the ARTDs, the regulation of RNA biology is mainly associated with stress conditions. Therein, certain stresses, including heat shock and oxidative stress, can induce SG assembly. SGs are membrane-less cytoplasmic bodies that form by liquid-liquid phase separation (LLPS) and sequester, stall and store mRNA/protein complex, for instance the translation machinery (Hofmann et al. 2021). In addition to classical SG markers like Ras GTPase-activating protein-binding protein (G3BP) or T-cell-restricted intracellular antigen-1 (TIA-1), several ARTD family members localize to SGs and facilitate their formation. This includes the mono-ARTDs ARTD7 (PARP15) and ARTD12 (PARP12), as well as the polymer-forming ARTD5 (Tankyrase/PARP5a) and two isoforms of the inactive ARTD13 (PARP13) (Leung et al. 2011; Leung et al. 2012). Overexpression of either of these ARTDs leads to SG

assembly partially dependent on their catalytic activity (Leung et al. 2012; Leung et al. 2011; Welsby et al. 2014). For ARTD8 (PARP14) it is controversially discussed whether it localizes to SGs. Antibody staining of endogenous protein suggested that it might reside in SGs, however overexpression studies rather indicated processing bodies (P-bodies) as the relevant foci even though co-localization with ARTD13 was observed (Leung et al. 2011; Carter-O'Connell et al. 2018). In the end, both propositions might be true depending on the context, as SGs and P-bodies are described to be functionally linked and share components and mRNAs (Kedersha et al. 2005; Anderson et al. 2009b). Of note is, that PARylation is discussed to have a role as a scaffold for LLPS and thus in SG assembly (Luscher et al. 2018; Leung et al. 2012). The PAR mediated SG assembly relies on the one hand on PARylation of SG components such as G3BP1, TIA-1, ARTD13 and Argonaut proteins (AGO1-4) and on the other hand recruitment of PAR binding proteins including poly(A) binding protein (PABP) (Leung et al. 2011; Leung et al. 2012; Gagné et al. 2008). Interestingly, several proteins have been described to be able to bind RNA as well as PAR due to their similarities in structure, further intertwining the roles of both molecules (Malet et al. 2009; Neuvonen et al. 2009; Leung et al. 2012; Butepage et al. 2018b). Therein, binding to RNA and PAR regulates the structure of SGs dynamically upon stress (Leung et al. 2012). In this context apart from PAR, MARYlation by the mono-ARTDs recruited to the SGs might either function as a seeding event for PARylation or MAR might have a role in LLPS itself, which still needs to be investigated (Luscher et al. 2018).

ARTD12 is described to inhibit translation dependent on several domains (Leung et al. 2011; Leung et al. 2012; Welsby et al. 2014; Atasheva et al. 2014). Upon oxidative stress or overexpression, ARTD12 is recruited to SGs, dependent on PAR and its PAR-binding WWE domain (Welsby et al. 2014; Catara et al. 2017). Further its ability to bind RNA via the Zinc fingers is required for the localization to SGs as well as the ability to inhibit translation (Leung et al. 2011; Welsby et al. 2014). Accordingly, an ARTD12 mutant lacking the Zinc fingers is excluded from SGs and rather localizes to cytoplasmic p62/ubiquitin bodies (Welsby et al. 2014). Additionally, even though no direct substrates have been identified to date, the catalytic activity of ARTD12 is likewise crucial to repress mRNA translation (Welsby et al. 2014). Because ARTD12 associates with mRNA, polysomes and translation initiation as well as elongation factors, it was proposed that it might modify and thus inhibit members of the translation machinery but this theory remains to be verified (Welsby et al. 2014; Atasheva et al. 2014).

The translation machinery comprises multiple enzymes and factors including elongation factor 2 (EF2). EF2 is a conserved GTPase, that mediates the movement of the growing peptide chain along the mRNA. For instance upon IL-1 β stimulation, EF2 is MARYlated which inhibits translation (Jäger et al. 2011; Bock et al. 2015; Haciosmanoğlu et al. 2016). The responsible transferase is not known, but ARTD8 and ARTD10 are promising candidates, since EF2 has been identified as a potential substrate in chemical genetics approaches for both proteins (Carter-O'Connell et al. 2018; Carter-O'Connell et al. 2016).

Generally, mass spectrometry analyses of ADP-ribosylated or ADP-ribose-binding proteins regularly identify many RNA binding proteins and GO enrichment of processes including RNA processing, splicing and decay as well as translation, which suggests a broad entanglement of RNA and ADP-ribosylation (Bock et al. 2015; Carter-O'Connell et al. 2016; Carter-O'Connell et al. 2018; Rodriguez et al. 2021). Only in recent years the amount of ADP-ribosylome studies in the absence of DNA damage inducing agents and under conditions for enrichment of MARYlation rather than PARylation have increased. Therefore, especially for MARYlation, many of the potential substrates have not been confirmed or investigated with regard to

functional consequences of the modification. However, the correlation of potential mono-ARTD interactors with RNA metabolism associated proteins and processes is striking and might help in unraveling the mechanism behind observed phenomena like the ARTD12-mediated inhibition of translation.

One of the confirmed substrates from mass spectrometry analyses of ARTD8 as well as ARTD14 are the two isoforms of the inactive ARTD13 (Carter-O'Connell et al. 2018; Rodriguez et al. 2021). For ARTD14, it was further determined that the acceptor sites are cysteine residues that are predominantly localized in the RNA-binding Zinc fingers. Interestingly, this includes six of the Zinc-coordinating cysteines which suggests consequences for the structure of the zinc fingers (Rodriguez et al. 2021). Further, within SGs both ARTD13 variants are PARylated, potentially by ARTD5, which also resides in these foci (Leung et al. 2011; Leung et al. 2012). Accordingly, even though ARTD13 itself is considered to be inactive, its functions might still be regulated by ADP-ribosylation (Leung et al. 2011; Leung et al. 2012; Karlberg et al. 2015; Carter-O'Connell et al. 2018; Rodriguez et al. 2021). ARTD13 has been implicated in the regulation of translation and mRNA stability by RNA decay as well as microRNA (miRNA) silencing (Leung et al. 2012; Bock et al. 2015; Kim et al. 2020). This regulation is however limited to RNAs that ARTD13 can specifically bind to via its CCCH Zinc finger domains and binding to the mRNA is a prerequisite (Todorova et al. 2015). ARTD13 can mediate repression of translation by binding to eukaryotic initiation factor 4A (eIF4A), a part of the translation initiation complex. The eIF4A-ARTD13-mRNA interaction blocks association with another component of the translation initiation complex, eIF4G and thus blocks protein synthesis (Zhu et al. 2012). All three proteins localize to SGs (Anderson et al. 2015; Hofmann et al. 2021). SGs can determine the fate of stalled mRNAs by either releasing the mRNA to resume translation or recruit P-bodies or exosomes to mediate RNA decay (Anderson et al. 2009b; Anderson et al. 2015). For instance, ARTD13 mediates the degradation of *TNF-related apoptosis-inducing ligand receptor 4 (TRAILR4)* mRNA (Todorova et al. 2014). Via its Zinc fingers, ARTD13 specifically binds to the 3' untranslated region (UTR) of the *TRAILR4* mRNA and subsequently recruits poly(A)-specific ribonuclease (PARN) which shortens the poly(A) tail and the exosome complex which executes 3' to 5' exonucleolytic RNA decay (Todorova et al. 2014). In addition, ARTD13 can also direct 5' to 3' RNA decay via its interaction partner DEAD-box RNA helicase DDX17, that can also reside in SGs (Todorova et al. 2015; Hirai et al. 2020). DDX17 recruits the mRNA-decapping enzyme subunit 1 and 2 (DCP1 and 2) as well as the 5' to 3' exoribonuclease 1 (XRN1), all of which are core components of P-bodies (Anderson et al. 2009b; Todorova et al. 2015; Anderson et al. 2015). Subsequently DCP1 and 2 remove the 7-methyl guanine cap and XRN1 degrades the mRNA 5' to 3' (Todorova et al. 2015). While the 5' to 3' RNA decay machinery is exclusive for P-bodies, SGs and P-bodies both share components of the miRNA silencing complex including AGO1-4 (Anderson et al. 2015). AGO proteins can be loaded with miRNA proteins that specifically base pair with their complementary target mRNA. AGO-miRNA complexes form the core of the RNA-induced Silencing Complex (RISC) which leads to translational silencing and degradation of the target mRNA (Nowak et al. 2021). Here ARTD13 inhibits AGO activity and thus miRNA silencing by inducing AGO PARylation through ARTD5 recruitment (Leung et al. 2011; Leung et al. 2012). As ARTD13 is involved in translation repression, SG assembly, miRNA silencing and exosomal as well as XRN1-mediated RNA decay, it is conceivable that it can regulate and determine mRNA fate upon stress. This ability might therein be regulated by interaction with different co-factors including ARTD5, ARTD8, ARTD12 and ARTD14 as well as its ADP-ribosylation status suggesting cooperativity between the different ARTD family members once more.

Apart from ARTD13, ARTD8 (PARP14) can regulate the mRNA stability of *Tissue Factor* (TF) in macrophages. To do so it interacts specifically with the 3' UTR of the TF mRNA as well as tristetraprolin (TTP), a protein known to destabilize specific mRNAs. This complex formation leads to destabilization of the TF mRNA and thus also less TF protein (Iqbal et al. 2014). It is not known whether TF mRNA decay relies on ARTD8 catalytic activity and MARYlation (Iqbal et al. 2014). Interestingly a similar mechanism could not be demonstrated for other TTP targets thus far (Iqbal et al. 2014). Of note is, that TTP can also localize to SGs and P-bodies dependent on the conditions, encouraging the hypothesis that ARTD8 might also be able to localize to both compartments (Stoecklin et al. 2004; Kedersha et al. 2005; Anderson et al. 2015). Further, a chemical genetics approach identified potential substrates of ARTD8 in cell lysates and interestingly a majority of these proteins, including ARTD13, was associated with RNA related GO terms including RNA metabolism, RNA processing and translation initiation (Carter-O'Connell et al. 2018). Similarly, the viability of ARTD8 knockdown cells was described to rely on genes involved in rRNA and mRNA processing and translation as well (Dhoonmoon et al. 2020). This suggests that ARTD8 function might be further intertwined with RNA biology which remains to be investigated in the future.

1.1.1.1.4 ARTD10

ARTD10 is one of the best studied mono-ARTDs with several identified substrates. ARTD10 was first identified as an interactor of c-Myc, where it prevents co-transformation by c-Myc and the adenoviral E1A of rat embryonic fibroblasts. This tumor suppressor function is independent of catalytic activity but requires nuclear localization (Yu et al. 2005). Generally, ARTD10 is able to shuttle between the nucleus and the cytosol and thus has functions and substrates in both compartments (Yu et al. 2005; Kleine et al. 2012). The export from the nucleus is dependent on Crm1 and the nuclear export sequence (NES) within ARTD10, however the transferase lacks a classical nuclear localization sequence (NLS) and the mechanism of nuclear import is not known (**Figure 6**)(Yu et al. 2005; Kleine et al. 2012). Within the nucleus, the activity of ARTD10 is regulated by cell cycle-dependent phosphorylation. Exclusively in the late G1 phase the cyclin E/cyclin-dependent kinase 2 (CDK2) complex phosphorylates ARTD10 at T101, which potentially boosts MARYlation activity (**Figure 6**)(Chou et al. 2006). Accordingly, this modification is only present in proliferating cells and it suggests a role for ARTD10 in cell cycle progression. Indeed, loss of ARTD10 led to G1 phase arrest of the cells and overall reduced viability (Chou et al. 2006). In this publication it was also first mentioned, that ARTD10 overexpression likewise led to growth arrest and cell death in HeLa cells, apparently independent of the phosphorylation status (Chou et al. 2006). In later studies, this finding was confirmed and analyzed in more detail (Herzog et al. 2013; Kleine et al. 2008). Upon overexpression, ARTD10 drives HeLa cells into apoptosis, dependent on catalytic activity (Herzog et al. 2013; Kleine et al. 2008). Therein, the capacity to MARYlate is required, but not sufficient as the deletion of the potential RNA recognition motif abolished the pro-apoptotic effect even though the protein remained catalytically active (**Figure 6**)(Herzog et al. 2013). An according deletion of the crucial N-terminus can be achieved by caspase 6-dependent cleavage at position 406 (**Figure 6**)(Herzog et al. 2013). Caspase-6 is an effector caspase, that can be activated under specific stress conditions, including inflammation and apoptosis (Zheng et al. 2020). It is comprehensible, that ARTD10 protein amount and activity need to be tightly regulated and balanced, since elevated as well as decreased levels hamper proliferation, survival and genomic integrity (Chou et al. 2006; Herzog et al. 2013; Kleine et al. 2008; Nicolae

et al. 2014; Shahrour et al. 2016; Venkannagari et al. 2016; Schleicher et al. 2018). Accordingly, next to phosphorylation by cyclin E/CDK2 and proteolytic cleavage by caspase-6, several mechanisms of transcriptional, post-transcriptional as well as post-translational regulation have been described, that will be further outlined in the following (**Figure 6**)(Kaufmann et al. 2015; Luscher et al. 2018; Gao et al. 2020; Nie et al. 2020; Tian et al. 2020a; Yahui et al. 2020).

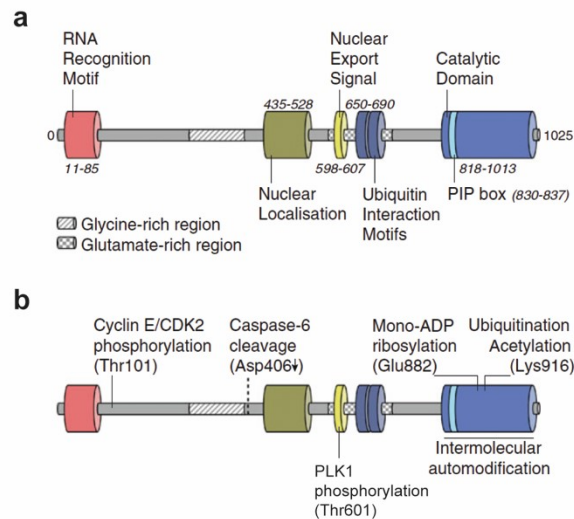


Figure 6: Schematic representation of the structure and post-translational modifications of ARTD10.

The figure is modified from Kaufman et al. 2015 (Kaufmann et al. 2015) (**a**) Depicted is the structural architecture of ARTD10 with the following motifs and domains: RNA Recognition motif (RRM; aa 11-85); Glycine-rich region (GRD; aa 281-399); broad nuclear localization region (aa 435-528); glutamate-rich region (aa 588-697); nuclear export signal (NES; aa 598-607); two ubiquitin interaction motifs (UIMs; aa 650-667 and 673-690); catalytic PARP domain (aa 818-1013) and PCNA interaction peptide box (PIP box; aa 830-837). (**b**) Depicted are the so far known post-translational modifications (PTMs) of ARTD10, that potentially modulate its function: Cyclin E/CDK2 phosphorylation at threonine 101; caspase-6 mediated cleavage after aspartate 406; PLK1 phosphorylation at threonine 601; auto-MARylation mostly takes place within the catalytic domain, with glutamate 882 as one identified site of modification; lysine 916 may be ubiquitinated or acetylated by unknown enzymes.

The ARTD10 protein levels are post-transcriptionally regulated. The *ARTD10* mRNA can be N⁶-methyladenosine (m⁶A) methylated by METTL3 (Gao et al. 2020). This modification can generally influence all stages of mRNA metabolism, including processing, translation and degradation (Zhao et al. 2017). In the case of *ARTD10*, m⁶A methylation leads to degradation of the mRNA and thus decreased protein levels (Gao et al. 2020). This can be antagonized by the non-coding cardiac-hypertrophy-associated PIWI-interacting RNA (CHAPIR) in complex with protein PIWIL4. As the name suggests, this is especially relevant in cardiac hypertrophy, where CHAPIR-PIWIL4 directly interacts with METTL3 to block m⁶A methylation of the *ARTD10* mRNA. This leads to increased levels of ARTD10 and promotes pathology (Gao et al. 2020). On a mechanistic level, ARTD10 may increase cardiac hypertrophy by regulation of glycogen synthase kinase-3 β (GSK3 β) activity (Gao et al. 2020). ARTD10 can MARylate GSK3 β and thereby inhibit its kinase activity (Feijs et al. 2013b). To resolve cardiac hypertrophy, GSK3 β phosphorylates nuclear factor of activated T cells 4 (NFATC4), which is consequently excluded from the nucleus prohibiting NFACT4-dependent expression of cardiac-hypertrophy-associated genes and thus restoring heart function (Antos et al. 2002). When CHAPIR and ARTD10 levels are increased, GSK3 β activity is decreases and NFACT4 can drive hypertrophy unopposed (Gao et al. 2020).

In addition to GSK3 β , other kinases are described to be regulated by ARTD10, hinting at a common modulatory mechanism for kinase activity and thus signaling (Feijs et al. 2013b; Zhao et al. 2018; Tian et al. 2020a; Tian et al. 2020b). In hippocampal neurons, ARTD10 MARylates protein kinase C delta (PKC δ), likewise inhibiting its kinase activity (Tian et al. 2020b). Because

PKC δ kinase activity is essential for the excitability of hippocampal neurons by regulating the voltage-gated K(+) channel Kv1.1, so is ARTD10. Inhibition of ARTD10 MARYlation activity increases the excitability neurons and thus stimulus transmission in the brain (Tian et al. 2020b).

Another central kinase controlled by ARTD10 MARYlation is Aurora kinase A (Zhao et al. 2018). This kinase was first identified as a potential substrate of ARTD10 in an *in vitro* Protoarray, along with many other kinases (Feijs et al. 2013b). This finding could be corroborated by in cell data in the context of several tumor cells and especially HCC. In metastatic HCC, ARTD10 is regularly downregulated and further it could be demonstrated that ARTD10-deficiency increase metastasis in other tumor cell lines (Zhao et al. 2018). These findings suggest that ARTD10 can suppress metastasis and indeed overexpression of ARTD10 could inhibit cell-migration dependent on its catalytic activity (Zhao et al. 2018). Furthermore, Aurora A was identified as the relevant substrate in this scenario. ARTD10 binds and MARYlates Aurora A, which abolishes kinase activity and thus downstream signaling (Zhao et al. 2018). Aurora A regulates multiple signaling pathways including NF- κ B, Hippo, Wnt/ β -catenin and mTOR signaling and has been broadly implicated as a driver of tumor metastasis in the past (Zhao et al. 2018; Lin et al. 2020). By regulation of Aurora A through MARYlation, ARTD10 is by extension able to control these pathways indicating a central role in the decision of cell fate dependent on catalytic activity. In a recent study, it has been suggested that ARTD10 activity can be boosted by the E3 ubiquitin ligase RNF114 (Yahui et al. 2020). RNF114 can directly interact with ARTD10 dependent on auto-MARYlation and therefore dependent on basal catalytic activity. Subsequently, RNF114 modifies ARDT10 with K27-linked polyubiquitination at an unknown position which is suggested to increase ARTD10 activity (Yahui et al. 2020). As K916, which is located in the catalytic domain, has been identified to be ubiquitinated in MS studies, this site could be a promising candidate (**Figure 6**)(Kaufmann et al. 2015). Comparable to ARTD10, RNF114 deficiency also promotes tumor metastasis, strengthening the hypothesis of a cooperative function (Yahui et al. 2020).

While RNF114 is described to positively influence ARTD10 activity, RNF146 proposedly targets ARTD10 for proteasomal degradation by K48-linked polyubiquitination. Interestingly, this function was described to be independent of Tankyrase activity, introducing a new mode of action for RNF146 (Nie et al. 2020). To date the site of modification is not known and neither is the Tankyrase-independent regulation of RNF146 activity (Nie et al. 2020). Generally, ARTD10 function is tightly coupled to ubiquitin and ubiquitination in several cases. Under basal conditions, ARTD10 predominantly localizes to cytoplasmic granules, that are neither stress granules, nor P-bodies or endosomes (Kleine et al. 2012; Mayo et al. 2018). Not much is known about the composition or function of these membraneless compartments, except that they contain ubiquitin, the ubiquitin-receptor p62/sequestosome 1 and glyceraldehyde 3-phosphate dehydrogenase (GAPDH) in addition to ARTD10 (Kleine et al. 2012; Mayo et al. 2018). GAPDH is further MARYlated but the functional consequences of the modification are unknown. The function of the association with ubiquitin and p62 is not understood, but it is conceivable that the “ARTD10 bodies” depict a sort of storage system to ensure availability upon stress. For example, it was proposed that they could fuse to autophagosomes when autophagy is induced, where p62 is known to play a crucial role in selective cargo recognition dependent on ubiquitination (Kleine et al. 2012; Lamark et al. 2017). However, to date there is no experimental data to support this hypothesis.

On top of autophagy, ubiquitination and p62 are involved in NF- κ B signaling, where p62 is suggested to be essential for the tumor necrosis factor receptor-associated factor 6 (TRAF6)-mediated ubiquitination of the NF- κ B essential modulator (NEMO) in response to IL-1 β (Zotti

et al. 2014). Interestingly, ARTD10 regulates the same central step within the pathway (Verheugd et al. 2013). After IL-1 β or tumor necrosis factor α (TNF α) stimulation, different TRAFs are recruited and activated downstream of the IL-1 receptor (IL-1R) or the TNF receptor (TNFR), respectively. One of them is TRAF6, an E3 ubiquitin ligase that transfers K63-linked polyubiquitin chains onto itself and downstream effectors (Shi et al. 2018; Adhikari et al. 2007). Auto-ubiquitination of TRAF6 functions as a scaffold for the recruitment of the I κ B kinase complex (IKK) and the transforming growth factor- β -activated kinase (TAK1) complex. IKK as well as TAK1 contain regulatory subunits, namely NEMO and TAK1-binding proteins 1 and 2 (TAB1/2), respectively, that contain UIMs that specifically bind to K63-linked ubiquitin chains (Shi et al. 2018; Adhikari et al. 2007). In addition to the regulatory subunits, both complexes contain catalytic subunits: the kinases IKK α and β or TAK1. Facilitated by proximity, TAK1 is able to phosphorylate the IKK β subunit, activating the IKK complex (Shi et al. 2018; Adhikari et al. 2007). Subsequently, TRAF6 conjugates K63-linked polyubiquitin to NEMO, which is likewise required for IKK activity. Activation of IKK activity leads to nuclear translocation of the NF- κ B transcription factor subunit p65/RelA and active gene transcription (Shi et al. 2018; Adhikari et al. 2007). Generally, the crosstalk between K63-linked polyubiquitination and phosphorylation plays a central role in the propagation of NF- κ B signaling (Karin et al. 2000). In addition to IKK and TAK1, ARTD10 can bind to the K63-linked auto-ubiquitination of TRAF6 via its UIMs (**Figure 6**) (Verheugd et al. 2013). Upon recruitment of NEMO to the same ubiquitin chains, ARTD10 interacts with and MARYlates NEMO. This modification prohibits K63-ubiquitination of NEMO and thus downstream signaling (Verheugd et al. 2013). Recently, a study described additional layers of regulation for the ARTD10-mediated inhibition of NF- κ B signaling (Tian et al. 2020a). Therein the polo-like kinase 1 (PLK1) and ARTD10 cross-regulate each other. PLK1 is an important regulator of mitosis, that can phosphorylate ARTD10 at T601 (**Figure 6**). Potentially, this modification is dependent on prior phosphorylation of T101 by CCNE/CDK2, that occurs in the G1 phase (Tian et al. 2020a; Chou et al. 2006). T601 phosphorylation of ARTD10 prevents its interaction with NEMO and therefore allows NEMO ubiquitination and promotes NF- κ B signaling (Tian et al. 2020a). Further, NF- κ B inhibits transcription from the *ARTD10* promoter and thus downregulates the ARTD10 protein levels (Tian et al. 2020a). To counteract this, ARTD10 can MARYlate PLK1, which decreases PLK1 kinase activity and T601 phosphorylation and hence promotes ARTD10-mediated inhibition of NEMO ubiquitination (Tian et al. 2020a). Further the PLK1-ARTD10-NF- κ B axis represents another example of crosstalk between MARYlation and ubiquitination as well as MARYlation and phosphorylation in a central signaling cascade.

1.2.3 ARTDs in immunity – a focus on mono-ADP-ribosylation

Generally, eukaryotic ADP-ribosylation is tightly coupled to cellular stress responses like DNA damage repair or the unfolded protein response (Beck et al. 2014; Dhoonmoon et al. 2020; Nicolae et al. 2015; Nicolae et al. 2014; Feijs et al. 2013c; Yang et al. 2020). Further, the previous chapters have demonstrated how crucial the regulation of ARTD expression and thus activity is in health and disease (Zhou et al. 2011; Aguiar et al. 2000; Arechederra et al. 2018; Chou et al. 2006; Tian et al. 2020a; Gao et al. 2020). Strong positive, meaning diversifying, selection during evolution is a hallmark for the relevance of proteins in host-pathogen conflicts. When a protein is a central part of the immune defense, it has to constantly develop to keep pace with the fast-evolving pathogens like viruses (Daugherty et al. 2014; Daugherty et al. 2012). These genes can be identified by analysis of the ratio between amino acid sequence altering to silent mutations during evolution (Daugherty et al. 2014). Therein it was

identified that nearly a third of the ARTDs evolve under strong positive selection in primates (Daugherty et al. 2014). This includes ARTD4, as well as ARTD7-9 and ARTD13 (Kerns et al. 2008; Daugherty et al. 2014). In ARTD4 an intrinsically disordered stretch is especially evolutionarily targeted and even though no direct anti-pathogenic functions have been described so far, the RNA vaults, that ARTD4 resides in, are implicated in immunity (Daugherty et al. 2014; Berger et al. 2009). For ARTD7 no roles have been identified in pathogen restriction yet, however ARTD8, ARTD9 and ARTD13 are well known for their role in the immune response, that will be discussed further hereafter (Fehr et al. 2020). Generally, the fast evolution of several ARTDs suggests, that ADP-ribosylation does not only have housekeeping functions like maintaining the genomic integrity of cells, but further is part of the biological arms race between host and pathogen (Kerns et al. 2008; Daugherty et al. 2014).

In line with this, several of the mono-ARTDs, that usually show only low abundance in healthy cells, are upregulated by infections, pathogen associated molecular patterns (PAMPs) as well as type I and II interferons (Fehr et al. 2020; Luscher et al. 2018). ARTD8 protein levels were elevated subsequent to *Mycobacterium tuberculosis* exposure of human monocytes, where it was even identified as a marker for clearance (Kaewseekhao et al. 2015). Further, infection of the same cells with *Borrelia burgdorferi*, a tick-borne gram-negative bacterium, induces the expression of *ARTD8*, *ARTD9*, *ARTD10*, and *ARTD12* by activation of Toll-like receptor 1 and 2 (TLR1/2) heterodimers (Salazar et al. 2009). Another common stimulus upon bacterial infection is lipopolysaccharides (LPS), which signals mainly through TLR4 (Lu et al. 2008). Prior to this thesis, Annika Gross could show in our lab, that LPS is also able to induce *ARTD10* mRNA as well as protein expression in activated human monocytes/macrophages (Eckei et al. 2017). This was corroborated by bulk RNA sequencing of murine bone marrow-derived macrophages with LPS, where *ARTD3*, *ARTD4*, *ARTD8-14* and *ARTD16* were upregulated (Curina et al. 2017; Caprara et al. 2018).

LPS/TLR4 signaling induces central proinflammatory cytokines as well as the type I interferon (IFN) response to activate and boost the immune response upon bacterial infection (Lu et al. 2008). In humans, 10 different TLRs have been described that recognize distinct PAMPs and localize to the plasma membrane or endosomes. In addition to components of the bacterial outer membrane like LPS and lipoproteins, they can also sense dsRNA, ssRNA and nonmethylated CpG oligonucleotide DNA, that constitute hallmarks for viral infections (Lu et al. 2008; Negishi et al. 2018). Generally, TLRs signal through adaptor proteins, including different IFN response factors (IRFs), to induce the type I IFN response (Negishi et al. 2018). IFNs can be subdivided into three subtypes, type I, II and III, depending on the receptors they bind to. Type I IFNs include for instance IFN α and β that bind to the IFN α/β receptor 1 and 2 (IFNAR1/2) heterodimer and signal through the Janus kinases JAK1 and TYK2 (Negishi et al. 2018). Besides bacterial infection and LPS, some mono-ARTDs can be activated directly by stimulation with type I IFNs. This has been shown for ARTD8-14 in several publications by now (Atasheva et al. 2012; Liu et al. 2012; Zhang et al. 2015; Atasheva et al. 2014; Shaw et al. 2017; Eckei et al. 2017). In fact, this activation of *mono-ARTD* genes in response to the type I IFN response is even evolutionary conserved. This was evaluated by RNA sequencing of fibroblast from 10 different vertebrate animals, reaching from microbats and bats, over chicken to rats, dogs and humans. On top of distinct interferon response genes (ISGs) for every species, 62 core ISGs could be identified in all vertebrates analyzed that included *ARTD8-9* and *ARTD12-13* (Shaw et al. 2017). Of note is, that *ARTD10* was still induced in 8 and *ARTD11* in 7 out of 10 species (Shaw et al. 2017). Additionally, *ARTD8-9* and *ARTD11-12* expression can be activated by type II IFNs as well (Juszczynski et al. 2006; Liu et al. 2012; Hu et al. 2020; Caprara et al. 2018). This subtype includes only a single gene, namely IFN γ , which is exclusively secreted in

the antiviral state of immune cells like T-cells, B-cells, natural killer (NK) cells, dendritic cells and macrophages, downstream of type I IFN or IL-12 exposure (Negishi et al. 2018). Apart from artificial stimulation with IFNs, *ARTD8-14* can also be up-regulated in response to actual viral infection by murine hepatitis virus (MHV), a coronavirus (Grunewald et al. 2019; Grunewald et al. 2020). Further, SARS-CoV-2 infection induced *ARTD8*, *ARTD10*, *ARTD12* and *ARTD14* (Heer et al. 2020), the new world alphavirus Venezuelan equine encephalitis virus (VEEV) led to expression of *ARTD12* (Atasheva et al. 2012) and Hantaan virus increases the mRNA levels of *ARTD10* (Lu et al. 2020).

Several ARTDs have already been described to restrict the propagation of several pathogens, including bacteria and viruses. ARTD8 restricts *Salmonella typhimurium* replication and *Mycobacterium tuberculosis* infection (Kaewseekhao et al. 2015; Caprara et al. 2018). Moreover, ARTD10, ARTD12 and ARTD14 can restrict VEEV replication, a positive single stranded RNA virus (Atasheva et al. 2014). The mechanism is not understood but it was shown that all three mono-ARTDs may inhibit cellular translation of the viral proteins (Atasheva et al. 2014). Further, for ARTD12 the direct binding to polysomes, as described above, seems to be relevant for its ability to counteract VEEV infection (Welsby et al. 2014; Atasheva et al. 2014). Apart from VEEV, ARTD14 is described to restrict another Alphavirus, SINV, and so does ARTD9 (Fehr et al. 2020). Further, multiple ARTDs have been described to inhibit MHV, including ARTD8, ARTD12 and ARTD14 (Fehr et al. 2020). In addition, knockdown of *ARTD10* increases Hantaan virus replication and inhibition of ARTD10 is pro-viral in avian influenza virus infection (AIV, H5N1) while overexpression is restricting (Yu et al. 2011; Lu et al. 2020). Interestingly, the AIV protein NS1 leads to decreased amounts of ARTD10 protein through direct interaction to promote cell cycle progression and thus viral replication, although it is not known how (Yu et al. 2011). This further highlights the importance of ARTD10 in the antiviral defense towards AIV. Moreover, ARTD13 is described to restrict multiple viral families including Alphaviruses, Orthomyxoviruses, like Influenza A virus (IAV), Flaviviruses, like ZIKA, Picornaviruses, Herpesviruses and Hepatitis B virus (Fehr et al. 2020). These findings support a broad role of ARTDs in antiviral responses to different pathogens, especially viruses.

Apart from the studies that solely examined the capacity of ARTDs to suppress replication of different pathogens, there is also research that studied the mechanisms of how this restriction takes place. The probably best studied PARP with antiviral activity is ARTD13/PARP13, that is accordingly also referred to as Zinc finger antiviral protein (ZAP). However, since ARTD13 does not have catalytic activity, it will only be introduced here briefly, as it is out of scope of this thesis (Karlberg et al. 2015; Kleine et al. 2008). The ZnF domains in ARTD13 can specifically bind to viral RNA dependent on high CG content to differentiate between self and foreign RNA (Takata et al. 2017; Fehr et al. 2020). Further, ARTD13 binds to the exosome and therefore recruits it to viral RNA that is consequently degraded (Guo et al. 2007; Fehr et al. 2020). In case of Alphaviruses however, the mechanism of viral RNA recognition is independent of the CG content and dependent on the SG association of ARTD13 (Fehr et al. 2020). For SINV it is also described, that ARTD14 can bind to the viral RNA and recruit the exosome to mediate degradation independent of catalytic activity, comparable to ARTD13 (Kim et al. 2020; Kozaki et al. 2017). Whether these ARTDs work cooperatively or redundantly is not known. Moreover, ARTD13 blocks translation of viral RNA by inhibition of eIF4G-eIF4A interaction (Zhu et al. 2012; Fehr et al. 2020). As a third well described mechanism to control viral replication, ARTD13 was described to induce proteasomal degradation of the IAV proteins PB2 and PA dependent on PARylation and ubiquitination (Liu et al. 2015; Fehr et al. 2020). Similarly, ARTD12 can MARYlate the NS1 and NS3 proteins of ZIKA virus which functions as a

seeding event for subsequent PARylation, ubiquitination and proteasomal degradation (Li et al. 2018). It can be speculated that both these mechanisms depend on the Tankyrase-RNF146 axis since it is PARylation- and ubiquitination-mediated. In a related fashion, the ARTD9/DTX3L complex can stimulate degradation of the 3C protease of Encephalomyocarditis virus (EMCV), which is likely dependent on the intrinsic ubiquitination activity of DTX3L and it is unknown whether ADP-ribosylation is important (Zhang et al. 2015). In addition to full-length ARTD13 (also ZAP-L) a shorter isoform exists that lacks the PARP domain (ARTD13.2, ZAP-S). This shorter isoform is described to interact with retinoic acid-inducible gene I (RIG-I), an intracellular receptor that senses dsRNA. This interaction promotes oligomerization of RIG-I and thus downstream antiviral and pro-inflammatory signaling (Leung et al. 2012; Fehr et al. 2020). However, depending on the context, ARTD13.2 may also downregulate IFN signaling by binding and destabilizing the *IFN- β* mRNA, potentially as a negative feedback loop (Schwerk et al. 2019; Fehr et al. 2020).

Many of the previously described functions of the different mono-ARTDs are also relevant in host-pathogen conflicts. For instance, regulation of signaling pathways like NF- κ B and IFN signaling. In addition to IL-1 β and TNF- α , NF- κ B signaling can be activated downstream of several TLRs or RIG-I, where it plays a central role in the induction of pro-inflammatory cytokines (Cui et al. 2014). Several ARTDs are known to regulate TLR and RIG-I signaling. As already mentioned ARTD13.2 promotes RIG-I signaling, however independent of MARylation (Leung et al. 2012; Fehr et al. 2020). Comparably, ARTD12 can increase NF- κ B and IRF signaling dependent on catalytic activity potentially by interaction with TIR domain-containing adapter inducing IFN- β (TRIF) (Welsby et al. 2014; Fehr et al. 2020). TRIF is a potential adaptor protein downstream of TLR3 and TLR4 that is necessary for the recruitment of TRAF3 and TRAF6 (Cui et al. 2014). Also, ARTD8 may promote NF- κ B signaling by an unknown mechanism in cancer cells (Yao et al. 2019). Apart from this, two other mono-ARTDs, ARTD10 and ARTD7, are described to rather inhibit NF- κ B signaling (Fehr et al. 2020). As described in more detail previously (Chapter 1.1.1.1.2), ARTD10 is recruited to TRAF6 by binding to TRAF6 auto-ubiquitination, just like NEMO. Subsequently, ARTD10 MARylates NEMO which prevents its poly-ubiquitination and thus downstream activation of the NF- κ B transcription factor (Verheugd et al. 2013). It is of note however, that it is unknown whether this happens during infection. Alternatively or additionally to NEMO, TRAF family-member-associated NF- κ B activator (TANK) binding kinase 1 (TBK1) can function downstream of TRIF and TRAFs. TBK1 phosphorylates IRF3 in order to activate IRF3-dependent Type I IFN signaling (Cui et al. 2014; Fehr et al. 2020). This step can be blocked by ARTD14, which MARylates TBK-1 and thereby inhibits its kinase activity (Yamada et al. 2016; Grunewald et al. 2020; Gozgit et al. 2021). This function of ARTD14 proposedly intended to avoid chronic inflammation and constitutive activation of IFN signaling. However, it has been reported that ARTD14 plays a proviral role in IAV and MHV infection (Yamada et al. 2016; Grunewald et al. 2020). But, as mentioned previously, ARTD14 also has antiviral functions. Accordingly, ARTD14 may play antiviral and proviral roles depending on the virus. In contrast to this, ARTD11 plays a strictly proviral role downstream of IFN. This mono-ARTD MARylates the E3 ubiquitin ligase β -transducin repeat-containing protein (β -TrCP) which can in turn ubiquitinate and target IFNAR1 for degradation (Guo et al. 2019). As it is strongly induced by IFN itself (Shaw et al. 2017; Grunewald et al. 2019), it is imaginable that it is supposed to function within a negative feedback loop that is exploited by viruses.

Furthermore, several of the ARTDs are described to directly influence signaling pathways on a transcriptional level and thus abundance of anti-pathogenic proteins. Within the nucleus, ARTD1, ARTD8, ARTD9 and the tankyrases have been described as direct transcriptional co-regulators of genes involved in the immune response (Welsby et al. 2012). Therein, ARTD8 and ARTD9/DTX3L are described to regulate STAT signaling, especially in macrophages and T-cells. For ARTD9/DTX3L a strictly pro-inflammatory function has been described and its loss acts anti-inflammatory (Iwata et al. 2016; Fehr et al. 2020). Expression of the complex leads to a broad induction of ISGs (Juszczynski et al. 2006; Zhang et al. 2015; Iwata et al. 2016). This is mediated on the one hand by direct interaction of ARTD9/DTX3L with STAT1, which increases its phosphorylation and transcription factor activity (Zhang et al. 2015; Iwata et al. 2016). Additionally, the complex can ubiquitinate the histone variant H2BJ, which subsequently remodels the chromatin to increase expression of ISGs (Zhang et al. 2015). In contrast to this, ARTD8 is rather described as the counter player of ARTD9/DTX3L that functions anti-inflammatory in differentiated macrophages. It MARYlates STAT1 which suppresses phosphorylation and hence downstream signaling (Iwata et al. 2016). Additionally, it shifts signaling rather towards the anti-inflammatory, pro-survival signaling of the IL-4-STAT6 pathway as a cofactor for STAT6 likewise dependent on its catalytic activity (Goenka et al. 2006; Goenka et al. 2007; Mehrotra et al. 2011).

In response to LPS and *S. typhimurium* in undifferentiated macrophages however ARTD8 is required to induce type I IFN signaling and to repress and clear infection (Caprara et al. 2018). Mechanistically, ARTD8 promotes the nuclear accumulation of several other ISGs and further enhances IRF3 transcription factor activity by increasing H3K27ac and RNA Pol II at the IRF3 promoter (Caprara et al. 2018). It is unknown whether this mechanism depends on catalytic activity of ARTD8 and whether this is different for viral infections. However, upon CoV infection ARTD8 was also crucial to rise an IFN I response (Grunewald et al. 2019). It is imaginable that the functions of ARTD8 vary between different cell type and infections. In line with this, ARTD9 and ARTD8 are described to function cooperatively in certain cancer cells, where ARTD9 rather represses STAT1 signaling through the STAT1 β isoform and promotes IL-4/STAT6 signaling and downregulation of IRF3 together with ARTD8, inducing pro-survival signaling (Camicia et al. 2013; Bachmann et al. 2014). This further emphasizes that the roles of ARTD8 and ARTD9 in the regulation of gene expression might be highly context dependent.

The subcellular localization of some mono-ARTDs further hints at potential functions in the innate immune defense. As described previously, the IFN-inducible ARTD7, ARTD12 and ARTD13 localize to stress granules and can even induce their assembly. Generally, these structures facilitate the antiviral state and stall viral replication and translation (McCormick et al. 2017). Additionally, ARTD8, ARTD10 and ARTD12 are associated with p62 (Kleine et al. 2012; Welsby et al. 2014; Caprara et al. 2018). P62 is a well-studied autophagy receptor, that also functions in xenophagy – pathogen associated autophagy. Therein xenophagy and p62 facilitate the clearance of certain intracellular viruses or bacteria (Bauckman et al. 2015; Kudchodkar et al. 2009). ARTD10 resides in p62 foci upon overexpression and potentially after IFN α -mediated expression (Kleine et al. 2012; Forst et al. 2013). For ARTD8 the interaction is inducible by LPS (Caprara et al. 2018). Similarly, ARTD12 co-localization with p62 cytoplasmic foci is increased downstream of TLR4 signaling (Welsby et al. 2014). Accordingly, it is imaginable that these mono-ARTDs function in the storage and release of p62 to facilitate fast induction of autophagy after infection. Furthermore, it is imaginable that p62-mediated autophagy leads to the clearance of stress granules containing pathogen components guided by ARTD12 which shuttles between these foci (Welsby et al. 2014). However, at this point

these functions are purely speculative and have to be investigated in the future. Comparably several identified substrates of mono-ARTDs play roles innate immunity, like GSK3 β , PKC δ and Aurora kinase A (Cui et al. 2014; Lin et al. 2020). These have all been identified as substrates of ARTD10 but they remain to be investigated in the context of infection (Feijs et al. 2013b; Zhao et al. 2018; Tian et al. 2020b).

Taken together, several mono-ARTDs as well as MARYlation seem to function in the innate immune response to pathogens as demonstrated by their expression patterns and broad restrictive capacities. Nonetheless, mechanistically little is known about the modes of action and there appear to be substantial differences between diverse cell types and pathogens. Further investigation of relevant interactors and substrates under specific infection conditions may lead to better understanding of the underlying mechanisms and may facilitate the development of anti-pathogenic treatments in the future.

1.2.4 Readers and Erasers of ADP-ribosylation

So far the previous chapters focused on the writers of ADP-ribosylation. However, in order to allow signal propagation, ADP-ribosylation requires specific readers that recognize the modification and promote recruitment of downstream factors. Equally important, signaling, especially stress signaling, needs to be terminated to enable the return to the basal state of the cells. Hence erasers that may revert the modification are likewise needed. As ADP-ribosylation is such a versatile PTM that comprises mono- as well as oligo-, poly- and branched poly-ADP-ribosylation on a multitude of amino acids, several specific and general readers and erasers are necessary to be able to remove and differentiate between the different bonds and species (Luscher et al. 2018)(**Figure 7**).

For instance there are several known binding motives that specifically recognize distinct regions within PAR chains (Luscher et al. 2018)(**Figure 7**). Therein, the WWE domain, the forkhead-associated (FHA) domain and the oligonucleotide/oligosaccharide binding (OB)-fold bind to *iso*-ADPr (Luscher et al. 2018). Meanwhile, the BRCA1 carboxy-terminal domain (BRCT), PAR-binding zinc finger (PBZ) domains and PAR-binding macrodomains bind to the terminal ADPr unit of the polymer (Luscher et al. 2018). Additionally, a specific PAR-binding peptide motif (PEP) and the PiIT N-terminal (PIN) domain have been identified as PAR readers (Luscher et al. 2018). Generally, these PAR readers propagate signaling downstream of the pARTDs, namely ARTD1 and 2 as well as the Tankyrases. For instance, these domains mediate the recruitment of DNA damage repair factors to sites of DNA damage (Luscher et al. 2018). In contrast, so far there is only one protein fold that can specifically bind to MARYlation: the macrodomain (**Figure 7**)(Luscher et al. 2018).

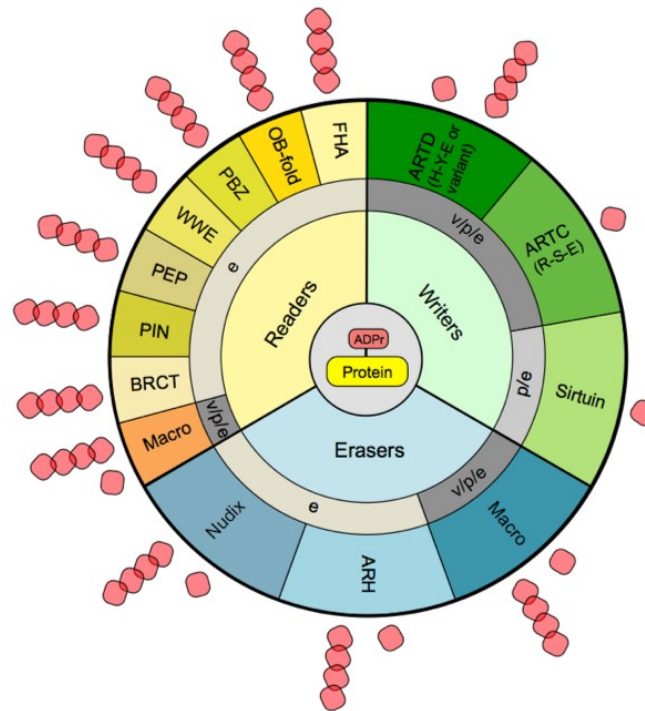


Figure 7: Writers, readers and erasers of protein ADP-ribosylation.

Depicted are the proteins and domains that are associated with ADP-ribosylation either as writers, readers or erasers of MAR- or PARYlation as indicated. Additionally, their distribution over different domains of life is shown. BRCT, BRCA1 C-terminal domain; e, eukaryotes; FHA, forkhead-associated domain; Macro, macrodomain; OB-fold, oligonucleotide/oligosaccharide binding fold; p, prokaryotes; PEP, PAR binding peptide motif; PBZ, PAR binding zinc finger; PIN, PiIT N-terminus domain; v, viruses; WWE, Tryptophan-Tryptophan-Glutamate domain (Luscher et al. 2018).

ADP-ribosylation is a fully reversible modification. Accordingly, there are specific erasers capable of removing MARYlation as well as PARYlation (**Figure 7**)(Luscher et al. 2018). Three protein families or domains have been described to be able to hydrolyze ADP-ribosylation: the nucleoside diphosphate linked to a variable moiety X (Nudix) proteins, the ADP-ribosylhydrolase (ARH) family as well as certain macrodomain-containing proteins (**Figure 7**)(Luscher et al. 2018). Additionally, the nucleotide pyrophosphatase/phosphodiesterase (NPP) protein family has been identified with potential hydrolase activity towards protein-conjugated ADP-ribosylation lately as well (Palazzo et al. 2016; O'Sullivan et al. 2019). While NUDT5 is restricted to processing free ADPr, NUDT9 and NUDT16 can catalyze partial removal of protein-conjugated PARYlation or PARYlation and MARYlation, respectively (O'Sullivan et al. 2019). Within the NPP family ENPP1 was described to have the same catalytic activity as NUDT9 and NUDT16 just without a Nudix domain (O'Sullivan et al. 2019).

The ARH family consists of three members: ARH1, ARH2 and ARH3 (Mashimo et al. 2014). ARH1 can specifically hydrolyse *N*-glycosidic bonds. Hence, it is able to completely remove arginine-linked MARYlation (Mashimo et al. 2014; Luscher et al. 2018; O'Sullivan et al. 2019). ARH1 was the first enzyme identified to be able to completely remove MARYlation from a protein (Moss et al. 1985). As ARH1 is restricted to arginine-linked MARYlation it can reverse the effect of the ecto-ARTCs as well as the eponymous cholera toxin (Luscher et al. 2018; O'Sullivan et al. 2019). Meanwhile, the second family member, ARH2, is considered to be catalytically inactive (Luscher et al. 2018; O'Sullivan et al. 2019). Finally, ARH3 acts as a specific hydrolase for *O*-glycosidic bonds of ADPr units. Accordingly, ARH3 is able to reduce PAR chains piece by piece to free ADPr units (O'Sullivan et al. 2019). Further research identified ARH3 as the hydrolase that can fully reverse serine-linked ADP-ribosylation by ARTD1/HPF1 as ADP-ribose is linked to the serine by an *O*-glycosidic bond as well (O'Sullivan et al. 2019). It is

assumed that ARH3 is restricted to exoglycosidic activity, meaning that it may only act on the terminal ADPr unit (Mueller-Dieckmann et al. 2006).

Finally, four macrodomain-containing proteins have been identified as erasers of ADP-ribosylation. Next to ARH3, PARG is the only enzyme capable of degrading PAR chains into single ADPr moieties by hydrolysis of the *O*-glycosidic bonds connecting the units (Hatakeyama et al. 1986; Luscher et al. 2018; O'Sullivan et al. 2019). However, the activity of PARG towards PAR chains is different from that of ARH3, as PARG possess exoglycosidic as well as endoglycosidic activity (Brochu et al. 1994). Consequently, it can produce protein free PAR chains as well as single ADPr units, preferably from long PAR chains (Hatakeyama et al. 1986; Brochu et al. 1994; Braun et al. 1994). PARG is unable to remove the final, amino acid-linked ADPr, even in the case of serine modification, resulting in MARYlation (Hatakeyama et al. 1986; Brochu et al. 1994; Braun et al. 1994; Luscher et al. 2018; O'Sullivan et al. 2019).

While the MARYlation of arginines and serines can be removed by ARH1 and ARH3, respectively, MARYlation of the acidic glutamate and aspartate residues is reverted by three other macrodomain-containing proteins: MacroD1, MacroD2 and the terminal ADP-ribose protein glycohydrolase (TARG1 aka C6orf130/OARD1) (Feijs et al. 2013a; Rosenthal et al. 2013; Jankevicius et al. 2013). Accordingly, these three enzymes are considered to be the cellular counter players of most ARTD modifications together with ARH3 and PARG. Additionally, for TARG1 it was described that it can remove entire PAR chains from the acceptor amino acid after ARTD1 activation through DNA damage, generating free PAR (Sharifi et al. 2013).

To date there is no enzyme known, that is able to remove lysine-linked MARYlation from proteins completely. However, there has been a great deal of discussion in the field whether modification of lysines actually occurs specifically or whether it is just an artefact of glycation, mass spectrometry and the analysis thereof (Luscher et al. 2018). Likewise, no enzyme has been identified that can entirely revert ARTD14-mediated cysteine MARYlation, although MacroD1 and MacroD2 have been suggested to counteract its cellular functions as discussed below (Ahmed et al. 2015; Bindesbøll et al. 2016). Further, partial activity against ARTD14 modification has been reported for MacroD2 (Rodriguez et al. 2021).

Interestingly, *O*-acetyl-ADPr (OAADPr), the byproduct of sirtuin deacetylation activity, can be hydrolyzed by ARH3, Nudix proteins and the cellular macrodomain-containing MARYhydrolases as well (Feijs et al. 2013a). This might be relevant as OAADPr is proposed to have functions as a second messenger in different cellular processes including regulation of reactive oxygen species and gene regulation (Imai et al. 2000; Jackson et al. 2002; Borra et al. 2004; Tong et al. 2010; Bheda et al. 2016).

1.2.4.1 Macrodomains as modulators of ADP-ribosylation

The macrodomain is a conserved globular protein fold that consists of a central β -sheet with six strands surrounded by five α -helices, that usually comprises 130-190 aa (**Figure 8a**). Depending on the macrodomain, it is noteworthy, that it can have more β -sheet strands and more α -helices, but these are the minimal requirements (Rack et al. 2016). In mammals, the macrodomain fold was first identified within rat macroH2A, a large histone variant, that possesses a typical histone fold at its N-terminus and the macrodomain at its C-terminus (**Figure 8b**)(Feijs et al. 2013a; Luscher et al. 2018). All subsequently defined homologues were accordingly named macrodomains. Generally, the macrodomain fold has been strongly linked to ADP-ribosylation and its variations and derivatives in a linked or free form (Rack et al. 2016). Different macrodomains can act as readers of MAR or PAR or as erasers of MAR and PAR, as mentioned previously (**Figure 7**)(Feijs et al. 2013a; Forst et al. 2013; Luscher et al. 2018).

Generally, ADPr derivatives are bound inside a cleft on the surface of the globular module, therein PAR readers bind the terminal ADPr moiety of the polymer (Rack et al. 2016; O'Sullivan et al. 2019). Within the binding cleft a conserved aromatic residue and an aspartate coordinate the adenosine. Additionally, two loops, loop 1 and loop 2, further stabilize the pyrophosphate and ribose part and are proposed to provide substrate specificity (Rack et al. 2016). A conserved glycine in loop 1 is readily essential for substrate binding and in case of the macrodomain hydrolases, the catalytic residues are localized in loop 1 as well (Rack et al. 2016; Butepage et al. 2018b; Forst et al. 2013). Generally, macrodomains can be divided into six different classes based on phylogenetic analyses: macro-H2A-like, ALC1-like, macro2-type, MacroD-like, PARG-like and SUD-M-like (Rack et al. 2016). Interestingly, the macrodomain is not necessarily evident on sequence level but there are cases where the fold was only identified after structural analyses like for PARG (Slade et al. 2011). Hence, it is imaginable that more macrodomains will be identified in the future when their structure is resolved.

Twelve human proteins were identified so far that possess macrodomains, encoded by eleven genes (**Figure 8b**) (Feijs et al. 2013a; Luscher et al. 2018). Amplified in liver cancer 1 (ALC1) and macroH2A1.1 are PAR binders, that are involved in the DNA-damage response subsequent to ARTD1 activation. Therein ALC1 is a chromatin remodeling factor, while macroH2A1.1 is incorporated into nucleosomes and leads to chromatin condensation and repression of gene expression (Ladurner 2003; Timinszky et al. 2009). The two other macroH2A variants, macroH2A1.2 and macroH2A2 however are unable to bind PAR or other ADPr derivatives (Feijs et al. 2013a; Neuvonen et al. 2009). Neither is ganglioside-induced differentiation-associated protein 2 (GDAP2 aka MacroD3), but it was described to bind poly(A) (Feijs et al. 2013a; Neuvonen et al. 2009).

PARG, the macrodomain-containing degrader of PAR, has five isoforms expressed from a single gene and resulting from alternative mRNA splicing. Three of the five isoforms possess catalytic activity (Meyer-Ficca et al. 2004; Luscher et al. 2018; O'Sullivan et al. 2019). Out of these three active isoforms, one, PARG110, resides in the nucleus where it is a major counter player of ARTD1 and thus prevents cellular energy exhaustion and allows the restart of transcription after the DNA damage response (Henning et al. 2018). The two other active isoforms, PARG99 and PARG102, localize to the cytoplasm where they may reverse tankyrase activity (Leung et al. 2012; Leung et al. 2011). During stress conditions, they localize to stress granules where they modulate their dynamic disassembly. In coherence with this, overexpression of these PARG isoforms represses assembly of SGs as opposed to ARTD overexpression (Leung et al. 2012; Leung et al. 2011). Loss of PARG is embryonically lethal (O'Sullivan et al. 2019).

In humans, three mono-ARTDs exist that possess multiple macrodomains in addition to their ART domains: ARTD7, ARTD8 and ARTD9. Therein, ARTD7 and ARTD9 possess two macrodomains and ARTD8 has three macrodomains N-terminally of the ART domains (**Figure 8b**) (Luscher et al. 2018). Especially, the macrodomains of these proteins have been described to be under strong positive selection, suggesting an essential role in host-pathogen conflicts (Daugherty et al. 2014). Further, phylogenetic analyses suggest, that these macrodomains have different specificities and functions as they do not cluster protein wise but rather macrodomains from different ARTDs cluster together (Aguar et al. 2005; Daugherty et al. 2014). Accordingly, macro2 and macro3 of ARTD8 and macro2 of ARTD7 were shown to bind specific protein-linked auto-MARylation of ARTD8, ARTD10 and ARTD12 catalytic domains *in vitro*, indicating some substrate specificity (Forst et al. 2013; Ekblad et al. 2018). Meanwhile, in neither molecule macro1 seems to have ADPr binding activity (Forst et al. 2013; Ekblad et al. 2018). For ARTD8 it was described that it can interact with catalytically active ARTD10 and

is recruited to ARTD10 foci in a MARYlation dependent manner (Forst et al. 2013). Furthermore, macro2 and macro3 were shown to interact with some ARTD10 substrates including Ran and NEMO (Forst et al. 2013; Verheugd et al. 2013). However, the function of these interactions remains elusive, but macro2-3 of human as well as mouse ARTD8/Artd8 have been established as important tools to study MARYlation (Forst et al. 2013; Gibson et al. 2017; Butepage et al. 2018a).

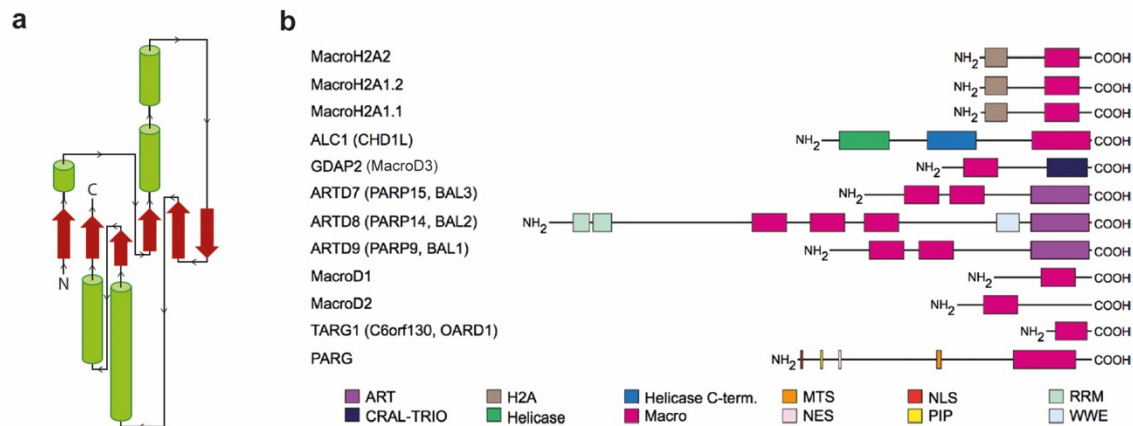


Figure 8: Schematic representation of the macrodomain fold and the 12 human, macrodomain-containing proteins.

(a) The conserved macrodomain fold consists of a β -sheet with a minimum of six strands in the center, that is surrounded by at least five α -helices. The β -sheet is depicted in red while the α -helices are green. 'N' marks the N-terminus and 'C' the C-terminus of the structure (Rack et al. 2016). **(b)** So far 12 human proteins, encoded by 11 genes, have been defined that possess macrodomains. These macrodomains can function as readers of PAR (macroH2A1.1, ALC1, ARTD9, MacroD1, TARG1) or MAR (ARTD8) and as erasers of PAR (PARG) or MAR (MacroD1, MacroD2 and TARG1). The following domains are depicted: ART, ADP-ribosyltransferase; CRAL-TRIO, cellular retinaldehyde binding protein triple functional domain protein; H2A, histone fold within macroH2A; Macro, macrodomain; MTS, mitochondrial targeting sequence; NES, nuclear export sequence; NLS, nuclear localization sequence; PIP, PCNA interacting peptide; RRM, RNA recognition motif; WWE, domain with conserved Tryptophan-Tryptophan-Glutamate (W-W-E) residues (Luscher et al. 2018).

In contrast, the macrodomains within ARTD9 recognize free ADPr, protein MARYlation and PAR (Yang et al. 2021; Karras et al. 2005; Camicia et al. 2013). Multiple of the cellular functions described for ARTD9 seem to depend on its macrodomains. Therein, macro2 of ARTD9 is responsible for PAR-dependent targeting to sites of DNA damage, where the ARTD9/DTX3L complex facilitates the recruitment of DNA damage response factors. Mechanistically, it is not known how ARTD9/DTX3L contribute to the DNA damage response but it was shown that they mediate chemoresistance of cancers (Yan et al. 2009; Yan et al. 2013; Camicia et al. 2013). Additionally, the previously described regulation of IFN signaling by ARTD9/DTX3L is mediated by ADP-ribosylation and macrodomain dependent interaction with STAT1 and STAT2 (Camicia et al. 2013). Further, both macrodomains within ARTD9 recognize the PARP7-mediated MARYlation of androgen receptor (AR) at cysteines which recruits the ARTD9/DTX3L complex. ARTD9/DTX3L are proposed to enhance AR signaling (Yang et al. 2021). Generally, the macrodomains in all macrodomain-containing ARTDs were shown to regulate transcription when associated with promoters, however in a rather artificial setup (Aguiar et al. 2005). The fact that multiple ARTDs possess reader domains that recognize different forms of ADP-ribosylation, like WWE and macrodomains, suggests crosstalk and potentially cooperativity between these molecules and generally a role for MAR- and PARYlation in the localization of the ARTDs (**Figure 5**) (Luscher et al. 2018; Forst et al. 2013; Kirby et al. 2018; Grimaldi et al. 2019; Wang et al. 2012; He et al. 2012; Welsby et al. 2014). This is for example described for ARTD8/ARTD9 in STAT signaling, ARTD7/ARTD9 in AR signaling and ARTD12/Tankyrase in stress granules as described previously (Bachmann et al. 2014; Iwata et al. 2016; Yang et al.

2021; Catara et al. 2017; Li et al. 2018). Interestingly, for ARTD11 it was described, that its own catalytic activity regulates its localization to the nuclear envelope (Kirby et al. 2018).

The last group of macrodomain-containing proteins in humans are the cellular MAR hydrolases MacroD1, MacroD2 and TARG1 (**Figure 8b**) (Feijs et al. 2013a; Luscher et al. 2018). While MacroD1 and TARG1 are rather ubiquitously expressed, MacroD2 has very low expression levels in all cells except neuroblastoma cells and certain tumors (Zaja et al. 2020; Luscher et al. 2018). MacroD1 can localize to mitochondria, the nucleus and the cytoplasm (Zaja et al. 2020). Loss of MacroD1 leads to defects in the mitochondrial morphology, however the function of MacroD1 in mitochondria remains elusive (Zaja et al. 2020). To date no convincing ART activity has been mapped to the mitochondria that would need to be regulated by MacroD1 MAR hydrolase activity. The proposed MARYlation activities of SIRT4 and NEURL4 in mitochondria are controversial (Du et al. 2009; Haigis et al. 2006; Cardamone et al. 2020). Alternatively, the hydrolytic activity of MacroD1 towards OAADPr may play a role in mitochondria (Feijs et al. 2013a). In the nucleus, MacroD1 is described to influence transcription through interaction with several transcription factors. This includes AHR, liver X receptor (LXR), AR, NF- κ B and estrogen receptor (ER) (Ahmed et al. 2015; Bindsbøll et al. 2016; Feijs et al. 2020). In case of AHR and LXR signaling MacroD1 was proposed to antagonize PARP7 MARYlation which leads to activation or suppression of AHR and LXR, respectively (Ahmed et al. 2015; Bindsbøll et al. 2016). It further enhances AR and NF- κ B, pathways that are likewise known to be regulated by MARYlation, however the mechanisms are not understood yet (Feijs et al. 2020; Fehr et al. 2020; Yang et al. 2021). The functions of MacroD2 are even less understood than those of MacroD1. Dysregulation of MacroD2 is associated with autism and cancer but the reasons are undetermined (Feijs et al. 2020; Luscher et al. 2018). Further, it is potentially excluded from the nucleus upon DNA damage and it may also counteract PARP7 in LXR signaling but not AHR signaling (Ahmed et al. 2015; Bindsbøll et al. 2016). TARG1 on the other hand can be detected in the nucleolus, the nucleoplasm and potentially in stress granules (Sharifi et al. 2013; Butepage et al. 2018b; Zaja et al. 2020). The shuttling between nucleus and nucleolus is governed by competitive binding to PAR and RNA (Butepage et al. 2018b). Under basal conditions TARG1 accumulates in the nucleolus while induction of DNA damage leads to PAR-mediated recruitment to the sites of DNA damage. Loss of TARG1 leads to disruption of the nucleolar structure and potentially increased sensitivity to DNA damage (Sharifi et al. 2013; Butepage et al. 2018b; Zaja et al. 2020). Unlike MacroD1 and MacroD2, TARG1 is proposed to be able to release complete PAR chains in addition of MAR hydrolase activity towards acidic residues (Sharifi et al. 2013; O'Sullivan et al. 2019).

Taken together the 12 macrodomain-containing human proteins regulate, propagate and counteract ADP-ribosylation signaling in multiple compartments and pathways in the cell and their functions are essential to maintain homeostasis.

1.2.5 ADP-ribosylation of nucleic acids

Thus far, ADP-ribosylation was only examined as a post-translation modification of proteins. However, recent studies found, that distinct sites within nucleic acids may likewise serve as acceptors of ADP-ribosylation (Weixler et al. 2021). Therein, the cellular transferases ARTD1, ARTD2 and ARTD3 were shown to modify ssDNA as well as dsDNA, potentially with implications for DNA damage repair (Weixler et al. 2021). Meanwhile ARTD10 and the catalytic domains of ARTD11 and ARTD15 could only MARYlate ssRNA efficiently (Weixler et al. 2021). Interestingly, the ARTD homologue tRNA 2'-phosphotransferase 1 (TRPT1) was the only

enzyme capable of MARylating ssDNA as well as ssRNA (Weixler et al. 2021). In any case phosphorylation was a mandatory prerequisite for the modification of RNA as well as DNA. Therefore, both molecules were exclusively modified at the 5' or 3' phosphorylated ends (Weixler et al. 2021).

Comparable to proteins, the PARylation and MARylation of nucleic acids is fully reversible. PARG can remove PARylation and MARylation from DNA, while TARG1, MACROD2 and ARH3 hydrolyze MARylation on DNA (Weixler et al. 2021). Similarly, PARG, TARG1, MACROD2, ARH3 can likewise remove MARylation of ssRNA, and additionally MACROD1 and NUDT16 are capable of erasing this as well (Weixler et al. 2021).

To date these modifications of RNA and DNA have only been studied *in vitro* or in cell free extracts and their abundance and functional relevance in cells remain to be investigated. However, these findings open a completely new perspective for the importance of ADP-ribosylation in the regulation of intracellular genome maintenance, transcription and translation as well as possibly in host-pathogen conflicts.

1.2.6 Non-eukaryotic ADP-ribosylation – a conserved modification

As the names of Diphtheria and Cholera toxin-like ARTs already suggest, ADP-ribosylation and its modulation are not unique for eukaryotes. In fact the bacterial ARTs as well as the hydrolases are discussed to be the ancestors of the eukaryotic counterparts (Aravind et al. 2015). Many non-eukaryotic organisms encode conserved structures that are associated with ADP-ribosylation (**Figure 7**) (Luscher et al. 2018). However, only very few of these organisms are predicted to be capable to completing a full cycle of ADP-ribosylation. Therein, the variety of genes associated with ADP-ribosylation generally correlates with the complexity of the species. This means most bacteria, archaea and viruses merely encode either for potential writers or erasers of ADP-ribosylation. Only eleven bacterial species are predicted to possess the necessary enzymes to transfer and remove ADP-ribosylation completely as investigated by domain searches and sequence similarity (Neuvonen et al. 2009; Daugherty et al. 2014; Perina et al. 2014; Rack et al. 2016). This suggests that most non-eukaryotes use isolated mediators of ADP-ribosylation to control ADP-ribosylation in their host cells. In line with this, several pathogens have been shown to rely on their capacity to modulate ADP-ribosylation for replication and propagation and/or pathogenesis and modulation of the host immune response (Eriksson et al. 2008; Kuri et al. 2011; Park et al. 2009; Rack et al. 2015; Simon et al. 2014; Luscher et al. 2018).

1.2.6.1 Viral macrodomains

Several viruses are described to require ADP-ribosylation for their propagation, including herpes simplex virus and vaccinia virus (Child et al. 1988; Li et al. 2012; Daugherty et al. 2014). In addition, some positive-sense, single stranded RNA ((+)ssRNA) viruses encode for structurally conserved macrodomains. These viruses belong to the viral family of Coronaviridae and the so-called alpha-like supergroup of viruses. This alpha-like supergroup contains the Alphaviruses and further includes hepatitis E viruses and Rubella virus (Eriksson et al. 2008; Egloff et al. 2006; Malet et al. 2009). For several viruses the macrodomain is also often called the X domain (Putics et al. 2005; Putics et al. 2006a; Putics et al. 2006b; Eriksson et al. 2008).

For Human coronavirus 229E (HCoV-229E), the functions of the macrodomain were first proposed to be dispensable as mutational studies showed no effects on viral replication (Putics et al. 2005). However, further research demonstrated that the macrodomain mutants of SARS and HCoV-229E led to increased sensitivity to the antiviral effects of interferon rather than effects on general genome replication (Kuri et al. 2011). Comparably, while mutations of the macrodomain in the mouse hepatitis virus strain A59 (MHV-A59) only led to slightly reduced viral loads, the production of proinflammatory cytokines like IL-6 was strongly decreased. In line with this, the induction of liver disease by MHV-59 was abolished when the macrodomain was mutated (Eriksson et al. 2008). In contrast to these viral families, mutations of the macrodomain in Sindbis virus (SINV), a prototypic Alphavirus, results in a decrease of viral RNA replication, especially in neuronal cells (Park et al. 2009). Consequentially, the virulence and lethality of SINV with mutations within the macrodomain is likewise reduced in mice (Park et al. 2009). Interestingly, in case of SINV, reversion of the mutations was readily observed, suggesting that the macrodomain is essential for the virus (Park et al. 2009). Though mutations of the viral macrodomains demonstrated functional relevance for replication or pathogenesis in several instances as described above, the biochemistry of these proteins remains poorly studied. Initially, it was proposed that the main function of viral macrodomains is phosphatase activity towards ADP-ribose-1''-monophosphate (Appr-1''-p) resulting in ADPr (ADRP activity). This activity was first shown for several coronaviruses including HCoV-229E, porcine, SARS-CoV and transmissible gastroenteritis virus (TGEV) (Putics et al. 2005; Saikatendu et al. 2005; Putics et al. 2006a; Putics et al. 2006b). Further, mutational studies revealed Asparagine 1302 (N1302), N1305, H1310, G1312, and G1313 as residues essential for the phosphatase activity of the HCoV-229E macrodomain (Putics et al. 2005; Putics et al. 2006b). In addition, ADRP activity was also demonstrated for the macrodomains of hepatitis E virus (HEV) and several Alphaviruses including Semliki Forest virus (SFV), VEEV and Chikungunya virus (CHIKV) (Egloff et al. 2006). However, it was proposed that other functions might be more relevant since the ADRP activity is rather weak (Egloff et al. 2006). Consistently, the macrodomains of SARS-CoV, HEV and SFV were shown to efficiently bind to free ADPr as well as PAR (Egloff et al. 2006). Furthermore, it was established that the macrodomains of the Alphaviruses SINV, VEEV and CHIKV can likewise bind to ADP-ribose and PAR via their conserved binding pocket (Malet et al. 2009; Park et al. 2009). In fact, it was determined that the binding affinity of Alphaviral macrodomains towards ADPr and PAR is even higher than that of coronaviruses (Malet et al. 2009). Moreover, it was illustrated that the conserved aspartic acid at position 10 (D10) of the CHIKV macrodomain is essential for the binding of adenine, while N24 and Y114 are required for ADRP activity (Malet et al. 2009). Additionally, the CHIKV macrodomain can bind negatively charged polymers like PAR and RNA independently of the ADPr binding pocket, potentially mediated by positive patches on its surfaces, comparable to the cellular TARG1 (Malet et al. 2009; Butepage et al. 2018b). Consistently, it was shown, that the N10A and N24A macrodomain mutants of SINV, that show defects in viral replication and decreased virulence, show no effects on PAR binding (Park et al. 2009), suggesting that another function of the macrodomain might be of relevance for the virus.

Taken together, previous studies of the relevance of the macrodomain for different viral families suggest that, even though the functions seem to differ between species, it appears to be important for the viral pathologies. If the viral pathology is decreased by modulation of the viral macrodomain, it might be a good target for antiviral therapy in the future. Therefore, further studies of the biochemistry are required to improve the understanding of relevance of

the macrodomain as only a more detailed biochemical characterization will allow unraveling of the effects of different mutants for binding or catalytic activity as well as molecular functions. Establishment of the viral macrodomains as a drug target is of particular importance because the viral families encoding macrodomains include many animal and human pathogens, that partially cause severe diseases. SARS-CoV and Middle East respiratory syndrome coronavirus (MERS-CoV) have been highlighted by the WHO for years, as diseases that should be prioritized for research due to a high potential to cause a global health emergency (WHO 2015, 2017, 2018a). Additionally, in the last 1.5 years, SARS-CoV-2 demonstrated how a coronavirus can cause a pandemic with nearly 200 million reported cases and almost 4 million deaths worldwide (WHO 2020c; Johns Hopkins University 2021). Generally, coronaviruses are zoonotic viruses that can cause respiratory, enteric, hepatic, and neurological diseases (Liu et al. 2020). Past and current outbreaks of SARS-CoV, MERS-CoV and SARS-CoV-2 presented a wide scope of severity in patients, ranging from asymptomatic, over flu-like symptoms to pneumonia, severe respiratory disease, and death (Liu et al. 2020). In case of SARS-CoV and MERS-CoV, the morbidity and mortality rates of endemic outbreaks were high, reaching 11% and 35%, respectively (Chan-Yeung et al. 2003; WHO 2021). HEV on the other hand remains the main cause for jaundice and hepatitis worldwide with about 20 million infections every year (Pérez-Gracia et al. 2014; Kamar et al. 2014; WHO 2020b). In immunosuppressed individuals, HEV infection can even lead to chronic hepatitis (Pérez-Gracia et al. 2014; Kamar et al. 2014). Even though a vaccine has been licensed in China in 2011, it has not been approved in other countries to date and the need for a vaccine or therapeutics remains unchanged (WHO 2020b). Alphaviruses in general as well as CHIKV, SINV, Mayaro virus and O'nyong'nyong virus (ONNV) in particular, were discussed by the WHO and experts to be prioritized for research as they pose severe health threats (WHO 2015, 2017, 2018c, 2018a). Generally, alphaviruses are arboviruses that are transmitted by mosquitoes and are currently reemerging worldwide due to globalization, travel, and climate changes (Baxter et al. 2020; Martinez et al. 2019; Semenza et al. 2017; Ryan et al. 2019; Kamal et al. 2018). The Alphavirus family can be subdivided into Old World Alphaviruses that mainly cause arthritis, fever and rashes and New World Alphaviruses that rather trigger encephalomyelitis (Baxter et al. 2020). Commonly, Alphaviruses can cause chronic diseases that can last months to years and so far no vaccines or specific therapeutics have been approved (Baxter et al. 2020). Chikungunya virus, an Old World Alphavirus, has been especially highlighted as an emerging health threat in recent years and it will be the focus of the following chapters (Cohen 2016; Janova 2019; McFee 2018; WHO 2018c).

1.3 Chikungunya virus – an emerging virus

Chikungunya virus (CHIKV) is a member of the *Togaviridae* family and the *Alphavirus* genus (International Committee on Taxonomy of Viruses 2020). Further, it is an arthropod-borne virus (Arbovirus), meaning it is transmitted by a vector to humans and other vertebrate animal hosts. In case of CHIKV, these vectors are mosquitoes, mainly *Aedes (Ae.) aegypti* and *albopictus* (Matusali et al. 2019). In the past, CHIKV was restricted to tropical regions in Africa, where it originated, causing small endemic outbreaks. In the last two decades however, it has emerged and spread across the whole equator as well as southwards and northwards to more than 60 countries (**Figure 9**)(WHO 2020a; Silva et al. 2017; Young 2018; Ruckert et al. 2018). Similar developments in emergence can be observed for other arboviruses including Zika and Dengue virus (Young 2018; Ruckert et al. 2018). This unprecedented emergence of mosquito-borne viruses has three main reasons: the spread of their vectors, increased travel around the

world and the evolution of the viruses (Silva et al. 2017; Young 2018; Ruckert et al. 2018). Climate change, urbanization and globalization greatly influenced all three of these factors.

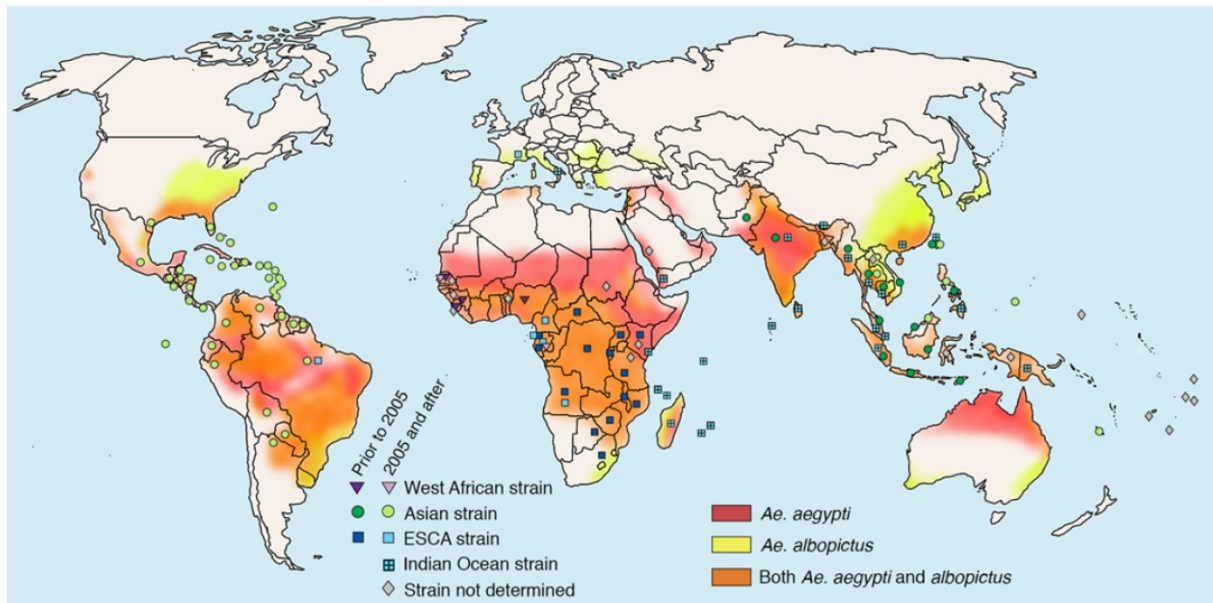


Figure 9: Geographical expansion of CHIKV outbreaks and *Ae. aegypti* and *albopictus*.

Countries, that are affected by endemic CHIKV outbreaks are marked with symbols. Different strains of CHIKV are depicted with different symbols as indicated: Purple triangles: West African strain; green circles: Asian Strain; blue squares: East/Central/South African (ECSA) strain; grey diamond: undetermined strain. Therein, darker shades implicate primary detection before and lighter shades after 2005. Blue squares with a cross represent the Indian Ocean strain, which is a subtype of the ESCA strain. The distribution of the two primary CHIKV vectors, *Ae. aegypti* and *albopictus*, is illustrated by shading. Areas with *Ae. aegypti* presence are marked in red, areas with *Ae. albopictus* presence are marked in yellow and areas where both species are present are marked in orange (Silva et al. 2017).

Rising temperatures and increased rainfall and humidity facilitated the spread of *Ae. aegypti* and *albopictus* and expanded the areas where the mosquitoes can breed and that the mosquito larvae can inhabit (Young 2018). Moreover, urbanization led to a further increase of stagnant water for mosquito breeding, as for instance dams were built, irrigation systems for farming were introduced and large amounts of water are stored in open containments (Young 2018). Hence, both mosquito species were able to spread extensively and they are expected to spread even further in the years to come, especially to the northern hemisphere and together with the mosquitoes the diseases they transmit can spread (Kamal et al. 2018; Ryan et al. 2019).

In 2004 one of the largest outbreaks of CHIKV originated in Kenya. This epidemic expanded to surrounding island in the Indian Ocean and over the course of the consecutive years to multiple countries including previously naïve areas like India, Europe, and the USA. Since 2004, several millions of people were infected with CHIKV and it became endemic in over 60 countries (Silva et al. 2017; WHO 2020a; Suhrbier 2019). This global expansion of CHIKV was promoted mainly by international air travel. Viremic travelers functioned as seeding events in previously unaffected countries like Italy, where they were stung by naïve mosquitoes, commencing a new cycle of human-mosquito-human transmission (Silva et al. 2017; WHO 2020a). Additionally, the fact that urban areas are very densely populated increases the contact between humans and mosquitoes. This accelerates transmission and increases the probability that CHIKV becomes endemic once introduced to a new region (Silva et al. 2017; Young 2018). It is estimated that upon an outbreak 30-75% of the local population can be infected with CHIKV (Suhrbier 2019).

During their life cycles, Arboviruses reside in two very distant hosts: vertebrates as well as arthropods and are therefore under high selective pressure from two evolutionary distinct directions (Ruckert et al. 2018). Further, Introduction of CHIKV and Arboviruses in general into naïve areas can drive evolution of the virus. Infection of different mosquito species, that are resident in new regions, can lead to evolution of the viral population in order to adapt to new vectors (Ruckert et al. 2018). For instance, one of the most prominent mutations in CHIKV is in the structural E1 protein of the envelope, that led to increased fitness in *Ae. albopictus* and thus allowed replication and transmission in areas, where *Ae. aegypti* is not present (Ruckert et al. 2018; Young 2018; Matusali et al. 2019). Therein, *Aedes aegypti* is transmitting the majority of cases in Africa, Asia and the American continents, while *Aedes albopictus* is the leading vector for the cases in Europe and the islands in the Indian Ocean (Matusali et al. 2019). Moreover, multiple mosquito strains all around the globe have been reported to have potential to serve as CHIKV vectors, enhancing its expansion potential (Matusali et al. 2019). Apart from the arthropod hosts, several non-human primates (NHPs) as well as other mammalian species like rodents and bats can serve as vertebrate hosts and potentially reservoirs for CHIKV in addition to humans (Matusali et al. 2019). Accordingly, the high evolutionary and adaptive capacity of CHIKV allowed for a large cellular, tissue and host tropism and therefore facilitated its spread.

Calculations and estimations predict, that in the next decades CHIKV will rather spread even further and become endemic in more countries due to the above summarized drivers (Silva et al. 2017; Kamal et al. 2018; Ryan et al. 2019; Young 2018). Therefore, it is generally considered a disease to watch and in need of research (Cohen 2016; WHO 2018a; Powers et al. 2017).

1.3.1 Chikungunya fever: symptoms, vaccines and therapy

CHIKV infection causes the disease called Chikungunya fever. Chikungunya fever can be subdivided into two phases: an acute and a chronic phase (Suhrbier 2019). Generally, most people affected by acute Chikungunya fever develop fever, (poly)arthralgia, (poly)arthritis, myalgia, headache, and rashes with about 85-95% of the cases being symptomatic (Hua et al. 2017; Suhrbier 2019). This acute phase usually lasts less than two weeks and is comparable to the flu or Dengue virus infections (Hua et al. 2017). However, atypical as well as severe forms of the acute phase have been reported and the disease can be aggravated by co-morbidities and –infections (Suhrbier 2019). Atypical symptoms often include neurological, cardiovascular, respiratory and renal manifestations, especially in elderly patients with co-morbidities (Suhrbier 2019). These atypical symptoms may in some cases develop into severe acute Chikungunya. Accordingly, severe forms of the disease can present with (meningo)encephalitis, cardiac failure, renal failure, multiorgan failure or septic shock that require hospitalization (Suhrbier 2019). Generally, upon Chikungunya infection the hospitalization rates vary from 0.6-13% and mortality rates from 0.024-0.7% and the disease presents with increased risks for infants (< 1 year) and geriatric patients (Suhrbier 2019).

The percentage of patients that develop chronic symptoms of Chikungunya fever is variable. In the first year post infection studies reported between 50 and 80% of chronic manifestations in patients. This number decreases over time and about a third of the cases still presents with persistent symptoms after more than 18 months (Hua et al. 2017). Generally, the risk of developing a chronic disease is increased in patients with strong symptoms in the acute phase, over the age of 45, in females, when high IgG levels are present and upon preexisting conditions of joint injuries or rheumatoid disorders (Hua et al. 2017; Suhrbier 2019). Chronic

Chikungunya is a musculoskeletal disease that is mainly characterized by persisting, rheumatoid arthritis or arthralgia of the joints and tenosynovitis (Hua et al. 2017; Suhrbier 2019; Almeida et al. 2020). The resulting joint pain can present as constant or as recurrent attacks and it can either migrate between affected locations or be non-migratory (Hua et al. 2017). The mechanism of chronic Chikungunya is not fully understood. However, it is common consent that residual viral material and remnants of dead host cells contribute to the persistence of the disease by activating the host immune system (Suhrbier 2019; McCarthy et al. 2016). Generally, it is demanding to isolate material from joints, therefore persistence of viral material is not readily tested in chronic Chikungunya patients. However, it is described in some studies, that residual viral RNA and antigen could be detected. Experiments with mice and NHPs further strengthen this hypothesis, viral RNA, capsid protein, antigen, and partially even infectious viruses could be detected in animals with chronic inflammation and disease manifestations (McCarthy et al. 2016; McCarthy et al. 2018).

Even though Chikungunya presents low mortality rates, the often debilitating joint pain, that accompanies the disease and potentially lasts for months or years, has a strong impact on the patients' quality of life. Moreover, the social and economic burden that this poses is extensive, especially considering that often a high percentage of the local population is affected by an outbreak (Silva et al. 2017; Suhrbier 2019).

To date, no vaccine or specific therapeutic is available to prevent or treat Chikungunya (WHO 2020a). However, several candidates for vaccines are in clinical trials that are based on different vaccine systems: live attenuated, whole-virus inactivated, virus-like particle, virus-vectored as well as mRNA-based vaccines are currently evaluated in phase I or II clinical trials (Schrauf et al. 2020; Goyal et al. 2018). Additionally, recently, the first CHIKV vaccine entered phase III clinical trials and preliminary, positive results have been reported. Therein, 98.5% of the over 4000 participants showed neutralizing antibodies against CHIKV 28 days after administration of the single dose vaccine VLA1553 from Valneva, while it was well tolerated (Valneva SE 2021). Definite results are expected within the next five months, but the vaccine candidate seems promising and has been awarded Fast Track and Breakthrough Therapy Designation by the FDA, which is supposed to accelerate the availability of drugs that are urgently needed (Valneva SE 2021; FDA 2018). This vaccine is based on a live attenuated virus that carries a large deletion of 61 aa at the C-terminus of the essential non-structural protein 3 (nsP3) (Hallengård et al. 2014). This suggests that a vaccine for CHIKV is finally within grasp and might slow down further expansion of CHIKV.

Another prevention strategy is the control of the mosquito vectors and thus the limitation of transmission (Ruckert et al. 2018; Achee et al. 2019; Suhrbier 2019). This is especially of interest, as it also limits the spread of other emerging Arboviruses like Zika and Dengue virus. But classical approaches like insecticides against the adult mosquitoes are often insufficient due to increased development of insecticide resistances (IR) in the *Aedes* populations (Achee et al. 2019; Suhrbier 2019). The elimination of breeding sites or mosquito larvae with larvicides or predatory microbes, copepod or fish is also common practice, however it is hard to accomplish as first all breeding sites need to be identified (Achee et al. 2019). This field of intervention is extensively researched, and alternative strategies are under development. For example, studies on the introduction of genetically modified *Wolbachia*, a symbiotic bacterium that infects mosquitoes, are promising in field studies. This strategy is for instance used to either limit the viability of the eggs or the life span of the mosquitoes or to decrease their capacity to replicate and transmit the pathogen (Achee et al. 2019). A second approach is the release of modified mosquitoes, either sterile males, or insects carrying gene drives or

dominant lethality (Achee et al. 2019). However, these approaches require further research and are partially self-limiting (Achee et al. 2019).

Still, additional specific antiviral treatments are urgently needed. On the one hand because a vaccination and vector control are purely prophylactic and do not improve the quality of life of already affected patients, and on the other hand because additional intervention strategies decrease the probability for the appearance of resistances as previously discussed (Chapter 1.1.3).

Apart from preventive measures, since there is no specific treatment available for Chikungunya, patients are usually medicated with general drugs that manage the pain and relieve the symptoms. Therein, the primary treatment is with standard painkillers like paracetamol to relieve the fever and pain of the acute phase as well as attacks of the chronic arthropathy (Suhrbier 2019).

Furthermore, there have been efforts to develop specific antivirals, that target viral entry into the host cells or replication (Battisti et al. 2021; Suhrbier 2019). These drugs function by directly targeting viral proteins or host factors that are essential for the virus. But to date few of these antivirals have been tested *in vivo* in animal models and none have been successful in clinical trials (Battisti et al. 2021; Suhrbier 2019). Further it is a challenge to find a therapeutic, that is effective subsequent to the acute, viremic phase when only few or no replication takes place anymore. In order to develop specific antivirals to target CHIKV in the acute as well as potentially the chronic phase, more knowledge about the viral life cycle and the functions of the viral proteins and host factors as well as the interaction between these is urgently needed.

1.3.2 The life cycle of CHIKV

After a blood meal of a CHIKV infected host, the virus is taken up into the mosquito, where it first replicates in the midgut epithelial cells. Afterwards it needs to escape the midgut through the basal lamina. Subsequently, the virus can replicate in secondary tissues of the mosquito until it reaches the salivary glands. From the salivary glands CHIKV can then be transmitted to a new vertebrate host via the next blood meal (Ruckert et al. 2018).

In humans, after the bite by an infected mosquito, the primary viral targets are the skin and the blood stream. Therein, skin fibroblast, keratinocytes and melanocytes are the main sites of initial viral replication (Matusali et al. 2019). Further, in the blood stream, CHIKV can infect peripheral blood mononuclear cells (PBMCs) including mainly monocytes but also B-cells and distinct dendritic cells (Matusali et al. 2019). Potentially, CHIKV can even infect platelets and blood cells (Matusali et al. 2019). From the blood stream, CHIKV is further transported to other target organs like the lymph nodes and spleen, skeletal muscles, joints and bone and in rare atypical cases also to the nervous system and the kidney or respiratory tract (Matusali et al. 2019). In skeletal muscles the target cells mainly comprise fibroblast, satellite cells and myotubes, while in joints and bone fibroblasts, macrophages, osteoblast and chondrocytes have been described to be infected (Matusali et al. 2019). Generally, fibroblast, monocytes and macrophages have been described to be the primary targets of CHIKV and these cells also play a role in the atypical infection of organs (Matusali et al. 2019). The wide variety of target cells again demonstrates the high tissue tropism of CHIKV and accordingly the range of adaptability and symptoms of the disease, as discussed previously (Chapter 1.3)(Matusali et al. 2019).

Generally, CHIKV enters the cell via receptor- and clathrin-mediated endocytosis conveyed by binding of the structural E2 glycoprotein in the viral envelope to host cell attachment factors, like prohibitin (PHB), and receptors (**Figure 10**) (Abdelnabi et al. 2015; De Caluwé et al. 2021). The responsible receptor in humans was long unknown, but recently matrix remodeling-associated protein 8 (MXRA8), was identified as a good candidate in several relevant cell types, including dermal and muscle fibroblasts, and in mouse models (Young et al. 2019; Zhang et al. 2019a; Zhang et al. 2018). Of note is, that macropinocytosis has also been discussed as an alternative entry mechanism (De Caluwé et al. 2021; Lee et al. 2019). Within the endosome, the low pH leads to remodeling of the viral envelope and fusion of the E1 envelope protein to the endosomal membrane (**Figure 10**) (Abdelnabi et al. 2015). Consequently, the free nucleocapsid is released into the cytoplasm, where it disassembles and thus liberates the 49S genomic RNA (**Figure 10**) (Abdelnabi et al. 2015).

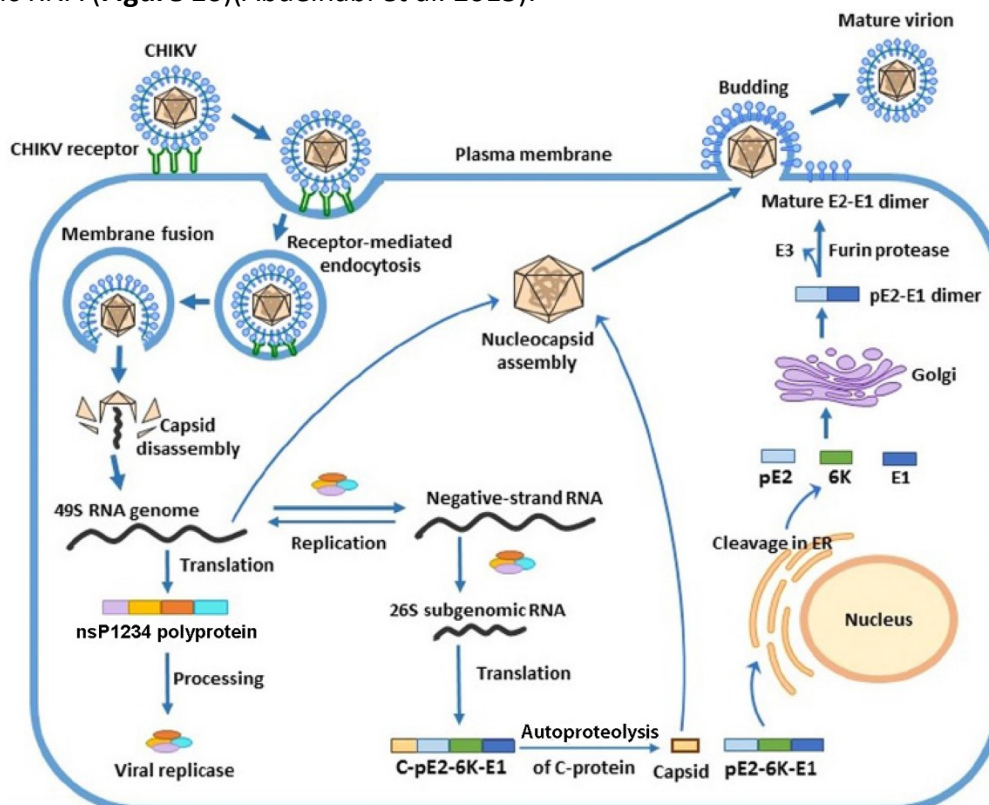


Figure 10: Replication cycle of CHIKV in the human host cell.

CHIKV enters a host cell via receptor-mediated endocytosis. Within the cell, the viral envelope fuses to the endosomal membrane, while the viral nucleocapsid is released into the cytoplasm, where it disassembles. Disassembly of the nucleocapsid in turn releases the viral genomic (49S) RNA. Host factors translate the first ORF of the viral genome into the non-structural polyprotein (nsP1234). This polyprotein is auto-proteolytically cleaved into the isolated nsPs by the viral protease in order to allow formation of the viral replication complex. This viral replicase synthesizes the negative-sense RNA, which serves as a template for subsequent replication of the full genome and transcription of the subgenomic (26S) RNA. Genome replication as well as transcription of the subgenomic RNA are also catalyzed by the viral replicase. Host factors translate the subgenomic RNA into the structural polyprotein (C-pE2-6K-E1). The structural polyprotein is auto-processed by the C-protein to release the C-protein. The C-protein assembles with the newly synthesized genomic RNA to form the nucleocapsid. Meanwhile, the pE2-6K-E1 polyprotein translocates to the ER and is cleaved by the ER-Golgi secretory machinery. The pE2 is processed into mature E2 and E3 proteins by Furin. The nucleocapsid buds from the plasma membrane where it obtains its envelope of membrane-bound E2-E1 heterodimers. C, capsid; ER, endoplasmic reticulum; nsP, non-structural protein; ORF, open reading frame; pE2, precursor E2 (modified from Abdelnabi et al. 2015).

Subsequently, the genomic RNA is translated into the non-structural (ns) polyprotein (nsP1234) by the host cell translation machinery. Stepwise, autoprolytic cleavage processes the polyprotein into the individual ns proteins (nsP1-nsP4), that assemble the viral replication complex (**Figure 10**) (Abdelnabi et al. 2015). This viral replicase thereafter produce

negative-sense, minus-strand RNA from the genomic RNA, which is in turn used as a template for the synthesis of new, full-length genomic RNA as well as the positive-sense, subgenomic 26S RNA (**Figure 10**)(Abdelnabi et al. 2015). Subsequently, the subgenomic RNA is translated into the structural polyprotein (C-pE2-6K-E1) by the host cell machinery (**Figure 10**)(Abdelnabi et al. 2015). Again this structural polyprotein must be processed into the individual structural proteins. First, the capsid protein (C-protein) is auto-proteolytically separated from the rest of the polyprotein. The free C-protein can then assemble the icosahedral nucleocapsid together with the newly synthesized full-length genomic RNA in the cytoplasm of the cell (**Figure 10**)(Abdelnabi et al. 2015; Yap et al. 2017). Meanwhile, the residual pE2-6K-E1 polyprotein is transported through the endoplasmic reticulum (ER) where it is processed into precursor E2 (pE2, also referred to as p62), 6K and E1 by signal peptidases (**Figure 10**)(Abdelnabi et al. 2015; Snyder et al. 2013). Via the ER-Golgi secretory pathway these structural proteins are further transported towards the cell surface. Within the secretory vesicles, the preformed pE2-E1 heterodimers are further processed by the cellular Furin protease into E3 and the mature E2-E1 glycoprotein heterodimers that trimerize into the viral spikes and are deposited within the plasma membrane (**Figure 10**)(Abdelnabi et al. 2015; Yap et al. 2017; De Caluwé et al. 2021). At the plasma membrane, the nucleocapsid is then engulfed into its envelope, consisting of the E2-E1 spikes and lipid membrane, and buds from the cell (**Figure 10**)(Abdelnabi et al. 2015; Yap et al. 2017). The 6K protein is proposed to facilitate glycoprotein processing and folding as well as virus assembly, but remains to be studied in more detail (Silva et al. 2017). It is of note, that in 10-18% of the cases a -1 frameshift of the ribosome within the 6K coding sequence occurs during the translation of the structural polyprotein. This leads to the translation of an additional structural protein instead of 6K: the transframe (TF) protein (Firth et al. 2008; Snyder et al. 2013). It is discussed that TF is likewise important for efficient virus particle assembly and that it is actually more frequently incorporated into the virions than 6K (Firth et al. 2008; Snyder et al. 2013).

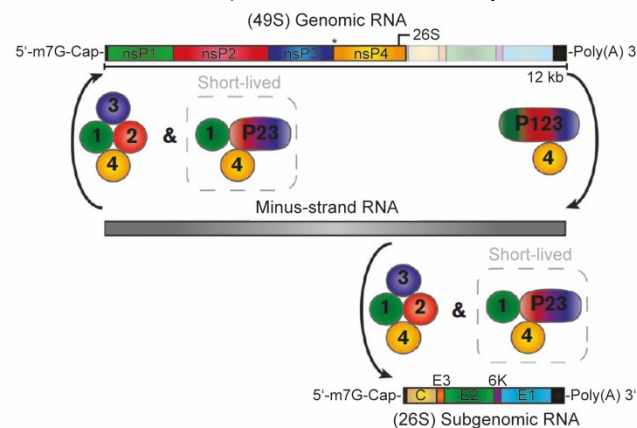


Figure 11: Organization and replication of the CHIKV genome.

CHIKV genome consists of a ≈ 12 kb long, (+)ssRNA, the 49S genomic RNA. It is subdivided into two ORFs. The first ORF encodes nsP1-nsP4 that are translated as a polyprotein that needs to be proteolytically processed. Processing into nsP123 and isolated nsP4 results in the minus-strand replication complex, which synthesizes the minus-strand RNA. Further processing of the polyprotein into the short-lived nsP1, nsP23 and nsP4 and the mature nsP1/nsP2/nsP3/nsP4 replication complex is required to allow subsequent synthesis of new genomic 49S RNA as well as subgenomic 26S RNA with the minus-strand RNA as a template. The asterisk (*) marks the premature stop codon within the first ORF that is suppressed in about 10% of the cases. m7G, 7-methylguanosine; nsP, non-structural protein (modified from Rupp et al. 2015).

CHIKV is encoded by a linear, about 12 kb long (+)ssRNA genome with a 5' 7-methylguanosine (m7G) cap and a 3' poly(A) tail (**Figure 11**)(Solignat et al. 2009; Rupp et al. 2015; De Caluwé et al. 2021). Further, the genome is subdivided into two open reading frames (ORFs)(**Figure 11**)(Rupp et al. 2015). Therein, the first ORF encodes the non-structural proteins (nsPs), nsP1-

4, which possess catalytic activities and mediate processes like genome replication and regulation of the host cell immune response (Ahola et al. 2016). This ORF can be immediately translated by the host cell machinery from the genomic RNA (Abdelnabi et al. 2015). The second ORF on the other hand is under the control of a subgenomic promoter. In order to translate the second ORF a subgenomic 26S mRNA must be generated from the minus-strand RNA (**Figure 11**)(Rupp et al. 2015). The second ORF encodes the structural proteins of CHIKV, C, E1-3 and 6K/TF (**Figure 11**)(Abdelnabi et al. 2015; Snyder et al. 2013). The different steps of viral genome replication are governed by the composition of the viral replication complex and the processing of the ns polyprotein is essential for replication (**Figure 11**)(Rupp et al. 2015). The unprocessed nsP1234 polyprotein does not process RNA synthesis activity until it is auto-proteolytically cleaved (Rupp et al. 2015). The early replication complex or minus-strand replication complex, comprising nsP123 and isolated nsP4, first produce the negative-sense, minus-strand RNA from the genomic RNA (**Figure 11**)(Rupp et al. 2015). Further cleavage is necessary for the subsequent steps in replication. First nsP1 is cleaved of the yield the very short-lived nsP1, nsP23, nsP4 complex. This leads to a shift from minus-strand synthesis towards positive-sense RNA synthesis, more precisely synthesis of the genomic full-length and the subgenomic RNAs (**Figure 11**)(Rupp et al. 2015). The nsP23 protein is almost instantaneously processed into isolated nsP2 and nsP3, resulting in the mature viral replication complex of the individual nsPs, which further produces genomic and subgenomic mRNA with a preference for subgenomic RNA synthesis (**Figure 11**)(Rupp et al. 2015).

1.3.3 Functions of the CHIKV non-structural proteins

The CHIKV viral genome encodes four non-structural proteins (nsP1-4), that possess multiple domains and catalytic activities necessary for viral persistence, including genome replication and host cell modulation (**Figure 12**)(Rupp et al. 2015; Ahola et al. 2016). All nsPs are essential for CHIKV replication and are highly conserved between Alphaviruses (**Figure 12**)(Rupp et al. 2015; Ahola et al. 2016). Notably, in the Alphavirus field it is common practice, that properties, that are documented for one species are assumed to be true for other Alphaviruses as well and are stated as facts without further validation. Often, aspects have been investigated for prototypic Alphaviruses like Sindbis virus (SINV), Semliki Forest virus (SFV) or Venezuelan Equine Encephalitis virus (VEEV) and are presumed for CHIKV as well, as systems to study these viruses are better established. However, multiple differences between different Alphaviral species, especially between Old and New World Alphaviruses, have been demonstrated and therefore careful evaluation of the primary literature is often necessary. Chikungunya is an Old World Alphavirus (Ahola et al. 2016; Garmashova et al. 2007; Kim et al. 2016b).

NsP4 is the first nsP that is cleaved of from the polyprotein (**Figure 11 and 13**)(Rupp et al. 2015). Notably, about 90% of the translation of the genomic RNA results in the nsP123 polyprotein due to a premature stop codon within the first ORF. Only in 10% of the cases stop codon suppression leads to read through translation of the full-length nsP1234 ns polyprotein (**Figure 13**)(Rupp et al. 2015). Therefore, nsP4 is commonly the least abundant viral nsP in infected cells. Generally, nsP4 catalytic activities are hard to study, due to the disordered N-terminus that leads to insolubility and degradation of isolated nsP4 in bacteria and eukaryotic cells, respectively. It is proposed, that nsP4 is stabilized by incorporation into the viral replication complex together with the other nsPs (**Figure 12**)(Rupp et al. 2015; Ahola et al. 2016). Within the replication complex, nsP4 is the RNA-dependent RNA polymerase (RdRp), that due to sequence analyses is predicted to have the typical structure of RNA polymerases

with the conserved GDD catalytic triade and mutation of GDD to GAA abolishes RNA replication (**Figure 12**)(Rupp et al. 2015; Ahola et al. 2016). However, nsP4 implicitly requires the other three nsPs in different configurations in order to carry out its RNA synthesis activity (Rupp et al. 2015). Further, studies showed that nsP4 has promoter binding properties at the genomic and subgenomic promoters, which potentially determines the site of RNA synthesis (Rupp et al. 2015). In addition to RdRp activity, nsP4 potentially possesses terminal adenylyltransferase (TATase) activity that might produce the poly(A) tail of the genomic and subgenomic mRNAs (**Figure 11 and 13**)(Rupp et al. 2015; Ahola et al. 2016).

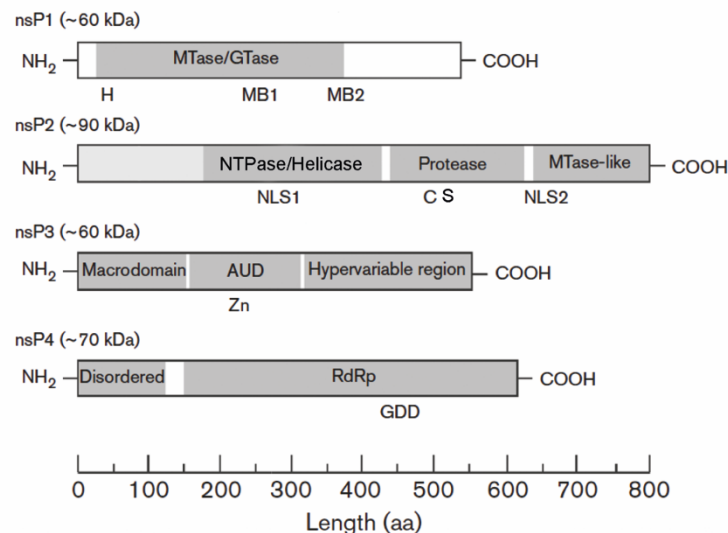


Figure 12: Schematic representation of the Alphavirus non-structural proteins.

The domain architecture and catalytic activities of the four individual Alphaviral non-structural proteins nsP1, nsP2, nsP3 and nsP4 are depicted. The domains were defined by structural studies or conserved sequences and are depicted as grey boxes. Additionally, special features within the domains are shown underneath the protein. Generally, all characteristics are shown relative to their positions in the protein. NsP1 possesses MTase and GTase activity and interacts with membranes via an amphiphatic helix (MB1) and a palmitoylation site (MB2). The depicted H is described to covalently bind the 7-methylguanosine moiety for the RNA cap. NsP2 contains a NTPase and Helicase, a cysteine protease and a MTase-like domain. The active site C and S of the protease are shown. Additionally, the two NLS within nsP2 are marked. NsP3 consists of a macrodomain of so far unknown function, the AUD that coordinates a Zn ion and a hypervariable region that mediates multiple host factor interactions. NsP4 possesses a disordered N-terminus that leads to degradation of the isolated nsP4 but is essential for its activity and the viral RdRp. AUD, Alphavirus unique domain; C, cysteine; GDD, glycine-aspartate-aspartate catalytic triade; GTase, guanylyltransferase; H, histidine; MB, membrane-binding; MTase, methyltransferase; NLS, nuclear localization sequence; nsP, non-structural protein; NTPase, nucleoside triphosphatase; RdRp, RNA-dependent RNA polymerase; Zn, zinc (modified from Rupp et al. 2015).

The next protein released from the ns polyprotein is nsP1 (**Figure 11 and 13**)(Rupp et al. 2015). NsP1 is responsible for the capping of the viral, positive-sense genomic and subgenomic RNAs in order to shield it from degradation. It possesses S-adenosyl methionine(SAM)-dependent methyltransferase (MTase) and guanylyltransferase (GTase) activity within its central domain containing a potential Rossman fold (**Figure 12**)(Bullard-Feibelman et al. 2016; Feibelman et al. 2018; Kaur et al. 2018; Mudgal et al. 2019; Rupp et al. 2015; Ahola et al. 2016). NsP1 first transfers a methylgroup from SAM onto the 7-N position of GTP via its MTase activity. Subsequently, 7-methylguanosine (m7G) is covalently bound by a conserved histidine within nsP1 creating the m7G-nsP1 intermediate under release of pyrophosphate by GTase activity (**Figure 12**)(Rupp et al. 2015; Ahola et al. 2016). Finally, the m7G is transferred to the 5'-diphosphate RNA (ppRNA) resulting in the final m7G-capped viral RNA (Rupp et al. 2015; Ahola et al. 2016). In case of CHIKV, the GTase activity might be independent of SAM as opposed to other Alphaviruses (Bullard-Feibelman et al. 2016). Additionally, nsP1 anchors the polyprotein

and replication complexes of CHIKV to the plasma membrane, the main site of viral replication (Rupp et al. 2015; Ahola et al. 2016). To do so, it interacts with the cytoplasmic part of the plasma membrane lipids via an amphiphatic alpha helix and palmitoylated cysteines (**Figure 12**)(Rupp et al. 2015; Ahola et al. 2016). For some Alphaviral nsP1 proteins, like SFV nsP1, it is described that lipid association is necessary for efficient capping activity, while other nsP1 versions, like SINV nsP1 are independent of this (Rupp et al. 2015). For CHIKV it has not been well studied whether lipid binding boosts capping activity, but several studies work without the addition of lipids (Bullard-Feibelman et al. 2016; Kaur et al. 2018). However, a recent studies implies that formation of a dodecameric ring of nsP1 as well as membrane binding may be crucial for nsP1 capping activity (Jones et al. 2021). NsP1 interacts with the other nsPs within the replication complex, but they are not well studied (Rupp et al. 2015; Rana et al. 2014). However, it was shown that nsP1 and its association for nsP4 are essential for minus-strand replication and that interaction with nsP2 boosts ATPase activity, that will be described in more detail hereafter (Rupp et al. 2015; Kumar et al. 2018). Meanwhile, host-factor interactions of nsP1 are poorly understood. It is described that nsP1 interacts with and restricts tetherin, a host protein that limit virus budding (Jones et al. 2013; Ahola et al. 2016). But this finding is debated in the field (Wan et al. 2019). Furthermore, nsP1 plays roles in cytoskeletal reorganization and transmission of the virus to other cells (Rupp et al. 2015).

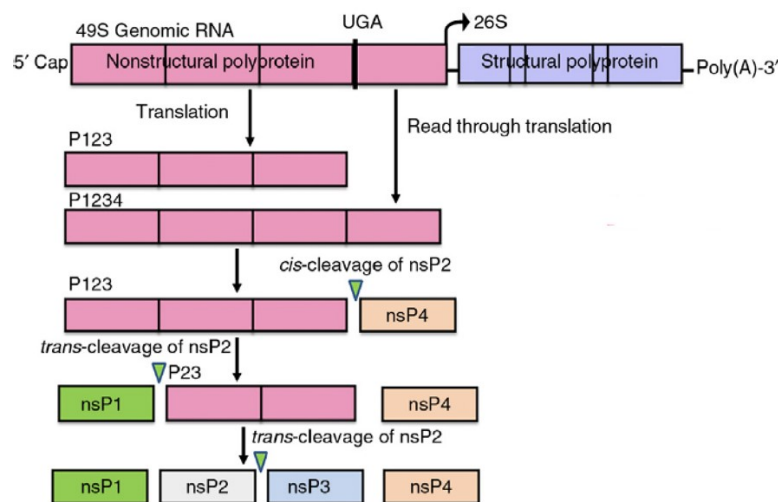


Figure 13: Schematic representation of non-structural polyprotein processing in CHIKV.

The non-structural polyprotein is translated from the genomic RNA via the host machinery, either as the shorter version nsP123 due to a premature stop codon (UGA) or as the full-length nsP1234 by stop codon suppression and read through translation. Subsequently, the polyprotein is gradually processed into the individual nsPs by *cis*- and *trans*-cleavage of the protease within nsP2. nsP, non-structural protein (modified from Tomar et al. 2017).

The probably best studied nsP of CHIKV is nsP2. Comparable to the other nsPs, it is a multi-domain and multifunctional protein. It is the only CHIKV nsP that localizes to the nucleus as well as the cytoplasm (Rupp et al. 2015; Ahola et al. 2016). Modeling based on the sequence predicts two RecA-like domains that are described to have nucleoside triphosphatase (NTPase), helicase and 5'-RNA triphosphatase (RTPase) activity near its N-terminus. The C-terminal half of the protein has been structurally resolved and consists of a protease and an MTase-like domain (**Figure 12**)(Rupp et al. 2015; Ahola et al. 2016). Therein, nsP2 is the viral protease responsible for the essential cleavage of the ns polyprotein (**Figure 13**)(Rupp et al. 2015; Ahola et al. 2016). It was previously suggested that all Alphaviral proteases are papain-like proteases with a cysteine and histidine catalytic diad. However, for the CHIKV nsP2 it was demonstrated that it is not a papain-like protease and that it might switch between a catalytic cysteine and a catalytic serine nearby (**Figure 12**)(Saisawang et al. 2015; Tomar et al. 2017). In

order to block protease activity completely, it was proposed that both residues need to be mutated or targeted (Saisawang et al. 2015). CHIKV nsP2 is able to cleave in *cis*- and in *trans*- in order to perform proteolytic processing of the ns polyprotein at three different sites (**Figure 13**)(Tomar et al. 2017; Rupp et al. 2015). The processing of the nsP3/4 site most likely happens in *cis* while the proteolysis of the nsP1/2 and nsP2/3 sites is proposed to happen in *trans* due to sterical hindrance (Tomar et al. 2017; Rupp et al. 2015). Generally, the features of the protease of CHIKV differ from that of other Alphaviruses, for instance it can efficiently cleave small peptide substrates, especially the nsP3/4 cleavage site (Tomar et al. 2017; Ahola et al. 2016). Additionally, there are differences between nsP2 as part of different polyproteins, full-length, mature nsP2 and the isolated protease with regard to substrate specificity and efficiency (Tomar et al. 2017; Rupp et al. 2015). These differences and the concentration of nsP2 govern the gradual processing of the polyprotein to regulate the different steps of viral replication (**Figure 11 and 13**)(Rupp et al. 2015). The initially low concentration of polyprotein favors in *cis* cleavage and therefore the release of nsP4. In turn, increase of the proteins over time promotes in *trans* cleavage. Meanwhile, presence of nsP1 in the polyprotein (e.g. nsP123) hampers cleavage of the nsP2/3 site, therefore the nsP1/2 is cleaved first and only after nsP1 release, the nsP2/3 site is cleaved later in infection (Rupp et al. 2015). Additionally, other domains within nsP2, besides the protease domain, were shown to be important for nsP2 protease activity. For instance, the C-terminus containing the MTase-like domain is generally essential for nsP2 protease activity (Ahola et al. 2016). For some Alphaviruses it was demonstrated that the macrodomain within nsP3 is essential to allow proteolysis of the nsP2/3 cleavage site by nsP2, however this is still debated in the case of CHIKV (Tomar et al. 2017; Ahola et al. 2016).

Apart from protease activity, nsP2 possesses NTPase activity without preference for specific canonical dNTPs, that is boosted by RNA and DNA binding (Karpe et al. 2011; Das et al. 2014; Ahola et al. 2016). Additionally, ATPase activity might be increased by interaction with nsP1 as mentioned previously (Kumar et al. 2018). This activity is provided by the RecA-like helicase domain in the N-terminal part of the protein (Rupp et al. 2015; Ahola et al. 2016).

Moreover, nsP2 exhibits RTPase activity. Therein it can remove the γ -phosphate from RNA, turning 5'-pppRNA into 5'-ppRNA, which is required in order to cap the viral positive sense RNAs. The RTPase activity of nsP2 uses the same active site as the NTPase activity (Rupp et al. 2015; Ahola et al. 2016). Further, the RecA-like domain within nsP2 transfers helicase activity towards dsRNA in 5' to 3' direction. The helicase is dependent on the C-terminal part of nsP2 and on its intrinsic NTPase activity in order to generate energy. The C-terminus of nsP2 may provide RNA binding activity (Das et al. 2014; Rupp et al. 2015; Ahola et al. 2016). The helicase activity is described to function in complex with nsP4 and thereby facilitate the RdRp activity of nsP4 by unwinding dsRNA (Rupp et al. 2015; Law et al. 2019). Nsp2 further regulates the RdRp activity of nsP4 to avoid nucleotide depletion in the cell (Stapleford et al. 2015). Additionally, the helicase domain is proposed to have RNA annealing activity (Das et al. 2014; Ahola et al. 2016). Besides, it was proposed, that nsP2 might act as a transcription factor for the subgenomic RNA by binding to the subgenomic promoter and hence targeting of the replication complex. However, polyprotein processing was also affected in the conditions investigated, which therefore might already alter subgenomic RNA synthesis (Rupp et al. 2015).

In addition to direct effects on viral replication, nsP2 is also known to regulate host cell factors and thereby antagonize the antiviral immune response. Many of these functions are rather interaction mediated than dependent on catalytic activities of nsP2 (Akhrymuk et al. 2012; Ahola et al. 2016; Fros et al. 2016; Goertz et al. 2018; Meshram et al. 2019). For instance, the

catalytic subunit of RNA polymerase II complex Rpb1 is targeted for ubiquitin- and proteasome-mediated degradation by nsP2 independent of its protease activity. Instead, this activity requires the intact helicase and MTase-like domains. The degradation of Rpb1 leads to a shutoff of host cell transcription and therefore antagonizes the antiviral response of the cell (Akhrymuk et al. 2012; Fros et al. 2016). In addition to the general inhibition of overall host transcription, nsP2 is also described to specifically abolish JAK/STAT and thus IFN signaling by decreasing the amount of phosphorylated STAT1 (pSTAT1) in the nucleus (Goertz et al. 2018). This is especially relevant as CHIKV infection is described to induce a massive IFN response in infected cells (Matusali et al. 2019; Fros et al. 2016). One proposed mechanism is, that nsP2 promotes the nuclear export of pSTAT1 dependent on nsP2 nuclear localization and its MTase-like domain (Goertz et al. 2018; Meshram et al. 2019; Ahola et al. 2016). Apart from transcriptional shutoff, CHIKV is also described to mediate translational shutoff in an independent manner. Some findings propose that nsP2 is also involved in this host cell regulatory mechanism, however it remains unknown how (Ahola et al. 2016; Fros et al. 2016). Another host factor targeted by nsP2 is the ubiquitin-conjugating enzyme E2 L3 (UBE2L3), that is downregulated by nsP2 dependent on protease activity. UBE2L3 is a restriction factor for CHIKV infection, which potentially influences the expression of structural proteins and thus viral infectivity (Ramphan et al. 2018). Moreover, nsP2 is described to interact with multiple other proteins involved in transcription, cytoskeletal organization and protein degradation or autophagy, however these factors were not essential for viral replication (Ahola et al. 2016; Bourai et al. 2012).

CHIKV nsP3 consist of three domains: the N-terminal macrodomain, the Alphavirus unique domain (AUD) and the hypervariable, proposedly unstructured C-terminus (**Figure 12**) (Rupp et al. 2015; Ahola et al. 2016). Generally, the exact function of nsP3 in viral replication remains elusive, but it is essential for RNA synthesis and polyprotein processing and it appears to be a determinant for vector and cell specificity (Rupp et al. 2015; Ahola et al. 2016; Meshram et al. 2018; Matusali et al. 2019). Furthermore, nsP3 is discussed to play a role in chronic manifestation of Chikungunya (Remenyi et al. 2018). As described previously (Chapter 1.2.6.1), the function of the conserved macrodomain remains to be studied in detail. Prior to this thesis, it was known to bind polymers like PAR and RNA as well as single ADPr units. Furthermore, weak ADP-ribose-1"-monophosphate (Appr-1"-p) activity was demonstrated for the CHIKV macrodomain (Malet et al. 2009; Ahola et al. 2016). While this was not studied in CHIKV preceding this thesis, mutations of functionally important residues in the SINV macrodomain led to reduced replication and pathologies (Park et al. 2009). However, the underlying mechanism is unknown. (Rupp et al. 2015; Ahola et al. 2016; Fros et al. 2016). Whether the macrodomain is essential to promote nsP2/3 proteolysis by nsP2, like it is shown for some other Alphaviruses, is still under debate (Tomar et al. 2017; Ahola et al. 2016).

Comparable to the macrodomain, the functions of the AUD are poorly studied. This is a domain that coordinates a Zinc (Zn) ion between to conserved cysteines and so far, it has only been described for Alphaviruses (Rupp et al. 2015; Ahola et al. 2016; Fros et al. 2016). Mutational studies propose that the AUD is relevant for CHIKV replication and synthesis of subgenomic RNA resulting in defect in virus assembly, but the reason is undetermined (Gao et al. 2019). Additionally, several interactions with host cell proteins have been mapped lately, however the mechanistic relevance is not known (Ghildiyal et al. 2021).

The probably best studied domain within nsP3 is the hypervariable domain (HVD), which is not well conserved among Alphaviruses, highly phosphorylated at serines and an interaction hub for multiple host factors (Rupp et al. 2015; Ahola et al. 2016; Fros et al. 2016; Meshram

et al. 2018). In infected cells, nsP3 resides in the replication complex as well as in cytoplasmic granules dependent on its C-terminus. These cytoplasmic granules are specific nsP3 granules, that sequester selected components from stress granules, while others are excluded. On the one hand this prohibits the assembly of bona fide stress granules that may act antiviral and on the other hand it allows the utilization of desired factors for viral replication (Fros et al. 2012; Scholte et al. 2015; Gotte et al. 2019; Meshram et al. 2018).

Best studied is probably, that nsP3 interacts with Ras-GAP SH3 domain-binding protein 1 and 2 (G3BP1 and G3BP2) via two conserved FGDF motives its hypervariable domain (Panas et al. 2014; Schulte et al. 2016; Meshram et al. 2018). Loss of both, G3BP1 and G3BP2, hampers viral replication, comparable to deletion of both FGDF motifs from nsP3 (Schulte et al. 2016; Kim et al. 2016b). This interaction is conserved and likewise essential in mosquito cells, where nsP3 interacts with the mosquito analogue Rasputin (Fros et al. 2015a; Meshram et al. 2018). For SFV it was shown, that G3BP (G3BP1 and G3BP2) orchestrates the recruitment of the translation machinery, for instance the 40S ribosomal subunit, to viral replication hubs (Gotte et al. 2019). Additionally, G3BP may facilitate the transition from ns polyprotein translation to negative-sense RNA synthesis, by removal of translation factors and thus clearance of the RNA for the viral replication complex (Scholte et al. 2015; Ahola et al. 2016). Even though interaction with G3BP is essential, it is not sufficient to promote viral replication. Therein, interaction of nsP3 HVD with further host factors is required. Depending on the cell line, nsP3 HVD is described to interact with amphiphysin-2 (BIN1), CD2-associated protein (CD2AP), nucleosome assembly protein 1 like 1 and 4 (NAP1L1 and NAP1L4) for instance (Tossavainen et al. 2016; Meshram et al. 2018; Mutso et al. 2018; Dominguez et al. 2021). The binding of some of these proteins is dependent on the phosphorylation state of nsP3 HVD which is linked to the cellular background (Dominguez et al. 2021). All of the before mentioned factors play additive pro-viral roles for CHIKV replication and are partially redundant (Tossavainen et al. 2016; Meshram et al. 2018; Mutso et al. 2018; Dominguez et al. 2021). Therefore, further investigation of the post-translational modifications of the nsP3 HVD may add a layer of information of the regulation of host factor interaction.

1.4 Aims of this work

Fast-evolving RNA viruses are a major health threat due to their high adaptability. In order to generate effective and potentially combinatory treatments, a better understanding of the mechanisms they use to circumvent the immune response and to induce pathogenicity is urgently needed. The viral non-structural proteins play crucial roles in the pursuit and especially highly conserved modules, like the largely uncharacterized viral macrodomain, are promising candidates. This is particularly interesting, as modulation of the macrodomain already showed effects in several relevant pathogenic virus families, including Coronaviruses, Alphaviruses and Hepatitis E viruses. The first aim of this work was to further understand the function and relevance of the viral macrodomains by biochemical characterization. Since the macrodomain fold is closely linked to ADP-ribosylation and the cellular erasers MacroD1, MacroD2, TARG1 and PARG, several viral macrodomains were tested for their ability to hydrolyze MAR- and PARYlation. Therefore, isolated macrodomains from CHIKV, VEEV, Feline Infectious Peritonitis virus (FIPV), HEV and O'nyong'nyong virus (ONNV) were subjected to *in vitro* hydrolase assays. Substrate-specificity was assessed by using different substrates, including ARTD10, NEMO and ARTD1. More detailed analyses were subsequently performed with a focus on the CHIKV macrodomain. These comprised mutational studies to identify residues that are essential for catalysis as well as *in vitro* hydrolase assays in the context of the full-length nsP3 protein. Finally, the capacity of CHIKV nsP3 and the isolated macrodomain to remove MARYlation in cells was addressed analyzing ARTD10 as a substrate.

The subsequent chapters, containing the second part of the work, thrived to understand the mechanistic function of the macrodomain for CHIKV replication in more detail. To do so, a replicon-based system was established to assess CHIKV replication. First, the influence of IFN-inducible ARTDs as potential counter players of the macrodomain were addressed in knockdown and overexpression experiments. Further, the consequence of previously characterized macrodomain mutants for CHIKV was tested. The experiments were corroborated by setups using different ADP-ribosylation inhibitors. For comparison, additional replicon mutants were established, that lacked protease or RdRp activity. The replication of the different CHIKV replicons was studied by Luciferase assays, Western blot and flow cytometry analyses. Additionally, several systems were tested to perform rescue experiments of mutant replicons.

In order to understand the functional relevance of the macrodomain as well as the defects of the macrodomain mutant replicons, common substrates of the macrodomain and ARTDs were researched. First the non-structural proteins, nsP1-nsP3 were tested as substrates of ADP-ribosylation by different ARTDs and hydrolase activity of nsP3 *in vitro* and in cells. Further experiments focused on nsP2 and ARTD10 and the functional consequences of MARYlation on protease activity *in vitro*.

The last part of the thesis aimed at identifying common cellular substrates of the macrodomain within CHIKV nsP3 and ARTD10 that may function as host factors in CHIKV replication. Therefore, complementary mass spectrometry (MS) approaches were carried out. On the one hand, the interactome of the isolated macrodomain and full-length nsP3 was determined using BioID and tandem affinity purification (TAP) techniques. This was compared to the interactomes of ARTD10 and its inactive mutant identified with BioID and GFP-Trap. Additionally, an influence of IFN α treatment on the ARTD10 interactors was addressed. The overlaps of all experiments were considered and initial co-immunoprecipitation, co-localization experiments as well as *in vitro* ADPr assays were performed to verify the results.

2 Results and Discussion

The following chapter presents the results of this thesis including their discussion and is subdivided into three parts. The first section focuses on the biochemical characterization of the macrodomains of a subset of positive single stranded RNA ((+)ssRNA) viruses as mono-ADP-ribosyl(MAR)-hydrolases. The second part investigates the Chikungunya virus (CHIKV) non-structural proteins (nsPs) 1-3 as substrates of cellular mono-ADP-ribosylation (MARylation) with a focus on the consequences of the modification for the viral protease within nsP2. Additionally, the functional relevance of MARylation on CHIKV replication is examined in the context of diverse viral replicon constructs. The third and final part of the results aims at identifying common substrates of the cellular ADP-ribosyltransferases and the CHIKV macrodomain utilizing a complementary mass spectrometry analyses approach.

2.1 The viral macrodomains of Chikungunya virus and other pathogenic (+)ssRNA viruses are (protein) mono-ADP-ribosyl-hydrolases

This chapter depicts the biochemical characterization of several viral macrodomains as MAR hydrolases with a focus on the Chikungunya macrodomain. The macrodomain is an evolutionary conserved protein fold that is strongly associated with ADP-ribosylation. A subset of (+)ssRNA viruses encodes macrodomains in their genomes with thus far unknown function. To test for potential MAR reverting abilities a group of isolated viral macrodomains from different virus families was initially tested in *in vitro* hydrolase assays with cellular ADP-ribosyltransferases and substrates in endpoint and time course experiments. The specificity was tested on mono- as well as poly-ADP-ribosylation (PARylation) and compared to known cellular hydrolases. Additionally, actual MAR hydrolase activities were confirmed by competition assays with ADP-ribose (ADPr) as well as analyses of the released products of hydrolase assays. Furthermore, catalytically important amino acids of the CHIKV macrodomain were identified using mutational analysis. The characterization of the isolated macrodomain of CHIKV was complemented by analyses of the full-length nsP3 protein, which harbors the macrodomain near the N-terminus. Finally, the *in vitro* MAR hydrolase activities of CHIKV macrodomain and full-length nsP3 were confirmed in cells with the help of murine Artd8-macro2-3 constructs in immunofluorescence and co-immunoprecipitation experiments. These results have previously been published in Eckeï, Krieg et al. 2017.

2.1.1 Viral macrodomains exhibit hydrolase activity towards protein mono-ADP-ribosylation *in vitro*

In contrast to PARylation, cellular MARylation is only poorly studied to date, due to a lack of efficient tools for intracellular detection of the modification and only a limited number of known substrates. Hence, the molecular function of MARylation remains mainly elusive. The starting point for this thesis was the finding that the expression of several cellular mono-ADP-ribosyltransferases (ARTDs) was induced by interferon α and/or β . Prior work from our lab described *ARTD10* and *ARTD8* to be induced by interferon α (Eckeï et al. 2017), while others described interferon β inducibility of *ARTD7*, *ARTD10* and *ARTD12* (Atasheva et al. 2012). These findings hint at a potential function of MARylation in the antiviral innate immune response. Additionally, the macrodomain protein fold was identified as a regulator of

MARylation with cellular macrodomain-containing proteins as “readers” and “erasers” of this modification (Feijs et al. 2013a).

The macrodomain fold is evolutionary conserved and can be found in all domains of life as well as a subset of (+)ssRNA viruses (Rack et al. 2016)(**Figure 14**). So far, the viral macrodomains (vMDs) are only poorly characterized biochemically but show high homology to known regulators of ADP-ribosylation like the cellular erasers MacroD1 and MacroD2 (**Figure 14**).

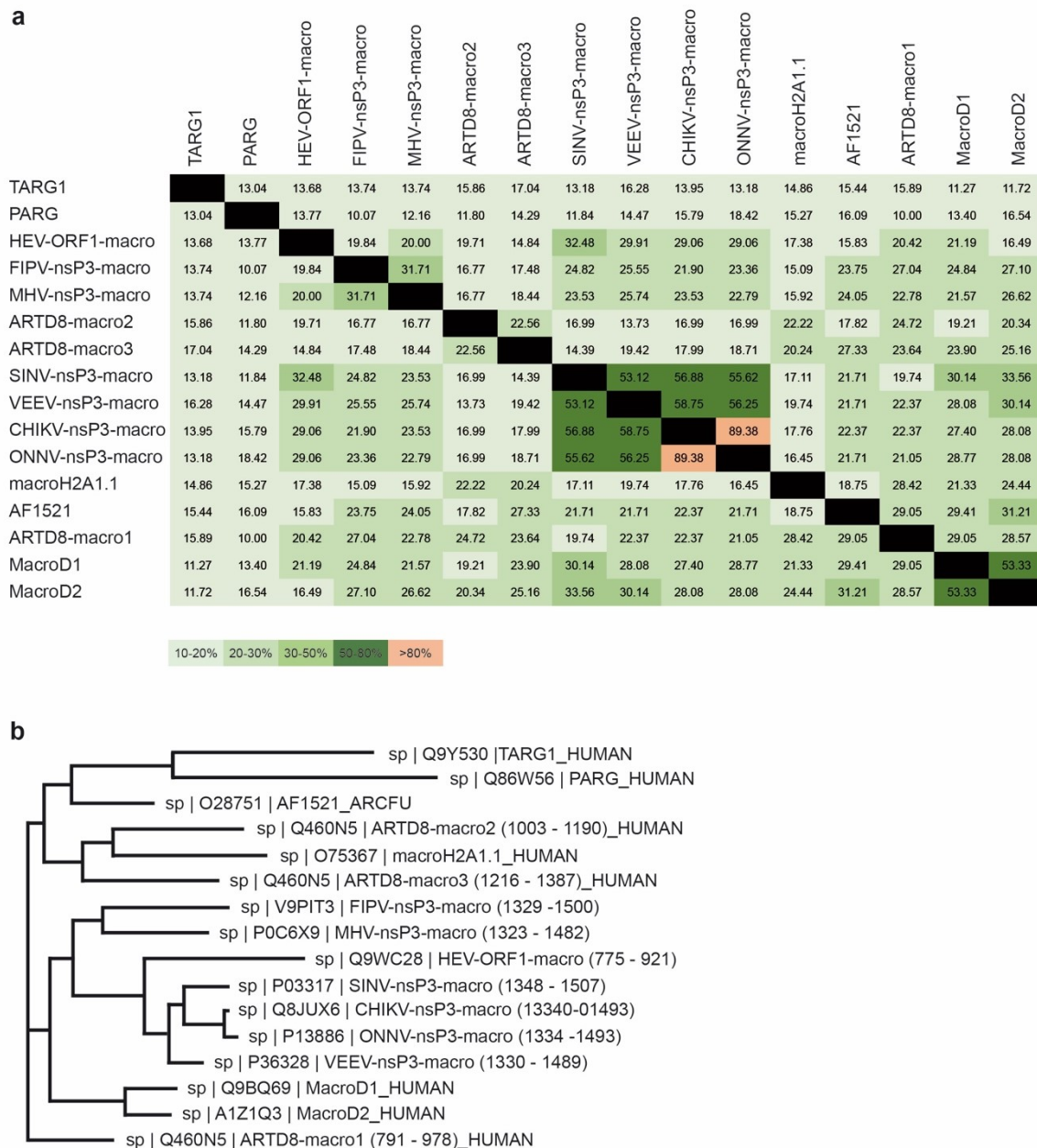


Figure 14: The macrodomain fold is highly conserved.

This figure is from Ecke, Krieg et al. 2017. I created these graphs. **(a)** Percent identity matrix of the indicated macrodomains generated with Clustal multiple sequence alignment based on sequence comparison. **(b)** Phylogenetic tree of the indicated macrodomains created by using ClustalW2. HEV, hepatitis E virus; FIPV, Feline Infectious Peritonitis virus; MHV, mouse hepatitis virus; ARTD8-macro2, macrodomain 2 of human ARTD8; ARTD8-macro3, macrodomain 3 of human ARTD8; SINV, Sindbis virus; VEEV, Venezuelan Equine Encephalitis virus; CHIKV, Chikungunya virus; ONNV, O’nyong’nyong virus; AF, *Archaeoglobus fulgidus*; ARTD8-macro1, macrodomain 1 of human ARTD8; ORF1, open reading frame 1 protein; nsP3, nonstructural protein 3.

contrast to that the negative control His-Artd8-macro2 showed no decrease in signal after 60 min of incubation (**Figure 15a**). The same could be demonstrated for ARTD7 and ARTD8 by colleagues (Ecke et al. 2017). This hints at a broad MAR-hydrolase activity of all tested viral MDs towards several substrates of protein MArYlation, including three cellular ARTDs and the known substrate NEMO.

To expand on the biochemical characterization of the hydrolase activity, time course experiments were performed with the isolated SINV macrodomain on the GST-ARTD10cat domain. After automodification of ARTD10 in the presence of radioactive ^{32}P -NAD $^{+}$, the reactions were incubated with the SINV macrodomain for the indicated times. A sample where the reaction was immediately stopped (0 min) and a sample that was incubated for 240 min without addition of the SINV macrodomain served as controls. Compared to the control samples the majority of incorporated label was already removed after 10 min on the autoradiogram. The ^{32}P label further decreased over time until most of the signal was gone at 180 min. The MArYlation itself was stable over time in the absence of the SINV MD (**Figure 15b**). Comparable results were achieved for the CHIKV, FIPV and ONNV MDs on ARTD10 and ARTD8 as well as the SINV MD on ARTD8 with only slight differences between the different macrodomains (Ecke et al. 2017).

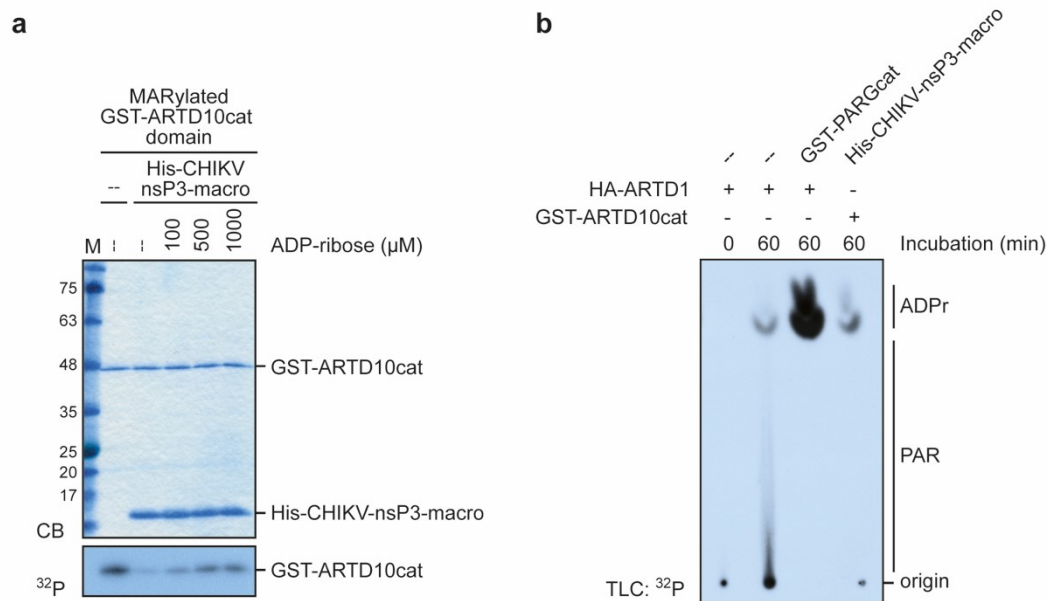


Figure 16: Viral macrodomains are specific MAR-hydrolases.

This figure is modified from Ecke, Krieg et al. 2017. (a) Bacterially expressed GST-ARTD10cat was coupled to GST-sepharose and incubated in the presence of radioactively labelled ^{32}P -NAD $^{+}$ for 30 min at 30°C to allow automodification. Subsequently, the reactions were washed to remove free NAD $^{+}$ prior to addition of the bacterially expressed His-tagged CHIKV-nsP3-macrodomain. The reactions were further incubated in the presence of increasing amounts of ADP-ribose as indicated for 60 min at 30°C (n = 2, SK_B_25, I performed these experiments). (b) Immunoprecipitated HA-ARTD1 or bacterially expressed GST-sepharose-coupled GST-ARTD10cat domain were incubated in the presence of radioactively labelled ^{32}P -NAD $^{+}$ for 30 min at 30°C. Subsequently, the reactions were washed to remove free NAD $^{+}$ prior to the addition of GST-PARGcat or His-CHIKV-nsP3 macro as indicated. The reactions were further incubated for the indicated times at 30°C. Afterwards supernatants of the reactions were subjected to thin layer chromatography (TLC) to analyze the released, radioactively labelled products using autoradiography (^{32}P) (n = 1, SK_B_50, I performed these experiments). CB, Coomassie blue; TLC, thin layer chromatography; ^{32}P , autoradiogram.

To investigate the specificity of the removal of the radioactive label by the vMDs, further *in vitro* assays were performed with the isolated CHIKV-nsP3-macro on the GST-ARTD10cat domain (**Figure 16**). Because some viral macrodomains were previously described to bind free ADPr, ADPr was used as a competitive inhibitor as described for MacroD2 (Malet et al. 2009;

Rosenthal et al. 2013). Increasing amounts of ADPr were added to the hydrolase reactions containing MARylated GST-ARTD10cat domain and His-CHIKV-nsP3-macro. It can be observed that ADPr was able to inhibit the CHIKV macrodomain's MAR-hydrolase activity in a concentration dependent manner (**Figure 16a**). This means free ADPr was able to compete with the protein-linked mono-ADP-ribose for binding to the active site of the viral macrodomain. Additionally, the released products of the reaction were analyzed using thin layer chromatography (TLC) and subsequent autoradiography (^{32}P). For comparison automodified HA-ARTD1 was incubated in the presence or absence of GST-PARG catalytic domain (GST-PARGcat). PARG is known to cleave the ribose-ribosyl glycosidic bond between individual ADPr units in PAR chains, resulting in free ADPr units. The autoradiogram showed that the products resulting from the hydrolase assay with the CHIKV macrodomain on ARTD10cat exhibited the same mobility as the ADPr released from PARG treatment of ARTD1. Incubation of ARTD1 alone showed a smear of released PAR chains due to intrinsic instability of protein PARylation (**Figure 16b**). Hence it was demonstrated that the CHIKV-nsP3-macro is a specific MAR-hydrolase releasing ADPr units and thus cleaving the bond between the substrate amino acid side chain and ADPr.

2.1.2 Viral macrodomains are ineffective hydrolases of protein poly-ADP-ribosylation *in vitro*

All tested viral macrodomains have been established as efficient and specific MAR-hydrolases. As the next step in their biochemical characterization, the ability to degrade PARylation by ARTD1 was addressed (**Figure 17**). To do so, HA-ARTD1 was overexpressed in HEK293 cells, immunoprecipitated from lysates and allowed to auto-PARylate in the presence of $\beta\text{-NAD}^+$ and double stranded oligonucleotides. Afterwards, hydrolase assays were carried out comparable to the reactions with MARylated substrates. In addition to the viral macrodomains, TARG1 and PARGcat were included. As mentioned above, PARG is able to cleave the ribose-ribosyl glycosidic bond within PAR chains resulting in MARylated ARTD1 and free, single ADPr units. TARG1 on the other hand was described to release intact PAR by hydrolyzing the bond between PAR and the linked amino acid, even though this activity is rather weak (Sharifi et al. 2013). The PAR signal was analyzed by immunoblotting with an ADP-ribose-specific antibody (**Figure 17a**). The addition of $\beta\text{-NAD}^+$ to the reaction allowed a robust auto-PARylation of ARTD1, that was visible on the $\alpha\text{-PAR}$ immunoblot as a high molecular weight shift above 135 kDa. Moreover, the detection of the HA-tag verified that a substantial amount of the ARTD1 molecules was modified, because the distinct band in the absence of NAD^+ shifted completely upon PARylation. Compared to the sample without macrodomains there was only a slight reduction in PARylation after the treatment with viral macrodomains or TARG1 that was not significant according to quantification and application of a *t*-test (**Figure 17b**). The incubation with GST-PARGcat on the other hand, led to a nearly complete and significant reduction of the PAR signal and a reversion to the distinct HA-ARTD1 band detected with the $\alpha\text{-HA}$ -Antibody (**Figure 17a-b**). For comparison the reduction of MARylation of GST-ARTD10cat after macrodomain treatment was quantified as well (**Figure 17c**). In contrast to the PAR signal, the MAR signal was decreased significantly by all viral macrodomain after 60 min of hydrolase reaction. In fact, compared to the human MAR-hydrolase TARG1, the viral hydrolases seemed to be more effective in reverting MARylation, suggesting that this is their main activity and the de-PARylating ability seemed inefficient, especially compared to PARG. It is of note, however, that even though there was no significant decrease in the measured PAR signal, there was some increase in the HA-ARTD1 band at 135 kDa that corresponds to

unmodified ARTD1 (**Figure 17a**). This speaks for an inefficient but existent activity of the tested viral macrodomains towards PARylation, that has to be investigated further.

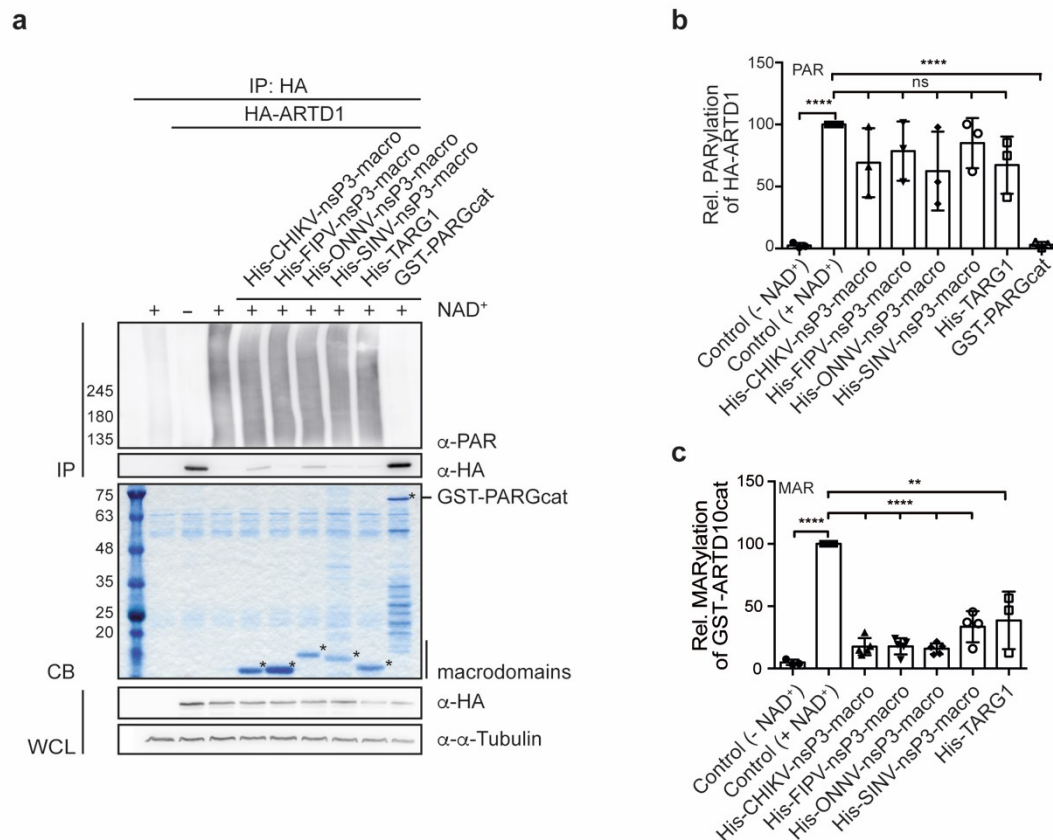


Figure 17: Viral macrodomains inefficiently remove protein poly-ADP-ribosylation *in vitro*.

This figure is modified from Ecke, Krieg et al. 2017. **(a)** Plasmids encoding HA-ARTD1 were transiently transfected into HEK293 cells. 48 h post transfection cells were lysed in TAP lysis buffer and HA-ARTD1 was immunoprecipitated using an anti-HA-antibody (Covance). Subsequently, HA-ARTD1 was activated by addition of double stranded DNA oligos to the reactions and allowed automodification in the presence or absence β -NAD⁺ as indicated for 30 min at 30°C. Afterwards, the reactions were washed to remove free NAD⁺ prior to addition of the indicated bacterially expressed His-tagged macrodomains or GST-PARGcat. The reactions were further incubated for 60 min at 30°C. The PAR signal was quantified by immunoblotting with an ADP-ribose-specific antibody (Trevigen), while total protein amounts were visualized by Coomassie blue (CB) staining. Equal expression of HA-ARTD1 was verified by immunoblotting with HA- and α -tubulin-specific antibodies in whole cell lysates (WCL) (n = 3, SK_B_20; two out of three experiments were performed by Patricia Korn, née Verheugd, I performed the third experiment). **(b)** Quantification of relative PAR signal of three independent experiments performed as in panel a (n = 3, mean value \pm SD, I performed the evaluation). **(c)** Quantification of relative MAR signal of GST-ARTD10cat after 60 min of hydrolase assay (n = 3-5, mean value \pm SD, I performed the evaluation). CB, Coomassie blue; IP, immunoprecipitation; WCL, whole cell lysate. **** p < 0.0001; ** p < 0.01; ns, not significant when an unpaired student's *t*-test was applied.

To address the hydrolase activity of the viral macrodomains against PARylated ARTD1 in more detail, time course experiments were performed with the CHIKV and the FIPV macrodomains, representatives of the alphavirus genus and the Alphacoronavirus genus, respectively, to determine whether there are differences between the individual hydrolases (**Figure 18**). The time course was carried out for 240 min on immunoprecipitated, *in vitro* PARylated ARTD1 to evaluate whether a potentially weak activity becomes apparent over longer periods of time (**Figure 15b**). While the CHIKV macrodomain seemed to exhibit slight activity on HA-ARTD1-PARylation after 240 min compared to the sample incubated without macrodomain, the FIPV macrodomain did not (**Figure 18**). What was even more apparent in these assays, however, was the intrinsic instability of the PAR chains, because solely the incubation over 240 min already robustly decreased the PAR signal compared to the control samples that was not incubated. This effect was also visible in the TLC analysis, which showed a substantial amount of released PAR chains in the absence of PARG (**Figure 16b**) and it renders it difficult to

distinguish between innate decay of PAR chains due to instability and actual hydrolase activity conveyed by viral macrodomains.

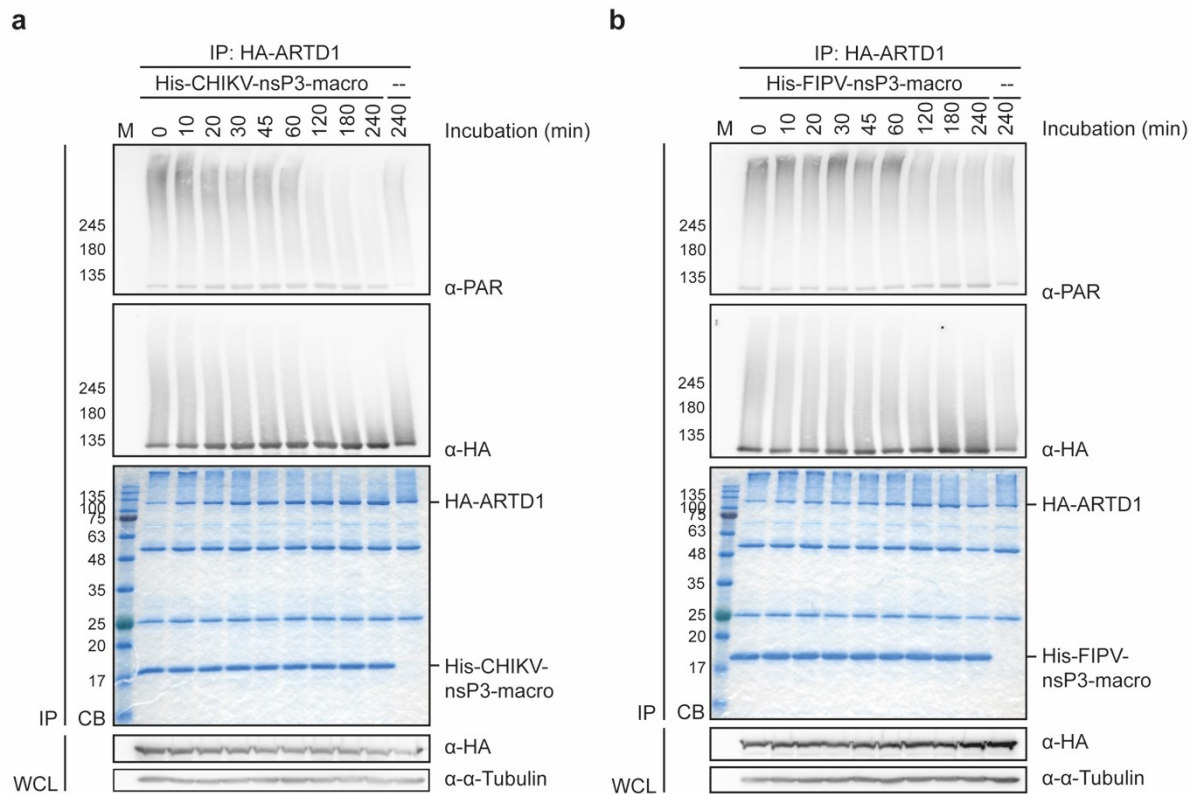


Figure 18: Hydrolase activity of CHIKV and FIPV macrodomains on PARylated HA-ARTD1 over time.

This figure is modified from Ecke, Krieg et al. 2017. **(a-b)** Plasmids encoding HA-ARTD1 were transiently transfected into HEK293 cells. 48 h post transfection cells were lysed in TAP lysis buffer and HA-ARTD1 was immunoprecipitated using an anti-HA-antibody (Covance). Subsequently, HA-ARTD1 was activated by addition of double stranded DNA oligos to the reactions and allowed automodification in the presence β -NAD⁺ for 30 min at 30°C. Afterwards, the reactions were washed to remove free NAD⁺ prior to addition of the bacterially expressed His-tagged CHIKV **(a)** or FIPV **(b)** macrodomains for the indicated times. The PAR signal was quantified by immunoblotting with an ADP-ribose-specific antibody (Trevigen), while total protein amounts were visualized by Coomassie blue (CB) staining. Equal expression of HA-ARTD1 was verified by immunoblotting with HA- and α -tubulin-specific antibodies in whole cell lysates (WCL) ($n = 1$, SK_B_40, I performed this experiment). CB, Coomassie blue; IP, immunoprecipitation; WCL, whole cell lysate.

To circumvent the challenge of differentiating between intrinsic PAR deterioration and actual PAR-hydrolase activity of the viral macrodomains another approach was employed. Instead of monitoring the decrease of PARylated HA-ARTD1 (**Figure 17 and 18**), the released products were analyzed directly, which might be more sensitive (**Figure 19**). Therefore, HA-ARTD1 was auto-PARylated in the presence of radioactive ³²P-NAD⁺ and subjected to 60 min hydrolase assays with the macrodomains of CHIKV, VEEV, FIPV, HEV, SINV and ONNV, while TARG1 and PARGcat served as controls. The supernatants were collected and analyzed using TLC or sequencing PAGE to analyze released PAR and ADPr (**Figure 19a-b**). As a control ³²P-NAD⁺ was included, which was distinguishable from ADPr as well as PAR chains of different lengths in both approaches. Furthermore, both autoradiograms showed that PAR chains were released from ARTD1 exclusively by incubation for 60 min, as observed previously (**Figure 16 and 18**). This effect was slightly increased by the addition of the viral macrodomains, except the FIPV macrodomain, that seemed inactive again. While PARGcat degraded the PAR chains to individual ADPr units as expected, TARG1 was inactive compared to the control. These results were validated by the residual PARylation of ARTD1 on the beads (**Figure 19c**).

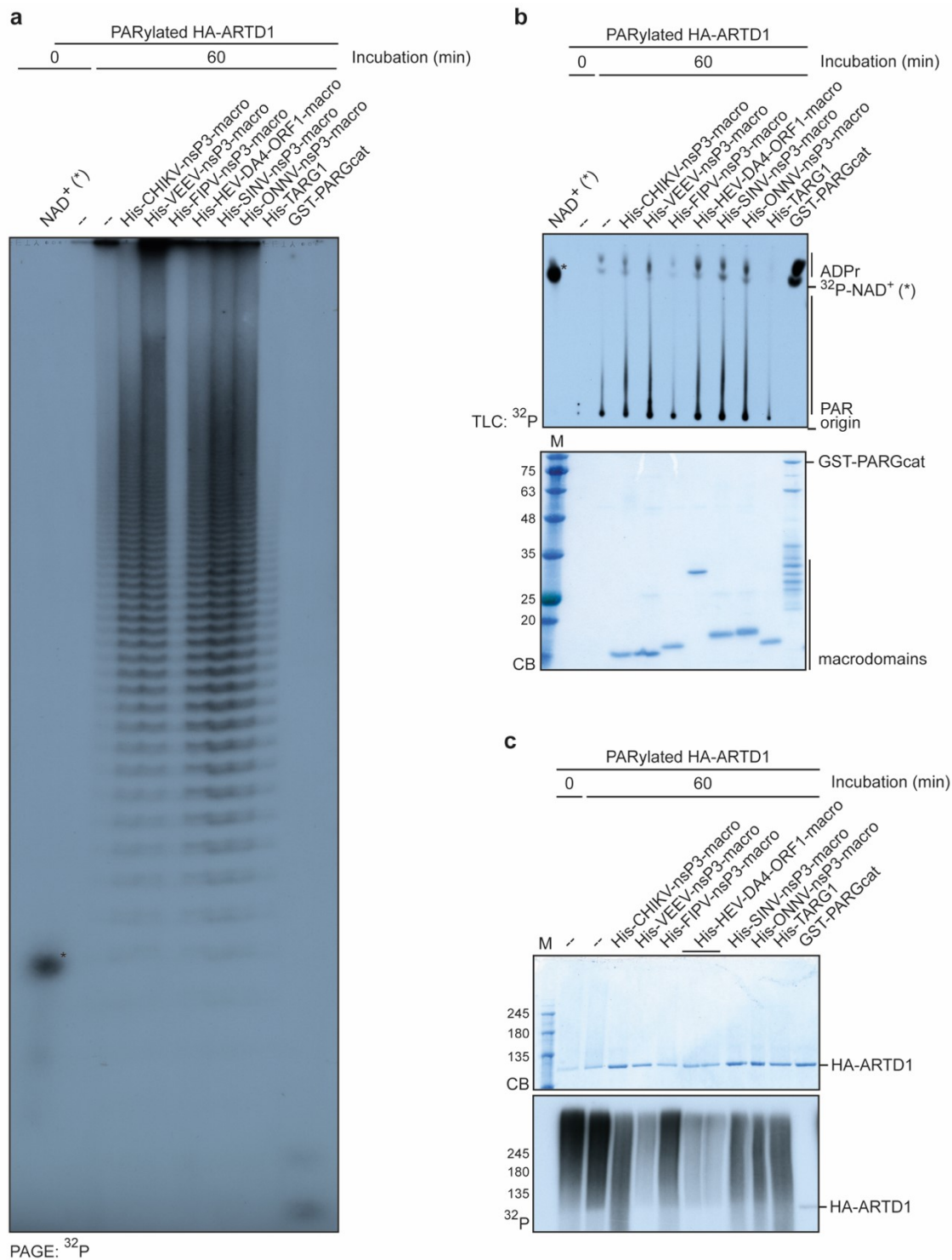


Figure 19: Analysis of products released from hydrolase assays on PARylated HA-ARTD1.

This figure is modified from Ecke, Krieg et al. 2017. **(a-c)** Plasmids encoding HA-ARTD1 were transiently transfected into HEK293 cells. 48 h post transfection cells were lysed in TAP lysis buffer and HA-ARTD1 was immunoprecipitated using an anti-HA-antibody (Covance). Subsequently, HA-ARTD1 was activated by addition of double stranded DNA oligos to the reactions and automodification in the presence radioactive ³²P-NAD⁺ for 30 min at 30°C was allowed. Afterwards, the reactions were washed to remove free NAD⁺ prior to addition of the indicated bacterially expressed His-tagged macrodomains or GST-PARGcat. The reactions were further incubated for 60 min at 30°C. Supernatants were collected (n = 2, SK_B_50, I performed these experiments). **(a)** Fractions of supernatant were analyzed by sequencing PAGE with ³²P-NAD⁺ as control (left lane, indicated with *) to visualize the released radioactively labelled ADP-ribose and PAR by autoradiography (³²P). **(b)** Fractions of supernatant were analyzed by Coomassie blue (CB) staining to visualize the macrodomains and by thin layer chromatography (TLC) to visualize released radioactively labelled ADP-ribose and PAR chains from hydrolase reactions by autoradiography (³²P). ³²P-NAD⁺ was used as a control (left lane, indicated with *). **(c)** Residual PARylation of HA-ARTD1 (on the beads) was analyzed by SDS-PAGE and autoradiography (³²P). Total protein was visualized by Coomassie blue (CB) staining. CB, Coomassie blue; TLC, thin layer chromatography; ³²P, autoradiogram.

Taken together the findings of this chapter suggests that de-MARylation rather than de-PARylation of ADP-ribosylated proteins is the biochemical activity of viral macrodomains, even though some showed weak activity towards PARylation as well. Compared to the actual PAR-hydrolase PARG however, this activity seems neglectable, and the ribose-ribosyl glycosidic bond cannot be cleaved efficiently.

2.1.3 Identification of catalytically essential amino acids of the CHIKV macrodomain by mutational analysis

The catalytic mechanism of macrodomains as ADP-ribosylhydrolases has not been characterized in detail (Rosenthal et al. 2013; Slade et al. 2011; Jankevicius et al. 2013). For further elucidation catalytically relevant amino acids of the CHIKV macrodomain were identified. To do so, Giulia Rosetti performed *in silico* analysis based on the published crystal structure of the macrodomain in complex with ADP-ribose (ADPr) (Malet et al. 2009). *In silico* alanine (A) scanning was applied to a set of amino acids facing the substrate binding pocket within a distance of 5 Å from the ADPr. The resulting amino acids were ranked by their potential effect on ADPr binding with asparagine at position 24 (N24), valine at position 33 (V33) and tyrosine at position 114 (Y114) being the top three hits. In addition to the alanine mutations, it was evaluated which other amino acid replacements would lead to a more substantial effect on ADPr binding by calculating the free energy ($\Delta\Delta G$) of the ligand/substrate interaction of every possible substitution. As a result, three mutants were created for each position by site directed mutagenesis. N24 was mutated to alanine (A), arginine (R) and tyrosine (Y), V33 was replaced by alanine (A), glutamic acid (E) and phenylalanine (F), and finally Y114 was substituted by alanine (A), valine (V) and tryptophan (W) (Ecke et al. 2017). To validate the results of the *in silico* studies, the mutants were subjected to *in vitro* hydrolase assays on MARylated ARTD10 as a substrate (**Figure 20**). As controls the WT macrodomain and samples in the absence of macrodomain were included. The substitution of the original amino acids by alanines resulted in a decreased catalytic activity for N24A and Y114V compared to the WT controls but especially at the later times there was still a reduction in MARylation visible and thus these mutants possessed residual hydrolase activity. The V33A mutant on the other hand only showed a very faint reduction of catalytic activity. Evaluation of the mutations with higher $\Delta\Delta G$ values showed that all mutants exhibited reduced hydrolase activity while N24R, N24Y, V33E and Y114W were completely inactive (**Figure 20**).

This proves that the three residues, N24, V33 and Y114, are indeed essential for binding and hydrolysis of MARylation by the CHIKV macrodomain. Evaluation of the crystal structure of the CHIKV macrodomain in complex with ADPr (Malet et al. 2009) suggests that N24 is directed towards the binding pocket where it forms a hydrogen bond with the ribose ring that connects to the substrate. Substitution of this asparagine with alanine, arginine or tyrosine leads to a loss of that hydrogen bond. Furthermore, arginine and tyrosine are predicted to alter ligand positioning and might thus reduce substrate binding, explaining the increased effect compared to the alanine mutation. V33 on the other hand is submerged entirely within the binding pocket and is linked to the diphosphate of ADPr and the nitrogen backbone of the substrate by hydrogen bonding. Unlike for N24, this hydrogen bond can still be formed in the alanine mutant, explaining its activity (**Figure 20b**). Meanwhile, the insertion of larger amino acids such as glutamic acid and phenylalanine at this position will obstruct the binding pocket for the substrate. In addition, the negative charge of glutamic acid might result in electrostatic repulsion of the likewise negatively charged phosphate groups of ADPr.

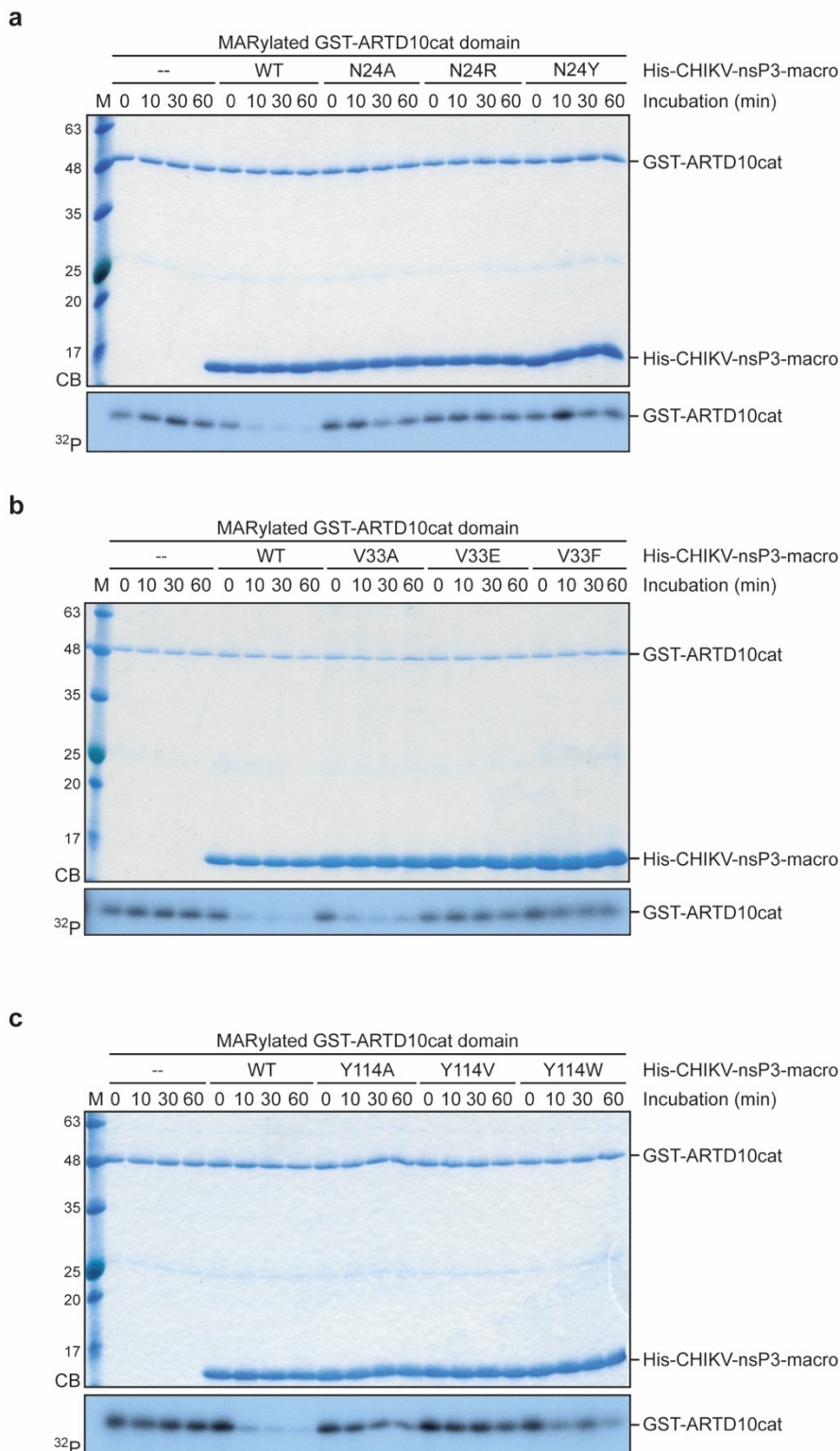


Figure 20: Characterization of catalytically inactive CHIKV macrodomain mutants.

This figure is modified from Ecke, Krieg et al. 2017. **(a-c)** Bacterially expressed GST-ARTD10cat was coupled to GST-sepharose and incubated in the presence of radioactively-labelled ^{32}P -NAD⁺ for 30 min at 30°C to allow automodification. Subsequently, the reactions were washed to remove free NAD⁺ prior to addition of the bacterially expressed His-tagged CHIKV-nsP3-macrodomain or mutants thereof. The reactions were further incubated for the indicated times at 30°C. Total proteins were stained with Coomassie blue (CB) and the incorporated radioactive label was analyzed using autoradiography (^{32}P). **(a)** Hydrolase assays with focus on asparagine at position 24 (N24) with mutations to alanine (N24A), arginine (N24R) and tyrosine (N24Y) (n = 2, SK_B_11, I performed these experiments). **(b)** Hydrolase assays with focus on valine at position 33 (V33) with mutations to alanine (V33A), glutamic acid (V33E) and phenylalanine (V33F) (n = 2, SK_B_11, I performed these experiments). **(c)** Hydrolase assays with focus on tyrosine at position 114 (Y114) with mutations to alanine (Y114A), valine (Y114V) and tryptophan (Y114W) (n = 2, SK_B_11, I performed these experiments). CB, Coomassie blue; ^{32}P , autoradiogram.

The function of Y114 remained elusive from mere inspection of the crystal structure. Complementation with molecular dynamics modeling revealed that Y114 interacts with the diphosphate and the terminal ribose ring of the ADPr through hydrogen bonds (Rungrotmongkol et al. 2010). Hence, Y114 might also be involved in substrate recognition. All three mutations resulted in a loss of the hydrogen bond formed with the terminal ribose ring (Ecke et al. 2017).

In conclusion, the *in silico* analysis led to the identification of catalytically dead mutants of the CHIKV macrodomain. We chose the V33E and the Y114V mutants for future experiments because they affect different binding modes to the substrate.

The *in vitro* hydrolase assays on GST-ARTD10cat domain demonstrated that the V33E and the Y114V macrodomain mutants of CHIKV were inactive towards MARYlation. Furthermore, the activity towards PARylation was tested by analyzing the released products of *in vitro* auto-PARYlated HA-ARTD1 as substrate (Figure 21a). The analysis of the supernatants by TLC demonstrated that the V33E and the Y114V mutants of the CHIKV macrodomain were also inactive towards PARylation, because the signal did not exceed the signal released from HA-ARTD1 in the absence of macrodomains.

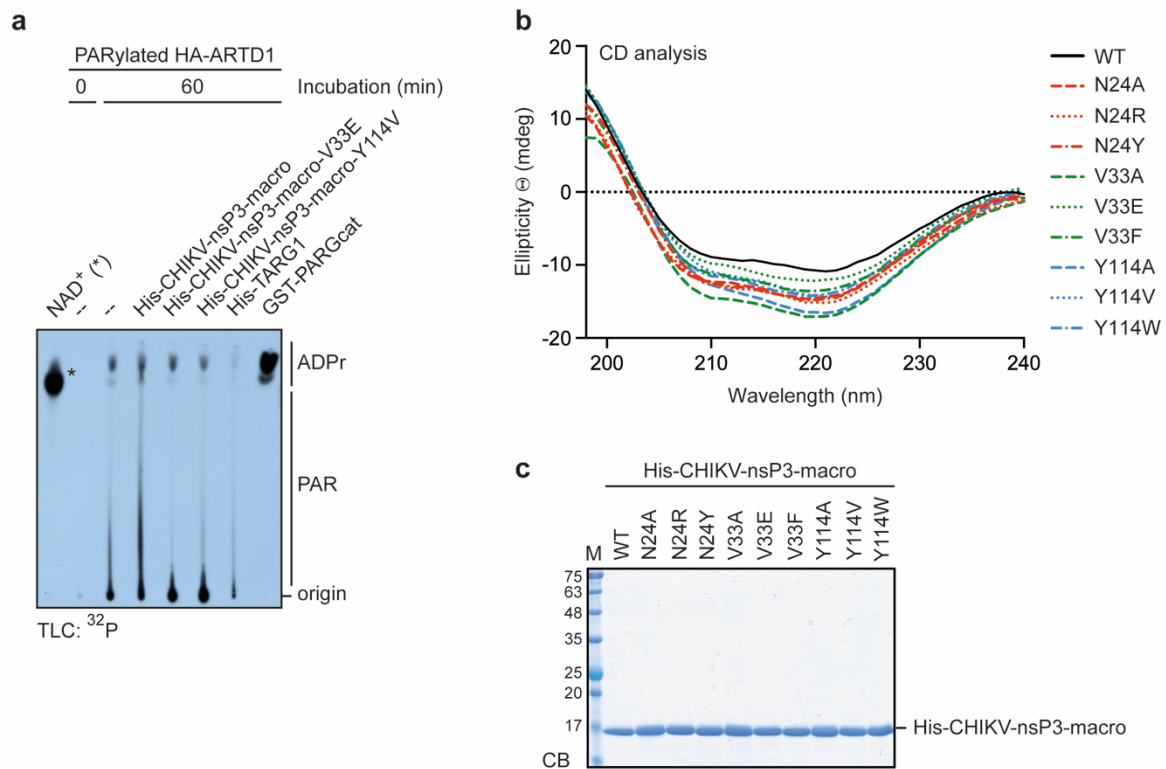


Figure 21: Investigation of the integrity of the CHIKV macrodomain mutants.

This figure is modified from Ecke, Krieg et al. 2017. **(a)** Plasmids encoding HA-ARTD1 were transiently transfected into HEK293 cells. 48 h post transfection cells were lysed in TAP lysis buffer and HA-ARTD1 was immunoprecipitated using an anti-HA-antibody (Covance). Subsequently, HA-ARTD1 was activated by addition of double stranded DNA oligos to the reactions and allowed automodification in the presence radioactive ³²P-NAD⁺ for 30 min at 30°C. Afterwards, the reactions were washed to remove free NAD⁺ prior to addition of the indicated bacterially expressed His-tagged macrodomains or GST-PARGcat. The reactions were further incubated for 60 min at 30°C. Supernatants were collected and fractions were subjected to thin layer chromatography (TLC) to visualize released radioactively labelled ADP-ribose and PAR chains from hydrolase reactions by autoradiography (³²P). ³²P-NAD⁺ was used as a control (left lane, indicated with *) (n = 1, SK_B_50, I performed this experiment). **(b)** Analysis of CHIKV macrodomain wt and mutants by circular dichroism (CD) to assess their folding (n = 1, SK_B_16, I performed this experiment with support by Alexander R. Grimm). The CD analysis was supported by Alexander R. Grimm (Institute of Biotechnology, RWTH Aachen University). **(c)** His-CHIKV-nsP3-macro wt and mutants used for CD analysis were subjected to SDS-PAGE and stained with Coomassie blue (CB) to confirm comparable protein concentrations and purity of the samples (n = 1, SK_B_16, I performed this experiment). CB, Coomassie blue; CD, circular dichroism; TLC, thin layer chromatography; ³²P, autoradiogram.

Because the single site mutations change the properties of the original amino acids, the changes in hydrolase activity may also result from incorrect folding of the macrodomain. Therefore, the folding of all macrodomain mutants was analyzed compared to the wt employing circular dichroism spectroscopy (**Figure 21b**). The spectra of the mutants resemble the wt spectrum closely, indicating that the structural integrity of the mutants remained unaffected. Hence, the observed changes of the catalytic activity were indeed due to impaired binding of the ADPr or the substrate and not defective protein folding. Therefore, the mutational analysis of the CHIKV macrodomain provides new insights into the mechanism of ADP-ribosylation hydrolysis. In addition, completely inactive mutants can be used as controls for further studies, for example to explore the functional relevance of de-MARylation activity for the virus.

2.1.4 The full-length CHIKV nsP3 protein possesses similar hydrolase properties to the isolated macrodomain *in vitro*

In the preceding experiments, isolated macrodomains have been characterized. In CHIKV, the macrodomain is not a self-contained protein, but it is located within the bigger non-structural protein 3 (nsP3). nsP3 consists of the N-terminal macrodomain, the alphavirus unique domain and an unstructured, hypervariable C-terminal region (Rana et al. 2014). So the question arose, whether the macrodomain has the same biochemical properties when part of the full-length nsP3 protein. To address this, His₆-tagged full-length CHIKV nsP3 was expressed in bacteria and subjected to *in vitro* hydrolase assays with automodified GST-ARTD10cat domain as substrate (**Figure 22**). In a time course experiment, the full-length nsP3 protein showed a comparable capacity to de-MARylate ARTD10 as the isolated macrodomain (**Figure 15, 16 and 22a**). Additionally, free ADPr also inhibited the hydrolase activity of nsP3 in a dose-dependent manner as well (**Figure 22b**).

Furthermore, the previously identified single site macrodomain mutants V33E and Y114V were introduced into the full-length nsP3 as well and bacterially expressed as His-tagged fusion proteins. In an *in vitro* hydrolase assay nsP3 harboring these mutations proved to be catalytically inactive towards ARTD10-mediated MARylation similar to the isolated macrodomain (**Figure 22c**).

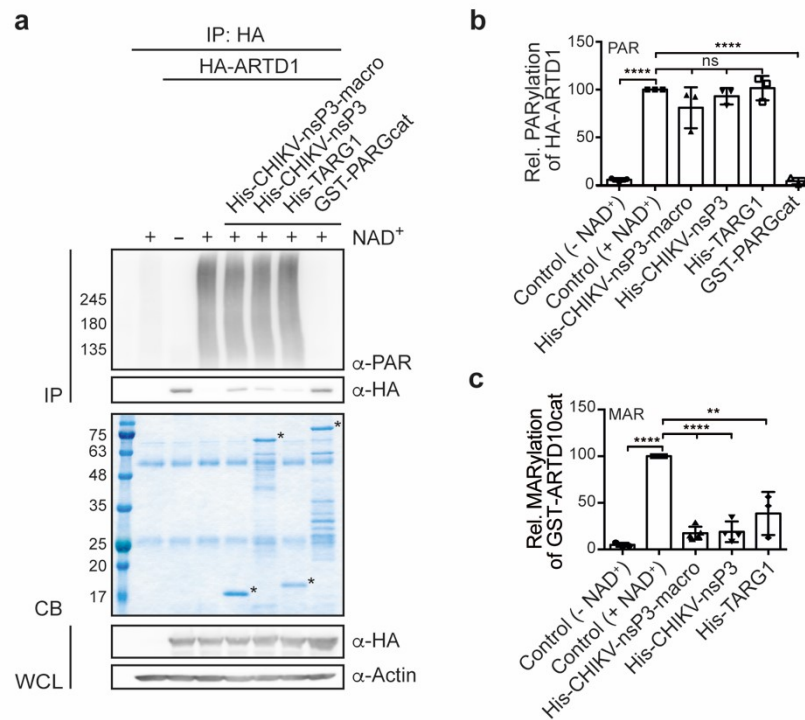


Figure 23: The full-length nsP3 protein of CHIKV is inefficient in removing protein poly-ADP-ribosylation.

This figure is modified from Ecke, Krieg et al. 2017. **(a)** Plasmids encoding HA-ARTD1 were transiently transfected into HEK293 cells. 48 h post transfection cells were lysed in TAP lysis buffer and HA-ARTD1 was immunoprecipitated using an anti-HA-antibody (Covance). Subsequently, HA-ARTD1 was activated by addition of double stranded DNA oligos to the reactions and automodification in the presence or absence β -NAD⁺ as indicated for 30 min at 30°C was allowed. Afterwards, the reactions were washed to remove free NAD⁺ prior to addition of bacterially expressed His-tagged CHIKV nsP3 full-length or isolated macrodomains as well as His-TARG1 or GST-PARGcat as indicated. The reactions were further incubated for 60 min at 30°C. The PAR signal was quantified by immunoblotting with an ADP-ribose-specific antibody (Trevigen), while total protein amounts were visualized by Coomassie blue (CB) staining. Equal expression of HA-ARTD1 was verified by immunoblotting with HA- and α -tubulin-specific antibodies in whole cell lysates (WCL) ($n = 3$, SK_B_20, I performed these experiments). **(b)** Quantification of relative PAR signal of three independent experiments performed as in panel a ($n = 3$, mean value \pm SD, I performed this evaluation). **(c)** Quantification of relative MAR signal of GST-ARTD10cat after 60 min of hydrolase assay ($n = 3-5$, mean value \pm SD, I performed this evaluation). CB, Coomassie blue; IP, immunoprecipitation; WCL, whole cell lysate. **** $p < 0.0001$; ** $p < 0.01$; ns, not significant when an unpaired student's t -test was applied.

2.1.5 The Chikungunya virus macrodomain can hydrolyze ARDT10-mediated mono-ADP-ribosylation in cells

The previous chapters contain a detailed biochemical characterization of the full-length nsP3 and the isolated macrodomain of CHIKV as efficient and specific hydrolases of protein MARYlation *in vitro*. The robustness of the effects and the inclusion of positive and negative controls for each assay render it unlikely that the observed activity is an artifact of the *in vitro* assays. Still, to determine whether the hydrolase activity can be validated in cells a system was employed that indirectly visualizes intracellular MARYlation (Forst et al. 2013; Butepage et al. 2018a). It uses the specific binding of murine Artd8-macro2-3 to automodified ARTD10. In co-immunoprecipitation and co-localization studies the effect of co-expression of the CHIKV macrodomain on the MARYlation status of ARTD10 was evaluated (**Figure 24**).

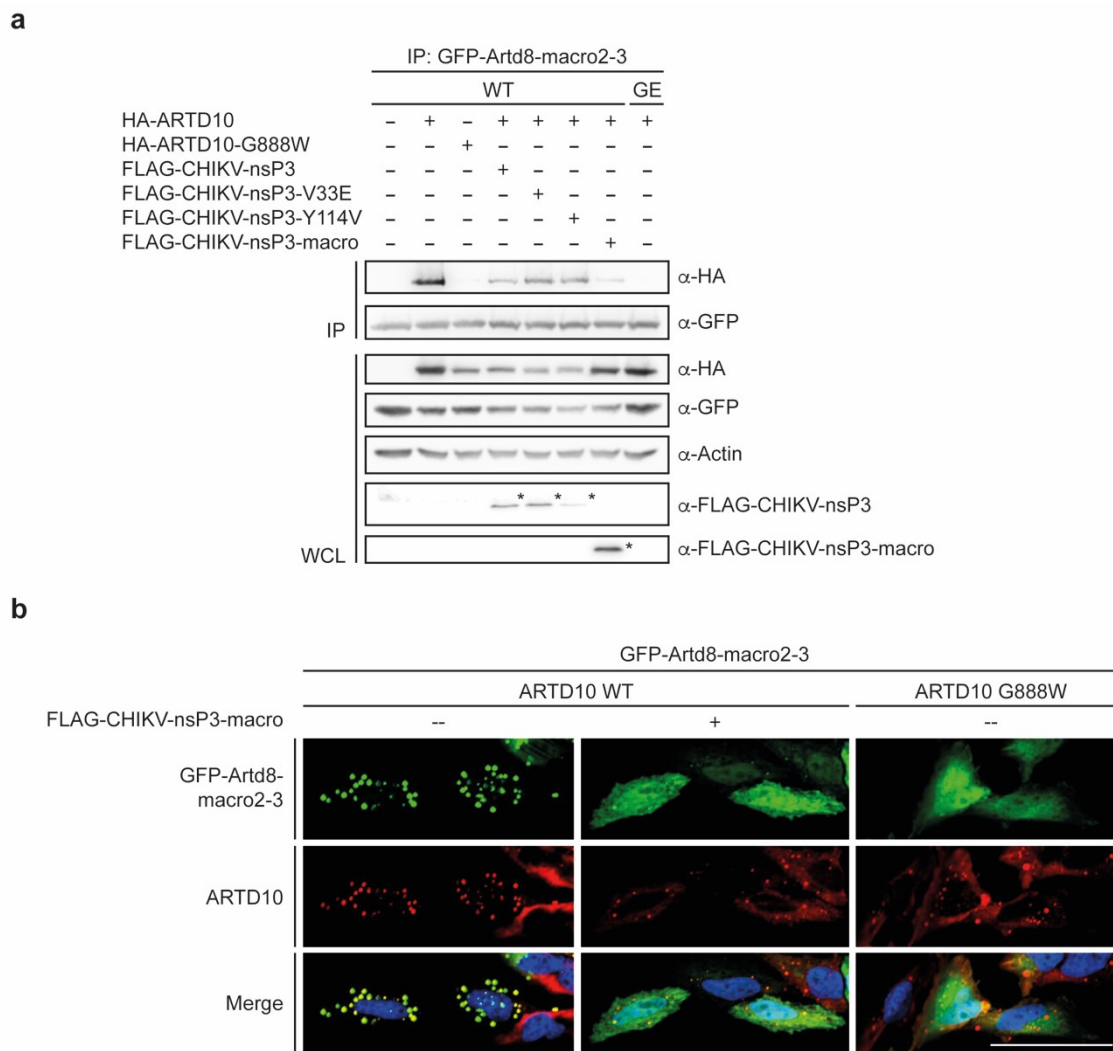


Figure 24: The CHIKV macrodomain is able to remove MARYlation intracellularly.

This figure is modified from Ecke, Krieg et al. 2017. **(a)** Plasmids encoding HA-ARTD10, wt or inactive G888W mutant, and FLAG-CHIKV-nsP3, full-length or isolated macrodomain in active or inactive versions, were transiently transfected into HEK293 Flp-IN T-Rex cells stably expressing murine GFP-Artd8-macro2-3 constructs. The GFP-Artd8-macro2-3 MAR-binding deficient GA mutant was used as a control. Cells were lysed in TAP lysis buffer and GFP-Artd8-macro2-3 were immunoprecipitated using a GFP-specific antibody (Rockland). Co-immunoprecipitated HA-ARTD10 was analyzed by immunoblotting with α -HA antibodies and total protein amounts were evaluated in whole cell lysates (WCL) by immunoblotting ($n = 2$, SK_B_31, I performed these experiments). **(b)** Plasmids encoding GFP-Artd8-macro2-3 and FLAG-CHIKV-nsP3-macro were transiently transfected into HeLa- Flp-IN T-Rex cells stably expressing ARTD10 wt or G888W as indicated. Cells were fixed with PFA and ARTD10 was stained with a monoclonal antibody (5H11). GFP-Artd8-macro2-3 and ARTD10 localization were analyzed using confocal microscope. GFP-Artd8-macro2-3 is shown in green and ARTD10 in red. Nuclei were stained with Hoechst and are shown in blue. Scale bar: 50 μ m ($n = 1$, SK_B_33, I performed this experiment). IP, immunoprecipitation; WCL, whole cell lysate.

First of all, HEK293 cells stably expressing murine Artd8 macrodomain 2 and 3 GFP-fusion proteins (GFP-Artd8-macro2-3) were co-transfected with plasmids encoding either full-length nsP3 or the isolated macrodomain of CHIKV as well as HA-ARTD10 wt or inactive G888W mutant. Afterwards, the expression of GFP-Artd8-macro2-3 wt or the MAR-binding deficient G1055E (macro2) G1268E (macro3) double mutant (GE) was induced with doxycycline (Dox). To evaluate the interaction between Artd8-macro2-3 and ARTD10, the GFP-fusion proteins were immunoprecipitated using GFP-specific antibodies and the amount of co-immunoprecipitated ARTD10 was analyzed by immunoblotting with anti-ARTD10 monoclonal antibodies. Because the wt macro2-3 construct is described to specifically bind to MARYlated ARTD10, the amount of co-immunoprecipitated ARTD10 can be used as a measure for

modification. This was verified by a robust signal for ARTD10 wt in the IP using Artd8-macro2-3 wt, while there was no signal for the catalytically inactive ARTD10 G888W mutant. Also, the MAR-binding deficient Artd8-macro2-3 GE mutant was unable to interact with ARTD10 wt (**Figure 24a**). Upon overexpression of the full-length nsP3 or the isolated macrodomain of CHIKV, the amount of co-immunoprecipitated ARTD10 was strongly reduced. ARTD10 expression was decreased when co-expressed with the viral proteins. Therefore, the inactive V33E and Y114V mutants were included in the assay as additional controls, which showed an increase in co-immunoprecipitated ARTD10 wt compared to the active macrodomains. This suggests de-MARylation of ARTD10 by the active CHIKV macrodomain and full-length nsP3 in cells and thus reduced binding of Artd8-macro2-3 (**Figure 24a**).

As a second approach to confirm intracellular MAR-hydrolase activity of the CHIKV macrodomain, co-localization studies were performed using immunofluorescence (**Figure 24b**). Therefore, stable ARTD10 wt or ARTD10-G888W expressing HeLa cells (Herzog et al. 2013) were transiently transfected with plasmids encoding GFP-Artd8-macro2-3 wt. While almost complete co-localization with ARTD10 wt dots was observed, the distribution of GFP-Artd8-macro2-3 was diffuse when catalytically inactive ARTD10-G888W was co-expressed. Upon co-expression of the isolated CHIKV macrodomain the macro2-3 constructs were largely redistributed towards a more diffuse localization comparable to the ARTD10-G888W control and only partial co-localization with the ARTD10 wt dots remained (**Figure 24b**). This suggested robust, though not complete, de-MARylation of ARTD10 by the CHIKV macrodomain, reducing the binding of Artd8-macro2-3. Hence, two independent approaches complemented the *in vitro* studies by validating intracellular MAR-hydrolase activity of the CHIKV macrodomain towards automodified ARTD10.

Taken together this chapter (2.1) identifies the CHIKV macrodomain as an efficient and specific hydrolase of mono-ADP-ribosylation not only *in vitro* but also in cells, while the activity towards poly-ADP-ribosylation is inefficient. Additionally, inactive macrodomains could be established by single site mutations shedding light on the catalytically relevant residues within the ADP-ribose binding pocket. Furthermore, the macrodomains of VEEV, SINV, ONNV, HEV and FIPV could also be defined as MAR-hydrolases *in vitro*. Because all tested viral macrodomains robustly removed MARylation from several substrates that contain multiple sites of modification, a broad activity towards protein MARylation can be proposed. These findings are in line with the fact that also multiple mono-ARTDs are induced by interferon signaling.

Around the same time our paper was released (Eckei et al. 2017), other groups published similar studies characterizing the hydrolase activity of viral macrodomains on protein ADP-ribosylation (Li et al. 2016a; McPherson et al. 2017; Fehr et al. 2016). These confirm the observed de-MARylation activity of CHIKV, VEEV, and HEV *in vitro* (Li et al. 2016a; McPherson et al. 2017), and additionally identify the severe acute respiratory syndrome coronavirus (SARS-CoV) and the human coronavirus 229E (HCoV229E) macrodomains as MAR-hydrolases *in vitro* (Fehr et al. 2016; Li et al. 2016a). Of note is that in contrast to our findings Li et al. also describe hydrolase activity of the VEEV and the SARS macrodomains on ARTD5(Tankyrase 1)- and ARTD1-mediated auto-PARylation, but the assays show strong background and thus render interpretation challenging. All in all, we suggest that the main activity of the viral macrodomains is de-MARylation.

After the biochemical characterization, in the next steps it needs to be addressed what the functional relevance of the de-MARylation activity is for viral replication. In the following chapters this will be addressed by analyzing the consequences of macrodomain inactive

mutants in the context of viral replicons, the effects of ARTDs on viral replication as well as the investigation of relevant substrates of (de-)MARylation (see chapters 2.2 and 2.3).

2.2 Mono-ADP-ribosylation restricts Chikungunya virus replication by inhibiting the auto-proteolytic activity of nsP2

Based on the results from the previous chapter 2.1, this chapter focuses on deciphering the functional role of the de-MARylation activity of the Chikungunya virus (CHIKV) macrodomain for the viral life cycle in more detail and on a more mechanistic level. First of all, a replicon based system was established to monitor replication of different CHIKV variants under diverse conditions through gaussia luciferase activity (based on Glasker et al. 2013). Exploiting this system, it was demonstrated that the interferon-inducible mono-ADP-ribosyltransferases ARTD10 and ARTD12 acted as restriction factors for CHIKV replication in cell culture while their knockdown facilitated replication. However, the degree of restriction depended on the timing of treatment in regard to the viral life cycle and on the catalytic activity of the transferases. Moreover, the inactive and ADP-ribose-(ADPr-)binding deficient macrodomain mutants V33E (**Figure 20 and 22**) as well as D10A (Malet et al. 2009; McPherson et al. 2017) were tested in the CHIKV replicon system and displayed a defect in viral replication that can be partially rescued by co-expression of a functionally active macrodomain. Further investigation revealed a decrease in processed non-structural proteins (nsPs) of CHIKV upon overexpression of ARTD10 and ARTD12 as well as in the macrodomain mutant replicons comparable to a protease-deficient virus. These processed nsPs originate from a polyprotein that needs to be auto-proteolytically processed by the viral protease which is part of nsP2. Cleavage of the polyprotein depicts an essential step for viral replication and our findings suggest that the activity of the macrodomain is somehow necessary for polyprotein processing. Therefore, it was tested whether the macrodomain and MARylation influence the protease activity of nsP2. Indeed, *in vitro* studies with bacterially expressed, recombinant proteins uncovered that nsP2 was a substrate of robust MARylation by several interferon-induced mono-ARTDs that was reversed by the macrodomain of nsP3. Furthermore, it was demonstrated that the MARylation of nsP2 hampers its protease activity *in vitro* in a dose-dependent manner. This inhibition can be antagonized by the de-MARylation activity of the viral macrodomain. The results in this chapter were partially published as a preprint in Krieg et al. 2020.

2.2.1 The interferon-induced ARTD10 and ARTD12 restrict viral replication of CHIKV

With establishing the catalytic activity of the macrodomain, the question about the functional relevance of de-MARylation for viral replication arose. For hepatitis E virus (HEV) a previous study of the macrodomain G48S/G49S/G50A triple mutant, which lost more than 90% of its MAR-hydrolase activity, showed a severe decrease in replication of the HEV replicon (Li et al. 2016a). The structural integrity of this triple mutation was never assessed. Thus, a structural effect cannot be excluded in that case. Furthermore, the severe acute respiratory syndrome coronavirus (SARS-CoV) was investigated in a similar manner. The catalytically inactive N1040A macrodomain mutant was introduced in the viral genome. But this mutation had no effect on viral replication in cell culture. However, in mouse infection models the macrodomain mutant virus presented a slight reduction in viral load and more importantly a strong increase in survival of the SARS-CoV infected animals. This effect may result from an increase of the innate immune response via enhanced interferon signaling and proinflammatory cytokine production (Fehr et al. 2016).

Both studies indicate a functional relevance for MARYlation in the viral life cycle and the necessity of the de-MARYlating activity of the macrodomain. But they also suggest that the mechanism of regulation is probably very different and needs to be assessed for every virus individually. For CHIKV, McPherson and colleagues introduced the single G32S, G32A, T11A and Y114A macrodomain mutations into the viral genome. *In vitro* these mutants showed decreased MAR-hydrolase activity compared to the wt but still retained significant activity, in line with our findings for the Y114A mutant (**Figure 20c**). In a mouse infection model these mutants exhibited decreased replication and virulence but the mechanism was not further investigated (McPherson et al. 2017).

To investigate the functional relevance for the hydrolase activity of CHIKV nsP3 in more detail, first of all a CHIKV replicon system was established based on Glasker et al. 2013. The Chikungunya genome consists of two open reading frames (ORFs). The first ORF encodes the non-structural proteins (nsPs) that are essential for viral replication and that modulate the host cell functions to optimize propagation. The second ORF is under the control of a subgenomic promoter that requires a functional replication complex consistent of the nsPs and encodes the structural proteins. The structural proteins form the viral envelope and are thus necessary for a fully functional, infectious virus. In the utilized replicon system, the ORF for structural proteins are replaced by a transgene encoding *Gaussia* luciferase. Therefore, the replicon cannot form intact virus but the luciferase activity can be used as a measure for replication. Because the *Gaussia* luciferase is secreted, samples from the supernatant can be measured at different hours post transfection (hpt) without interrupting the experiment (Glasker et al. 2013).

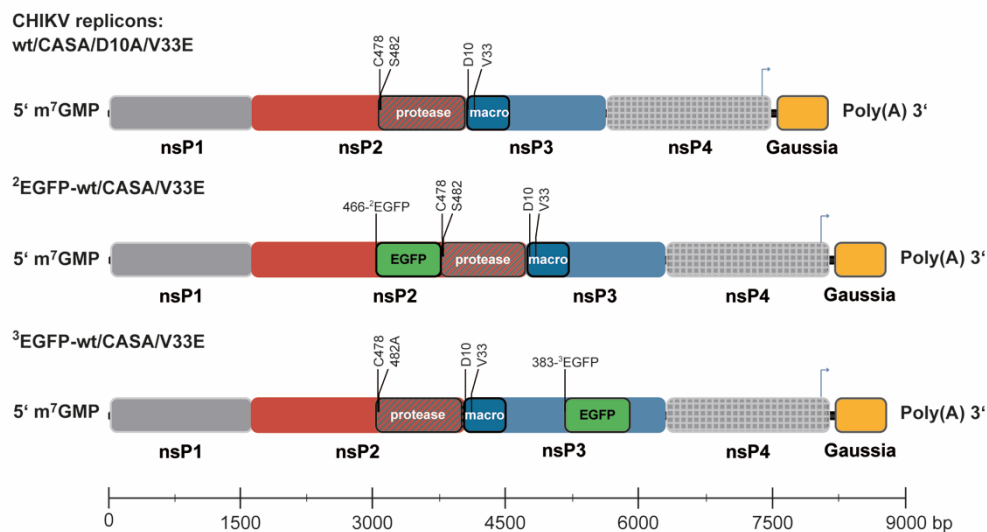


Figure 25: Schematic representation of CHIKV replicon constructs used in the following experiments.

The scale bar indicates the length of the RNA-based replicons in base pairs (bp). This figure was created by Patricia Korn, née Verheugd. This figure is adapted from Krieg et al. 2020.

In addition to the wildtype (wt) replicon several variants were created (**Figure 25**). On the one hand, we introduced the D10A (Malet et al. 2009; McPherson et al. 2017) and the V33E (**Figure 20 and 22**) inactive macrodomain mutants. On the other hand, we mutated the cysteine 478 (C478) and serine 482 (S482) to alanines. These residues are located within the protease domain of nsP2 and are essential for proteolytic activity (Saisawang et al. 2015). Additionally, we created EGFP insertions into nsP2 and nsP3 at the positions 466 and 383, respectively, according to Utt et al. 2016. In the following, these EGFP insertions will be referred to as ²EGFP and ³EGFP replicons. They were used for detection and immunoprecipitation of the replicon

proteins. This circumvented the lack of commercially available, good antibodies and to increase sensitivity. Furthermore, this allowed visualization of the replicon in immunofluorescence studies. All replicon constructs were transcribed *in vitro* and equipped with a 5'-m⁷G-cap prior to transfection of the recombinant RNA, to mimic viral infection as realistically as possible.

As no CHIKV-nsP2-specific antibodies were commercially available at the time, we ordered a custom, affinity purified rabbit polyclonal antibody directed against the protease domain of nsP2 from Eurogentec (**Figure 26**). To characterize it, recombinant, bacterially expressed His₆-fusion proteins of full-length nsP2 and the isolated protease domain (His-nsP2-459-798) were separated by SDS-PAGE, immunoblotted, and then incubated with the nsP2-specific antibody. The immunoblot shows, that the polyclonal antibody recognizes both proteins (**Figure 26a**). Furthermore, the antibody was tested on whole cell lysates. To do so, HEK293 cells were transiently transfected with an empty control plasmid, plasmids encoding Flag-nsP2 or the replicon wt RNA. After lysis the whole cell lysates were separated by SDS-PAGE, immunoblotted, and incubated with the nsP2-specific antibody. Even though there were unspecific bands visible in the whole cell lysates, upon the expression of nsP2 a specific protein species appeared at the expected molecular weight of around 75 kDa that is not present in the control whole cell lysate (**Figure 26b**). Hence, the nsP2-specific antibody recognized plasmid as well as replicon based nsP2 in whole cell lysates. Immunoprecipitation with the nsP2-specific antibody was not successful (data not shown).

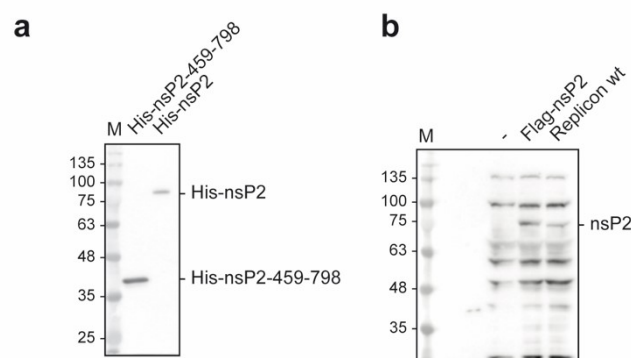


Figure 26: Characterization of the custom-designed CHIKV nsP2 antibody.

This figure is modified from Krieg et al. 2020. Rabbits were simultaneously immunized with two peptides located in the protease domain of CHIKV nsP2 (peptide 1 (570-584) CERKYPFTKGKWNINK, and peptide 2 (740-755): CVLGRKFRSSRALKPP) to create polyclonal, purified CHIKV-nsP2-specific antibodies (Eurogentec). **(a)** Bacterially expressed, His₆-tagged fusion proteins of the full-length CHIKV nsP2 and the isolated protease domain (459-798) were immunoblotted with the nsP2-specific antibody (SK_C_53, I performed this experiment). **(b)** HEK293 cells were transiently transfected with plasmids encoding Flag-nsP2 or with the replicon wt. After lysis the whole cell lysates were immunoblotted with nsP2-specific antibody (SK_C_53, I performed this experiment).

After establishment of the necessary tools (**Figure 25 and 26**), the influence of ADP-ribosylation on CHIKV replication was investigated. First of all, HEK293 cells were treated with siRNA pools targeting several interferon-inducible mono-ARTDs (Eckei et al. 2017; Krieg et al. 2020) including *ARTD10*, *ARTD12*, *ARTD8* and *ARTD7* prior to transfection with the CHIKV ³EGFP replicon (**Figure 27**). Analysis of the Gaussia luciferase activity in the supernatant, revealed that knockdown of *ARTD10* and *ARTD12* led to a significant increase of luciferase activity 9 hours post transfection (hpt) compared to *siControl* treated cells. This effect decreased over time. Meanwhile, *ARTD8* and *ARTD7* knockdown only allowed a marginal increase in CHIKV replication. Furthermore, simultaneous knockdown of *ARTD10* and *ARTD12*

was tested, but no further increase of replication could be achieved compared to the single knockdowns (**Figure 27**).

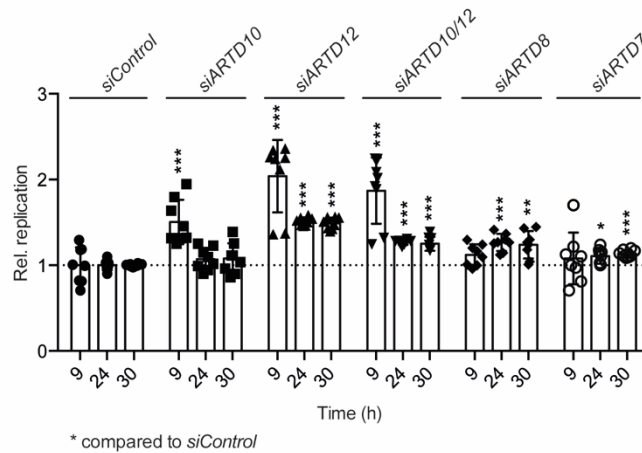


Figure 27: The knockdown of interferon-inducible mono-ARTDs increases CHIKV replication.

This figure is modified from Krieg et al. 2020. HEK293 cells were transfected with siRNA oligo pools targeting *ARTD10*, *ARTD12*, *ARTD7* or *ARTD8* or a combination as indicated. A non-targeting siRNA pools was used as a control. 72 h after transfection of the siRNA pools, the cells were transfected with *in vitro* transcribed $^3\text{EGFP}$ replicon RNA and the supernatant was collected at 9, 24 and 30 hours post transfection (hpt). The Gaussia luciferase activity in the supernatant was quantified as a measure for replication, normalized to *siControl* treated cells ($n = 4$, two technical replicates were measured per n , two-tailed Mann-Whitney test was applied, SK_D_13, I performed these experiments). *** $p < 0.001$; ** $p < 0.01$; * $p < 0.05$ when a two-tailed Mann-Whitney test was applied.

Because the knockdowns of ARTD10 and ARTD12 showed the largest effects on replication (**Figure 27**), the following experiments focus on these two mono-ARTDs. To further investigate their influence on CHIKV replication, overexpression studies were performed (**Figure 28**). Stable HEK293 Flp-IN T-REx cell lines were used in which the expression of the transgene can be induced by doxycycline (Dox). For control the effect of Dox on CHIKV replication was initially assessed. Analysis of the Gaussia luciferase activity in the supernatant, indicated that Dox had slightly repressing effects (**Figure 28a**). In all subsequent experiments, control cells were always treated with doxycycline. The CHIKV replicon RNA was transfected into HEK293 Flp-IN T-REx cells stably expressing ARTD10 or inactive ARTD10-GW mutant (Kleine et al. 2008), or ARTD12 or inactive ARTD12-HY mutant (Krieg et al. 2020). Subsequently, the Gaussia luciferase activity was measured at different times after transfection (**Figure 28b,c**). Compared to the control cells, overexpression of active ARTD10 as well as ARTD12 diminished the replication by about 50% 24 hpt while the inactive variants had only minor effects (**Figure 28c**). The expression of the different proteins was comparable (**Figure 28d**). Looking at the progression of replication over time, there appears to be a change in the slope of the curve between 12 and 24 hpt, implicating that the effect of MARYlation changes over time (**Figure 28b**). This will be addressed further in later experiments. However, overexpression experiments show that ARTD10 and ARTD12 are significantly restrictive for CHIKV replication dependent on their catalytic activity 24 hpt.

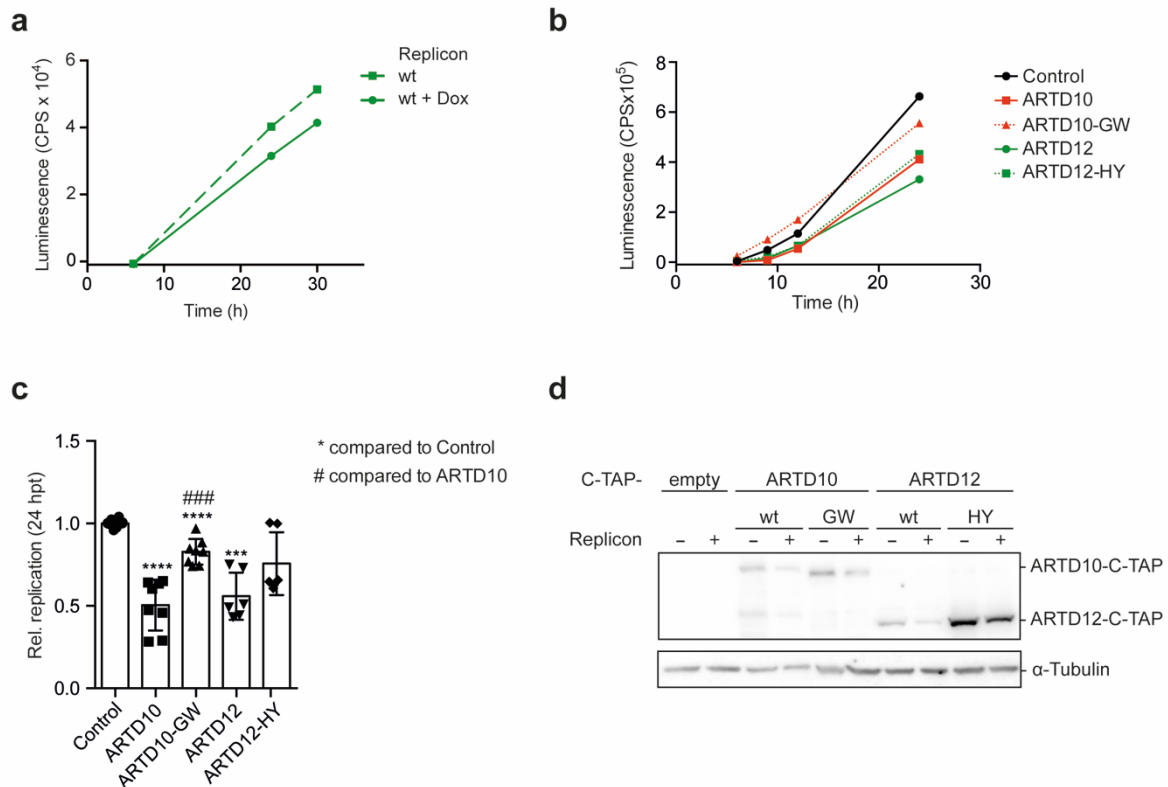


Figure 28: Overexpression of ARTD10 and ARTD12 restricts CHIKV replication in a catalytic activity-dependent manner.

This figure is modified from Krieg et al. 2020. **(a)** HEK293 Flp-IN T-REx cells stably expressing the TAP-tag alone were transfected with *in vitro* transcribed CHIKV replicon RNA with or without prior induction by doxycycline (Dox) as indicated. Supernatant was collected at the indicated times after transfection and Gaussia luciferase activity was analyzed as a measure for replication (mean of two technical replicates is shown, I performed this experiment). **(b-d)** HEK293 Flp-IN T-REx cells stably expressing the TAP-tag alone, ARTD10-C-TAP, wt or inactive GW mutant, or ARTD12-C-TAP, wt or inactive HY mutant, as indicated. Expression was induced with Dox 16 h prior to transfection with the *in vitro* transcribed replicon wt RNA (n = 3-4, SK_C_51, I performed these experiments). **(b)** Representative measurement of Gaussia luciferase activity in the supernatant collected at the indicated times after transfection (mean of two technical replicates is shown). **(c)** Quantification of Gaussia luciferase activity relative to the TAP-tag control cells at 24 hours post transfection (hpt) (n = 3-4, mean value \pm SD, two technical replicates were measured per n, two-tailed Mann-Whitney test was applied, SK_C_51, I performed these experiments). **(d)** Cells were harvested 24 hpt and expression of the TAP-tagged fusion proteins was analyzed in whole cell lysates by immunoblotting with ARTD10- (5H11) and ARTD12-specific (Sigma) antibodies compared to α -tubulin as a loading control 24 hpt. CPS, counts per second; Dox, doxycycline; hpt, hours post transfection; TAP, tandem affinity purification. **** $p < 0.0001$; ***/### $p < 0.001$ when a two-tailed Mann-Whitney test was applied.

To address whether the observed effect is potentially specific for interferon-regulated MARYlation, transient overexpression experiments were performed with ARTD1 and IFN-insensitive ARTD14 (Krieg et al. 2020) (**Figure 29**). While ARTD1 PARYlates its substrates, ARTD14 is restricted to MARYlation (Luscher et al. 2018). The immunoblot of whole cell lysates confirmed that HA-ARTD1 expression is comparable to HA-ARTD10 expression. HA-ARTD14 expression on the other hand was considerably lower but still higher than that of HA-ARTD12 (**Figure 29a**). Measurement of the Gaussia luciferase activity however, showed that only ARTD10 and ARTD12 restricted viral replication significantly and ARTD1 and ARTD14 had no effect (**Figure 29b**). Hence, restriction of CHIKV seemed to be selective for interferon-regulated mono-ARTDs.

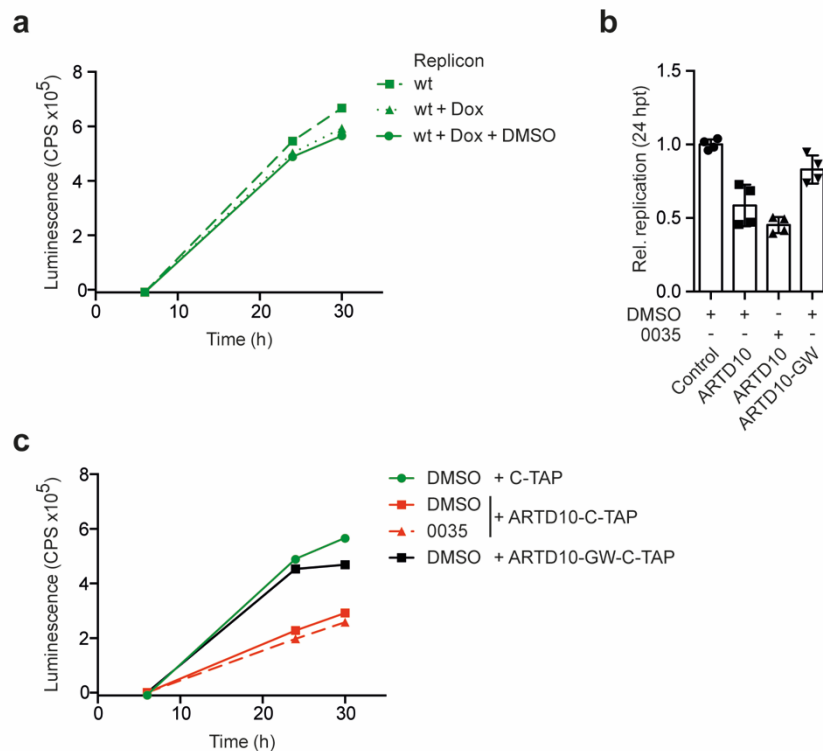


Figure 30: The specific ARTD10 inhibitor 0035 cannot rescue ARTD10 overexpression effects on CHIKV replication.

(a) HEK293 Flp-IN T-REx control cells, only expressing the TAP-tag alone, were incubated in the presence or absence of doxycycline (DOX) and the vehicle dimethyl sulfoxide (DMSO) as indicated prior to transfection with the *in vitro* transcribed CHIKV replicon RNA. Gaussia luciferase activity in the supernatant was measured at the indicated times post transfection (mean of two technical replicates is shown, I performed this experiment). **(b,c)** HEK293 Flp-IN T-REx cells stably expressing the TAP-tag alone or ARTD10-C-TAP, wt or inactive GW mutant, were either treated with 10 μ M of the ARTD10-specific inhibitor 0035 or the vehicle DMSO as indicated. 24 h later, the cells were transfected with *in vitro* transcribed CHIKV replicon RNA (n = 2, SK_C_51, SK_D_2, I performed these experiments). **(b)** Quantification of Gaussia luciferase activity relative to the TAP-tag control cells treated with DMSO at 24 hpt (n = 2, mean value \pm SD, two technical replicates were measured per n, I performed these experiments). **(c)** Representative measurement of Gaussia luciferase activity in the supernatant collected at the indicated times after transfection (mean of two technical replicates is shown, I performed this experiment). DMSO, dimethyl sulfoxide.

To investigate this further, the restrictive effect of MARYlation by ARTD10 and ARTD12 was assessed in more detail at different time points. Additionally, a potential cooperative effect of these two interferon-induced mono-ARTDs was tested (**Figure 31**). For that purpose, stable HEK293 cells expressing either the TAP-tag only or ARTD10-C-TAP were transiently transfected with a plasmid encoding HA-ARTD12 that proved to be active and restrictive before (**Figure 29**) prior to transfection with the ³EGFP replicon that contained the EGFP-tag within the unstructured region of nsP3 (**Figure 25**). Like in previous experiments, ARTD10 and ARTD12 decreased Gaussia luciferase activity in the supernatant at 9 as well as 30 hpt. Furthermore, addition of ARTD12 to ARTD10 did not increase the effects at 9 hpt but the transferases showed cooperativity at 30 hpt. Interestingly, the HY mutant of ARTD12 depicted a comparable level of restriction as the wt at 9 hpt, with a significant difference only at 30 hpt. Furthermore, the inactive ARTD10-GW mutant gained repressing effects at later time points (**Figure 31a**). These fluctuations in impact on CHIKV replication again hint at a more complex role of MARYlation in the viral life cycle. On the one hand the different ARTDs seem to play diverse roles, potentially through MARYlation of distinct substrates, and on the other hand there seems to be a switch in relevance, possibly from a restrictive to a proviral role of MARYlation. Moreover, ARTD12 seemed to have a MAR-independent function as well, that appeared to lose effect over time. To observe an earlier time point in the viral life cycle prior to expression from the subgenomic promoter, we used the EGFP insertion of the replicon to

visualize the amount of processed nsP3 in whole cell lysates under the same setup. The immunoblot showed, comparable to the luciferase activity, that presence of active mono-ARTDs decreased the amount of nsP3, even cooperatively when ARTD10 and ARTD12 were both present. Meanwhile the inactive mutants had only small effects (**Figure 31b**). This suggested an earlier point of inhibition than the translation from the subgenomic promoter, potentially in the processing of the polyprotein.

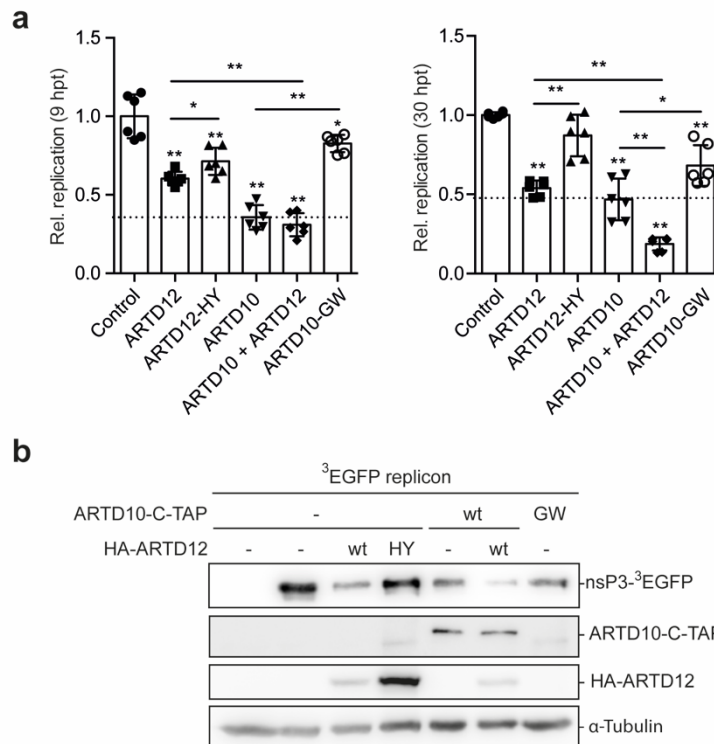


Figure 31: ARTD10 and ARTD12 partially cooperate in restricting CHIKV replication and nsP3 protein levels.

This figure is modified from Krieg et al. 2020. **(a,b)** HEK293 Flp-IN T-REx cells stably expressing the TAP-tag alone or ARTD10, wt or inactive GW mutant, were transiently transfected with plasmids encoding HA-ARTD12, wt or inactive HY mutant, as indicated. 24 h later, the cells were additionally transfected with *in vitro* transcribed ³EGFP replicon RNA ($n = 3$, SK_C_51, I performed these experiments). **(a)** Quantification of Gaussia luciferase activity relative to the TAP-tag control cells without HA-ARTD12 at 9 or 30 hpt ($n = 3$, mean value \pm SD, two technical replicates were measured per n , I performed these experiments). **(b)** Cells were harvested 30 hpt and whole cell lysates were immunoblotted with ARTD10- (5H11), HA- (Covance) and GFP-specific (Rockland) antibodies, to control expression of ARTDs and the viral nsP3 compared to the loading control α -tubulin. $**p < 0.01$; $*p < 0.05$ when a two-tailed Mann-Whitney test was applied.

In addition to the experiments depicted in this thesis, in cooperation with Fabian Pott and Christine Goffinet (Charité, Berlin) the findings above were complemented with live virus studies (Krieg et al. 2020). These experiments confirmed the inhibitory effect of ARTD10 on CHIKV replication dependent on its catalytic activity, while the inactive ARTD10-GW mutant showed a dominant-negative effect. The restriction was more pronounced at earlier times after the infection. Furthermore, ARTD12 inhibited the full-length virus, but in contrast to ARTD10 the inactive ARTD12-HY mutant restricted the virus to the same extent hinting at an additional MAR-independent mechanism of inhibition again.

All in all, this chapter defines ARTD10 and ARTD12 as restriction factors for CHIKV replication, that is for ARTD10 dependent on its ability to MARYlate, while the effect of ARTD12 was independent of MARYlation.

2.2.2 Mono-ADP-ribosylation affects CHIKV polyprotein processing

The fact that ARTD10- and ARTD12-mediated inhibition of CHIKV replication was most prominent at early times and leads to decreased levels of processed nsP3, suggested a role for MARYlation early in the viral life cycle. To further elucidate this, the role of the macrodomain's hydrolase function for viral replication was addressed. Hence, the inactive macrodomain mutants were tested in replicon assays (**Figure 32**). To test the hypothesis of MARYlation influencing polyprotein processing, the nsP2 C478A/S482A mutant, referred to as CASA in the latter, was included in the assays. This mutant was described to be proteolytically inactive (Saisawang et al. 2015). Looking at the Gaussia luciferase activity, the replicons carrying the macrodomain mutants D10A and V33E showed no replication activity comparable to the protease mutant (**Figure 32a,b**). Still, there seemed to be a small, but significant difference between the CASA mutant and the hydrolase inactive mutants at 30 hpt (**Figure 32b**). Additional to analyzing the luciferase activity, the whole cell lysates of the replicon transfected cells were investigated by immunoblotting with the custom-designed, nsP2-specific antibody described before (**Figure 26**). The immunoblot showed, that processed nsP2 was only detectable for the replicon wt, but for neither of the mutants (**Figure 32c**). This suggested a potential defect in polyprotein processing in the presence of inactive macrodomains. This is in line with the effects of processed nsP3 in the previous overexpression experiments with ARTD10 and ARTD12 (**Figure 31b**).

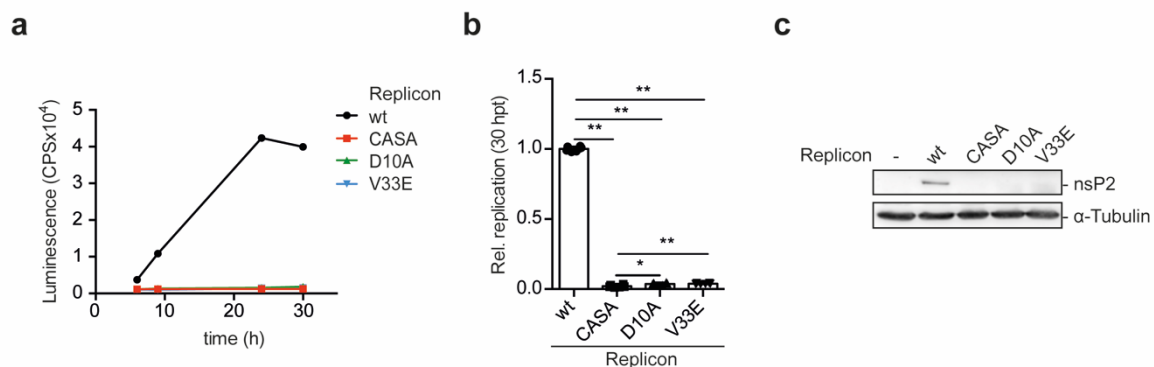


Figure 32: CHIKV hydrolase inactive mutants cannot replicate and resemble the proteolytically inactive CASA mutant.

This figure is modified from Krieg et al. 2020. **(a-c)** HEK293 cells were transfected with *in vitro* transcribed CHIKV replicon RNA, wt or mutants, as indicated. The CASA mutant is the proteolytically inactive nsP2 C478A S482A mutant, while the D10A and V33E mutants are located within the macrodomain and abolish hydrolase activity ($n = 3$, SK_D_9, I performed these experiments). **(a)** Representative measurement of Gaussia luciferase activity in the supernatant collected at the indicated times after transfection (mean of two technical replicates is shown, I performed this experiment). **(b)** Quantification of Gaussia luciferase activity relative to the control cells with wt replicon at 30 hpt ($n = 3$, mean value \pm SD, two technical replicates were measured per n , I performed these experiments). **(c)** Cells were harvested 30 hpt and whole cell lysates were immunoblotted with CHIKV nsP2-specific antibodies (Eurogentec), to control expression of the viral nsP2 compared to the loading control α -tubulin. ** $p < 0.01$; * $p < 0.05$ when a two-tailed Mann-Whitney test was applied.

Since the nsP2-specific antibody showed unspecific bands and the signal for nsP2 was rather weak (**Figure 26**), the results from Figure 32 were complemented with replicons carrying EGFP insertions and thus provided more sensitivity with a GFP-specific antibody (**Figure 33**). Again, the macrodomain V33E mutant was investigated compared to the proteolytically inactive CASA mutant, for the ²EGFP as well as the ³EGFP replicon, containing EGFP within nsP2 or nsP3, respectively. Of note is, that the replication activity of both replicons with EGFP insertions was significantly reduced in comparison to the wt replicon (**Figure 33a,b**). This is contradictory to previous reports, where no differences between replicons with and without insertions were observed. However, these studies were performed with plasmid-based trans replication systems, which might explain the discrepancies (Utt et al. 2016). Nonetheless, the

²EGFP as well as the ³EGFP still exhibited replication curves comparable to the wt and were thus used for further analysis. Also the introduction of the CASA and the V33E mutants led to the same replication defect as for the replicons without EGFP insertions (**Figure 33a,b**). The analysis of the whole cell lysates of the transfected cells by immunoblotting revealed that the untagged, processed nsP2 was only detectable for the wt replicon. Immunoblotting with a GFP-specific antibody on the other hand, increased the sensitivity and thus allowed detection of processed nsP2-²EGFP and nsP3-³EGFP for the ²EGFP and ³EGFP replicons, respectively (**Figure 33c**). As expected, the CASA mutant of both EGFP replicons showed no detectable bands for processed nsPs, as this mutant is proteolytically inactive. Furthermore, while there was no processed nsP2-²EGFP detectable for the ²EGFP V33E mutant, the ³EGFP V33E replicon displayed a distinct band for processed nsP3-³EGFP, although much weaker than for the ³EGFP wt replicon (**Figure 33c**). The discrepancy between the V33E mutant of ²EGFP and the ³EGFP replicons was probably due to lower replication of the ²EGFP replicon in general, leaving the signal for the processed nsP2-²EGFP just at the limit of sensitivity. The fact that there was weak signal for processed nsP3-³EGFP in the V33E mutant provides evidence that polyprotein was synthesized from this replicon. Thus, the lack of processed protein was not due to a lack of translation, for example due to incorrectly folded viral RNA. Moreover, the higher proteolytic activity compared to the CASA mutant suggests that the nsP2 protease is inhibited by MARYlation. This would be consistent with some residual protease activity because the MARYlation may not be complete.

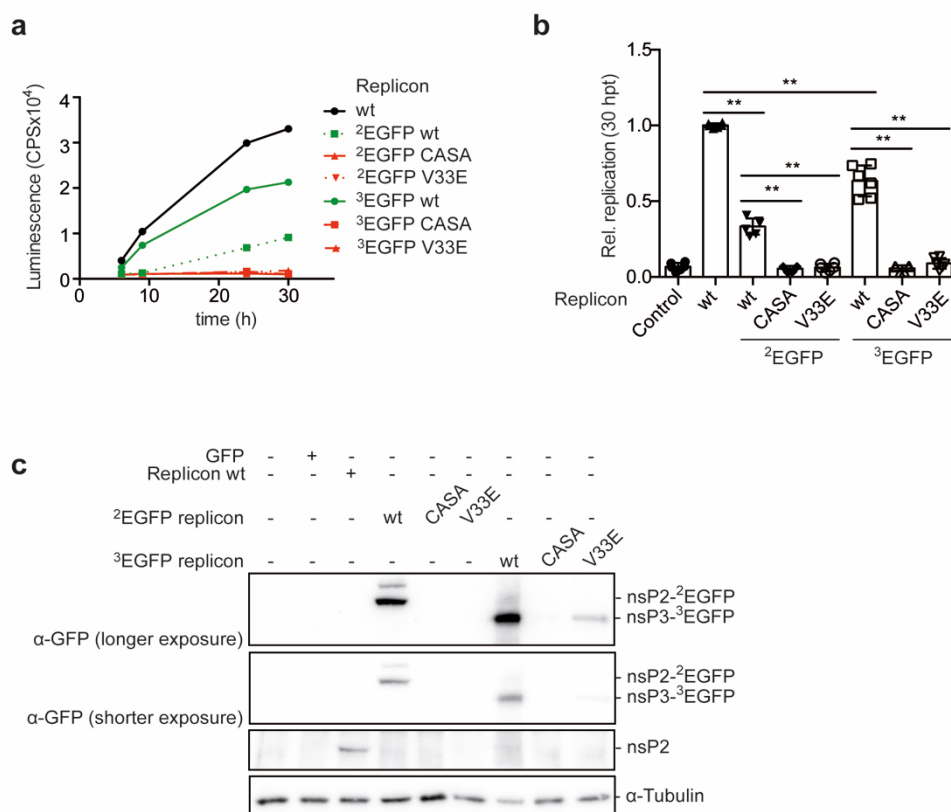


Figure 33: The EGFP replicons containing macrodomain mutants exhibit similar properties to the untagged replicon.

This figure is modified from Krieg et al. 2020. **(a-c)** HEK293 cells were transfected with *in vitro* transcribed CHIKV wt, ²EGFP and ³EGFP replicon RNA and the indicated protease (CASA) and macrodomain (V33E) mutants thereof (n = 3, SK_D_11, I performed these experiments). **(a)** Representative measurement of Gaussia luciferase activity in the supernatant collected at the indicated times after transfection (mean of two technical replicates is shown). **(b)** Quantification of Gaussia luciferase activity relative to the control cells with wt replicon at 30 hpt (n = 3, mean value \pm SD, two technical replicates were measured per n, I performed these experiments). **(c)** The cells were harvested 30 hpt and whole cell lysates were immunoblotted with CHIKV nsP2-specific or GFP-specific antibodies (Eurogentec; Rockland), to control expression of the viral nsP2 and nsP3 compared to the loading control α -tubulin. ***p* < 0.01 when a two-tailed Mann-Whitney test was applied.

A defect in polyprotein processing is not the only explanation for decreased levels of processed viral nsPs. For Zika virus (ZIKV) it was shown that expression of ARTD12 led to PARylation and ubiquitination of the viral nsPs NS1 and NS3, which resulted in their proteasomal degradation (Li et al. 2018). Because ARTD12 was restricted to MARylation but its catalytic activity is essential for this effect, the MARylation might be a seeding event for the subsequent PARylation and ubiquitination. A similar mode of action, would also explain the decrease in processed nsPs of the CHIKV macrodomain mutants. It would suggest that there is no decrease in processing, but that the polyprotein or the processed nsPs are degraded when MARylation cannot be antagonized by the macrodomain. To test this hypothesis, HEK293 cells were transfected with $^3\text{EGFP}$ replicons, wt or mutants, and treated either with the proteasomal inhibitor MG132 or the vehicle DMSO. As another major degradation machinery of the cell, the autophagic cascade was blocked, by inhibiting the fusion of the autophagosome and the lysosome with Bafilomycin A1 (Baf. A1) (**Figure 34**). If the decrease in processed nsPs of CHIKV was due to degradation, treatment with MG132 or Baf. A1 should lead to an increase in replication and amounts of protein for the V33E mutant and potentially also for the wt, as it was the case for ZIKV (Li et al. 2018). However, neither treatment could increase replication or amounts of processed proteins. If anything it rather seemed to inhibit replication of the $^3\text{EGFP}$ wt replicon and further decreased the amounts of processed nsP3- $^3\text{EGFP}$ in the V33E mutants (**Figure 34**). Therefore, the mechanism of MAR-mediated regulation of CHIKV seems to be distinct from ZIKV and the decrease of viral nsPs is not due to degradation by the proteasome or autophagy.

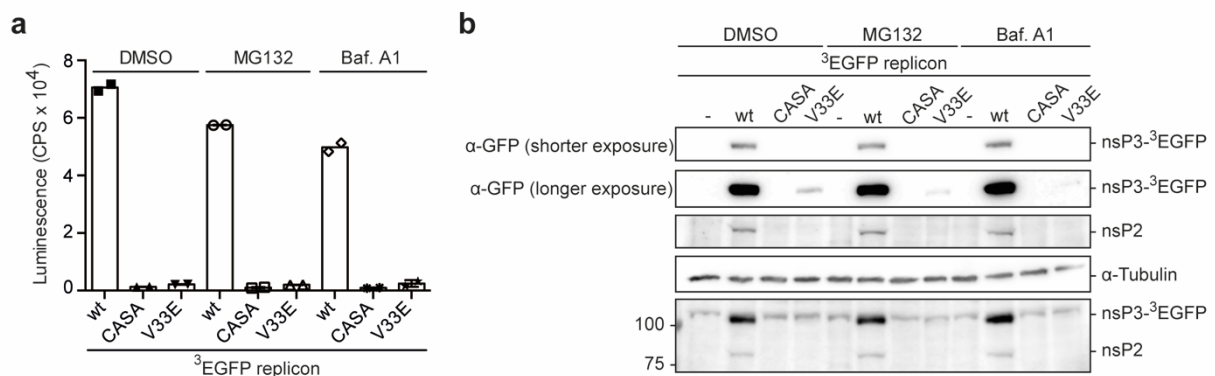


Figure 34: Inhibition of the proteasome or the autophagic flux does not rescue the defect of the CHIKV V33E mutant.

This figure is modified from Krieg et al. 2020. **(a-b)** HEK293 cells were transfected with *in vitro* transcribed $^3\text{EGFP}$ replicon wt, CASA or V33E mutant RNA. 24 hpt the cells were treated with 25 μM MG132, 200 nM Bafilomycin A1 (Baf.A1) or the vehicle DMSO for 6 h ($n = 1$, SK_D_1, I performed this experiment). **(a)** Quantification of Gaussia luciferase activity at 30 hpt ($n = 1$, mean value, two technical replicates were measured, I performed this experiment). **(b)** The cells were harvested 30 hpt and whole cell lysates were immunoblotted with CHIKV nsP2-specific or GFP-specific antibodies (Eurogentec; Rockland), to control expression of the viral nsP2 and nsP3 compared to the loading control α -tubulin.

If the polyprotein is properly translated from the viral RNA and MARylation inhibits the viral life cycle later, it should be possible to rescue the defect of the CHIKV V33E macrodomain mutant. The first attempt was to treat $^3\text{EGFP}$ wt or V33E replicon transfected cells with inhibitors of ADP-ribosylation (**Figure 35**). On the one hand, the ARTD10-specific inhibitor 0035 was employed (Venkannagari et al. 2013; Venkannagari et al. 2016), because ARTD10 showed effects on CHIKV replication in the previous chapter 2.2.1. On the other hand, the broad inhibitor 3-aminobenzamide (3-AB) was used. As its structure resembles NAD^+ , it is capable of inhibiting all ARTD enzymes to different degrees and should thus inhibit ADP-ribosylation in general (Wahlberg et al. 2012b). If MARylation restricts viral replication, and the V33E mutant shows a defect in replication due to its inability to reverse MARylation,

depletion of ADP-ribosylation with inhibitors might rescue this effect. However, analysis of the replication by measuring Gaussia luciferase activity revealed, that neither treatment with 0035, nor with 3-AB was able to reverse the effect of the mutation of the macrodomain (**Figure 35a,c**). On the $^3\text{EGFP}$ wt replicon the inhibitors showed a slight restrictive effect, that was not due to the vehicle DMSO (**Figure 35a-c**). Furthermore, evaluation of the viral proteins in whole cell lysates via immunoblot indicated that treatment with either ARTD inhibitor rather decreased the amounts of processed viral nsP2 and nsP3 for the wt as well as the V33E mutant replicon (**Figure 35d**). Comparable to the experiments with the ARTD10 cells (**Figure 30**), inhibition of ARTD10 and more broadly all ARTDs did not show a proviral effect. Again, the regulation of CHIKV replication through ARTDs seemed to be more complex than just proviral or restrictive. The fact that inhibition of ADP-ribosylation showed a slightly restrictive effect further strengthens the hypothesis that MARYlation might to some extent be necessary for viral replication. Thus, simple inhibition of ARTDs is unlikely to reveal simple reactions patterns. The hydrolase activity of the macrodomain might on the other hand be specific and only de-MARYlate certain substrates whose modifications restrict the virus. Furthermore, initial ADP-ribosylation might be necessary for targeting or recruiting of the viral replication machinery to host factors that are exploited.

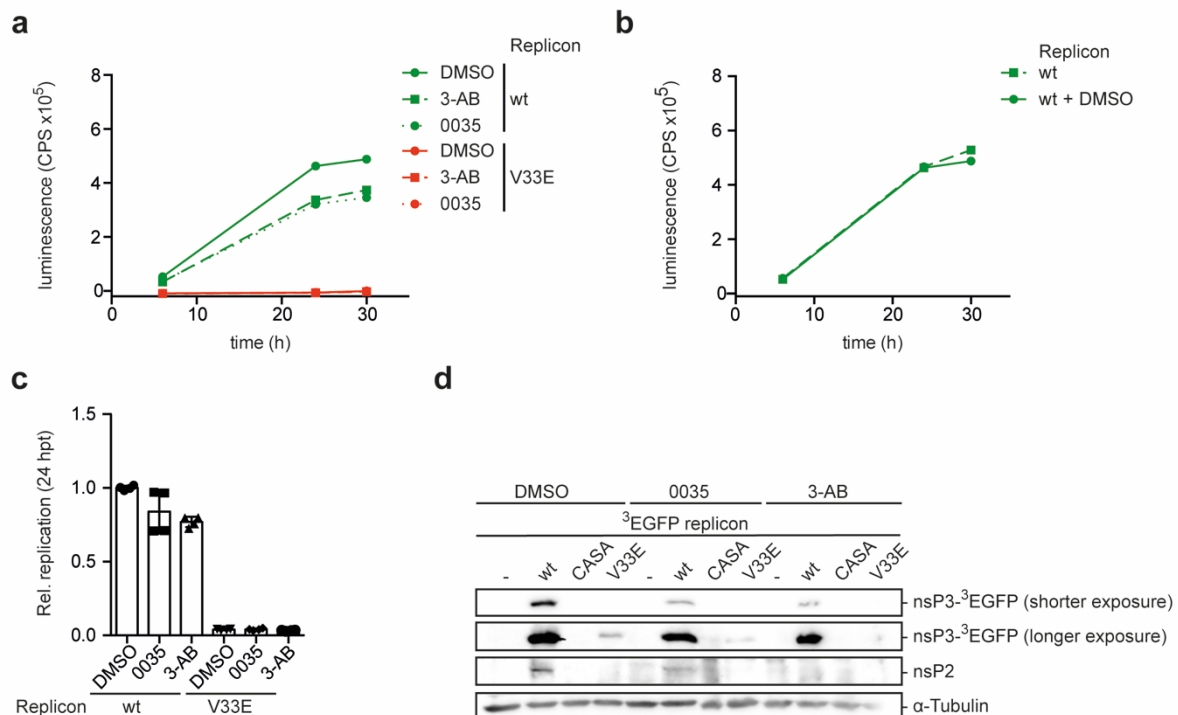


Figure 35: Treatment with ARTD inhibitors cannot rescue the defect of the CHIKV V33E macrodomain mutant.

(a-d) HEK293 cells were treated with the vehicle DMSO, 10 μM of the ARTD10-specific inhibitor 0035 or 2.5 mM of the broad ARTD inhibitor 3-aminobenzamide (3-AB). 24 h later, the cells were transfected with *in vitro* transcribed $^3\text{EGFP}$ replicon wt or the V33E macrodomain mutant RNA ($n = 2$, SK_C_6, I performed these experiments). (a) Representative measurement of Gaussia luciferase activity in the supernatant collected at the indicated times after transfection (mean of two technical replicates is shown, I performed this experiment). (b) Representative measurement of Gaussia luciferase activity in the supernatant collected at the indicated times after transfection of *in vitro* transcribed CHIKV replicon RNA in the presence or absence of DMSO, to test the effect of the vehicle on replication (mean of two technical replicates is shown, I performed this experiment). (c) Quantification of Gaussia luciferase activity relative to the control cells transfected with wt replicon and treated with DMSO at 24 hpt ($n = 2$, mean value \pm SD, two technical replicates were measured per n , I performed these experiments). (d) Cells were harvested at 24 hpt and whole cell lysates were immunoblotted with CHIKV nsP2-specific or GFP-specific antibodies (Eurogentec; Rockland), to control expression of the viral nsP2 and nsP3 compared to the loading control α -tubulin.

Because inhibition of ADP-ribosylation seems to be to imprecise, more specific complementation approaches were employed in the following. First, a prove-of-principle experiment was performed. Therefore, the proteolytically inactive CASA mutant replicon was complemented with plasmid encoded GFP-tagged nsP2-459-798. This fragment of nsP2 harbors the protease domain (**Figure 36**). For control, the GFP-tag alone and the inactive GFP-nsP2-459-798-CASA mutant were co-expressed. As expected, the CASA mutant replicon was replication defective in the presence of the GFP-tag alone. Co-expression of the active protease rescued replication of the CASA replicon, while GFP did not. This effect was dependent on protease activity, because the inactive GFP-nsP2-459-798-CASA construct did not increase luciferase activity (**Figure 36a,b**). Expression of the fusion proteins was controlled by immunoblotting of whole cell lysates (**Figure 36c**). Of note was that the GFP-tag alone was expressed at much higher levels than the protease fusion proteins. Therefore, they are depicted separately with different exposure times. Importantly, the expression levels of the protease domain and the CASA mutant were very similar and thus the effects on replication are comparable. The low expression levels of the protease domain might also explain why the replication could not be fully restored. In general, these experiments demonstrated that a mutant replicon can at least partially be rescued by co-expression of active protease.

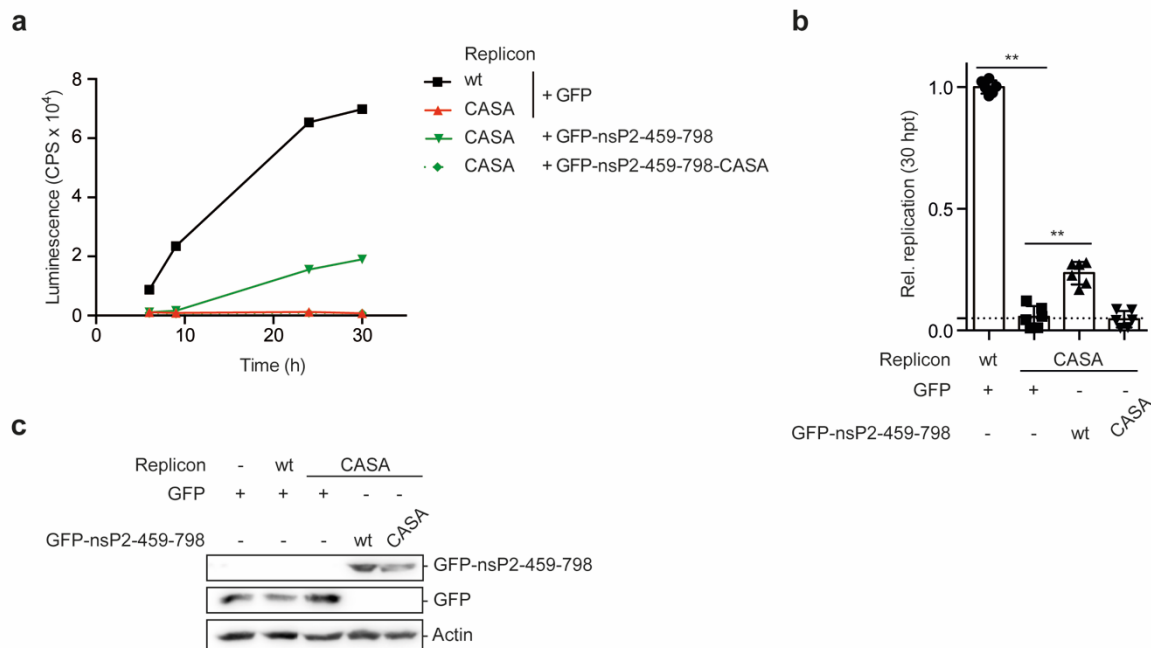


Figure 36: The proteolytically inactive CASA mutant of the CHIKV replicon can partially be rescued by addition of exogenous protease domain.

This figure is modified from Krieg et al. 2020. **(a-c)** HEK293 cells were transiently transfected with plasmids encoding GFP-tagged fusion proteins of nsP2-459-798 or CASA mutant or the GFP-tag alone. The deletion nsP2-459-798 comprises the C-terminal part of nsP2 and the protease domain. 24 h later, the cells were transfected with *in vitro* transcribed CHIKV replicon wt or CASA mutant RNA ($n = 3$, SK_D_3, I performed these experiments). **(a)** Representative measurement of Gaussia luciferase activity in the supernatant collected at the indicated times after transfection (mean of two technical replicates is shown, I performed this experiment). **(b)** Quantification of Gaussia luciferase activity relative to the control cells transfected with wt replicon and GFP-tag alone at 30 hpt ($n = 3$, mean value \pm SD, two technical replicates were measured per n , I performed these experiments). **(c)** Cells were harvested at 30 hpt and expression of the GFP-fusion proteins was checked by immunoblotting of whole cell lysates with GFP-specific antibodies (Rockland) compared to the loading control α -tubulin. $**p < 0.01$ when a two-tailed Mann-Whitney test was applied.

A similar experiment was performed for the V33E macrodomain mutant. HEK293 Flp-IN T-REx cells stably expressing TAP-tagged nsP3 full-length or isolated macrodomain were transfected with the V33E replicon. For control, cells only expressing the TAP-tag alone were used and the wt replicon was included as a reference (**Figure 37**). However, analysis of the Gaussia

luciferase activity revealed that expression of exogenous, active macrodomain did not rescue the V33E-dependent replication defect (**Figure 37a,b**), even though the fusion proteins were expressed (**Figure 37c**). To exclude that the TAP-tag renders the macrodomains inactive, we repeated the experiment with transiently transfected Flag-constructs that showed activity in cells before (**Figure 24**). But again, no rescue of replication was observed (data not shown). Furthermore, no effect on the amount of processed nsP2 or nsP3 could be detected (data not shown, SK_D_9). It is not clear, why active macrodomain was unable to rescue the effects of the V33E mutation within the replicon. Potentially, a rescue with exogenous protein is not possible for the macrodomain, because nsP3 localizes to distinct, dot-like foci in the cytoplasm and is partly responsible for inclusion or exclusion of proteins from these viral replication hubs (Gotte et al. 2018; Schulte et al. 2016; Fros et al. 2012). A possibility is that nsP3 when expressed from a plasmid does not localize to the same spots as replicon-based nsP3.

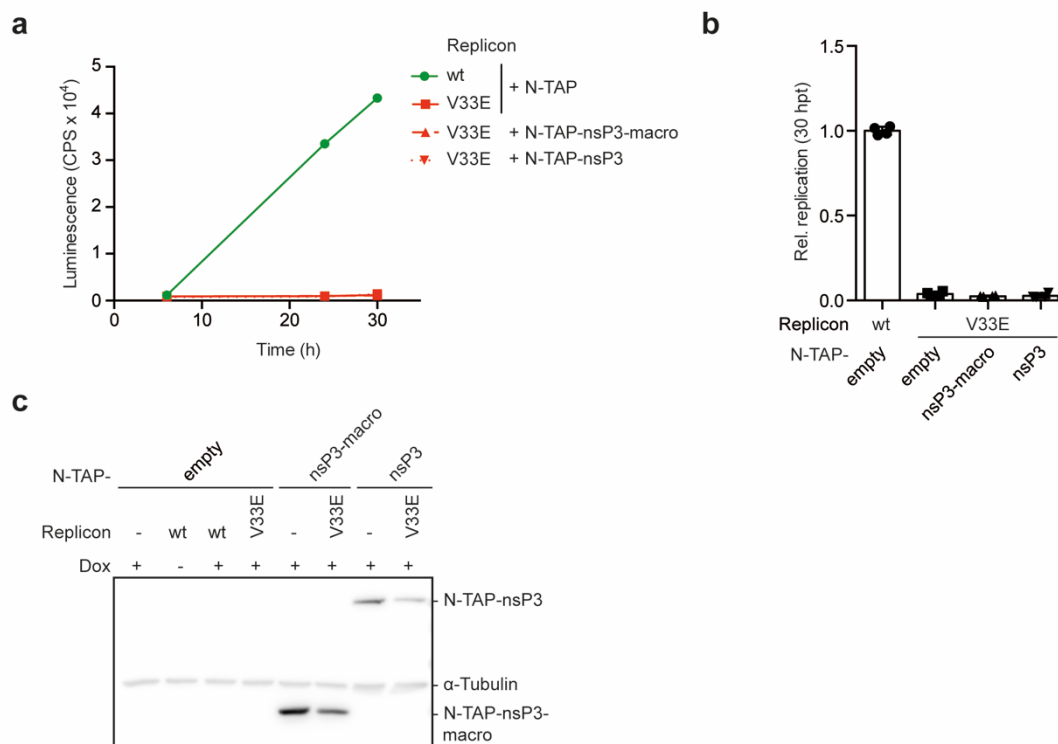


Figure 37: Addition of the exogenous CHIKV macrodomain or full-length nsP3 cannot rescue the CHIKV V33E mutant.

This figure is modified from Krieg et al. 2020. **(a-c)** HEK293 Flp-IN T-REx cells stably expressing N-TAP-nsP3, N-TAP-nsP3-macro or the TAP-tag alone as a control were transfected with *in vitro* transcribed CHIKV replicon wt or inactive macrodomain mutant (V33E) replicon RNA. (n = 2, SK_C_51, I performed these experiments) **(a)** Representative measurement of Gaussia luciferase activity in the supernatant collected at the indicated times after transfection (mean of two technical replicates is shown, I performed this experiment). **(b)** Quantification of Gaussia luciferase activity relative to the control N-TAP-cells transfected with wt replicon RNA at 30 hpt (n = 2, mean value ± SD, two technical replicates were measured per n, I performed these experiments). **(c)** Cells were harvested at 30 hpt and expression of the N-TAP-fusion proteins was checked by immunoblotting of whole cell lysates with anti-rabbit secondary antibodies compared to the loading control α -tubulin.

To circumvent the obstacle of targeting the DNA-encoded nsP3 to replication hubs, complementation of the V33E replicon was attempted with another replicon construct (**Figure 38**). To be able to observe effects on polyprotein processing, complementation was performed with the proteolytically inactive CASA mutant replicon that harbors a functional macrodomain. To increase sensitivity and allow differentiation between the two replicon constructs, for the V33E mutant the GFP-tagged ³EGFP replicon was used, while the CASA replicon was transfected as the untagged version. Indeed, the replication of mutant replicons, represented by Gaussia luciferase activity, was restored to about 80% upon co-transfection of the V33E and the CASA replicons (**Figure 38a,b**). However, evaluation of the luciferase activity

alone, does not allow to discriminate between replicons, as both constructs contain the Gaussia luciferase under the control of the subgenomic promoter. Therefore, the amount of processed, GFP-tagged nsP3 was assessed by immunoblotting. In line with the replication, the amount of processed nsP3-³EGFP was increased upon co-transfection of the CASA replicon, suggesting more polyprotein processing of the V33E replicon (**Figure 38c**). Because only the nsP3 derived from the V33E mutant replicon carries a GFP-tag, it can be assigned unambiguously to a rescue of the macrodomain mutant that is not due to proteolytic activity of the CASA replicon.

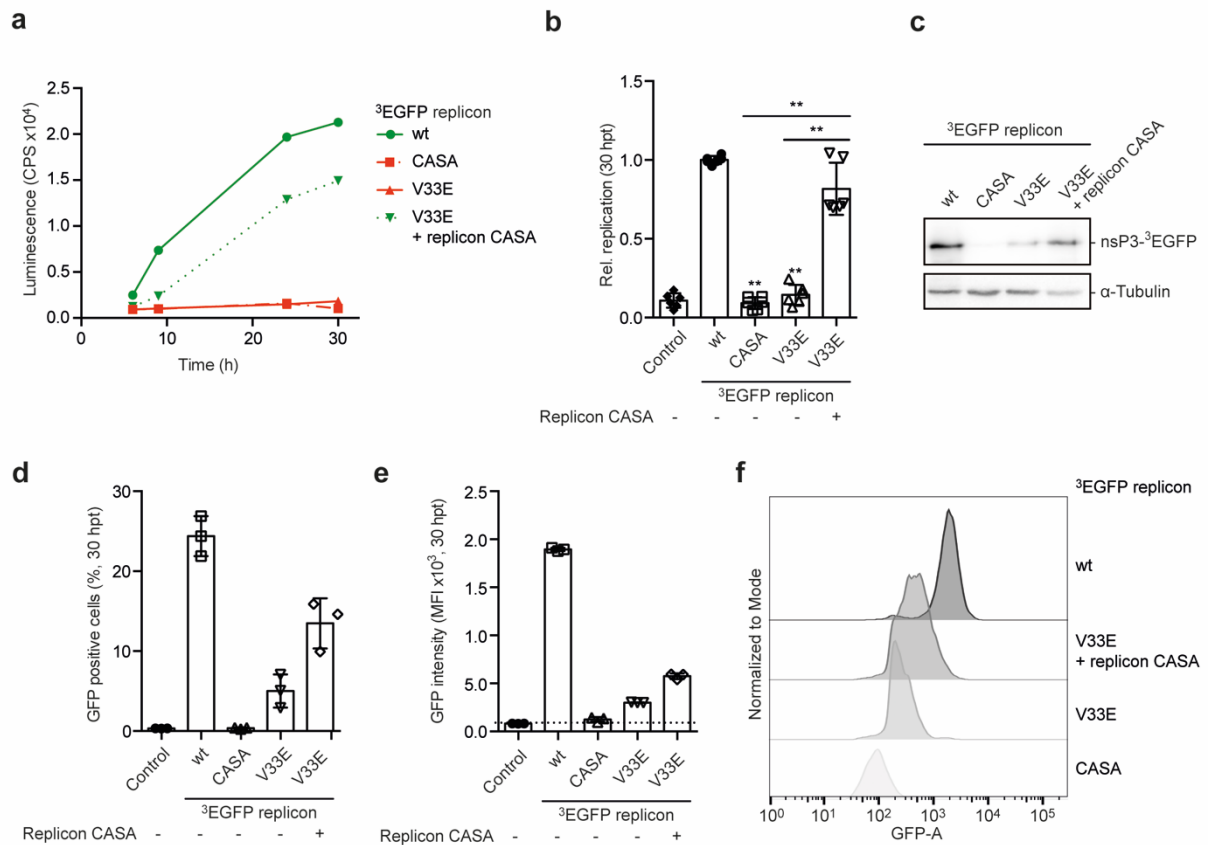


Figure 38: Co-transfection of the proteolytically inactive CASA replicon can partially rescue the replication and processing defect of the macrodomain inactive V33E replicon.

This figure is modified from Krieg et al. 2020. **(a-f)** HEK293 cells were transfected with *in vitro* transcribed ³EGFP replicon wt, CASA or V33E RNA or co-transfected with *in vitro* transcribed ³EGFP V33E and untagged CASA replicon RNA as indicated (n = 3, SK_D_11, I performed these experiments). **(a)** Representative measurement of Gaussia luciferase activity in the supernatant collected at the indicated times after transfection (mean of two technical replicates is shown, I performed this experiment). **(b)** Quantification of Gaussia luciferase activity relative to the control cells transfected with ³EGFP wt replicon RNA at 30 hpt (n = 3, mean value \pm SD, two technical replicates were measured per n, I performed these experiments). **(c)** Cells were harvested at 30 hpt and subjected to flow cytometry analysis (d-f). Subsequently the cells were lysed and whole cells lysates were immunoblotted with GFP-specific antibodies (Rockland) to check the amounts of processed nsP3-³EGFP compared to the loading control α -tubulin. **(d,e)** Thirty hpt the cells were subjected to flow cytometry analysis to determine the percentage of GFP positive cells **(d)** and their mean fluorescence intensity (MFI) **(e)**. **(f)** “Modal” representation of the GFP fluorescence intensity of the GFP positive cells **(d)**, scaling all samples to the maximum count. MFI, mean fluorescence intensity. ***p* < 0.01 when a two-tailed Mann-Whitney test was applied.

The immunoblotting is further corroborated by flow cytometry analysis of the cells, to further increase sensitivity of the GFP signal and to exclude effects from replication of the CASA replicon (**Figure 38d-f**). A gating strategy was established with control cells to be able to analyze only live, single cells using propidium iodide (PI) staining (**Figure 39**). The depicted gates were further used for all flow cytometry experiments containing these fluorescent labels. Furthermore, gating of GFP positive cells was set up with scatter plots of untransfected

control cells and untagged wt replicon transfected cells as negative control as well as GFP expressing cells as positive controls (**Figure 40**). These gates were likewise transferred to all other samples. Quantification of the percentage of GFP positive cells showed an increase after complementation with the CASA mutant (**Figure 38d**). Furthermore, within the GFP-positive cell population the mean fluorescence intensity (MFI) of the GFP signal was enhanced when both replicon variants were co-transfected, suggesting that the amount of nsP3-³EGFP per cell rose due to more processing (**Figure 38e,f**).

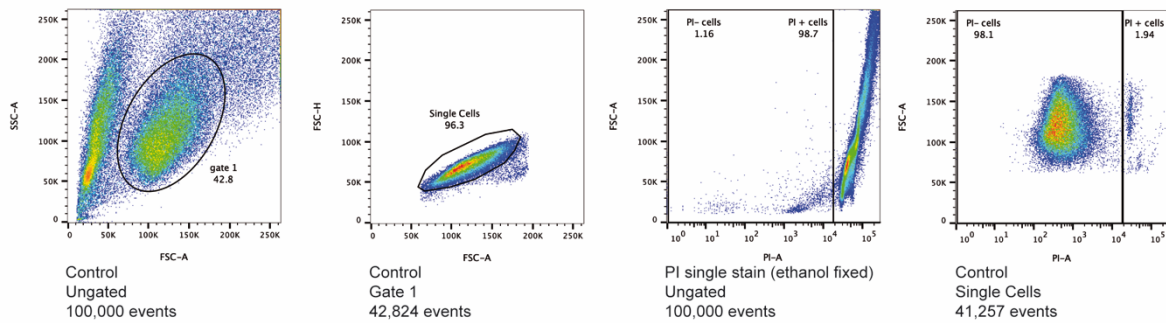


Figure 39: Representative gating strategy of control cells for the flow cytometry analysis of GFP-tagged CHIKV replicons.

This figure is modified from Krieg et al. 2020. First, the cell population was gated with SSC-A and FSC-A. Subsequently, single cells were gated with FSC-H and FSC-A. To determine the appropriate propidium iodide (PI) gate, control cells were fixed and permeabilized with ethanol. The corresponding PI gate was applied to non-fixed cells as well. The same gates were applied for all samples (SK_D_11, I performed this experiment). SSC, side scatter; FSC, forward scatter; A, area; H, height; PI, propidium iodide.

Like the summarized values from multiple experiments (**Figure 38d-f**), the single, representative scatter plots of the different CHIKV replicon constructs can be considered to visualize the GFP signal for individual cells and their distribution (**Figure 40**). Compared to the EGFP control, the ²EGFP and ³EGFP wt replicon showed a more defined population of GFP positive cells and the GFP intensity was overall more constant, with a clear separation from the GFP-negative cells. In general, the scatter plots of the flow cytometry analysis reflected the results of the immunoblots (**Figure 33c**). The protease deficient mutants did not show GFP positive cells. While the ²EGFP-V33E replicon was at the detection limit, the ³EGFP-V33E replicon displayed low but clearly detectable numbers of GFP positive cells. The intensity was lower than for the wt replicon transfected cells. Co-transfection of the untagged CASA replicon did not only increase the percentage and intensity of GFP positive cells, but the population also resembled the distribution of the wt replicon more closely (**Figure 40**).

Taken together, this complementation experiment demonstrates that the polyprotein itself was properly translated from the mutant replicons and that the hydrolase deficient V33E replicon could be rescued by a replicon with a functional macrodomain. Addition of a functional hydrolase increased processed nsP3 and thus further strengthened the hypothesis that the hydrolase function promotes nsP2 protease activity.

Even though the proteolytic activity of nsP2 was removed from the equation by the CASA mutation, the complementation using a complete replicon still contained three other nsPs in addition to nsP3 with many more catalytic activities and functions. This makes the system rather complex and difficult to molecularly assign the rescue to the hydrolytic function of the macrodomain. Hence, another system was employed to more specifically evaluate a macrodomain-mediated rescue of the V33E defect. To eliminate potential obstruction of targeting to the replication hubs, the macrodomain was fused to a GFP-specific nanobody (GFP-nanobody) that is supposed to be recruited to the GFP-tag of nsP3 encoded by the ³EGFP replicon. In this scenario the nanobody-macrodomain fusion protein should be located to the

replicon-encoded fusion proteins and might thus be able to substitute the hydrolase deficiency of the V33E mutant (**Figure 41**).

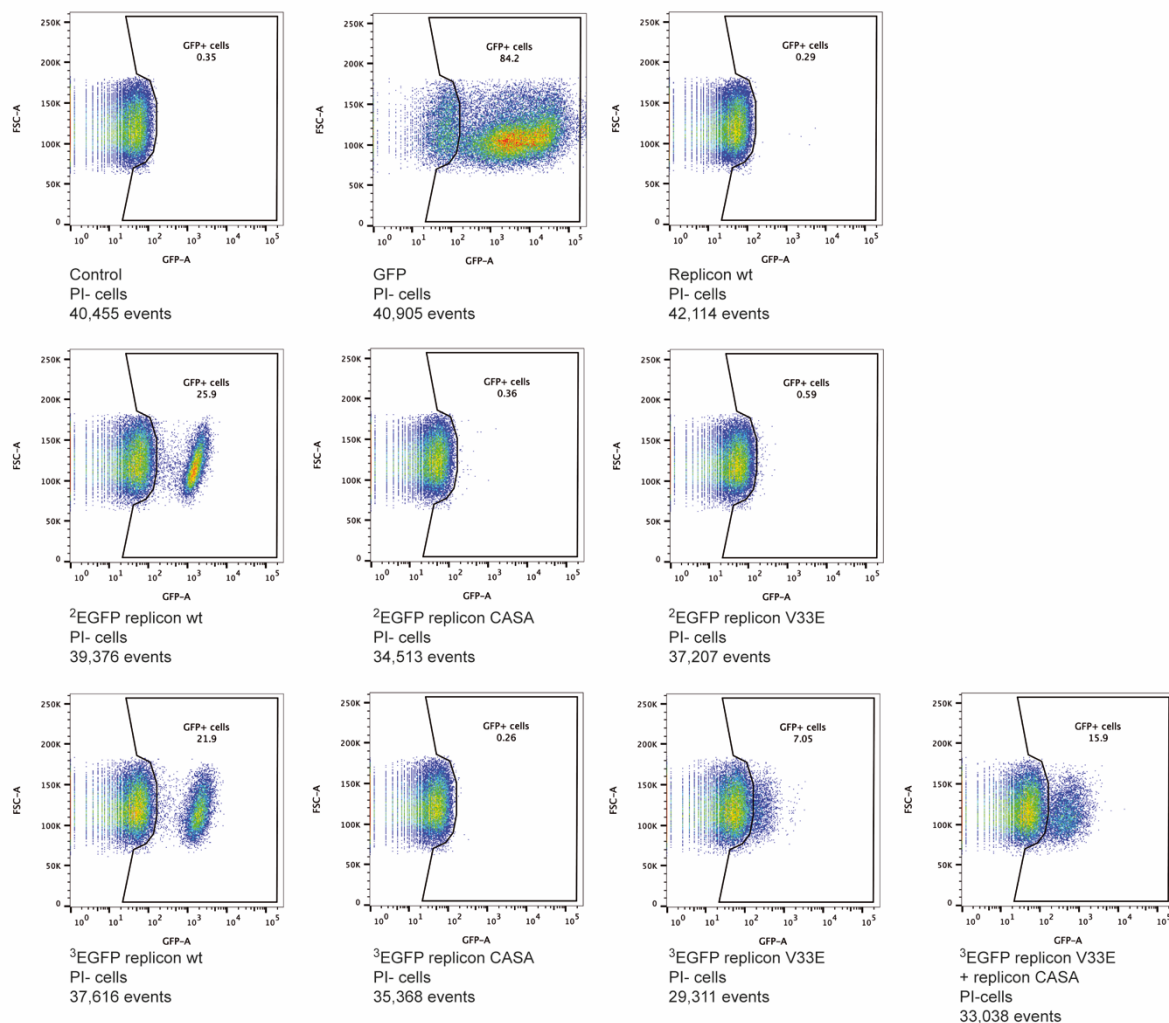


Figure 40: Representative scatter plots for gating GFP positive cells of ²EGFP and ³EGFP variants and co-transfection of the CASA replicon.

This figure is modified from Krieg et al. 2020. Cells were transfected with a plasmid encoding EGFP or *in vitro* transcribed replicon RNA variants as indicated. Thirty hpt the cells were analyzed by flow cytometry analysis. Within the population of live (PI-), single cells (**Figure 39**), the gates for GFP positive cells were set according to transfected control cells and cells transfected with a plasmid encoding GFP. This gate was applied to all other samples. Depicted is the percentage of GFP positive cells within this gate for each sample (SK_D_11, I performed this experiment).

Indeed, while the percentage of GFP positive cells remains unaffected, the intensity of GFP fluorescence was increased in the presence of active GFP-nanobody-nsP3-macro but not the inactive V33E mutant (**Figure 41a-c**). For the flow cytometry analysis the same gating strategy for live, single cells was employed as established previously (**Figure 39**), and the GFP positive cells were gated within this population (**Figure 42**). Because the percentage of GFP positive cells for the ³EGFP V33E replicon was so low, even lower than in previous experiments (**Figure 38 and 40**), it was difficult to see the difference in GFP intensity in the scatter plots. It was best visualized in mean fluorescence intensity (MFI) (**Figure 41b**) and the overlay of the GFP signal distributions (**Figure 41c**). Even though the amount of cells in the GFP positive populations and the intensity of the GFP signal was low, the effects are reproducible and especially the fact that they were exclusive for the catalytic activity of the GFP-nanobody fused macrodomain renders them unlikely to be artefacts.

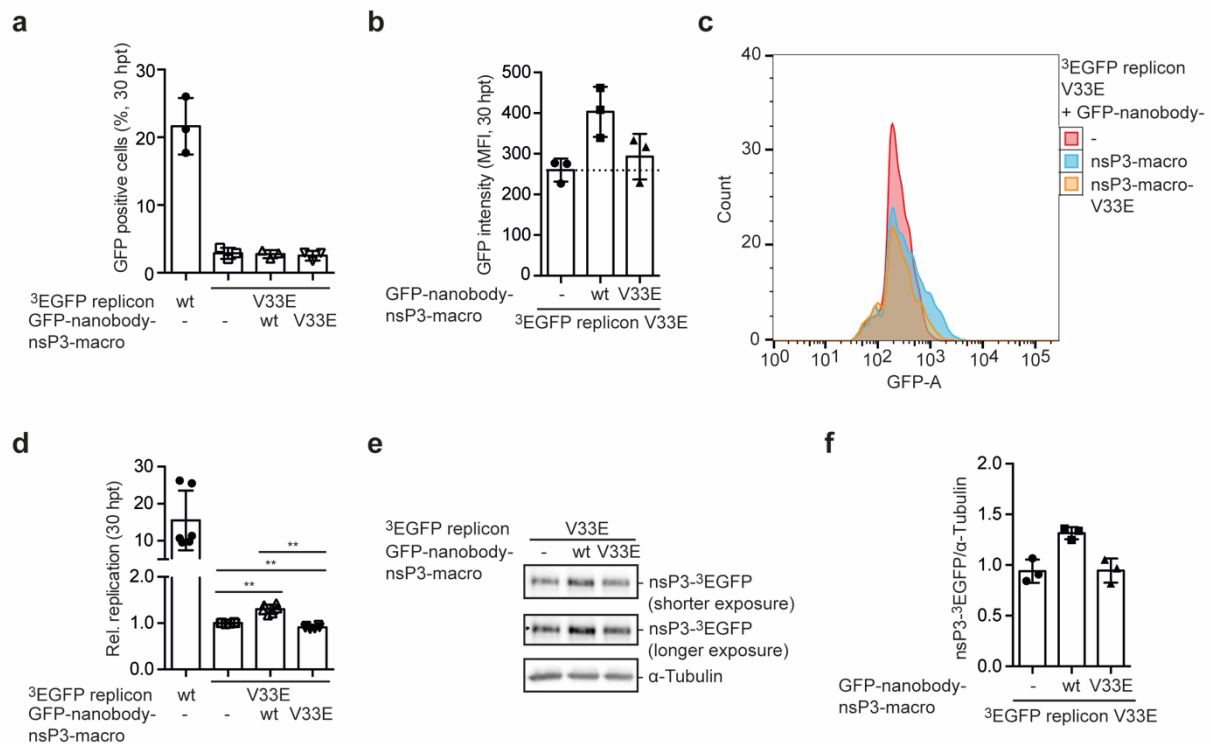


Figure 41: GFP-nanobody-mediated targeting of exogenous macrodomain to the ³EGFP V33E replicon can partially rescue its defect.

This figure is modified from Krieg et al. 2020. **(a-f)** HEK293 cells were transiently transfected with plasmids encoding for the GFP-nanobody-nsP3-macro, wt or inactive V33E mutant, as indicated. Twenty-four h later, the cells were transfected with *in vitro* transcribed ³EGFP replicon RNA, wt or V33E mutant ($n = 3$, SK_D_16, I performed these experiments). **(a,b)** Cells were subjected to flow cytometry analysis 30 hpt to determine the percentage of GFP positive cells **(a)** and their mean fluorescence intensity (MFI) **(b)**. **(c)** Representative visualization of the GFP fluorescence intensity of the GFP positive cells **(a)**. **(d)** Quantification of Gaussia luciferase activity relative to cells transfected with ³EGFP V33E replicon RNA at 30 hpt ($n = 3$, mean value \pm SD, two technical replicates were measured per n , I performed these experiments). **(e)** Subsequent to flow cytometry analysis the cells were lysed and whole cells lysates were immunoblotted with GFP-specific antibodies (Rockland) to check the amounts of processed nsP3-³EGFP compared to the loading control α -tubulin. **(f)** Quantification of processed GFP-tagged nsP3 by densitometry analysis in relation to the loading control α -tubulin ($n = 3$, mean \pm SD). ** $p < 0.01$ when a two-tailed Mann-Whitney test was applied.

In addition to the flow cytometry analysis, the replication of the samples was measured via luciferase activity. The relative replication corresponds to the MFI: compared to the V33E replicon alone, co-expression of the active nanobody-macrodomain increased the replication significantly while the inactive variant did not. Even though the gain in replication was significant, it was minor compared to the wt (**Figure 41d**). These findings were corroborated with immunoblot analysis of processed, GFP-tagged nsP3, which showed a quantifiable increase dependent on hydrolase activity (**Figure 41e,f**). These experiments support the notion that targeting of an active macrodomain can rescue effects on polyprotein processing as well as replication at least to some extent, potentially by eliminating effects of a protective layer of the viral replication hub.

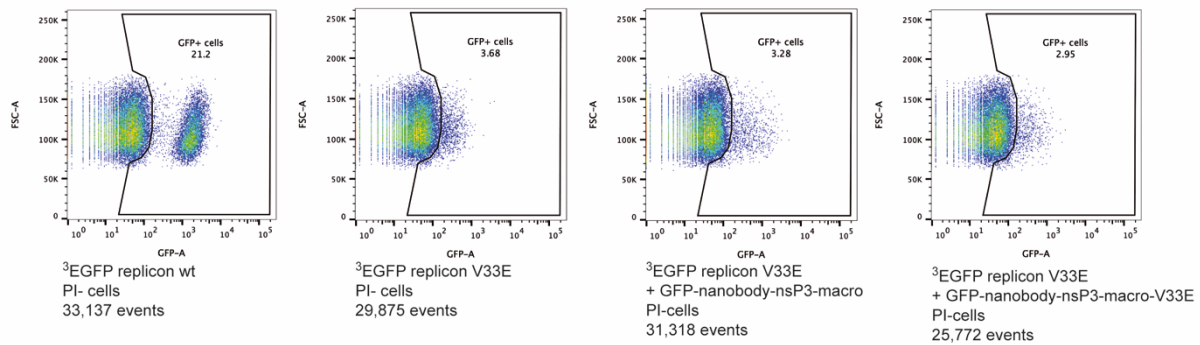


Figure 42: Representative scatter plots for gating GFP positive cells of ³EGFP V33E replicon complementation with the GFP-nanobody-nsP3 macro.

This figure is modified from Krieg et al. 2020. HEK293 cells were transiently transfected with plasmids encoding for the GFP-nanobody-nsP3-macro, wt or inactive V33E mutant, as indicated. Twenty-four h later, the cells were transfected with *in vitro* transcribed ³EGFP replicon RNA, wt or V33E mutant. The gate for GFP positive cells from **Figure 40** was applied within the population of live, single cells (**Figure 39**) of all samples. Depicted is the percentage of GFP positive cells within this gate for each sample (SK_D_16, I performed this experiment).

Although the targeting effects were most likely abolished by fusion of the nsP3 macrodomain to the GFP-nanobody, the rescue of replication and processing of the polyprotein of the V33E mutant was only partial. The same was the case for the rescue of the proteolytically inactive CASA replicon with exogenous nsP2 protease domain (**Figure 36**). Because nsP2 and nsP3 are described to inhibit host transcription and translation (Akhrymuk et al. 2018), the question arises whether these properties might complicate the interpretation of co-expression of replicons and these proteins. Therefore, the co-expression efficiency was assessed by flow cytometry and replication analyses (**Figure 43**). To do so, HEK293 cells were co-transfected with plasmid-encoded mCherry or mCherry-nsP2 or -nsP3 fusion proteins and *in vitro* transcribed ²EGFP or ³EGFP replicon RNA. EGFP alone was co-expressed from a plasmid as control. This allowed detection of the expression of the different proteins by their fluorescent tags in flow cytometry (**Figure 43a**). Because this experiment required the detection of mCherry, DAPI staining replaced PI staining for the gating of live cells. Hence, a different gating strategy was established (**Figure 44**). First, DAPI stained control cells were used to gate for live, single cells (**Figure 44a**). Afterwards, EGFP, mCherry and double positive cells were gated compared to DAPI stained untransfected, EGFP only and mCherry only transfected cells (**Figure 44b**). Samples containing only one dye were used for compensation. Evaluation of the fluorescent cells revealed that transfection of single plasmids led to a 70-80% transfection rate, while the replicon RNA alone transfected about 30% of the cells. Co-transfection of two plasmids resulted in a solid co-transfection (yellow) of around 50%. However, when replicon RNA was co-transfected with plasmids encoding mCherry or mCherry-nsP2 or -nsP3 fusion proteins, hardly any co-transfected cells were detectable and in general the amount of GFP positive, hence nsP-expressing cells, was decreased (**Figure 43a**). This marginal co-transfection and co-expression rate of replicons with plasmids might explain why the rescue experiments were only partially successful. If the exogenous protein is merely co-expressed with replicon derived proteins in 2-10% of the cells, a rescue effect can also only be expected in 2-10% of the cells. Yet, it is of note here, that this experiment was preformed once so far and the co-transfection took place simultaneously. Usually in rescue experiments the cells were transfected with plasmids or induced prior to transfection with replicon RNA; therefore, this experiment will have to be repeated and the effect of step-wise transfection needs to be assessed. Nonetheless, this suggests a drawback of inefficient co-transfection in complementation experiments and thus strengthens the relevance of a partial rescue in the performed assays.

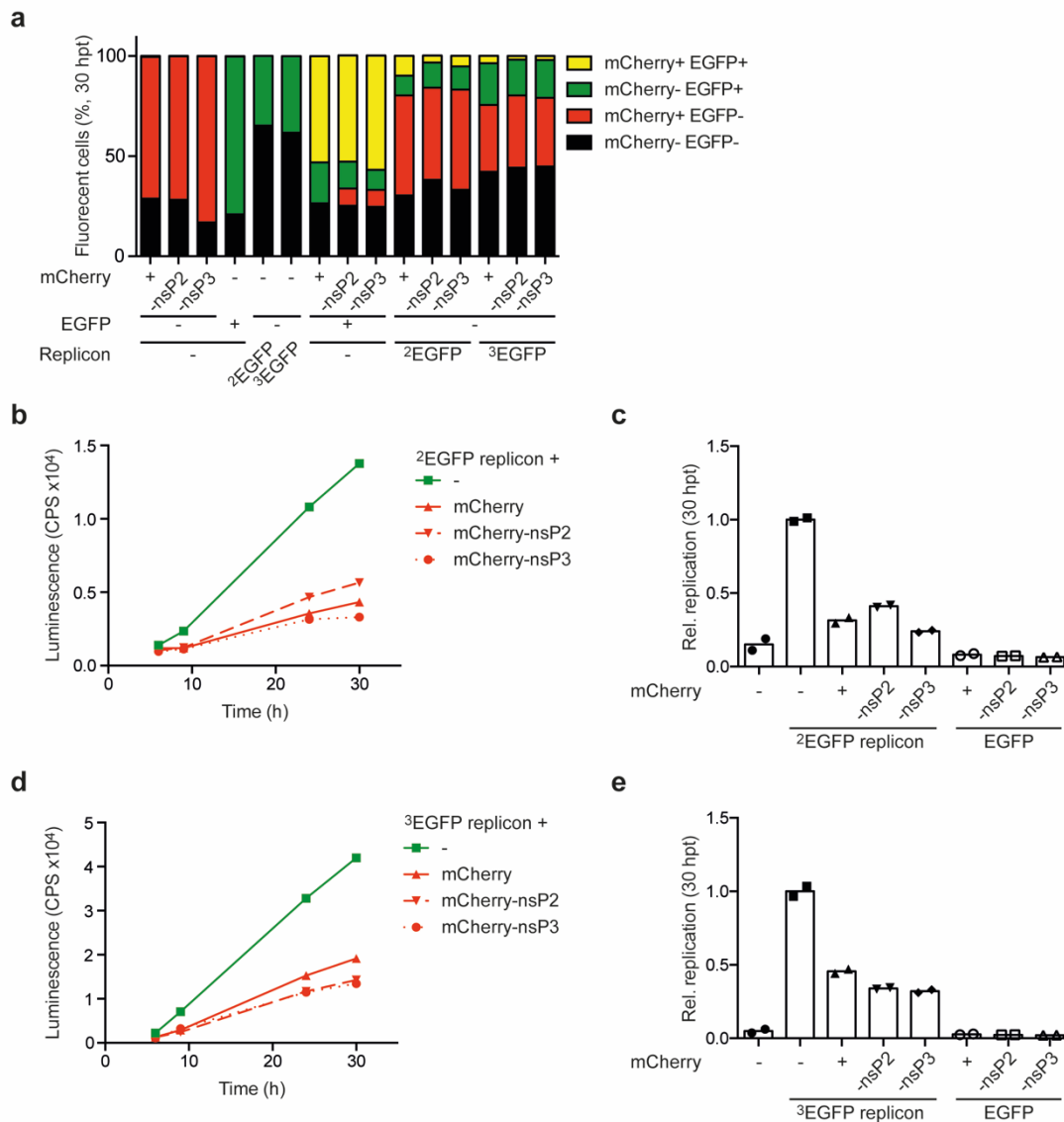


Figure 43: Co-expression of plasmids reduces expression of viral proteins and replication from replicon constructs.

(a-e) HEK293 cells were co-transfected with plasmids encoding EGFP, mCherry, mCherry-nsP2 or mCherry-nsP3 and *in vitro* transcribed ²EGFP or ³EGFP replicon RNA (n = 1, SK_D_18, I performed this experiment). (a) Thirty hpt the cells were subjected to flow cytometry analysis and the percentage of mCherry positive, GFP positive, double negative and double positive cells was determined. Gating was performed according to control and single transfected cells (Figure 44). The flow cytometry measurements were performed by me with support of Fabian Peiser. (b-e) Additionally to evaluation of the fluorescence, replication of the ²EGFP (b,c) and the ³EGFP (d,e) was measured by Gaussia luciferase activity in the supernatant. (b,d) Representative measurement of Gaussia luciferase activity of the ²EGFP (b) or the ³EGFP (d) replicon in the supernatant collected at the indicated times after transfection (mean of two technical replicates is shown, I performed this experiment). (c,e) Quantification of Gaussia luciferase activity of ²EGFP (c) or ³EGFP (e) replicon relative to cells transfected with replicon RNA only at 30 hpt (n = 1, mean value, two technical replicates were measured, I performed this experiment).

Because the amount of replicon expressing cells seemed to decrease upon co-transfection of plasmids, the luciferase activity was evaluated as well to determine potential effects on viral replication (Figure 43b-e). The results are depicted separately for the ²EGFP (Figure 43b,c) and the ³EGFP (Figure 43d,e) replicon for clarity purposes and because they exhibited different basal replication capacities. Still, both EGFP replicon variants showed strongly decreased replication when plasmids were co-expressed in line with the flow cytometry data. This again suggested that rescue experiments might not be straight forward and depended strongly on the setup. In general, it is possible though, because prior expression of some ARTDs did not affect viral replication (Figure 28 and 29).

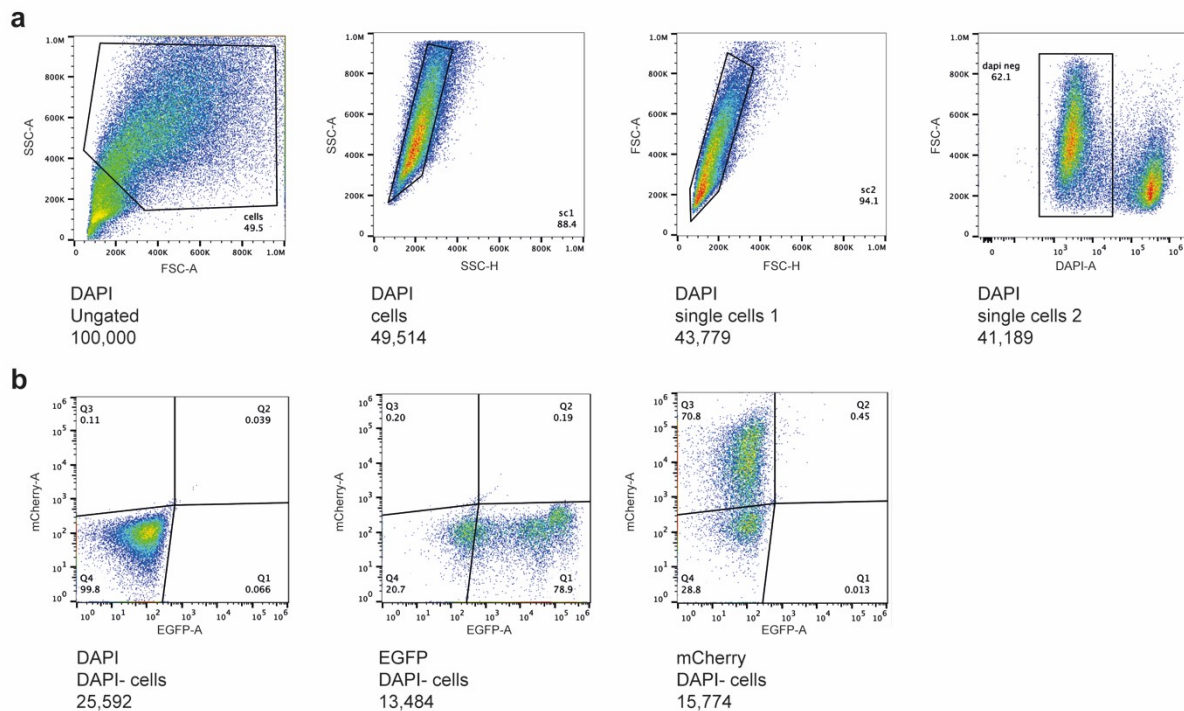


Figure 44: Representative scatter plots for gating EGFP, mCherry and double positive cells of co-expression experiment with plasmids and replicons.

(a) First, the cell population was gated with SSC-A and FSC-A. Subsequently, single cells were gated with SSC-A and SSC-H and thereafter with FSC-A and FSC-H. Live cells were gated with the help of DAPI staining, in which live cells were DAPI negative. Fluorescent signals were compensated with the help of DAPI, EGFP and mCherry single samples. **(b)** EGFP, mCherry and double positive cells were gated compared to DAPI stained untransfected, EGFP only and mCherry only samples. The same gates were applied for all samples (**Figure 43**, SK_D_18, I performed this experiment). Depicted is the percentage of cells in each gate. DAPI, 4',6-diamidino-2-phenylindole.

Taken together, the V33E macrodomain mutant replicon constructs showed less processed nsPs compared to the wt in several setups and this effect was partially reversible by co-expression of functional macrodomain (**Figure 32, 33, 38 and 41**). A complementary result was observed by overexpression of catalytically active ARTD10 and ARTD12 (**Figure 31**). One explanation for a reduced amount of processed nsPs is a MARYlation-mediated defect of auto-catalytic polyprotein processing resulting from a lack of viral hydrolase activity. However, there is also another hypothesis. When an intact, functional replication complex is formed from partially processed nsP1-3 and nsP4 new viral (-)ssRNA is made. Subsequently, viral replication complex generates new full-length (+)ssRNA as well as subgenomic RNA (**Figure 11**) (Rupp et al. 2015). This newly synthesized genomic RNA is used as a template for further rounds of ns polyprotein translation followed by cleavage. This results in more processed nsPs. Hence, a defect in replication of the viral genome would also lead to a decrease in processed viral proteins.

To explore this line of explanation, a new replicon construct was established (**Figure 45**). The GAA mutation was introduced into the ²EGFP replicon. In this mutant D466 and D467 of nsP4 were both mutated to alanines rendering the viral RNA-dependent RNA polymerase (RdRp) inactive (Utt et al. 2016). The G465 was not mutated, however as this mutant is commonly referred to as the GAA mutant, this nomenclature was adopted. These mutations prevent synthesis of new full-length genomic RNA and restrict translation to the initially transfected, *in vitro* transcribed RNA as a template. In addition to the GAA mutation, the V33E macrodomain and the CASA protease mutants were introduced as well (**Figure 45**). Hence, effects of genome replication are eliminated and the amount of processed nsPs can be assessed from comparable amount of template that was transfected.

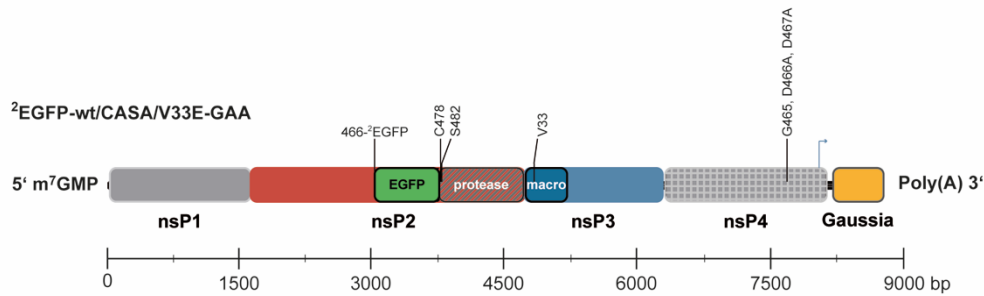


Figure 45: Schematic representation of CHIKV replicon GAA constructs used in the following experiments.

The scale bar indicates the length of the RNA-based replicons in base pairs (bp). This figure was modified from **Figure 25**, created by Patricia Korn, née Verheugd. This figure is adapted from Krieg et al. 2020.

The GAA constructs were subsequently used to transfect HEK293 cells. The ²EGFP wt and V33E mutant were used for comparison. This setup was analyzed to be able to distinguish between polyprotein processing and genome replication effects (**Figure 46**). To determine polyprotein processing of the individual constructs the cells were subjected to flow cytometry analysis 30 hpt (**Figure 46a-c**). The gating was performed as described previously (**Figure 39**). In line with previous flow cytometry experiments (**Figure 40**), the ²EGFP replicon transfected about 30% of cells while the ²EGFP V33E replicon only led to around 1% of GFP positive cells. Looking at the introduction of the GAA mutant, the fraction of GFP positive cells was even further decreased and interestingly, the ²EGFP-CASA-GAA and -V33E-GAA double mutants showed even less GFP positive cells (**Figure 46a**). Analysis of the mean fluorescence intensity (MFI) of the GFP positive cells showed a similar pattern: the V33E single mutation possessed the highest MFI, the GAA mutation had a lower average GFP signal and this was even further decreased by introduction of the V33E or the CASA mutations into the GAA background (**Figure 46b**). The difference between the GAA replicon and the V33E-GAA and CASA-GAA replicons was further observable when the GFP intensity of the GFP positive cells was visualized as a distribution instead of a mean value (**Figure 46c**). In this representation the peaks of the double mutants superposed with the control cells, while the ²EGFP-GAA replicon showed a higher peak that was shifted to higher intensity of the GFP signal. The fact that the GFP percentage as well as the intensity of the signal was further decreased by introduction of the V33E mutant to the GAA replicon demonstrated that the defect resulting from a lack of viral hydrolase activity took place prior and additional to the impact of genome replication on the amount of processed nsPs. As expected, inactivation of the RdRp abolished viral replication measured by Gaussia luciferase activity, which was comparable to the V33E mutant (**Figure 46d**), but still differences were measurable in the amount of GFP detected by flow cytometry. To strengthen the conclusion from the flow cytometry, the analysis was corroborated by immunoblotting of whole cell lysates with GFP-specific antibodies to visualize the processed nsP2-²EGFP (**Figure 46e**). Whereas there was a strong protein band visible for the wt, only faint nsP2 signals were detected for the V33E and the GAA replicons. However, no nsP2 was detected upon the transfection of the ²EGFP-CASA-GAA or ²EGFP-V33E-GAA replicons. These findings validated the flow cytometry results. Consequently, hydrolase deficiency decreased the amount of processed nsPs independent of genome amplification, comparable to the protease inactive CASA mutant. This suggested that MARYlation indeed controls polyprotein processing.

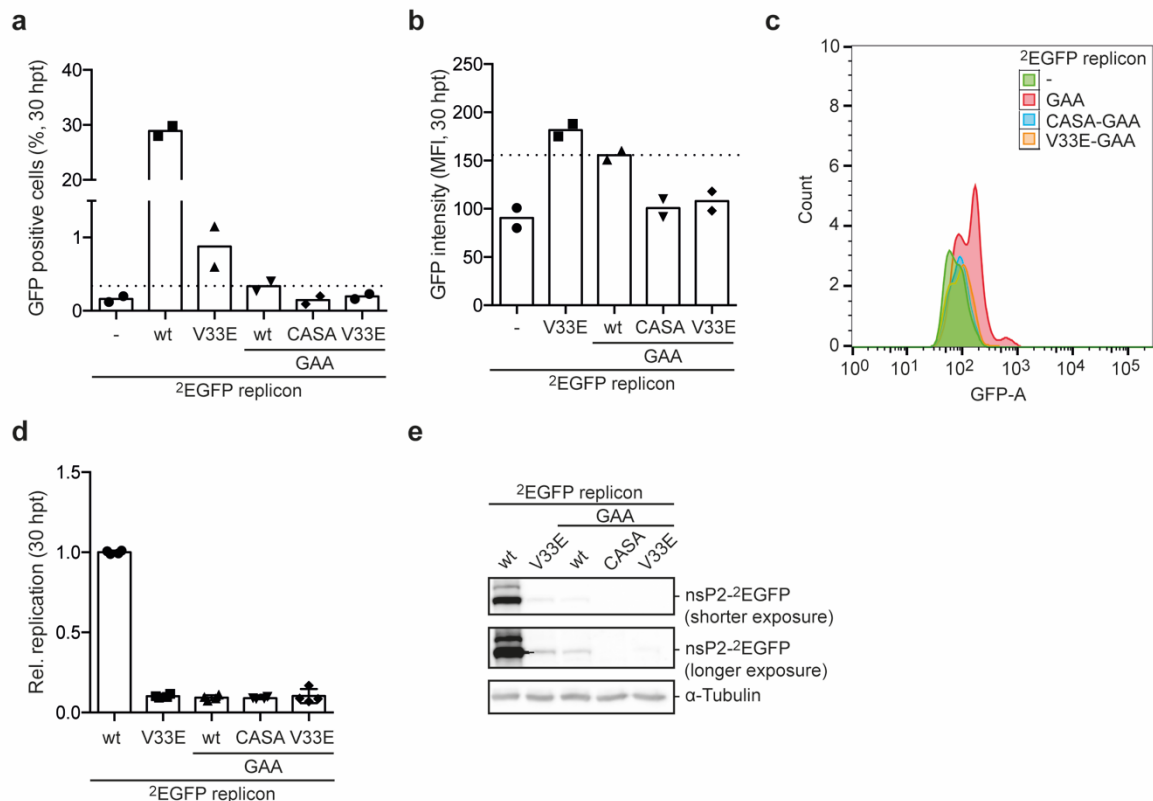


Figure 46: Introduction of the V33E macrodomain mutant into the GAA replicon construct further decreases the amount of processed nsP3.

(a-e) HEK293 cells were transfected with *in vitro* transcribed RNA of ²EGFP replicon variants as indicated (n = 2, SK_D_17, I performed these experiments). (a-c) Thirty hpt cells were subjected to flow cytometry analysis to determine the percentage of GFP positive cells (a) and the mean fluorescence intensity (MFI) within the population of GFP positive cells (b). (c) Representative visualization of the GFP fluorescence intensity of the GFP positive cells (a). (d) Quantification of Gaussia luciferase activity relative to cells transfected with ²EGFP replicon RNA at 30 hpt (n = 2, mean value \pm SD, two technical replicates were measured per n, I performed these experiments). (e) Subsequent to flow cytometry analysis the cells were lysed and whole cells lysates were immunoblotted with GFP-specific antibodies (Rockland) to check the amounts of processed nsP2-2EGFP compared to the loading control α -tubulin.

While the number of GFP positive cells that was very low in these experiments, the fact that the results were reproducible with two different methods, flow cytometry and immunoblotting, as well as in two independent experiments argues for their reliability. Nonetheless, further validation of the conclusion might be obtained by employing a trans-replication system (Utt et al. 2016). In this system the polyprotein is expressed from a plasmid under the control of a cytomegalovirus (CMV) promoter. This should result in more robust expression of the polyprotein. The replication can be measured by co-expression of a second construct with Firefly luciferase under control of the CHIKV 5' UTR and Gaussia luciferase and/or mCherry under the control of the subgenomic promoter. This allows distinguishing between transcription of the full-length and the subgenomic RNA. Introduction of the hydrolase-deficient V33E mutant in this system, potentially in addition to the GAA mutation, would allow to verify a polyprotein processing defect instead of erroneous genome replication with potentially stronger signals for the processed proteins and more cells to evaluate. Furthermore, an increased expression from the CMV promoter-based plasmid might allow visualization of the full-length polyprotein that failed so far and that should be more abundant in the V33E and CASA mutants compared to the wt.

2.2.3 CHIKV nsP2 is a substrate of mono-ADP-ribosylation *in vitro* and in cells

It has been reported before, e.g. for the kinase GSK3 β , that modification of proteins with MAR may have allosteric effects on their catalytic activity (Feijs et al. 2013b). Because MARylation seems to influence auto-catalytic polyprotein processing of CHIKV, the hypothesis arose that nsP2 might be a substrate of MARylation by the interferon-inducible mono-ARTDs and that this modification is reversed by the macrodomain.

To test this hypothesis, recombinant nsP2 as well as nsP2-459-798 truncation, which contains the protease domain, were subjected to *in vitro* ADP-ribosylation assays with ARTD10 (**Figure 47**). The bacterially expressed, isolated catalytic domain of ARTD10 modified nsP2 as well as the protease domain. No MARylation was observed in the presence of ARTD10-GW. Especially compared to previously described substrates of mono-ADP-ribosylation the modification was quite strong. Furthermore, co-incubation with either the isolated macrodomain or full-length nsP3 antagonized the MARylation of nsP2. Interestingly, the full-length nsP3 revealed a slight bias towards de-modifying nsP2 compared to GST-ARTD10cat (**Figure 47a**). Because the isolated catalytic domain of ARTD10 might lack specificity in *in vitro* assays, the experiments were corroborated with full-length ARTD10. To do so, HA-ARTD10, wt or GW, was transiently expressed in HEK293 cells and immunoprecipitated prior to *in vitro* ADP-ribosylation assays. Analogous to the catalytic domain, full-length ARTD10 strongly MARylated nsP2 and the protease domain, while the GW mutant did not. Moreover, this modification was efficiently removed by addition of the viral nsP3 hydrolase. In these experiments, comparison to the previously described substrate NEMO (Verheugd et al. 2013) emphasized the intensity of modification of the viral proteins (**Figure 47b**).

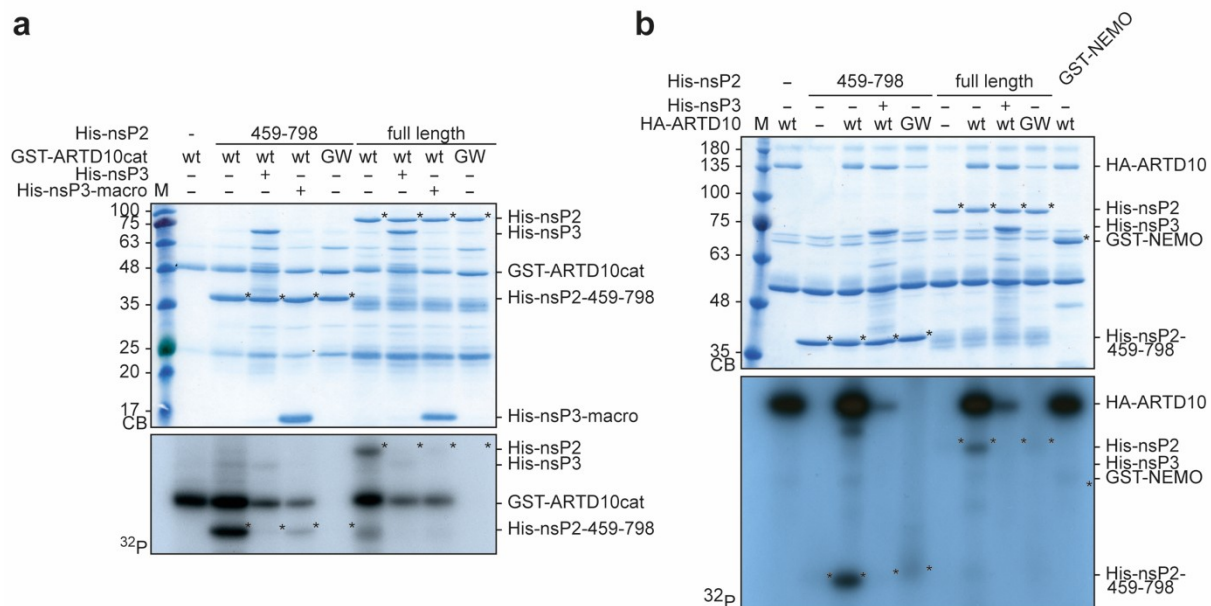


Figure 47: NsP2 is a substrate of ARTD10-mediated MARylation *in vitro* that can be reversed by the nsP3 macrodomain. This figure is modified from Krieg et al. 2020. **(a)** Bacterially expressed, His₆-tagged full-length nsP2 or the nsP2-459-798 C-terminal deletion containing the protease domain were incubated with GST-ARTD10cat, wt or inactive GW mutant, as indicated in the presence of radioactively labelled ³²P-NAD⁺ for 30 min at 30°C to allow auto- as well as substrate-modification. Furthermore, bacterially expressed, His₆-tagged full-length nsP3 or the isolated macrodomain were co-incubated as indicated (n = 2, SK_C_3, I performed these experiments). **(b)** HEK293 cells were transiently transfected with plasmids encoding HA-ARTD10 wt or GW mutant. Forty-eight h later, the cells were lysed in TAP lysis buffer and HA-ARTD10 was immunoprecipitated using an anti-HA-antibody (Covance). Subsequently, HA-ARTD10 incubated in the presence radioactively labelled ³²P-NAD⁺ and full-length or truncated His-nsP2 as a substrate for 30 min at 30°C to allow auto- as well as substrate-modification. Furthermore, bacterially expressed, His₆-tagged full-length nsP3 or the isolated macrodomain were co-incubated as indicated. Total proteins were stained with Coomassie blue (CB) and the incorporated label was analyzed by autoradiography (³²P) (n = 2, SK_C_3, I performed these experiments).

In addition to ARTD10, other mono-ARTDs are also regulated by interferon upon viral infection. These include ARTD7, ARTD8 and ARTD12 (Ecke et al. 2017; Krieg et al. 2020), which also showed effects on CHIKV replication (**Figure 27 and 28**). Interferon-independent ARTDs on the other hand, did not restrict the replicon (**Figure 29**). Hence, the question came up whether other ARTD family members were likewise able to transfer ADPr onto nsP2. To test this, catalytic domains of ARTD7, ARTD8 and ARTD12 were included in *in vitro* ADP-ribosylation assays with nsP2-459-798 and nsP2 as substrates (**Figure 48**). Furthermore, His-ARTD15cat was included as a transferase where expression is not triggered by interferon (Krieg et al. 2020). The variable intrinsic activities of the individual ARTD catalytic domains required different exposure times of the autoradiograms for visualization. While ARTD10 and ARTD7 showed rather robust auto-modification, ARTD8, ARTD12 and ARTD15 were less active. Nonetheless all transferases included in the experiment auto-modified and could thus be evaluated for their ability to MARylate nsP2. Indeed, in line with the replication experiments, all interferon-inducible ARTDs modified nsP2 *in vitro*, while ARTD15 did not. Even though the activity of ARTD15 was weak, its auto-modification was comparable to ARTD12, which MARylated nsP2 to a detectable level. Therefore, nsP2 can be dismissed as a substrate of ARTD15. Interestingly, even though only isolated catalytic domains were employed in the assays, they still depicted distinct specificities towards nsP2. Whereas ARTD10 and ARTD12 modified nsP2 and nsP2-459-798 to an equal extent, ARTD7 seemed to prefer the full-length protein as substrate. In contrast, ARTD8 modified the truncation stronger, strikingly even to a higher amount than itself (**Figure 48**). This suggests substrate specificity of the different catalytic domains. In the past, this has been questioned, but apparently the highly conserved PARP domains are to some extent intrinsically restraint to certain substrates, amino acids or consensus sequences.

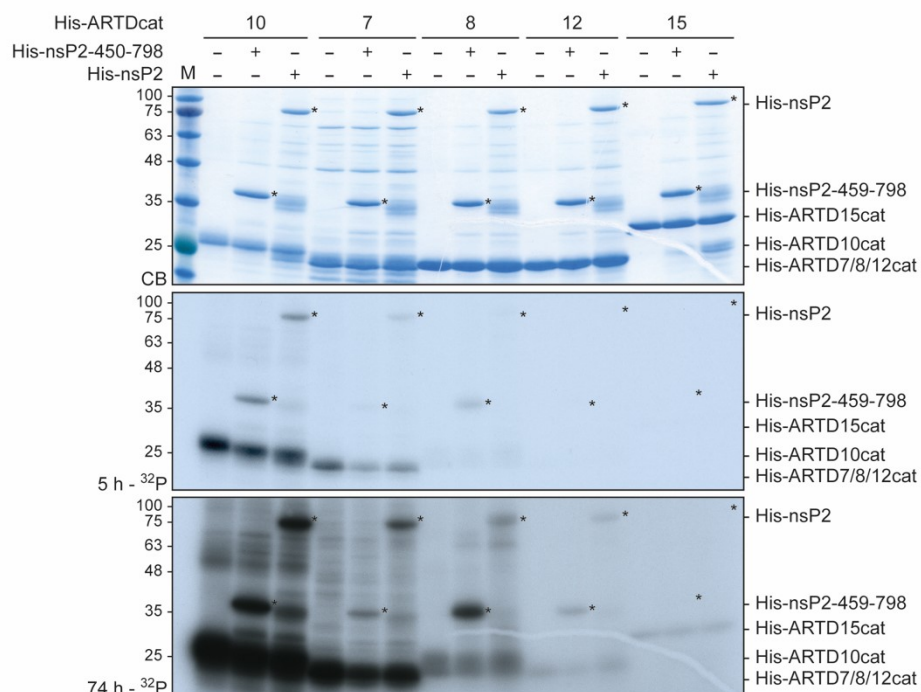


Figure 48: Interferon-inducible mono-ARTDs MARylate nsP2 *in vitro*.

This figure is modified from Krieg et al. 2020. Bacterially expressed, His₆-tagged full-length nsP2 or the nsP2-459-798 C-terminal deletion containing the protease domain were incubated with the bacterially expressed, His₆-tagged catalytic domains of interferon-regulated ARTD10, ARTD7, ARTD8 and ARTD12 or the interferon-independent ARTD15 as indicated. The reactions took place in the presence of radioactively labelled ³²P-NAD⁺ at 30°C for 30 min. Total proteins were stained with Coomassie blue (CB) and the incorporated label was analyzed by autoradiography (³²P) (n = 2, SK_C_3, I performed these experiments).

Although the ADP-ribosylation assays displayed a certain level of specificity, the MARylation of nsP2 might still be an artefact of the synthetic nature of *in vitro* studies. While these enforce proximity of the proteins involved in the assay, in cells a modification might not take place due to for instance different localization of the components. Therefore, it needs to be demonstrated that nsP2 is MARylated in cells. Two approaches were used to do so (**Figure 49**). The ²EGFP replicon was transfected into cells to be able to immunoprecipitate replicon-derived nsP2 via GFP-Trap. To detect MARylation of nsP2, the GFP-Trap was immunoblotted with a MAR-binding-reagent. This reagent is based on bacterially expressed Macro2-3 of human ARTD8 fused to a rabbit Fc tag (Gibson et al. 2017). Because, in contrast to the murine Artd8-macro2-3, the human macrodomains of ARTD8 were described to partially interact independent of MARylation though (Butepage et al. 2018a), treatment with recombinant nsP3 macrodomain was included (**Figure 47**). The MAR-binding-reagent showed a signal for the replicon derived nsP2 that was removed by incubation with the macrodomain while the amounts of total nsP2 were comparable (**Figure 49a**). This indicated that nsP2 was MARylated in cells under replicon conditions. In addition, DNA-encoded, plasmid-derived GFP-nsP2 was transiently expressed in HEK293 cells and subsequent to GFP-Trap immunoblotted with the MAR-binding reagent. Interestingly, GFP-nsP2 MARylation was increased upon co-transfection of the replicon V33E RNA, containing the hydrolase-deficient macrodomain mutant (**Figure 49b**). This finding suggested that viral infection conditions were essential to trigger modification of nsP2 by mono-ARTDs. The replicon might induce interferon signaling and thus expression of mono-ARTDs. Additionally, the localization to replication hubs and association of nsP2 with viral RNA might be necessary to target ARTD-mediated MARylation. The fact that several ARTDs, including ARTD10, possess potential RNA recognition motives (RRM) strengthens this hypothesis. It was demonstrated for ARTD10 that the RRM is essential for targeting to characteristic cytoplasmic foci (Kleine et al. 2012). It is possible that the viral RNA is recognized by the RRM of ARTD10 and likewise modulates targeting.

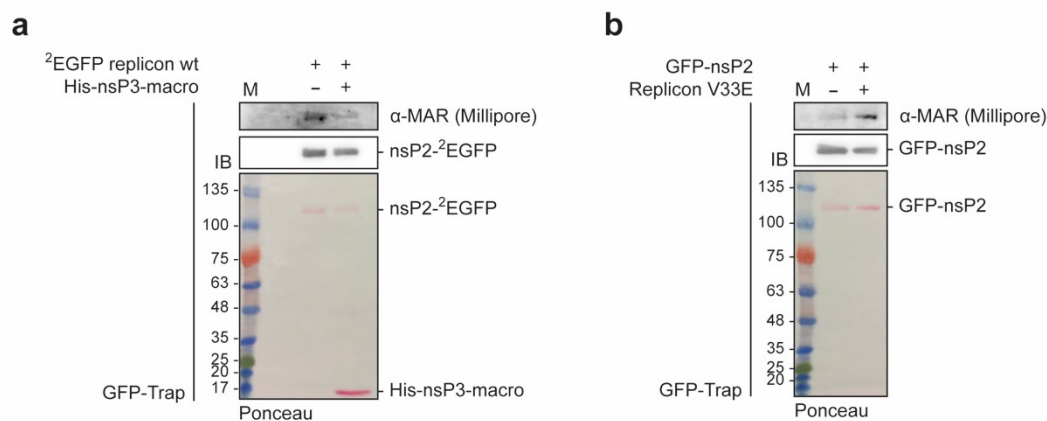


Figure 49: NsP2 is a substrate of MARylation in cells.

This figure is modified from Krieg et al. 2020. **(a)** HEK293 cells were transfected with *in vitro* transcribed ²EGFP replicon RNA. Thirty hpt the cells were lysed and nsP2-²EGFP was immunoprecipitated using GFP-Trap (Chromotek). Subsequently, the GFP-Traps were incubated in the presence or absence of recombinant His-nsP3-macro as indicated at 30°C for 30 min. The samples were subjected to immunoblotting and MARylation was detected with a MAR-binding-reagent (Millipore) while the total amount of nsP2-²EGFP was visualized with GFP-specific antibodies (Rockland). Additionally, all total proteins were visualized with Ponceau staining (n = 1, SK_D_12, I performed this experiment). **(b)** HEK293 cells were transiently transfected with plasmids encoding GFP-nsP2 fusion protein. Twenty-four h later, the cells were co-transfected with *in vitro* transcribed replicon V33E RNA, the hydrolase deficient variant. Thirty hpt the cells were lysed and GFP-nsP2 was immunoprecipitated using GFP-Trap (Chromotek). Subsequently, the GFP-Traps were subjected to immunoblotting and MARylation was detected with a MAR-binding-reagent (Millipore) while the total amount of GFP-nsP2 was visualized with GFP-specific antibodies (Rockland) and Ponceau staining (n = 1, SK_D_12, I performed this experiment).

To further support intracellular MARYlation of nsP2, the co-localization of ARTD10 and replicon-derived nsP2-²EGFP was studied by immunofluorescence confocal microscopy in ARTD10 HeLa cells (Herzog et al. 2013)(**Figure 50**). The untagged ARTD10 was stained with ARTD10-specific antibodies and secondary antibodies coupled to Alexa555. In the classic confocal images, taken with the LSM 710, ARTD10 was exclusively detectable upon doxycycline induction and appeared in cytoplasmic foci as described before (Kleine et al. 2012)(**Figure 50a**). The ²EGFP replicon showed a diffuse cytoplasmic and nuclear distribution, foci in the cytoplasm, nucleolar accumulation and accumulation around the nuclear envelop, possibly the ER, and the cytoplasmic membrane (**Figure 50a**). These various localizations might account for different stages of polyprotein processing and association with different cellular proteins. NsP2 is described to associate with the cytoplasmic replication hubs as well as for instance Rbp1, a subunit of RNA polymerase II complex, in the nucleus (Akhrymuk et al. 2012; Utt et al. 2015; Goertz et al. 2018). ARTD10 partially co-localized with nsP2-²EGFP (**Figure 50a**). The classical confocal microscopy was corroborated with Airyscan processed images using an LSM 980 confocal microscope that has a higher resolution (**Figure 50b**). In these pictures the structure of the ARTD10 and the nsP2-²EGFP foci became more pronounced and the co-localization was more distinct. Profiling of the fluorescent intensities in a merged image of EGFP and the Alexa555 fluorophore along an axis (**Figure 50b**), further showed overlapping peaks of ARTD10 and nsP2 indicating co-localization (**Figure 50c**). Of note, the fluorescent intensity of the ARTD10 staining was much weaker than the GFP signal, therefore different y-axes were used for the graph. In addition, evaluation of the Gaussia luciferase activity in the supernatant revealed, that catalytically active ARTD10 inhibits CHIKV replication in HeLa cells, comparable to HEK293 cells, while the inactive GW mutant does not (**Figure 50d**).

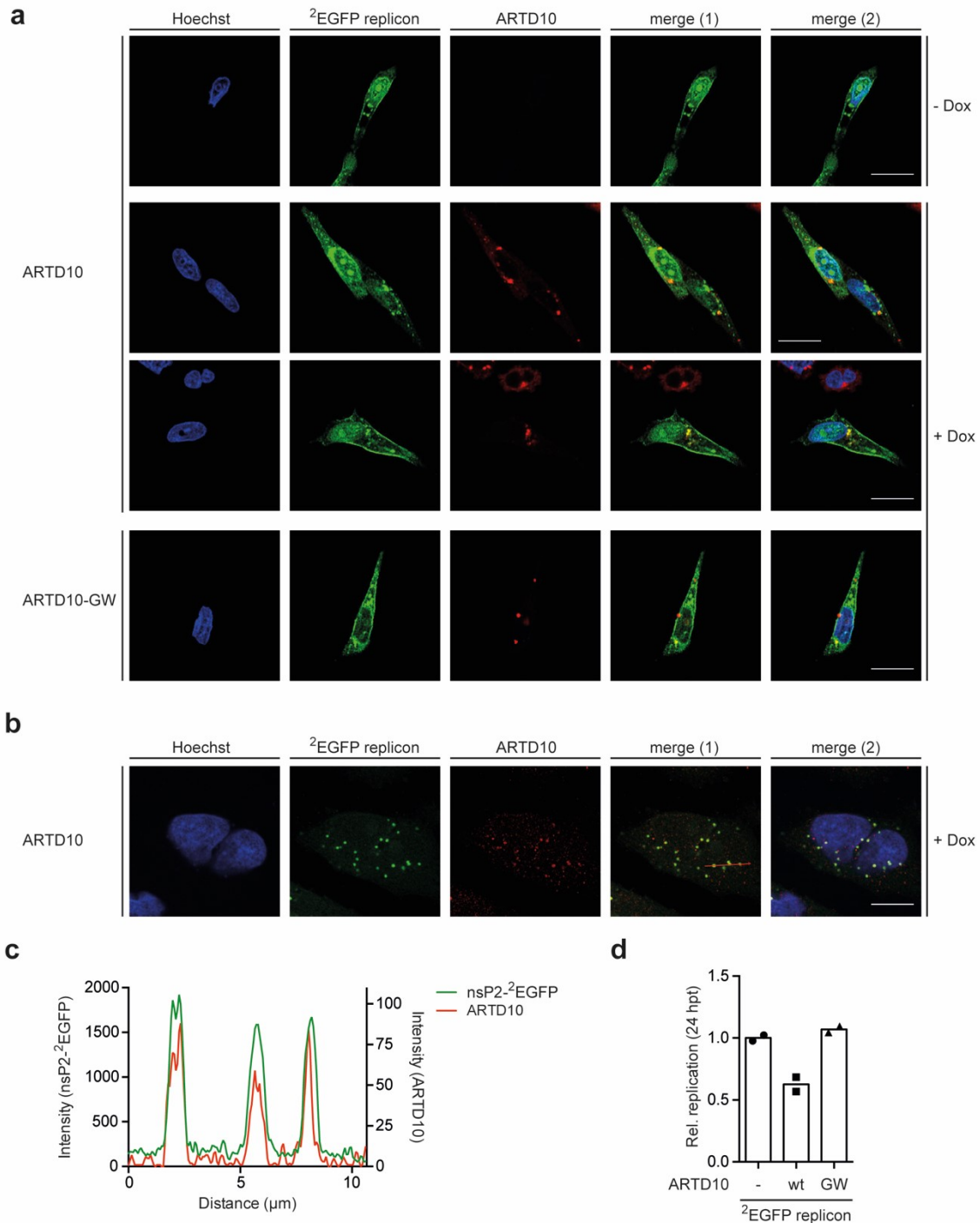


Figure 50: ARTD10 partially co-localizes with replicon derived nsP2 in cells.

(a-c) HeLa Flp-IN T-REx cells stably expressing untagged ARTD10 wt or inactive GW mutant were either induced with doxycycline (Dox) or used as control cells as indicated. Subsequent to induction, the cells were transfected with *in vitro* transcribed ²EGFP replicon RNA (n = 1, SK_C_54, I performed this experiment). **(a,b)** Twenty-four hpt the cells were fixed with glyoxal solution and ARTD10 was stained with monoclonal ARTD10-specific antibodies (5H11). The ²EGFP replicon/nsP2-²EGFP is shown in green and ARTD10 in red. Nuclei were stained with Hoechst and are shown in blue. **(a)** (Co)localization of ARTD10 and nsP2-²EGFP was analyzed by confocal microscope with an LSM 710 confocal. I performed this experiment. Scale bar: 20 μm. **(b)** (Co-)localization of ARTD10 and nsP2-²EGFP was analyzed by confocal microscope using the Airyscan processing technology of the LSM 980. The Airyscan images were taken by Sabrina Ernst and Karla Feijs. Scale bar: 10 μm. **(c)** Intensity profiles of nsP2-²EGFP and ARTD10 (Alexa555) fluorescence measured along the arrows depicted in the merge (1) picture **(b)**. I performed this analysis. **(d)** Quantification of Gaussia luciferase activity relative to cells transfected with ²EGFP replicon RNA without Dox induction at 24 hpt (n = 1, mean value, two technical replicates were measured, I performed this experiment).

In conclusion this chapter defines CHIKV nsP2 as a substrate for MARYlation *in vitro* and in cells by interferon-inducible mono-ARTDs. Furthermore, a condition similar to viral infection was necessary to induce modification of nsP2, potentially to target and activate the respective transferases. Immunofluorescence studies revealed that ARTD10 partially co-localized with nsP2, supporting the concept that ARTD10 MARYlates nsP2.

2.2.4 Mono-ADP-ribosylation inhibits the proteolytic activity of nsP2 reversibly

After confirming nsP2 as a substrate for MARYlation *in vitro* as well as in cells, the question of the functional consequence of this modification needed to be addressed. Therefore, an *in vitro* protease assay activity was established. First, an artificial substrate was created based on the junction between nsP3 and nsP4, which has been described to be the best *in vitro* substrate for nsP2 and its cleavage constitutes the earliest step in polyprotein processing (Rausalu et al. 2016). For visualization purposes, the cleavage site was embedded between a GST- and an EGFP-tag and a polylinker was introduced to increase its accessibility (**Figure 51a**). This substrate was expressed in *E. coli* and subsequently subjected to a protease assay using His-nsP2-459-798. For control the inactive His-nsP2-459-798-CASA mutant was included. Cleavage of the substrate was monitored by Coomassie blue staining. While in the presence of the active protease domain the substrate was progressively cleaved, the CASA mutant showed no activity. Meanwhile. The substrate was stable in the absence of protease. Moreover, neither of the resulting fragments was further cleaved (**Figure 51b**). Together, these results demonstrated activity and specificity of the viral protease.

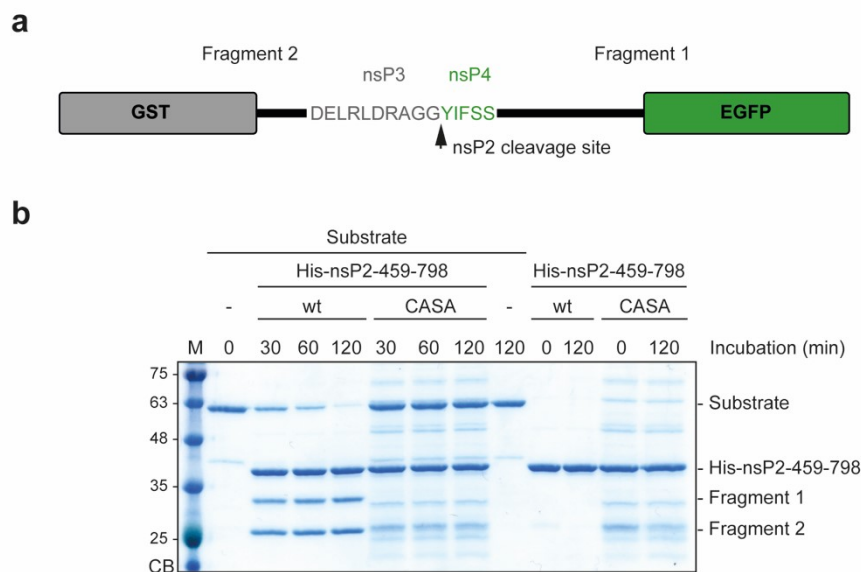


Figure 51: Establishment of the nsP2 protease assay *in vitro*.

This figure is modified from Krieg et al. 2020. **(a)** Schematic representation of the substrate for the nsP2 protease assay. A peptide comprising the cleavage site between nsP3 and nsP4, that is described to be the best *in vitro* substrate for the nsP2 protease (Rausalu et al. 2016), was cloned flanked by a GST- and an EGFP-tag for visualization. To increase accessibility of the cleavage site a polylinker was introduced between the peptide and EGFP. Patricia Korn, née Verheugd, made this figure. **(b)** The bacterially expressed substrate was incubated with recombinant, His⁶-tagged nsP2-459-798, containing the protease domain, at 30°C for the indicated times. As a control the inactive CASA mutant was included and all recombinant proteins were incubated separately for 120 min to exclude instability issues. The reactions were subjected to SDS-PAGE and the total proteins were stained with Coomassie blue (CB) (n = 2, SK_C_4, I performed these experiments).

The generation of a specific protease assay allowed testing of the effect of MARYlation on the catalytic activity of nsP2 (**Figure 52**). For this purpose, His-nsP2-459-798 was modified by ARTD10cat in the presence of β -NAD⁺ for 30 min prior to addition of the substrate. Samples

without GST-ARTD10cat were likewise incubated with β -NAD⁺ and the catalytically inactive GW mutant served as a further control (**Figure 52a**). In the Coomassie blue staining, strong MARYlation of nsP2-459-798 was visible by a mobility shift of the protein. This was exclusive for co-incubation with ARTD10cat, confirming a successful and specific ADP-ribosylation assay. Evaluation of the unprocessed substrate revealed, that the protease alone can still process the substrate effectively over time. In the presence of GST-ARTD10cat, the proteolytic activity of nsP2 was strongly inhibited. This was dependent on MARYlation, as the ARTD10cat-GW mutant had no effect (**Figure 52a**). In addition to time-dependent processing, the influence of the degree of modification on protease activity was assessed. Therefore, active GST-ARTD10cat was titrated in the presence of radioactively labelled ³²P-NAD⁺ to allow more precise measurement of the amount of MARYlation. The autoradiogram showed that modification of His-nsP2-459-798 correlated with the amount of GST-ARTD10cat in the reaction. Analogously, the quantity of unprocessed substrate decreased congruently with the incorporated label (**Figure 52b**). Because the amount of unprocessed substrate was inversely proportionate to catalytic activity MARYlation inhibits nsP2 protease activity in a dose-dependent manner.

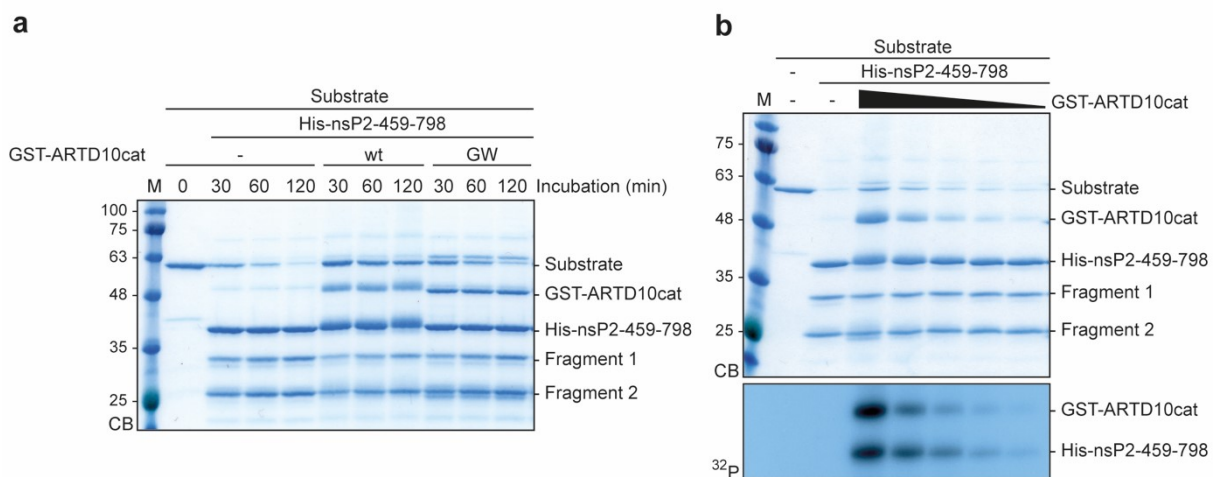


Figure 52: ARTD10-mediated MARYlation inhibits nsP2 protease activity in a dose-dependent manner.

This figure is modified from Krieg et al. 2020. **(a)** Recombinant His-nsP2-459-798 was incubated with or without bacterially expressed GST-ARTD10cat, wt or inactive GW mutant, in the presence of β -NAD⁺ at 30°C for 30 min. Subsequently, the recombinant substrate was added to the reactions and further incubation at 30°C took place for the indicated times. The samples were subjected to SDS-PAGE and the total protein amount were stained with Coomassie blue (CB) (n = 3, SK_C_35, I performed these experiments). **(b)** Recombinant His-nsP2-459-798 was incubated with increasing amounts of bacterially expressed GST-ARTD10cat in the presence of radioactively labelled ³²P-NAD⁺ at 30°C for 30 min. Subsequently, the recombinant substrate was added to the reactions and further incubation at 30°C took place for 120 min. The samples were subjected to SDS-PAGE and the total protein amount were stained with Coomassie blue (CB) while the incorporated radioactive label was visualized with autoradiography (³²P) (n = 1, SK_C_35, I performed this experiment).

The hypothesis was that MARYlation is a mechanism of the innate immune response, which is antagonized by the nsP3 macrodomain. Hence, the question arises whether the inhibitory effect of nsP2 modification on protease activity can be reversed by the hydrolase activity of nsP3. Consequently, recombinant His-nsP3 and His-nsP3-macro were tested for their capacity to reverse the effect of GST-ARTD10cat-mediated MARYlation. For comparison, the inactive GST-ARTD10cat-GW and the His-nsP2-459-798-CASA mutants were included. Because the increase of processed fragments was difficult to distinguish when analyzed by Coomassie blue staining, the fragments were detected and quantified by immunoblotting (**Figure 53**). Furthermore, immunoblotting with the MAR-binding reagent enabled a more sensitive detection of the MARYlation state of nsP2 (**Figure 53a**). The MAR blot illustrates that His-nsP2-459-798 was MARYlated in the presence of GST-ARTD10cat. This MARYlation signal decreased

upon addition of His-nsP3 or His-nsP3-macro with the former being more efficient. The same tendency was visible by examination of the motility shifts in the Coomassie blue staining. Reactivation of the protease activity by de-MARylation was assessed by the amount of unprocessed substrate and processed fragments using Coomassie blue staining and immunoblotting. The samples containing the macrodomain variants showed a decreased amount of full-length substrate compared to fully MARylated sample and the CASA control, while an increase was detectable in relation to the inactive GW mutant or the active protease domain alone (**Figure 53a**).

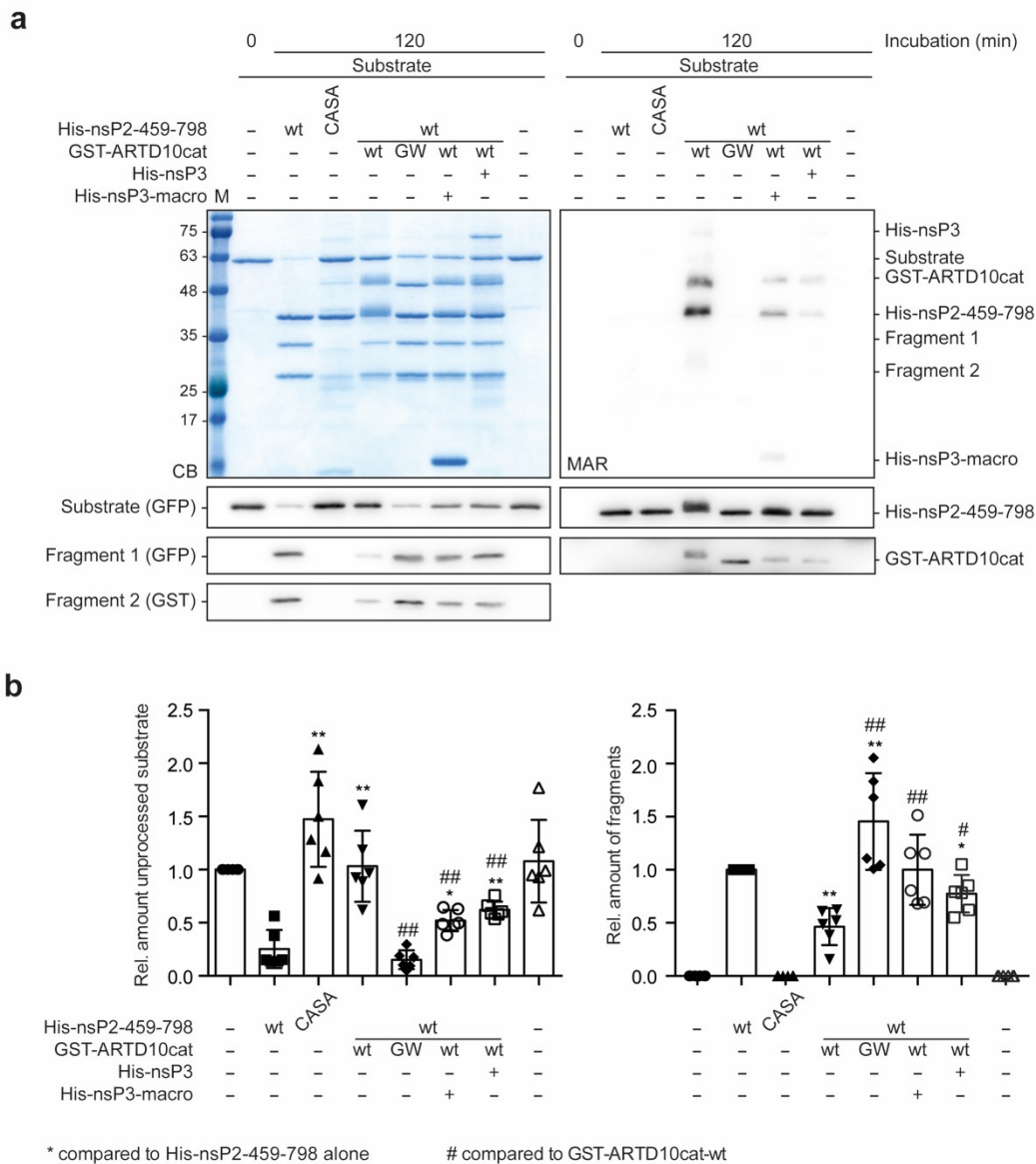


Figure 53: The inhibitory effect of MARylation on nsP2 protease activity can be reversed by the viral nsP3 macrodomain. This figure is modified from Krieg et al. 2020. **(a,b)** Bacterially expressed His-nsP2-459-798, wt or CASA, GST-ARTD10cat, wt or GW, and His-nsP3, full-length or isolated macro, were incubated as indicated in the presence β -NAD⁺ at 30°C for 30 min. Subsequently, the recombinant substrate was added to the reactions and further incubation at 30°C took place for 120 min (n = 6, SK_C_35, I performed these experiments). **(a)** Total protein amounts were stained with Coomassie blue (CB) and immunoblotted with GFP- (Rockland), GST- (Sigma), ARTD10 (5H11) or nsP2-specific (Eurogentec) antibodies. Furthermore, MARylation was assessed by immunoblotting with the MAR-binding-reagent (Millipore). **(b)** Quantification of the unprocessed substrate (left) or the sum of processed fragments (right) by densitometry (n = 6, mean \pm SD, I performed these experiments). **/##p < 0.01, */#p < 0.05 when a two-tailed Mann-Whitney test was applied.

This visual examination was supplemented by quantification by densitometry and statistical evaluation to translate the conveyed impression into relative values (**Figure 53b**). The quantification confirmed that hydrolysis of the MARylation significantly reactivated the

protease activity of nsP2. However, the rescue was only partial, potentially due to residual MARYlation (**Figure 53a**) in line with the dose-dependent inhibition (**Figure 52b**).

In summary, the biochemical characterization of nsP2 as a substrate for MARYlation and the functional consequences of the modification for protease activity provide a first mechanistic explanation for the phenotype of the CHIKV macrodomain mutants as well as the inhibitory effect of the interferon-induced mono-ARTDs. The *in vitro* data thus supports the hypothesis that nsP2-mediated polyprotein processing is hampered by MARYlation and reactivated by the de-MARYlating activity of the viral macrodomain.

2.2.5 Investigation of the CHIKV Y114V macrodomain mutant

Besides the V33E macrodomain mutant, mutation of Y114 to valine (Y114V) was identified hydrolase deficient (Chapter 2.1.3). In addition to investigation of the catalytic activity, the former master student Catharina Voigt evaluated the capability of different CHIKV mutants to bind ADPr using thermal shift assays. While the V33E mutant was not able to bind ADPr anymore, the Y114V variant of the macrodomain exhibited the same capacity to bind ADPr as the wt (data not shown). Like the V33E mutant, the D10A mutation abolished ADPr binding (Malet et al. 2009; McPherson et al. 2017). While the V33E and the D10A macrodomain mutants have already been assessed with regard to their influence on CHIKV replication (Chapter 2.2.2), this chapter will focus on the preliminary examination of the Y114V mutant. Interestingly, measurement of luciferase activity of the different replicon mutants revealed, that unlike the hydrolase- and binding-deficient mutants, the Y114V mutant was still able to replicate (**Figure 54a,b**). Time course experiments demonstrated reduced replication compared to the wt at early times post transfection, but there was no difference at late time points (**Figure 54a,b**). This switch in the slope of replication resembled findings obtained with ARTD10 and ARTD12 (**Figure 28**). Additionally, immunoblotting of processed nsP2 with the nsP2-specific antibody showed unaffected polyprotein processing of the Y114V macrodomain mutant (**Figure 54c**).

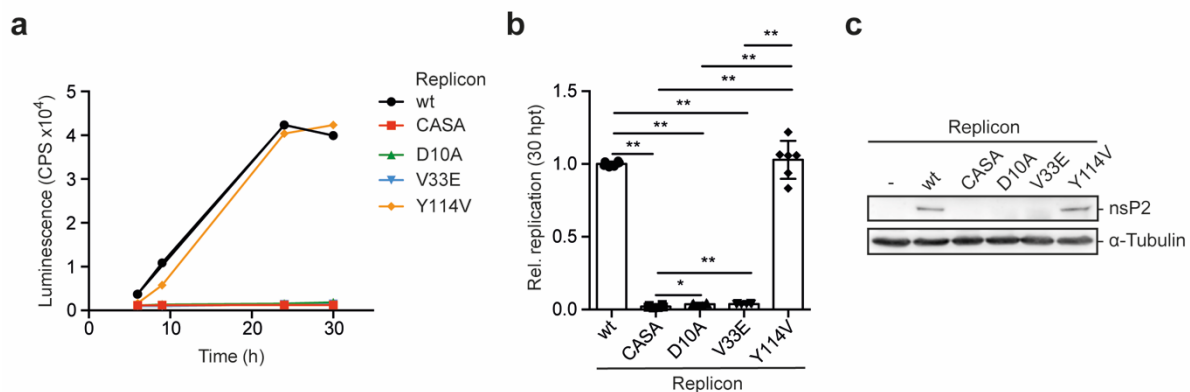


Figure 54: Investigation of the replication ability of the CHIKV replicon Y114V macrodomain mutant.

This figure is modified from Krieg et al. 2020. **(a-c)** HEK293 cells were transfected with *in vitro* transcribed replicon RNA, wt or the indicated mutants. The CASA mutant is a protease activity deficient mutant while the D10A, V33E and Y114V mutants are located within the macrodomain ($n = 3$, SK_D_9, I performed these experiments). **(a)** Representative measurement of Gaussia luciferase activity in the supernatant collected at the indicated times after transfection (mean of two technical replicates is shown, I performed this experiment). **(b)** Quantification of Gaussia luciferase activity relative to the control cells with wt replicon at 30 hpt ($n = 3$, mean value \pm SD, two technical replicates were measured per n , I performed these experiments). **(c)** Cells were harvested 30 hpt and whole cell lysates were immunoblotted with CHIKV nsP2-specific antibodies (Eurogentec), to control expression of the viral nsP2 compared to the loading control α -tubulin. ** $p < 0.01$; * $p < 0.05$ when a two-tailed Mann-Whitney test was applied.

Because the Y114V mutant replicon behaved differently from the other investigated macrodomain mutants, the influence of modulating MArlylation was further studied (**Figure 55**). On the one hand, treatment with inhibitors of ADP-ribosylation was assessed. HEK293 cells were treated with the vehicle DMSO, the ARTD10 specific inhibitor OUL35 (0035) or the broad inhibitor 3-AB prior to transfection with the Y114V replicon. Additionally, the wt and V33E replicons were included for reference. Interestingly, the Y114V replicon seemed to be less sensitive to inhibitor treatment than the wt was in these experiments, where replication was decreased (**Figure 55a; Figure 35**). In contrast to that, overexpression of active ARTD10 hampered replication of the Y114V mutant even stronger than the wt (**Figure 55b**). Even though these experiments were only performed once so far, they support the finding that the Y114V mutant behaved differently from the wt as well as the V33E macrodomain mutant.

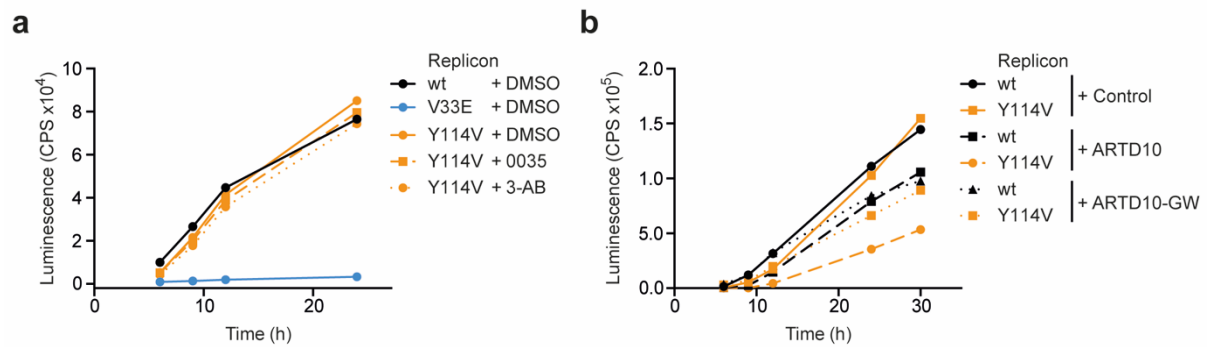


Figure 55: Influence of MARYlation on replication of the CHIKV Y114V replicon.

(a) HEK293 cells were treated with the vehicle DMSO, 10 μ M of the ARTD10-specific inhibitor 0035 or 2.5 mM of the broad ARTD inhibitor 3-aminobenzamide (3-AB). 24 h later, the cells were transfected with *in vitro* transcribed ³EGFP replicon wt or the V33E macrodomain mutant RNA. Representative measurement of Gaussia luciferase activity in the supernatant collected at the indicated times after transfection ($n = 1$, SK_C_6, mean of two technical replicates is shown, I performed this experiment). **(b)** HEK293 Flp-IN T-REx cells stably expressing the TAP-tag alone, ARTD10-C-TAP, wt or inactive GW mutant, as indicated, were induced with Dox 16 h prior to transfection with the *in vitro* transcribed replicon wt or Y114V mutant RNA. Representative measurement of Gaussia luciferase activity in the supernatant collected at the indicated times after transfection ($n = 1$, SK_D_2, mean of two technical replicates is shown, I performed this experiment).

Taken together, preliminary characterization of the Y114V mutant and experiments with the interferon-inducible mono-ARTDs and the inhibitors of ADP-ribosylation point to a more complex role of MARYlation for CHIKV replication. Together these findings suggest that ADP-ribosylation not only represses or activates replication, but that it may control individual steps of replication distinctly. For example, there seems to be a switch from antiviral to a proviral role during the viral life cycle indicated by differential accumulation of Gaussia luciferase activity over time. Furthermore, in addition to hydrolysis, binding to ADPr might be functionally relevant. The *in vitro* studies demonstrated distinct specificities of nsP3 towards different substrates. Therefore, it is conceivable that the binding is necessary for targeting the replication complex and nsP3 to MARYlated host factors. Moreover, it is imaginable that the hydrolase activity is necessary to release the macrodomain from its substrate. The lack of hydrolase activity might trap the Y114V mutant bound to the substrate and thus prevent further modification by restricting accessibility. As the protease assays demonstrated, the MAR-mediated inhibition of nsP2 is dose-dependent and thus restricting MARYlation by binding of the Y114V mutant might likewise restrict the inhibition. Comparably, the Y114V mutant might bind to the MAR-transferase itself and thus hamper its activity. There are several lines of arguments that seem conclusive, but this potential dual role of the macrodomain needs to be investigated in future experiments for clarification. Potentially, the identification of more viral infection-dependent substrates of MARYlation could uncover different impacts of the modification on different substrates.

2.2.6 CHIKV nsP1 and nsP3 are substrates for mono-ADP-ribosylation *in vitro*

In the previous chapters, nsP2 was identified as a new substrate of MARylation *in vitro* and in cells. This modification inhibited the protease activity and thus polyprotein processing. This was counteracted by the de-MARylation activity of the viral macrodomain. Nonetheless it was apparent that there are more effects of MARylation on CHIKV replication that introduce complexity to the system. In the past the identification of MAR substrates turned out to be challenging, for instance due to the low abundance of MARylation compared to PARylation. Furthermore, the previously described substrates displayed only weak signals for MARylation compared to the auto-modification of the ARTDs. The facts that a trigger for mono-ARTD expression was identified with interferon and that viral nsP2 represents a good substrate for MARylation instigates the idea that additional viral proteins might be bona fide substrates for interferon-induced mono-ARTDs. In addition to nsP2 and nsP3, Chikungunya encodes two more non-structural proteins. NsP1 is the RNA capping enzyme and nsP4 functions as the RdRp. His₆-tagged nsP1 was produced recombinantly, while bacterial expression of nsP4 could not be achieved. In fact, nsP4 was never expressed in bacteria successfully, probably due to solubility issues (Rupp et al. 2015; Ahola et al. 2016). Therefore, only nsP1, nsP2 and nsP3 were subjected to *in vitro* ADP-ribosylation assays with full-length, TAP-purified ARTD10 (**Figure 56**). For nsP3 the inactive V33E mutant was used to prevent de-MARylation. Furthermore, the nsPs were incubated with ³²P-NAD⁺ without a transferase or with inactive ARTD10-GW as controls.

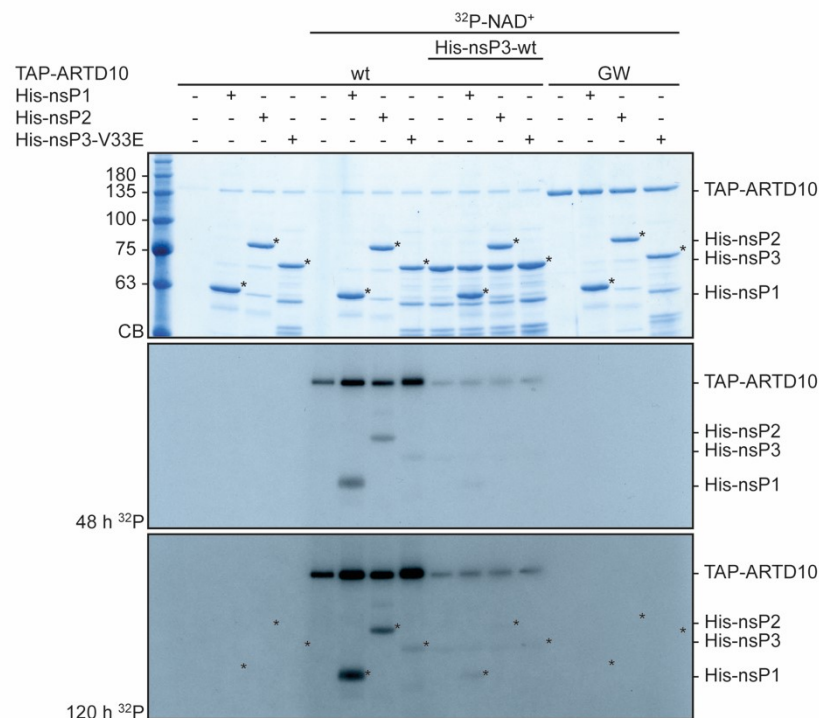


Figure 56: Full-length ARTD10 reversibly MARylates CHIKV nsP1, nsP2 and nsP3 *in vitro*.

Bacterially expressed, His₆-tagged nsP1, nsP2 and nsP3 V33E were incubated with TAP-purified ARTD10 full-length, wt or inactive GW mutant, in the presence or absence of radioactively labelled ³²P-NAD⁺ as indicated at 30°C for 30 min. Furthermore, active, recombinant His-nsP3 was co-incubated as indicated. Total proteins were stained with Coomassie blue (CB) and the incorporated label was analyzed by autoradiography (³²P) (n = 2, SK_C_3, I performed these experiments).

The autoradiogram demonstrated that nsP1 is a robust substrate of ARTD10-mediated MARylation. Further exposure also unveiled a signal of the inactive nsP3, while none of the negative controls showed modifications (**Figure 56**). Further, the macrodomain was assessed

for its ability to de-MARylate nsP1-nsP3. Indeed, de-MARylation of nsP1, nsP2 and nsP3-V33E was efficient (**Figure 56**).

In addition to ARTD10, ARTD7cat and ARTD8cat were tested for their capacity to modify nsP1 and nsP3-V33E. Subjection to further *in vitro* ADP-ribosylation assays demonstrated that both were able to MARylate nsP1, nsP2 and nsP3. Of note, the modification of nsP1 was very efficient (**Figure 57**).

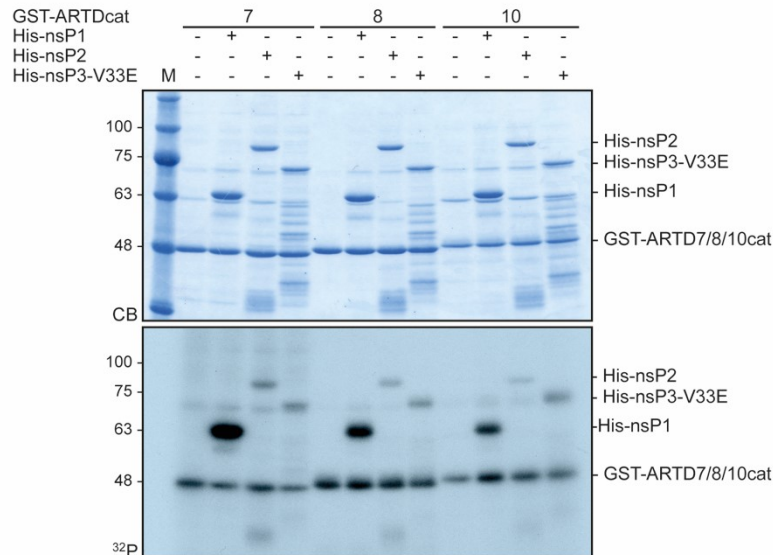


Figure 57: Interferon-inducible mono-ARTDs modify CHIKV nsP1, nsP2 and nsP3 *in vitro*.

Bacterially expressed, His₆-tagged nsP1, nsP2 or inactive nsP3 V33E were incubated with the bacterially expressed, GST-tagged catalytic domains of interferon-regulated ARTD7, ARTD8 and ARTD10 as indicated. The reactions took place in the presence of radioactively labelled ³²P-NAD⁺ at 30°C for 30 min. Total proteins were stained with Coomassie blue (CB) and the incorporated label was analyzed by autoradiography (³²P) (n = 2, SK_C_3, I performed these experiments).

To investigate the specificity of the assays and to examine whether the modification of the CHIKV non-structural proteins is exclusive for interferon-regulated MARylation, they were further evaluated as substrates for ARTD1-mediated PARylation *in vitro* (**Figure 58**). Therefore, His-nsP1, -nsP2 and -nsP3-V33E were incubated in the presence of radioactively labelled ³²P-NAD⁺ and recombinant His-ARTD1, which was activated by addition of double stranded DNA oligomers. Recombinant histone H3 was included in the experiment as a positive control. Additionally, all reactions were incubated in the presence and absence of His-HPF1, which was identified as a co-factor of ARTD1. Association of ARTD1 with HPF1 shifts its substrate specificity from auto-modification to substrate modification and from glutamate and aspartate to serine (Bonfiglio et al. 2017). Assessment of the PAR signal in the autoradiogram revealed that while H3 was a substrate of ARTD1, enhanced by HPF1, the viral nsPs were not modified. Moreover, as expected, HPF1 was modified and a shift from auto-modification to substrate modification was visible in the presence of HPF1 and H3. No such decrease in auto-modification was detectable when the nsPs were present (**Figure 58**).

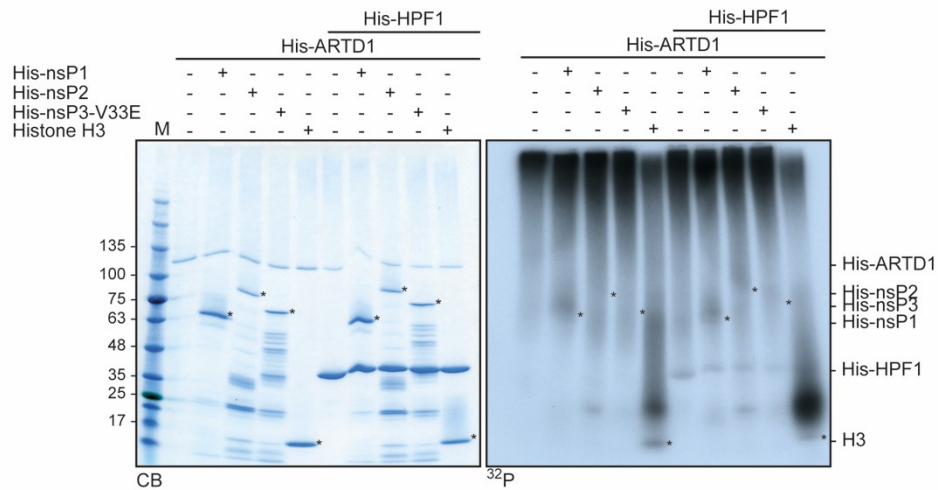


Figure 58: ARTD1 does not PARylate CHIKV nsP1, nsP2 or nsP3 *in vitro*.

Bacterially expressed, His6-tagged nsP1, nsP2 or inactive nsP3 V33E were incubated with recombinant, His-ARTD1 in the presence or absence of its co-factor HPF1 as indicated. Furthermore, commercial histone H3 was included as a positive control. ARTD1 was activated by addition of double stranded DNA oligomers and the reactions took place in the presence of radioactively labelled ^{32}P -NAD $^{+}$ at 30°C for 30 min. Total proteins were stained with Coomassie blue (CB) and the incorporated label was analyzed by autoradiography (^{32}P) (n = 2, SK_C_10, I performed these experiments).

This suggested broader relevance for modification of viral proteins by interferon-induced mono-ARTDs, particularly as at least 3 of 4 CHIKV nsPs are substrates. Further studies need to address the modifications in cells and functional relevance.

2.3 Identification of common cellular interactors and substrates of ARTD10 and the CHIKV nsP3 macrodomain

Investigation of the phenotype of hydrolase-deficient macrodomain mutant replicons as well as the effect of ARTD10 overexpression on CHIKV replication indicated that MARYlation plays a complex role in the viral life cycle. This might be explained by a multitude of cellular substrates of mono-ARTD-mediated MARYlation. The different substrates could display pro- or antiviral functions dependent on their state of modification. Furthermore, ARTD10 substrates can potentially be recognized by the viral macrodomain. This might affect targeting, can be hijacked by the virus or the MARYlation can be counteracted by the hydrolase activity of nsP3. To elucidate the various possibilities of regulation by (de-)MARYlation, the cellular interactors and potential substrates need to be identified. The following chapter describes the approach used to characterize interactors of CHIKV nsP3 and ARTD10 in cells. Tandem affinity purifications (TAP) or GFP-Trap purifications and the BioID system were employed. The interactors were identified using mass spectrometry (MS) and the results of the different approaches were compared and evaluated. The generated overlap of shared protein interactions between nsP3 and ARTD10 was tested for its ability to discover new substrates of MARYlation using the example of Ras GTPase-activating protein-binding protein 1 (G3BP1). In fact, *in vitro* ADP-ribosylation assays revealed G3BP1 to be a robust substrate for ARTD10-mediated MARYlation and de-MARYlation by nsP3.

2.3.1 Identification of cellular interactors of the CHIKV nsP3 macrodomain by MS analysis

To uncover new substrates of mono-ADP-ribosylation in a CHIKV infection context, the ability of the viral macrodomain to interact with MARYlated proteins was utilized. If upon viral infection, the hydrolase indeed counteracts intracellular MARYlation as part of the innate immunity, it should interact with these substrates. Hence two independent approaches were used (**Figure 59**). NsP3 was fused to an N-terminal TAP-tag, consisting of a protein A and a calmodulin binding protein (CBP), separated by a Tobacco Etch virus (TEV) cleavage site (**Figure 59**)(Puig et al. 2001). Stable HEK293 Flp-IN T-REx cells lines were created expressing either the TAP-tag alone (Kleine et al. 2008), TAP-nsP3 or TAP-nsP3-macro (**Supplementary Figure S65b**). Subsequent to Dox induced protein expression, the TAP-fusion protein containing complexes were firstly immunoprecipitated via IgG beads using their protein A tag. Thereafter the proteins of interest were detached from the beads by TEV protease-mediated cleavage, leaving only the protein A tag bound to the beads. In a second purification step, a pull down was performed using the CBP tag and calmodulin beads. Afterwards the bead-bound protein complexes were subjected to MS analysis for identification (**Figure 59**).

As enzyme-substrate interactions are often transient, a second approach was employed, that potentially allows for the identification of more dynamic and weaker interactions. In this case, the proteins of interest, nsP3 or nsP3-macro, were fused to a mutant BirA* biotin ligase. This BirA* variant carries an arginine to glycine mutation at position 118 (R118G) compared to the *E. coli* wt protein. The R118G substitution renders the biotin ligase highly promiscuous and allows for quick biotinylation of all proteins in close proximity. If fused to a protein of interest, BirA* is expected to biotinylate interaction partners of set protein, even if an interaction is dynamic (**Figure 59**)(Roux et al. 2012). To characterize the interactome of the viral macrodomain in this setup, HEK293 cells were transiently transfected with plasmids encoding C-terminally fused nsP3-BirA*-HA, nsP3-macro-BirA*-HA or BirA*-HA. After transfection the cells were further incubated in the absence or presence of biotin overnight, to be able to

distinguish BirA*-mediated biotinylation from basal biotinylation in cells (**Supplementary Figure S65a**). Afterwards the cells are lysed, and the biotinylated proteins were enriched using streptavidin beads. Because the highly stable, covalent biotin label was used for purification, the lysis conditions can be very stringent and thus decrease solubility issues. Increased solubility might be of relevance for nsP3 interaction partners, as nsP3 is associated with dot-like structures and potentially membranes (Gotte et al. 2018; Schulte et al. 2016; Fros et al. 2012). Thereafter, the purified proteins were eluted from the beads with biotin supplemented SDS loading buffer at 95°C, subjected to SDS-PAGE and gel fragments were prepared for MS analysis (**Figure 59**; for a control immunoblot see **Supplementary Figure S66**).

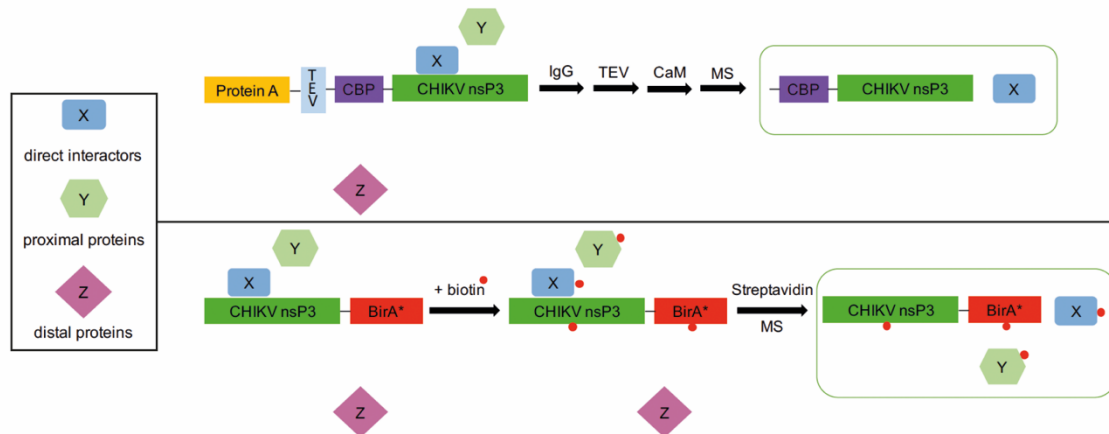


Figure 59: Schematic representation of the mass spectrometry analysis approaches used to identify potentially MAR-dependent interactors of the nsP3 macrodomain.

Depicted are the TANDem affinity purification (TAP) method (upper panel) and the BioID approach (lower panel) (Puig et al. 2001; Roux et al. 2012). For the TAP method the protein of interest, in this case CHIKV nsP3, is fused N-terminally to protein A and calmodulin binding protein (CBP) tags that are connected through a Tobacco Etch virus (TEV) cleavage site. This allows the subsequent affinity purification of direct, relatively stable interactors via two independent tags. The BioID approach on the other hand is based on the C-terminal fusion of a promiscuous, mutant biotin ligase (BirA*) to nsP3, that upon addition of biotin leads to biotinylation of direct stable and more dynamic interactors as well as proteins in close proximity. All biotinylated proteins are immunoprecipitated via streptavidin beads. In both approaches the interactors are identified by mass spectrometry (MS) analysis. I made this figure.

Liquid chromatography tandem mass spectrometry (LC-MS/MS) measurements and primary filter steps were performed by Christian Preisinger and afterwards the data was evaluated with regard to relative enrichment compared to controls (Cox et al. 2014; Tyanova et al. 2016). Therefore, the intensities of peptides from proteins that co-purified with TAP-nsP3 or TAP-nsP3-macro were averaged over the technical duplicates of the three independent experiments and set in relation to the averaged intensities for the TAP tag alone. Proteins that were enriched equal to or higher than 5 times were included in the interactome (**Figure 60a**).

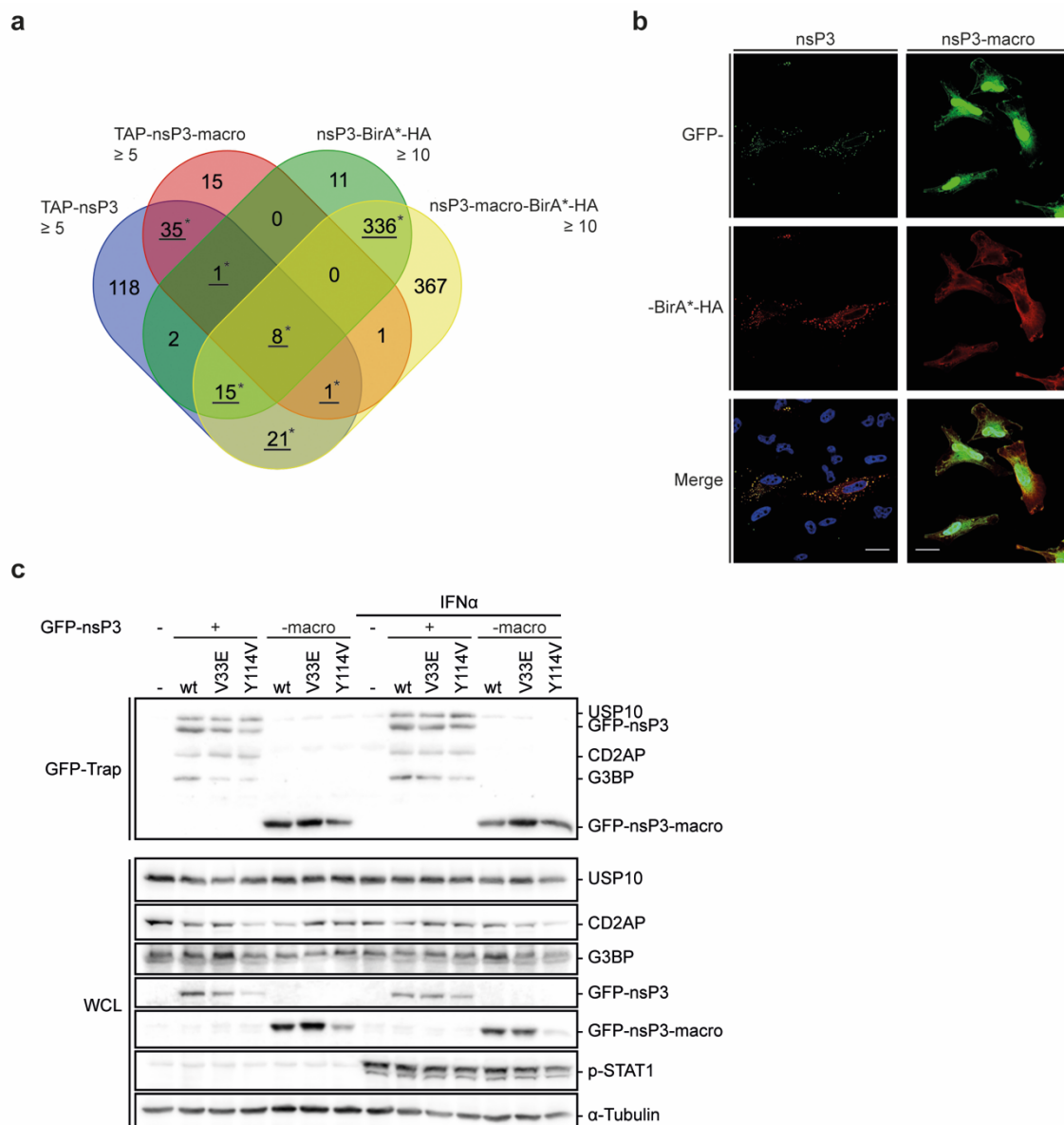


Figure 60: Analysis of potentially macrodomain-dependent interactors of nsP3 identified by MS.

(a) Venn diagram of interactors of full-length nsP3 or the isolated macrodomain identified by MS. For the TAP approach, stable TAP-tag, TAP-nsP3 or TAP-nsP3-macro HEK293 Flp-IN T-REx cells were induced with doxycycline. Sixteen h later the TAP-fusion proteins and their binding partners were co-purified using both tags successively prior to MS analysis. For the BioID, HEK293 cells were transiently transfected with plasmids encoding BirA*-HA alone, nsP3-BirA*-HA or nsP3-macro-BirA*-HA. Subsequently the cells were incubated in the presence or absence of biotin for 16 h, lysed and biotinylated proteins were immunoprecipitated with streptavidin beads before MS analysis. Depicted are the number of unique proteins co-purified with TAP-nsP3 or TAP-nsP3-macro ($n = 3$, enrichment ≥ 5 , SK_B_30) or biotinylated by nsP3-BirA*-HA or nsP3-macro-BirA*-HA ($n = 2$, enrichment ≥ 10 vs. BirA* control and ≥ 10 vs. absence of biotin, SK_B_17) and the numbers of overlapping proteins thereof. I performed the experiments until MS analysis. The mass spectrometry measurements and initial data analysis with MaxQuant were performed by Christian Preisinger. Further analysis was performed by me. The proteins that were used for further analysis are underlined and marked with an asterisk. **(b)** HeLa cells were transiently transfected with plasmids encoding GFP-nsP3 full-length or isolated macrodomain and nsP3-BirA*-HA or nsP3-macro-BirA*-HA as indicated. Forty-eight h after transfection the cells were fixed with PFA and stained with HA-specific antibodies (Covance). GFP-fusion proteins are shown in green while BirA*-HA-fusions are red. The nuclei were stained with Hoechst and are shown in blue. NsP3 and nsP3-macro localization was analyzed using confocal microscopy. Scale bar: 20 μm ($n = 1$, SK_B_19, I performed this experiment). **(c)** Validation of selected interactors of nsP3 by GFP-Trap. HEK293 cells were transiently transfected with plasmids encoding GFP-nsP3 full-length or isolated macrodomain and mutants thereof as indicated. Twenty-four h after transfection the cells were treated with 180 U of IFN α and further 24 h later the cells were lysed and the GFP-fusion proteins were immunoprecipitated using GFP-Trap (Chromotek). Co-immunoprecipitated interactors were analyzed by immunoblotting with specific antibodies. As control endogenous as well as overexpressed GFP-fusion protein were visualized in whole cell lysates (WCL) compared to the loading control α -tubulin ($n = 2$, SK_C_24, I performed these experiments).

For BioID two controls were considered. The BirA*-HA was used to exclude unspecific biotinylation of the ligase and no addition of biotin served to exclude basal, cellular biotinylation. For nsP3-BirA*-HA as well as nsP3-macro-BirA*-HA proteins were included in the proteome that showed a relative enrichment of ten or more compared to both controls (**Figure 60a**). For BioID the enrichment score was chosen higher than for the TAP approach because it generally showed more background. The resulting four datasets were subsequently examined for their overlap (**Figure 60a, Table 1**). As expected when comparing the data from the two techniques, the BioID generally resulted in more interactors than the TAP approach. However, the TAP procedure also comprised unique proteins. These might be too far away from the ligase, because they were part of bigger protein complexes or the interaction was N-terminal. When comparing the results from the full-length nsP3 with the isolated macro proteomes, two things need to be taken into account: The C-terminus of nsP3 contains the alphavirus unique domain (AUD) and a hypervariable domain (HVD). The latter is described as the main interaction hub of nsP3 with host cell proteins and it is responsible for its subcellular localization (Rana et al. 2014; Gotte et al. 2018; Fros et al. 2012; Schulte et al. 2016; Mutso et al. 2018). Therefore, proteins only enriched with the full-length nsP3 were excluded from further investigation as potential substrates, because their interaction was probably independent of the macrodomain and thus MARYlation. The isolated macrodomain on the other hand, did not localize to the characteristic foci like the intact nsP3 (**Figure 60b**). Accordingly, all interactors identified exclusively for the detached macrodomain were likewise eliminated, as incorrect localization might lead to artificial results, particularly for the BioID approach. Of course, this may also lead to exclusion of bona fide substrates, but it decreases the risk of false positives greatly. These considerations resulted in a subset of 417 potential cellular substrates of de-MARYlation that will be further explored in the following. These proteins were identified at least in one screen for nsP3 as well as for the isolated macrodomain (**Figure 60a** underlined and marked with an asterisk, excerpt in **Table 1**). Among newly identified proteins, this list also includes known interactors of nsP3 like G3BP1 and CD2-associated protein (CD2AP) (Mutso et al. 2018; Panas et al. 2014), supporting the credibility of the findings.

Furthermore, selected proteins were verified in independent pull-down experiments with GFP-nsP3 and GFP-nsP3-macro as bait proteins (**Figure 60c**). In addition, the macrodomain V33E and Y114V mutants were included in the assays and the influence of IFN α treatment was assessed. The G3BP-specific antibody recognizes both G3BP1 and G3BP2, which are collectively referred to as G3BP. In line with the proteome analyses G3BP, CD2AP and USP10 co-immunoprecipitated with the full-length nsP3, while USP10 also showed weak interaction with the isolated macrodomain. The macrodomain mutations only appeared to alter the interaction with G3BP, as slightly less G3BP co-purified with nsP3. The immunoblots of IFN α treated cells suggested an increased binding of nsP3 to G3BP and USP10 (**Figure 60c**). However, these are only weak tendencies that need to be addressed in more detailed studies. Nevertheless, it is a first interesting suggestion that MARYlation might influence the interactions. This is especially interesting considering that nsP3 itself was identified as a substrate of MARYlation in initial *in vitro* studies (**Figure 56 and 57**). Still, the pull-down assays verified the MS analysis of G3BP1, CD2AP and USP10 and colleagues could likewise confirm MAGED2 as an interactor of nsP3 (data not shown)(Kruttt 2018).

Table 1: Overview of nsP3 interacting proteins identified in at least three MS approaches (TAP or BioID as indicated)

Protein name	Gene ID	TAP-		-BirA*-HA		CRAPome
		nsP3	macro	nsP3	macro	
SAFB-like transcription modulator	SLTM	+	+	+	+	47 / 411
Fragile X mental retardation syndrome-related protein 2	FXR2	+	+	+	+	46 / 411
Protein-methionine sulfoxide oxidase MICAL3	MICAL3	+	+	+	+	6 / 411
Double-stranded RNA-binding protein Staufen homolog 1	STAU1	+	+	+	+	58 / 411
Metastasis-associated protein MTA1	MTA1	+	+	+	+	53 / 411
Four and a half LIM domains protein 1	FHL1	+	+	+	+	35 / 411
TBC1 domain family member 23	TBC1D23	+	+	+	+	1 / 411
Nucleosome assembly protein 1-like 1	NAP1L1	+	+	+	+	152 / 411
Ubiquitin carboxyl-terminal hydrolase 10	USP10	+	+	+		35 / 411
Myosin-9	MYH9	+	+		+	203 / 411
Ras GTPase-activating protein-binding protein 1	G3BP1	+		+	+	141 / 411
Nuclear fragile X mental retardation-interacting protein 2	NUFIP2	+		+	+	94 / 411
Protein FAM207A	FAM207A	+		+	+	16 / 411
SWI/SNF complex subunit SMARCC1	SMARCC1	+		+	+	66 / 411
Caprin-1	CAPRIN1	+		+	+	120 / 411
U4/U6 small nuclear ribonucleoprotein Prp31	PRPF31	+		+	+	145 / 411
Nuclear cap-binding protein subunit 3	NCBP3	+		+	+	22 / 411
ATP-dependent RNA helicase DDX1	DDX1	+		+	+	125 / 411
Antigen KI-67	MKI67	+		+	+	80 / 411
La-related protein 1	LARP1	+		+	+	78 / 411
CD2-associated protein	CD2AP	+		+	+	33 / 411
Ataxin-2	ATXN2	+		+	+	33 / 411
Proline Rich Coiled-Coil 2C	PRRC2C	+		+	+	67 / 411
Melanoma-associated antigen D2	MAGED2	+		+	+	43 / 411
Ataxin-2-like protein	ATXN2L	+		+	+	127 / 411

Apart from verification by pull-downs, the reliability of the data was further evaluated with the CRAPome tool (version 1.1)(Mellacheruvu et al. 2013). This web-based application comprises a contaminant repository for interactome studies from affinity purification as well as BioID studies. It gives a score for how often an identified protein is found in MS analyses and thus provides information about how likely a protein is a contaminant or a bone fide interaction partner. For instance, heat shock protein 70 (HSP70, gene ID HSPA1A) is a frequent false positive in MS studies and exhibits a score of 395 hits within 411 studies in the repository. Except for Myosin-9 however, which was found in roughly half of the studies, the interactors found for nsP3 show rather low CRAPome scores indicating that the negative controls for the experiments were adequate. Classical pull-down experiments might not provide a suitable verification method for proteins that were found exclusively via BioID, because this technique

was explicitly chosen to identify transient interactions. Therefore, in addition to the CRAPome analysis, these proteins need to be validated by different approaches. For example, cross-linking prior to GFP-Trap might conserve dynamic interactions and allow a snapshot of the network. Additionally, co-localization studies can verify interaction in cells. To further restrict the amounts of potential substrates, which need to be validated, the interactome of ARTD10 was investigated. Creation of the overlap between the 417 macrodomain-dependent nsP3 interactors (**Figure 60a** underlined and marked with an asterisk, excerpt in **Table 1**) and the ARTD10 screens might provide further evidence that the resulting proteins are potentially regulated by MARYlation and worth more comprehensive studies.

2.3.2 Identification of ARTD10 interactors dependent on interferon and catalytic activity

The ARTD10 interactome was explored using BioID. The aim was to identify ARTD10 substrates. BirA*-HA, absence of exogenous biotin and the inactive ARTD10-GW mutant served as controls. The catalytic domain is located near the C-terminus of ARTD10. Because the BirA* ligase is fused to the C-terminus of the protein, the integrity of the construct was initially investigated to ensure catalytic activity and proper localization (**Figure 61a,b**). Therefore, the subcellular localizations of BirA*-HA, ARTD10-BirA*-HA and ARTD10-GW-BirA*-HA were analyzed. While the biotin ligase alone exhibited a diffuse distribution in the cytoplasm, the ARTD10 fusion proteins displayed characteristic cytoplasmic foci (**Figure 61a**) (Kleine et al. 2012). Furthermore, the catalytic activity of ARTD10 was assessed by co-localization with the murine GFP-Artd8-macro2-3 construct (Forst et al. 2013; Butepage et al. 2018a). The GFP-Artd8-macro2-3 showed a clear co-localization the ARTD10-BirA*-HA dots, while it appeared diffuse and largely nuclear in the absence of a catalytically active transferase. Moreover, the MAR-binding deficient GFP-Artd8-macro2-3-GE mutant did not co-localize with ARTD10-BirA*-HA (**Figure 61a**). This argues for a functional ARTD10 fusion protein. In a second, more direct approach, the MAR transferase activity of the ARTD10-BirA*-HA was verified in an *in vitro* ADP-ribosylation assay. Transiently expressed BirA*-HA, ARTD10-BirA*-HA and ARTD10-GW-BirA*-HA were immunoprecipitated from HEK293 cells using HA-specific antibodies. Subsequently the IPs were incubated in the presence or absence of radioactively labelled NAD⁺. The resulting autoradiograms demonstrated auto-modification of ARTD10-BirA*-HA in the presence of NAD⁺, while the other samples did not show a signal for MARYlation (**Figure 61b**). Taken together, the integrity of the BirA* fusion proteins could be validated and hence assessment of their interactome was pursued in the following.

HEK293 cells were transiently transfected with plasmids encoding either BirA*-HA, ARTD10-BirA*-HA or inactive ARTD10-GW-BirA*-HA and subsequently incubated in the presence or absence of biotin (**Supplementary Figure S65d**). Following stringent lysis, the biotinylated proteins were immunoprecipitated using streptavidin beads. After extensive washing steps, the beads were eluted with biotin saturated SDS loading buffer at 95°C, subjected to SDS-PAGE and afterwards gel fragments were prepared for MS analysis (for a control immunoblot see **Supplementary Figure S67**).

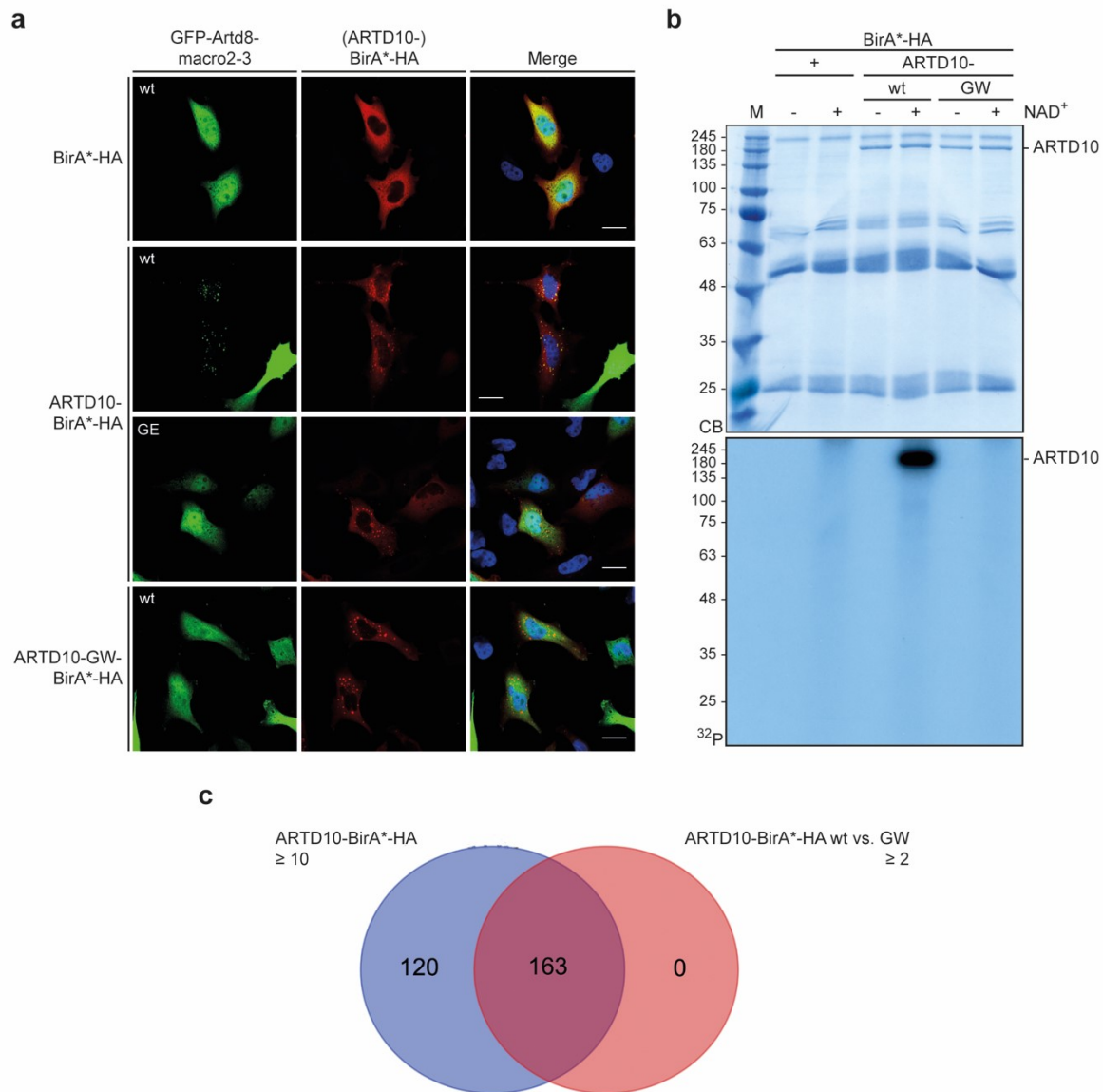


Figure 61: Characterization of the ARTD10-BirA*-HA construct and its interactors.

(a) HeLa cells were transiently transfected with plasmids encoding BirA*-HA alone or ARTD10-BirA*-HA, wt or inactive GW mutant, in combination with GFP-Artd8-macro2-3, wt or binding-deficient GW mutant, as indicated. Forty-eight h after transfection the cells were fixed with PFA and stained with HA-specific antibodies (Covance). GFP-Artd8-macro2-3 and ARTD10 localization were analyzed using confocal microscopy. GFP-fusion proteins are shown in green while BirA*-HA-fusions are red. The nuclei were stained with Hoechst and are shown in blue. Scale bar: 20 μ m ($n = 1$, SK_C_33, I performed this experiment). **(b)** HEK293 cells were transiently transfected with plasmids encoding BirA*-HA alone or ARTD10-BirA*-HA, wt or inactive GW mutant. Forty-eight h after transfection the cells were lysed and the BirA*-fusion proteins were immunoprecipitated using HA-specific antibodies (Covance). Subsequently the IPs were incubated in the presence or absence of radioactively labelled ³²P-NAD⁺ as indicated at 30°C for 30 min. Total proteins were stained with Coomassie blue (CB) and the incorporated label was analyzed by autoradiography (³²P) ($n = 1$, SK_C_33, I performed this experiment). **(c)** Venn diagram of interactors of ARTD10-BirA*-HA identified by MS. HEK293 cells were transiently transfected with plasmids encoding BirA*-HA alone or ARTD10-BirA*-HA, wt or inactive GW mutant. Subsequently the cells were incubated in the presence or absence of biotin for 16 h, lysed and biotinylated proteins were immunoprecipitated with streptavidin beads before MS analysis. Depicted are the number of unique proteins biotinylated by ARTD10-BirA*-HA ($n = 1$, enrichment ≥ 10 vs. BirA* control and ≥ 5 vs. absence of biotin, SK_B_21) and the overlap with proteins that are enriched for wt ARTD10 compared to the inactive GW mutant and normalized to the amount of ARTD10 ($n = 1$, enrichment ≥ 2 vs. GW, ≥ 10 vs. BirA* control and ≥ 5 vs. absence of biotin, SK_B_21). I performed the experiments until MS analysis. The mass spectrometry measurements and initial data analysis with MaxQuant were performed by Christian Preisinger. Further analysis was performed by me.

Next, Christian Preisinger performed LC-MS/MS measurements of the samples and applied primary filter steps (Cox et al. 2014; Tyanova et al. 2016). To identify bona fide interactors of ARTD10, the intensities were analyzed for their relative enrichment compared to control

samples for each protein. Accordingly, proteins that were enriched 10 fold or higher compared to the BirA*-HA control and 5 fold or higher compared to ARTD10-BirA*-HA without biotin treatment were included in the interactome ARTD10 (**Figure 61c**). Furthermore, the relative enrichment of proteins identified for ARTD10 was assessed compared to the inactive GW mutant. Intensities that were 2 fold or higher increased in the wt measurements compared to the GW mutant, when normalized to the amount of ARTD10 itself, were considered to be dependent on MAR transferase activity (**Figure 61c** and **Table 2**). This is the case for around half of the interactors of ARTD10 identified by BioID. The top ten of these wt enriched proteins were further subjected to scoring in the CRAPome contaminant repository (**Table 2**). Apart from KRT6A and KRT77 the hits were only rarely found in other MS screens.

Table 2: Overview of the top 10 proteins enriched for ARTD10-BirA*-HA wt compared to the inactive GW mutant

Protein name	Gene ID	Enrichment fold	LFQ ratio		CRAPome
			vs. Control	vs. -biotin	
Keratin, type II cytoskeletal 6A	KRT6A	8241493.81	6922500.00	6.67	283 / 411
Rab11 family-interacting protein 2	RAB11FIP2	5219196.06	4383900.00	4383900.00	11 / 411
Poly(ADP-ribose) glycohydrolase	PARG	4692026.18	3941100.00	3941100.00	7 / 411
Calmodulin-regulated spectrin-associated protein 1	CAMSAP1	4586425.53	3852400.00	3852400.00	16 / 411
Kinesin light chain 4	KLC4	3358267.35	2820800.00	2820800.00	13 / 411
Keratin, type II cytoskeletal 1b	KRT77	2697519.20	2265800.00	2265800.00	325 / 411
Ras-related C3 botulinum toxin substrate 1	RAC1	1688538.92	1418300.00	1418300.00	15 / 411
Metastasis-associated protein MTA1	MTA1	1451860.12	1219500.00	1219500.00	53 / 411
Uncharacterized protein C20orf194	C20orf194	634294.41	532780.00	532780.00	n/a
Segment polarity protein dishevelled homolog DVL-1	DVL1	633913.44	532460.00	532460.00	18 / 411

Of note, due to deterioration of one sample, only one out of two biological replicates of the experiment could be evaluated. Hence, the BioID will have to be repeated to acquire more reliable results. However, the dataset will be used in the following for comparison with the other MS screens, since only overlaps with reproduced proteins will be incorporated. Therefore, presuming critical review, the BioID for ARTD10 may still provide valuable information to restrict the macrodomain-dependent nsP3 interactome and to characterize common substrates.

The dataset generated by BioID was complemented with an affinity purification approach for ARTD10. As establishment of a TAP system for ARTD10 was unsuccessful in the past, a GFP-Trap was established instead. Therefore, GFP-ARTD10 and inactive GFP-ARTD10-GW were transiently expressed in HEK293 cells. Comparable to the TAP system, the GFP-tag served as a negative control. In addition, all GFP constructs were treated with IFN α , to potentially be able to enrich for binding partners that are important in the context of viral infection. Forty-eight h after transfection and IFN α treatment for 24 h, the cells were lysed and the GFP-fusion proteins were immunoprecipitated using GFP-Trap (**Supplementary Figure S65c**). The enriched proteins were prepared for and subjected to LC-MS/MS measurement performed by Christian Preisinger following primary filter steps (Cox et al. 2014; Tyanova et al. 2016).

Subsequently the label-free quantification (LFQ) intensities were evaluated for their relative enrichment compared to the GFP control, separately for interferon treated and untreated cells. Proteins with a relative enrichment of 5 fold or higher were considered ARTD10 interactors (**Figure 62**).

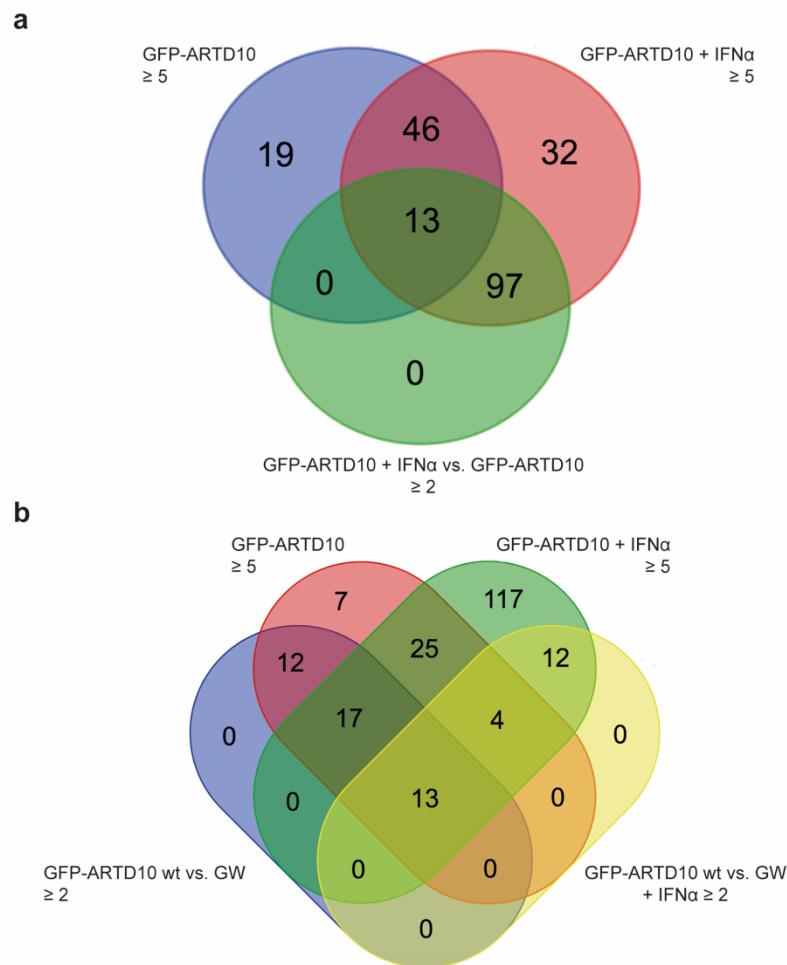


Figure 62: Investigation of ARTD10 binding partners dependent on interferon α and catalytic activity via GFP-Trap and MS. (a,b) HEK293 cells were transiently transfected with plasmids encoding GFP, GFP-ARTD10 or GFP-ARTD10-GW. Twenty-four h after transfection the cells were treated with 180 U/ml of IFN α for 24 h and subsequently the cells were lysed and the GFP-fusion proteins were immunoprecipitated using GFP-Trap (Chromotek). Co-immunoprecipitated interactors were analyzed by MS analysis ($n = 3$, SK_B_48). I performed the experiments until MS analysis. The mass spectrometry measurements and initial data analysis with MaxQuant were performed by Christian Preisinger. Further analysis was performed by me. **(a)** Venn diagram of the binding partners of GFP-ARTD10 identified by MS analysis with a focus on the influence of IFN α treatment. Depicted are the number of unique proteins co-purified with GFP-ARTD10 in the presence or absence of IFN α ($n = 3$, enrichment ≥ 5 vs. GFP control), their overlap and the overlap with proteins that are enriched for IFN treated compared to untreated cells and normalized to the amount of ARTD10 ($n = 3$, enrichment ≥ 2 vs. untreated, ≥ 5 vs. GFP control). **(b)** Venn diagram of the binding partners of GFP-ARTD10 identified by MS analysis with a focus on the influence of catalytic activity. Depicted are the number of unique proteins co-purified with GFP-ARTD10 in the presence or absence of IFN α ($n = 3$, enrichment ≥ 5 vs. GFP control), their overlap and the overlap with proteins that are enriched for wt ARTD10 compared to the inactive GW mutant and normalized to the amount of ARTD10 in the presence or absence of IFN α ($n = 3$, enrichment ≥ 2 vs. GW mutant, ≥ 5 vs. GFP control).

After establishing the general binding partners, the influence of IFN α treatment was assessed by evaluating the enrichment fold between the intensities of the interacting proteins of IFN treated versus untreated GFP-ARTD10 screens. As a result 110 proteins were identified that were enriched at least 2 fold (**Figure 62a, Table 3**), with 97 binding partners that were unique for interferon conditions. Closer examination of the 13 proteins that constantly bound to ARTD10 but increased upon induction of an antiviral state revealed low scores for the CRAPome analysis, suggesting reliability of the results (**Table 3**). Interestingly, this set of

proteins contains several ubiquitin-associated enzymes, in line with previous findings placing MARYlation in general and ARTD10 in particular at the interface with ubiquitination (Verheugd et al. 2013; Kleine et al. 2012). This suggested once more a crosstalk between these two modifications that needs to be further addressed in future experiments. Potentially ARTD10-mediated MARYlation might regulate ubiquitination and thus degradation of proviral or viral proteins as suggested for ARTD12 and ZIKA virus (Li et al. 2018). Even though it was not enriched for a certain condition, RPS27A aka ubiquitin itself was also detected in the ARTD10 interactome. In previous studies ubiquitin has been identified as the only measurable interactor in the ARTD10 inducible HeLa cells (H. Kleine and M. Nielsen, personal communication) and it has been shown to be ADP-ribosylated in cells (Higashi et al. 2019). The fact that ARTD10 possesses N-terminal ubiquitin interacting motifs (UIMs), extends the evidence for a broader relevance of an interaction between MAR and ubiquitin. Furthermore, DTX3L and ARTD9 (aka PARP9) were identified in this set of proteins. These two proteins were previously described to form a complex that renders the otherwise inactive ARTD9 able to MARYlate. Moreover, they are associated with antiviral activity, inflammation and STAT signaling (Bachmann et al. 2014; Higashi et al. 2019; Iwata et al. 2016; Juszczynski et al. 2006; Yang et al. 2017; Zhang et al. 2015).

Table 3: Overview of the interferon-enriched binding partners of GFP-ARTD10 that were identified by MS in the presence and absence of IFN α .

Protein name	Gene ID	Enrichment fold	LFQ ratio	CRAPome
E3 ubiquitin-protein ligase DTX3L	DTX3L	5.58	5749916.67	4 / 411
V-type proton ATPase subunit B, brain isoform	ATP6V1B2	5.25	1006780.00	40 / 411
Poly [ADP-ribose] polymerase 9	PARP9	5.13	3683066.67	1 / 411
Promyelocytic leukemia protein	PML	4.65	376621.67	9 / 411
Probable E3 ubiquitin-protein ligase HERC1	HERC1	3.97	5041833.33	1 / 411
DDB1- and CUL4-associated factor 8	DCAF8	3.41	391880.00	5 / 411
Transcription elongation factor B polypeptide 2	TCEB2	3.23	315865.00	18 / 411
Nucleoporin Nup43	NUP43	2.72	5.41	21 / 411
RING finger protein 166	RNF166	2.57	397653.33	0 / 411
Ragulator complex protein LAMTOR1	LAMTOR1	2.57	10.30	4 / 411
Single-stranded DNA-binding protein 3	SSBP3	2.29	725813.33	0 / 411
Ribosomal RNA processing protein 36 homolog	RRP36	2.28	420316.67	4 / 411
Macrophage migration inhibitory factor	MIF	2.09	16.24	49 / 411

In addition to interferon-dependence, the reliance on catalytic activity of ARTD10 was investigated for the identified binding partners (**Figure 62b, Table 4**). Consequently, the relative enrichment compared to the GFP-ARTD10-GW samples was assessed, separately for interferon-treated and –untreated conditions, and proteins with a score of 2-fold or higher normalized to the amount of ARTD10 were included in the list of wt enriched proteins. Taken together, the association of 58 binding partners was increased when ARTD10 was able to MARYlate, including 13 proteins that were mutual for the absence and presence of IFN signaling (**Figure 62b, Table 4**). Analysis of the CRAPome score of these 13 interactors revealed

reasonably low values with 107 out of 411 experiments with the highest value for 3-hydroxyacyl-CoA dehydrogenase type-2 (HSD17B10), a mainly mitochondrial protein. It is discussed to have dehydrogenase independent functions apart of mitochondrial ribonuclease P complex that regulates mitochondrial integrity and apoptosis (Oerum et al. 2018; Yang et al. 2005). Although this interaction seems improbable, it might be worth further investigation as ARTD10 has been linked to mitochondrial function in the past (Marton et al. 2018). Additionally, this subset contains once more several ubiquitin associated proteins including the DTX3L/ARTD9 complex and RNF114. In line with this, RNF114 has recently been described to interact with ARTD10 dependent on auto-modification and is suggested to boost ARTD10 activity by transferring K27-linked poly-ubiquitination on ARTD10 (Yahui et al. 2020). This interaction might additionally be interesting to investigate in the future, since RNF114 has been described to inhibit swine fever as well as porcine reproductive and respiratory syndrome virus replication and regulate NF- κ B signaling (Lin et al. 2018; Rodriguez et al. 2014; Zhang et al. 2019b; Bai et al. 2020). Furthermore, MAGED2, that was identified as a macrodomain-dependent nsP3 interactor as well, was identified as a binding partner of ARTD10 dependent on catalytic activity (**Table 4**). This interaction was initially confirmed in a bachelor thesis (Krut 2018).

Table 4: Overview of the wt-enriched binding partners of GFP-ARTD10 that were identified by MS in the presence and absence of IFN α .

Protein name	Gene ID	Enrichment fold	LFQ ratio	CRAPome
RING finger protein 114	RNF114	8666485.57	17377833.33	3 / 411
3-hydroxyacyl-CoA dehydrogenase type-2	HSD17B10	4184993.16	8391650.00	107 / 411
Melanoma-associated antigen D2	MAGED2	1183902.42	2373933.33	43 / 411
Probable E3 ubiquitin-protein ligase DTX2	DTX2	901483.40	1807633.33	0 / 411
Probable E3 ubiquitin-protein ligase HERC1	HERC1	729071.31	1461916.67	1 / 411
Opioid growth factor receptor	OGFR	665160.06	1333763.33	5 / 411
Prostate tumor-overexpressed gene 1 protein	PTOV1	597340.60	1197773.33	0 / 411
E3 ubiquitin-protein ligase DTX3L	DTX3L	591327.82	1185716.67	4 / 411
Poly [ADP-ribose] polymerase 9	PARP9	412341.09	826816.67	1 / 411
V-type proton ATPase catalytic subunit A	ATP6V1A	186060.10	373083.33	62 / 411
V-type proton ATPase subunit B, brain isoform	ATP6V1B2	110006.94	220583.33	40 / 411
CREB-binding protein	CREBBP	3.50	6187350.00	2 / 411
Calcyclin-binding protein	CACYBP	2.09	1538733.33	67 / 411

So far there is little known about regulation, localization, and substrate-specificity of ARTD10. Although interferon has been described to drive ARTD10 expression (Atasheva et al. 2012; Ecker et al. 2017), the functional consequences for catalytic activity or binding partners remain elusive. While the ARylation levels of ARTD8 and ARTD9 increased upon IFN γ treatment in macrophages, it was detectable but not altered for ARTD10 (Higashi et al. 2019). This data now suggests a potential shift in interactors upon induction of the antiviral state that will need to be addressed in future experiments. Also, the BioID and GFP-Trap studies together might finally resolve the nature of the ARTD10 foci in cells. So far it has been established that they are neither classical P-bodies nor stress granules (SGs) but that they can contain

glyceraldehyde-3-phosphate dehydrogenase (GAPDH), the ubiquitin receptor p62 and ubiquitin itself (Kleine et al. 2012; Mayo et al. 2018). Strikingly, GAPDH is enriched for the catalytically active ARTD10 in the BioID as well as the GFP-Trap. Also, ubiquitin (aka RPS27A) was identified in both screens although the interaction was not influenced by different conditions. Immunofluorescence imaging showed that even though the ARTD10-GW mutant still localized to cytoplasmic foci, they appeared bigger and structurally different (**Figure 24b**, **Figure 61a**). Further evaluation of the wt-enriched proteins might shed light on this enigmatic feature of ARTD10.

2.3.3 Identification of common, cellular interactors of ARTD10 and nsP3

Although all interactomes contained distinct interactors that have the potential to identify new functions of ARTD10 and host factors for nsP3, the aim of this thesis was to find common interactors and possibly substrates of ARTD10 and the CHIKV macrodomain. Therefore, instead of validating the isolated proteomes, the focus of this chapter will lay on the intersection of all screens. Hence, the macrodomain-dependent interactors of nsP3 were compared with both ARTD10 screens, containing all identified proteins independent of enrichment. The results are depicted in a Venn diagram stating the number of unique proteins, that are shared or exclusive for each of the datasets (**Figure 63a**). To incorporate the enrichment information, the number of enriched proteins and the nature of the enrichment are depicted for each intersection, with the wt enrichment derived from the BioID and the GFP-Trap and the IFN α enrichment resulting only from the GFP-Trap of ARTD10 (**Figure 63a**). All datasets have a fair amount of unique proteins. This might be on the one hand rooted in the different principles of the techniques used. Furthermore, nsP3 as well as ARTD10 are expected to have interactions that are independent of each other. However, there were also overlapping interactors. Among these were two proteins that are found in all three groups, namely Programmed cell death protein 5 (PDCD5) and Cirhin (aka CIRH1A or UTP4). They were also enriched for wt ARTD10 or IFN α , respectively (**Figure 63a**, **Table 5**). PDCD5 is associated with the regulation of apoptosis and inflammation and its expression negatively correlates with multiple types of cancer. Its functions are for instance regulated by NF- κ B signaling that is in turn described to be regulated by ARTD10 through NEMO and plays a role in inflammation (Li et al. 2016b; Wang et al. 2016a; Verheugd et al. 2013). Cirhin, a ribosomal protein, is less well studied. It is associated with proliferation of colorectal cancer cells, it positively regulates NF- κ B signaling and it is part of the small subunit (SSU) processome that is responsible for rRNA processing and assembly and integrity of the SSU of eukaryotic ribosomes (Guo et al. 2017; Wada et al. 2014; Wilkins et al. 2013; Yu et al. 2009). What further supports the relevance of Cirhin and the SSU processome is the fact that other complex members were likewise identified in the overlap between the ARTD10 and the CHIKV interactomes and enriched upon interferon treatment, including WD repeat-containing proteins 43 and 46 (WDR43/46) (**Table 5**)(Wada et al. 2014). Therefore, it will be interesting to study PDCD5 as well as Cirhin in future experiments to validate the interaction and to test them as substrates of (de-)MARylation *in vitro* and in cells. Apart from these two proteins, there was also an overlap of 15 proteins exclusively between the GFP-Trap of ARTD10 and the macrodomain-dependent interactome of nsP3 (**Figure 63a**). Interestingly, the majority of these proteins was enriched for wt ARTD10 and/or interferon treatment (**Table 5**), indicating that these might be substrates of ARTD10 relevant for the virus, which are antagonized by the viral macrodomain. This hypothesis will have to be tested in future ADP-ribosylation and hydrolase assays. The CHIKV interactome shares the highest overlap with the BioID of ARTD10 including 119 proteins

with most of them enriched for active ARTD10, pointing towards a bias for MARYlation (**Figure 63a, Table 5**). There is also an overlap exclusive for the two independent ARTD10 screens that will be neglected in the following, because it does not suggest a relevance for CHIKV infection.

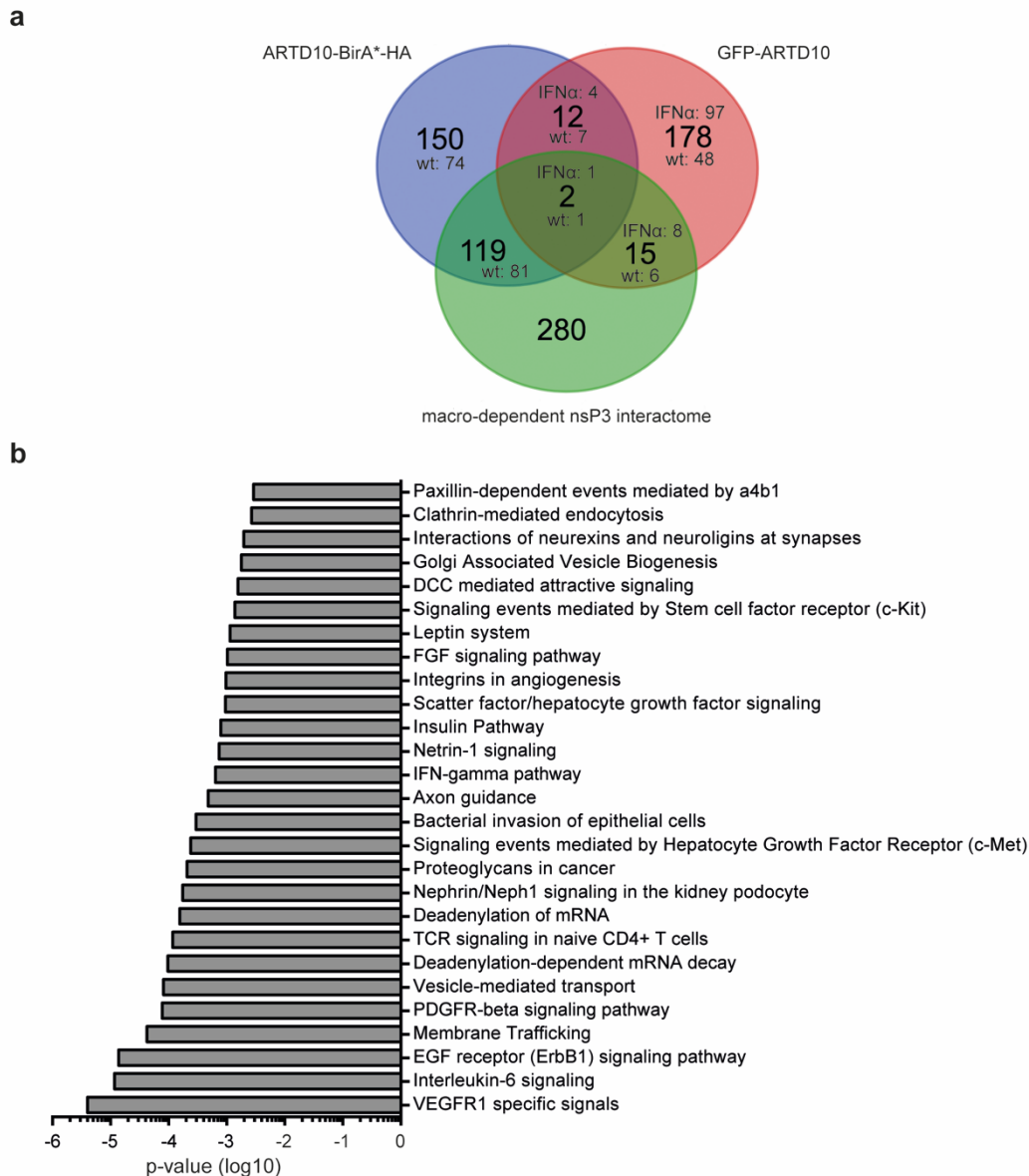


Figure 63: Identification of common interactors of ARTD10 and CHIKV nsP3 in four independent MS approaches.

(a) Venn diagram of the interactors of ARTD10-BirA*-HA and GFP-ARTD10 together with overlap between nsP3 and nsP3 macrodomain derived from the TAP and BioID methods identified by MS analysis. Depicted are the number of unique proteins for each setup as well as their overlaps. Furthermore, the amounts of IFN α - or wt-enriched proteins within each intersection are displayed, that were identified in the GFP-Trap or BioID experiments of ARTD10. I performed this analysis. **(b)** Proteins that were enriched for wt-ARTD10 in the GFP-Trap and/or the BioID approach that were also identified as interactors of nsP3 and the nsP3 macrodomain were analyzed for statistical overrepresentation of certain pathways by gene enrichment analysis using the ToppFun application from the ToppGene Suite (Reference list: Homo sapiens; ToppGene Build Information: 2020-Jun-11 18:03 / #25 / fda0c76b4231e1b5533a2568a14cff7286a5d88) with regard to Pathways (Chen et al. 2009). Depicted are selected Pathways with a p -value ≤ 0.05 using the probability density function method. I performed this analysis.

To obtain an impression of the processes potentially oppositely regulated by (de-)MARYlation of ARTD10 and the nsP3 macrodomain, the 88 wt-enriched proteins shared between at least one ARTD10 screens and the macrodomain-dependent nsP3 interactome were subjected to statistical Pathway enrichment analysis using the ToppFun application from the ToppGene Suite (Reference list: Homo sapiens; ToppGene Build Information: 2020-Jun-11 18:03 / #25 /

fda0c76b4231e1b5533a2568a14cfff7286a5d88) (**Figure 63b**). This examination revealed several pathways that are associated with inflammation and infection like “interleukin-6 signaling”, “TCR signaling in naïve CD4⁺ T cells”, “Bacterial invasion of epithelial cells” and “IFN-gamma pathway” containing proteins like PTPN11, CBL, STAT3, NCK1, DBNL, SEPTIN9, CD2AP and CTTN. These might be interesting to investigate as substrates, because their regulation by MARYlation could influence inflammation during CHIKV infection. Furthermore, there were several terms involved in RNA regulation and vesicle biology that might be relevant for viral genome replication and virus entry and shedding from the cell. Moreover, there were several pathways included that relate to signaling in the liver. These might be worth assessing, because NF- κ B signaling in general and NEMO in particular have been linked to liver homeostasis. Their inhibition results in spontaneous liver damage, fibrosis and carcinogenesis (Luedde et al. 2007; Liedtke et al. 2012; Hsin et al. 2016; Kondylis et al. 2017) (**Figure 63b**).

The 81 proteins found by wt -enriched ARTD10 BioID and the nsP3 interactome were grouped using the STRING Database (Version 11.0, Organism: Homo sapiens) and *k* means clustering (Szkarczyk et al. 2019). This revealed, among other clusters, two sets of interactors à 16 and 5 proteins (**Table 5**). These clustered together because they interacted or were part of the same protein network. This increases the chance of their relevance in comparison to hits that do not show connections to any other proteins identified in the screen. To decide which proteins from this intersection to focus on might be particularly interesting, because the wt-enriched ARTD10-BirA*-HA interactors have the highest probability to be MARYlated. In addition to the proteins that have already been highlighted through the Pathway analysis, this clustering approach also spotlighted for example G3BP1.

Table 5: Overview of selected, common interactors of CHIKV nsP3 and ARTD10 identified by MS analysis.

Protein name	Gene ID	nsP3 overlap	ARTD10		Enrichment type	CRAPome
			GFP-	-BirA*		
Programmed cell death protein 5	PDCD5	+	+	+	wt	68 / 411
Cirhin	CIRH1A	+	+	+	IFN α	15 / 411
Single-stranded DNA-binding protein 3	SSBP3	+	+		wt & IFN α	0 / 411
Nuclear pore complex protein Nup153	NUP153	+	+		wt & IFN α	48 / 411
U4/U6 small nuclear ribonucleoprotein Prp3	PRPF3	+	+		wt & IFN α	59 / 411
Replication protein A 70 kDa DNA-binding subunit	RPA1	+	+		wt	84 / 411
RNA-binding protein 27	RBM27	+	+		wt	62 / 411
Melanoma-associated antigen D2	MAGED2	+	+		wt	43 / 411
WD repeat-containing protein 46	WDR46	+	+		IFN α	5 / 411
WD repeat-containing protein 43	WDR43	+	+		IFN α	27 / 411
Transcription factor 20	TCF20	+	+		IFN α	29 / 411
Protein Red	IK	+	+		IFN α	53 / 411
Nuclear pore complex protein Nup50	NUP50	+	+		IFN α	38 / 411
E3 ubiquitin-protein ligase CBL	CBL	+		+	wt/cluster 1	2 / 411
Signal transducer and activator of transcription 3	STAT3	+		+	wt/cluster 1	36 / 411

Tight junction protein ZO-1	TJP1	+		+	wt/cluster 1	35 / 411
Drebrin	DBN1	+		+	wt/cluster 1	87 / 411
Cytoplasmic protein NCK1	NCK1	+		+	wt/cluster 1	5 / 411
Sorting nexin-9	SNX9	+		+	wt/cluster 1	12 / 411
Src substrate cortactin	CTTN	+		+	wt/cluster 1	73 / 411
CD2-associated protein	CD2AP	+		+	wt/cluster 1	33 / 411
Caldesmon	CALD1	+		+	wt/cluster 1	55 / 411
Epidermal growth factor receptor substrate 15-like 1	EPS15L1	+		+	wt/cluster 1	27 / 411
Tyrosine-protein phosphatase non-receptor type 11	PTPN11	+		+	wt/cluster 1	41 / 411
Ankyrin-2	ANK2	+		+	wt/cluster 1	14 / 411
Zyxin	ZYX	+		+	wt/cluster 1	67 / 411
Coronin-1B	CORO1B	+		+	wt/cluster 1	38 / 411
Drebrin-like protein	DBNL	+		+	wt/cluster 1	37 / 411
Palladin	PALLD	+		+	wt/cluster 1	23 / 411
Polyadenylate-binding protein-interacting protein 1	PAIP1	+		+	wt/cluster 2	7 / 411
Eukaryotic translation initiation factor 4B	EIF4B	+		+	wt/cluster 2	167 / 411
Eukaryotic translation initiation factor 5	EIF5	+		+	wt/cluster 2	40 / 411
Ras GTPase-activating protein-binding protein 1	G3BP1	+		+	wt/cluster 2	141 / 411
182 kDa tankyrase-1-binding protein	TNKS1BP1	+		+	wt/cluster 2	25 / 411

As G3BP1 was not only identified in the macrodomain-associated nsP3 interactome, but also interacted preferentially with catalytically active ARTD10-BirA*-HA (**Table 5**), G3BP1 was analyzed more closely (**Figure 64**). In previous studies, the SG associated G3BP1 has already been described to be essential for CHIKV replication in combination with the closely related G3BP2 (Kim et al. 2016b). Interestingly, these proteins, jointly referred to as G3BP, are described to have proviral as well as antiviral roles depending on the virus. Originally, G3BP was identified as part of the cellular stress response to viral infection and essential for SG assembly (Tourriere et al. 2003; Kedersha et al. 2016). However, many viruses have evolved to modulate and exploit the immune response. CHIKV nsP3 for instance recruits G3BP to cytosolic foci and thus blocks SG formation and even hijacks G3BP functions for translation of the viral genome (Fros et al. 2012). This recruitment was clearly visible in immunofluorescence studies. Upon overexpression of Flag-nsP3 in U2OS cells the endogenous G3BP showed a dot-like localization in the cytoplasm while the signal was diffuse in the absence of nsP3 (**Figure 64a**). That fact that G3BP1 was not only associated with the full-length nsP3 but also identified as an interactor of the macrodomain and of ARTD10, enriched for the wt, in the BioID screens, suggested that it might be a mutual substrate. Therefore, His-G3BP1 was bacterially expressed and subjected to *in vitro* ADP-ribosylation assays in the presence of radioactively labelled NAD⁺ and GST-ARTD10cat (**Figure 64b**). The inactive GST-ARTD10-GW mutant was included as a control. Strikingly, the autoradiogram revealed that G3BP1 was efficiently MARYlated. To explore whether G3BP1 was in fact a mutual substrate, recombinant His-nsP3 was likewise included. Importantly, MARYlated G3BP1 was substrate to the viral macrodomain (**Figure**

64b). Hence, this assay did not only characterize G3BP1 as a good substrate of ARTD10 and of nsP3, but it also suggested specificity for the viral macrodomain towards the SG component. Based on these findings, the question arises whether MARYlation also effects G3BP1 in cells. Initially, the influence of ARTD10 co-expression on nsP3-dependent recruitment of G3BP1 to mutual condensates was assessed. U2OS cells were transiently transfected with plasmids encoding GFP-G3BP1 and mCherry-nsP3 in the presence or absence of HA-ARTD10. Confocal microscopy demonstrated that nsP3 and G3BP1 efficiently co-localized in cytoplasmic foci independently of ARTD10 (**Figure 64c**). To expand on this, the localization of ARTD10 in relation to G3BP was analyzed. In this case, Flag-nsP3 was expressed to convey G3BP recruitment to foci and GFP-ARTD10 was co-expressed. Furthermore, endogenous G3BP, G3BP1 and G3BP2, was stained to study co-localization with ARTD10. While ARTD10 and G3BP did not seem to co-localize per se, the ARTD10 foci frequently depicted close proximity to the G3BP/nsP3 dots (**Figure 64d**). However, this initial experiment did not reveal any obvious effects. Still, this did not discard a potential role of G3BP1 MARYlation for CHIKV replication. As these experiments were exclusively conducted with plasmid-based expression, a drawback is the lack of the replicon context. For nsP2 it was already demonstrated that MARYlation depended on the transfection of replicon RNA (**Figure 49**). This might be relevant for induction of an antiviral state in the cell that potentially shifts the substrate specificity of the transferases or to recruit mono-ARTDs to the viral RNA via RNA recognition motifs (RRMs). Hence, the effect of ARTD10 co-expression on G3BP1 or G3BP localization should be reevaluated in the presence of CHIKV replicon RNA, also with a macrodomain mutant replicon. Meanwhile MARYlation of G3BP1 needs to be confirmed in cells. As G3BP1 is only essential for CHIKV replication in combination with G3BP2 (Kim et al. 2016b), it is of note that a recent master thesis also identified G3BP2 as a substrate of (de-)MARYlation *in vitro* (Kaesler 2020). These results likewise need to be corroborated with studies in cells.

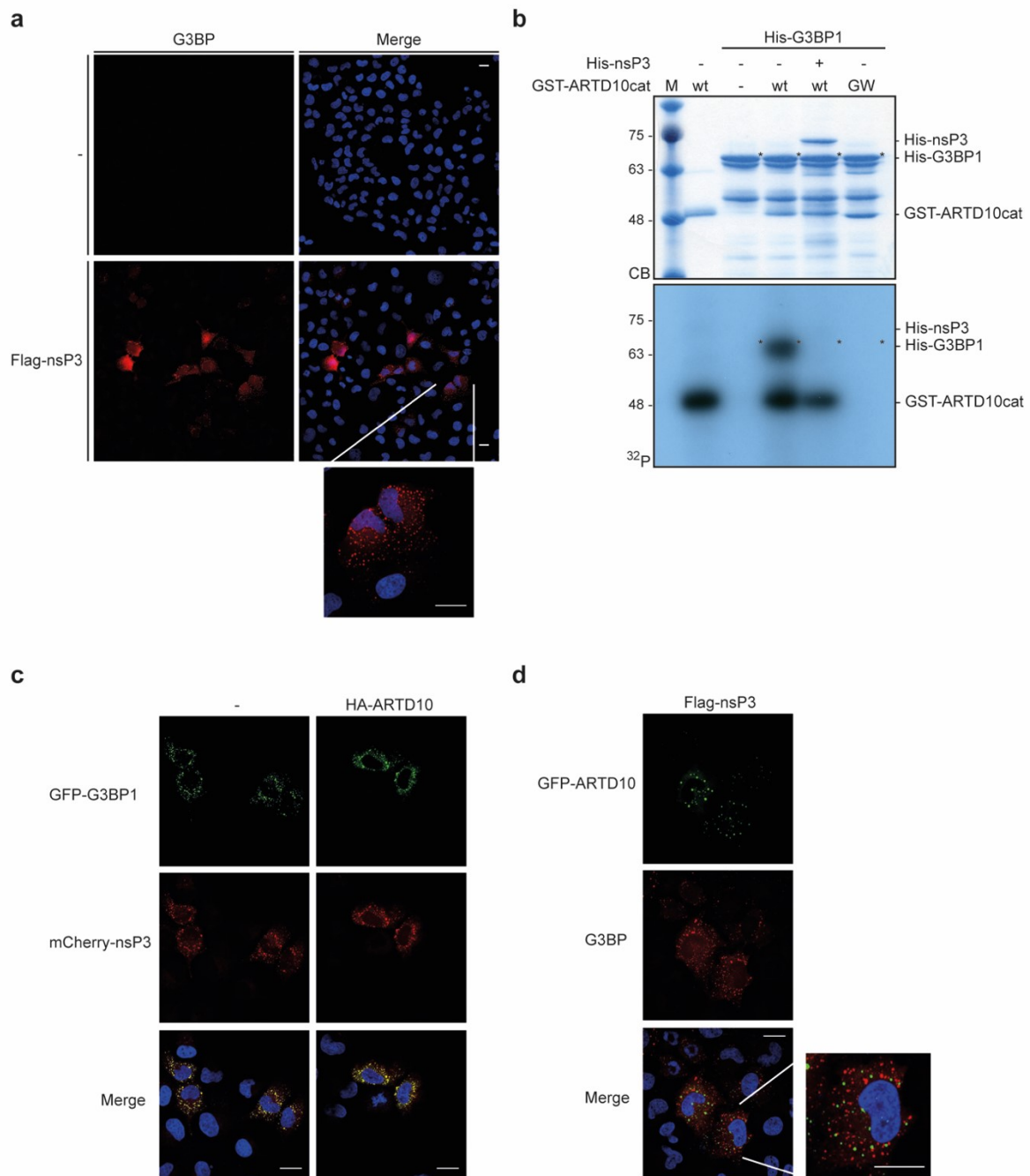


Figure 64: G3BP1 is a substrate of ARTD10-mediated MARYlation *in vitro* reversed by nsP3.

(a) U2OS cells were transiently transfected with plasmids encoding Flag-nsP3 as indicated. Forty-eight h after transfection the cells were fixed with PFA and endogenous pan G3BP (comprising G3BP1 and G3BP2) was stained with specific antibodies (BD). G3BP localization was analyzed using confocal microscopy. G3BP is red while the nuclei were stained with Hoechst and are shown in blue. Scale bar: 20 μm ($n = 1$, SK_C_46, I performed this experiment). **(b)** Bacterially expressed, His₆-tagged G3BP1 was incubated with GST-ARTD10cat, wt or inactive GW mutant, as indicated in the presence of radioactively labelled ³²P-NAD⁺ for 30 min at 30°C to allow auto- as well as substrate-modification. Furthermore, bacterially expressed, His₆-tagged full-length nsP3 was co-incubated as indicated ($n = 1$, SK_C_45, I performed this experiment). Total proteins were stained with Coomassie blue (CB) and the incorporated radioactive label was analyzed using autoradiography (³²P). **(c)** U2OS cells were transiently transfected with plasmids encoding GFP-G3BP1 and mCherry-nsP3 with or without HA-ARTD10 as indicated. Forty-eight h after transfection the cells were fixed with PFA. G3BP1 and nsP3 localization were analyzed using confocal microscopy. GFP-G3BP1 is shown in green while mCherry-nsP3 is red. The nuclei were stained with Hoechst and are shown in blue. Scale bar: 20 μm ($n = 1$, SK_C_46, I performed this experiment). **(d)** U2OS cells were transiently transfected with plasmids encoding GFP-ARTD10 and Flag-nsP3 with or without HA-ARTD10 as indicated. Forty-eight h after transfection the cells were fixed with PFA and endogenous pan G3BP (comprising G3BP1 and G3BP2) was stained with specific antibodies (BD). ARTD10 and G3BP localization were analyzed using confocal microscopy. GFP-ARTD10 is shown in green while G3BP is red. The nuclei were stained with Hoechst and are shown in blue. Scale bar: 20 μm ($n = 1$, SK_C_46, I performed this experiment).

If intracellular MARYlation of G3BP can be confirmed, it will be interesting to define the sites of modification because the recruitment to nsP3 foci is not the only imaginable function that might be affected. Both G3BP proteins are highly conserved and comprise several domains. The N-terminal NTF2-domain interacts with the double FGDF motif in nsP3 and the viral replication complex (Panas et al. 2015; Schulte et al. 2016). However a different domain, the arginine glycine rich RGG motif, is responsible for the recruitment of the host translation machinery that translates the viral genome (Gotte et al. 2019). Furthermore, G3BP is suggested to play a role in the switch from genome translation to replication of the negative sense RNA, by clearing the viral genome from translating ribosomes to ensure accessibility for the viral RNA-dependent RNA polymerase nsP4 (Scholte et al. 2015). Depending on the site of modification all of the above mentioned proviral functions might be influenced and it would be interesting to address different steps in the viral life cycle that might be affected.

Although the results for G3BP1 preliminary, they demonstrated that the employed complementary MS approach can be used to identify novel substrates of MARYlation with relevance for CHIKV replication. The continuous evaluation of additional proteins identified in the screens has a good probability for discovering further mutual substrates of ARTD10 and nsP3. The enrichment studies focusing on active transferase and interferon treatment might further facilitate the determination of relevant proteins.

3 Conclusion and Future Perspectives

The aim of this thesis was to elucidate the function of mono-ADP-ribosylation (MARylation) at the host-pathogen interface with a focus on antiviral immunity, particularly against Chikungunya virus (CHIKV). The interferon inducibility of several mono-ADP-ribosyltransferases, including ARTD10 and ARTD12, suggested that they are part of the cellular innate immune response to viral infection (Atasheva et al. 2012; Atasheva et al. 2014; Eckeï et al. 2017; Krieg et al. 2020). As the name suggests, these enzymes transfer mono-ADP-ribose onto substrate proteins, a modification that is fully reversible (Kleine et al. 2008; Hottiger et al. 2010; Rosenthal et al. 2013; Feijs et al. 2013a). Hydrolysis of MARylation is, among others, associated with the highly conserved macrodomain fold that can be found in all domains of life (Rosenthal et al. 2013; Feijs et al. 2013a; Rack et al. 2016). Additionally, a subset of positive single stranded RNA ((+)ssRNA) viruses encodes macrodomains in their genomes, including alpha-, corona- and orthohepeviruses. Thus far the function of these viral macrodomains remained elusive, it was only known that they can bind free ADP-ribose (ADPr), poly-ADP-ribose (PAR), DNA and RNA *in vitro* and that they possess weak ADP-ribose 1''-phosphohydrolase activity (Egloff et al. 2006; Malet et al. 2009). In this thesis, the macrodomains of several alphaviruses, namely CHIKV, Sindbis virus (SINV), O'nyong'nyong virus (ONNV) and Venezuelan Equine Encephalitis virus (VEEV), an alphacoronavirus, Feline Infectious Peritonitis virus (FIPV), and from two orthohepeviruses, Hepatitis E virus (HEV) strains DA4 and DD12, were characterized as efficient hydrolases of protein MARylation *in vitro*. This activity was shown on a broad range of substrates, comprising ARTD7, ARTD8, ARTD10 and NEMO (Eckeï et al. 2017). Other groups confirmed similar properties and additionally attributed de-MARylation activity to the macrodomains of Severe Acute Respiratory Syndrome coronavirus SARS-CoV and human coronavirus 229E (HCoV-229E) (Li et al. 2016a; Fehr et al. 2016; McPherson et al. 2017). Furthermore, the activity of the viral macrodomains towards PARylation was neglectable, especially in comparison to the PAR-hydrolase PARG and considering the intrinsic instability of protein-linked PAR chains (Eckeï et al. 2017). Moreover, computational analysis facilitated the identification of catalytically essential amino acids and as a result the generation of the inactive CHIKV macrodomain mutants V33E and Y114V. Finally, the findings for the isolated macrodomain were verified with *in vitro* studies of the full-length non-structural protein 3 (nsP3) of CHIKV that contains the macrodomain near its N-terminus. The first chapter of the results, covering the biochemical characterization of the viral macrodomains, concludes with the confirmation that the MAR-hydrolase activity of the CHIKV macrodomain as well as the full-length nsP3 is not restricted to *in vitro* assays but can also be measured on the auto-modification of ARTD10 in cells (Eckeï et al. 2017). This attributes a completely new function to the previously enigmatic nsP3.

Based on the results of the first part, the functional consequences of MARylation for CHIKV replication and the mechanistic relevance of the macrodomain's de-MARylation activity was further investigated in the following chapters. Herein, the cellular mono-ARTDs ARTD10 and ARTD12 were identified as restriction factors for CHIKV replication in overexpression and knockdown experiments with *in vitro* transcribed replicon RNA. Especially for ARTD10 this was dependent on catalytic activity. Introduction of the hydrolase- and DNA-binding deficient V33E and D10A (Malet et al. 2009; McPherson et al. 2017) macrodomain mutants in turn rendered the replicon inactive with regard to replication. Both findings suggested that MARylation inhibits CHIKV replication, which is antagonized by the macrodomain.

Furthermore, it became apparent that this inhibition interferes early in the viral life cycle, affecting production of processed non-structural proteins and genome replication (Krieg et al. 2020). This result was corroborated by other groups that described a correlation between the MAR-hydrolase activity and CHIKV replication. The interference was suggested to affect the genome replication complex assembly and genome replication (McPherson et al. 2017; Abraham et al. 2018). This implicates the CHIKV macrodomain as a potential target for pharmacological intervention. Comparably, mutational inactivation of the macrodomain of HEV also led to a replication deficient virus (Li et al. 2016a). Worldwide, HEV is still the most frequent cause for jaundice and acute hepatitis and can lead to chronic hepatitis in immunosuppressed patients (Pérez-Gracia et al. 2014; Kamar et al. 2014). In contrast, the hydrolase-deficient N1040A macrodomain mutant of SARS-CoV did not influence replication in cell culture. However the lethality in mice was decreased due to an enhanced immune response (Fehr et al. 2016). However, macrodomain mutation of Murine Hepatitis coronavirus (MHV) in combination with ARTD knockdown or inhibition increased the replication of mutant but not wt virus and interferon signaling (Grunewald et al. 2019). Interestingly, the macrodomain of the Middle East Respiratory Syndrome coronavirus (MERS-CoV) and the new SARS-CoV-2, causing COVID-19, were recently described to have MAR-hydrolase activity (Alhammad et al. 2021). The fact that three diseases currently prioritized by the WHO (WHO 2020c) and further pathogens regularly considered for this list (WHO 2018a) rely on MAR-hydrolase activity for replication or more serious disease, attributes a broad application range for specific macrodomain inhibitors in antiviral therapies. However, the evolutionary conservation of this protein fold results in a high sequence similarity between pathogenic macrodomains and the cellular versions thereof complicating the discovery of specific compounds. Nonetheless, recent developments in medium- to high-throughput screening techniques for small molecule inhibitor testing have retrieved the first selective, allosteric inhibitors with low micromolar affinity for macrodomains, namely the macrodomain 2 of ARTD8 (Schuller et al. 2017; Ekblad et al. 2018; Wazir et al. 2021). In combination with evolution of these compounds and analysis of the information with bioinformatics tools like QSAR for structure activity relationship modeling (Cherkasov et al. 2014; Moustakim et al. 2018), the development of specific inhibitors for the viral macrodomains becomes achievable. Interestingly, the treatment with selective inhibitors for macrodomains might possess even broader medical applicability, since several strains of bacteria have been shown to depend on MAR-hydrolysis as part of toxin-antitoxin systems consisting of an ADP-ribosyltransferase and a macrodomain (Rack et al. 2016; Jankevicius et al. 2016; Harms et al. 2016). This system is conserved in a number of bacterial pathogens including *Mycobacterium tuberculosis*, *Klebsiella pneumoniae* and enteropathogenic *Escherichia coli* (EPEC) (Jankevicius et al. 2016; Gldenpfennig 2018).

In the following the mechanistic explanation for the influence of hydrolase deficiency on CHIKV replication is discussed. The defect for the macrodomain mutant replicons could be traced to impaired polyprotein processing that consequentially prevented the assembly of the viral replication complexes, synthesis of the negative strand RNA, replication of the viral genome and translation from the subgenomic promoter. The inhibition of proteolytic cleavage of the polyprotein could be reversed by complementation with a functional macrodomain, either as part of an additional replicon that lacked protease activity or a targeted, exogenous macrodomain. The processing of the polyprotein is executed by the viral protease domain of nsP2, that was identified as a substrate of MARylation *in vitro* and in cells under replicon conditions. This modification could be mediated by several interferon-regulated ARTDs,

namely, ARTD7, ARTD8, ARTD10 and ARTD12, while nsP2 was not a substrate of ARTD15 and the PARYlating ARTD1. Finally, it was demonstrated that ARTD10-mediated MARYlation of nsP2 inhibited its protease activity towards an artificial substrate in a dose-dependent manner, whereas de-MARYlation by the viral macrodomain reversed the effect. This describes the first mechanistic function and substrate of the CHIKV macrodomain (Krieg et al. 2020). However, there are still pieces of the puzzle missing. Application of inhibitors of cellular MARYlation could not rescue the replication defect of the V33E macrodomain mutant replicon. Furthermore, the hydrolase-deficient Y114V mutant, that is still able to bind ADP-ribose, could replicate and process the viral polyprotein. Moreover, there appears to be a time dependence for the restriction of CHIKV replication by ARTD10, with the effect decreasing over time (Krieg et al. 2020). All these facts hint at additional consequences of MARYlation within the viral life cycle and a potential role for binding of ADP-ribose by the viral macrodomain. The first explanation that comes to mind is that other functions of nsP2 apart from polyprotein processing are affected by the modification. A protease activity-dependent function is the downregulation of cellular Ubiquitin-Conjugating Enzyme E2 L3 (UBE2L3). While the function of this degradation is not fully understood, it could function as a readout of nsP2 protease activity and for the effect of MARYlation (Ramphan et al. 2018). Besides the protease domain, nsP2 also features an N-terminal domain that possesses NTPase, RNA triphosphatase and helicase activity (Karpe et al. 2011; Das et al. 2014), and a non-functional S-adenosylmethionine (SAM)-dependent methyltransferase-like (MTL) domain with a potential nuclear localization sequence (NLS) near the C-terminus (Akhrymuk et al. 2012; Fros et al. 2013). Mapping of the sites of modification of nsP2 would allow to draw conclusion about potential effects on other functions of nsP2. Mapping of MARYlation sites by MS is still challenging despite various advances in the field (Luscher et al. 2018). An alternative is to investigate potential functional consequences of MARYlation on the *in vitro* NTPase, RNA triphosphatase and helicase activities of nsP2 in parallel (Das et al. 2014). The helicase domain is necessary for RNA recognition and affects genome replication and infectivity of the virus by unwinding of double stranded RNA (dsRNA) to facilitate the transcription by nsP4 (Law et al. 2019). The helicase and the MTL domain together also regulate the ubiquitin-dependent degradation of the catalytic subunit of RNA polymerase II, Rpb1, to inhibit the antiviral response of the host cell during the first 6 hpi (Akhrymuk et al. 2012). In general, nsP2, especially its C-terminal region, is involved in the modulation of the host innate immune response to CHIKV infection. It is involved in host cell transcriptional and translational shut-off and the cytopathic effect of CHIKV infection. nsP2 also interferes with interferon signaling, largely independent of enzymatic activity but dependent on interactions and nuclear translocation (Bourai et al. 2012; Fros et al. 2013; Fros et al. 2015b; Fros et al. 2016; Bhalla et al. 2016; Akhrymuk et al. 2019; Goertz et al. 2018). Apart from direct effects on enzymatic activities, MARYlation might influence the necessary interactions or the intracellular localization of nsP2 (Luscher et al. 2018), both of which are shown to be essential for its functions. In conclusion, MARYlation of the multifunctional nsP2 protein might have far more implications than a defect in polyprotein processing that could be investigated by indirect readouts for its effects in the absence and presence of MARYlation on Rpb1 abundance, host cell transcription and translation and interferon signaling.

In addition to nsP2, nsP1 and nsP3 were likewise substrates of mono-ARTDs *in vitro*. Again this feature seemed to be exclusive for IFN-regulated mono-ARTDs and the modification was reversed by the hydrolase activity of the CHIKV macrodomain. The MARYlation of nsP1 and nsP3 needs to be confirmed in cells under replicon conditions. nsP1 encodes the RNA capping

enzyme that transfers a 7-methyl-GMP-cap to the 5' end of newly synthesized viral RNA to shield it from recognition by host nucleases (Ahola et al. 1995; Ahola et al. 2016). Hence MARYlation could affect the GTPase or methyltransferase activity of nsP1, which can be tested separately *in vitro* following ADP-ribosylation assays (Tomar et al. 2011; Li et al. 2015a; Bullard-Feibelman et al. 2016; Delang et al. 2016). Furthermore, nsP1 is responsible for anchoring of the replication complex to membranes mediated by its alpha-helical membrane-binding peptide and palmitoylation (Laakkonen et al. 1996; Ahola et al. 1999; Ahola et al. 2000). This membrane association is essential for viral replication and might influence capping activity (Spuul et al. 2007; Ahola et al. 1999), which might be disturbed by MARYlation. This can be studied with the help of *in vitro* model membrane platforms like giant unilamellar vesicles (GUVs), potentially of a defined, favorable composition of lipids, by monitoring the binding of bacterially expressed nsP1 in the presence and absence of MARYlation using confocal microscopy or co-sedimentation and -flotation assays (Sezgin et al. 2012; Zhao et al. 2012; Lorenz et al. 2015; Bhatia et al. 2015). This system might even allow investigation of the membrane association of the replication complex and consequences for viral replication dependent on MARYlation (Kovalev et al. 2020).

Besides the macrodomain and its hydrolase function, nsP3 is best studied for various host factor interactions, for instance with G3BP, mediated by the C-terminal unstructured, hypervariable domain (HVD)(Fros et al. 2012; Panas et al. 2014; Kim et al. 2016b). Many of the described interactions are known to be essential for viral replication, because they e.g. involve recruitment of the translation machinery (Scholte et al. 2015; Schulte et al. 2016; Gotte et al. 2019; Agback et al. 2019; Meertens et al. 2019). Furthermore, nsP3 localizes to cytoplasmic foci that shield the replication complex from unwanted antiviral factors and blocks stress granule assembly while in turn sequestering desired interactors (Fros et al. 2012; Gotte et al. 2018). These crucial interactions might be disturbed by MARYlation of nsP3 as indicated by the co-immunoprecipitation assays with the nsP3 V33E mutant and G3BP from cells. This should be further studied by *in vitro* pull-downs with bacterially expressed nsP3 and interactors in the MARYlated and de-MARYlated state and confirmed in cells.

Apart from enzymatic activities and modulation of host factors, the viral nsPs also possess an intricate network of interactions amongst each other (Rana et al. 2014). Different compositions of the replication complex and gradual processing of the polyprotein govern different steps in the viral life cycle (Rupp et al. 2015). For instance, nsP1 interaction boosts the ATPase activity of nsP2 (Kumar et al. 2018) and association of the nsP2 helicase domain with nsP4 regulates the polymerase activity of nsP4 to prevent nucleotide depletion (Stapleford et al. 2015). These essential interactions are also likely to be influenced by MARYlation, especially since at least three out of four of the nsPs are modified. It is of note, that the influence of MARYlation on the interaction does not necessarily need to be inhibitory, but might also lead to recruitment of nsP3 by binding to the modification and thus be exploited by the virus. This would in turn explain the apparent dual, time-dependent effect of MARYlation on CHIKV replication and would likewise become visible in *in vitro* or in cell pull-down assays using nsP3 wt, the binding-deficient V33E or the binding-active Y114V mutant. So far, CHIKV nsP4 was not tested as a substrate for *in vitro* ADP-ribosylation because its expression in bacteria was unsuccessful due to solubility and stability issues (Rupp et al. 2015; Ahola et al. 2016). Even deletion of the first 97 amino acids, that are proposed to cause degradation, did not yield recombinant protein. However, expression of tagged nsP4 in HEK293 cells was achieved. Therefore, it could be immunoprecipitated from lysates and subsequently subjected to *in vitro* ADP-ribosylation assays or the modification could be immediately evaluated in cells with specific antibodies, potentially under replicon conditions.

In general, the MARYlation of viral proteins appears to be a broader phenomenon that is not restricted to CHIKV. In fact, the structural nucleocapsid protein N of coronaviruses has been described to be ADP-ribosylated; this has been demonstrated for MHV, SARS-CoV and MERS-CoV (Grunewald et al. 2017). Interestingly, this modification was only observed under infection conditions, comparable to the results for nsP2, indicating again that the viral context is necessary to target or activate the mono-ARTDs. However, the transferase responsible for the modification of the protein N remains to be identified. Furthermore, ADP-ribosylation of the N protein was not reversed by the nsP3 macrodomain (Grunewald et al. 2017), even though they were described to interact (Hurst et al. 2013). This supports the hypothesis that the viral macrodomain possess selectivity and did not inevitably remove all MARYlation. Actually, it was demonstrated that the N protein was ADP-ribosylated within virions suggesting that the modification might have a regulatory function (Grunewald et al. 2017). This might be the case for other MAR sites as well and needs to be addressed in the future.

In addition to CoV and CHIKV proteins, recent reports have described the protease subunits PA and PB2 of Influenza A virus and the non-structural NS1 and NS3 proteins of Zika virus as substrates of ADP-ribosylation (Liu et al. 2015; Li et al. 2018). Yet again, the mechanism of regulation is different: For PA and PB2 the association with inactive ARTD13 (aka Zinc finger antiviral protein or ZAPL) and for NS1 and NS3 MARYlation by ARTD12 led to PARYlation, possibly by tankyrases, marking them for ubiquitination and finally proteasomal degradation (Liu et al. 2015; Li et al. 2018). This mode of action for the ARTD-mediated inhibition of CHIKV was excluded, since proteasomal inhibition had no effect.

Lastly, novel findings from our own group suggest that the E7 proteins of several Human Papillomavirus (HPV) strains are substrates for *in vitro* MARYlation by IFN-regulated ARTDs (Eckei-Potthoff 2020). Even though the functional consequences of the modification have not been determined yet, it might explain the induction of apoptosis in HeLa cells upon overexpression of ARTD10 dependent on catalytic activity (Kleine et al. 2008; Herzog et al. 2013). This effect has been used as a tool to identify inhibitors of ARTD10 (Venkannagari et al. 2016; Murthy et al. 2018), but the cause for the induction of apoptosis remains elusive. HeLa cells are HPV transformed cervical cancer cells that still rely on E6 and E7 for maintaining proliferation (Mittal et al. 2017). If MARYlation of E7 by ARTD10 hampered its various functions, mainly mediated by interaction with host proteins, this would explain the phenotype observed in HeLa cells. Until today about 20% of human cancers are caused by pathogens and within these HPV-transformed malignancies comprise around 30%, resulting in about 5% of all cancers (Araldi et al. 2018; Mittal et al. 2017).

These few examples of viral proteins from multiple virus families and classes as substrates of ADP-ribosylation provide evidence for broad implications of this post-translational modification, especially in combination with interferon-regulated mono-ARTDs, in the modulation of viral infections. Interestingly, several mechanistic consequences have been described, antiviral as well as proviral. These propose that the effect of ADP-ribosylation has to be assessed separately for each viral family, potentially even for each viral strain. It is not uncommon though that modifications or pathways have different consequences for different viruses. This concept is already well established, for instance for autophagy or cyclic GMP-AMP synthase (cGAS)/stimulator of interferon genes (STING) pathway, that are initially antiviral but are inhibited or even hijacked in different ways by evolved pathogens (Cong et al. 2020; Eaglesham et al. 2020). Nonetheless, this highlights (mono-)ADP-ribosylation as a promising, new target for extensive antiviral therapies by activation or inhibition depending on the individual virus. It is likely that with more detailed investigation of further pathogens

and ARTD enzymes that are still poorly studied, and through refinement of detection techniques even more mechanisms will come to light.

Besides the viral proteins themselves, it is imaginable that cellular host factors are regulated by ARTD-mediated MARYlation or nsP3-mediated de-MARYlation. Therefore, the third part of this thesis strived at the identification of common intracellular substrates of ARTD10 and the CHIKV macrodomain using complementary approaches. For both, nsP3 as well as ARTD10, affinity purification, TAP (Puig et al. 2001) and GFP Trap, and proximity labelling approaches, BioID (Roux et al. 2012), were used to identify more robust and more transient interactors, respectively. In addition, the constructs and conditions were varied to be able to analyze the enrichment for favored states. For instance, for nsP3 the full-length construct and the isolated macrodomain were employed for the interactome analysis. In the following only proteins that interacted with nsP3 as well as the isolated macrodomain were considered to exclude artefacts of the localization along with binding mediated by C-terminal HVD of nsP3. Similarly, active ARTD10 was compared to the transferase-deficient GW mutant to allow enrichment analysis for interactors that depend on ARTD10-mediated MARYlation. Finally, the effect of interferon α treatment on the ARTD10 interactome was evaluated to mimic an antiviral state in the cell and identify relevant binding partners in these conditions. Taken together, all approaches resulted in a robust overlap of interactors, especially between the BioID experiments of nsP3 and ARTD10. These were used to characterize more dynamic interactions, like enzyme-substrate binding. These need to be validated and tested for *in vitro* and in cell MARYlation in future experiments. However, initial testing revealed Ras GTPase-activating protein-binding protein 1 (G3BP1) as a strong substrate of ARTD10-mediated MARYlation and de-MARYlation by nsP3. It was identified in the macrodomain-dependent interactome of nsP3 and was also enriched with ARTD10 compared to the GW mutant. Together the follow-up of the common interactors of nsP3 and ARTD10 has good prospects for characterizing further substrates relevant to CHIKV infection.

Apart from G3BP1, that was already described as a C-terminal binding partner of nsP3 and was found to be essential for replication in combination with the highly conserved G3BP2 (Panas et al. 2015; Kim et al. 2016b; Gotte et al. 2019), 135 additional proteins were identified that interacted with nsP3, dependent on the macrodomain, and ARTD10. 87 of these proteins were wt-enriched for ARTD10 and 9 were enriched for IFN α treatment. With statistical enrichment analysis with regard to “Pathways”, the choice of proteins to focus on may be facilitated, by investigating members of relevant pathways only. Further clustering with the *k* means method on the basis of described interactions between the enriched proteins may likewise allow the reduction of candidates for continued validation.

Additionally, selection of promising interactors can be achieved by comparison with preexisting screens from the literature. For instance, our group performed an *in vitro* ProtoArray with ARTD8 and ARTD10 that revealed glycogen synthase kinase 3 β (GSK3 β) as a novel ARTD10 substrate that is regulated by MARYlation (Feijs et al. 2013b). But the screen identified far more potential hits for both ARTDs that have not been functionally characterized. Similarly, the Cohen group performed chemical genetics based mass spectrometry screens to characterize new, specific substrate candidates of ARTD10 and ARTD11 (Carter-O’Connell et al. 2016). To do so, they orthogonally engineered the catalytic site of the transferases to be able to use bulkier NAD $^+$ analogs as co-substrates. These analogs allowed click-chemistry based addition of tags for purification (via biotin) or visualization (via fluorescent dyes) of the substrates post modification. Because the analogs cannot penetrate the membrane, they were added to whole cell lysates and modified proteins were

subsequently purified and analyzed by MS recovering unique as well as shared potential substrates. Interestingly, production of ARTD10 and ARTD11 chimeras composed of different catalytic and regulatory subunits showed that both, the PARP domain itself and N-terminal motifs, influence substrate specificity (Carter-O'Connell et al. 2016). This is in line with the *in vitro* assays that depicted varying modification of the CHIKV nsPs already for the isolated catalytic domains of different ARTDs. Lastly, the ARTD10 interactome derived from this thesis, can be compared with an approach that aimed at identifying intracellularly ADP-ribosylated proteins after IFN γ treatment of THP-1 macrophages (Higashi et al. 2019). In this study, the ADP-ribosylome was investigated by Af1521 macrodomain-dependent enrichment of MARYlated peptides after PARG treatment and subsequent MS analysis. This allowed the identification of sites of MARYlation in addition to the mere information on the identity of the substrates. For example, ARTD8 and ARTD9 showed increased MARYlation upon interferon stimulation (Higashi et al. 2019). Although this dataset was derived from nearly physiological conditions and even suggested relevance for the antiviral state due to IFN γ involvement, the PARG treatment prohibits discrimination between PAR- and MARYlation. Also the setup lacks information on the responsible ARTD enzyme. However, complementary comparison *in vitro*, transferase-specific ProtoArray (Feijs et al. 2013b), a chemical genetics approach, that is situated at the interface between *in vitro* and in cells and investigates individual ARTDs, (Carter-O'Connell et al. 2016) and an in cell ADP-ribosylome study (Higashi et al. 2019) might support validation of the ARTD10 screens from this thesis and allow conclusions about differences between *in vitro* and in cell studies and about their specificities and biases.

Besides the validation that remains to be done for the interactomes, new findings and developments suggest that altered MS approaches might be beneficial and more efficient to answer arising questions about relevant substrates of MARYlation during CHIKV infection. On one hand, binding- and hydrolase-deficient macrodomain V33E and Y114V mutants have been established; a comparison of their interactomes would potentially allow conclusions on the relevance of MAR hydrolase versus binding activity. On the other hand, we have learned that MARYlation of contextual substrates at least partially depends on the presence of the complete replication machinery and viral RNA (Grunewald et al. 2017; Krieg et al. 2020) and that MARYlation might play a time-resolved dual role in the viral life cycle that can be pro- and antiviral. In addition to the progress in MAR-associated virology, proximity dependent biotinylation (PDB) as the basis of the initial BioID approach used in this thesis has been advanced (Roux et al. 2012; Samavarchi-Tehrani et al. 2020). In general, approaches based on peroxidases, like APEX and APEX2 can be excluded, because they rely on hydrogen peroxide (H₂O₂) supplementation for activity (Lam et al. 2015; Martell et al. 2012; Rhee et al. 2013). H₂O₂ is known to induce DNA damage and thus PARYlation, which would in turn impact localization and activity of ARTDs and macrodomains (Blenn et al. 2006; Malet et al. 2009; Ecker et al. 2017; Butepage et al. 2018b). The BioID system on the other hand employs the *Escherichia coli* derived, mutated biotin ligase BirA* (R118G) (Roux et al. 2012) and these biotin protein ligases (PBLs) for PDB proteomics have likewise been improved in recent years. BirA* contains an N-terminal DNA binding domain that might result in unwanted chromatin associated background but could not be removed without accompanied decrease in catalytic activity. However, the PBL from *Bacillus subtilis* could be N-terminally truncated (referred to as BaSu)(Ramanathan et al. 2018) and the respective enzyme from the thermophilic *Aquifex aeolicus* naturally lacks this domain (referred to as BioID2)(Kim et al. 2016a). The BioID2 enzyme, displays a higher affinity towards biotin and thus requires less supplementation, however it is suggested to also be able to scavenge biotin from the serum or medium

(Samavarchi-Tehrani et al. 2020). The biotinylation efficiency of neither BaSu nor BioID2 strongly surpasses that of BirA*. But an error-prone PCR approach with BirA* as a template coupled with yeast display did not only allow to remove the N-terminal domain but it also resulted in two enzymes, TurboID and miniTurbo, with a 3-6 fold increased activity and specific biotinylation within minutes instead of hours (Branon et al. 2018). This would allow a time resolved identification of interactors that could shed light on the switch in the effect of MARYlation over the viral life cycle. Therefore, ARTD10 or other interferon-regulated mono-ARTDs, could be fused to TurboID or miniTurbo and co-transfected with the hydrolase-deficient V33E mutant replicon, to simulate CHIKV infection conditions and shift ARTD10 specificity to the relevant substrates. Thereafter, biotinylation could be induced by incubation with exogenous biotin for 15-30 min, which is sufficient for these enzymes (Branon et al. 2018), at 9 and 24 hpt, where the effect of ARTD10 overexpression seems to change. Comparison of the interactors at both time points might reveal the reason for this. A comparable approach could likewise be performed for the CHIKV macrodomain. Because the miniTurbo protein is much smaller than BirA* it could be introduced into the replicon nsP3 sequence comparable to EGFP insertions used in this thesis (Krieg et al. 2020; Utt et al. 2016). With the V33E and the Y114V mutants for comparison, this could reveal the different interactors of nsP3 at 9 and 24 hpt depend on MAR hydrolase and binding functions in a context where antiviral cellular MARYlation is induced. It might also reveal differences in replication complex formation discussed above. Of note, TurboID and miniTurbo are described to utilize biotin from the medium and therefore produce significant background biotinylation especially over longer periods of time (May et al. 2020; Samavarchi-Tehrani et al. 2020). The use of biotin depleted medium and the short exposures to exogenous biotin of only 15-30 min however would circumvent this drawback.

Along this line of thought, another approach is also imaginable. Instead of finding interactors of the macrodomain or the ARTD10, one could immediately identify MARYlated proteins under different conditions as described for IFN γ treatment of THP-1 macrophages (Higashi et al. 2019). Instead one could transfect HEK293 cells with CHIKV replicons, wt, V33E or Y114V mutants and harvest the cells at 9 or 24 hpt. This is especially interesting as the Af1521 macrodomain has been evolved to a “superbinder” that displays much stronger affinity towards MARYlated proteins and lacks catalytic activity (Nowak et al. 2020). Additionally, the establishment of a negative control that lacks MAR binding ability was recently established in our lab. Besides the identification of MARYlated proteins under these conditions, not just interactors, this approach can also reveal the sites of modification. As discussed above, information on the MAR sites might in turn immediately allow conclusion about the function that is influenced. Furthermore, if the frequently performed PARG treatment steps (Higashi et al. 2019) were skipped in the enrichment process, the usually more abundant PARYlation would be removed from the equation and exclusively MARYlation could be examined. Comparison to the interactome of ARTD10 or knockdown/inhibition of individual mono-ARTDs in the validation process could thereafter enable identification of the responsible transferase.

This thesis and the outlook so far have focused exclusively on protein ADP-ribosylation. However, recent studies revealed that DNA and RNA likewise serve as substrates for MARYlation, mediated by bacterial transferases as well as the cellular transferases ARTD3, ARTD10, ARTD11 and ARTD15 (Jankevicius et al. 2016; Munnur et al. 2017; Munnur et al. 2019). Furthermore, the modifications can be removed by several cellular hydrolases, their bacterial equivalents and some viral macrodomains including VEEV and SARS-CoV (Munnur et al. 2017; Munnur et al. 2019). The physiological abundance and relevance of these

modification is yet to be determined. A potential substrate that immediately comes to mind, apart from the cellular RNA, is viral RNA, especially since (+)ssRNA viruses encode macrodomains. Additionally, several of the IFN-induced mono-ARTDs possess potential RNA recognition motives, including the RRM of ARTD8 and ARTD10. Previous approaches to identify RNAs that interact with ARTD10 were unsuccessful, potentially because it recognizes foreign instead of cellular molecules. Preliminary investigations in this direction have already been performed *in vitro* but remained inconclusive so far (Güldenpfennig 2018). In future experiments, it will be interesting to investigate whether viral RNA is MARYlated in the cell and if so, which transferases mediate the modification and what functional consequences result from it. This could potentially be achieved by sequence-specific precipitation of the replicon RNA and subsequent probing for MARYlation. Complementary to this, one could perform Af1521 superbinder pull-downs and extract potentially co-precipitated RNA by sequencing or sequence specific qRT-PCR from cells transfected with CHIKV replicon RNA. Consequences of RNA MARYlation for CHIKV replication and translation could be studied by *in vitro* polyprotein translation assays subsequent to *in vitro* ADP-ribosylation assays of the *in vitro* transcribed replicon RNA. This would provide a completely new perspective of MARYlation with respect to the antiviral immune response.

Taken together this thesis provides the macrodomain as a new therapeutic target for antiviral therapy of Chikungunya virus, supported by research from other groups defining similarly promising application opportunities for HEV and several Coronaviruses including SARS. Furthermore, a mechanistic explanation for the functional role of the hydrolase of the CHIKV macrodomain was described with the viral protease nsP2 as an essential substrate. Finally, more potential common substrates of cellular ARTDs and nsP3 were identified that will have to be explored in the future

4 Material and Methods

This chapter summarizes the applied material and methods of this research project. In addition to a listing of the used materials the molecular methods are depicted that were employed to work with pro- and eukaryotic cells and to analyze DNA, RNA and proteins. The materials and methods are described according to standard protocols used in the Institute of Biochemistry and Molecular Biology, RWTH Aachen University, and modified with regard to individual differences in experimental procedures.

4.1 Material

The following central reagents were used in this work:

³²P-NAD⁺ (Perkin-Elmer); AcTEV™ protease (Thermo Fisher Scientific); ADPr (Adenosine 5' diphosphoribose sodium-salt, Sigma); β-NAD⁺ (Sigma); Biotin (AppliChem); Blasticidin S (Invivogen); Calmodulin sepharose 4B (GE Healthcare Life Sciences); Dynabeads™ MyOne™ Streptavidin C1 (Invitrogen); GFP-Trap magnetic agarose beads (Chromotek, gtm); GFP-Trap magnetic beads (Chromotek, gtm); Glutathione-sepharose (Sigma); Glyoxal (Sigma); HiPerFect Transfection Reagent (Qiagen); Hoechst 33258 (SigmaAldrich); Hygromycin B (Invivogen); Interferon-α (Peprotech, discontinued); Lipofectamine 2000 Transfection Reagent (Invitrogen); Mowiol 4–88 (SigmaAldrich); Opti-MEM™, Reduced Serum Medium, no phenol red (Gibco); Pierce™ Glutathione Agarose (Thermo Fisher Scientific); Propidium Iodide (PI) solution (Sigma); Protein G sepharose FastFlow (GE Healthcare Life Sciences); recombinant Human Histone H3 (New England BioLabs (NEB)); TALON metal affinity resin (BD Bioscience)

4.1.1 Kits

The following ready-to-use kits were used according to the manufacturer's instructions if not stated otherwise in the methods section.

Kit	Product number	Supplier
BioLux® Gaussia Luciferase Assay Kit	E3300, discontinued	NEB
DC™ Proteinassay Kit I	5000111	Bio-Rad
Gateway™ BP Clonase™ Enzyme Mix	11789021	Invitrogen
Gaussia Luciferase Assay Reagent	GAR-2B	Targeting Systems
Gateway™ LR Clonase™ Enzyme Mix	11791043	Invitrogen
mMESSAGE mMACHINE™ SP6 Transcription Kit	AM1340	Invitrogen
NucleoBond® Xtra Maxi Kit	740414	Macherey Nagel
NucleoSpin Plasmid EasyPure Mini Kit	740727	Macherey Nagel
Q5® Site-Directed Mutagenesis Kit	E0554	NEB
StrataClone Blunt Cloning Kit	240207	Agilent
Zymoclean Gel DNA Recovery Kit	D4001	Zymo Research

4.1.2 Synthetic oligonucleotides

Oligonucleotides (oligos) were purchased from Integrated DNA Technologies (IDT). Oligos were generally dissolved in TE buffer according to the manufacturer's instructions if not stated otherwise.

TE buffer: 10 mM Tris base (pH 8.0); 1mM EDTA

Primers for molecular cloning	
Primer name	Sequence 5'-3'
CHIKV macro <i>attB1</i> fw	GGGGACAAGTTTGTACAAAAAAGCAGGCTCGATGGCA CCGTCGTACCGGGTAAAACG
CHIKV macro <i>attB2</i> rev	GGGGACCACTTTGTACAAGAAAGCTGGGTCTCAGGTCC GCATCTGTATGGCCTC
<i>attB</i> <i>EcoRI</i> CHIKV nsP3 fw	GGGGACAAGTTTGTACAAAAAAGCAGGCTTCGAATTC ATGGCACCGTCGTACCGGG
CHIKV nsP3 <i>BamHI</i> <i>attB</i> rev	GGGGACCACTTTGTACAAGAAAGCTGGGTCTCACCTA GGGGATCCTAACTCGTCGTCCGT
CHIKV nsP1 <i>attB</i> fw	GGGGACAAGTTTGTACAAAAAAGCAGGCTTCATGGAT CCTGTGTACGTGGACATA
CHIKV nsP1 <i>attB</i> rev	GGGGACCACTTTGTACAAGAAAGCTGGGTCTCATGCGC CCGCTCTGTCTC
<i>NdeI</i> CHIKV nsP1 fw	CATATGGATCCTGTGTACGTGGACATAG
CHIKV nsP1 <i>XhoI</i> rev	CTCGAGTGCGCCGCTCTGTCCTCA
CHIKV nsP2 <i>attB</i> fw	GGGGACAAGTTTGTACAAAAAAGCAGGCTTCATGGGAA TAATAGAGACTCCGAGAGGA
CHIKV nsP2 <i>attB</i> rev	GGGGACCACTTTGTACAAGAAAGCTGGGTCTCAACATCC TGCTCGGGTGACCT
CHIKV nsP4 <i>attB</i> fw	GGGGACAAGTTTGTACAAAAAAGCAGGCTTCATGTATAT ATTCTCGTCGGACACCGGT
CHIKV nsP4 <i>attB</i> rev	GGGGACCACTTTGTACAAGAAAGCTGGGTCTTATTAGG ACCGCCGTACAAAGT
CHIKV nsP4 d1-97 <i>attB</i> fw	GGGGACAAGTTTGTACAAAAAAGCAGGCTTCATGTACCG GACTACATATCCGGCG
<i>EcoRI</i> nsP3/4 <i>BamHI</i> fw	AATTCGACGAGTTAAGACTAGACAGGGCAGGTGGGTATATA TTCTCGTCGGAG
<i>EcoRI</i> nsP3/4 <i>BamHI</i> rev	GATCCTCCGACGAGAATATATACCCACCTGCCCTGTCTAGTC TTAACTCGTCTG
<i>EcoRI</i> nsP3/4 polylinker <i>NcoI</i> fw	AATTCGACGAGTTAAGACTAGACAGGGCAGGTGGGTATATAT TCTCGTCGGAGGATCCACCGGTCGCCACCGGCTCTGCCGCTG CCACAAGAGGCTCTGCTGGAAGCGGCGGATCTGCCACAGGC TCTGGATCTGCAGCTGGCTCTGGCGACTCTGTGGCTGCCGGA TCTGGCGGAGGAAGCGGCTCTAC
<i>EcoRI</i> nsP3/4 polylinker <i>NcoI</i> rev	CATGGTAGAGCCGCTTCTCCGCCAGATCCGGCAGCCACAGAG TCGCCAGAGCCAGCTGCAGATCCAGAGCCTGTGGCAGATCCG CCGCTTCCAGCAGAGCCTTGTGGCAGCGGAGCCGGTG GCGACCGGTGGATCCTCCGACGAGAATATATACCCACCTGCC CTGTCTAGTCTTAACTCGTCTG

<i>attB2</i> -CHIKV-nsP2-459-798_for	GGGGACAAGTTTGTACAAAAAAGCAGGCTCGATGGCGGGCA TCTGCAGTCACC
<i>attB2</i> -CHIKV-nsP2-1-468_rev	GGGGACCACTTTGTACAAGAAAGCTGGGTCTCAGAAGGTCA TTTGGTGACTGC
<i>EcoRV</i> GST fw	GATATCCATGTCCCCTATACTAGGTTATTGGA
EGFP <i>NotI</i> rev	GATGCGGCCGCTTTACTTGTACAGC
<i>attB</i> nsP2 1-455 fw	GGGGACAAGTTTGTACAAAAAAGCAGGCTTCGGAATAATAG AGACTCCGAGAGGAG
nsP2 1-455 <i>attB</i> rev	GGGGACCACTTTGTACAAGAAAGCTGGGTCTCATGCATGCT CCACCTCCCACT
G3BP1 <i>attB</i> fw	GGGGACAAGTTTGTACAAAAAAGCAGGCTTCATGGTGATGG AGAAGCCTAGTCCCC
G3BP1 <i>attB</i> rev	GGGGACCACTTTGTACAAGAAAGCTGGGTCTCACTGCCGTGG CGCAAGCCC
MAGED2 <i>attB</i> fw	GGGGACAAGTTTGTACAAAAAAGCAGGCTTCATGTCTGACAC AAGCGAGAGTGGTG
MAGED2 <i>attB</i> rev	GGGGACCACTTTGTACAAGAAAGCTGGGTCTCACTTGTAGGA GAAACCACAGGCA
USP10 <i>attB</i> fw	GGGGACAAGTTTGTACAAAAAAGCAGGCTTCATGGCCCTCC ACAGCCCGCAGTA
USP10 <i>attB</i> rev	GGGGACCACTTTGTACAAGAAAGCTGGGTCTTACAGCAGGT CCTACTCGGCGGTA
<i>SpeI</i> Gly Gly EGFP fw	ACTAGTGGTGGTGTGAGCAAGGGCGAG
EGFP Gly Gly <i>XhoI</i> rev	CTCGAGACCACCTTGTACAGCTCGTCC

Mutagenesis primers were designed using the NEBaseChanger tool from NEB.

Mutagenesis primers	
Primer name	Sequence 5'-3'
Q5_ATG_BirA_CHIKV_for	TACGACGGTGCCATTTTTCGAATCCGGAGACGTACG
Q5_ATG_BirA_CHIKV_rev	CGTACGTCTCCGGATTTCGAAATGGCACCGTCGTA
Q5 CHIKV D10A <i>EcoRV</i> fw	AAAACGCATGGCTATCGCGAAGAACGATG
Q5 CHIKV D10A <i>EcoRV</i> rev	ACCCGGTACGACGGTGCC
Q5 CHIKV N24R <i>XhoI</i> fw	TCGAGGGTTACCAGGTGACGGTG
Q5 CHIKV N24R <i>XhoI</i> rev	GGCCTGGCGGCGTTGACTACGCA
Q5 CHIKV N24Y <i>SmaI</i> fw	CCGGGGTTACCAGGTGACGGTG
Q5 CHIKV N24Y <i>SmaI</i> rev	GGGTAGGCGGCGTTGACTACGCA
Q5 CHIKV V33E <i>BsrGI</i> fw	GGCAGTGTACAAAAAATGGCCGGAGTC
Q5 CHIKV V33E <i>BsrGI</i> rev	TTGCACTACCGTCACCTGGTAACCC
Q5 CHIKV V33F <i>StuI</i> fw	GTGACGGTTTTTGTCAAGGCAGTATACAAAAAATGGCC
Q5 CHIKV V33F <i>StuI</i> rev	CTGGTAGGCCTCGAGGGTTGGCGGCGTTG
Q5 CHIKV Y114V <i>BspEI</i> fw	CACAGGTGTAGTCTCCGGAGGGAAAGAC
Q5 CHIKV Y114V <i>BspEI</i> rev	GAGAGGAGAGGTATAGCTAC
Q5 CHIKV Y114W <i>AgeI</i> fw	GTATGGTCAGGAGGGAAAGACAGG

Q5 CHIKV Y114W Agel rev	ACCGGTGGAGAGGAGAGGTATAGC
nsP2 C478A S482A fw	TAAGGCCTTGGTCCCTATCCTCGAAAC
nsP2 C478A S482A rev	GCCCAAGCAACGTTGGCTTTATTTTGGAAATG
Q5 nsP2 linker fw	GAGCTCGAGACCTTCGATACATTCCAAAATAAAG
Q5 nsP2 linker rev	GGAAGTAGTCATTTGGTGACTGCAGATG
Q5 nsP3 linker fw	GAGCTCGAGGGAAACCTTGCGGCCGTG
Q5 nsP3 linker rev	GGAAGTAGTGGTTGTGGATGGCAGCGTG

Double stranded oligonucleotides: gBlocks	
Primer name	Sequence 5'-3'
CHIKV D10A Minigene	CACCCGAGCAGGATGTGCACCGTCGTACCGGGTAAAACGCATGG CCATCGCGAAGAACGATGAAGAGTGCCTAGTCAACGCCGCTAAC CCTCGCGGGTTACCGGGTGGCGGTGTTTGCAAGGCAGTATACAA AAAATGGCCGGAGTCCTTTAAGAACAGTGCAACACCAGTGGGAA CCGCAAAAACAGTTATGTGCGGTACGTATCCAGTAATCCACGCTG TTGGACCAAACCTTCTCTAATTATTCGGAGTCTGAAGGGGACCGGG AATTGGCAGCTGCCTATCGAGAAGTCGCAAAGGAAGTAAGTAGG CTGGGAGTAAATAGTGTAGCTATACCTCTCCTCTCCACAGGTGTAT ACTCAGGAGGGAAAGACAGGCTGACCCAGTCACTGAACCACCTCT TTACAGCCATGGACTCGACGGATGCAGACGTGGTCATCTACTGCCG CGACAAAGAATGGGAGAAGAAAATATCTGAGGCCATACAGATGCG GACCCAAGTAGAGCTGCTGGATGAGCACATCTCCATAGACTGCGAT ATTGTTTCGCGTGCACCCTGACAGCAGCTTGGCAGGCAGAAAAGGA TACAGCACCAAGGAAGGCGCACTGTACTCATATCTAGAAGGGACCC GTTTTTCATCAGACGGCTGTGGATATGGCGGAGATACATACTATGTG GCCAAAGCAAACAGAGGCCAATGAGCAAGTCTGCCTATATGCCCTG GGGGAAAGTATTGAATCGATAAGG
CHIKV V33E Minigene	CACCCGAGCAGGATGTGCACCGTCGTACCGGGTAAAACGCATGGA CATCGCGAAGAACGATGAAGAGTGCCTAGTCAACGCCGCTAACCT CGCGGGTTACCGGGTGGCGGTGAGTGCAAGGCAGTATACAAAAA TGCCCGGAGTCCTTTAAGAACAGTGCAACACCAGTGGGAACCGCAA AACAGTTATGTGCGGTACGTATCCAGTAATCCACGCTGTTGGACCA AACTTCTCTAATTATTCGGAGTCTGAAGGGGACCGGGAATTGGCAG CTGCCTATCGAGAAGTCGCAAAGGAAGTAAGTAGGCTGGGAGTAAA TAGTGTAGCTATACCTCTCCTCTCCACAGGTGTATACTCAGGAGGGA AAGACAGGCTGACCCAGTCACTGAACCACCTCTTTACAGCCATGGAC TCGACGGATGCAGACGTGGTCATCTACTGCCGCGACAAAGAATGGG AGAAGAAAATATCTGAGGCCATACAGATGCGGACCCAAGTAGAGCT GCTGGATGAGCACATCTCCATAGACTGCGATATTGTTTCGCGTGCACC CTGACAGCAGCTTGGCAGGCAGAAAAGGATACAGCACCAAGGAGG CGCACTGTACTCATATCTAGAAGGGACCCGTTTTTCATCAGACGGCTGT GGATATGGCGGAGATACATACTATGTGGCCAAAGCAAACAGAGGCC AATGAGCAAGTCTGCCTATATGCCCTGGGGGAAAGTATTGAATCGAT AAGG
CHIKV Y114V Minigene	CACCCGAGCAGGATGTGCACCGTCGTACCGGGTAAAACGCATGGACA TCGCGAAGAACGATGAAGAGTGCCTAGTCAACGCCGCTAACCTCG CGGGTTACCGGGTGGCGGTGTTTGCAAGGCAGTATACAAAAATGG CCGGAGTCCTTTAAGAACAGTGCAACACCAGTGGGAACCGCAAAAAC

	<p>AGTTATGTGCGGTACGTATCCAGTAATCCACGCTGTTGGACCAA CTCTAATTATTCGGAGTCTGAAGGGGACCGGGAATTGGCAGCTGCCT ATCGAGAAGTCGCAAAGGAAGTAACTAGGCTGGGAGTAAATAGTGT AGCTATACTCTCCTCTCCACAGGTGTAGTCTCAGGAGGGAAAGACA GGCTGACCCAGTCACTGAACCACCTCTTTACAGCCATGGACTCGACGG ATGCAGACGTGGTCATCTACTGCCGACAAAGAATGGGAGAAGAAA ATATCTGAGGCCATACAGATGCGGACCCAAGTAGAGCTGCTGGATGA GCACATCTCCATAGACTGCGATATTGTTGCGGTGCACCCTGACAGCAG CTTGGCAGGCAGAAAAGGATACAGCACCACGGAAGGGCAGCTGTACT CATATCTAGAAGGGACCCGTTTTTCATCAGACGGCTGTGGATATGGCG AGATACATACTATGTGGCCAAAGCAAACAGAGGCCAATGAGCAAGTC TGCCTATATGCCCTGGGGGAAAGTATTGAATCGATAAGG</p>
<p>CHIKV nsP4 GAA Minigene</p>	<p>GGACACCGGTCCAGGTCATTTACAACAGAAGTCAGTACGCCAGTCAGT GCTGCCGGTGAACACCCTGGAGGAAGTCCACGAGGAGAAGTGTACC CACCTAAGCTGGATGAAGCAAAGGAGCAACTATTACTTAAGAACTCC AGGAGAGTGCATCCATGGCCAACAGAAGCAGGTATCAGTCGCGCAAA GTAGAAAACATGAAAGCAGCAATCATCCAGAGACTAAAGAGAGGCTG TAGACTATACTTAATGTCAGAGACCCAAAAGTCCCTACTTACCGGACT ACATATCCGGCGCCTGTGTACTCGCTCCGATCAACGTCCGATTGTCCA ATCCCGAGTCCGCAGTGGCAGCATGCAATGAGTTCTTAGCTAGAACT ATCCAAGTGTCTCATCATACCAAATTACCGACGAGTATGATGCATATCT AGACATGGTGGACGGGTCGGAGAGTTGCCTGGACCGAGCGACATTCA ATCCGTCAAACTCAGGAGCTACCCGAAACAGCACGCTTACCACGCGC CCTCCATCAGAAGCGCTGTACCGTCCCCATTCCAGAACACACTACAGAA TGTAAGTGGCAGCAGCCACGAAAAGAACTGCAACGTACACAGATGA GGGAATTACCCACTTTGGACTCAGCAGTATTCAACGTGGAGTGTTC AAAATTCGCATGCAACCAAGAATACTGGGAAGAATTTGCTGCCAGCCCT ATTAGGATAAACAAGTGAAGATTTAGCAACCTATGTTACTAACTAAAAG GGCCAAAAGCAGCAGCGCTATTGCAAAAACCCATAATCTACTGCCACT ACAGGAAGTACCAATGGATAGGTTACAGTAGATATGAAAAGGGACGT AAAGGTGACTCCTGGTACAAAGCATAACAGAGGAAAGACCTAAGGTGCA GGTTATACAGGCGGCTGAACCCCTGGCGACAGCATACTATGTGGGATT CACAGAGAGCTGGTTAGGAGGCTGAACGCCGTCTCCTACCCAATGTAC ATACACTATTTGACATGTCTGCCGAGGATTTGATGCCATCATAGCCGCA CACTTTAAGCCAGGAGACTGTTTTGGAAACGGACATAGCCTCCTTTGA TAAGAGCCAAGATGATTCACTTGCCTTACTGCTTTGATGCTGTTAGAGG ATTTAGGGTGGATCACTCCCTGCTGGACTTGATAGAGGCTGCTTTCCGA GAGATTTCCAGCTGTCACTACCGACAGGTACGCGCTTCAAGTTCGGCGC CATGATGAAATCAGGTATGTTCTAACTCTGTTGTC AACACATTGTTAAA CATCACCATCGCCAGCCGAGTGTGGAAGATCGTCTGACAAAATCCGCGT GCGCGGCCTTCATCGGCGCCGCAACATAACATGGAGTGTCTCCGA TGAATTGATGGCAGCCAGATGTGCCACTTGATGAACATGGAAGTGAAGA TCATAGATGCAGTTGTATCCTTGAAAGCCCTTACTTTTGTGGAGGGTTTAT ACTGCACGATACTGTGACAGGAACAGCTTGACAGAGTGGCAGACCCGCTAA AAAGGCTTTTTAACTGGGCAAACCGCTAGCGGCAGGTGACGAACAAGAT GAAGATAGAAGACGAGCGCTGGCTGACGAAGTGTGATGATGGCAACGAA CAGGGCTAATTGATGAGCTGGAGAAAGCGGTATACTCTAGGTACGAAGTG CAGGGTATATCAGTTGTGGTAATGTCCATGGCCACCTTTGCAAGCTCCAGA</p>

	TCCAACCTTCGAGAAGCTCAGAGGACCCGTCATAACTTTGTACGGCGGTCCT AAATAGGTACGCACTACAGCTACCTATTTTGCAGAAGCCGACAGCAAGTAT CTAAACACTAATC
GFPnanobody <i>AgeI XhoI</i> hs optimized Minigene	ACCGGTCGCCACCATGCAGGTGCAGTTGGTAGAGAGTGGGGGAGCACTTG TTCAACCTGGAGGAAGTCTGCGGCTGTCATGCGCCGCTCAGGCTTCCCGG TGAACAGATATTCCATGCGCTGGTACCGGCAAGCACCTGGCAAGGAGAGA GAATGGGTTGCAGGAATGAGTTCCGCAGGAGACAGAAGCAGCTATGAGG ATTCTGTGAAAGGAAGTTCACTATTAGCCGGGACGATGCACGGAACACT GTGTATCTCCAGATGAATTCCCTGAAGCCGGAGGATACGGCTGTCTACTAT TGTAATGTAAATGTTGGATTCGAGTACTGGGGTCAAGGAACGCAAGTGAC AGTATCCAGCTCCGGACTCAGATCTCGAG

Custom sequencing primers were directly ordered and synthesized at SeqLab/Microsynth in case of the SP6-CHIKV-Replicon-SG-GLuc constructs where the Standard Primer List was not sufficient (chapter 4.2.1.10).

Sequencing primers	Sequence 5'-3'
Primer 1 SP6 backbone fw	ATGGCTGCGTGAGACACA
Primer 2 nsP1 fw	GAACATAGGATTATGTTCAACA
Primer 3 nsP1 fw	AAGGTTTCAGGCCGAGTTTG
Primer 4 nsP2 fw	GATGCTGTAAGAAGGAAGAAG
Primer 5 nsP2 fw	ATACGAGGTCATGACAGCA
Primer 6 nsP2 fw	AGACTACCACACTCATTAGTG
Primer 7 nsP3 fw	CGGAGTCCTTTAAGAACAG
Primer 8 nsP3 fw	GCTTCGCATGAACCACGT
Primer 9 nsP3 fw	ACAGACAGCGACTGGTC
Primer 10 nsP4 fw	TGAGGGAATTACCCACTTTG
Primer 11 nsP4 fw	CATCGCCAGCCGAGTG

Annealed double stranded oligos were added to *in vitro* ADP-ribosylation assays with ARTD1 in order to stimulate its PARylating activity (chapter 4.2.4.14).

Annealed double stranded oligonucleotides	Sequence 5'-3'
For ARTD1 activation	CACCGTGTGAGGACCACTAGCCTCT

Dharmacon/Horizon Discovery siRNA oligonucleotides	
Name	Catalogue number
siGENOME Non-targeting siRNA Control Pool #2	D-001206-14
siGENOME Human PARP10 (84875) siRNA - SMARTpool	M-014997-03
siGENOME Human PARP12 (64761) siRNA - SMARTpool	M-013740-01
siGENOME Human PARP14 (54625) siRNA - SMARTpool	M-023583-02
siGENOME Human PARP15 (165631) siRNA - SMARTpool	M-017186-00

4.1.3 Plasmids

Gateway entry vectors	
Plasmid name	Description
pDONR/Zeo	Empty Gateway vector (Invitrogen) for generation of Gateway entry clones. The vector contains the <i>ccdB</i> for negative selection that is replaced by the gene of interest through recombination by BP reaction. Contains a zeocin resistance gene.
pDONR/Zeo-CHIKV-nsP3-macro	Gateway entry vector containing the isolated macro domain of CHIKV. The CDS was amplified from pDEST14-CHIKV-nsP3-macro (gift from B. Coutard) using primers with <i>attB</i> sites (P. Korn, née Verheugd).
pDONR/Zeo-CHIKV-nsP3-macro-V33E	Generated by site directed mutagenesis of pDONR/Zeo-CHIKV-nsP3-macro.
pDONR/Zeo-CHIKV-nsP3-macro-Y114V	
pDONR/Zeo-CHIKV-nsP3	Gateway entry vector containing the fulllength nsP3 of CHIKV. The CDS was amplified from SP6-CHIKV-Replicon-SG-GLuc (gift from B. Kümmerer) using primers with <i>attB</i> sites.
pDONR/Zeo-CHIKV-nsP3-V33E	Generated by site directed mutagenesis of pDONR/Zeo-CHIKV-nsP3 (P. Korn, née Verheugd).
pDONR/Zeo-CHIKV-nsP3-Y114V	
pDONR/Zeo-CHIKV-nsP1	Gateway entry vector containing nsP1 of CHIKV. The CDS was amplified from SP6-CHIKV-Replicon-SG-GLuc (gift from B. Kümmerer) using primers with <i>attB</i> sites.
pDONR/Zeo-CHIKV-nsP2	Gateway entry vector containing nsP2 of CHIKV. The CDS was amplified from SP6-CHIKV-Replicon-SG-GLuc (gift from B. Kümmerer) using primers with <i>attB</i> sites.
pDONRZeo-CHIKV-nsP2-CASA	Generated by site directed mutagenesis of pDONR/Zeo-CHIKV-nsP2.
pDONR/Zeo-CHIKV-nsP4	Gateway entry vector containing nsP4 of CHIKV. The CDS was amplified from SP6-CHIKV-Replicon-SG-GLuc (gift from B. Kümmerer, Bonn) using primers with <i>attB</i> sites.
pDONR/Zeo-CHIKV-nsP4-Δ1-97	Gateway entry vector containing nsP4 of CHIKV with an N-terminal deletion of the first 97 amino acids. The CDS was amplified from SP6-CHIKV-Replicon-SG-GLuc (gift from B. Kümmerer) using primers with <i>attB</i> sites.
pDONR/Zeo-CHIKV-nsP2-1-455	Gateway entry vector containing amino acids 1-455 of nsP2 of CHIKV. The CDS was amplified from pDONR/Zeo-CHIKV-nsP2 using primers with <i>attB</i> sites.

pDONR/Zeo-CHIKV-nsP2-1-468	Gateway entry vector containing amino acids 1-468 of nsP2 of CHIKV. The CDS was amplified from pDONR/Zeo-CHIKV-nsP2 using primers with <i>attB</i> sites (P. Korn, née Verheugd).
pDONR/Zeo-CHIKV-nsP2-459-798	Gateway entry vector containing amino acids 459-798 of nsP2 of CHIKV. The CDS was amplified from pDONR/Zeo-CHIKV-nsP2 using primers with <i>attB</i> sites (P. Korn, née Verheugd).
pDONR/Zeo-CHIKV-nsP2-459-798-CASA	Generated by site directed mutagenesis of pDONR/Zeo-CHIKV-nsP2-459-798.
pDONR/Zeo-G3BP1	Gateway entry vector containing human G3BP1. The CDS was amplified from pDNR-LIB-G3BP1 (Dharmacon) using primers with <i>attB</i> sites
pDONR/Zeo-MAGED2	Gateway entry vector containing human MAGED2. The CDS was amplified from pOTB7-MAGED2 (Dharmacon) using primers with <i>attB</i> sites
pDONR/Zeo-USP10iso1	Gateway entry vector containing human USP10 isoform 1. The CDS was amplified from Flag-HA-USP10 (Addgene) using primers with <i>attB</i> sites

Bacterial expression vectors	
Plasmid name	Description
GW-pDest14-CHIKV-nsP3-macro	Vector for bacterial expression of N-terminally His ₆ -tagged CHIKV nsP3 macro (gift from B. Coutard, Marseille).
GW-pDest14-CHIKV-nsP3-macro-D10A	Generated by site directed mutagenesis of GW-pDest14-CHIKV-nsP3-macro (J. Fechner).
GW-pDest14-CHIKV-nsP3-macro-N24A	Generated by site directed mutagenesis of GW-pDest14-CHIKV-nsP3-macro (B. Lippok).
GW-pDest14-CHIKV-nsP3-macro-N24R	Generated by site directed mutagenesis of GW-pDest14-CHIKV-nsP3-macro.
GW-pDest14-CHIKV-nsP3-macro-N24Y	
GW-pDest14-CHIKV-nsP3-macro-V33A	Generated by site directed mutagenesis of GW-pDest14-CHIKV-nsP3-macro (B. Lippok).
GW-pDest14-CHIKV-nsP3-macro-V33E	Generated by site directed mutagenesis of GW-pDest14-CHIKV-nsP3-macro.
GW-pDest14-CHIKV-nsP3-macro-V33F	
GW-pDest14-CHIKV-nsP3-macro-Y114A	Generated by site directed mutagenesis of GW-pDest14-CHIKV-nsP3-macro (B. Lippok).
GW-pDest14-CHIKV-nsP3-macro-Y114V	Generated by site directed mutagenesis of GW-pDest14-CHIKV-nsP3-macro.
GW-pDest14-CHIKV-nsP3-macro-Y114W	
GW-pDEST14-FIPV-nsP3-macro	Vector for bacterial expression of N-terminally His ₆ -tagged FIPV nsP3 macro (gift from B. Coutard, Marseille).
GW-pDEST14-VEEV-nsP3-macro	Vector for bacterial expression of N-terminally His ₆ -tagged VEEV nsP3 macro (gift from B. Coutard, Marseille).
GW-pDest17	Empty Gateway vector for the bacterial expression of N-terminally His ₆ -tagged fusion

	proteins (Invitrogen). The vector contains the <i>ccdB</i> for negative selection that is replaced by the gene of interest through recombination by LR reaction. Contains an ampicillin resistance gene.
GW-pDest17-ARTD10-818-1025	Vector for bacterial expression of N-terminally His ₆ -tagged ARTD10cat (818-1025) (M. Bütepage)
GW-pDest17-ARTD10-818-1025-GW	Vector for bacterial expression of N-terminally His ₆ -tagged ARTD10cat GW (818-1025) (B. Lippok).
GW-pDest17-ARTD12cat	Vector for bacterial expression of N-terminally His ₆ -tagged ARTD12cat (L. Ecker-Potthoff).
GW-pDest17-ARTD15cat	Vector for bacterial expression of N-terminally His ₆ -tagged ARTD15cat (L. Ecker-Potthoff).
GW-pDest17-ARTD7cat	Vector for bacterial expression of N-terminally His ₆ -tagged ARTD7cat (L. Ecker-Potthoff).
GW-pDest17-ARTD8cat	Vector for bacterial expression of N-terminally His ₆ -tagged ARTD8cat (L. Ecker-Potthoff).
GW-pDest17-CHIKV-nsP1	Vector for bacterial expression of N-terminally His ₆ -tagged of CHIKV nsP1. Generated by Gateway recombination of pDONR/Zeo-CHIKV-nsP1 with GW-pDest17.
GW-pDest17-CHIKV-nsP2	Vector for bacterial expression of N-terminally His ₆ -tagged of CHIKV nsP2. Generated by Gateway recombination of pDONR/Zeo-CHIKV-nsP2 with GW-pDest17.
GW-pDest17-CHIKV-nsP2-1-455	Vector for bacterial expression of N-terminally His ₆ -tagged of CHIKV nsP2 1-455. Generated by Gateway recombination of pDONR/Zeo-CHIKV-nsP2-1-455 with GW-pDest17.
GW-pDest17-CHIKV-nsP2-1-468	Vector for bacterial expression of N-terminally His ₆ -tagged of CHIKV nsP2 1-468. Generated by Gateway recombination of pDONR/Zeo-CHIKV-nsP2-1-468 with GW-pDest17.
GW-pDest17-CHIKV-nsP2-459-798	Vector for bacterial expression of N-terminally His ₆ -tagged of CHIKV nsP2 459-468. Generated by Gateway recombination of pDONR/Zeo-CHIKV-nsP2-459-798 with GW-pDest17.
GW-pDest17-CHIKV-nsP2-459-798-CASA	Generated by site directed mutagenesis of GW-pDest17-CHIKV-nsP2-459-798.
GW-pDest17-CHIKV-nsP3	Vector for bacterial expression of N-terminally His ₆ -tagged of CHIKV nsP3. Generated by Gateway recombination of pDONR/Zeo-CHIKV-nsP3 with GW-pDest17.
GW-pDest17-CHIKV-nsP3-V33E	Generated by site directed mutagenesis of GW-pDest17-CHIKV-nsP3.
GW-pDest17-CHIKV-nsP3-Y114V	

GW-pDest17-CHIKV-nsP4	Vector for bacterial expression of N-terminally His ₆ -tagged of CHIKV nsP4. Generated by Gateway recombination of pDONR/Zeo-CHIKV-nsP4 with GW-pDest17.
GW-pDest17-CHIKV-nsP4-Δ1-97	Vector for bacterial expression of N-terminally His ₆ -tagged of CHIKV nsP4 Δ1-97. Generated by Gateway recombination of pDONR/Zeo-CHIKV-nsP4-Δ1-97 with GW-pDest17.
GW-pDest17-G3BP1	Vector for bacterial expression of N-terminally His ₆ -tagged of G3BP1. Generated by Gateway recombination of pDONR/Zeo-G3BP1 with GW-pDest17.
GW-pDest17-HPF1	Vector for bacterial expression of N-terminally His ₆ -tagged HPF1 (B. Lippok).
GW-pDest17-MAGED2	Vector for bacterial expression of N-terminally His ₆ -tagged of MAGED2. Generated by Gateway recombination of pDONR/Zeo-MAGED2 with GW-pDest17.
GW-pDest17-mParp14 Macro2	Vector for bacterial expression of N-terminally His ₆ -tagged mParp14 Macro2 (Forst et al. 2013).
GW-pDest17-TARG1	Vector for bacterial expression of N-terminally His ₆ -tagged TARG1 (M. Bütepage).
GW-pDest17-USP10-iso1	Vector for bacterial expression of N-terminally His ₆ -tagged of USP10 isoform1. Generated by Gateway recombination of pDONR/Zeo-USP10-iso1 with GW-pDest17.
GW-pGST	Empty Gateway vector for the bacterial expression of N-terminally GST-tagged fusion proteins (Invitrogen). The vector contains the <i>ccdB</i> for negative selection that is replaced by the gene of interest through recombination by LR reaction. Contains an ampicillin resistance gene.
GW-pGST-ARTD10-818-1025	Vector for bacterial expression of N-terminally GST-tagged ARTD10cat (818-1025) (Kleine et al. 2008).
GW-pGST-ARTD10-818-1025-GW	Vector for bacterial expression of N-terminally GST-tagged ARTD10cat GW (818-1025) (H. Kleine).
GW-pGST-ARTD7cat	Vector for bacterial expression of N-terminally GST-tagged ARTD7cat (P. Korn, née Verheugd).
GW-pGST-ARTD8cat	Vector for bacterial expression of N-terminally GST-tagged ARTD8cat (P. Korn, née Verheugd).
GW-pGST-CHIKV-nsP3	Vector for bacterial expression of N-terminally GST-tagged CHIKV nsP3 (P. Korn, née Verheugd).
GW-pGST-NEMO	Vector for bacterial expression of N-terminally GST-tagged NEMO (Verheugd et al. 2013).

pET-22b(+)-CHIKV-nsP1	Vector for bacterial expression of C-terminally His ₆ -tagged CHIKV nsP1. CHIKV nsP1 was amplified from SP6-CHIKV-Replicon-SG-GLuc (gift from B. Kümmerer) using primers <i>NdeI</i> CHIKV nsP1 fw and CHIKV nsP1 <i>XhoI</i> fw. It was introduced into pET-22b(+) by restriction with <i>NdeI</i> and <i>XhoI</i> and ligation.
pGEX2T-PARGcat	Vector for bacterial expression of N-terminally GST-tagged PARGcat (Kleine et al. 2008).
pGEX4T1-nsP3_4site-EGFP	Vector for the bacterial expression of N-terminally GST-tagged and C-terminally EGFP-tagged artificial protease substrate of nsP2 containing the long nsP3/nsP4 junction (Rausalu et al. 2016). The oligos <i>EcoRI</i> nsP3/4 <i>BamHI</i> fw and rev were annealed. EGFP was isolated from pEGFP-N1 by restriction with <i>BamHI</i> and <i>NotI</i> . The oligos and EGFP were inserted into pGEX4T1 by restriction with <i>EcoRI</i> and <i>NotI</i> and ligation.
pGEX4T1-nsP3_4site-polylinker-EGFP	Vector for the bacterial expression of N-terminally GST-tagged and C-terminally EGFP-tagged artificial protease substrate of nsP2 containing a polylinker for better accessibility and the long nsP3/nsP4 junction (Rausalu et al. 2016). The oligos <i>EcoRI</i> nsP3/4 polylinker <i>NcoI</i> fw and rev were annealed and introduced into pGEX4T1-nsP3_4site-EGFP by restriction with <i>EcoRI</i> and <i>NcoI</i> and ligation (B. Lippok).
pMCox20A-HEPEXDA4-ORF1-macro	Vector for bacterial expression of N-terminally His ₆ -tagged HEPEXDA4 and DD12 ORF1 macro (gift from B. Coutard, Marseille).
pMCox20A-HEPEXDD12-ORF1-macro	
pNIC-Bsa4-ONNV-nsP3-macro	Vector for bacterial expression of N-terminally His ₆ -tagged SINV and ONNV macros. Plasmids encoding the macros of SINV and ONNV were generated by LIC and cloned into pNIC-Bsa4 (P. Korn, née Verheugd).
pNIC-Bsa4-SINV-nsP3-macro	

Eukaryotic expression vectors	
Plasmid name	Description
pEQ176P2	This vector was used to adjust the amount of plasmids in calcium phosphate precipitation based transfection of mammalian cells. The β -galactosidase coding sequence was removed (J. Lüscher-Firzlaff).
GW-pcDNA5/FRT/TO/GS/N-TAP	Empty Gateway vector for the CMV/TetO2 driven expression the TAP tag or generation of plasmids for N-terminally TAP-tagged fusion proteins (Invitrogen). The vector contains the <i>ccdB</i> for negative selection that is replaced by the gene of

	interest through recombination by LR reaction. Vector can be used for FRT recombination into FlpIn T-Rex cell lines. The vector contains a hygromycin resistance gene.
GW-pcDNA5/FRT/TO/GS/N-TAP-CHIKV-nsP3	Vector for CMV/TetO2 driven expression of N-terminally TAP-tagged CHIKV nsP3. Vector can be used for FRT recombination into FlpIn T-Rex cell lines. The vector contains a hygromycin resistance gene. Generated by Gateway recombination of pDONR/Zeo-CHIKV-nsP3 with GW-pcDNA5/FRT/TO/GS/N-TAP.
GW-pcDNA5/FRT/TO/GS/N-TAP-CHIKV-nsP3-macro	Vector for CMV/TetO2 driven expression of N-terminally TAP-tagged CHIKV nsP3. Vector can be used for FRT recombination into FlpIn T-Rex cell lines. The vector contains a hygromycin resistance gene (P. Korn, née Verheugd).
GW-pDest-mCherry-C1	Empty Gateway vector for the expression of mCherry or the generation of plasmids for N-terminally mCherry-tagged fusion proteins. The vector contains the <i>ccdB</i> for negative selection that is replaced by the gene of interest through recombination by LR reaction (J. Vervoorts-Weber).
GW-pDest-mCherry-C1-CHIKV-nsP1	Vector for the expression of N-terminally mCherry-tagged CHIKV nsP1, nsP2, nsP3 or nsP4. Generated by Gateway recombination of pDONR/Zeo-CHIKV-nsP1/-nsP2/-nsP3/-nsP4 with GW-pDest-mCherry-C1.
GW-pDest-mCherry-C1-CHIKV-nsP2	
GW-pDest-mCherry-C1-CHIKV-nsP3	
GW-pDest-mCherry-C1-CHIKV-nsP4	
GW-pEGFP	Empty Gateway vector for the expression of EGFP or the generation of plasmids for N-terminally EGFP-tagged fusion proteins. The vector contains the <i>ccdB</i> for negative selection that is replaced by the gene of interest through recombination by LR reaction (Kleine et al. 2012).
GW-pEGFP-ARTD10	Vector for expression of N-terminally EGFP-tagged ARTD10 or the GW mutant (N. Herzog).
GW-pEGFP-ARTD10-GW	
GW-pEGFP-CHIKV-nsP2	Vector for expression of N-terminally EGFP-tagged CHIKV nsP2 and variants thereof. Generated by Gateway recombination of pDONR/Zeo-CHIKV-nsP2/-nsP2-459-798 and the according CASA mutants with GW-pEGFP.
GW-pEGFP-CHIKV-nsP2-459-798	
GW-pEGFP-CHIKV-nsP2-459-798-CASA	
GW-pEGFP-CHIKV-nsP2-CASA	
GW-pEGFP-CHIKV-nsP3	
GW-pEGFP-CHIKV-nsP3-macro	Vector for expression of N-terminally EGFP-tagged CHIKV nsP3 and variants thereof. Generated by Gateway recombination of pDONR/Zeo-CHIKV-nsP3/-nsP3-macro and the according macro mutants with GW-pEGFP.
GW-pEGFP-CHIKV-nsP3-macro-V33E	
GW-pEGFP-CHIKV-nsP3-macro-Y114V	
GW-pEGFP-CHIKV-nsP3-V33E	
GW-pEGFP-CHIKV-nsP3-Y114V	

GW-pEGFP-G3BP1	Vector for expression of N-terminally EGFP-tagged G3BP1. Generated by Gateway recombination of pDONR/Zeo-G3BP1 with GW-pEGFP.
GW-pFlag	Empty Gateway vector for the expression of N-terminally Flag-tagged fusion proteins. The vector was modified from pcDNA3 (Invitrogen) by introduction of the Gateway cassette which contains the <i>ccdB</i> for negative selection that is replaced by the gene of interest through recombination by LR reaction (J. Lüscher-Firzlaff).
GW-pFlag-CHIKV-nsP2	Vector for expression of N-terminally Flag-tagged CHIKV nsP2 and the CASA mutant. Generated by Gateway recombination of pDONR/Zeo-CHIKV-nsP2/-nsP2-CASA with GW-pFlag.
GW-pFlag-CHIKV-nsP2-CASA	
GW-pFlag-CHIKV-nsP3	Vector for expression of N-terminally Flag-tagged CHIKV nsP3. Generated by Gateway recombination of pDONR/Zeo-CHIKV-nsP3 with GW-pFlag.
GW-pFlag-CHIKV-nsP3-macro	Vector for expression of N-terminally Flag-tagged CHIKV nsP3 macro. Generated by Gateway recombination of pDONR/Zeo-CHIKV-nsP3-macro with GW-pFlag (P. Korn, née Verheugd).
GW-pFlag-CHIKV-nsP3-macro-V33E	Vector for expression of N-terminally Flag-tagged CHIKV nsP3 macro mutants. Generated by Gateway recombination of pDONR/Zeo-CHIKV-nsP3-macro-V33E/-Y114V with GW-pFlag.
GW-pFlag-CHIKV-nsP3-macro-Y114V	
GW-pFlag-CHIKV-nsP3-V33E	Vector for expression of N-terminally Flag-tagged CHIKV nsP3 with mutations in the macro. Generated by Gateway recombination of pDONR/Zeo-CHIKV-nsP3-V33E/-Y114V with GW-pFlag (P. Korn, née Verheugd).
GW-pFlag-CHIKV-nsP3-Y114V	
GW-pGFPnanobody	Empty Gateway vector for the expression of anti-GFP-nanobody or the generation of plasmids for N-terminally anti-GFP-nanobody-fused proteins. The vector contains the <i>ccdB</i> for negative selection that is replaced by the gene of interest through recombination by LR reaction. The human sequence optimized gBlock GFPnanobody <i>AgeI XhoI</i> hs optimized was inserted into GW-pEGFP by restriction with <i>XhoI</i> and <i>AgeI</i> and ligation, replacing the EGFP.
GW-pGFPnanobody-CHIKV-nsP3	Vector for the expression of N-terminally anti-GFP-nanobody-fused CHIKV nsP3 and variants thereof. The gBlock GFPnanobody <i>AgeI XhoI</i> hs optimized was inserted into GW-pEGFP-nsP3/-nsP3-macro/-nsP3-macro-V33E/-nsP3-V33E, respectively, by restriction with <i>XhoI</i> and <i>AgeI</i> and ligation, replacing the EGFP.
GW-pGFPnanobody-CHIKV-nsP3-macro	
GW-pGFPnanobody-CHIKV-nsP3-macro-V33E	
GW-pGFPnanobody-CHIKV-nsP3-V33E	

GW-pHA-PARP12	Vector for the expression of N-terminally HA-tagged ARTD12 wt or H567Y mutant (A. Forst).
GW-pHA-PARP12 H564Y	
pcDNA3-CHIKV-Replicon-CASA-nsP3-383-EGFP-SG-Gluc	
pcDNA3-CHIKV-Replicon-CASA-SG-Gluc	
pcDNA3-CHIKV-Replicon-nsP3-383-EGFP-SG-Gluc	
pcDNA3-CHIKV-Replicon-SG-Gluc	
pcDNA3-CHIKV-Replicon-V33E-nsP3-383-EGFP-SG-Gluc	
pcDNA3-CHIKV-Replicon-V33E-SG-Gluc	Vector for the mammalian expression of N-terminally Flag- and GST-tagged and C-terminally EGFP-tagged artificial protease substrate of nsP2 containing a polylinker for better accessibility and the long nsP3/nsP4 junction (Rausalu et al. 2016). GST-nsP3_4site-polylinker-EGFP was amplified from pGEX4T1-nsP3_4site-polylinker-EGFP with the primers <i>EcoRV</i> GST fw and EGFP <i>NotI</i> rev and inserted into pcDNA3 (Invitrogen) by restriction with <i>EcoRV</i> and <i>NotI</i> and ligation.
pcDNA3-Flag-GST-nsP3_4site-polylinker-EGFP	
pcDNA3.1-MCS*-BirA(R118G)-HA	Vector for the expression of C-terminally HA-tagged BirA(R118G). BirA is a biotin ligase derived <i>E. coli</i> that was mutated to R118G to increase promiscuity (Roux et al. 2012). Generated from pcDNA3.1-MCS-BirA(R118G)-HA (Addgene) by extension of the MCS by introduction of custom oligos (K. Feijs).
pcDNA3.1-ARTD10GW-BirA(R118G)-HA	Vector for the expression of C-terminally BirA(R118G)-HA-fused ARTD10 or the GW mutant (J. Wozniak).
pcDNA3.1-ARTD10wt-BirA(R118G)-HA	
pcDNA3.1-CHIKV-nsP3-BirA(R118G)-HA	Vector for the expression of C-terminally BirA(R118G)-HA-fused CHIKV nsP3. Generated by restriction of pcDNA3.1-MCS*-BirA(R118G)-HA and pDONR/Zeo-CHIKV-nsP3 by with <i>EcoRI</i> and <i>BamHI</i> and ligation.
pcDNA3.1-ATG-CHIKV-nsP3-macro-BirA(R118G)-HA	Vector for the expression of C-terminally BirA(R118G)-HA-fused CHIKV nsP3 macro. Generated by site directed mutagenesis of pcDNA3.1-CHIKV-nsP3-macro-BirA(R118G)-HA (C. Kocyigit) using the primers Q5_ATG_BirA_CHIKV_for and rev introducing and ATG.
pcDNA5/FRT/TO-GFP-mParp14 Macro2-3	Vector for CMV/TetO2 driven expression of N-terminally EGFP-tagged mParp14-Macro2-3 or the

pcDNA5/FRT/TO-GFP-mParp14 Macro2-3 G1055E G1268E	G1055E G1268E mutant (M. Bütepage). The vector contains a hygromycin resistance gene.
pCMV-HA-PARP7	Vector for the expression of N-terminally HA-tagged PARP7/ARTD14 (gift from A. Ladurner, München).
pEVRF0-HA-PARP10	Vector for the expression of N-terminally HA-tagged ARTD10 or the GW mutant (Kleine et al. 2008).
pEVRF0-HA-PARP10-GW	
pHA.NE-PARP1	Vector for the expression of N-terminally HA-tagged ARTD1 (gift from M. Hottiger, Zürich).

Plasmids for <i>in vitro</i> transcription	
Plasmid name	Description
SP6-CHIKV-Replicon-SG-GLuc	Vector for the <i>in vitro</i> transcription of the CHIKV Replicon with Gaussia Luciferase under the control of the subgenomic promoter (gift from B. Kümmerer, Bonn)(Glasker et al. 2013).
SP6-CHIKV-Replicon-D10A-SG-GLuc	Vector for the <i>in vitro</i> transcription of the CHIKV Replicon with mutations in the macro and with Gaussia Luciferase under the control of the subgenomic promoter. Generated from SP6-CHIKV-Replicon-SG-GLuc (gift from B. Kümmerer, Bonn) by restriction with <i>Clal</i> and <i>BstAPI</i> and insertion of the gBlocks CHIKV D10A/V33E/Y114V Minigene.
SP6-CHIKV-Replicon-V33E-SG-GLuc	
SP6-CHIKV-Replicon-Y114V-SG-GLuc	
SP6-CHIKV-Replicon-CASA-SG-GLuc	Vector for the <i>in vitro</i> transcription of the CHIKV Replicon with the CASA mutation and with Gaussia Luciferase under the control of the subgenomic promoter. Generated from SP6-CHIKV-Replicon-SG-GLuc (gift from B. Kümmerer, Bonn) and GW-pFlag-CHIKV-nsP2-CASA by restriction with <i>NdeI</i> and ligation.
SP6-CHIKV-Replicon-nsP2-466-EGFP-SG-Gluc	Vector for the <i>in vitro</i> transcription of the CHIKV Replicon (wt, CASA or V33E, respectively) containing an insertion of EGFP at position 466 of nsP2 according to Utt et al. 2016 and with Gaussia Luciferase under the control of the subgenomic promoter. Linkers were introduced into the according SP6-CHIKV-Replicon-SG-GLuc variants by site directed mutagenesis using the primers Q5 nsP2 linker fw and rev containing <i>SpeI</i> and <i>XhoI</i> restriction sites. The EGFP sequence was amplified from pEGFP-C1 using the primers <i>SpeI</i> Gly Gly EGFP fw and EGFP Gly Gly <i>XhoI</i> rev and inserted into the replicons by restriction with <i>SpeI</i> and <i>XhoI</i> and ligation.
SP6-CHIKV-Replicon-CASA-nsP2-466-EGFP-SG-Gluc	
SP6-CHIKV-Replicon-V33E-nsP2-466-EGFP-SG-Gluc	
SP6-CHIKV-Replicon-GAA-nsP2-466-EGFP-SG-Gluc	Vector for the <i>in vitro</i> transcription of the CHIKV Replicon containing the EGFP insertion within nsP2

SP6-CHIKV-Replicon-CASA-GAA-nsP2-466-EGFP-SG-Gluc	as well as the GAA mutation or a combination of the GAA mutation with the CASA or V33E mutation. Generated from SP6-CHIKV-Replicon-nsP2-466-EGFP-SG-Gluc (wt, CASA or V33E) by restriction with <i>AgeI</i> and <i>AvrII</i> and insertion of the gBlock CHIKV nsP4 GAA Minigene.
SP6-CHIKV-Replicon-V33E-GAA-nsP2-466-EGFP-SG-Gluc	
SP6-CHIKV-Replicon-nsP3-383-EGFP-SG-Gluc	Vector for the <i>in vitro</i> transcription of the CHIKV Replicon (wt, CASA or V33E, respectively) containing an insertion of EGFP at position 383 of nsP3 according to Utt et al. 2016 and with Gaussia Luciferase under the control of the subgenomic promoter. Linkers were introduced into the according SP6-CHIKV-Replicon-SG-GLuc variants by site directed mutagenesis using the primers Q5 nsP3 linker fw and rev containing <i>SpeI</i> and <i>XhoI</i> restriction sites. The EGFP sequence was amplified from pEGFP-C1 using the primers <i>SpeI</i> Gly Gly EGFP fw and EGFP Gly Gly <i>XhoI</i> rev and inserted into the replicons by restriction with <i>SpeI</i> and <i>XhoI</i> and ligation.
SP6-CHIKV-Replicon-CASA-nsP3-383-EGFP-SG-Gluc	
SP6-CHIKV-Replicon-V33E-nsP3-383-EGFP-SG-Gluc	
SP6-CHIKV-Replicon-GAA-nsP3-383-EGFP-SG-Gluc	Vector for the <i>in vitro</i> transcription of the CHIKV Replicon containing the EGFP insertion within nsP3 as well as the GAA mutation or a combination of the GAA mutation with the CASA or V33E mutation. Generated from SP6-CHIKV-Replicon-nsP3-383-EGFP-SG-Gluc (wt, CASA or V33E) by restriction with <i>AgeI</i> and <i>AvrII</i> and insertion of the gBlock CHIKV nsP4 GAA Minigene.
SP6-CHIKV-Replicon-CASA-GAA-nsP3-383-EGFP-SG-Gluc	
SP6-CHIKV-Replicon-V33E-GAA-nsP3-383-EGFP-SG-Gluc	

4.1.4 Antibodies

Primary Antibodies or Antibody-likes			
Antigen	Clone/Product number	Supplier	Description/Application
Actin	C4/69100	MP Biomedicals	Monoclonal mouse WB: 1:200 TBS-T
ARTD10	5H11	E. Kremmer	Monoclonal rat WB: 1:500 TBS-T IF: 1:50
Avidin D-HRP	A-2004	Vector Laboratories	HRP-conjugated Avidin D WB: 1:10,000 5% BSA TBS-T
CD2AP	A599/5478	Cell Signaling	Monoclonal rabbit WB: 1:1,000 5% BSA TBS-T
CHIKV nsP2		Eurogentec	Polyclonal rabbit, raised against two peptides of nsP2: aa570-584: CERKYPFTKGKWNINK, aa740-755: CVLGRKFRSSRALKPP WB: 1:5,000 5% BSA TBS-T

FLAG	M2	Sigma	Monoclonal mouse WB: 1:5,000 TBS-T
G3BP	23/G3BP/611126	BD	Monoclonal mouse WB: 1:1,000 TBS-T IF: 1:50
GFP	600-301-215	Rockland	Monoclonal mouse WB: 1:2,000 TBS-T IP: 1 µl per IP
GFP	600-101-215	Rockland	Polyclonal goat WB: 1:2,000 TBS-T
GST	6G9	E. Kremmer	Monoclonal rat WB: 1:500 TBS-T
HA	16B12	Covance/ Biolegend	Monoclonal mouse WB: 1:1,000 TBS-T IF: 1:1,000 IP: 1 µl per IP
MAR	MABE1076	Merck Millipore	Monoclonal antibody-like with rabbit Fc tag, produced in E. coli WB: 0.4 µg/ml TBS-T
p-STAT1	58D6/9167	Cell Signaling	Monoclonal rabbit WB: 1:1,000 5% BSA TBS-T
PAR	4336-BPC-100	Trevigen	Polyclonal rabbit WB: 1:2,000 TBS-T
PARP12	SAB2104087	Sigma	Polyclonal rabbit WB: 1:1,000 TBS-T
Tubulin - α	B-5-1-2/T-5168	Sigma	Monoclonal mouse WB: 1:5,000 TBS-T
Tubulin - α	B-5-1-2/sc-23948	Santa Cruz	Monoclonal mouse WB: 1:1,000 TBS-T
USP10	D7A5/8501	Cell Signaling	Monoclonal rabbit WB: 1:1,000 5% BSA TBS-T
ARTD8		Eurogentec	Polyclonal rabbit, raised against a peptide of ARTD8: aa1193–1207: NLVSDKIPKAKDTQG WB: 1:1,000 5% BSA TBS-T

Secondary Antibodies			
Antigen	Product number	Supplier	Application
Alexa Fluor 555-conjugated goat anti-mouse IgG (H+L)	A-21422	Invitrogen	IF: 1:1,000
Alexa Fluor 555-conjugated goat anti-rat IgG (H+L)	A-21434	Invitrogen	IF: 1:1,000
Peroxidase-conjugated goat α -mouse IgG (H+L)	115-036-068	Jackson Immunoresearch	WB: 1:10,000
Peroxidase-conjugated goat α -rabbit IgG (H+L)	111-035-144	Jackson Immunoresearch	WB: 1:10,000

Peroxidase-conjugated goat α -rat IgG (H+L)	112-035-068	Jackson Immunoresearch	WB: 1:10,000
Peroxidase-conjugated rabbit α -goat IgG (H+L)	sc-2768	Santa Cruz	WB: 1:5,000

4.1.5 Inhibitors

Reagent	Product number	Supplier	Application
OUL35/0035	6344	Tocris	10 μ M
3-Aminobenzamide	sc-3501	Santa Cruz	2.5 mM
MG132	C2211	Sigma	25 μ M
Bafilomycin A1	BML-CM110	Enzo Life Sciences	200 nM

4.1.6 Bacterial strains

Strain	Source	Genotype
<i>E. coli</i> BL21 (DE3) pLysS	Stratagene	<i>B Fdcm ompT hsdS (rB- mB-) gal (DE3) [pLysS Camr]</i>
<i>E. coli</i> DB3.1	Invitrogen	<i>gyrA462 endA1 Δ(sr1-recA) mcrB mrr hsdS20 glnV44 (=supE44) ara14 galK2 lacY1 proA2 rpsL20 xyl5 leuB6 mtl1</i>
<i>E. coli</i> DH5 α	Invitrogen	<i>F-, ϕ80dlacZΔM15, Δ(lacZYA-argF)U169, deoR, recA1, endA1, hsdR17(rK -, mK+), phoA, supE44, λ-, thi-1, gyrA96, relA1</i>
<i>E. coli</i> GM2163		<i>F-dam-13::Tn 9 dcm-6 hsdR2 leuB6 his-4 thi-1 ara-14 lacY1 galK2 galT22 xyl-5 mtl-1 rpsL136 tonA31 tsx-78 supE44McrA - McrB-</i>
<i>E. coli</i> Lemo21 (DE3)	NEB	<i>fhuA2 [lon] ompT gal (λ DE3) [dcm] ΔhsdS/ pLemo(CamR) λ DE3 = λ sBamHlo ΔEcoRI-B int::(lacI::PlacUV5::T7 gene1) i21 Δnin5 pLemo = pACYC184-PrhaBAD-lysY</i>
<i>E. coli</i> One Shot™ Stbl3™	Invitrogen	<i>F-mcrB mrrhsdS20(rB-, mB-) recA13 supE44 ara-14 galK2 lacY1 proA2 rpsL20(StrR) xyl-5 λ-leumtl-1</i>
<i>E. coli</i> XL10 Gold	Stratagene	<i>TetrD(mcrA)183 D(mcrCB-hsdSMR-mrr)173 endA1 supE44 thi-1 recA1 gyrA96 relA1 lac Hte [F' proAB lacIqZDM15 Tn10 (Tetr) Amy Camr]</i>
StrataClone SoloPack Gold Competent Cells	Agilent	<i>TetrΔ(mcrA)183 Δ(mcrCB-hsdSMR-mrr)173 endA1 supE44 thi-1 recA1 gyrA96 relA1 lac Hte [F' proAB lacIqZDM15 Tn10 (Tetr) Amy Camr]</i>

E. coli DB3.1 were used for the amplification of empty Gateway vectors. *E. coli* DH5 α or One Shot™ Stbl3™ were used for plasmid amplification for Gateway recombination based cloning. *E. coli* One Shot™ Stbl3™ or XL10 Gold were used for the amplification of plasmids generated by conventional restriction-ligation-based cloning. *E. coli* One Shot™ Stbl3™ were used to amplify all SP6-CHIKV-Replicon-SG-GLuc constructs and variants thereof. The *E. coli* GM2163 strain was used to produce plasmids without dam methylation to be able to digest with methylation sensitive restriction enzymes. This was necessary for the introduction of the

macro mutants into SP6-CHIKV-Replicon-SG-GLuc. StrataClone SoloPack Gold Competent Cells were used for blunt end cloning using the StrataClone Blunt Cloning Kit (Agilent).

E. coli BL21 (DE3) pLysS or Lemo21 (DE3) were used for the production of recombinant proteins. Only the His-HEPEXDA4-ORF1-macro and His-HEPEXDD12-ORF1-macro were produced in *E. coli* XL10 Gold.

4.1.7 Eukaryotic cell lines

Strain		Source/Reference	Description
HEK293		ATCC CRL-1573™	Adenovirus transformed cell line from human embryonic kidney
HEK293 FlpIn T-REx		Invitrogen #R780-07	HEK293 cell line for stable integration and Dox-inducible expression of proteins. The insert was stably integrated from pcDNA5/FRT/TO constructs via FRT recombination. CMV/TetO2 driven expression can be induced by addition of Dox as the cell line constitutively expresses the Tetracycline repressor (pcDNA6/TR based; Invitrogen).
Insert	ARTD10-C-TAP	(Kleine et al. 2008)	
	ARTD10-GW-C-TAP		
	ARTD12-C-TAP	A. Forst	
	ARTD12-HY-C-TAP	(Krieg et al. 2020)	
	GFP-mParp14-macro2-3	M. Bütepage (Ecke et al. 2017)	
	GFP-mParp14-macro2-3 G1055E G1268E		
	N-TAP	(Kleine et al. 2008)	
	N-TAP-CHIKV-nsP3	B. Lippok (Ecke et al. 2017)	
N-TAP-CHIKV-nsP3-macro			
HeLa		ATCC CCL-2™	Human cervix adenocarcinoma cell line containing HPV18 (human papillomavirus 18)
HeLa FlpIn T-REx		Stephen Taylor, University of Manchester	HeLa cell line for stable integration and Dox-inducible expression of proteins. The insert was stably integrated from pcDNA5/FRT/TO constructs via FRT recombination. CMV/TetO2 driven expression can be induced by addition of Dox as the cell line constitutively expresses the Tetracycline repressor (pcDNA6/TR based; Invitrogen).
Insert	ARTD10	(Herzog et al. 2013)	
	ARTD10 GW		
U2-OS		ATCC HTB-96™	Human osteosarcoma cell line

4.2 Experimental Procedures

4.2.1 Work with nucleic acids

4.2.1.1 Restriction digestion of DNA

Restriction enzymes and buffers (NEB) were used according to the manufacturer's instructions. Generally, 0.25 μ l of each enzyme were used per 10 μ l of reaction volume and the reaction was incubated for 1 h. For preparative restrictions for molecular cloning 2-5 μ g of plasmid were digested in a volume of 40 μ l, while analytical restrictions were performed in 10 μ l reaction volume with 1 μ g of DNA. In preparative restrictions 1 μ l of alkaline phosphatase (NEB) was added exclusively to the vector backbone to prohibit religation. For restriction digests employing multiple restriction enzymes the reaction conditions were adjusted according to the Double Digest Finder/NEBcloner (NEB). The resulting DNA fragments were analyzed using agarose gel electrophoresis (chapter 4.2.1.2).

4.2.1.2 Agarose gel electrophoresis

TBE buffer:	89 mM Tris base (pH 8.0); 89 mM boric acid; 2 mM EDTA
10x DNA/RNA loading buffer:	50 mM Tris base (pH 8.0); 50 mM EDTA; 50% (v/v) glycerol; 0.25% (w/v) Bromophenol blue; 0.25% (w/v) xylencyanole
Agarose	Low EEO (Sigma); 0.7-2% (w/v)
Ethidium bromide:	Applichem; 0.5 μ g/ml
Size marker:	GeneRuler™ 1 kb Plus DNA Ladder (MBI Fermentas)

Agarose gel electrophoresis was used to analyze DNA products from PCR reactions (chapter 4.2.1.4), DNA fragments from restriction digests of plasmid DNA (chapter 4.2.1.1) or RNA from *in vitro* transcription (chapter 4.2.1.11). The samples were mixed with 10x loading buffer and subjected to electrophoresis in a 0.7-2% agarose gel containing ethidium bromide, depending on the expected product sizes. Separation took place at 80-120 V for 15-30 min in comparison to the size marker. The Nucleic acid fragments were visualized on a UV transilluminator (E-BOX VX2, Peqlab)(wavelength $\lambda=302$ nm).

4.2.1.3 Gel purification of DNA from an agarose gel

Subsequent to agarose gel electrophoresis of DNA fragments from restriction digests or PCRs, desired DNA fragments were purified from the agarose gel by excision with a scalpel under UV light. Thereafter the DNA was purified using the ZymoClean™ Gel DNA Recovery Kit (Zymo Research) according to the manufacturer's instructions. The DNA was eluted in 10 μ l TE buffer and used for molecular cloning.

4.2.1.4 Polymerase chain reaction (PCR)

PCRs were performed to amplify DNA inserts for Gateway or blunt end cloning (chapters 4.2.1.5 and 4.2.1.6). The inserts were amplified using forward (fw) and reverse (rev) primers contained extensions with the desired restriction sites or *attB* sites. The PCR was performed using the Phusion® High-Fidelity DNA Polymerase (NEB) according to the manufacturer's

instructions in a reaction volume of 50 μ l. The PCR product was analyzed via agarose gel electrophoresis and subsequently purified from the agarose gel (chapters 4.2.1.2 and 4.2.1.3). Purified PCR products containing *attB* sites were immediately used for Gateway cloning (chapter 4.2.1.5), while those for classical cloning via restriction were processed by blunt end cloning (chapter 4.2.1.6).

4.2.1.5 Gateway cloning

Gateway cloning (Invitrogen) comprises a cloning technique that is based on the sequence specific recombination of the bacteriophage λ . Recombinase enzymes, the BP clonase and the LR clonase, recombine specific attachment (*att*) sites. The former recombined *attB* and *attP* sites to create *attL* and *attR* sites, which the latter recombines and vice versa. This system is used to create entry clones, where a pDONR vector (Invitrogen) containing *attP* sites is recombined with a *attB* site flanked PCR product (chapter 4.2.1.4) or gBlock. The flanking sequences were designed according to the Gateway manual (Invitrogen). In the resulting entry clone the gene of interest is flanked by *attL* sites that can be recombined with various destination vectors with *attR* sites carrying diverse tags and selection markers. Empty gateway vectors, both entry and destination vectors, contain selection cassettes in between the *attP* and *attR* sites that allow for negative selection of negative clones via the *ccdB* gene. The *ccdB* gene is replaced by the gene of interest after successful recombination.

The BP and LR reactions were performed overnight at 25°C using half of the reagents suggested by the manual (10 μ l reaction volume). Five μ l of the BP reaction were subsequently transformed into competent bacteria, either *E. coli* DH5 α or Stbl3 (chapter 4.2.2.2). After plasmid preparation (chapter 4.2.1.9) the integrity of the Gateway constructs was controlled by restriction digest and sequencing (chapters 4.2.1.1 and 4.2.1.10).

4.2.1.6 Blunt end cloning

For classical molecular cloning using PCR products or gBlocks in combination with restriction digestion and ligation, the DNA inserts were generally initially cloned into the pSC-B-amp-kan vector via the StrataClone Blunt Cloning Kit (Agilent) according to the manufacturer's instructions. This intermediate step increases the efficiency of the restriction digestion and therefore the ligation into the desired vector (chapters 4.2.1.1 and 4.2.1.7). After blunt end cloning the PCR product or gBlock was always sequenced within the pSC-B-amp-kan prior to further processing (chapter 4.2.1.10).

4.2.1.7 Ligation of DNA fragments

Ligation of gel-purified, digested DNA fragments was performed using the T4 DNA ligase (NEB) according to the manufacturer's instructions in a volume of 20 μ l. 200 ng of vector backbone were used per reaction and the insert was added in a 5:1 molar ratio to the backbone. The ligation reaction was performed overnight at 25°C.

4.2.1.8 Site-directed mutagenesis

Mutations were introduced into plasmids using site-directed mutagenesis PCR using the Q5[®] Site-Directed Mutagenesis Kit (NEB) according to the manufacturer's instructions. Forward and reverse primers were designed using the NEBaseChanger tool (NEB). Generally, in

addition to the desired mutations, silent mutations were introduced. These did not alter the amino acid sequence but allowed for specific restriction digestion to identify successful mutation of the plasmids. Five μl of the KLD reaction were transformed into competent bacteria (chapter 4.2.2.2) and after plasmid preparation the introduction of the correct mutations was controlled via restriction digest and sequencing (chapter 4.2.1.1 and 4.2.1.10).

4.2.1.9 Plasmid preparation from bacterial cultures

On a small scale, DNA plasmids were purified from 4 ml of bacterial culture using the NucleoSpin Plasmid EasyPure Mini Kit (Macherey Nagel) according to the manufacturer's instructions. On a large scale, DNA plasmids were purified from 300 ml bacterial culture using the NucleoBond® Xtra Maxi Kit (Macherey Nagel) according to the manufacturer's instructions. Generally, the integrity of the resulting plasmids was controlled by restriction digestion and if necessary sequencing (chapter 4.2.1.1 and 4.2.1.10). The concentration and the purity of the plasmids was analyzed using the NanoDrop™ 1000 (Thermo Fisher Scientific).

4.2.1.10 Sequencing of DNA

The integrity of new vectors was controlled by Sanger Sequencing performed by SeqLab/Microsynth. Therefore, 1.2 μg of plasmids in a volume of 12 μl were analyzed using the standard primers provided by the company dependent on the plasmid backbone. If necessary, custom primers were directly ordered from and synthesized by SeqLab/Microsynth (chapter 4.1.2). The sequencing results were analyzed with the SerialCloner software (SerialBasic).

4.2.1.11 *In vitro* transcription of m⁷G-capped replicon RNA

First, 2 μg of the plasmid encoding the desired replicon variant were linearized using *Nde*I in 30 μl reaction volume (chapter 4.2.1.1). Subsequently the linearized plasmid was precipitated by addition of 71 μl ddH₂O, 5 μl 0.5 M EDTA, 10 μl 3 M sodium acetate (NaOAc) and 250 μl ice cold ethanol (EtOH) and incubation at -20°C for 30 min. The DNA was pelleted by centrifugation at full speed and 4°C for 15 min. The DNA pellet was dried and dissolved in 4.2 μl of RNase free water. The linearization and precipitation was controlled by agarose gel electrophoresis (chapter 4.2.1.2). Thereafter *in vitro* transcription was performed using the mMESSAGING mMACHINE™ SP6 Transcriptions Kit (Invitrogen) according to the manufacturer's instructions. Cap analog and GTP were added to the reaction in order to produce 5'-capped m⁷G-RNA and the reaction was carried out at 37°C for 2 h. Subsequently, the template DNA was digested addition of TURBO DNase from the kit at 37°C for another 15 min. The resulting RNA was precipitated using lithium chloride (LiCl) precipitation protocol according to the manufacturer's instructions. Finally, the dried RNA pellet was dissolved in 20 μl elution buffer from the High Pure RNA Isolation Kit (Roche). The *in vitro* transcription was controlled using agarose gel electrophoresis (chapter 4.2.1.2) and the concentration and purity of the RNA was analyzed using the NanoDrop™ 1000 (Thermo Fisher Scientific). Subsequently, the RNA was stored at -80°C until transfection (chapter 4.2.1.11).

4.2.2 Work with prokaryotic cells

4.2.2.1 Cultivation of bacterial cells

LB medium;	1% (w/v) tryptone; 0.5% (w/v) yeast extract; 1% (w/v) NaCl optional: 100 µg/ml ampicillin or 30 µg/ml kanamycin
Low salt LB medium:	1% (w/v) tryptone; 0.5% (w/v) yeast extract; 0.5% (w/v) NaCl 50 µg/ml zeocin
Agar plates:	LB medium; 1.5% (w/v) bacto agar optional: 100 µg/ml ampicillin or 30 µg/ml kanamycin
Low salt agar plates:	Low salt LB medium; 1.5% (w/v) bacto agar 50 µg/ml zeocin

All bacterial cultures generally contained the respective antibiotics, dependent on the transformed plasmid. Agar plates were incubated overnight at 37°C until colonies became visible. Liquid bacterial cultures were incubated overnight at 37°C under constant agitation of 130-160 rpm. For small scale plasmids preparation 5 ml of bacterial culture were grown in a test tube, while bacterial cultures for large scale plasmid preparation were grown in 300 ml in an Erlenmeyer flask (chapter 4.2.1.9). For purification of recombinant proteins, bacterial starter cultures were grown overnight in 25 ml in an Erlenmeyer flask. These were used for inoculation of the main culture the next morning. The main culture was grown in 400-500 ml until the desired OD was reached (chapters 4.2.4.1 and 4.2.4.2).

4.2.2.2 Heat shock transformation

Bacteria were transformed with DNA plasmids using heat shock transformation. One-hundred µl of chemically competent bacteria were thawed on ice. Subsequently, 5 µl of BP/LR reaction or Mutagenesis/KLD reaction or 7 µl of ligation reaction were added to the cell suspension. After incubation for 30 min on ice, the heat shock was performed at 42°C for 47 sec. Thereafter, the reaction was chilled on ice for 2 min prior to addition of 900 µl pre-warmed LB medium. The bacteria were regenerated at 37°C and 160 rpm for 1 h. Subsequently, the bacteria were pelleted at 5000 rpm for 3 min and the supernatant was discarded except 50-100 µl. The bacterial were resuspended in the remaining medium, completely plated onto agar plates containing the respective antibiotics and incubated overnight at 37°C.

For the retransformation of pre-existing plasmids, the transformation protocol was shortened. 1 µl of plasmid was transformed and the regeneration after the heat shock was omitted. After the 2 min incubation on ice, 50 µl of the transformation reaction were immediately plated onto agar plates containing the according antibiotics.

4.2.3 Work with eukaryotic cells

4.2.3.1 Cultivation of eukaryotic cells

1x PBS: 140 mM NaCl; 2.6 mM KCl; 2 mM Na₂HPO₄; 1.45 mM KH₂PO₄
Dulbecco's modified Eagle Medium (DMEM), high Glucose, + GlutaMAX™, - Pyruvate (Gibco)
Fetal calve serum (FCS), heat-inactivated (Gibco)
Trypsin/EDTA (0.05 %) (TrypLE™ Express, Gibco)
Penicillin/streptomycin (P/S) 10.000 Units/ 10.000 µg/ml (Gibco)
1 mg/ml Doxycycline in PBS
Interferone α (Peprotech, discontinued)

All cell lines were cultivated in DMEM supplemented with 10% (v/v) FCS and 1% (v/v) P/S at 37°C in an incubator providing saturated and 5% CO₂. The cells grew in 10 cm dishes in 10 ml medium and they were generally passaged every 3-5 days before they reached confluency. To passage the cells, they were washed with 1x PBS and incubated with Trypsin/EDTA for 5-10 min until they detached. Trypsinization was stopped by addition of fresh medium and a fraction of the cells suspension was transferred to a new 10 cm dish with fresh medium in a ratio dependent on the cell type. The stable HeLa and HEK293 FlpIn T-REx cells lines containing inserts were cultivated in 15 µg/ml blasticidin S (Invivogen) and 200 µg/ml hygromycin B (Invivogen). Protein expression of the stable FlpIn T-REx cells lines was induced with 1 µg/ml Doxycycline (Dox) 16 h prior to transfection with replicon RNA (chapter 4.2.3.5) or harvesting/fixation. Further, cells were treated with 180 U/ml Interferone α (IFNα) 24 h prior to harvesting.

4.2.3.2 Cryoconservation of eukaryotic cells

Cryoconservation medium: 90% heat-inactivated FCS, 10% DMSO

For long term conservation cells were detached from a 10 cm dish after reaching 80-90% confluency using trypsinization. The cells were pelleted at 500 xg and 4°C for 3 min and the medium was removed. Subsequently, the pellet was resuspended in 1 ml of cryoconservation medium and transferred to a cryo tube (Nalgene). Afterwards the cell suspension was slowly cooled at -80°C in a styrofoam box for 3-5 days until it was moved to -150°C for long term storage.

For thawing, the cell suspension was quickly warmed to 37°C and transferred into 10 ml of pre-warmed DMEM. The cells were pelleted at 500 xg and 4°C for 3 min, the medium was discarded and the cells were resuspended in fresh, pre-warmed medium before transfer to a 10 cm dish.

4.2.3.3 Cell seeding

For seeding cells, the cells were trypsinized and the cell concentration of the suspension was determined using the CASY cell counter (OMNI Life science) with a cell type-specific program. Cells were seeded into cell culture dishes or multi-well plates dependent on the experiment. Generally, HeLa and U2-OS cell lines were seeded 1 day prior to transfection or induction, while HEK293 cell lines were seeded 2 days before further treatment except for siRNA

transfection (chapter 4.2.3.6). The following amount of cells was seeded for the specific cell line:

Cell line	Dish format / Cultivation time	Number of cells
HEK293 cell lines	10 cm / 5 days	1.5×10^6
HeLa cell lines	10 cm / 4 days	$0.8-1 \times 10^6$
U2-OS	10 cm / 4 days	$0.8-1 \times 10^6$

The amount of cells was scaled up or down dependent on the length of the cultivation time in the experiment and of the size of the cell culture dishes/well in the following way:

Dish format / Cultivation time	Factor
15 cm	3
6 cm	1/2
6 well	1/5
12 well	1/10
Per day longer	1/2
Per day shorter	2

4.2.3.4 Calcium phosphate transfection of plasmid DNA

1x HBS buffer: 17 mM HEPES; 138 mM NaCl; 5 mM KCl; 0.71 mM Na_2HPO_4 ; pH 6.95
 1x HEPES buffer: 10 mM HEPES; 142 mM NaCl; 6.7 mM KCl; pH 7.3
 2.5 M CaCl_2

Cells were seeded as described previously (chapter 4.2.3.3). For transient overexpression, HEK293, HeLa and U2-OS cells were transfected with plasmid DNA using the calcium phosphate (CaPO_4) method. For a 10 cm dish, 20 μg of total DNA were mixed with 950 μl 1x HBS buffer. The amount of plasmid encoding the respective proteins of interests varied between constructs and the total amount of DNA was adjusted using pEQ176P2. Thereafter, 50 μl of CaCl_2 were added dropwise. After vortexing, the transfection mixture was incubated at room temperature (RT) for 30 min before it was added dropwise to the cell culture dish under gentle rocking. After approx. 1 h DNA- CaPO_4 precipitates became visible in the dish. The cells were incubated under normal cultivation conditions for 6 h (HEK293) or 24 h (HeLa or U2-OS). Subsequently, the cells were gently washed with pre-warmed HEPES buffer and incubated at RT for 5-10 min until the precipitates dissolved. Finally, transient protein expression was allowed for at least 48 h until harvesting or for 24 h until transfection with *in vitro* transcribed replicon RNA.

In smaller culture dishes, the amount of plasmid DNA, buffers and solutions was adjusted according to the volume of medium as follows:

Dish format	DNA amount per dish/well	1x HBS and 2.5 M CaCl_2 volume per dish/well
10 cm	20 μg	950 μl HBS + 50 μl CaCl_2
6 cm	10 μg	475 μl HBS + 25 μl CaCl_2
6 well	4 μg	190 μl HBS + 10 μl CaCl_2
12 well	2 μg	95 μl HBS + 5 μl CaCl_2

4.2.3.5 Transfection of *in vitro* transcribed replicon RNA

Cells were seeded as described previously (chapter 4.2.3.3). Lipofectamine 2000 transfection reagent (Thermo Fisher Scientific) was used according to the manufacturer's instructions in order to transfect cells with *in vitro* transcribed replicon RNA (chapter 4.2.1.11). In 12 well plates, 3 µg of *in vitro* transcribed replicon RNA were mixed with 100 µl Opti-MEM and 5 µl Lipofectamine 2000 by vortexing. The transfection mixture was incubated at RT for 5-10 min before it was added to the cells dropwise under gentle rocking. In a 10 cm dish, the ingredients were scaled up according to the volume of medium. Accordingly, 30 µg of replicon RNA were mixed with 1 ml of Opti-MEM and 50 µl Lipofectamine 2000. During the experiment the cells were incubated under normal cultivation conditions and 100 µl of supernatant were collected at 6, 9, 12, 24 and/or 30 h post transfection (hpt) in order to measure Gaussia luciferase activity and viral replication (chapter 4.2.3.7). Thirty hpt the cells were harvested. In the case of the analysis of co-transfection analysis of replicon RNA with plasmid DNA, both were transfected with Lipofectamine 2000 as described above.

4.2.3.6 Transfection of siRNA

Opti-MEM™, Reduced Serum Medium, no phenol red (Gibco)
HiPerFect Transfection Reagent (Qiagen)
20 µM siRNA stock

Cells were seeded in 12 wells or 6 wells as described previously (chapter 4.2.3.3). For transient siRNA transfection, the cells were transfected immediately after seeding. In the short time between seeding and the preparation of the transfection mixture, the cells were incubated under normal cultivation conditions. For a 12 well 3 µl of 20 µM siRNA stock was mixed with 55 µl of Opti-MEM and 5 µl of HiPerFect transfection reagent, resulting in a final siRNA concentration of 50 nM in the cell culture dish. Accordingly, for 6 wells, 6 µl of 20 µM siRNA stock was mixed with 110 µl of Opti-MEM and 10 µl of HiPerFect transfection reagent. The transfection mixtures were incubated at RT for 10 min until dropwise addition to the wells. Thereafter, the cells were incubated at normal cultivation conditions for 72 h when they were either harvested or further transfected with replicon RNA (chapter 4.2.3.5).

4.2.3.7 Viral replication assay

Cells were transfected with *in vitro* transcribed replicon RNA as described previously (chapter 4.2.3.5). One-hundred µl of supernatant were collected 6, 9, 12, 24 and/or 30 hpt. In the CHIKV replicon constructs, Gaussia luciferase replaces the structural polyprotein under the control of the subgenomic promoter and is secreted into the supernatant upon expression. Hence, Gaussia luciferase activity in the supernatant was analyzed as a measure for replication and cells that were only treated with transfection reagent without replicon RNA functioned as a negative control. To do so, either the BioLux® Gaussia Luciferase Assay Kit (NEB, discontinued) or the GAR-2B Gaussia Luciferase Assay (Targeting Systems) were used according to the manufacturer's instructions. Therein, 5 µl of supernatant for each sample were analyzed in technical duplicates 96-well plate (opaque, white) and measured according to the "Stabilized Assay Protocol I". After 35-40 sec of incubation with 50 µl stabilized substrate solution, the counts per second (CPS) were analyzed in each well with a VICTOR² 1420 multilabel counter

(Perkin Elmer) measuring luminescence without a filter over an interval of 10 sec. Statistical analysis was performed using the GraphPad Prism software.

4.2.3.8 Flow cytometry analysis

1x PBS: see chapter 4.2.3.1
Washing buffer: 1x PBS; 2% (v/v) heat-inactivated FCS

Cells were transfected with *in vitro* transcribed replicon RNA and/or plasmid DNA in 12 wells as described previously (chapters 4.2.3.4 and 4.2.3.5). Thirty hpt the cells were transferred into a 1.5 ml reaction tube by washing the cells of the plate in medium. Afterwards the cells were washed with 1x PBS and resuspended in 500 μ l washing buffer. For the propidium iodide (PI) staining control, cells were permeabilized and fixed in 80% EtOH at -20°C for 30 min and afterwards washed twiced and resuspended in 500 μ l washing buffer. The other samples were not fixed or permeabilized. Thereafter 50 μ g/ml of PI solution was added to all samples and incubated in the dark at RT for 20 min. Subsequently, flow cytometry analysis was performed with the FACSCanto II (BD Bioscience) measuring 100,000 events per sample per experiment.

In the experiment for the evaluation of co-transfection and co-expression efficiency of plasmid DNA and replicon RNA, mCherry was used. Therefore, 4',6-diamidino-2-phenylindole (DAPI) was used instead of PI to stain dead cells. In that case, all samples were treated with 0.1 μ g/mL DAPI solution immediately prior to the measurement. Flow cytometry analysis was performed with the Sony SH800 Cell Sorter because the FACSCanto II did not possess the necessary laser or filter to analyze mCherry. Again 100,000 events were measured per sample.

The data was analyzed using the FlowJo software (BD Bioscience).

4.2.4 Protein chemical methods

4.2.4.1 Purification of glutathione S transferase (GST-)tagged fusion proteins from bacteria

1x PBS:	see chapter 4.2.3.1
2xYT Medium:	1.6% (w/v) tryptone; 1% (w/v) yeast extract; 0.5% (w/v) NaCl
20% (w/v) Glucose solution, sterilely filtered	
1 M isopropyl- β -D-thiogalactopyranoside (IPTG)	
TNE lysis buffer:	20 mM Tris base, pH 8.0; 150 mM NaCl; 1 mM EDTA; 10% glycerol; 0.5-2 mM TCEP; add freshly: 1x PIC
GST wash buffer:	100 mM Tris base, pH 8.0; 120 mM NaCl; 0.5-2 mM TCEP
GST elution buffer:	GST wash buffer; add freshly: 20 mM glutathione
Pierce™ Glutathione Agarose (Thermo Fisher Scientific)	

E. coli BL21 or Lemo21 were transformed with plasmids for bacterial expression of the desired N-terminally tagged proteins via the shortened heat shock transformation protocol (chapter 4.2.2.2). A starter culture of 25 ml LB medium or 2xYT medium was inoculated with 4-5 clones from the agar plate and incubated at 37°C and 160 rpm overnight. The next morning a main culture of 400-500 ml LB medium supplemented with 0.4% (w/v) glucose or 2xYT medium was inoculated with the starter culture and incubated at normal growing conditions. The main cultures in supplemented LB were grown until an OD₆₀₀ of 0.4-0.6 and subsequently induced with 1 mM IPTG. After induction the cells were incubated at 20°C and 160 rpm overnight. The main cultures in 2xYT medium were grown until an OD₆₀₀ of 1.0-1.2 and subsequently induced with 0.1 mM IPTG. Thereafter these cultures were grown at 20°C and 160 rpm for 5 h. After the expression the bacteria were pelleted by centrifugation at 5000 rpm and 4°C for 10 min and the pellets were stored at -80°C or immediately used for the purification.

The bacteria pellet was resuspended in 20 ml TNE lysis buffer with PIC and transferred to a 50 ml reaction tube. The cell suspension was sonicated for 5-10 min with an interval of 30 sec/30 sec and an amplitude of 15-25% with the Branson digital sonifier 250D until the suspension showed a color change. Thereafter the lysate was incubated on ice for 10 min to allow the proteins to go into solution and subsequently the soluble fraction was cleared by centrifugation at 16,000 xg and 4°C for 30 min. Meanwhile 250 μ l of glutathione agarose (500 μ l slurry) were washed twice in 5 ml TNE lysis buffer by centrifugation at 500 xg and 4°C for 3 min. After centrifugation, the soluble fraction of the cell lysate was filtered with a 45 μ m filter, added to the equilibrated beads and incubated on an overhead shaker at 4°C for 1 h. Thereafter, the suspension was transferred into a Poly-Prep® Chromatography Column (Bio-Rad). All subsequent washing steps and the elution were performed in the chromatography column. The beads were washed once with 10 ml ice-cold PBS and afterwards 1x with 10 ml ice-cold GST wash buffer. The recombinant proteins were eluted by addition of 300 μ l elution buffer and incubation for 10 min. The elution step was repeated twice and all elution fractions were collected separately in 1.5 ml reaction tubes. The purity and the concentration of the elution fractions was analyzed by SDS-PAGE and Coomassie blue staining (chapters 4.2.4.3 and 4.2.4.4) and the recombinant proteins were aliquoted to avoid repeated freezing and thawing and stored at -80°C.

4.2.4.2 Purification of hexahistidine-(His-)tagged fusion proteins from bacteria

1x PBS:	see chapter 4.2.3.1
IMAC lysis buffer:	100 mM HEPES, pH 8.0; 500 mM NaCl; 10% Glycerol; 10 mM imidazole; 0.5-2 mM TCEP; add freshly: 1x PIC
IMAC wash buffer:	20 mM HEPES, pH 7.5; 500 mM NaCl; 10% Glycerol; 10 mM imidazole; 0.5-2 mM TCEP
IMAC elution buffer:	20 mM HEPES, pH 7.5; 500 mM NaCl; 10% Glycerol; 500 mM imidazole; 0.5-2 mM TCEP
TALON metal affinity resin (BD Bioscience)	

The expression of recombinant proteins in bacteria was performed as described in the previous chapter (chapter 4.2.4.1).

The purification was performed as described in the previous chapter as well (chapter 4.2.4.1), expect that the buffers were exchanged for the ion metal affinity chromatography (IMAC) buffers listed above and instead of GST agarose TALON metal affinity resin was used.

During the purification of His-CHIKV-nsP2, His-CHIKV-nsP2-459-798 and the respective CASA mutants no PIC was added to the lysis buffer.

4.2.4.3 Sodium dodecyl sulfate polyacrylamide gel electrophoresis (SDS-PAGE)

4x sample buffer (4x SB):	320 mM Tris-HCl, pH 6.8; 40% (v/v) glycerol; 20% (w/v) SDS; 0.5% bromophenol blue; 200 mM β -mercaptoethanol
SDS running buffer:	25 mM Tris base, pH 8.3; 250 mM glycine; 0.1% (w/v) SDS
Size marker:	protein marker VI, 10-245 kDa (AppliChem)

Proteins can be separated according to their molecular weight by denaturing, discontinuous SDS-PAGE. SDS_PAGE was performed using either the Mini-PROTEAN Tetra Cell system (Bio-Rad) or the Multigel-Long system (Biometra). The gels consisted of a 5% polyacrylamide (PAA) stacking gel and for the separation gel the PAA concentration varied from 7.5% to 15%, depending on the molecular weight of the proteins. In cases where the molecular weight of the proteins to be visualized was not compatible for separation on a classical PAA gel, a gradient gel with a PAA concentration from 15% on the bottom to 7.5% at the top was made and used. The samples were mixed with 4x SB to a final concentration of 1xSB and denatured at 95°C for 5 min. A protein size marker was used to allow estimation of the molecular weight of the proteins. Mini-PROTEAN gels were run at 150-200 V while Multigel-Long gels were run at 25-30 mA until the running front reached the end of the gel. The gels were immediately used for CB staining or Western blotting (chapters 4.2.4.4, 4.2.4.8 and 4.2.4.9).

4.2.4.4 Coomassie Blue (CB) staining

CB staining solution:	0.006% (w/v) Coomassie brilliant blue G-250; 10% (v/v) acetic acid
-----------------------	--

Subsequent to SDS-PAGE, total proteins were stained with CB staining. Therefore, the gel was incubated in CB staining solution at RT under gentle agitation for 1 h. Subsequently, the background was destained using ddH₂O and lint-free tissues overnight. Afterwards, gels were dried using a vacuum-drier and Whatman filter paper.

4.2.4.5 Circular dichroism (CD) analysis

CD buffer: 10 mM potassium phosphate, pH 7.5; 100 mM (NH₄)₂SO₄; 10% glycerol

Amicon Ultra-0.5 centrifugal filter, 10K NMWL/MWCO Device, (Merck Millipore)

In order to perform CD analysis of the His-tagged CHIKV-nsP3-macro and its mutants, the IMAC elution buffer was exchanged for CD buffer by using the Amicon centrifugal device with a MWCO of 10 kDa according to the manufacturer's instructions. All samples were centrifuged at 14,000 xg and 4°C for 15 min. Thereafter, the protein concentrations were determined using the DC™ Protein assay Kit I (Bio-Rad) according to the manufacturer's instructions and the concentration was adjusted to 0.5 mg/ml with CD buffer. The concentration and the purity of the samples was assessed with SDS-PAGE and Coomassie blue staining (chapters 4.2.4.3 and 4.2.4.4).

For the CD analysis 140 µl of each sample were transferred into a Hellma® SUPRASIL cuvette (Hellma GmbH & Co. KG) with a pathlength of 0.5 mm. CD buffer alone was used as a baseline. The measurement was performed at RT in the Olis SDM 17 CD (Olis). Each sample was scanned in technical triplicates from 195 to 240 nm. The analysis was performed using the Olis Global Works software package (Olis) and the spectra were smoothed with the Savitzky-Golay filter and a filter size of 10 (Gorry 1990). The CD analysis was supported by Alexander R. Grimm (Institute of Biotechnology, RWTH Aachen University).

4.2.4.6 Preparation of protein lysates from eukaryotic cells

1x PBS: see chapter 4.2.3.1

RIPA buffer: 10 mM Tris base, pH 7.4; 150 mM NaCl; 1% NP-40; 1% deoxycholate; 0.1% SDS

TAP lysis buffer: 50 mM Tris base, pH 7.5; 150 mM NaCl; 1 mM EDTA; 10% glycerol; 1% NP-40; 2 mM TCEP

1% SDS lysis buffer: 10 mM Tris base, pH 8.0; 1% SDS; 1 mM EDTA

Protease inhibitors: 1x Protease Inhibitor Cocktail (PIC, Sigma) containing AEBSF, Aprotinin, Bestatin, E-64d, Leupeptin and Pepstatin A

Phosphatase inhibitors: 20 mM β-glycerol phosphate; 0.1 mM sodium vanadate (NaVO₄); 50 nM oicadaic acid

Before preparation of lysates, the cells were washed with ice-cold 1x PBS. HeLa cell lines and U2-OS cells were washed on the plate. Because HEK293 are less adherent, they were washed from the plate in medium, transferred into a reaction tube and washed with ice-cold 1x PBS in the centrifuge. All lysis buffers were supplemented with PIC and phosphatase inhibitors directly prior to use in the above listed concentrations. The amount of lysis buffer used was scaled according to the dish/well. Therein, 10 cm dishes were lysed in 500 µl, 6 cm dishes in 300 µl, 6 well plates in 200 µl and 12 wells in 100 µl lysis buffer. In the case of HeLa cell lines and U2-OS cells, the lysis buffer was added directly to the plate and the cells were subsequently scraped and transferred to a 1.5 ml reaction tube. HEK293 cell lines were resuspended in lysis buffer and if necessary transferred to a 1.5 ml reaction tube as well.

Generally, RIPA lysates were prepared as a standard using supplemented RIPA buffer. The samples were sonicated in a water bath sonicator if the volume of the lysate was below 250 µl at 4°C, an interval of 1 sec/1 sec and an amplitude of 70% for 5 min. If the volume was above

250 μ l the samples were sonicated on ice with the Branson digital sonifier 250D at an amplitude of 10% for 30 sec. Subsequently the lysates were incubated on ice for 10 min to allow the proteins to go into solution prior to centrifugation in a tabletop centrifuge at full speed and 4°C for 30 min. The soluble fraction was transferred to a new reaction tube and used for further for SDS-PAGE and western blot Analysis or for immunoprecipitation (chapters 4.2.4.3, 4.2.4.7, 4.2.4.8 and 4.2.4.9).

If the lysates were prepared for co-immunoprecipitations or *in vitro* ADPr assays, TAP lysates were prepared instead of RIPA lysates to preserve protein-protein interactions and catalytic activity. Therefore, the cells were resuspended in supplemented TAP lysis buffer and incubated on an overhead shaker at 4°C for 30 min. Cells debris and insoluble proteins were subsequently pelleted by centrifugation in a tabletop centrifuge at full speed and 4°C for 30 min. Again the soluble WCL was transferred to a new reaction tube for further use.

To improve the solubility of membrane proteins, such as potentially CHIKV nsP1 and the viral polyprotein, 1% SDS lysis buffer was used to prepare lysates according to a protocol from PhosphoSolutions. In short, the supplemented 1% SDS lysis buffer was pre-heated to 95°C before addition to the cells. Thereafter the cells were resuspended, sonicated and centrifuged as described for RIPA lysates.

4.2.4.7 (Co-)immunoprecipitation

RIPA buffer:	see chapter 4.2.4.6
TAP lysis buffer	see chapter 4.2.4.6
Protein-G sepharose beads (Amersham Pharmacia) + primary antibody	
GFP-Trap magnetic agarose beads (Chromotek, gtma)	
2x SB	160 mM Tris-HCl, pH 6.8; 20% (v/v) glycerol; 10% (w/v) SDS; 0.25% bromophenol blue; 100 mM β -mercaptoethanol

Immunoprecipitation (IP) was performed from RIPA lysates, while the co-immunoprecipitation (co-IP) of protein-protein complexes was performed from TAP lysates. After the preparation of WCLs (chapter 4.2.4.6), 60 μ l of input sample were mixed with 4x SB and used for SDS-PAGE and Western blotting (chapters 4.2.4.3, 4.2.4.8 and 4.2.4.9). The residual lysate was used for the (co-)IP. To IP HA-tagged proteins, 1 μ l of anti-HA antibody (Covance/Biolegend) was used with 10-15 μ l of Protein-G sepharose slurry. For GFP-tagged proteins on the other hand, 1 μ l of anti-GFP antibody (monoclonal, Rockland) was used with 15 μ l of Protein-G sepharose slurry or 5 μ l of GFP-Trap bead slurry was used. In any case the beads were washed twice in 500 μ l of the according lysis buffer before addition to the lysate, while the potential primary antibody was immediately added. Afterwards, the mixture was incubated on an overhead shaker at 4°C for 1 h. Subsequently, the supernatant was discarded and the beads were washed three times with 1 ml of the according lysis buffer. The buffer was completely removed and the beads were resuspended in 20 μ l 2x SB, incubated at 95°C for 5 min and subjected to SDS-PAGE and Western blot analysis (chapters 4.2.4.3, 4.2.4.8 and 4.2.4.9).

4.2.4.8 Semidry Western blot

Semidry transfer buffer: 25 mM Tris base; 192 mM glycine; 20% (v/v) methanol
 Amersham™ Protran® Western blotting membranes, nitrocellulose, 0.2 μ m pore size (Cytiva)
 Whatman® Qualitative Filter Paper, Grade 3

Ponceau S solution: 0.05% (w/v) Ponceau S; 1% (v/v) acetic acid

For immunodetection of proteins with specific antibodies after SDS-PAGE (chapters 4.2.4.3 and 4.2.4.10), the proteins were typically transferred to nitrocellulose membranes using the semidry Western blotting technique. The gel, 6 filter papers and the membrane were incubated in semidry transfer buffer for a few minutes. Afterwards, everything was stacked from bottom (cathode) to top (anode) starting with 3 filter papers, the gel, the membrane and again 3 filter papers on a Semidry blotting apparatus (PEGASUS model, PHASE GmbH). The transfer took place at 2 mA/cm² of membrane for 75 min. Afterwards, the transfer efficiency was evaluated by staining of the membrane in Ponceau S solution under gentle rocking for a few minutes. The blot was further used for immunodetection of proteins and modifications via specific antibodies (chapter 4.2.4.10).

4.2.4.9 Tank Western blot

Tank blot transfer buffer: 25 mM Tris base; 192 mM glycine; 0.01% (w/v) SDS
Amersham™ Protran® Western blotting membranes, nitrocellulose, 0.2 µm pore size (Cytiva)
Whatman® Qualitative Filter Paper, Grade 3
Ponceau S solution: see chapter 4.2.4.8

In order to transfer proteins with a high molecular weight more efficiently, a wet/tank blot was performed instead of a semidry blot after SDS-PAGE (chapter 4.2.4.3). The tank blot was performed using the Mini Trans-Blot® Module (Bio-Rad). The two sponges, the gel, 6 filter papers and the membrane were incubated in ice-cold tank blot transfer buffer for a few minutes. The blotting cassette was assembled from black to see-through starting with a sponge, 3 filter papers, the gel, the membrane, 3 filter papers and a sponge and the cassette was placed into the blotting chamber with black facing black. The frozen cooling element and a magnetic stirring fish were placed in the blotting chamber and the blotting chamber was filled up with ice-cold tank blot transfer buffer. Then, the apparatus was placed in an ice bucket on a magnetic stirrer. While stirring the transfer took place at 100 V for 1 h. Afterwards, the transfer efficiency was evaluated by staining of the membrane in Ponceau S solution under gentle rocking for a few minutes. The blot was further used for immunodetection of proteins and modifications via specific antibodies (chapter 4.2.4.10).

4.2.4.10 Immunodetection of proteins and modifications

1x TBS: 50 mM Tris base, pH 7.5; 150 mM NaCl
1x TBS-T: 0.05% (v/v) Tween-20 in TBS
Blocking solution: 5% (w/v) non-fat dry milk powder in TBS-T

Subsequent to Semidry or Tank Western blot (chapters 4.2.4.8 and 4.2.4.9), the transferred proteins or modifications were detected using specific antibodies. After Ponceau S staining, the blot was incubated in blocking solution at RT and under gentle rocking for 1 h to block unspecific binding sites. The blocking solution was removed by washing 3 times with 1x TBS-T for 5 min each. Thereafter, the primary antibody was added to the membrane in a dilution specific to the antibody (chapter 4.1.4) and incubated at 4°C and under gentle rocking overnight. The next morning, to remove excess, unbound antibody, the membrane was washed 3 times in TBS-T for 5 min each. Thereafter, the secondary, HRP-coupled antibody was

added to the membrane in a dilution specific to the antibody (chapter 4.1.4) and incubated at RT and under gentle rocking for 1 h. Again, to remove excess, unbound antibody, the membrane was washed 3 times in TBS-T for 10 min each. The membranes were either developed using ECL solutions (SuperSignal™ West Pico PLUS Substrate or SuperSignal™ West Femto Maximum Sensitivity Substrate, Thermo Fisher Scientific) and a LAS3000 luminescence imaging device (Fuji) for detection, or using the WesternBright Quantum HRP substrate (Advansta) and the Azure c600 (Azure Biosystems) for detection.

If Biotinylation was assessed, the membrane was blocked in 5% BSA TBS-T instead of the normal blocking solution and no secondary antibody was used as the Avidin-D was directly coupled to HRP.

Immunoblots were quantified using the ImageJ software (NIH, Bethesda, USA) and statistical analysis was performed with GraphPad Prism software.

4.2.4.11 *In vitro* ADP-ribosylation assay with recombinant proteins

10x ADPr buffer	500 mM Tris base, pH 8.0; 20 mM TCEP; 40 mM MgCl ₂
1x ADPr buffer:	50 mM Tris base, pH 8.0; 2 mM TCEP; 4 mM MgCl ₂
10 mM β-NAD ⁺ (Sigma)	
³² P-NAD ⁺ (Perkin-Elmer)	
4x SB	see chapter 4.2.4.3

In vitro ADP-ribosylation (ADPr) assays were carried out in a reaction volume of 30 μl in ADPr buffer. One μg of recombinant, bacterially expressed His- or GST-tagged ARTDs or TAP-ARTD10, wt or GW, were subjected to *in vitro* ADP-ribosylation assays with or without 1 μg of recombinant substrates and/or hydrolases. The reactions were incubated in the presence or absence of 50-500 μM β-NAD⁺ and 1 μCi of ³²P-NAD⁺ at 30°C and 1,400 rpm for 30 min. In the case of His-ARTD1 5 pmol of annealed oligos were also added to the reaction to activate the PARylating activity. The reactions were stopped by addition of 4x SB and incubation at 95°C for 5 min. Thereafter, the samples were subjected to SDS-PAGE and CB staining or semidry western blotting (chapters 4.2.4.3 and 4.2.4.4) and the vacuum dried gel was developed by autoradiography.

4.2.4.12 *In vitro* ADP-ribosylation assay with immunoprecipitated HA-ARTD10

ADPr buffer:	see chapter 4.2.4.11
10 mM β-NAD ⁺ (Sigma)	
³² P-NAD ⁺ (Perkin-Elmer)	
4x SB	see chapter 4.2.4.3

HA-tagged ARTD10 or the GW mutant were expressed in HEK293 cells for 48 h and immunoprecipitated from TAP lysates as described previously (chapters 4.2.3.4, 4.2.4.6 and 4.2.4.7). After two washing steps with 1 ml TAP lysis buffer, the IPs were equilibrated with 1 ml of ADPr buffer. The IPs were either stored at -80°C in residual buffer or the buffer was completely removed and the beads were subjected to *in vitro* ADPr assays as described previously (chapter 4.2.4.11).

4.2.4.13 Hydrolase assay with recombinant proteins

Pulldown buffer: 100 mM Tris base, pH 7.6; 250 mM NaCl; 50 mM KCl; 5 mM MgCl₂; 0.5% NP-40; 0.1% Triton X-100
ADPr buffer: see chapter 4.2.4.11
Pierce™ Glutathione Agarose (Thermo Fisher Scientific)
10 mM β-NAD⁺ (Sigma)
³²P-NAD⁺ (Perkin-Elmer)
4x SB see chapter 4.2.4.3

One μg of bacterially expressed, GST-tagged ARTD10cat and/or NEMO were coupled to 30 μl of GST agarose slurry in pulldown buffer on an overhead shaker at 4°C for 1 h. Subsequently the beads were washed with pulldown buffer and equilibrated in ADPr buffer. The ADPr assay was carried out as described previously (chapter 4.2.4.11). The reaction was stopped by washing twice with 1 ml ADPr buffer. For the hydrolase assay the reactions were incubated with or without 1 μg of His-tagged hydrolase or His-Artd8-macro2 in 30 μl ADPr buffer for 0, 10, 20, 30, 60, 120, 180 or 240 min. The reactions were stopped by addition of 4x SB and incubation at 95°C for 5 min. Thereafter, the samples were subjected to SDS-PAGE and CB staining (chapters 4.2.4.3 and 4.2.4.4) and the vacuum dried gel was developed by autoradiography.

4.2.4.14 Hydrolase assay with immunoprecipitated HA-ARTD1

ADPr buffer: see chapter 4.2.4.11
10 mM β-NAD⁺ (Sigma)
³²P-NAD⁺ (Perkin-Elmer)
4x SB see chapter 4.2.4.3

HA-tagged ARTD1 was expressed in HEK293 cells for 48 h and immunoprecipitated from TAP lysates as described previously (chapters 4.2.3.4, 4.2.4.6 and 4.2.4.7). After two washing steps with 1 ml TAP lysis buffer, the IPs were equilibrated with 1 ml of ADPr buffer. The IPs were either stored at -80°C in residual buffer or the buffer was completely removed and the beads were subjected to *in vitro* hydrolase assays as described previously (chapter 4.2.4.11). In short, HA-ARTD1 bound to the beads was allowed automodification in the presence of 5 pmol annealed oligos and 50-500 μM β-NAD⁺ with or without 1 μCi of ³²P-NAD⁺ at 30°C and 1,400 rpm for 30 min. The reactions were stopped by washing twice with 1 ml ADPr buffer. For the hydrolase assay the reactions were incubated with or without 1 μg of respective His-tagged hydrolase in 30 μl ADPr buffer for 0, 10, 20, 30, 60, 120, 180 or 240 min. The reactions were stopped by addition of 4x SB and incubation at 95°C for 5 min. Thereafter, the samples were subjected to SDS-PAGE and CB staining or semidry Western blotting (chapters 4.2.4.3, 4.2.4.4 and 4.2.4.8). The modification was analyzed by autoradiography of the vacuum-dried gel or immunodetection with an anti-PAR antibody (Trevigen) (chapter 4.2.4.10). The released products were analyzed by TLC or PAGE (chapters 4.2.4.15 and 4.2.4.16).

4.2.4.15 Thin Layer Chromatography (TLC) of released products from hydrolase assays

TLC buffer: 0.3 M LiCl; 0.9 M acetic acid
PEI-F cellulose plates (20 cm × 20 cm, Merck)

A TLC chamber was filled with TLC buffer and shut air-tight with the help of silicon paste. The atmosphere was allowed to build at RT for at least 24 h prior to the experiment. Subsequent to the hydrolase assay in the presence of radioactively labelled $^{32}\text{P-NAD}^+$ (chapters 4.2.4.13 and 4.2.4.14), the supernatant was removed from the beads. In order to analyze the released products, the supernatant was subjected to TLC. The samples were spotted onto PEI-F cellulose plates and $^{32}\text{P-NAD}^+$ was spotted as a control. The TLC was developed in the TLC chamber containing the TLC buffer and the products were visualized by exposure to X-Ray films. The beads and a fraction of the supernatant were subjected to SDS-PAGE and CB staining (chapters 4.2.4.3 and 4.2.4.4). As a control for the hydrolase assay the vacuum-dried gel resulting from the bead-bound fraction was likewise exposed to X-Ray films.

4.2.4.16 Sequencing PAGE of released products from hydrolase assays

Urea loading buffer 50% (w/v) urea; 25 mM NaCl; 4 mM EDTA; 0.02% xylene cyanol;
0.02% bromophenol blue

As an alternative to TLC (chapter 4.2.4.15), the products released from hydrolase assays were analyzed using sequencing PAGE. This allows the differentiation between various lengths of release ADPr polymers including single moieties (Panzeter et al. 1990). The samples to be analyzed were generated as described previously (chapter 4.2.4.15). The supernatant was dried in a Speed-Vac and resuspended in 5 μl of urea loading buffer. The 20% PAA sequencing gel (60 cm x 20 cm x 0.35 mm, in TBE buffer) was pre-heated to 55°C degrees by pre-electrophoresis at 55 W for about 1 h. Then, the samples were loaded and PAGE was carried out at 55 W until the running front had migrated about 30 cm. The gel was vacuum-dried and developed by autoradiography.

4.2.4.17 *In vitro* protease assay with nsP2

ADPr buffer: see chapter 4.2.4.11
4x SB see chapter 4.2.4.3

The reaction was carried out in 15 μl ADPr buffer. Recombinant His-CHIKV-nsP2-459-798 or the respective CASA mutant were incubated in the presence of bacterially expressed, synthetic substrate at 30°C for 0, 30, 60 or 120 min. As negative controls the protease or the substrate were incubated at 30°C for 0 and 120 min. The reaction was stopped by addition of 4x SB and incubation at 95°C for 5 min. The protease assay was analyzed by SDS-PAGE and CB staining (chapters 4.2.4.3 and 4.2.4.4).

4.2.4.18 ADP-ribosylation assay with subsequent *in vitro* protease assay

ADPr buffer: see chapter 4.2.4.11
10 mM $\beta\text{-NAD}^+$ (Sigma)
 $^{32}\text{P-NAD}^+$ (Perkin-Elmer)
4x SB see chapter 4.2.4.3

Bacterially expressed, His-tagged ARTD10cat, wt or GW, was incubated in the presence of His-CHIKV-nsP2-459-798 with or without hydrolase. The ADPr assay was carried out in 30 μl ADPr buffer with 500 μM $\beta\text{-NAD}^+$ and in the presence or absence of 1 μCi of $^{32}\text{P-NAD}^+$ at 30°C for

30 min. Afterwards, the synthetic protease substrate was added and the reactions were further incubated at 30°C for 0, 30, 60 or 120 min. As controls the substrate was incubated alone for 0 and 120 min and the inactive CASA mutant of the protease was included. The reactions were terminated by addition of 4x SB and incubation at 95°C for 5 min. The assay was either analyzed by SDS-PAGE and CB staining and optionally autoradiography if $^{32}\text{P-NAD}^+$ was used, or by SDS-PAGE, semidry Western blotting and immunodetection of the proteins and modifications (chapters 4.2.4.3, 4.2.4.4, 4.2.4.8 and 4.2.4.10).

4.2.4.19 BioID Assay

1x PBS	see chapter 4.2.3.1
BioID lysis buffer:	50 mM Tris base, pH 7.5; 500 mM NaCl; 0.2% SDS; 5 mM EDTA; 1 mM DTT
10% Triton X-100 solution	
50 mM Tris base, pH 7.5 (at 4°C)	
Dynabeads™ MyOne™ Streptavidin C1 (Invitrogen)	
BioID wash buffer 1:	2% SDS
BioID wash buffer 2:	50 mM HEPES, pH 7.5; 500 mM NaCl; 2% SDS; 1 mM EDTA; 1% Triton X-100
BioID wash buffer 3:	10 mM Tris base, pH 8.0; 250 mM LiCl; 0.5% SDS; 1 mM EDTA; 0.5% NP-40
BioID wash buffer 4:	50 mM Tris base, pH 7.5; 50 mM NaCl
BioID elution buffer:	30 mM biotin; 100 mM NaCl; 2% SDS; 6 M urea; 2 M thiourea; in PBS
4x SB:	see chapter 4.2.4.3

The BioID system was used to identify interactors of CHIKV nsP3 and the isolated macro as well as ARTD10 compared to its inactive GW mutant. Therefore, the proteins of interest are fused to BirA carrying the R118G mutation. This promiscuous biotin ligase biotinylates proteins in close proximity and therefore potentially stable as well as dynamic interactors, that can be identified by mass spectrometry (MS) after Streptavidin-mediated enrichment (**Figure 59**) (Roux et al. 2012).

Eight 10 cm dishes of HEK293 cells were seeded per condition and transiently transfected with plasmids encoding the desired fusion proteins or BirA alone as described previously (chapters 4.2.3.3 and 4.2.3.4). The day after transfection, the cells were treated with 50 μM biotin overnight. For every BirA-fusion protein a condition with and without biotin was generated. Forty-eight h after transfection and 16 h after the addition of biotin, the cells were washed from the plate in medium and transferred into Falcon tubes. The eight plates from each condition were pooled. The cells were washed three times with ice-cold 1x PBS by centrifugation at 4°C and 500 xg for 3 min to remove excess biotin from the medium. The subsequent steps were performed at RT. The cells were resuspended in 2 ml lysis buffer and sonicated for 15 sec with an interval of 1 sec/1 sec and an amplitude of 10-15% using a Branson digital sonifier 250D. After addition of 500 μl of 10% Triton X-100 solution, resulting in a final concentration of 2% Triton X-100, the sonification step was repeated. Finally, 2.5 ml of ice-cold 50 mM Tris base pH 7.5 were added and the sonification step was repeated once more. Thereafter the lysate was centrifuged at 4°C and 16,000 xg for 30 min. Sixty μl of the lysate were collected as an input sample and the protein concentration was determined using the DC™ Protein assay Kit I (Bio-Rad) according to the manufacturer's instruction. For the input

control 20 µg of total protein were subjected to SDS-PAGE, semidry Western blotting and immunodetection (chapters 4.2.4.3, 4.2.4.8 and 4.2.4.10). The following steps were performed at 4°C or on ice. Per sample 600 µl of Dynabeads™ MyOne™ Streptavidin C1 slurry were washed twice with 50 mM Tris base, pH 7.5 for equilibration. The lysate was added to the beads and was incubated on an overhead shaker at 4°C overnight. All subsequent steps were performed at RT again. An aliquot of the supernatant was collected to analyze the flow-through. Generally, the washing steps were performed on an overhead shaker for 8 min to allow thorough washing of the high amount of beads. For removal of the washing buffer the reaction tubes were placed on a magnetic rack for 2 min before pipetting. The beads were washed twice with 1 ml of wash buffer 1, once with 1 ml of wash buffer 2 and once with 1 ml of wash buffer 3. Finally, the beads were washed 4 times with 1 ml of wash buffer 4 to remove residual detergent prior to MS analysis. To elute the bound proteins from the beads, 50 µl of elution buffer were added and incubated at RT for 15 min. Thereafter, 17 µl of 4x SB were added and the samples were incubated at 95°C for additional 15 min. Finally, 6 µl of the elution was analyzed by SDS-PAGE, semidry Western blotting and immunodetection (chapters 4.2.4.3, 4.2.4.8 and 4.2.4.10). The rest of the elution fractions was subjected to MS analysis performed by Stefanie Gostek and Christian Preisinger. The samples were subjected to SDS-PAGE and silver staining and digested from gel pieces prior to the measurement.

4.2.4.20 Tandem-Affinity Purification

1x PBS	see chapter 4.2.3.1
1 mg/ml Dox in PBS	
TAP lysis buffer:	see chapter 4.2.4.6
Olaparib (Selleckchem)	
Protein G sepharose FastFlow (GE Healthcare Life Sciences)	
TEV buffer:	50 mM Tris base, pH 7.5; 150 mM NaCl; 0.5 mM EDTA; 1 mM DTT
AcTEV™ protease (Thermo Fisher Scientific)	
Calmodulin sepharose 4B (GE Healthcare Life Sciences)	
CaM binding buffer:	10 mM Tris base, pH 7.5; 150 mM NaCl; 0.2% (v/v) NP-40; 1 mM magnesium acetate; 1 mM CaCl ₂ ; 1 mM imidazole; 10 mM β-mercaptoethanol
1 M CaCl ₂	
CaM washing buffer:	50 mM ammonium bicarbonate, pH 8.0; 75 mM NaCl; 1 mM magnesium acetate; 1 mM imidazole; 2 mM CaCl ₂

Tandem affinity purification (TAP) allows the highly specific co-IP of protein complexes that interact with a protein of interest. The protein of interest is fused to two tags and therefore allows the precipitation with two affinity purification steps instead of just one. Here, this technique was used to identify interactors of CHIKV nsP3 or the isolated macro via subsequent MS analysis. The proteins of interest were fused to the classical TAP-tag consisting of Protein A, a Tobacco Etch Virus (TEV) protease cleavage site and a Calmodulin (CaM) binding peptide (CaBP; **Figure 59**)(Puig et al. 2001). The TAP tag alone was used as a negative control. Large-scale spinner suspension cultures were inoculated in 500 ml medium with 20x 90% confluent 10 cm dishes each of HEK293 FlpIn T-REx cells with stably integrated, Dox-inducible N-TAP, N-TAP-CHIKV-nsP3 or N-TAP-CHIKV-nsP3-macro (chapter 4.1.7)(Krieg et al. 2020; Kleine et al. 2008). The cells were expanded and fresh medium was added until a total volume of 1 l was reached. When the cultures became dense, the expression of the transgenes was

induced by addition of 1 µg/ml Dox for 16 h. The cells were harvested by centrifugation at 4°C and 500 xg for 10 min. Thereafter the cells were washed once with 20 ml of ice-cold 1x PBS by centrifugation and the pellet was resuspended in 20 ml TAP lysis buffer containing PIC, phosphatase inhibitors and 10 µM Olaparib. The lysis took place on an overhead shaker at 4°C for 30 min. The lysates were cleared by centrifugation at 16,000 xg and 4°C for 30 min. Meanwhile 160 µl of Protein G sepharose FastFlow slurry were equilibrated in TAP lysis buffer. The soluble fraction of the lysate was added to the beads and incubated on an overhead shaker at 4°C for 1 h. The beads were pelleted and washed three times with 2.5 ml TEV buffer by centrifugation. Thereafter, the beads were resuspended in 300 µl TEV buffer and incubated with 30 U of AcTEV protease (3 µl) on an overhead shaker at 4°C for 3 h. Meanwhile 50 µl of Calmodulin sepharose 4B slurry were equilibrated in CaM binding buffer. The Protein G sepharose were pelleted by centrifugation and the 300 µl of supernatant were transferred to the equilibrated CaM sepharose. Thereafter the Protein G sepharose was resuspended in 900 µl of CaM binding buffer, pelleted and the supernatant was again transferred to the CaM sepharose. Further, 6 µl (0.5% (v/v)) of 1 M CaCl₂ was added and the mixture was incubated on an overhead shaker at 4°C for 1.5 h. After the incubation the beads were washed three times with 300 µl of CaM washing buffer by centrifugation. The supernatant was completely removed and the beads were subjected to MS analysis. The MS analysis was performed by Stefanie Gostek and Christian Preisinger. The peptides were generated by on-bead-digest.

4.2.4.21 GFP-Trap of GFP-ARTD10 for mass spectrometry analysis

1x PBS	see chapter 4.2.3.1
Frackelton buffer:	20 mM HEPES, pH 7.4; 50 mM NaCl; 30 mM Na ₄ P ₂ O ₇ ; 50 mM NaF; 0.2% (v/v) Triton [®] X-100; 10% (v/v) glycerol; 5 µM ZnCl ₂ ; PIC
GFP-Trap magnetic beads (Chromotek, gtm)	
4x SB:	see chapter 4.2.4.3

Two 10 cm dishes of HEK293 cells were seeded per condition and transiently transfected with plasmids encoding GFP, GFP-ARTD10 or GFP-ARTD10GW as described previously (chapters 4.2.3.3 and 4.2.3.4). Twenty-four h after transfection the desired cells were treated with 180 U/ml of IFN α for 24 h. Forty-eight h after transfection and 24 h after IFN α treatment the cells were lysed in Frackelton buffer as described previously for TAP lysis buffer (chapter 4.2.4.6). In short, the cells were washed from the plates in medium and the 2 plates from the same condition were pooled. The cells were washed with ice-cold 1x PBS and resuspended in 1 ml of Frackelton buffer. Lysis took place on an overhead shaker at 4°C for 30 min and afterwards the lysates were cleared by centrifugation at 4°C and 16,000 xg for 30 min. Meanwhile 20 µl of GFP-Trap magnetic beads were equilibrated in TAP lysis buffer. Sixty µl of lysate were analyzed by SDS-PAGE and immunoblotting as input control (chapters 4.2.4.3, 4.2.4.8 and 4.2.4.10). The remaining lysate was incubated with the equilibrated beads on an overhead shaker at 4°C for 1.5 h. After the incubation time, the beads were washed 2 times with 1 ml Frackelton buffer and 2 times with 1x PBS to remove the residual detergent prior to MS analysis. The MS analysis was performed by Stefanie Gostek and Christian Preisinger. The peptides were generated by on-bead-digest.

4.2.4.22 Mass spectrometry analysis

Mass spectrometry measurements and initial analysis with MaxQuant and first filtering steps were performed by Christian Preisinger (Tyanova et al. 2016). Final analysis was performed using Microsoft Excel. For the TAP interactomes of CHIKV nsP3 and the isolated macropeptides that were enriched at least 5 times over the TAP-tag control were regarded as interactors. For the GFP-Trap interactome of ARTD10, peptides that were enriched at least 5 times compared to the GFP-tag control were regarded as interactors. Further, the peptides that were enriched at least 2 times over the condition without IFN α or with the ARTD10 GW mutant normalized to the amount of ARTD10 itself were considered enriched for IFN α treatment or the wt, respectively. When the BioID screens were evaluated, peptides with an intensity lower than 10^7 were dismissed. For the residual hits, peptides that were enriched at least 10 times over the BirA alone (with biotin) and at least 10 times over the fusion protein without addition of biotin were regarded as interactors. Moreover, the peptides that were enriched at least 2 times over the ARTD10 GW mutant normalized to the amount of ARTD10 itself were considered enriched for the wt.

4.2.5 Microscopic methods

4.2.5.1 Fixation and immunofluorescence (IF) staining of adherent cells

1x PBS	see chapter 4.2.3.1
3.7% (w/v) paraformaldehyde (PFA) in PBS	
Permeabilization solution:	40 µg/ml Digitonin in PBS
Blocking solution:	3% (w/v) BSA in PBS
Antibody dilution solution:	1% BSA (w/v) in PBS
Primary and secondary antibodies	see chapter 4.1.4
10 mg/ml Hoechst33258 (Sigma)	
Mowiol 4-88 (Sigma)	
40% glyoxal stock solution (Sigma)	
glyoxal solution mix:	3.2% (v/v) glyoxal; 20% EtOH; 0.8% glacial acetic acid; pH adjusted to 5.0 by addition of 5 N NaOH
Quenching solution:	100 mM NH ₄ Cl in PBS

HeLa cell lines were seeded, induced and/or transfected on coverslips (CS) in 12 well plates as described above (chapters 4.2.3.1, 4.2.3.3, 4.2.3.4 and 4.2.3.5). Sixteen h after induction, 30 hpt with replicon RNA and/or 48 h after transfection with plasmids, the cells were washed twice with 1x PBS. Thereafter, the cells were either fixed using PFA or glyoxal.

For PFA fixation, 500 µl of 3.7% PFA were added to the wells and incubated at RT for 20 min. After fixation, the cells were washed with 1x PBS and permeabilized by incubation with permeabilization solution at RT for 15 min. Thereafter, the CS was blocked in blocking solution at RT for 30 min before addition of the primary antibody diluted in antibody dilution solution with a dilution dependent on the used antibody (chapter 4.1.4). The cells were incubated with the primary antibody in a humid box and at 37°C for 1 h. Afterwards, the CS were washed three times with antibody dilution solution and the secondary, fluorophore-coupled antibody was added diluted in antibody dilution solution and incubated in a humid box, in the dark and at 37°C for 1 h. The cells were washed twice with 1x PBS and once with ddH₂O before the DNA was stained with 10 µg/ml Hoechst33258 (diluted 1:1,000 in ddH₂O) at RT for 5 min. Finally, the CS were washed twice with ddH₂O and mounted on an object slide with 12 µl Mowiol 4-88. The slides were stored at 4°C in the dark until microscopy.

Glyoxal is proposed to conserve the morphology of the cell more accurately, while providing stronger fixation of proteins and RNA (Richter et al. 2018). For fixation with glyoxal, first the glyoxal solution mix was prepared freshly (Richter et al. 2018). Five-hundred µl of glyoxal solution mix were added to the CS and first incubated one ice for 30 min and then at RT for another 30 min. The samples were washed twice with 1x PBS and optionally quenched with quenching solution at RT for 20 min. After additional washing, twice with 1x PBs and once with ddH₂O the CS were stained with Hoechst33258 and mounted with Mowiol 4-88 as described above. Image acquisition took place with laser-scanning confocal microscopy (chapter 4.2.5.2).

4.2.5.2 Fluorescence laser-scanning confocal microscopy of fixed cells

Confocal microscopy was performed at the IZKF core facility. If not indicated otherwise, images were captured using a Zeiss LSM 710 Confocal Laser Scanning Microscope with an AxioCam (Zeiss) and a C-Apochromat 40x water immersion objective. For all pictures the

pinhole was set to 1 airy unit (AU). The resolution was chosen at 1024x1024 pixels. The Hoechst33258 staining of the nuclei (emission maximum: 455 nm) was excited with a UV-laser at a wavelength of 352 nm and detected with a 454–553 nm bandpass filter. The EGFP fluorochrome (emission maximum: 509 nm) was excited with an argon laser with at a wavelength of 488 nm and it was detected using a 488 nm single channel photomultiplier (PTM) and a 495–550 nm bandpass filter. The fluorochromes Alexa Fluor 555 or mCherry (emission maximum: 580/610 nm) were excited at a wavelength of 561 nm using a helium-neon-laser and were detected using a 562–630 nm bandpass filter.

Confocal microscope images using the Airyscan processing technology of the LSM 980 were taken by Sabrina Ernst and Karla Feijs.

The Zen 2012 software (Zeiss) and the ImageJ software (NIH, Bethesda, USA) were used for analysis and image editing. Brightness and contrast of images were only adjusted in a linear range and settings were always applied to the complete images and with the same settings for all images of the same experiment.

5 References

- Abdelnabi, R., J. Neyts, and L. Delang. 2015. 'Towards antivirals against chikungunya virus', *Antiviral Res*, 121: 59-68.
- Abraham, R., D. Hauer, R. L. McPherson, A. Utt, I. T. Kirby, M. S. Cohen, A. Merits, A. K. L. Leung, and D. E. Griffin. 2018. 'ADP-ribosyl-binding and hydrolase activities of the alphavirus nsP3 macrodomain are critical for initiation of virus replication', *Proc Natl Acad Sci U S A*, 115: E10457-E66.
- Achee, N. L., J. P. Grieco, H. Vatandoost, G. Seixas, J. Pinto, L. Ching-Ng, A. J. Martins, W. Juntarajumnonng, V. Corbel, C. Gouagna, J. P. David, J. G. Logan, J. Orsborne, E. Marois, G. J. Devine, and J. Vontas. 2019. 'Alternative strategies for mosquito-borne arbovirus control', *PLoS Negl Trop Dis*, 13: e0006822.
- Adams, M. J., E. J. Lefkowitz, A. M. King, B. Harrach, R. L. Harrison, N. J. Knowles, A. M. Kropinski, M. Krupovic, J. H. Kuhn, A. R. Mushegian, M. L. Nibert, S. Sabanadzovic, H. Sanfacon, S. G. Siddell, P. Simmonds, A. Varsani, F. M. Zerbini, R. J. Orton, D. B. Smith, A. E. Gorbalenya, and A. J. Davison. 2017. '50 years of the International Committee on Taxonomy of Viruses: progress and prospects', *Arch Virol*, 162: 1441-46.
- Adhikari, A., M. Xu, and Z. J. Chen. 2007. 'Ubiquitin-mediated activation of TAK1 and IKK', *Oncogene*, 26: 3214-26.
- Agback, P., F. Dominguez, Y. Pustovalova, T. Lukash, N. Shiliaev, V. Y. Orekhov, I. Frolov, T. Agback, and E. I. Frolova. 2019. 'Structural characterization and biological function of bivalent binding of CD2AP to intrinsically disordered domain of chikungunya virus nsP3 protein', *Virology*, 537: 130-42.
- Aguiar, R. C., K. Takeyama, C. He, K. Kreinbrink, and M. A. Shipp. 2005. 'B-aggressive lymphoma family proteins have unique domains that modulate transcription and exhibit poly(ADP-ribose) polymerase activity', *J Biol Chem*, 280: 33756-65.
- Aguiar, R. C., Y. Yakushijin, S. Kharbanda, R. Salgia, J. A. Fletcher, and M. A. Shipp. 2000. 'BAL is a novel risk-related gene in diffuse large B-cell lymphomas that enhances cellular migration', *Blood*, 96: 4328-34.
- Ahel, D., Z. Horejsí, N. Wiechens, S. E. Polo, E. Garcia-Wilson, I. Ahel, H. Flynn, M. Skehel, S. C. West, S. P. Jackson, T. Owen-Hughes, and S. J. Boulton. 2009. 'Poly(ADP-ribose)-dependent regulation of DNA repair by the chromatin remodeling enzyme ALC1', *Science*, 325: 1240-3.
- Ahmed, S., D. Bott, A. Gomez, L. Tamblyn, A. Rasheed, T. Cho, L. MacPherson, K. S. Sugamori, Y. Yang, D. M. Grant, C. L. Cummins, and J. Matthews. 2015. 'Loss of the Mono-ADP-ribosyltransferase, Tiparp, Increases Sensitivity to Dioxin-induced Steatohepatitis and Lethality', *J Biol Chem*, 290: 16824-40.
- Ahola, T., and L. Kaariainen. 1995. 'Reaction in alphavirus mRNA capping: formation of a covalent complex of nonstructural protein nsP1 with 7-methyl-GMP', *Proc Natl Acad Sci U S A*, 92: 507-11.
- Ahola, T., P. Kujala, M. Tuittila, T. Blom, P. Laakkonen, A. Hinkkanen, and P. Auvinen. 2000. 'Effects of palmitoylation of replicase protein nsP1 on alphavirus infection', *J Virol*, 74: 6725-33.
- Ahola, T., A. Lampio, P. Auvinen, and L. Kaariainen. 1999. 'Semliki Forest virus mRNA capping enzyme requires association with anionic membrane phospholipids for activity', *Embo j*, 18: 3164-72.
- Ahola, Tero, and Andres Merits. 2016. 'Functions of Chikungunya Virus Nonstructural Proteins.' in Chioma M. Okeoma (ed.), *Chikungunya Virus: Advances in Biology, Pathogenesis, and Treatment* (Springer International Publishing: Cham).
- Akhrymuk, I., I. Frolov, and E. I. Frolova. 2018. 'Sindbis Virus Infection Causes Cell Death by nsP2-Induced Transcriptional Shutoff or by nsP3-Dependent Translational Shutoff', *J Virol*, 92: e01388-18.

- Akhrymuk, I., S. V. Kulemzin, and E. I. Frolova. 2012. 'Evasion of the innate immune response: the Old World alphavirus nsP2 protein induces rapid degradation of Rpb1, a catalytic subunit of RNA polymerase II', *J Virol*, 86: 7180-91.
- Akhrymuk, I., T. Lukash, I. Frolov, and E. I. Frolova. 2019. 'Novel mutations in nsP2 abolish chikungunya virus-induced transcriptional shutoff and make virus less cytopathic without affecting its replication rates', *J Virol*, 93: e02062-18.
- Alhammad, Yousef M. O., Maithri M. Kashipathy, Anuradha Roy, Jean-Philippe Gagné, Peter McDonald, Philip Gao, Louis Nonfoux, Kevin P. Battaile, David K. Johnson, Erik D. Holmstrom, Guy G. Poirier, Scott Lovell, and Anthony R. Fehr. 2021. 'The SARS-CoV-2 Conserved Macrodomain Is a Mono-ADP-Ribosylhydrolase', *Journal of Virology*, 95: e01969-20.
- Alkhatib, H. M., D. F. Chen, B. Cherney, K. Bhatia, V. Notario, C. Giri, G. Stein, E. Slattery, R. G. Roeder, and M. E. Smulson. 1987. 'Cloning and expression of cDNA for human poly(ADP-ribose) polymerase', *Proc Natl Acad Sci U S A*, 84: 1224-8.
- Almeida, D. E., E. Costa, A. S. Pinto, J. L. Silva, J. S. Neves, A. R. Ribeiro, and M. Cerqueira. 2020. 'Chikungunya arthritis - should we expect it to become more common in Portuguese rheumatology?', *Acta Reumatol Port*, 45: 298-300.
- Amé, J. C., V. Rolli, V. Schreiber, C. Niedergang, F. Apiou, P. Decker, S. Muller, T. Höger, J. Ménissier-de Murcia, and G. de Murcia. 1999. 'PARP-2, A novel mammalian DNA damage-dependent poly(ADP-ribose) polymerase', *J Biol Chem*, 274: 17860-8.
- Amé, J. C., C. Spenlehauer, and G. de Murcia. 2004. 'The PARP superfamily', *Bioessays*, 26: 882-93.
- Anderson, J., C. Schiffer, S. K. Lee, and R. Swanstrom. 2009a. 'Viral protease inhibitors', *Handb Exp Pharmacol*, 189: 85-110.
- Anderson, Paul, and Nancy Kedersha. 2009b. 'Stress granules', *Current Biology*, 19: R397-R98.
- Anderson, Paul, Nancy Kedersha, and Pavel Ivanov. 2015. 'Stress granules, P-bodies and cancer', *Biochimica et Biophysica Acta (BBA) - Gene Regulatory Mechanisms*, 1849: 861-70.
- Antos, Christopher L, Timothy A McKinsey, Norbert Frey, William Kutschke, John McAnally, John M Shelton, James A Richardson, Joseph A Hill, and Eric N Olson. 2002. 'Activated glycogen synthase-3 β suppresses cardiac hypertrophy in vivo', *Proceedings of the National Academy of Sciences*, 99: 907-12.
- Araldi, R. P., T. A. Sant'Ana, D. G. Módolo, T. C. de Melo, D. D. Spadacci-Morena, R. de Cassia Stocco, J. M. Cerutti, and E. B. de Souza. 2018. 'The human papillomavirus (HPV)-related cancer biology: An overview', *Biomed Pharmacother*, 106: 1537-56.
- Aravind, L., D. Zhang, R. F. de Souza, S. Anand, and L. M. Iyer. 2015. 'The natural history of ADP-ribosyltransferases and the ADP-ribosylation system', *Curr Top Microbiol Immunol*, 384: 3-32.
- Arechederra, Maria, Fabrice Daian, Annie Yim, Sehrish K. Bazai, Sylvie Richelme, Rosanna Dono, Andrew J. Saurin, Bianca H. Habermann, and Flavio Maina. 2018. 'Hypermethylation of gene body CpG islands predicts high dosage of functional oncogenes in liver cancer', *Nature Communications*, 9: 3164.
- Atasheva, S., M. Akhrymuk, E. I. Frolova, and I. Frolov. 2012. 'New PARP gene with an anti-alphavirus function', *J Virol*, 86: 8147-60.
- Atasheva, S., E. I. Frolova, and I. Frolov. 2014. 'Interferon-stimulated poly(ADP-Ribose) polymerases are potent inhibitors of cellular translation and virus replication', *J Virol*, 88: 2116-30.
- Aylward, R. B., H. F. Hull, S. L. Cochi, R. W. Sutter, J. M. Olive, and B. Melgaard. 2000. 'Disease eradication as a public health strategy: a case study of poliomyelitis eradication', *Bulletin of the World Health Organization*, 78: 285-97.
- Azarm, K., and S. Smith. 2020. 'Nuclear PARPs and genome integrity', *Genes Dev*, 34: 285-301.
- Bachmann, Samia B., Sandra C. Frommel, Rosalba Camicia, Hans C. Winkler, Raffaella Santoro, and Paul O. Hassa. 2014. 'DTX3L and ARTD9 inhibit IRF1 expression and mediate in cooperation with ARTD8 survival and proliferation of metastatic prostate cancer cells', *Molecular Cancer*, 13: 125.
- Bai, Y., L. Li, T. Shan, Y. Zhang, X. Chen, F. Gao, Y. Jiang, Y. Zhou, G. Li, L. Yu, N. Kong, Z. Ma, and G. Tong. 2020. 'Proteasomal degradation of nonstructural protein 12 by RNF114 suppresses porcine reproductive and respiratory syndrome virus replication', *Vet Microbiol*, 246: 108746.

- Bailey-Elkin, B. A., R. C. M. Knaap, M. Kikkert, and B. L. Mark. 2017. 'Structure and Function of Viral Deubiquitinating Enzymes', *J Mol Biol*, 429: 3441-70.
- Baltimore, D. 1971. 'Expression of animal virus genomes', *Bacteriol Rev*, 35: 235-41.
- Barbarulo, A., V. Iansante, A. Chaidos, K. Naresh, A. Rahemtulla, G. Franzoso, A. Karadimitris, D. O. Haskard, S. Papa, and C. Bubici. 2013. 'Poly(ADP-ribose) polymerase family member 14 (PARP14) is a novel effector of the JNK2-dependent pro-survival signal in multiple myeloma', *Oncogene*, 32: 4231-42.
- Barry, S. M., M. A. Johnson, and G. Janossy. 2000. 'Cytopathology or immunopathology? The puzzle of cytomegalovirus pneumonitis revisited', *Bone Marrow Transplant*, 26: 591-7.
- Battisti, Verena, Ernst Urban, and Thierry Langer. 2021. 'Antivirals against the Chikungunya Virus', *Viruses*, 13: 1307.
- Bauckman, K. A., N. Owusu-Boaitey, and I. U. Mysorekar. 2015. 'Selective autophagy: xenophagy', *Methods*, 75: 120-7.
- Baxter, V. K., and M. T. Heise. 2020. 'Immunopathogenesis of alphaviruses', *Adv Virus Res*, 107: 315-82.
- Bayas, A., and P. Rieckmann. 2000. 'Managing the adverse effects of interferon-beta therapy in multiple sclerosis', *Drug Saf*, 22: 149-59.
- Beck, C., I. Robert, B. Reina-San-Martin, V. Schreiber, and F. Dantzer. 2014. 'Poly(ADP-ribose) polymerases in double-strand break repair: focus on PARP1, PARP2 and PARP3', *Exp Cell Res*, 329: 18-25.
- Beck, C., J. M. Rodriguez-Vargas, C. Boehler, I. Robert, V. Heyer, N. Hanini, L. R. Gauthier, A. Tissier, V. Schreiber, M. Elofsson, B. Reina San Martin, and F. Dantzer. 2019. 'PARP3, a new therapeutic target to alter Rictor/mTORC2 signaling and tumor progression in BRCA1-associated cancers', *Cell Death Differ*, 26: 1615-30.
- Beijerinck, M. W. 1898. 'Concerning a contagium vivum fluidum as a cause of the spot-disease of tobacco leaves.', *Verh. Akad. Wet. Amsterdam*, II: 3-21.
- Berger, W., E. Steiner, M. Grusch, L. Elbling, and M. Micksche. 2009. 'Vaults and the major vault protein: novel roles in signal pathway regulation and immunity', *Cell Mol Life Sci*, 66: 43-61.
- Bhalla, N., C. Sun, L. K. Metthew Lam, C. L. Gardner, K. D. Ryman, and W. B. Klimstra. 2016. 'Host translation shutoff mediated by non-structural protein 2 is a critical factor in the antiviral state resistance of Venezuelan equine encephalitis virus', *Virology*, 496: 147-65.
- Bhardwaj, A., Y. Yang, B. Ueberheide, and S. Smith. 2017. 'Whole proteome analysis of human tankyrase knockout cells reveals targets of tankyrase-mediated degradation', *Nat Commun*, 8: 2214.
- Bhatia, T., P. Husen, J. Brewer, L. A. Bagatolli, P. L. Hansen, J. H. Ipsen, and O. G. Mouritsen. 2015. 'Preparing giant unilamellar vesicles (GUVs) of complex lipid mixtures on demand: Mixing small unilamellar vesicles of compositionally heterogeneous mixtures', *Biochim Biophys Acta*, 1848: 3175-80.
- Bheda, P., H. Jing, C. Wolberger, and H. Lin. 2016. 'The Substrate Specificity of Sirtuins', *Annu Rev Biochem*, 85: 405-29.
- Bindesbøll, C., S. Tan, D. Bott, T. Cho, L. Tamblyn, L. MacPherson, L. Grønning-Wang, H. I. Nebb, and J. Matthews. 2016. 'TCDD-inducible poly-ADP-ribose polymerase (TIPARP/PARP7) mono-ADP-ribosylates and co-activates liver X receptors', *Biochem J*, 473: 899-910.
- Blenn, C., F. R. Althaus, and M. Malanga. 2006. 'Poly(ADP-ribose) glycohydrolase silencing protects against H₂O₂-induced cell death', *Biochem J*, 396: 419-29.
- Bock, F. J., T. T. Todorova, and P. Chang. 2015. 'RNA Regulation by Poly(ADP-Ribose) Polymerases', *Mol Cell*, 58: 959-69.
- Boehler, C., L. R. Gauthier, O. Mortusewicz, D. S. Biard, J. M. Saliou, A. Bresson, S. Sanglier-Cianferani, S. Smith, V. Schreiber, F. Boussin, and F. Dantzer. 2011. 'Poly(ADP-ribose) polymerase 3 (PARP3), a newcomer in cellular response to DNA damage and mitotic progression', *Proc Natl Acad Sci U S A*, 108: 2783-8.
- Bonfiglio, J. J., P. Fontana, Q. Zhang, T. Colby, I. Gibbs-Seymour, I. Atanassov, E. Bartlett, R. Zaja, I. Ahel, and I. Matic. 2017. 'Serine ADP-Ribosylation Depends on HPF1', *Mol Cell*, 65: 932-40.e6.

- Borra, M. T., M. R. Langer, J. T. Slama, and J. M. Denu. 2004. 'Substrate specificity and kinetic mechanism of the Sir2 family of NAD⁺-dependent histone/protein deacetylases', *Biochemistry*, 43: 9877-87.
- Bourai, M., M. Lucas-Hourani, H. H. Gad, C. Drosten, Y. Jacob, L. Tafforeau, P. Cassonnet, L. M. Jones, D. Judith, T. Couderc, M. Lecuit, P. Andre, B. M. Kummerer, V. Lotteau, P. Despres, F. Tangy, and P. O. Vidalain. 2012. 'Mapping of Chikungunya virus interactions with host proteins identified nsP2 as a highly connected viral component', *J Virol*, 86: 3121-34.
- Branon, T. C., J. A. Bosch, A. D. Sanchez, N. D. Udeshi, T. Svinkina, S. A. Carr, J. L. Feldman, N. Perrimon, and A. Y. Ting. 2018. 'Efficient proximity labeling in living cells and organisms with TurboID', *Nat Biotechnol*, 36: 880-87.
- Braun, S. A., P. L. Panzeter, M. A. Collinge, and F. R. Althaus. 1994. 'Endoglycosidic cleavage of branched polymers by poly(ADP-ribose) glycohydrolase', *Eur J Biochem*, 220: 369-75.
- Brochu, G., C. Duchaine, L. Thibeault, J. Lagueux, G. M. Shah, and G. G. Poirier. 1994. 'Mode of action of poly(ADP-ribose) glycohydrolase', *Biochim Biophys Acta*, 1219: 342-50.
- Bullard-Feibelman, K. M., B. P. Fuller, and B. J. Geiss. 2016. 'A Sensitive and Robust High-Throughput Screening Assay for Inhibitors of the Chikungunya Virus nsP1 Capping Enzyme', *PLoS One*, 11: e0158923.
- Butepage, M., L. Eckeï, P. Verheugd, and B. Luscher. 2015. 'Intracellular Mono-ADP-Ribosylation in Signaling and Disease', *Cells*, 4: 569-95.
- Butepage, M., S. Krieg, L. Eckeï, J. Li, G. Rossetti, P. Verheugd, and B. Luscher. 2018a. 'Assessment of Intracellular Auto-Modification Levels of ARTD10 Using Mono-ADP-Ribose-Specific Macrod domains 2 and 3 of Murine Artd8', *Methods Mol Biol*, 1813: 41-63.
- Butepage, M., C. Preisinger, A. von Kriegsheim, A. Scheufen, E. Lausberg, J. Li, F. Kappes, R. Feederle, S. Ernst, L. Eckeï, S. Krieg, G. Muller-Newen, G. Rossetti, K. L. H. Feijs, P. Verheugd, and B. Luscher. 2018b. 'Nucleolar-nucleoplasmic shuttling of TARG1 and its control by DNA damage-induced poly-ADP-ribosylation and by nucleolar transcription', *Sci Rep*, 8: 6748.
- Cai, T., D. Sun, Y. Duan, Y. Qiu, C. Dai, J. Yang, and W. He. 2018. 'FHL2 promotes tubular epithelial-to-mesenchymal transition through modulating β -catenin signalling', *J Cell Mol Med*, 22: 1684-95.
- Callow, Marinella G., Hoanh Tran, Lilian Phu, Ted Lau, James Lee, Wendy N. Sandoval, Peter S. Liu, Sheila Bheddah, Janet Tao, Jennie R. Lill, Jo-Anne Hongo, David Davis, Donald S. Kirkpatrick, Paul Polakis, and Mike Costa. 2011. 'Ubiquitin Ligase RNF146 Regulates Tankyrase and Axin to Promote Wnt Signaling', *PLoS One*, 6: e22595.
- Camicia, R., S. B. Bachmann, H. C. Winkler, M. Beer, M. Tinguely, E. Haralambieva, and P. O. Hassa. 2013. 'BAL1/ARTD9 represses the anti-proliferative and pro-apoptotic IFN γ -STAT1-IRF1-p53 axis in diffuse large B-cell lymphoma', *J Cell Sci*, 126: 1969-80.
- Caprara, G., E. Prosperini, V. Piccolo, G. Sigismondo, A. Melacarne, A. Cuomo, M. Boothby, M. Rescigno, T. Bonaldi, and G. Natoli. 2018. 'PARP14 Controls the Nuclear Accumulation of a Subset of Type I IFN-Inducible Proteins', *J Immunol*, 200: 2439-54.
- Cardamone, Maria Dafne, Yuan Gao, Julian Kwan, Vanessa Hayashi, Megan Sheeran, Junxiang Xu, Justin English, Joseph Orofino, Andrew Emili, and Valentina Perissi. 2020. 'ADP-ribosylation of mitochondrial proteins is mediated by Neuralized-like protein 4 (NEURL4)', *bioRxiv*: 2020.12.28.424513.
- Carter-O'Connell, I., H. Jin, R. K. Morgan, R. Zaja, L. L. David, I. Ahel, and M. S. Cohen. 2016. 'Identifying Family-Member-Specific Targets of Mono-ARTDs by Using a Chemical Genetics Approach', *Cell Rep*, 14: 621-31.
- Carter-O'Connell, I., A. Vermehren-Schmaedick, H. Jin, R. K. Morgan, L. L. David, and M. S. Cohen. 2018. 'Combining Chemical Genetics with Proximity-Dependent Labeling Reveals Cellular Targets of Poly(ADP-ribose) Polymerase 14 (PARP14)', *ACS Chem Biol*, 13: 2841-48.
- Catara, G., G. Grimaldi, L. Schembri, D. Spano, G. Turacchio, M. Lo Monte, A. R. Beccari, C. Valente, and D. Corda. 2017. 'PARP1-produced poly-ADP-ribose causes the PARP12 translocation to stress granules and impairment of Golgi complex functions', *Sci Rep*, 7: 14035.

- Chambon, P., J. D. Weill, J. Doly, M. T. Strosser, and P. Mandel. 1966. 'On the formation of a novel adenylic compound by enzymatic extracts of liver nuclei', *Biochem Biophys Res Commun*, 25: 638-43.
- Chambon, P., J. D. Weill, and P. Mandel. 1963. 'Nicotinamide mononucleotide activation of new DNA-dependent polyadenylic acid synthesizing nuclear enzyme', *Biochem Biophys Res Commun*, 11: 39-43.
- Chan-Yeung, Moira, and Rui-Heng XU. 2003. 'SARS: epidemiology', *Respirology*, 8: S9-S14.
- Chang, P. C., M. Campbell, and E. S. Robertson. 2016. 'Human Oncogenic Herpesvirus and Post-translational Modifications - Phosphorylation and SUMOylation', *Frontiers in Microbiology*, 7: 962.
- Chang, P., M. Coughlin, and T. J. Mitchison. 2009. 'Interaction between Poly(ADP-ribose) and NuMA contributes to mitotic spindle pole assembly', *Mol Biol Cell*, 20: 4575-85.
- Chang, William, Jasmin N Dynek, and Susan Smith. 2005. 'NuMA is a major acceptor of poly(ADP-ribosylation) by tankyrase 1 in mitosis', *Biochemical Journal*, 391: 177-84.
- Channappanavar, R., and S. Perlman. 2017. 'Pathogenic human coronavirus infections: causes and consequences of cytokine storm and immunopathology', *Semin Immunopathol*, 39: 529-39.
- Chatrin, C., M. Gabrielsen, L. Buetow, M. A. Nakasone, S. F. Ahmed, D. Sumpton, G. J. Sibbet, B. O. Smith, and D. T. Huang. 2020. 'Structural insights into ADP-ribosylation of ubiquitin by Deltex family E3 ubiquitin ligases', *Sci Adv*, 6: eabc0418.
- Chen, J., E. E. Bardes, B. J. Aronow, and A. G. Jegga. 2009. 'ToppGene Suite for gene list enrichment analysis and candidate gene prioritization', *Nucleic Acids Res*, 37: W305-11.
- Chen, L., O. T. Keppler, and C. Scholz. 2018. 'Post-translational Modification-Based Regulation of HIV Replication', *Frontiers in Microbiology*, 9: 2131.
- Cheng, L., Z. Li, Y. Z. Huang, X. Zhang, X. Y. Dai, L. Shi, P. W. Xi, J. F. Wei, and Q. Ding. 2019. 'TCDD-Inducible Poly-ADP-Ribose Polymerase (TIPARP), A Novel Therapeutic Target Of Breast Cancer', *Cancer Manag Res*, 11: 8991-9004.
- Cherkasov, A., E. N. Muratov, D. Fourches, A. Varnek, Baskin, II, M. Cronin, J. Dearden, P. Gramatica, Y. C. Martin, R. Todeschini, V. Consonni, V. E. Kuz'min, R. Cramer, R. Benigni, C. Yang, J. Rathman, L. Terfloth, J. Gasteiger, A. Richard, and A. Tropsha. 2014. 'QSAR modeling: where have you been? Where are you going to?', *J Med Chem*, 57: 4977-5010.
- Child, S. J., C. A. Franke, and D. E. Hruby. 1988. 'Inhibition of vaccinia virus replication by nicotinamide: evidence for ADP-ribosylation of viral proteins', *Virus Res*, 9: 119-32.
- Cho, S. H., S. Goenka, T. Henttinen, P. Gudapati, A. Reinikainen, C. M. Eischen, R. Lahesmaa, and M. Boothby. 2009. 'PARP-14, a member of the B aggressive lymphoma family, transduces survival signals in primary B cells', *Blood*, 113: 2416-25.
- Chou, H. Y., H. T. Chou, and S. C. Lee. 2006. 'CDK-dependent activation of poly(ADP-ribose) polymerase member 10 (PARP10)', *J Biol Chem*, 281: 15201-7.
- Cohen, J. 2016. 'Unfilled Vials', *Science*, 351: 16-9.
- Cong, Y., N. Dinesh Kumar, M. Mauthe, P. Verlhac, and F. Reggiori. 2020. 'Manipulation of selective macroautophagy by pathogens at a glance', *J Cell Sci*, 133: jcs240440.
- Cook, Brandoch D., Jasmin N. Dynek, William Chang, Grigoriy Shostak, and Susan Smith. 2002. 'Role for the Related Poly(ADP-Ribose) Polymerases Tankyrase 1 and 2 at Human Telomeres', *Mol Cell Biol*, 22: 332-42.
- Cox, Jürgen, Marco Y. Hein, Christian A. Luber, Igor Paron, Nagarjuna Nagaraj, and Matthias Mann. 2014. 'Accurate Proteome-wide Label-free Quantification by Delayed Normalization and Maximal Peptide Ratio Extraction, Termed MaxLFQ', *Molecular & Cellular Proteomics*, 13: 2513-26.
- Crow, M. S., K. K. Lum, X. Sheng, B. Song, and I. M. Cristea. 2016. 'Diverse mechanisms evolved by DNA viruses to inhibit early host defenses', *Crit Rev Biochem Mol Biol*, 51: 452-81.
- Cui, J., Y. Chen, H. Y. Wang, and R. F. Wang. 2014. 'Mechanisms and pathways of innate immune activation and regulation in health and cancer', *Hum Vaccin Immunother*, 10: 3270-85.
- Curina, A., A. Termanini, I. Barozzi, E. Prosperini, M. Simonatto, S. Polletti, A. Silvola, M. Soldi, L. Austenaa, T. Bonaldi, S. Ghisletti, and G. Natoli. 2017. 'High constitutive activity of a broad

- panel of housekeeping and tissue-specific cis-regulatory elements depends on a subset of ETS proteins', *Genes Dev*, 31: 399-412.
- Cyrklaff, M., C. Risco, J. J. Fernández, M. V. Jiménez, M. Estéban, W. Baumeister, and J. L. Carrascosa. 2005. 'Cryo-electron tomography of vaccinia virus', *Proc Natl Acad Sci U S A*, 102: 2772-7.
- d'Herelle, F. H. 1917. 'Sur un microbe invisible antagoniste des bacilles dysenteriques.', *C.R. Acad. Sci.*, 165: 373-75.
- Das, P. K., A. Merits, and A. Lulla. 2014. 'Functional cross-talk between distant domains of chikungunya virus non-structural protein 2 is decisive for its RNA-modulating activity', *J Biol Chem*, 289: 5635-53.
- Daugherty, M. D., and H. S. Malik. 2012. 'Rules of engagement: molecular insights from host-virus arms races', *Annu Rev Genet*, 46: 677-700.
- Daugherty, M. D., J. M. Young, J. A. Kerns, and H. S. Malik. 2014. 'Rapid evolution of PARP genes suggests a broad role for ADP-ribosylation in host-virus conflicts', *PLoS Genet*, 10: e1004403.
- Dawicki-McKenna, J. M., M. F. Langelier, J. E. DeNizio, A. A. Riccio, C. D. Cao, K. R. Karch, M. McCauley, J. D. Steffen, B. E. Black, and J. M. Pascal. 2015. 'PARP-1 Activation Requires Local Unfolding of an Autoinhibitory Domain', *Mol Cell*, 60: 755-68.
- Dawood, Fatimah S., Philip Ricks, Gibril J. Njie, Michael Daugherty, William Davis, James A. Fuller, Alison Winstead, Margaret McCarron, Lia C. Scott, Diana Chen, Amy E. Blain, Ron Moolenaar, Chaoyang Li, Adebola Popoola, Cynthia Jones, Puneet Anantharam, Natalie Olson, Barbara J. Marston, and Sarah D. Bennett. 2020. 'Observations of the global epidemiology of COVID-19 from the prepandemic period using web-based surveillance: a cross-sectional analysis', *The Lancet Infectious Diseases*, 20: 1255-62.
- De Caluwé, L., K. K. Ariën, and K. Bartholomeeusen. 2021. 'Host Factors and Pathways Involved in the Entry of Mosquito-Borne Alphaviruses', *Trends Microbiol*, 29: 634-47.
- De Clercq, E. 2019. 'New Nucleoside Analogues for the Treatment of Hemorrhagic Fever Virus Infections', *Chem Asian J*, 14: 3962-68.
- Delang, L., C. Li, A. Tas, G. Querat, I. C. Albuлесcu, T. De Burghgraeve, N. A. Guerrero, A. Gigante, G. Piorkowski, E. Decroly, D. Jochmans, B. Canard, E. J. Snijder, M. J. Perez-Perez, M. J. van Hemert, B. Coutard, P. Leyssen, and J. Neyts. 2016. 'The viral capping enzyme nsP1: a novel target for the inhibition of chikungunya virus infection', *Sci Rep*, 6: 31819.
- Dhoonmoon, A., E. M. Schleicher, K. E. Clements, C. M. Nicolae, and G. L. Moldovan. 2020. 'Genome-wide CRISPR synthetic lethality screen identifies a role for the ADP-ribosyltransferase PARP14 in DNA replication dynamics controlled by ATR', *Nucleic Acids Res*, 48: 7252-64.
- Di Girolamo, M., and G. Fabrizio. 2019. 'Overview of the mammalian ADP-ribosyl-transferases clostridia toxin-like (ARTCs) family', *Biochem Pharmacol*, 167: 86-96.
- Diani-Moore, S., P. Ram, X. Li, P. Mondal, D. Y. Youn, A. A. Sauve, and A. B. Rifkind. 2010. 'Identification of the aryl hydrocarbon receptor target gene TiPARP as a mediator of suppression of hepatic gluconeogenesis by 2,3,7,8-tetrachlorodibenzo-p-dioxin and of nicotinamide as a corrective agent for this effect', *J Biol Chem*, 285: 38801-10.
- Dominguez, F., N. Shiliaev, T. Lukash, P. Agback, O. Palchevska, J. R. Gould, C. D. Meshram, P. E. Prevelige, T. J. Green, T. Agback, E. I. Frolova, and I. Frolov. 2021. 'NAP1L1 and NAP1L4 Binding to Hypervariable Domain of Chikungunya Virus nsP3 Protein Is Bivalent and Requires Phosphorylation', *J Virol*, 95: e0083621.
- Dong, Ensheng, Hongru Du, and Lauren Gardner. 2020. 'An interactive web-based dashboard to track COVID-19 in real time', *The Lancet Infectious Diseases*, 20: 533-34.
- Dowdle, W. R. 1998. 'The principles of disease elimination and eradication', *Bulletin of the World Health Organization*, 76 Suppl 2: 22-25.
- Du, J., H. Jiang, and H. Lin. 2009. 'Investigating the ADP-ribosyltransferase activity of sirtuins with NAD analogues and 32P-NAD', *Biochemistry*, 48: 2878-90.
- Eaglesham, J. B., and P. J. Kranzusch. 2020. 'Conserved strategies for pathogen evasion of cGAS-STING immunity', *Curr Opin Immunol*, 66: 27-34.
- Ecke, Laura, Sarah Krieg, Mareike Bütepage, Anne Lehmann, Annika Gross, Barbara Lippok, Alexander R. Grimm, Beate M. Kümmerer, Giulia Rossetti, Bernhard Lüscher, and Patricia Verheugd.

2017. 'The conserved macrodomains of the non-structural proteins of Chikungunya virus and other pathogenic positive strand RNA viruses function as mono-ADP-ribosylhydrolases', *Scientific Reports*, 7: 41746.
- Eckei-Potthoff, L. 2020. 'Characterization of an Artd10 knockdown mouse model and Interplay between interferon-regulated mono-ADP-ribosylation and human papillomavirus E6 and E7 proteins', RWTH Aachen University.
- Egloff, M. P., H. Malet, A. Putics, M. Heinonen, H. Dutartre, A. Frangeul, A. Gruez, V. Campanacci, C. Cambillau, J. Ziebuhr, T. Ahola, and B. Canard. 2006. 'Structural and functional basis for ADP-ribose and poly(ADP-ribose) binding by viral macro domains', *J Virol*, 80: 8493-502.
- Eisemann, T., and J. M. Pascal. 2020. 'Poly(ADP-ribose) polymerase enzymes and the maintenance of genome integrity', *Cell Mol Life Sci*, 77: 19-33.
- Ekblad, T., P. Verheugd, A. E. Lindgren, T. Nyman, M. Elofsson, and H. Schuler. 2018. 'Identification of Poly(ADP-Ribose) Polymerase Macrodomain Inhibitors Using an AlphaScreen Protocol', *SLAS Discov*, 23: 353-62.
- Eriksson, K. K., L. Cervantes-Barragan, B. Ludewig, and V. Thiel. 2008. 'Mouse hepatitis virus liver pathology is dependent on ADP-ribose-1''-phosphatase, a viral function conserved in the alpha-like supergroup', *J Virol*, 82: 12325-34.
- Farmer, H., N. McCabe, C. J. Lord, A. N. Tutt, D. A. Johnson, T. B. Richardson, M. Santarosa, K. J. Dillon, I. Hickson, C. Knights, N. M. Martin, S. P. Jackson, G. C. Smith, and A. Ashworth. 2005. 'Targeting the DNA repair defect in BRCA mutant cells as a therapeutic strategy', *Nature*, 434: 917-21.
- FDA. 2018. 'Fast Track, Breakthrough Therapy, Accelerated Approval, Priority Review'. <https://www.fda.gov/patients/learn-about-drug-and-device-approvals/fast-track-breakthrough-therapy-accelerated-approval-priority-review>.
- Fehr, A. R., R. Channappanavar, G. Jankevicius, C. Fett, J. Zhao, J. Athmer, D. K. Meyerholz, I. Ahel, and S. Perlman. 2016. 'The Conserved Coronavirus Macrodomain Promotes Virulence and Suppresses the Innate Immune Response during Severe Acute Respiratory Syndrome Coronavirus Infection', *MBio*, 7: e01721-16.
- Fehr, A. R., S. A. Singh, C. M. Kerr, S. Mukai, H. Higashi, and M. Aikawa. 2020. 'The impact of PARPs and ADP-ribosylation on inflammation and host-pathogen interactions', *Genes Dev*, 34: 341-59.
- Feibelman, K. M., B. P. Fuller, L. Li, D. V. LaBarbera, and B. J. Geiss. 2018. 'Identification of small molecule inhibitors of the Chikungunya virus nsP1 RNA capping enzyme', *Antiviral Res*, 154: 124-31.
- Feijs, K. L., A. H. Forst, P. Verheugd, and B. Luscher. 2013a. 'Macrodomain-containing proteins: regulating new intracellular functions of mono(ADP-ribosyl)ation', *Nat Rev Mol Cell Biol*, 14: 443-51.
- Feijs, K. L., H. Kleine, A. Braczynski, A. H. Forst, N. Herzog, P. Verheugd, U. Linzen, E. Kremmer, and B. Luscher. 2013b. 'ARTD10 substrate identification on protein microarrays: regulation of GSK3beta by mono-ADP-ribosylation', *Cell Commun Signal*, 11: 5.
- Feijs, K. L., P. Verheugd, and B. Luscher. 2013c. 'Expanding functions of intracellular resident mono-ADP-ribosylation in cell physiology', *FEBS J*, 280: 3519-29.
- Feijs, Karla, Christopher Cooper, and Roko Žaja. 2020. 'The Controversial Roles of ADP-Ribosyl Hydrolases MACROD1, MACROD2 and TARG1 in Carcinogenesis', *Cancers*, 12: 604.
- Firth, A. E., B. Y. Chung, M. N. Fleeton, and J. F. Atkins. 2008. 'Discovery of frameshifting in Alphavirus 6K resolves a 20-year enigma', *Virology*, 5: 108.
- Fontana, P., J. J. Bonfiglio, L. Palazzo, E. Bartlett, I. Matic, and I. Ahel. 2017. 'Serine ADP-ribosylation reversal by the hydrolase ARH3', *Elife*, 6: e28533.
- Forst, A. H., T. Karlberg, N. Herzog, A. G. Thorsell, A. Gross, K. L. Feijs, P. Verheugd, P. Kursula, B. Nijmeijer, E. Kremmer, H. Kleine, A. G. Ladurner, H. Schuler, and B. Luscher. 2013. 'Recognition of mono-ADP-ribosylated ARTD10 substrates by ARTD8 macrodomains', *Structure*, 21: 462-75.
- Francki, RIB, CM Fauquet, DL Knudson, and F Brown. 2012. *Classification and Nomenclature of Viruses: Fifth Report of the International Committee on Taxonomy of Viruses. Virology Division of the International Union of Microbiological Societies* (Springer Science & Business Media).

- Fros, J. J., N. E. Domeradzka, J. Baggen, C. Geertsema, J. Flipse, J. M. Vlak, and G. P. Pijlman. 2012. 'Chikungunya virus nsP3 blocks stress granule assembly by recruitment of G3BP into cytoplasmic foci', *J Virol*, 86: 10873-9.
- Fros, J. J., C. Geertsema, K. Zouache, J. Baggen, N. Domeradzka, D. M. van Leeuwen, J. Flipse, J. M. Vlak, A. B. Failloux, and G. P. Pijlman. 2015a. 'Mosquito Rasputin interacts with chikungunya virus nsP3 and determines the infection rate in *Aedes albopictus*', *Parasit Vectors*, 8: 464.
- Fros, J. J., L. D. Major, F. E. M. Scholte, J. Gardner, M. J. van Hemert, A. Suhrbier, and G. P. Pijlman. 2015b. 'Chikungunya virus non-structural protein 2-mediated host shut-off disables the unfolded protein response', *J Gen Virol*, 96: 580-89.
- Fros, J. J., and G. P. Pijlman. 2016. 'Alphavirus Infection: Host Cell Shut-Off and Inhibition of Antiviral Responses', *Viruses*, 8: 166.
- Fros, J. J., E. van der Maten, J. M. Vlak, and G. P. Pijlman. 2013. 'The C-terminal domain of chikungunya virus nsP2 independently governs viral RNA replication, cytopathicity, and inhibition of interferon signaling', *J Virol*, 87: 10394-400.
- Gagné, Jean-Philippe, Maxim Isabelle, Ken Sin Lo, Sylvie Bourassa, Michael J. Hendzel, Valina L. Dawson, Ted M. Dawson, and Guy G. Poirier. 2008. 'Proteome-wide identification of poly(ADP-ribose) binding proteins and poly(ADP-ribose)-associated protein complexes', *Nucleic Acids Research*, 36: 6959-76.
- Gao, Xiang-Qian, Yu-Hui Zhang, Fang Liu, Murugavel Ponnusamy, Xue-Mei Zhao, Lu-Yu Zhou, Mei Zhai, Cui-Yun Liu, Xin-Min Li, Man Wang, Chan Shan, Pei-Pei Shan, Yin Wang, Yan-Han Dong, Li-Li Qian, Tao Yu, Jie Ju, Tao Wang, Kai Wang, Xin-Zhe Chen, Yun-Hong Wang, Jian Zhang, Pei-Feng Li, and Kun Wang. 2020. 'The piRNA CHAPIR regulates cardiac hypertrophy by controlling METTL3-dependent N6-methyladenosine methylation of Parp10 mRNA', *Nat Cell Biol*, 22: 1319-31.
- Gao, Y., N. Goonawardane, J. Ward, A. Tuplin, and M. Harris. 2019. 'Multiple roles of the non-structural protein 3 (nsP3) alphavirus unique domain (AUD) during Chikungunya virus genome replication and transcription', *PLoS Pathog*, 15: e1007239.
- García-Saura, Antonio Ginés, and Herwig Schüler. 2021. 'PARP10 Multi-Site Auto- and Histone MARYlation Visualized by Acid-Urea Gel Electrophoresis', *Cells*, 10: 654.
- Garmashova, Natalia, Rodion Gorchakov, Eugenia Volkova, Slobodan Paessler, Elena Frolova, and Ilya Frolov. 2007. 'The Old World and New World Alphaviruses Use Different Virus-Specific Proteins for Induction of Transcriptional Shutoff', *Journal of Virology*, 81: 2472-84.
- Gelderblom, HR. 1996. 'Structure and Classification of Viruses.' in Baron S. (ed.), *Medical Microbiology. 4th edition.* (University of Texas Medical Branch at Galveston: Galveston (TX)).
- Gerrish, P. J., and J. G. García-Lerma. 2003. 'Mutation rate and the efficacy of antimicrobial drug treatment', *Lancet Infect Dis*, 3: 28-32.
- Ghildiyal, R., and R. Gabrani. 2021. 'Deciphering the human cellular interactors of alphavirus unique domain of chikungunya virus', *Virus Res*, 295: 198288.
- Gibson, B. A., L. B. Conrad, D. Huang, and W. L. Kraus. 2017. 'Generation and Characterization of Recombinant Antibody-Like ADP-Ribose Binding Proteins', *Biochemistry*, 56: 6305-16.
- Gill, D. M., A. M. Pappenheimer, Jr., R. Brown, and J. T. Kurnick. 1969. 'Studies on the mode of action of diphtheria toxin. VII. Toxin-stimulated hydrolysis of nicotinamide adenine dinucleotide in mammalian cell extracts', *J Exp Med*, 129: 1-21.
- Glasker, S., A. Lulla, V. Lulla, T. Couderc, J. F. Drexler, P. Liljestrom, M. Lecuit, C. Drosten, A. Merits, and B. M. Kummerer. 2013. 'Virus replicon particle based Chikungunya virus neutralization assay using *Gaussia luciferase* as readout', *Virology*, 453: 235.
- Glowacki, G., R. Braren, M. Cetkovic-Cvrlje, E. H. Leiter, F. Haag, and F. Koch-Nolte. 2001. 'Structure, chromosomal localization, and expression of the gene for mouse ecto-mono(ADP-ribosyl)transferase ART5', *Gene*, 275: 267-77.
- Glowacki, G., R. Braren, K. Firner, M. Nissen, M. Kuhl, P. Reche, F. Bazan, M. Cetkovic-Cvrlje, E. Leiter, F. Haag, and F. Koch-Nolte. 2002. 'The family of toxin-related ecto-ADP-ribosyltransferases in humans and the mouse', *Protein Sci*, 11: 1657-70.

- Goenka, S., and M. Boothby. 2006. 'Selective potentiation of Stat-dependent gene expression by collaborator of Stat6 (CoaSt6), a transcriptional cofactor', *Proc Natl Acad Sci U S A*, 103: 4210-5.
- Goenka, S., S. H. Cho, and M. Boothby. 2007. 'Collaborator of Stat6 (CoaSt6)-associated poly(ADP-ribose) polymerase activity modulates Stat6-dependent gene transcription', *J Biol Chem*, 282: 18732-9.
- Goertz, G. P., K. L. McNally, S. J. Robertson, S. M. Best, G. P. Pijlman, and J. J. Fros. 2018. 'The MTase-like domain of chikungunya virus nsP2 inhibits the interferon response by promoting the nuclear export of STAT1', *J Virol*, 92: e01008-18.
- Gomez, Alvin, Christian Bindesbøll, Somisetty V. Satheesh, Giulia Grimaldi, David Hutin, Laura MacPherson, Shaimaa Ahmed, Laura Tamblyn, Tiffany Cho, Hilde Irene Nebb, Anders Moen, Jan Haug Anonsen, Denis M. Grant, and Jason Matthews. 2018. 'Characterization of TCDD-inducible poly-ADP-ribose polymerase (TIPARP/ARTD14) catalytic activity', *Biochemical Journal*, 475: 3827-46.
- Goode, E. L., G. Chenevix-Trench, H. Song, S. J. Ramus, M. Notaridou, K. Lawrenson, M. Widschwendter, R. A. Vierkant, M. C. Larson, S. K. Kjaer, M. J. Birrer, A. Berchuck, J. Schildkraut, I. Tomlinson, L. A. Kiemeny, L. S. Cook, J. Gronwald, M. Garcia-Closas, M. E. Gore, I. Campbell, A. S. Whittemore, R. Sutphen, C. Phelan, H. Anton-Culver, C. L. Pearce, D. Lambrechts, M. A. Rossing, J. Chang-Claude, K. B. Moysich, M. T. Goodman, T. Dörk, H. Nevanlinna, R. B. Ness, T. Rafnar, C. Hogdall, E. Hogdall, B. L. Fridley, J. M. Cunningham, W. Sieh, V. McGuire, A. K. Godwin, D. W. Cramer, D. Hernandez, D. Levine, K. Lu, E. S. Iversen, R. T. Palmieri, R. Houlston, A. M. van Altena, K. K. Aben, L. F. Massuger, A. Brooks-Wilson, L. E. Kelemen, N. D. Le, A. Jakubowska, J. Lubinski, K. Medrek, A. Stafford, D. F. Easton, J. Tyrer, K. L. Bolton, P. Harrington, D. Eccles, A. Chen, A. N. Molina, B. N. Davila, H. Arango, Y. Y. Tsai, Z. Chen, H. A. Risch, J. McLaughlin, S. A. Narod, A. Ziogas, W. Brewster, A. Gentry-Maharaj, U. Menon, A. H. Wu, D. O. Stram, M. C. Pike, J. Beesley, P. M. Webb, X. Chen, A. B. Ekici, F. C. Thiel, M. W. Beckmann, H. Yang, N. Wentzensen, J. Lissowska, P. A. Fasching, E. Despierre, F. Amant, I. Vergote, J. Doherty, R. Hein, S. Wang-Gohrke, G. Lurie, M. E. Carney, P. J. Thompson, I. Runnebaum, P. Hillemanns, M. Dürst, N. Antonenkova, N. Bogdanova, A. Leminen, R. Butzow, T. Heikkinen, K. Stefansson, P. Sulem, S. Besenbacher, T. A. Sellers, S. A. Gayther, and P. D. Pharoah. 2010. 'A genome-wide association study identifies susceptibility loci for ovarian cancer at 2q31 and 8q24', *Nat Genet*, 42: 874-9.
- Gorbalenya, A. E. 2018. 'Increasing the number of available ranks in virus taxonomy from five to ten and adopting the Baltimore classes as taxa at the basal rank', *Arch Virol*, 163: 2933-36.
- Gorry, Peter A. 1990. 'General least-squares smoothing and differentiation by the convolution (Savitzky-Golay) method', *Anal Chem*, 62: 570-73.
- Gotte, B., L. Liu, and G. M. McInerney. 2018. 'The Enigmatic Alphavirus Non-Structural Protein 3 (nsP3) Revealing Its Secrets at Last', *Viruses*, 10: 105.
- Gotte, B., M. D. Panas, K. Hellstrom, L. Liu, B. Samreen, O. Larsson, T. Ahola, and G. M. McInerney. 2019. 'Separate domains of G3BP promote efficient clustering of alphavirus replication complexes and recruitment of the translation initiation machinery', *PLoS Pathog*, 15: e1007842.
- Goyal, M., A. Chauhan, V. Goyal, N. Jaiswal, S. Singh, and M. Singh. 2018. 'Recent development in the strategies projected for chikungunya vaccine in humans', *Drug Des Devel Ther*, 12: 4195-206.
- Gozgit, J. M., M. M. Vasbinder, R. P. Abo, K. Kunii, K. G. Kuplast-Barr, B. Gui, A. Z. Lu, J. R. Molina, E. Minissale, K. K. Swinger, T. J. Wigle, D. J. Blackwell, C. R. Majer, Y. Ren, M. Niepel, Z. A. Varsamis, S. P. Nayak, E. Bamberg, J. R. Mo, W. D. Church, A. S. A. Mady, J. Song, L. Utley, P. E. Rao, T. J. Mitchison, K. W. Kuntz, V. M. Richon, and H. Keilhack. 2021. 'PARP7 negatively regulates the type I interferon response in cancer cells and its inhibition triggers antitumor immunity', *Cancer Cell*, 39: 1214-26.e10.
- Grimaldi, G., and D. Corda. 2019. 'ADP-ribosylation and intracellular traffic: an emerging role for PARP enzymes', *Biochem Soc Trans*, 47: 357-70.

- Grimaldi, Giovanna, Laura Schembri, Matteo Lo Monte, Daniela Spano, Rosaria Di Martino, Andrea R Beccari, Carmen Valente, and Daniela Corda. 2020. 'PARP12-catalyzed mono-ADP-ribosylation of Golgin-97 controls the transport of E-cadherin', *bioRxiv*: 2020.05.05.078097.
- Grundy, G. J., L. M. Polo, Z. Zeng, S. L. Rulten, N. C. Hoch, P. Paomephan, Y. Xu, S. M. Sweet, A. W. Thorne, A. W. Oliver, S. J. Matthews, L. H. Pearl, and K. W. Caldecott. 2016. 'PARP3 is a sensor of nicked nucleosomes and monoribosylates histone H2B(Glu2)', *Nat Commun*, 7: 12404.
- Grünewald, Kay, and Marek Cyrklaff. 2006. 'Structure of complex viruses and virus-infected cells by electron cryo tomography', *Curr Opin Microbiol*, 9: 437-42.
- Grunewald, M. E., Y. Chen, C. Kuny, T. Maejima, R. Lease, D. Ferraris, M. Aikawa, C. S. Sullivan, S. Perlman, and A. R. Fehr. 2019. 'The coronavirus macrodomain is required to prevent PARP-mediated inhibition of virus replication and enhancement of IFN expression', *PLoS Pathog*, 15: e1007756.
- Grunewald, M. E., A. R. Fehr, J. Athmer, and S. Perlman. 2017. 'The coronavirus nucleocapsid protein is ADP-ribosylated', *Virology*, 517: 62-68.
- Grunewald, M. E., M. G. Shaban, S. R. Mackin, A. R. Fehr, and S. Perlman. 2020. 'Murine Coronavirus Infection Activates the Aryl Hydrocarbon Receptor in an Indoleamine 2,3-Dioxygenase-Independent Manner, Contributing to Cytokine Modulation and Proviral TCDD-Inducible-PARP Expression', *J Virol*, 94: e01743-19.
- Guerrero-Preston, R., C. Michailidi, L. Marchionni, C. R. Pickering, M. J. Frederick, J. N. Myers, S. Yegnasubramanian, T. Hadar, M. G. Noordhuis, V. Zizkova, E. Fertig, N. Agrawal, W. Westra, W. Koch, J. Califano, V. E. Velculescu, and D. Sidransky. 2014. 'Key tumor suppressor genes inactivated by "greater promoter" methylation and somatic mutations in head and neck cancer', *Epigenetics*, 9: 1031-46.
- Güldenpfennig, A. 2018. 'Mono-ADP-ribosylation at the host-pathogen interface', Bachelor Thesis, RWTH Aachen University.
- Guo, F., J. J. Chen, and W. J. Tang. 2017. 'CIRH1A augments the proliferation of RKO colorectal cancer cells', *Oncol Rep*, 37: 2375-81.
- Guo, G., L. Ye, K. Pan, Y. Chen, D. Xing, K. Yan, Z. Chen, N. Ding, W. Li, H. Huang, L. Zhang, X. Li, and X. Xue. 2020. 'New Insights of Emerging SARS-CoV-2: Epidemiology, Etiology, Clinical Features, Clinical Treatment, and Prevention', *Front Cell Dev Biol*, 8: 410.
- Guo, T., J. Liu, X. Chen, L. Jin, F. Huang, and H. Zheng. 2019. 'PARP11 regulates total levels of type-I interferon receptor IFNAR1', *Nat Microbiol*, 4: 1771-73.
- Guo, X., J. Ma, J. Sun, and G. Gao. 2007. 'The zinc-finger antiviral protein recruits the RNA processing exosome to degrade the target mRNA', *Proc Natl Acad Sci U S A*, 104: 151-6.
- Haag, F., F. Koch, and H. G. Thiele. 1990. 'Nucleotide and deduced amino acid sequence of the rat T-cell alloantigen RT6.1', *Nucleic Acids Res*, 18: 1047.
- Haag, F., F. Koch-Nolte, M. Kuhl, S. Lorenzen, and H. G. Thiele. 1994. 'Premature stop codons inactivate the RT6 genes of the human and chimpanzee species', *J Mol Biol*, 243: 537-46.
- Haciosmanoğlu, E., B. Varol, BÖ Edis, and M. Bektaş. 2016. 'Interleukin-1 β effect on the endogenous ADP-ribosylation and phosphorylation of eukaryotic elongation factor 2', *Cytotechnology*, 68: 2659-66.
- Haigis, M. C., R. Mostoslavsky, K. M. Haigis, K. Fahie, D. C. Christodoulou, A. J. Murphy, D. M. Valenzuela, G. D. Yancopoulos, M. Karow, G. Blander, C. Wolberger, T. A. Prolla, R. Weindruch, F. W. Alt, and L. Guarente. 2006. 'SIRT4 inhibits glutamate dehydrogenase and opposes the effects of calorie restriction in pancreatic beta cells', *Cell*, 126: 941-54.
- Hallengård, D., M. Kakoulidou, A. Lulla, B. M. Kümmerer, D. X. Johansson, M. Mutso, V. Lulla, J. K. Fazakerley, P. Roques, R. Le Grand, A. Merits, and P. Liljeström. 2014. 'Novel attenuated Chikungunya vaccine candidates elicit protective immunity in C57BL/6 mice', *J Virol*, 88: 2858-66.
- Hanada, K., Y. Suzuki, and T. Gojobori. 2004. 'A large variation in the rates of synonymous substitution for RNA viruses and its relationship to a diversity of viral infection and transmission modes', *Mol Biol Evol*, 21: 1074-80.

- Harms, A., and K. Gerdes. 2016. 'Back to the Roots: Deep View into the Evolutionary History of ADP-Ribosylation Opened by the DNA-Targeting Toxin-Antitoxin Module DarTG', *Mol Cell*, 64: 1020-21.
- Harrison, Stephen C., Bruce Alberts, Ellie Ehrenfeld, Lynn Enquist, Harvey Fineberg, Steven L. McKnight, Bernard Moss, Michael O'Donnell, Hidde Ploegh, Sandra L. Schmid, K. Peter Walter, and Julie Theriot. 2004. 'Discovery of antivirals against smallpox', *Proc Natl Acad Sci U S A*, 101: 11178-92.
- Hatakeyama, K., Y. Nemoto, K. Ueda, and O. Hayaishi. 1986. 'Purification and characterization of poly(ADP-ribose) glycohydrolase. Different modes of action on large and small poly(ADP-ribose)', *J Biol Chem*, 261: 14902-11.
- He, F., K. Tsuda, M. Takahashi, K. Kuwasako, T. Terada, M. Shirouzu, S. Watanabe, T. Kigawa, N. Kobayashi, P. Guntert, S. Yokoyama, and Y. Muto. 2012. 'Structural insight into the interaction of ADP-ribose with the PARP WWE domains', *FEBS Lett*, 586: 3858-64.
- Heaton, S. M. 2019. 'Harnessing host-virus evolution in antiviral therapy and immunotherapy', *Clin Transl Immunology*, 8: e1067.
- Heer, C. D., D. J. Sanderson, L. S. Voth, Y. M. O. Alhammad, M. S. Schmidt, S. A. J. Trammell, S. Perlman, M. S. Cohen, A. R. Fehr, and C. Brenner. 2020. 'Coronavirus infection and PARP expression dysregulate the NAD metabolome: An actionable component of innate immunity', *J Biol Chem*, 295: 17986-96.
- Henning, R. J., M. Bourgeois, and R. D. Harbison. 2018. 'Poly(ADP-ribose) Polymerase (PARP) and PARP Inhibitors: Mechanisms of Action and Role in Cardiovascular Disorders', *Cardiovasc Toxicol*, 18: 493-506.
- Herzog, N., J. D. Hartkamp, P. Verheugd, F. Treude, A. H. Forst, K. L. Feijs, B. E. Lippok, E. Kremmer, H. Kleine, and B. Luscher. 2013. 'Caspase-dependent cleavage of the mono-ADP-ribosyltransferase ARTD10 interferes with its pro-apoptotic function', *FEBS J*, 280: 1330-43.
- Hicks, A. L., and S. Duffy. 2014. 'Cell tropism predicts long-term nucleotide substitution rates of mammalian RNA viruses', *PLoS Pathog*, 10: e1003838.
- Higashi, H., T. Maejima, L. H. Lee, Y. Yamazaki, M. O. Hottiger, S. A. Singh, and M. Aikawa. 2019. 'A study into the ADP-ribosylome of IFN-gamma-stimulated THP-1 human macrophage-like cells identifies ARTD8/PARP14 and ARTD9/PARP9 ADP-ribosylation', *J Proteome Res*, 18: 1607-22.
- Hill, L., G. Browne, and E. Tulchinsky. 2013. 'ZEB/miR-200 feedback loop: at the crossroads of signal transduction in cancer', *Int J Cancer*, 132: 745-54.
- Hirai, Yuya, Eisuke Domae, Yoshihiro Yoshikawa, and Keizo Tomonaga. 2020. 'Differential roles of two DDX17 isoforms in the formation of membraneless organelles', *The Journal of Biochemistry*, 168: 33-40.
- Hofmann, S., N. Kedersha, P. Anderson, and P. Ivanov. 2021. 'Molecular mechanisms of stress granule assembly and disassembly', *Biochim Biophys Acta Mol Cell Res*, 1868: 118876.
- Holmes, Edward C. 2009. *The evolution and emergence of RNA viruses* (Oxford University Press).
- Honjo, T., Y. Nishizuka, and O. Hayaishi. 1968. 'Diphtheria toxin-dependent adenosine diphosphate ribosylation of aminoacyl transferase II and inhibition of protein synthesis', *J Biol Chem*, 243: 3553-5.
- Hottiger, M. O., P. O. Hassa, B. Luscher, H. Schuler, and F. Koch-Nolte. 2010. 'Toward a unified nomenclature for mammalian ADP-ribosyltransferases', *Trends Biochem Sci*, 35: 208-19.
- Hsiao, S. J., and S. Smith. 2008. 'Tankyrase function at telomeres, spindle poles, and beyond', *Biochimie*, 90: 83-92.
- Hsin, I. F., E. Montano, and E. Seki. 2016. 'Finding a new role for NEMO: A key player in preventing hepatocyte apoptosis and liver tumorigenesis by inhibiting RIPK1', *Hepatology*, 64: 295-7.
- Hu, B., Q. Wei, X. Li, M. Ju, L. Wang, C. Zhou, L. Chen, Z. Li, M. Wei, M. He, and L. Zhao. 2020. 'Development of an IFN γ response-related signature for predicting the survival of cutaneous melanoma', *Cancer Med*, 9: 8186-201.
- Hua, C., and B. Combe. 2017. 'Chikungunya Virus-Associated Disease', *Curr Rheumatol Rep*, 19: 69.

- Huang, H., Y. Zheng, L. Li, W. Shi, R. Zhang, H. Liu, Z. Chen, and L. Wu. 2020. 'The roles of post-translational modifications and coactivators of STAT6 signaling in tumor growth and progression', *Future Med Chem*, 12: 1945-60.
- Hui, Kenrie P. Y., Man-Chun Cheung, Ranawaka A. P. M. Perera, Ka-Chun Ng, Christine H. T. Bui, John C. W. Ho, Mandy M. T. Ng, Denise I. T. Kuok, Kendrick C. Shih, Sai-Wah Tsao, Leo L. M. Poon, Malik Peiris, John M. Nicholls, and Michael C. W. Chan. 2020. 'Tropism, replication competence, and innate immune responses of the coronavirus SARS-CoV-2 in human respiratory tract and conjunctiva: an analysis in ex-vivo and in-vitro cultures', *The Lancet Respiratory Medicine*, 8: 687-95.
- Hull, Roger, and Hans Will. 1989. 'Molecular biology of viral and nonviral retroelements', *Trends in Genetics*, 5: 357-59.
- Hurst, K. R., C. A. Koetzner, and P. S. Masters. 2013. 'Characterization of a critical interaction between the coronavirus nucleocapsid protein and nonstructural protein 3 of the viral replicase-transcriptase complex', *J Virol*, 87: 9159-72.
- Hutin, D., L. Tamblyn, A. Gomez, G. Grimaldi, H. Soedling, T. Cho, S. Ahmed, C. Lucas, C. Kanduri, D. M. Grant, and J. Matthews. 2018. 'Hepatocyte-Specific Deletion of TIPARP, a Negative Regulator of the Aryl Hydrocarbon Receptor, Is Sufficient to Increase Sensitivity to Dioxin-Induced Wasting Syndrome', *Toxicol Sci*, 165: 347-60.
- Iansante, V., P. M. Choy, S. W. Fung, Y. Liu, J. G. Chai, J. Dyson, A. Del Rio, C. D'Santos, R. Williams, S. Chokshi, R. A. Anders, C. Bubici, and S. Papa. 2015. 'PARP14 promotes the Warburg effect in hepatocellular carcinoma by inhibiting JNK1-dependent PKM2 phosphorylation and activation', *Nat Commun*, 6: 7882.
- Imai, S., C. M. Armstrong, M. Kaerberlein, and L. Guarente. 2000. 'Transcriptional silencing and longevity protein Sir2 is an NAD-dependent histone deacetylase', *Nature*, 403: 795-800.
- International Committee on Taxonomy of Viruses. 2020. "VMR: Virus Metadata Resource." In.
- International Committee on Taxonomy of Viruses Executive, Committee. 2020. 'The new scope of virus taxonomy: partitioning the virosphere into 15 hierarchical ranks', *Nat Microbiol*, 5: 668-74.
- Iqbal, M. B., M. Johns, J. Cao, Y. Liu, S. C. Yu, G. D. Hyde, M. A. Laffan, F. P. Marchese, S. H. Cho, A. R. Clark, F. N. Gavins, K. J. Woollard, P. J. Blackshear, N. Mackman, J. L. Dean, M. Boothby, and D. O. Haskard. 2014. 'PARP-14 combines with tristetraprolin in the selective posttranscriptional control of macrophage tissue factor expression', *Blood*, 124: 3646-55.
- Ivanovsky, D. 1882. 'Concerning the mosaic disease of the tobacco plant.', *St. Petersburg Acad. Imp. Sci. Bul.*, 35: 67-70.
- Ivashkiv, L. B., B. Zhao, K. H. Park-Min, and M. Takami. 2011. 'Feedback inhibition of osteoclastogenesis during inflammation by IL-10, M-CSF receptor shedding, and induction of IRF8', *Ann N Y Acad Sci*, 1237: 88-94.
- Iwata, H., C. Goettsch, A. Sharma, P. Ricchiuto, W. W. Goh, A. Halu, I. Yamada, H. Yoshida, T. Hara, M. Wei, N. Inoue, D. Fukuda, A. Mojcher, P. C. Mattson, A. L. Barabasi, M. Boothby, E. Aikawa, S. A. Singh, and M. Aikawa. 2016. 'PARP9 and PARP14 cross-regulate macrophage activation via STAT1 ADP-ribosylation', *Nat Commun*, 7: 12849.
- Jackson, M. D., and J. M. Denu. 2002. 'Structural identification of 2'- and 3'-O-acetyl-ADP-ribose as novel metabolites derived from the Sir2 family of beta -NAD⁺-dependent histone/protein deacetylases', *J Biol Chem*, 277: 18535-44.
- Jäger, D., K. Werdan, and U. Müller-Werdan. 2011. 'Endogenous ADP-ribosylation of elongation factor-2 by interleukin-1 β ', *Mol Cell Biochem*, 348: 125-8.
- Jankevicius, G., A. Ariza, M. Ahel, and I. Ahel. 2016. 'The Toxin-Antitoxin System DarTG Catalyzes Reversible ADP-Ribosylation of DNA', *Mol Cell*, 64: 1109-16.
- Jankevicius, G., M. Hassler, B. Golia, V. Rybin, M. Zacharias, G. Timinszky, and A. G. Ladurner. 2013. 'A family of macrodomain proteins reverses cellular mono-ADP-ribosylation', *Nat Struct Mol Biol*, 20: 508-14.
- Janova, E. 2019. 'Emerging and threatening vector-borne zoonoses in the world and in Europe: a brief update', *Pathog Glob Health*, 113: 1-9.

- Jayaweera, M., H. Perera, B. Gunawardana, and J. Manatunge. 2020. 'Transmission of COVID-19 virus by droplets and aerosols: A critical review on the unresolved dichotomy', *Environ Res*, 188: 109819.
- Johns Hopkins University. 2021. 'COVID-19 Dashboard by the Center for Systems Science and Engineering (CSSE) at Johns Hopkins University (JHU)', Accessed August 3, 2020. <https://gisanddata.maps.arcgis.com/apps/opsdashboard/index.html#/bda7594740fd40299423467b48e9ecf6>.
- Jones, P. H., M. Maric, M. N. Madison, W. Maury, R. J. Roller, and C. M. Okeoma. 2013. 'BST-2/tetherin-mediated restriction of chikungunya (CHIKV) VLP budding is counteracted by CHIKV non-structural protein 1 (nsP1)', *Virology*, 438: 37-49.
- Jones, R., G. Bragagnolo, R. Arranz, and J. Reguera. 2021. 'Capping pores of alphavirus nsP1 gate membranous viral replication factories', *Nature*, 589: 615-19.
- Juszczynski, P., J. L. Kutok, C. Li, J. Mitra, R. C. Aguiar, and M. A. Shipp. 2006. 'BAL1 and BBAP are regulated by a gamma interferon-responsive bidirectional promoter and are overexpressed in diffuse large B-cell lymphomas with a prominent inflammatory infiltrate', *Mol Cell Biol*, 26: 5348-59.
- Kaesler, F. 2020. 'Post-Translational Modifications in the Interaction of Host Proteins and Non-Structural Proteins of Chikungunya Virus', Master Thesis, RWTH Aachen University.
- Kaewseekhao, B., V. Naranbhai, S. Roytrakul, W. Namwat, A. Paemanee, V. Lulitanond, A. Chaiprasert, and K. Faksri. 2015. 'Comparative Proteomics of Activated THP-1 Cells Infected with Mycobacterium tuberculosis Identifies Putative Clearance Biomarkers for Tuberculosis Treatment', *PLoS One*, 10: e0134168.
- Kalejta, R. F. 2008. 'Tegument proteins of human cytomegalovirus', *Microbiol Mol Biol Rev*, 72: 249-65.
- Kamal, M., M. A. Kenawy, M. H. Rady, A. S. Khaled, and A. M. Samy. 2018. 'Mapping the global potential distributions of two arboviral vectors Aedes aegypti and Ae. albopictus under changing climate', *PLoS One*, 13: e0210122.
- Kamar, N., H. R. Dalton, F. Abravanel, and J. Izopet. 2014. 'Hepatitis E virus infection', *Clin Microbiol Rev*, 27: 116-38.
- Karin, M., and Y. Ben-Neriah. 2000. 'Phosphorylation meets ubiquitination: the control of NF- κ B activity', *Annu Rev Immunol*, 18: 621-63.
- Karlberg, T., M. Klepsch, A. G. Thorsell, C. D. Andersson, A. Linusson, and H. Schüler. 2015. 'Structural basis for lack of ADP-ribosyltransferase activity in poly(ADP-ribose) polymerase-13/zinc finger antiviral protein', *J Biol Chem*, 290: 7336-44.
- Karpe, Y. A., P. P. Aher, and K. S. Lole. 2011. 'NTPase and 5'-RNA triphosphatase activities of Chikungunya virus nsP2 protein', *PLoS One*, 6: e22336.
- Karras, G. I., G. Kustatscher, H. R. Buhecha, M. D. Allen, C. Pugieux, F. Sait, M. Bycroft, and A. G. Ladurner. 2005. 'The macro domain is an ADP-ribose binding module', *Embo j*, 24: 1911-20.
- Kaufmann, M., K. L. Feijs, and B. Luscher. 2015. 'Function and regulation of the mono-ADP-ribosyltransferase ARTD10', *Curr Top Microbiol Immunol*, 384: 167-88.
- Kaur, R., R. Mudgal, M. Narwal, and S. Tomar. 2018. 'Development of an ELISA assay for screening inhibitors against divalent metal ion dependent alphavirus capping enzyme', *Virus Res*, 256: 209-18.
- Kausche, G. A., Ruska, H. 1939. 'Die Struktur der "kristallinen Aggregate" des Tabakmosaikvirus-proteins.', *Biochem. Z.*, 303: 211.
- Kedersha, N., M. D. Panas, C. A. Achorn, S. Lyons, S. Tisdale, T. Hickman, M. Thomas, J. Lieberman, G. M. McInerney, P. Ivanov, and P. Anderson. 2016. 'G3BP-Caprin1-USP10 complexes mediate stress granule condensation and associate with 40S subunits', *J Cell Biol*, 212: 845-60.
- Kedersha, N., G. Stoecklin, M. Ayodele, P. Yacono, J. Lykke-Andersen, M. J. Fritzler, D. Scheuner, R. J. Kaufman, D. E. Golan, and P. Anderson. 2005. 'Stress granules and processing bodies are dynamically linked sites of mRNP remodeling', *J Cell Biol*, 169: 871-84.
- Keenan, E. K., D. K. Zachman, and M. D. Hirschey. 2021. 'Discovering the landscape of protein modifications', *Mol Cell*, 81: 1868-78.

- Kerns, J. A., M. Emerman, and H. S. Malik. 2008. 'Positive selection and increased antiviral activity associated with the PARP-containing isoform of human zinc-finger antiviral protein', *PLoS Genet*, 4: e21.
- Kim, D. I., S. C. Jensen, K. A. Noble, B. Kc, K. H. Roux, K. Motamedchaboki, and K. J. Roux. 2016a. 'An improved smaller biotin ligase for BioID proximity labeling', *Mol Biol Cell*, 27: 1188-96.
- Kim, D. S., S. Challa, A. Jones, and W. L. Kraus. 2020. 'PARPs and ADP-ribosylation in RNA biology: from RNA expression and processing to protein translation and proteostasis', *Genes Dev*, 34: 302-20.
- Kim, D. Y., J. M. Reynaud, A. Rasalouslykaya, I. Akhrymuk, J. A. Mobley, I. Frolov, and E. I. Frolova. 2016b. 'New World and Old World Alphaviruses Have Evolved to Exploit Different Components of Stress Granules, FXR and G3BP Proteins, for Assembly of Viral Replication Complexes', *PLoS Pathog*, 12: e1005810.
- Kirby, I. T., A. Kojic, M. R. Arnold, A. G. Thorsell, T. Karlberg, A. Vermehren-Schmaedick, R. Sreenivasan, C. Schultz, H. Schuler, and M. S. Cohen. 2018. 'A Potent and Selective PARP11 Inhibitor Suggests Coupling between Cellular Localization and Catalytic Activity', *Cell Chem Biol*, 25: 1547-53.e12.
- Kiselevsky, D. B. 2020. 'Granzymes and Mitochondria', *Biochemistry (Mosc)*, 85: 131-39.
- Kleine, H., A. Herrmann, T. Lamark, A. H. Forst, P. Verheugd, J. Luscher-Firzlaff, B. Lippok, K. L. Feijs, N. Herzog, E. Kremmer, T. Johansen, G. Muller-Newen, and B. Luscher. 2012. 'Dynamic subcellular localization of the mono-ADP-ribosyltransferase ARTD10 and interaction with the ubiquitin receptor p62', *Cell Commun Signal*, 10: 28.
- Kleine, H., E. Poreba, K. Lesniewicz, P. O. Hassa, M. O. Hottiger, D. W. Litchfield, B. H. Shilton, and B. Luscher. 2008. 'Substrate-assisted catalysis by PARP10 limits its activity to mono-ADP-ribosylation', *Mol Cell*, 32: 57-69.
- Komori, T. 2018. 'Runx2, an inducer of osteoblast and chondrocyte differentiation', *Histochem Cell Biol*, 149: 313-23.
- Kondylis, V., S. Kumari, K. Vlantis, and M. Pasparakis. 2017. 'The interplay of IKK, NF- κ B and RIPK1 signaling in the regulation of cell death, tissue homeostasis and inflammation', *Immunol Rev*, 277: 113-27.
- Kovalev, Nikolay, Judit Pogany, and Peter D. Nagy. 2020. 'Reconstitution of an RNA virus replicase in artificial giant unilamellar vesicles supports full replication and provides protection for the dsRNA replication intermediate', *J Virol*, 94: e00267-20.
- Kozaki, T., J. Komano, D. Kanbayashi, M. Takahama, T. Misawa, T. Satoh, O. Takeuchi, T. Kawai, S. Shimizu, Y. Matsuura, S. Akira, and T. Saitoh. 2017. 'Mitochondrial damage elicits a TCDD-inducible poly(ADP-ribose) polymerase-mediated antiviral response', *Proc Natl Acad Sci U S A*, 114: 2681-86.
- Krieg, Sarah, Fabian Pott, Laura Eckei, Maud Verheirstraeten, Mareike Bütepage, Barbara Lippok, Christine Goffinet, Bernhard Lüscher, and Patricia Verheugd. 2020. 'Mono-ADP-ribosylation by ARTD10 restricts Chikungunya virus replication by interfering with the proteolytic activity of nsP2', *bioRxiv*: 2020.01.07.896977.
- Krupovic, Mart, Jonas Blomberg, John M. Coffin, Indranil Dasgupta, Hung Fan, Andrew D. Geering, Robert Gifford, Balázs Harrach, Roger Hull, Welkin Johnson, Jan F. Kreuze, Dirk Lindemann, Carlos Llorens, Ben Lockhart, Jens Mayer, Emmanuelle Muller, Neil E. Olszewski, Hanu R. Pappu, Mikhail M. Pooggin, Katja R. Richert-Pöggeler, Sead Sabanadzovic, H  l  ne Sanfa  on, James E. Schoelz, Susan Seal, Livia Stavalone, Jonathan P. Stoye, Pierre-Yves Teycheney, Michael Tristem, Eugene V. Koonin, and Jens H. Kuhn. 2018. 'Ortervirales: New Virus Order Unifying Five Families of Reverse-Transcribing Viruses', *Journal of Virology*, 92: e00515-18.
- Krutt, L. 2018. 'Validierung und Charakterisierung potenzieller Interaktionspartnern von ARTD10 und CHIKV-nsP3', Bachelor Thesis, RWTH Aachen University
- Kudchodkar, S. B., and B. Levine. 2009. 'Viruses and autophagy', *Rev Med Virol*, 19: 359-78.
- Kumar, S., A. Kumar, P. Mamidi, A. Tiwari, S. Kumar, A. Mayavannan, S. Mudulli, A. K. Singh, B. B. Subudhi, and S. Chattopadhyay. 2018. 'Chikungunya virus nsP1 interacts directly with nsP2 and modulates its ATPase activity', *Sci Rep*, 8: 1045.

- Kuri, T., K. K. Eriksson, A. Putics, R. Zust, E. J. Snijder, A. D. Davidson, S. G. Siddell, V. Thiel, J. Ziebuhr, and F. Weber. 2011. 'The ADP-ribose-1'-monophosphatase domains of severe acute respiratory syndrome coronavirus and human coronavirus 229E mediate resistance to antiviral interferon responses', *J Gen Virol*, 92: 1899-905.
- Kurosaki, T., H. Ushiro, Y. Mitsuchi, S. Suzuki, M. Matsuda, Y. Matsuda, N. Katunuma, K. Kangawa, H. Matsuo, T. Hirose, and et al. 1987. 'Primary structure of human poly(ADP-ribose) synthetase as deduced from cDNA sequence', *J Biol Chem*, 262: 15990-7.
- Kurt Yilmaz, N., R. Swanstrom, and C. A. Schiffer. 2016. 'Improving Viral Protease Inhibitors to Counter Drug Resistance', *Trends Microbiol*, 24: 547-57.
- Laakkonen, P., T. Ahola, and L. Kaariainen. 1996. 'The effects of palmitoylation on membrane association of Semliki forest virus RNA capping enzyme', *J Biol Chem*, 271: 28567-71.
- Ladurner, A. G. 2003. 'Inactivating chromosomes: a macro domain that minimizes transcription', *Mol Cell*, 12: 1-3.
- Lam, S. S., J. D. Martell, K. J. Kamer, T. J. Deerinck, M. H. Ellisman, V. K. Mootha, and A. Y. Ting. 2015. 'Directed evolution of APEX2 for electron microscopy and proximity labeling', *Nat Methods*, 12: 51-4.
- Lamark, T., S. Svenning, and T. Johansen. 2017. 'Regulation of selective autophagy: the p62/SQSTM1 paradigm', *Essays Biochem*, 61: 609-24.
- Langelier, M. F., J. L. Planck, S. Roy, and J. M. Pascal. 2012. 'Structural basis for DNA damage-dependent poly(ADP-ribosylation) by human PARP-1', *Science*, 336: 728-32.
- Law, Y. S., A. Utt, Y. B. Tan, J. Zheng, S. Wang, M. W. Chen, P. R. Griffin, A. Merits, and D. Luo. 2019. 'Structural insights into RNA recognition by the Chikungunya virus nsP2 helicase', *Proc Natl Acad Sci U S A*, 116: 9558-67.
- Lee, C. H. R., K. Mohamed Hussain, and J. J. H. Chu. 2019. 'Macropinocytosis Dependent Entry of Chikungunya Virus into Human Muscle Cells', *PLoS Negl Trop Dis*, 13: e0007610.
- Lee, M. K., H. S. Cheong, Y. Koh, K. S. Ahn, S. S. Yoon, and H. D. Shin. 2016. 'Genetic Association of PARP15 Polymorphisms with Clinical Outcome of Acute Myeloid Leukemia in a Korean Population', *Genet Test Mol Biomarkers*, 20: 696-701.
- Leung, A. K., S. Vyas, J. E. Rood, A. Bhutkar, P. A. Sharp, and P. Chang. 2011. 'Poly(ADP-ribose) regulates stress responses and microRNA activity in the cytoplasm', *Mol Cell*, 42: 489-99.
- Leung, A., T. Todorova, Y. Ando, and P. Chang. 2012. 'Poly(ADP-ribose) regulates post-transcriptional gene regulation in the cytoplasm', *RNA Biol*, 9: 542-8.
- Li, C., Y. Debing, G. Jankevicius, J. Neyts, I. Ahel, B. Coutard, and B. Canard. 2016a. 'Viral Macro Domains Reverse Protein ADP-ribosylation', *J Virol*, 90: 8478-86.
- Li, C., J. Guillen, N. Rabah, A. Blanjoie, F. Debart, J. J. Vasseur, B. Canard, E. Decroly, and B. Coutard. 2015a. 'mRNA Capping by Venezuelan Equine Encephalitis Virus nsP1: Functional Characterization and Implications for Antiviral Research', *J Virol*, 89: 8292-303.
- Li, G., D. Ma, and Y. Chen. 2016b. 'Cellular functions of programmed cell death 5', *Biochim Biophys Acta*, 1863: 572-80.
- Li, Lili, Hui Zhao, Ping Liu, Chunfeng Li, Natalie Quanquin, Xue Ji, Nina Sun, Peishuang Du, Cheng-Feng Qin, Ning Lu, and Genhong Cheng. 2018. 'PARP12 suppresses Zika virus infection through PARP-dependent degradation of NS1 and NS3 viral proteins', *Sci Signal*, 11: eaas9332.
- Li, Nan, Yajie Zhang, Xin Han, Ke Liang, Jiadong Wang, Lin Feng, Wenqi Wang, Zhou Songyang, Chunru Lin, Liuqing Yang, Yonghao Yu, and Junjie Chen. 2015b. 'Poly-ADP ribosylation of PTEN by tankyrases promotes PTEN degradation and tumor growth', *Genes Dev*, 29: 157-70.
- Li, Z., Y. Yamauchi, M. Kamakura, T. Murayama, F. Goshima, H. Kimura, and Y. Nishiyama. 2012. 'Herpes simplex virus requires poly(ADP-ribose) polymerase activity for efficient replication and induces extracellular signal-related kinase-dependent phosphorylation and ICP0-dependent nuclear localization of tankyrase 1', *J Virol*, 86: 492-503.
- Liedtke, C., and C. Trautwein. 2012. 'The role of TNF and Fas dependent signaling in animal models of inflammatory liver injury and liver cancer', *Eur J Cell Biol*, 91: 582-9.
- Lin, B., Q. Ke, D. W. Leaman, V. Goel, and A. Agarwal. 2018. 'Regulation of RANKL-induced osteoclastogenesis by RING finger protein RNF114', *J Orthop Res*, 36: 159-66.

- Lin, L., D. Wang, N. Cao, Y. Lin, Y. Jin, and C. Zheng. 2013. 'Whole-transcriptome analysis of hepatocellular carcinoma', *Med Oncol*, 30: 736.
- Lin, X., X. Xiang, L. Hao, T. Wang, Y. Lai, M. Abudoureyimu, H. Zhou, B. Feng, X. Chu, and R. Wang. 2020. 'The role of Aurora-A in human cancers and future therapeutics', *Am J Cancer Res*, 10: 2705-29.
- Liu, C. H., L. G. Zhou, G. F. Chen, and R. M. Krug. 2015. 'Battle between influenza A virus and a newly identified antiviral activity of the PARP-containing ZAPL protein', *Proc Natl Acad Sci U S A*, 112: 14048-53.
- Liu, J., X. Zheng, Q. Tong, W. Li, B. Wang, K. Sutter, M. Trilling, M. Lu, U. Dittmer, and D. Yang. 2020. 'Overlapping and discrete aspects of the pathology and pathogenesis of the emerging human pathogenic coronaviruses SARS-CoV, MERS-CoV, and 2019-nCoV', *J Med Virol*, 92: 491-94.
- Liu, S. Y., D. J. Sanchez, R. Aliyari, S. Lu, and G. Cheng. 2012. 'Systematic identification of type I and type II interferon-induced antiviral factors', *Proc Natl Acad Sci U S A*, 109: 4239-44.
- Loh, C. Y., J. Y. Chai, T. F. Tang, W. F. Wong, G. Sethi, M. K. Shanmugam, P. P. Chong, and C. Y. Looi. 2019. 'The E-Cadherin and N-Cadherin Switch in Epithelial-to-Mesenchymal Transition: Signaling, Therapeutic Implications, and Challenges', *Cells*, 8: 1118.
- Lorenz, M., B. Vollmer, J. D. Unsay, B. G. Klupp, A. J. Garcia-Saez, T. C. Mettenleiter, and W. Antonin. 2015. 'A single herpesvirus protein can mediate vesicle formation in the nuclear envelope', *J Biol Chem*, 290: 6962-74.
- Los, M., M. Mozoluk, D. Ferrari, A. Stepczynska, C. Stroh, A. Renz, Z. Herceg, Z. Q. Wang, and K. Schulze-Osthoff. 2002. 'Activation and caspase-mediated inhibition of PARP: a molecular switch between fibroblast necrosis and apoptosis in death receptor signaling', *Mol Biol Cell*, 13: 978-88.
- Lu, S., N. Zhu, W. Guo, X. Wang, K. Li, J. Yan, C. Jiang, S. Han, H. Xiang, X. Wu, Y. Liu, H. Xiong, L. Chen, Z. Gong, F. Luo, and W. Hou. 2020. 'RNA-Seq Revealed a Circular RNA-microRNA-mRNA Regulatory Network in Hantaan Virus Infection', *Front Cell Infect Microbiol*, 10: 97.
- Lu, Y. C., W. C. Yeh, and P. S. Ohashi. 2008. 'LPS/TLR4 signal transduction pathway', *Cytokine*, 42: 145-51.
- Luedde, T., N. Beraza, V. Kotsikoris, G. van Loo, A. Nenci, R. De Vos, T. Roskams, C. Trautwein, and M. Pasparakis. 2007. 'Deletion of NEMO/IKKgamma in liver parenchymal cells causes steatohepatitis and hepatocellular carcinoma', *Cancer Cell*, 11: 119-32.
- Lüscher, B., I. Ahel, M. Altmeyer, A. Ashworth, P. Bai, P. Chang, M. Cohen, D. Corda, F. Dantzer, M. D. Daugherty, T. M. Dawson, V. L. Dawson, S. Deindl, A. R. Fehr, K. L. H. Feijs, D. V. Filippov, J. P. Gagné, G. Grimaldi, S. Guettler, N. C. Hoch, M. O. Hottiger, P. Korn, W. L. Kraus, A. Ladurner, L. Lehtiö, A. K. L. Leung, C. J. Lord, A. Mangerich, I. Matic, J. Matthews, G. L. Moldovan, J. Moss, G. Natoli, M. L. Nielsen, M. Niepel, F. Nolte, J. Pascal, B. M. Paschal, K. Pawłowski, G. G. Poirier, S. Smith, G. Timinszky, Z. Q. Wang, J. Yélamos, X. Yu, R. Zaja, and M. Ziegler. 2021. 'ADP-ribosyltransferases, an update on function and nomenclature', *FEBS J*.
- Luscher, B., M. Butepage, L. Eckeï, S. Krieg, P. Verheugd, and B. H. Shilton. 2018. 'ADP-Ribosylation, a Multifaceted Posttranslational Modification Involved in the Control of Cell Physiology in Health and Disease', *Chem Rev*, 118: 1092-136.
- Lustig, A., and A. J. Levine. 1992. 'One hundred years of virology', *J Virol*, 66: 4629-31.
- MacPherson, L., L. Tamblyn, S. Rajendra, F. Bralha, J. P. McPherson, and J. Matthews. 2013. '2,3,7,8-Tetrachlorodibenzo-p-dioxin poly(ADP-ribose) polymerase (TiPARP, ARTD14) is a mono-ADP-ribosyltransferase and repressor of aryl hydrocarbon receptor transactivation', *Nucleic Acids Res*, 41: 1604-21.
- Malet, Helene, Bruno Coutard, Said Jamal, Helene Dutartre, Nicolas Papageorgiou, Maarit Neuvonen, Tero Ahola, Naomi Forrester, Ernest A. Gould, Daniel Lafitte, Francois Ferron, Julien Lescar, Alexander E. Gorbalenya, Xavier de Lamballerie, and Bruno Canard. 2009. 'The Crystal Structures of Chikungunya and Venezuelan Equine Encephalitis Virus nsP3 Macro Domains Define a Conserved Adenosine Binding Pocket', *Journal of Virology*, 83: 6534-45.

- Martell, J. D., T. J. Deerinck, Y. Sancak, T. L. Poulos, V. K. Mootha, G. E. Sosinsky, M. H. Ellisman, and A. Y. Ting. 2012. 'Engineered ascorbate peroxidase as a genetically encoded reporter for electron microscopy', *Nat Biotechnol*, 30: 1143-8.
- Martinez, J. D., J. A. C. Garza, and A. Cuellar-Barboza. 2019. 'Going Viral 2019: Zika, Chikungunya, and Dengue', *Dermatol Clin*, 37: 95-105.
- Marton, J., T. Fodor, L. Nagy, A. Vida, G. Kis, A. Brunyanszki, M. Antal, B. Luscher, and P. Bai. 2018. 'PARP10 (ARTD10) modulates mitochondrial function', *PLoS One*, 13: e0187789.
- Mashimo, M., J. Kato, and J. Moss. 2014. 'Structure and function of the ARH family of ADP-ribosyl-acceptor hydrolases', *DNA Repair (Amst)*, 23: 88-94.
- Matsumoto, T. 1982. 'Assembly of paramyxoviruses', *Microbiol Immunol*, 26: 285-320.
- Matusali, G., F. Colavita, L. Bordi, E. Lalle, G. Ippolito, M. R. Capobianchi, and C. Castilletti. 2019. 'Tropism of the Chikungunya Virus', *Viruses*, 11: 175.
- May, D. G., K. L. Scott, A. R. Campos, and K. J. Roux. 2020. 'Comparative Application of BioID and TurboID for Protein-Proximity Biotinylation', *Cells*, 9: 1070.
- Mayer, A. 1886. 'Concerning the mosaic disease of tobacco.', *Landivertschaftlichen Versuchs-Stationen*, 32: 451-567.
- Mayo, Emilia, Gaia Fabrizio, Emanuele Scarpa, Annalisa Stilla, Nadia Dani, Fulvio Chiacchiera, Henning Kleine, Francesca Attanasio, Bernhard Lüscher, and Maria Di Girolamo. 2018. 'ARTD10/PARP10 Induces ADP-Ribosylation of GAPDH and Recruits GAPDH into Cytosolic Membrane-Free Cell Bodies When Overexpressed in Mammalian Cells', *Challenges*, 9: 22.
- McCarthy, M. K., B. J. J. Davenport, and T. E. Morrison. 2018. 'Chronic Chikungunya Virus Disease.' in Mark Heise (ed.), *Chikungunya Virus* (Springer International Publishing: Cham).
- McCarthy, M. K., and T. E. Morrison. 2016. 'Chronic chikungunya virus musculoskeletal disease: what are the underlying mechanisms?', *Future Microbiol*, 11: 331-4.
- McCormick, Craig, and Denys A. Khapersky. 2017. 'Translation inhibition and stress granules in the antiviral immune response', *Nature Reviews Immunology*, 17: 647-60.
- McFee, R. B. 2018. 'Emerging Infectious Diseases - Overview', *Dis Mon*, 64: 163-69.
- McGurk, L., E. Gomes, L. Guo, J. Mojsilovic-Petrovic, V. Tran, R. G. Kalb, J. Shorter, and N. M. Bonini. 2018. 'Poly(ADP-Ribose) Prevents Pathological Phase Separation of TDP-43 by Promoting Liquid Demixing and Stress Granule Localization', *Mol Cell*, 71: 703-17 e9.
- McPherson, R. L., R. Abraham, E. Sreekumar, S. E. Ong, S. J. Cheng, V. K. Baxter, H. A. Kistemaker, D. V. Filippov, D. E. Griffin, and A. K. Leung. 2017. 'ADP-ribosylhydrolase activity of Chikungunya virus macrodomain is critical for virus replication and virulence', *Proc Natl Acad Sci U S A*, 114: 1666-71.
- Meertens, L., M. L. Hafirassou, T. Couderc, L. Bonnet-Madin, V. Kril, B. M. Kummerer, A. Labeau, A. Brugier, E. Simon-Loriere, J. Burlaud-Gaillard, C. Doyen, L. Pezzi, T. Goupil, S. Rafasse, P. O. Vidalain, A. Bertrand-Legout, L. Gueneau, R. Juntas-Morales, R. Ben Yaou, G. Bonne, X. de Lamballerie, M. Benkirane, P. Roingard, C. Delaugerre, M. Lecuit, and A. Amara. 2019. 'FHL1 is a major host factor for chikungunya virus infection', *Nature*, 574: 259-63.
- Mehrotra, P., J. P. Riley, R. Patel, F. Li, L. Voss, and S. Goenka. 2011. 'PARP-14 functions as a transcriptional switch for Stat6-dependent gene activation', *J Biol Chem*, 286: 1767-76.
- Mellacheruvu, D., Z. Wright, A. L. Couzens, J. P. Lambert, N. A. St-Denis, T. Li, Y. V. Miteva, S. Hauri, M. E. Sardi, T. Y. Low, V. A. Halim, R. D. Bagshaw, N. C. Hubner, A. Al-Hakim, A. Bouchard, D. Faubert, D. Fermin, W. H. Dunham, M. Goudreault, Z. Y. Lin, B. G. Badillo, T. Pawson, D. Durocher, B. Coulombe, R. Aebersold, G. Superti-Furga, J. Colinge, A. J. Heck, H. Choi, M. Gstaiger, S. Mohammed, I. M. Cristea, K. L. Bennett, M. P. Washburn, B. Raught, R. M. Ewing, A. C. Gingras, and A. I. Nesvizhskii. 2013. 'The CRAPome: a contaminant repository for affinity purification-mass spectrometry data', *Nat Methods*, 10: 730-6.
- Ménissier de Murcia, J., M. Ricoul, L. Tartier, C. Niedergang, A. Huber, F. Dantzer, V. Schreiber, J. C. Amé, A. Dierich, M. LeMeur, L. Sabatier, P. Chambon, and G. de Murcia. 2003. 'Functional interaction between PARP-1 and PARP-2 in chromosome stability and embryonic development in mouse', *Embo j*, 22: 2255-63.

- Menzel, S., T. Koudelka, B. Rissiek, F. Haag, C. Meyer-Schwesinger, A. Tholey, and F. Koch-Nolte. 2021. 'ADP-Ribosylation Regulates the Signaling Function of IFN- γ ', *Front Immunol*, 12: 642545.
- Meshram, C. D., P. Agback, N. Shiliaev, N. Urakova, J. A. Mobley, T. Agback, E. I. Frolova, and I. Frolov. 2018. 'Multiple Host Factors Interact with Hypervariable Domain of Chikungunya Virus nsP3 and Determine Viral Replication in Cell-Specific Mode', *J Virol*, 92: e00838-18.
- Meshram, C. D., T. Lukash, A. T. Phillips, I. Akhrymuk, E. I. Frolova, and I. Frolov. 2019. 'Lack of nsP2-specific nuclear functions attenuates chikungunya virus replication both in vitro and in vivo', *Virology*, 534: 14-24.
- Meyer-Ficca, M. L., R. G. Meyer, D. L. Coyle, E. L. Jacobson, and M. K. Jacobson. 2004. 'Human poly(ADP-ribose) glycohydrolase is expressed in alternative splice variants yielding isoforms that localize to different cell compartments', *Exp Cell Res*, 297: 521-32.
- Mittal, Suruchi, and Lawrence Banks. 2017. 'Molecular mechanisms underlying human papillomavirus E6 and E7 oncoprotein-induced cell transformation', *Mutation Research/Reviews in Mutation Research*, 772: 23-35.
- Mocarski, ES, T Shenk, and RF Pass. 2007. 'Cytomegalovirus.' in DM Knipe, Howley, PM, Griffin, DE, et al., (ed.), *Fields virology* (Lippincott Williams & Wilkins: Philadelphia, PA).
- Moldovan, G. L., B. Pfander, and S. Jentsch. 2007. 'PCNA, the maestro of the replication fork', *Cell*, 129: 665-79.
- Monath, T. P. 2008. 'Treatment of yellow fever', *Antiviral Res*, 78: 116-24.
- Morandi, L., D. Gissi, A. Tarsitano, S. Asioli, A. Gabusi, C. Marchetti, L. Montebugnoli, and M. P. Foschini. 2017. 'CpG location and methylation level are crucial factors for the early detection of oral squamous cell carcinoma in brushing samples using bisulfite sequencing of a 13-gene panel', *Clin Epigenetics*, 9: 85.
- Moss, J., M. K. Jacobson, and S. J. Stanley. 1985. 'Reversibility of arginine-specific mono(ADP-ribose)ylation: identification in erythrocytes of an ADP-ribose-L-arginine cleavage enzyme', *Proc Natl Acad Sci U S A*, 82: 5603-7.
- Moustakim, M., K. Riedel, M. Schuller, A. P. Gehring, O. P. Monteiro, S. P. Martin, O. Fedorov, J. Heer, D. J. Dixon, J. M. Elkins, S. Knapp, F. Bracher, and P. E. Brennan. 2018. 'Discovery of a novel allosteric inhibitor scaffold for polyadenosine-diphosphate-ribose polymerase 14 (PARP14) macrodomain 2', *Bioorg Med Chem*, 26: 2965-72.
- Mudgal, R., S. Mahajan, and S. Tomar. 2019. 'Inhibition of Chikungunya virus by an Adenosine Analog targeting the SAM-dependent nsP1 methyltransferase', *FEBS Lett*, 594: 678-94.
- Mueller-Dieckmann, C., S. Kernstock, M. Lisurek, J. P. von Kries, F. Haag, M. S. Weiss, and F. Koch-Nolte. 2006. 'The structure of human ADP-ribosylhydrolase 3 (ARH3) provides insights into the reversibility of protein ADP-ribosylation', *Proc Natl Acad Sci U S A*, 103: 15026-31.
- Munnur, D., and I. Ahel. 2017. 'Reversible mono-ADP-ribosylation of DNA breaks', *FEBS J*, 284: 4002-16.
- Munnur, Deeksha, Edward Bartlett, Johannes Gregor Matthias Rack, Ivan Ahel, Andreja Mikoč, Petra Mikolčević, Ilsa T Kirby, and Michael S Cohen. 2019. 'Reversible ADP-ribosylation of RNA', *Nucleic Acids Research*, 47: 5658-69.
- Murthy, S., J. Desantis, P. Verheugd, M. M. Maksimainen, H. Venkannagari, S. Massari, Y. Ashok, E. Obaji, Y. Nkizinkinko, B. Luscher, O. Tabarrini, and L. Lehtio. 2018. '4-(Phenoxy) and 4-(benzyloxy)benzamides as potent and selective inhibitors of mono-ADP-ribosyltransferase PARP10/ARTD10', *Eur J Med Chem*, 156: 93-102.
- Mutso, M., A. M. Morro, C. Smedberg, S. Kasvandik, M. Aquilimeba, M. Teppor, L. Tarve, A. Lulla, V. Lulla, S. Saul, B. Thaa, G. M. McInerney, A. Merits, and M. Varjak. 2018. 'Mutation of CD2AP and SH3KBP1 Binding Motif in Alphavirus nsP3 Hypervariable Domain Results in Attenuated Virus', *Viruses*, 10: 226.
- Negishi, H., T. Taniguchi, and H. Yanai. 2018. 'The Interferon (IFN) Class of Cytokines and the IFN Regulatory Factor (IRF) Transcription Factor Family', *Cold Spring Harb Perspect Biol*, 10: a028423.
- Neuvonen, M., and T. Ahola. 2009. 'Differential activities of cellular and viral macro domain proteins in binding of ADP-ribose metabolites', *J Mol Biol*, 385: 212-25.

- Nickoloff, J. A., D. Jones, S. H. Lee, E. A. Williamson, and R. Hromas. 2017. 'Drugging the Cancers Addicted to DNA Repair', *J Natl Cancer Inst*, 109: djx059.
- Nicolae, C. M., E. R. Aho, K. N. Choe, D. Constantin, H. J. Hu, D. Lee, K. Myung, and G. L. Moldovan. 2015. 'A novel role for the mono-ADP-ribosyltransferase PARP14/ARTD8 in promoting homologous recombination and protecting against replication stress', *Nucleic Acids Res*, 43: 3143-53.
- Nicolae, C. M., E. R. Aho, A. H. Vlahos, K. N. Choe, S. De, G. I. Karras, and G. L. Moldovan. 2014. 'The ADP-ribosyltransferase PARP10/ARTD10 interacts with proliferating cell nuclear antigen (PCNA) and is required for DNA damage tolerance', *J Biol Chem*, 289: 13627-37.
- Nie, Litong, Chao Wang, Nan Li, Xu Feng, Namsoo Lee, Dan Su, Mengfan Tang, Fan Yao, and Junjie Chen. 2020. 'Proteome-wide analysis reveals substrates of E3 ligase RNF146 targeted for degradation', *Molecular & Cellular Proteomics*, 19: 2015-30.
- Nishizuka, Y., K. Ueda, T. Honjo, and O. Hayaishi. 1968. 'Enzymic adenosine diphosphate ribosylation of histone and poly adenosine diphosphate ribose synthesis in rat liver nuclei', *J Biol Chem*, 243: 3765-7.
- Nishizuka, Y., K. Ueda, K. Nakazawa, and O. Hayaishi. 1967. 'Studies on the polymer of adenosine diphosphate ribose. I. Enzymic formation from nicotinamide adenine dinucleotide in mammalian nuclei', *J Biol Chem*, 242: 3164-71.
- Nowak, I., and A. A. Sarshad. 2021. 'Argonaute Proteins Take Center Stage in Cancers', *Cancers (Basel)*, 13: 788.
- Nowak, Kathrin, Florian Rosenthal, Tobias Karlberg, Mareike Bütepage, Ann-Gerd Thorsell, Birgit Dreier, Jonas Grossmann, Jens Sobek, Ralph Imhof, Bernhard Lüscher, Herwig Schüler, Andreas Plückthun, Deena M. Leslie Pedrioli, and Michael O. Hottiger. 2020. 'Engineering Af1521 improves ADP-ribose binding and identification of ADP-ribosylated proteins', *Nature Communications*, 11: 5199.
- O'Sullivan, J., M. Tedim Ferreira, J. P. Gagne, A. K. Sharma, M. J. Hendzel, J. Y. Masson, and G. G. Poirier. 2019. 'Emerging roles of eraser enzymes in the dynamic control of protein ADP-ribosylation', *Nat Commun*, 10: 1182.
- O'Carroll, I. P., and A. Rein. 2016. 'Viral Nucleic Acids.' in Ralph A. Bradshaw and Philip D. Stahl (eds.), *Encyclopedia of Cell Biology* (Academic Press: Waltham).
- Oei, S. L., J. Griesenbeck, M. Ziegler, and M. Schweiger. 1998. 'A novel function of poly(ADP-ribosylation): silencing of RNA polymerase II-dependent transcription', *Biochemistry*, 37: 1465-9.
- Oerum, S., M. Roovers, R. P. Rambo, J. Kopec, H. J. Bailey, F. Fitzpatrick, J. A. Newman, W. G. Newman, A. Amberger, J. Zschocke, L. Droogmans, U. Oppermann, and W. W. Yue. 2018. 'Structural insight into the human mitochondrial tRNA purine N1-methyltransferase and ribonuclease P complexes', *J Biol Chem*, 293: 12862-76.
- Otake, H., M. Miwa, S. Fujimura, and T. Sugimura. 1969. 'Binding of ADP-ribose polymer with histone', *J Biochem*, 65: 145-6.
- Otto, H., P. A. Reche, F. Bazan, K. Dittmar, F. Haag, and F. Koch-Nolte. 2005. 'In silico characterization of the family of PARP-like poly(ADP-ribosyl)transferases (pARTs)', *BMC Genomics*, 6: 139.
- Palazzo, L., C. M. Daniels, J. E. Nettleship, N. Rahman, R. L. McPherson, S. E. Ong, K. Kato, O. Nureki, A. K. Leung, and I. Ahel. 2016. 'ENPP1 processes protein ADP-ribosylation in vitro', *FEBS J*, 283: 3371-88.
- Panas, M. D., T. Ahola, and G. M. McInerney. 2014. 'The C-terminal repeat domains of nsP3 from the Old World alphaviruses bind directly to G3BP', *J Virol*, 88: 5888-93.
- Panas, M. D., T. Schulte, B. Thaa, T. Sandalova, N. Kedersha, A. Achour, and G. M. McInerney. 2015. 'Viral and cellular proteins containing FGDF motifs bind G3BP to block stress granule formation', *PLoS Pathog*, 11: e1004659.
- Pando, M. P., and I. M. Verma. 2000. 'Signal-dependent and -independent degradation of free and NF-kappa B-bound IkappaBalpha', *J Biol Chem*, 275: 21278-86.
- Panzeter, P. L., and F. R. Althaus. 1990. 'High resolution size analysis of ADP-ribose polymers using modified DNA sequencing gels', *Nucleic Acids Res*, 18: 2194.

- Pariante, N., S. Sierra, P. R. Lowenstein, and E. Domingo. 2001. 'Efficient virus extinction by combinations of a mutagen and antiviral inhibitors', *J Virol*, 75: 9723-30.
- Park, E., and D. E. Griffin. 2009. 'The nsP3 macro domain is important for Sindbis virus replication in neurons and neurovirulence in mice', *Virology*, 388: 305-14.
- Peck, K. M., and A. S. Luring. 2018. 'Complexities of Viral Mutation Rates', *J Virol*, 92: e01031-17.
- Pérez-Gracia, María Teresa, Beatriz Suay, and María Luisa Mateos-Lindemann. 2014. 'Hepatitis E: An emerging disease', *Infection, Genetics and Evolution*, 22: 40-59.
- Perina, D., A. Mikoc, J. Ahel, H. Cetkovic, R. Zaja, and I. Ahel. 2014. 'Distribution of protein poly(ADP-ribose)ylation systems across all domains of life', *DNA Repair (Amst)*, 23: 4-16.
- Pieper, A. A., A. Verma, J. Zhang, and S. H. Snyder. 1999. 'Poly (ADP-ribose) polymerase, nitric oxide and cell death', *Trends Pharmacol Sci*, 20: 171-81.
- Plantone, D., and T. Koudriavtseva. 2018. 'Current and Future Use of Chloroquine and Hydroxychloroquine in Infectious, Immune, Neoplastic, and Neurological Diseases: A Mini-Review', *Clin Drug Investig*, 38: 653-71.
- Powers, A. M., and S. H. Waterman. 2017. 'A decade of arboviral activity-Lessons learned from the trenches', *PLoS Negl Trop Dis*, 11: e0005421.
- Prieto-García, E., C. V. Díaz-García, I. García-Ruiz, and M. T. Agulló-Ortuño. 2017. 'Epithelial-to-mesenchymal transition in tumor progression', *Med Oncol*, 34: 122.
- Puig, O., F. Caspary, G. Rigaut, B. Rutz, E. Bouveret, E. Bragado-Nilsson, M. Wilm, and B. Séraphin. 2001. 'The tandem affinity purification (TAP) method: a general procedure of protein complex purification', *Methods*, 24: 218-29.
- Putics, A., W. Filipowicz, J. Hall, A. E. Gorbalenya, and J. Ziebuhr. 2005. 'ADP-ribose-1"-monophosphatase: a conserved coronavirus enzyme that is dispensable for viral replication in tissue culture', *J Virol*, 79: 12721-31.
- Putics, A., A. E. Gorbalenya, and J. Ziebuhr. 2006a. 'Identification of protease and ADP-ribose 1"-monophosphatase activities associated with transmissible gastroenteritis virus non-structural protein 3', *J Gen Virol*, 87: 651-6.
- Putics, A., J. Slaby, W. Filipowicz, A. E. Gorbalenya, and J. Ziebuhr. 2006b. 'ADP-ribose-1"-phosphatase activities of the human coronavirus 229E and SARS coronavirus X domains', *Adv Exp Med Biol*, 581: 93-6.
- Quan, J. J., J. N. Song, and J. Q. Qu. 2015. 'PARP3 interacts with FoxM1 to confer glioblastoma cell radioresistance', *Tumour Biol*, 36: 8617-24.
- Rack, J. G., R. Morra, E. Barkauskaite, R. Kraehenbuehl, A. Ariza, Y. Qu, M. Ortmayer, O. Leidecker, D. R. Cameron, I. Matic, A. Y. Peleg, D. Leys, A. Traven, and I. Ahel. 2015. 'Identification of a Class of Protein ADP-Ribosylating Sirtuins in Microbial Pathogens', *Mol Cell*, 59: 309-20.
- Rack, J. G., D. Perina, and I. Ahel. 2016. 'Macrodomains: Structure, Function, Evolution, and Catalytic Activities', *Annu Rev Biochem*, 85: 431-54.
- Ramanathan, Muthukumar, Karim Majzoub, Deepti S. Rao, Poornima H. Neela, Brian J. Zarnegar, Smarajit Mondal, Julien G. Roth, Hui Gai, Joanna R. Kovalski, Zurab Sipsrashvili, Theo D. Palmer, Jan E. Carette, and Paul A. Khavari. 2018. 'RNA-protein interaction detection in living cells', *Nature Methods*, 15: 207.
- Rambaut, A., E. C. Holmes, A. O'Toole, V. Hill, J. T. McCrone, C. Ruis, L. du Plessis, and O. G. Pybus. 2020. 'A dynamic nomenclature proposal for SARS-CoV-2 lineages to assist genomic epidemiology', *Nat Microbiol*, 5: 1403-07.
- Ramphan, S., S. Khongwichit, C. Saisawang, D. Kovanich, A. J. Ketterman, S. Ubol, P. Auewarakul, S. Roytrakul, D. R. Smith, and A. Kuadkitkan. 2018. 'Ubiquitin-Conjugating Enzyme E2 L3 is Downregulated by the Chikungunya Virus nsP2 Protease', *Proteomics Clin Appl*, 12: 1700020.
- Rana, J., S. Rajasekharan, S. Gulati, N. Dudha, A. Gupta, V. K. Chaudhary, and S. Gupta. 2014. 'Network mapping among the functional domains of Chikungunya virus nonstructural proteins', *Proteins*, 82: 2403-11.
- Rausalu, K., A. Utt, T. Quirin, F. S. Varghese, E. Zusinaite, P. K. Das, T. Ahola, and A. Merits. 2016. 'Chikungunya virus infectivity, RNA replication and non-structural polyprotein processing depend on the nsP2 protease's active site cysteine residue', *Sci Rep*, 6: 37124.

- Remenyi, R., Y. Gao, R. E. Hughes, A. Curd, C. Zothner, M. Peckham, A. Merits, and M. Harris. 2018. 'Persistent Replication of a Chikungunya Virus Replicon in Human Cells is Associated with Presence of Stable Cytoplasmic Granules Containing Non-structural Protein 3', *J Virol*, 92: e00477-18.
- Rhee, H. W., P. Zou, N. D. Udeshi, J. D. Martell, V. K. Mootha, S. A. Carr, and A. Y. Ting. 2013. 'Proteomic mapping of mitochondria in living cells via spatially restricted enzymatic tagging', *Science*, 339: 1328-31.
- Richter, K. N., N. H. Revelo, K. J. Seitz, M. S. Helm, D. Sarkar, R. S. Saleeb, E. D'Este, J. Eberle, E. Wagner, C. Vogl, D. F. Lazaro, F. Richter, J. Coy-Vergara, G. Coceano, E. S. Boyden, R. R. Duncan, S. W. Hell, M. A. Lauterbach, S. E. Lehnart, T. Moser, T. F. Outeiro, P. Rehling, B. Schwappach, I. Testa, B. Zapiec, and S. O. Rizzoli. 2018. 'Glyoxal as an alternative fixative to formaldehyde in immunostaining and super-resolution microscopy', *Embo j*, 37: 139-59.
- Rodriguez, K. M., S. C. Buch-Larsen, I. T. Kirby, I. R. Siordia, D. Hutin, M. Rasmussen, D. M. Grant, L. L. David, J. Matthews, M. L. Nielsen, and M. S. Cohen. 2021. 'Chemical genetics and proteome-wide site mapping reveal cysteine MARYlation by PARP-7 on immune-relevant protein targets', *Elife*, 10: e60480.
- Rodriguez, M. S., I. Egaña, F. Lopitz-Otsoa, F. Aillet, M. P. Lopez-Mato, A. Dorronsoro, S. Lobato-Gil, J. D. Sutherland, R. Barrio, C. Trigueros, and V. Lang. 2014. 'The RING ubiquitin E3 RNF114 interacts with A20 and modulates NF- κ B activity and T-cell activation', *Cell Death Dis*, 5: e1399.
- Rodriguez-Vargas, José Manuel, Léonel Nguekeu-Zebaze, and Françoise Dantzer. 2019. 'PARP3 comes to light as a prime target in cancer therapy', *Cell Cycle*, 18: 1295-301.
- Rosenthal, F., K. L. Feijs, E. Frugier, M. Bonalli, A. H. Forst, R. Imhof, H. C. Winkler, D. Fischer, A. Caflisch, P. O. Hassa, B. Luscher, and M. O. Hottiger. 2013. 'Macrodomain-containing proteins are new mono-ADP-ribosylhydrolases', *Nat Struct Mol Biol*, 20: 502-7.
- Rouleau, M., D. McDonald, P. Gagné, M. E. Ouellet, A. Droit, J. M. Hunter, S. Dutertre, C. Prigent, M. J. Hendzel, and G. G. Poirier. 2007. 'PARP-3 associates with polycomb group bodies and with components of the DNA damage repair machinery', *J Cell Biochem*, 100: 385-401.
- Roux, K. J., D. I. Kim, M. Raida, and B. Burke. 2012. 'A promiscuous biotin ligase fusion protein identifies proximal and interacting proteins in mammalian cells', *J Cell Biol*, 196: 801-10.
- Ruckert, C., and G. D. Ebel. 2018. 'How Do Virus-Mosquito Interactions Lead to Viral Emergence?', *Trends Parasitol*, 34: 310-21.
- Rulten, S. L., A. E. Fisher, I. Robert, M. C. Zuma, M. Rouleau, L. Ju, G. Poirier, B. Reina-San-Martin, and K. W. Caldecott. 2011. 'PARP-3 and APLF function together to accelerate nonhomologous end-joining', *Mol Cell*, 41: 33-45.
- Rungrotmongkol, T., N. Nunthaboot, M. Malaisree, N. Kaiyawet, P. Yotmanee, A. Meeprasert, and S. Hannongbua. 2010. 'Molecular insight into the specific binding of ADP-ribose to the nsP3 macro domains of chikungunya and Venezuelan equine encephalitis viruses: molecular dynamics simulations and free energy calculations', *J Mol Graph Model*, 29: 347-53.
- Rupp, J. C., K. J. Sokoloski, N. N. Gebhart, and R. W. Hardy. 2015. 'Alphavirus RNA synthesis and non-structural protein functions', *J Gen Virol*, 96: 2483-500.
- Ryan, S. J., C. J. Carlson, E. A. Mordecai, and L. R. Johnson. 2019. 'Global expansion and redistribution of Aedes-borne virus transmission risk with climate change', *PLoS Negl Trop Dis*, 13: e0007213.
- Rybicki, Edward. 1990. 'The classification of organisms at the edge of life or problems with virus systematics', *South African Journal of Science*, 86: 182.
- Ryu, Wang-Shick. 2017. 'Chapter 2 - Virus Structure.' in Wang-Shick Ryu (ed.), *Molecular Virology of Human Pathogenic Viruses* (Academic Press: Boston).
- Saikatendu, K. S., J. S. Joseph, V. Subramanian, T. Clayton, M. Griffith, K. Moy, J. Velasquez, B. W. Neuman, M. J. Buchmeier, R. C. Stevens, and P. Kuhn. 2005. 'Structural basis of severe acute respiratory syndrome coronavirus ADP-ribose-1''-phosphate dephosphorylation by a conserved domain of nsP3', *Structure*, 13: 1665-75.
- Saisawang, C., S. Saitornuang, P. Sillapee, S. Ubol, D. R. Smith, and A. J. Ketterman. 2015. 'Chikungunya nsP2 protease is not a papain-like cysteine protease and the catalytic dyad cysteine is interchangeable with a proximal serine', *Sci Rep*, 5: 17125.

- Salazar, J. C., S. Duhnam-Ems, C. La Vake, A. R. Cruz, M. W. Moore, M. J. Caimano, L. Velez-Climent, J. Shupe, W. Krueger, and J. D. Radolf. 2009. 'Activation of human monocytes by live *Borrelia burgdorferi* generates TLR2-dependent and -independent responses which include induction of IFN-beta', *PLoS Pathog*, 5: e1000444.
- Samavarchi-Tehrani, P., R. Samson, and A. C. Gingras. 2020. 'Proximity Dependent Biotinylation: Key Enzymes and Adaptation to Proteomics Approaches', *Mol Cell Proteomics*, 19: 757-73.
- Santaella, R. M., and F. W. Fraunfelder. 2007. 'Ocular adverse effects associated with systemic medications : recognition and management', *Drugs*, 67: 75-93.
- Schleicher, E. M., A. M. Galvan, Y. Imamura-Kawasawa, G. L. Moldovan, and C. M. Nicolae. 2018. 'PARP10 promotes cellular proliferation and tumorigenesis by alleviating replication stress', *Nucleic Acids Res*, 46: 8908-16.
- Scholte, F. E., A. Tas, I. C. Albulescu, E. Zusinaite, A. Merits, E. J. Snijder, and M. J. van Hemert. 2015. 'Stress granule components G3BP1 and G3BP2 play a proviral role early in Chikungunya virus replication', *J Virol*, 89: 4457-69.
- Schrauf, Sabrina, Roland Tschismarov, Erich Tauber, and Katrin Ramsauer. 2020. 'Current Efforts in the Development of Vaccines for the Prevention of Zika and Chikungunya Virus Infections', *Front Immunol*, 11: 592.
- Schreiber, V., J. C. Amé, P. Dollé, I. Schultz, B. Rinaldi, V. Fraulob, J. Ménissier-de Murcia, and G. de Murcia. 2002. 'Poly(ADP-ribose) polymerase-2 (PARP-2) is required for efficient base excision DNA repair in association with PARP-1 and XRCC1', *J Biol Chem*, 277: 23028-36.
- Schreiber, V., F. Dantzer, J. C. Ame, and G. de Murcia. 2006. 'Poly(ADP-ribose): novel functions for an old molecule', *Nat Rev Mol Cell Biol*, 7: 517-28.
- Schuller, M., K. Riedel, I. Gibbs-Seymour, K. Uth, C. Sieg, A. P. Gehring, I. Ahel, F. Bracher, B. M. Kessler, J. M. Elkins, and S. Knapp. 2017. 'Discovery of a selective allosteric inhibitor targeting macrodomain 2 of poly-adenosine-diphosphate-ribose polymerases 14', *ACS Chem Biol*, 12: 2866-74.
- Schulte, T., L. Liu, M. D. Panas, B. Thaa, N. Dickson, B. Gotte, A. Achour, and G. M. McNerney. 2016. 'Combined structural, biochemical and cellular evidence demonstrates that both FGDF motifs in alphavirus nsP3 are required for efficient replication', *Open Biol*, 6: 160078.
- Schwerk, J., F. W. Soveg, A. P. Ryan, K. R. Thomas, L. D. Hatfield, S. Ozarkar, A. Forero, A. M. Kell, J. A. Roby, L. So, J. L. Hyde, M. Gale, Jr., M. D. Daugherty, and R. Savan. 2019. 'RNA-binding protein isoforms ZAP-S and ZAP-L have distinct antiviral and immune resolution functions', *Nat Immunol*, 20: 1610-20.
- Semenza, J. C., and J. E. Suk. 2017. 'Vector-borne diseases and climate change: a European perspective', *FEMS Microbiol Lett*, 365: fnx244.
- Sezgin, E., and P. Schwille. 2012. 'Model membrane platforms to study protein-membrane interactions', *Mol Membr Biol*, 29: 144-54.
- Shahrour, M. A., C. M. Nicolae, S. Edvardson, M. Ashhab, A. M. Galvan, D. Constantin, B. Abu-Libdeh, G. L. Moldovan, and O. Elpeleg. 2016. 'PARP10 deficiency manifests by severe developmental delay and DNA repair defect', *Neurogenetics*, 17: 227-32.
- Shall, S., and G. de Murcia. 2000. 'Poly(ADP-ribose) polymerase-1: what have we learned from the deficient mouse model?', *Mutat Res*, 460: 1-15.
- Shao, C., Y. Qiu, J. Liu, H. Feng, S. Shen, H. Saiyin, W. Yu, Y. Wei, L. Yu, W. Su, and J. Wu. 2018. 'PARP12 (ARTD12) suppresses hepatocellular carcinoma metastasis through interacting with FHL2 and regulating its stability', *Cell Death Dis*, 9: 856.
- Sharifi, R., R. Morra, C. D. Appel, M. Tallis, B. Chioza, G. Jankevicius, M. A. Simpson, I. Matic, E. Ozkan, B. Golia, M. J. Schellenberg, R. Weston, J. G. Williams, M. N. Rossi, H. Galehdari, J. Krahn, A. Wan, R. C. Trembath, A. H. Crosby, D. Ahel, R. Hay, A. G. Ladurner, G. Timinszky, R. S. Williams, and I. Ahel. 2013. 'Deficiency of terminal ADP-ribose protein glycohydrolase TARG1/C6orf130 in neurodegenerative disease', *Embo j*, 32: 1225-37.
- Shaw, Andrew E., Joseph Hughes, Quan Gu, Abdelkader Behdenna, Joshua B. Singer, Tristan Dennis, Richard J. Orton, Mariana Varela, Robert J. Gifford, Sam J. Wilson, and Massimo Palmarini.

2017. 'Fundamental properties of the mammalian innate immune system revealed by multispecies comparison of type I interferon responses', *PLoS Biol*, 15: e2004086.
- Shi, Jian-Hong, and Shao-Cong Sun. 2018. 'Tumor Necrosis Factor Receptor-Associated Factor Regulation of Nuclear Factor κ B and Mitogen-Activated Protein Kinase Pathways', *Front Immunol*, 9: 1849.
- Shimizu, Y., S. Hasegawa, S. Fujimura, and T. Sugimura. 1967. 'Solubilization of enzyme forming ADPR polymer from NAD', *Biochem Biophys Res Commun*, 29: 80-3.
- Silva, Laurie A., and Terence S. Dermody. 2017. 'Chikungunya virus: epidemiology, replication, disease mechanisms, and prospective intervention strategies', *Journal of Clinical Investigation*, 127: 737-49.
- Simon, N. C., K. Aktories, and J. T. Barbieri. 2014. 'Novel bacterial ADP-ribosylating toxins: structure and function', *Nat Rev Microbiol*, 12: 599-611.
- Slade, Dea, Mark S. Dunstan, Eva Barkauskaite, Ria Weston, Pierre Lafite, Neil Dixon, Marijan Ahel, David Leys, and Ivan Ahel. 2011. 'The structure and catalytic mechanism of a poly(ADP-ribose) glycohydrolase', *Nature*, 477: 616-20.
- Smith, S. 2001. 'The world according to PARP', *Trends Biochem Sci*, 26: 174-9.
- Smith, S., and T. de Lange. 1999. 'Cell cycle dependent localization of the telomeric PARP, tankyrase, to nuclear pore complexes and centrosomes', *J Cell Sci*, 112: 3649-56.
- Smith, S., and T. de Lange. 2000. 'Tankyrase promotes telomere elongation in human cells', *Curr Biol*, 10: 1299-302.
- Snyder, J. E., K. A. Kulcsar, K. L. Schultz, C. P. Riley, J. T. Neary, S. Marr, J. Jose, D. E. Griffin, and R. J. Kuhn. 2013. 'Functional characterization of the alphavirus TF protein', *J Virol*, 87: 8511-23.
- Solignat, M., B. Gay, S. Higgs, L. Briant, and C. Devaux. 2009. 'Replication cycle of chikungunya: a re-emerging arbovirus', *Virology*, 393: 183-97.
- Spuul, P., A. Salonen, A. Merits, E. Jokitalo, L. Kääriäinen, and T. Ahola. 2007. 'Role of the amphipathic peptide of Semliki forest virus replicase protein nsP1 in membrane association and virus replication', *J Virol*, 81: 872-83.
- Stapleford, K. A., K. Rozen-Gagnon, P. K. Das, S. Saul, E. Z. Poirier, H. Blanc, P. O. Vidalain, A. Merits, and M. Vignuzzi. 2015. 'Viral Polymerase-Helicase Complexes Regulate Replication Fidelity To Overcome Intracellular Nucleotide Depletion', *J Virol*, 89: 11233-44.
- Steinhaus, E. A. 1949. 'Nomenclature and classification of insect viruses', *Bacteriol Rev*, 13: 203-23.
- Stoecklin, G., T. Stubbs, N. Kedersha, S. Wax, W. F. Rigby, T. K. Blackwell, and P. Anderson. 2004. 'MK2-induced tristetraprolin:14-3-3 complexes prevent stress granule association and ARE-mRNA decay', *Embo j*, 23: 1313-24.
- Strickfaden, H., D. McDonald, M. J. Kruhlak, J. F. Haince, J. P. Th'ng, M. Rouleau, T. Ishibashi, G. N. Corry, J. Ausio, D. A. Underhill, G. G. Poirier, and M. J. Hendzel. 2016. 'Poly(ADP-ribosyl)ation-dependent Transient Chromatin Decondensation and Histone Displacement following Laser Microirradiation', *J Biol Chem*, 291: 1789-802.
- Sugimura, T., S. Fujimura, S. Hasegawa, and Y. Kawamura. 1967. 'Polymerization of the adenosine 5'-diphosphate ribose moiety of NAD by rat liver nuclear enzyme', *Biochim Biophys Acta*, 138: 438-41.
- Suhrbier, Andreas. 2019. 'Rheumatic manifestations of chikungunya: emerging concepts and interventions', *Nature Reviews Rheumatology*, 15: 597-611.
- Sulkowski, M. S., C. Cooper, B. Hunyady, J. Jia, P. Ogurtsov, M. Peck-Radosavljevic, M. L. Shiffman, C. Yurdaydin, and O. Dalgard. 2011. 'Management of adverse effects of Peg-IFN and ribavirin therapy for hepatitis C', *Nat Rev Gastroenterol Hepatol*, 8: 212-23.
- Szklarczyk, D., A. L. Gable, D. Lyon, A. Junge, S. Wyder, J. Huerta-Cepas, M. Simonovic, N. T. Doncheva, J. H. Morris, P. Bork, L. J. Jensen, and C. V. Mering. 2019. 'STRING v11: protein-protein association networks with increased coverage, supporting functional discovery in genome-wide experimental datasets', *Nucleic Acids Res*, 47: D607-D13.
- Takata, M. A., D. Goncalves-Carneiro, T. M. Zang, S. J. Soll, A. York, D. Blanco-Melo, and P. D. Bieniasz. 2017. 'CG dinucleotide suppression enables antiviral defence targeting non-self RNA', *Nature*, 550: 124-27.

- Tallis, M., R. Morra, E. Barkauskaite, and I. Ahel. 2014. 'Poly(ADP-ribose)ylation in regulation of chromatin structure and the DNA damage response', *Chromosoma*, 123: 79-90.
- Thompson, L. H. 2012. 'Recognition, signaling, and repair of DNA double-strand breaks produced by ionizing radiation in mammalian cells: the molecular choreography', *Mutat Res*, 751: 158-246.
- Tian, L., K. Yao, K. Liu, B. Han, H. Dong, W. Zhao, W. Jiang, F. Qiu, L. Qu, Z. Wu, B. Zhou, M. Zhong, J. Zhao, X. Qiu, L. Zhong, X. Guo, T. Shi, X. Hong, and S. Lu. 2020a. 'PLK1/NF- κ B feedforward circuit antagonizes the mono-ADP-ribosyltransferase activity of PARP10 and facilitates HCC progression', *Oncogene*, 39: 3145-62.
- Tian, Y., P. Korn, P. Tripathi, D. Komnig, D. Wiemuth, A. Nikouee, A. Classen, C. Bolm, B. H. Falkenburger, B. Lüscher, and S. Gründer. 2020b. 'The mono-ADP-ribosyltransferase ARTD10 regulates the voltage-gated K(+) channel Kv1.1 through protein kinase C delta', *BMC Biol*, 18: 143.
- Timinszky, G., S. Till, P. O. Hassa, M. Hothorn, G. Kustatscher, B. Nijmeijer, J. Colombelli, M. Altmeyer, E. H. Stelzer, K. Scheffzek, M. O. Hottiger, and A. G. Ladurner. 2009. 'A macrodomain-containing histone rearranges chromatin upon sensing PARP1 activation', *Nat Struct Mol Biol*, 16: 923-9.
- Todorova, T., F. J. Bock, and P. Chang. 2014. 'PARP13 regulates cellular mRNA post-transcriptionally and functions as a pro-apoptotic factor by destabilizing TRAILR4 transcript', *Nat Commun*, 5: 5362.
- Todorova, T., F. J. Bock, and P. Chang. 2015. 'Poly(ADP-ribose) polymerase-13 and RNA regulation in immunity and cancer', *Trends Mol Med*, 21: 373-84.
- Tomar, S., M. Narwal, E. Harms, J. L. Smith, and R. J. Kuhn. 2011. 'Heterologous production, purification and characterization of enzymatically active Sindbis virus nonstructural protein nsP1', *Protein Expr Purif*, 79: 277-84.
- Tomar, Shailly, and Megha Aggarwal. 2017. 'Chapter 5 - Structure and Function of Alphavirus Proteases A2 - Gupta, Satya P.' in, *Viral Proteases and Their Inhibitors* (Academic Press).
- Tong, L., and J. M. Denu. 2010. 'Function and metabolism of sirtuin metabolite O-acetyl-ADP-ribose', *Biochim Biophys Acta*, 1804: 1617-25.
- Tossavainen, H., O. Aitio, M. Hellman, K. Saksela, and P. Permi. 2016. 'Structural Basis of the High-Affinity Interaction Between the Alphavirus Nonstructural Protein-3 (nsP3) and the SH3 Domain of Amphiphysin-2', *J Biol Chem*, 291: 16307-17.
- Tourriere, H., K. Chebli, L. Zekri, B. Courselaud, J. M. Blanchard, E. Bertrand, and J. Tazi. 2003. 'The RasGAP-associated endoribonuclease G3BP assembles stress granules', *J Cell Biol*, 160: 823-31.
- Tripathi, Ekta, and Susan Smith. 2016. 'Cell cycle-regulated ubiquitination of tankyrase 1 by RNF8 and ABRO1/BRCC36 controls the timing of sister telomere resolution', *Embo j*, 36: 503-19.
- Trofatter, K. F., Jr. 1987. 'Interferon', *Obstet Gynecol Clin North Am*, 14: 569-79.
- Tsai, C. H., P. Y. Lee, V. Stollar, and M. L. Li. 2006. 'Antiviral therapy targeting viral polymerase', *Curr Pharm Des*, 12: 1339-55.
- Tyanova, Stefka, Tikira Temu, and Juergen Cox. 2016. 'The MaxQuant computational platform for mass spectrometry-based shotgun proteomics', *Nature Protocols*, 11: 2301-19.
- Uchida, K., T. Morita, T. Sato, T. Ogura, R. Yamashita, S. Noguchi, H. Suzuki, H. Nyunoya, M. Miwa, and T. Sugimura. 1987. 'Nucleotide sequence of a full-length cDNA for human fibroblast poly(ADP-ribose) polymerase', *Biochem Biophys Res Commun*, 148: 617-22.
- Utt, A., P. K. Das, M. Varjak, V. Lulla, A. Lulla, and A. Merits. 2015. 'Mutations conferring a noncytotoxic phenotype on chikungunya virus replicons compromise enzymatic properties of nonstructural protein 2', *J Virol*, 89: 3145-62.
- Utt, A., T. Quirin, S. Saul, K. Hellstrom, T. Ahola, and A. Merits. 2016. 'Versatile Trans-Replication Systems for Chikungunya Virus Allow Functional Analysis and Tagging of Every Replicase Protein', *PLoS One*, 11: e0151616.
- Valneva SE. 2021. "Valneva Announces Positive Phase 3 Pivotal Results for its Single-Shot Chikungunya Vaccine Candidate [Press Release]." In.

- Venkannagari, H., A. Fallarero, K. L. Feijs, B. Lüscher, and L. Lehtiö. 2013. 'Activity-based assay for human mono-ADP-ribosyltransferases ARTD7/PARP15 and ARTD10/PARP10 aimed at screening and profiling inhibitors', *Eur J Pharm Sci*, 49: 148-56.
- Venkannagari, H., P. Verheugd, J. Koivunen, T. Haikarainen, E. Obaji, Y. Ashok, M. Narwal, T. Pihlajaniemi, B. Lüscher, and L. Lehtiö. 2016. 'Small-Molecule Chemical Probe Rescues Cells from Mono-ADP-Ribosyltransferase ARTD10/PARP10-Induced Apoptosis and Sensitizes Cancer Cells to DNA Damage', *Cell Chem Biol*, 23: 1251-60.
- Verheugd, P., A. H. Forst, L. Milke, N. Herzog, K. L. Feijs, E. Kremmer, H. Kleine, and B. Luscher. 2013. 'Regulation of NF-kappaB signalling by the mono-ADP-ribosyltransferase ARTD10', *Nat Commun*, 4: 1683.
- Virág, L., A. Robaszkievicz, J. M. Rodriguez-Vargas, and F. J. Oliver. 2013. 'Poly(ADP-ribose) signaling in cell death', *Mol Aspects Med*, 34: 1153-67.
- Vyas, S., I. Matic, L. Uchima, J. Rood, R. Zaja, R. T. Hay, I. Ahel, and P. Chang. 2014. 'Family-wide analysis of poly(ADP-ribose) polymerase activity', *Nat Commun*, 5: 4426.
- Vyas, Sejal, Melissa Chesarone-Cataldo, Tanya Todorova, Yun-Han Huang, and Paul Chang. 2013. 'A systematic analysis of the PARP protein family identifies new functions critical for cell physiology', *Nature Communications*, 4: 2240.
- Wada, K., M. Sato, N. Araki, M. Kumeta, Y. Hirai, K. Takeyasu, K. Furukawa, and T. Horigome. 2014. 'Dynamics of WD-repeat containing proteins in SSU processome components', *Biochem Cell Biol*, 92: 191-9.
- Wahlberg, E., T. Karlberg, E. Kouznetsova, N. Markova, A. Macchiarulo, A. G. Thorsell, E. Pol, Å Frostell, T. Ekblad, D. Öncü, B. Kull, G. M. Robertson, R. Pellicciari, H. Schüler, and J. Weigelt. 2012a. 'Family-wide chemical profiling and structural analysis of PARP and tankyrase inhibitors', *Nat Biotechnol*, 30: 283-8.
- Wahlberg, E., T. Karlberg, E. Kouznetsova, N. Markova, A. Macchiarulo, A. G. Thorsell, E. Pol, A. Frostell, T. Ekblad, D. Oncu, B. Kull, G. M. Robertson, R. Pellicciari, H. Schuler, and J. Weigelt. 2012b. 'Family-wide chemical profiling and structural analysis of PARP and tankyrase inhibitors', *Nat Biotechnol*, 30: 283-8.
- Wan, J. J., Y. S. Ooi, and M. Kielian. 2019. 'Mechanism of Tetherin Inhibition of Alphavirus Release', *J Virol*, 93: e02165-18.
- Wang, Shihang, Xuanyu Xu, Cai Wei, Sicong Li, Jingying Zhao, Yin Zheng, Xiaoyu Liu, Xiaomin Zeng, Wenliang Yuan, and Sihua Peng. 2021. 'Molecular evolutionary characteristics of SARS-CoV-2 emerging in the United States', *J Med Virol*, 94: 310-17.
- Wang, W., X. W. Song, and C. H. Zhao. 2016a. 'Roles of programmed cell death protein 5 in inflammation and cancer (Review)', *Int J Oncol*, 49: 1801-06.
- Wang, Y., R. An, G. K. Umanah, H. Park, K. Nambiar, S. M. Eacker, B. Kim, L. Bao, M. M. Harraz, C. Chang, R. Chen, J. E. Wang, T. I. Kam, J. S. Jeong, Z. Xie, S. Neifert, J. Qian, S. A. Andrabi, S. Blackshaw, H. Zhu, H. Song, G. L. Ming, V. L. Dawson, and T. M. Dawson. 2016b. 'A nuclease that mediates cell death induced by DNA damage and poly(ADP-ribose) polymerase-1', *Science*, 354: aad6872.
- Wang, Z., G. A. Michaud, Z. Cheng, Y. Zhang, T. R. Hinds, E. Fan, F. Cong, and W. Xu. 2012. 'Recognition of the iso-ADP-ribose moiety in poly(ADP-ribose) by WWE domains suggests a general mechanism for poly(ADP-ribosyl)ation-dependent ubiquitination', *Genes Dev*, 26: 235-40.
- Waterson, AP. 1965. 'The significance of viral structure', *Archiv für die gesamte Virusforschung*, 15: 275-300.
- Wazir, S., M. M. Maksimainen, H. I. Alanen, A. Galera-Prat, and L. Lehtiö. 2021. 'Activity-Based Screening Assay for Mono-ADP-Ribosylhydrolases', *SLAS Discov*, 26: 67-76.
- Weixler, Lisa, Katja Schäringer, Jeffrey Momoh, Bernhard Lüscher, Karla L. H. Feijs, and Roko Žaja. 2021. 'ADP-ribosylation of RNA and DNA: from in vitro characterization to in vivo function', *Nucleic Acids Research*, 49: 3634-50.
- Welsby, I., D. Hutin, C. Gueydan, V. Kruys, A. Rongvaux, and O. Leo. 2014. 'PARP12, an interferon-stimulated gene involved in the control of protein translation and inflammation', *J Biol Chem*, 289: 26642-57.

- Welsby, I., D. Hutin, and O. Leo. 2012. 'Complex roles of members of the ADP-ribosyl transferase super family in immune defences: looking beyond PARP1', *Biochem Pharmacol*, 84: 11-20.
- WHO. 2007. 'Smallpox', Accessed September 11, 2019. <http://www.who.int/mediacentre/factsheets/smallpox/en/>.
- WHO. 2015. "Blueprint for R&D preparedness and response to public health emergencies due to highly infectious pathogens." In.
- WHO. 2017. "2017 Annual review of diseases prioritized under the Research and Development Blueprint." In.
- WHO. 2018a. "2018 Annual review of diseases prioritized under the Research and Development Blueprint." In.
- WHO. 2018b. 'Global Health Estimates 2016: Disease burden by Cause, Age, Sex, by Country and by Region, 2000-2016.', Accessed July 13, 2020. <https://www.who.int/news-room/factsheets/detail/the-top-10-causes-of-death>.
- WHO. 2018c. 'List of Blueprint priority diseases', Accessed October 7, 2019. <https://www.who.int/blueprint/priority-diseases/en/>.
- WHO. 2019. 'Poliomyelitis', Accessed September 11, 2019. <https://www.who.int/en/news-room/factsheets/detail/poliomyelitis>.
- WHO. 2020a. 'Chikungunya', Accessed September 17, 2021. <https://www.who.int/news-room/factsheets/detail/chikungunya>.
- WHO. 2020b. 'Hepatitis E', Accessed July 1, 2021. <https://www.who.int/news-room/factsheets/detail/hepatitis-e>.
- WHO. 2020c. 'Prioritizing diseases for research and development in emergency contexts', Accessed July 16, 2020. <https://www.who.int/activities/prioritizing-diseases-for-research-and-development-in-emergency-contexts>.
- WHO. 2020d. "Q&A: Dexamethasone and COVID-19." In.
- WHO. 2020e. "WHO Director-General's opening remarks at the media briefing on COVID-19." In.
- WHO. 2021. 'Middle East respiratory syndrome coronavirus (MERS-CoV)', Accessed 01.07.2021. [https://www.who.int/health-topics/middle-east-respiratory-syndrome-coronavirus-mers - tab=tab_2](https://www.who.int/health-topics/middle-east-respiratory-syndrome-coronavirus-mers-tab=tab_2).
- Wilkins, B. J., K. Lorent, R. P. Matthews, and M. Pack. 2013. 'p53-mediated biliary defects caused by knockdown of cirh1a, the zebrafish homolog of the gene responsible for North American Indian Childhood Cirrhosis', *PLoS One*, 8: e77670.
- Xu, F., C. Zhao, Y. Li, J. Li, Y. Deng, and T. Shi. 2011. 'Exploring virus relationships based on virus-host protein-protein interaction network', *BMC Syst Biol*, 5 Suppl 3: S11.
- Yahui, Zhao, Liang Xiao, Wei Li, Liu Yao, Liu Juan, Feng Huan, Zheng Fen, Wang Ying, Ma Haijie, and Wu Jiayue. 2020. 'RNF114 suppresses tumour metastasis through the regulation of PARP10', *Research Square*.
- Yamada, M., M. Miwa, and T. Sugimura. 1971. 'Studies on poly (adenosine diphosphate-ribose). X. Properties of a partially purified poly (adenosine diphosphate-ribose) polymerase', *Arch Biochem Biophys*, 146: 579-86.
- Yamada, T., H. Horimoto, T. Kameyama, S. Hayakawa, H. Yamato, M. Dazai, A. Takada, H. Kida, D. Bott, A. C. Zhou, D. Hutin, T. H. Watts, M. Asaka, J. Matthews, and A. Takaoka. 2016. 'Constitutive aryl hydrocarbon receptor signaling constrains type I interferon-mediated antiviral innate defense', *Nat Immunol*, 17: 687-94.
- Yan, Q., S. Dutt, R. Xu, K. Graves, P. Juszczynski, J. P. Manis, and M. A. Shipp. 2009. 'BBAP monoubiquitylates histone H4 at lysine 91 and selectively modulates the DNA damage response', *Mol Cell*, 36: 110-20.
- Yan, Q., R. Xu, L. Zhu, X. Cheng, Z. Wang, J. Manis, and M. A. Shipp. 2013. 'BAL1 and its partner E3 ligase, BBAP, link Poly(ADP-ribose) activation, ubiquitylation, and double-strand DNA repair independent of ATM, MDC1, and RNF8', *Mol Cell Biol*, 33: 845-57.
- Yang, C. S., K. Jividen, T. Kamata, N. Dworak, L. Oostdyk, B. Remlein, Y. Pourfarjam, I. K. Kim, K. P. Du, T. Abbas, N. E. Sherman, D. Wotton, and B. M. Paschal. 2021. 'Androgen signaling uses a writer

- and a reader of ADP-ribosylation to regulate protein complex assembly', *Nat Commun*, 12: 2705.
- Yang, C. S., K. Jividen, A. Spencer, N. Dworak, L. Ni, L. T. Oostdyk, M. Chatterjee, B. Kusmider, B. Reon, M. Parlak, V. Gorbunova, T. Abbas, E. Jeffery, N. E. Sherman, and B. M. Paschal. 2017. 'Ubiquitin Modification by the E3 Ligase/ADP-Ribosyltransferase Dtx3L/Parp9', *Mol Cell*, 66: 503-16.e5.
- Yang, D., Q. Wang, G. Wei, J. Wu, Y. C. Zhu, Q. Zhu, T. Ni, X. Liu, and Y. Z. Zhu. 2020. 'Smyd3-PARP16 axis accelerates unfolded protein response and vascular aging', *Aging (Albany NY)*, 12: 21423-45.
- Yang, S. Y., X. Y. He, and H. Schulz. 2005. 'Multiple functions of type 10 17beta-hydroxysteroid dehydrogenase', *Trends Endocrinol Metab*, 16: 167-75.
- Yao, N., Q. Chen, W. Shi, L. Tang, and Y. Fu. 2019. 'PARP14 promotes the proliferation and gemcitabine chemoresistance of pancreatic cancer cells through activation of NF- κ B pathway', *Mol Carcinog*, 58: 1291-302.
- Yap, M. L., T. Klose, A. Urakami, S. S. Hasan, W. Akahata, and M. G. Rossmann. 2017. 'Structural studies of Chikungunya virus maturation', *Proc Natl Acad Sci U S A*, 114: 13703-07.
- Young, A. R., M. C. Locke, L. E. Cook, B. E. Hiller, R. Zhang, M. L. Hedberg, K. J. Monte, D. J. Veis, M. S. Diamond, and D. J. Lenschow. 2019. 'Dermal and muscle fibroblasts and skeletal myofibers survive chikungunya virus infection and harbor persistent RNA', *PLoS Pathog*, 15: e1007993.
- Young, P. R. 2018. 'Arboviruses: A Family on the Move', *Adv Exp Med Biol*, 1062: 1-10.
- Yu, Bin, Grant A. Mitchell, and Andrea Richter. 2009. 'Cirhin up-regulates a canonical NF- κ B element through strong interaction with Cirip/HIVeP1', *Exp Cell Res*, 315: 3086-98.
- Yu, M., S. Schreek, C. Cerni, C. Schamberger, K. Lesniewicz, E. Poreba, J. Vervoorts, G. Walsemann, J. Grotzinger, E. Kremmer, Y. Mehraein, J. Mertsching, R. Kraft, M. Austen, J. Luscher-Firzlauff, and B. Luscher. 2005. 'PARP-10, a novel Myc-interacting protein with poly(ADP-ribose) polymerase activity, inhibits transformation', *Oncogene*, 24: 1982-93.
- Yu, M., C. Zhang, Y. Yang, Z. Yang, L. Zhao, L. Xu, R. Wang, X. Zhou, and P. Huang. 2011. 'The interaction between the PARP10 protein and the NS1 protein of H5N1 AIV and its effect on virus replication', *Virology*, 8: 546.
- Zaja, R., G. Aydin, B. E. Lippok, R. Feederle, B. Luscher, and K. L. H. Feijs. 2020. 'Comparative analysis of MACROD1, MACROD2 and TARG1 expression, localisation and interactome', *Sci Rep*, 10: 8286.
- Zhang, Lu, Ji Cao, Longying Dong, and Hening Lin. 2020. 'TiPARP forms nuclear condensates to degrade HIF-1 α and suppress tumorigenesis', *Proceedings of the National Academy of Sciences*, 117: 13447-56.
- Zhang, R., A. S. Kim, J. M. Fox, S. Nair, K. Basore, W. B. Klimstra, R. Rimkunas, R. H. Fong, H. Lin, S. Poddar, J. E. Crowe, Jr., B. J. Doranz, D. H. Fremont, and M. S. Diamond. 2018. 'Mxra8 is a receptor for multiple arthritogenic alphaviruses', *Nature*, 557: 570-74.
- Zhang, Rong, James T. Earnest, Arthur S. Kim, Emma S. Winkler, Pritesh Desai, Lucas J. Adams, Gaowei Hu, Christopher Bullock, Beth Gold, Sara Cherry, and Michael S. Diamond. 2019a. 'Expression of the Mxra8 Receptor Promotes Alphavirus Infection and Pathogenesis in Mice and Drosophila', *Cell Reports*, 28: 2647-58.e5.
- Zhang, Y., D. Mao, W. T. Roswit, X. Jin, A. C. Patel, D. A. Patel, E. Agapov, Z. Wang, R. M. Tidwell, J. J. Atkinson, G. Huang, R. McCarthy, J. Yu, N. E. Yun, S. Paessler, T. G. Lawson, N. S. Omattage, T. J. Brett, and M. J. Holtzman. 2015. 'PARP9-DTX3L ubiquitin ligase targets host histone H2BJ and viral 3C protease to enhance interferon signaling and control viral infection', *Nat Immunol*, 16: 1215-27.
- Zhang, Y., H. Zhang, G. L. Zheng, Q. Yang, S. Yu, J. Wang, S. Li, L. F. Li, and H. J. Qiu. 2019b. 'Porcine RING Finger Protein 114 Inhibits Classical Swine Fever Virus Replication via K27-Linked Polyubiquitination of Viral NS4B', *J Virol*, 93: e01248-19.
- Zhang, Yue, Shanming Liu, Craig Mickanin, Yan Feng, Olga Charlat, Gregory A. Michaud, Markus Schirle, Xiaoying Shi, Marc Hild, Andreas Bauer, Vic E. Myer, Peter M. Finan, Jeffery A. Porter, Shih-Min A. Huang, and Feng Cong. 2011. 'RNF146 is a poly(ADP-ribose)-directed E3 ligase that regulates axin degradation and Wnt signalling', *Nat Cell Biol*, 13: 623-29.

- Zhao, B. S., I. A. Roundtree, and C. He. 2017. 'Post-transcriptional gene regulation by mRNA modifications', *Nat Rev Mol Cell Biol*, 18: 31-42.
- Zhao, H., and P. Lappalainen. 2012. 'A simple guide to biochemical approaches for analyzing protein-lipid interactions', *Mol Biol Cell*, 23: 2823-30.
- Zhao, Y., X. Hu, L. Wei, D. Song, J. Wang, L. You, H. Saiyin, Z. Li, W. Yu, L. Yu, J. Ding, and J. Wu. 2018. 'PARP10 suppresses tumor metastasis through regulation of Aurora A activity', *Oncogene*, 37: 2921-35.
- Zheng, M., R. Karki, P. Vogel, and T. D. Kanneganti. 2020. 'Caspase-6 Is a Key Regulator of Innate Immunity, Inflammasome Activation, and Host Defense', *Cell*, 181: 674-87.e13.
- Zhou, Z. D., C. H. Chan, Z. C. Xiao, and E. K. Tan. 2011. 'Ring finger protein 146/Iduna is a poly(ADP-ribose) polymer binding and PARsylation dependent E3 ubiquitin ligase', *Cell Adh Migr*, 5: 463-71.
- Zhou, Z. H., B. V. Prasad, J. Jakana, F. J. Rixon, and W. Chiu. 1994. 'Protein subunit structures in the herpes simplex virus A-capsid determined from 400 kV spot-scan electron cryomicroscopy', *J Mol Biol*, 242: 456-69.
- Zhu, Y., X. Wang, S. P. Goff, and G. Gao. 2012. 'Translational repression precedes and is required for ZAP-mediated mRNA decay', *Embo j*, 31: 4236-46.
- Zimmer, A. S., M. Gillard, S. Lipkowitz, and J. M. Lee. 2018. 'Update on PARP Inhibitors in Breast Cancer', *Curr Treat Options Oncol*, 19: 21.
- Zimmerlin, L., and E. T. Zambidis. 2020. 'Pleiotropic roles of tankyrase/PARP proteins in the establishment and maintenance of human naïve pluripotency', *Exp Cell Res*, 390: 111935.
- Zotti, T., I. Scudiero, P. Settembre, A. Ferravante, P. Mazzone, L. D'Andrea, C. Reale, P. Vito, and R. Stilo. 2014. 'TRAF6-mediated ubiquitination of NEMO requires p62/sequestosome-1', *Mol Immunol*, 58: 27-31.

6 Appendix

6.1 Supplementary Figures

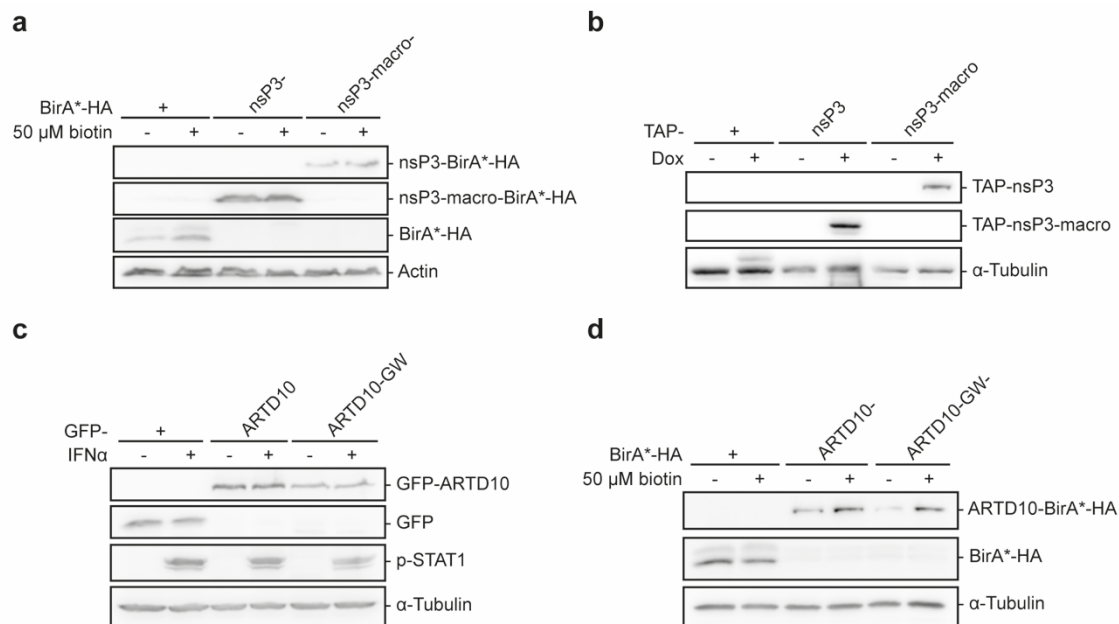


Figure S65: Expression and treatment controls for the MS experiments.

(a) HEK293 cells were transiently transfected with plasmids encoding BirA*-HA, nsP3-BirA*-HA or nsP3-macro-BirA*-HA. The day after transfection the cells were incubated in the presence or absence of 50 μ M biotin as indicated for 16 h. The cells were lysed and the WCLs were subjected to SDS-PAGE and immunoblotted with specific antibodies. The BirA*-fusion proteins were detected with an anti-HA antibody (Covance) and the expression was compared to the loading control actin (SK_B_17, I performed this experiment). **(b)** HEK293 FlpIn T-REx cell lines with stable integration of TAP, TAP-nsP3 or TAP-nsP3-macro were incubated in the presence or absence of 1 μ g/ml Dox for 24 h. Thereafter the cells were lysed and expression of the transgenes was evaluated by immunoblotting of the WCLs. The TAP fusion proteins were detected with an HRP-coupled anti-rabbit secondary antibody and the expression was compared to the loading control α -tubulin (SK_B_30, I performed this experiment). **(c)** HEK293 cells were transiently transfected with plasmids encoding GFP, GFP-ARTD10 or GFP-ARTD10-GW. The day after transfection the cells were incubated in the presence or absence of 180 U/ml IFN α as indicated for 24 h. The cells were lysed and the WCLs were subjected to SDS-PAGE and immunoblotted with specific antibodies. The GFP-fusion proteins were detected with an anti-GFP antibody (Rockland) and the expression was compared to the loading control α -tubulin. As a control for the IFN α treatment phosphorylated STAT1 was detected with a specific antibody (SK_B_48, I performed this experiment). **(d)** HEK293 cells were transiently transfected with plasmids encoding BirA*-HA, ARTD10-BirA*-HA or ARTD10-GW-BirA*-HA. The day after transfection the cells were incubated in the presence or absence of 50 μ M biotin as indicated for 16 h. The cells were lysed and the WCLs were subjected to SDS-PAGE and immunoblotted with specific antibodies. The BirA*-fusion proteins were detected with an anti-HA antibody (Covance) and the expression was compared to the loading control α -tubulin (SK_B_21, I performed this experiment).

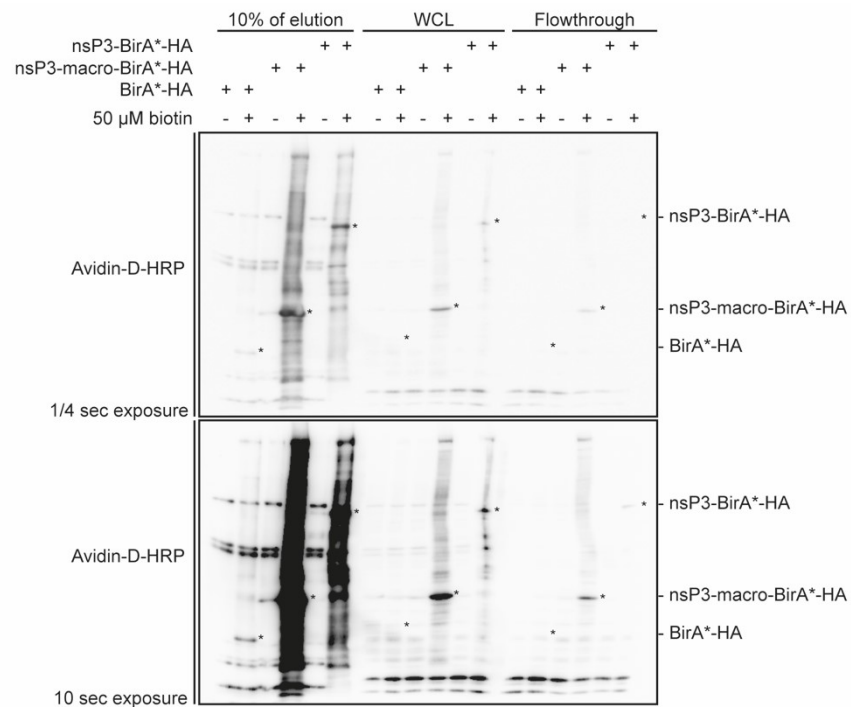


Figure S66: Biotinylation and streptavidin-enrichment of the nsP3- and nsP3-macro-BirA*-HA constructs.

HEK293 cells were transiently transfected with plasmids encoding BirA*-HA, nsP3-BirA*-HA or nsP3-macro-BirA*-HA. The day after transfection the cells were incubated in the presence or absence of 50 μ M biotin as indicated for 16 h. The cells were lysed and biotinylated proteins were enriched using streptavidin beads and eluted after IP. 10% of the elution fraction, the WCLs and the flowthrough from the IP were subjected to SDS-PAGE and immunoblotting. The biotinylation and the enrichment of biotinylated proteins was detected with Avidin-D-HRP (n = 2, SK_B_17_A I performed these experiments).

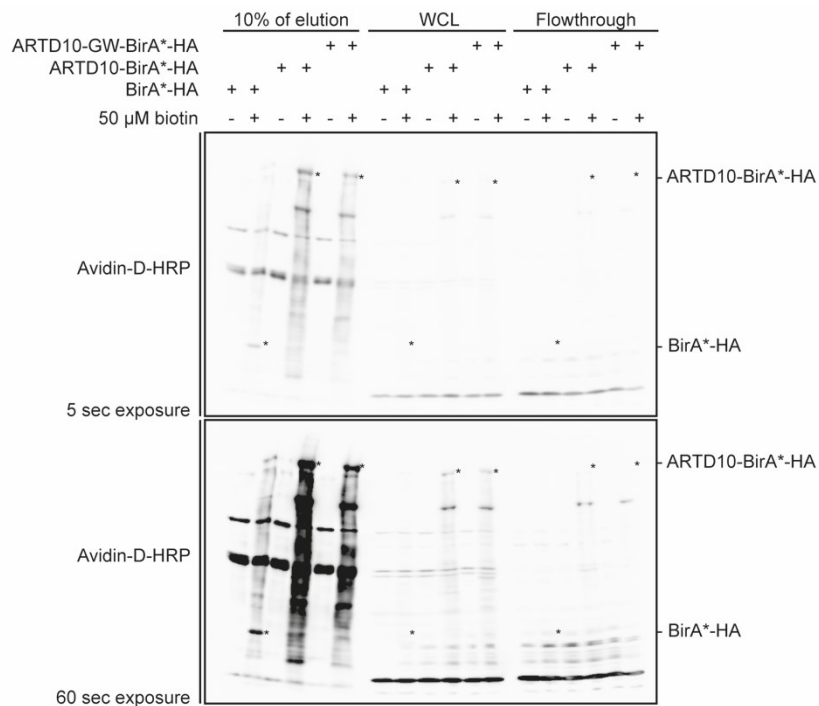


Figure S67: Biotinylation and streptavidin-enrichment of the ARTD10- and ARTD10-GW-BirA*-HA constructs.

HEK293 cells were transiently transfected with plasmids encoding BirA*-HA, ARTD10-BirA*-HA or ARTD10-GW-BirA*-HA. The day after transfection the cells were incubated in the presence or absence of 50 μ M biotin as indicated for 16 h. The cells were lysed and biotinylated proteins were enriched using streptavidin beads and eluted after IP. 10% of the elution fraction, the WCLs and the flowthrough from the IP were subjected to SDS-PAGE and immunoblotting. The biotinylation and the enrichment of biotinylated proteins was detected with Avidin-D-HRP (n = 1, SK_B_21_B, I performed this experiment).

6.2 Abbreviations

%	percent
°C	degree celsius
(+)ssRNA	positive sense single strand RNA
(-)ssRNA	negative sense single strand RNA
0035	OUL35
² EGFP	replicon with EGFP insertion in nsP2
3-AB	3-aminobenzamide
³ EGFP	replicon with EGFP insertion in nsP3
A	area
aa	amino acid
ADP	adenosine diphosphate
ADPr	ADP-ribose
ADRP	Appr-1"-p phosphatase
AF	Archaeoglobus fulgidus
AGO	argonaut
AHR	Aryl hydrocarbon receptor
AIF	Apoptosis -inducing factor
ALC1	Amplified in liver cancer 1
AMD	automodification domain
APEX1	apurinic/aprimidinic endodeoxyribonuclease 1
Appr-1"-p	ADP-ribose-1"-monophosphate
APS	ammonium persulfate
AR	Androgen receptor
Arbovirus	arthropod-borne virus
ARC	ankyrin repeat cluster
ARH	ADP-ribosyl-acceptor hydrolase
ART	ADP-ribosyltransferase
ARTC	ADP-ribosyltransferase cholera toxin-like
ARTD	ADP-ribosyltransferase diptheria toxin-like
ARTD10cat	ARTD10 catalytic domain
ATP	adenosine triphosphate
att	attachment acid
AU	airy unit
AUD	Alphavirus Unique Domain
Baf. A1	Bafilomycin A1
BAL	B-cell aggressive lymphoma
BBAP	B-lymphoma and BAL-associated protein
BIN1	amphiphysin-2
BioID	Proximity-dependent biotin identification
BirA*	Bifunctional ligase/repressor BirA with R118G mutation
bp	base pairs
BRCA	Breast cancer associated protein
BRCT	BRCA1 carboxy-terminal domain
BSA	Bovine serum albumin
C-protein	capsid protein
C-terminus	carboxy terminus
C6orf130	chromosome 6 open reading frame 130

CaM	calmodulin
CB	Coomassie blue
CBP	Calmodulin binding protein
CCN	cyclin
CD	circular dichroism
CD2AP	CD2-associated protein
CDK	cyclin-dependent kinase
CHIKV	Chikungunya virus
CHAPIR	cardiac-hypertrophy-associated PIWI-interacting RNA
CIRH1A	Cirhin
cm	centimeter
CMV	Cytomegalovirus
co-IP	co-immunoprecipitation
CoV	Coronavirus
COVID	Coronavirus disease
CPS	counts per second
ctrl	control
DAPI	4',6-diamidino-2-phenylindole
DdRp	DNA dependent RNA polymerase
DCP	mRNA-decapping enzyme subunit
DDX	DEAD-box helicase
DLBCL	Diffuse large B-cell lymphoma
DMARD	disease-modifying anti-rheumatic drugs
DMEM	Dulbecco's modified eagle medium
DMSO	dimethyl sulfoxide
DNA	Deoxyribonucleic acid
DNA pol	DNA polymerase
Dox	doxycycline
ds	double strand
DSB	double strand break
DTT	dithiothreitol
DTX3L	Deltex 3-like
<i>E. coli</i>	<i>Escherichia coli</i>
ECL	enhanced chemiluminescence
EDTA	ethylenediaminetetraacetic acid
eEF2	Eukaryotic elongation factor 2
eIF4A/G	eukaryotic initiation factor 4 A/G
EGFP	enhanced green fluorescent protein
EGTA	triethylene glycol diamine tetraacetic
EMCV	Encephalomyocarditis virus
EMT	epithelial-to-mesenchymal transition
ER	endoplasmatic reticulum
ER α	Estrogen receptor alpha
Fc	fragment crystallizable
FCS	fetal calf serum
FDA	U.S. Food and Drug Administration
FHA	Forkhead-associated
FHL	four and a half LIM domains protein
FIPV	Feline Infectious Peritonitis virus
FSC	forward scatter

g	gram
G3BP	Ras GTPase-activating protein-binding protein
GAPDH	glyceraldehyde-3-phosphate dehydrogenase
GDAP2	Ganglioside-induced differentiation-associated protein 2
GO	gene ontology
GRD	glycine rich domain
GSK3 β	Glycogen synthase kinase-3 β
GST	Glutathione-S-transferase
GTase	guanylyltransferase
GTP	guanosine-5'-triphosphate
h	hour
H	height
H ₂ O ₂	hydrogen peroxide
HA	hemagglutinin
HCC	Hepatocellular carcinoma
HCoV229E	Human Coronavirus 229E
HCV	Hepatitis C virus
HEV	Hepatitis E virus
HIF-1	Hypoxia-induced factor 1
HIV-1	Human Immunodeficiency virus 1
HPF1	Histone PARylation factor 1
hpi	hours post infection
hpt	hours post transfection
HRP	Horseradish peroxidase
HSD17B10	3-hydroxyacyl-CoA dehydrogenase type-2
HSP70	heat shock protein 70
HVD	Hypervariable Domain
IAV	Influenza A virus
ICTV	Committee on Taxonomy of Viruses
IFN	interferon
IFNAR	IFN α/β receptor
Ig	immunoglobulin
IKK	I κ B kinase complex
IL	interleukin
IL-1R	IL-1 receptor
IP	immunoprecipitation
IPTG	isopropyl β -D-1-thiogalactopyranoside
IR	insecticide resistances
IRF	Interferon regulatory factor
ISG	interferon response gene
JAK	Janus kinase
JNK	c-Jun N-terminal kinase
kDa	kilo Dalton
KRT	keratin
LB	Lysogeny broth/Luria-Bertani
LC	Liquid chromatography
LFQ	label-free quantification

LLPS	liquid-liquid phase separation
LPS	lipopolysaccharides
LXR	Liver X receptor
m ⁶ A	N6-methyladenosine
m7G	7-methylguanosine
MAGED2	melanoma-associated antigen D2
MAR	mono-ADP-ribose
MARylation	mono-ADP-ribosylation
macro	macrodomain
MD	macrodomain
MERS	Middle East Respiratory Syndrome
MFI	mean fluorescence intensity
MIF	Macrophage-inhibitory factor
min	minutes
miRNA	micro RNA
MHV	Murine Hepatitis virus
ml	milliliter
mM	millimolar
mRNA	messenger RNA
MS	mass spectrometry
MTase	methyltransferase
MVP-ID	major vault particle interaction
MXRA8	matrix remodeling-associated protein 8
N-terminus	amino terminus
NAD ⁺	nicotinamide adenine dinucleotide
NAP1L	nucleosome assembly protein 1 like
NEMO	NF-κB essential modulator
NES	nuclear export sequence
NF-κB	Nuclear factor κB
NHEJ	non-homologous end-joining
NHP	non-human primate
NLS	nuclear localization signal
nm	nanometer
nM	nanomolar
NP-40	Nonidet P-40
ns	not significant
ns	non-structural
NSAID	nonsteroidal anti-inflammatory drugs
nsP	non-structural protein
nt	nucleotide
NTF2	Nuclear transport factor 2
NTPase	nucleoside triphosphatase
Nudix	Nucleoside diphosphate linked to a ribonucleoprotein variable moiety X
OAADPr	O-acetyl-ADP-ribose
OARD1	O-acyl-ADP-ribose-deacylase 1 protein 1
OB	oligonucleotide/oligosaccharide binding
ONNV	O'nyong'nyong virus
ORF	open reading frame
p-	phosphorylated

P-body	Processing body
PAGE	polyacrylamide gel electrophoresis
PAMP	pathogen associated molecular pattern
PAR	poly-ADP-ribose
PARG	Poly (ADP-ribose) glycohydrolase
PARN	poly(A)-specific ribonuclease
PARylation	poly-ADP-ribosylation
PBS	phosphate-buffered saline
PBZ	PAR binding zinc finger
PCNA	Proliferating cell nuclear antigen
PCR	polymerase chain reaction
PDCD5	Programmed cell death protein 5
PEP	PAR-binding peptide motif
PFA	para-formaldehyde
PHB	prohibitin
PI	propidium iodide
PIC	protease inhibitor cocktail
PIN	PiIT N-terminus domain
PKC δ	protein kinase C delta
PLK1	polo-like kinase 1
poly(A)	polymer of adenosine
ppRNA	diphosphate RNA
pppRNA	triphosphate RNA
PRD	PARP regulatory domain
PTM	post-translational modification
RAS	Rat sarcoma
RdRp	RNA-dependent RNA polymerase
RIPA	radioimmunoprecipitation assay
RISC	RNA-induced Silencing Complex
RNA	ribonucleic acid
RNAi	RNA interference
RNF	Ring finger protein
rpm	revolutions per minute
RPS27A	40S ribosomal protein S27a (ubiquitin)
RRM	RNA recognition motif
rRNA	ribosomal RNA
RT	reverse transcriptase
RTPase	5'-RNA triphosphatase
s	seconds
SAM	S-adenosyl methionine
SARS	severe acute respiratory syndrome
SB	sample buffer
SD	standard deviation
SDS	sodium dodecyl sulfate
SDS-PAGE	SDS-polyacrylamide gel electrophoresis
SFV	Semliki Forest virus
SG	stress granule
SINV	Sindbis virus
siRNA	short interfering RNA
ss	single strand
SSB	single strand break

SSC	side scatter
ssRNA	single strand RNA
SSU	small subunit
STAT	Signal transducer and activator of transcription 1
SUD	SARS unique domain
SV40	Semian virus 40
TAB	TAK1-binding protein
TAK1	transforming growth factor- β -activated kinase
TANK	TRAF family member-associated NF- κ B activator
TAP	tandem affinity purification
TARG1	Terminal ADP-ribose protein glycohydrolase 1
TATase	terminal adenylyltransferase
TBK1	TANK binding kinase 1
TCDD	2,3,7,8-tetrachlorodibenzo-p-dioxin
TCEP	tris(2-carboxyethyl)phosphine
TEMED	tetramethylethylenediamine
TEV	Tobacco etch virus
TF	Tissue Factor
TF protein	transframe protein
TGF	trnsforming growth factor
TGN	trans-Golgi network
TIA-1	T-cell-restricted intracellular antigen-1
TiPARP	TCDD-inducible PARP
TLC	thin layer chromatography
TLR	Toll-like receptor
TM	melting temperature
TMD	transmembrane domain
TMV	Tobacco mosaic virus
TNF	tumor necrosis factor
TNFR	TNF receptor
TRAF	tumor necrosis factor receptor-associated factor
TRAILR4	TNF-related apoptosis-inducing ligand receptor 4
TRPT1	tRNA 2'-phosphotransferase 1
TPH	Ti-PARP homologous zinc finger domain
tRNA	transfer RNA
TTP	tristetraprolin
UBE2L3	ubiquitin-conjugating enzyme E2 L3
UIM	ubiquitin interaction motif
USP10	Ubiquitin carboxyl-terminal hydrolase 10
UTR	untranslated region
v/v	volume per volume
VEEV	Venezuelan Equine Encephalitis virus
vMD	viral macrodomain
vWA	von Willebrand type A domain
WCL	whole cell lysate
WDR	WD repeat-containing protein
WGR	domain named after a conserved central motif Trp-Gly-Arg
WHO	World Health Organization
wt	wildtype

w/v	weight per volume
WWE	domain named after three conserved residues Trp-Trp-Glu
XRN1	exoribonuclease 1
ZAP	Zinc finger antiviral protein
ZIKV	Zika virus
ZnF/ZF	zinc finger domain
β -TrCP	β -transducin repeat-containing protein
μ g	microgram
μ M	micromolar
μ m	micrometer

Amino acids were generally abbreviated using the according three letter or one letter code.

6.3 List of figures

Figure 1: Classical virion morphologies.	10
Figure 2: Exemplary virion morphologies of complex viruses.	11
Figure 3: Baltimore classification of viruses.	12
Figure 4: Mono- and poly-ADP-ribosylation of proteins.	15
Figure 5: Schematic representation of the 17 human ARTD family members.	17
Figure 6: Schematic representation of the structure and post-translational modifications of ARTD10.	28
Figure 7: Writers, readers and erasers of protein ADP-ribosylation.	36
Figure 8: Schematic representation of the macrodomain fold and the 12 human, macrodomain-containing proteins.	39
Figure 9: Geographical expansion of CHIKV outbreaks and <i>Ae. aegypti</i> and <i>albopictus</i>.	44
Figure 10: Replication cycle of CHIKV in the human host cell.	48
Figure 11: Organization and replication of the CHIKV genome.	49
Figure 12: Schematic representation of the Alphavirus non-structural proteins.	51
Figure 13: Schematic representation of non-structural polyprotein processing in CHIKV. ...	52
Figure 14: The macrodomain fold is highly conserved.	58
Figure 15: Viral macrodomains possess hydrolase activity towards protein mono-ADP-ribosylation in vitro.	59
Figure 16: Viral macrodomains are specific MAR-hydrolases.	60
Figure 17: Viral macrodomains inefficiently remove protein poly-ADP-ribosylation in vitro.	62
Figure 18: Hydrolase activity of CHIKV and FIPV macrodomains on PARylated HA-ARTD1 over time.	63
Figure 19: Analysis of products released from hydrolase assays on PARylated HA-ARTD1. 64	
Figure 20: Characterization of catalytically inactive CHIKV macrodomain mutants.	66
Figure 21: Investigation of the integrity of the CHIKV macrodomain mutants.	67
Figure 22: The full-length CHIKV nsP3 protein is a specific and efficient MAR-hydrolase. ..	69
Figure 23: The full-length nsP3 protein of CHIKV is inefficient in removing protein poly-ADP-ribosylation.	70
Figure 24: The CHIKV macrodomain is able to remove MARylation intracellularly.	71

Figure 25: Schematic representation of CHIKV replicon constructs used in the following experiments.	74
Figure 26: Characterization of the custom-designed CHIKV nsP2 antibody.	75
Figure 27: The knockdown of interferon-inducible mono-ARTDs increases CHIKV replication.	76
Figure 28: Overexpression of ARTD10 and ARTD12 restricts CHIKV replication in a catalytic activity-dependent manner.	77
Figure 29: The restrictive effect on CHIKV replication might be specific for some interferon-induced mono-ARTDs.	78
Figure 30: The specific ARTD10 inhibitor 0035 cannot rescue ARTD10 overexpression effects on CHIKV replication.	79
Figure 31: ARTD10 and ARTD12 partially cooperate in restricting CHIKV replication and nsP3 protein levels.	80
Figure 32: CHIKV hydrolase inactive mutants cannot replicate and resemble the proteolytically inactive CASA mutant.	81
Figure 33: The EGFP replicons containing macrodomain mutants exhibit similar properties to the untagged replicon.	82
Figure 34: Inhibition of the proteasome or the autophagic flux does not rescue the defect of the CHIKV V33E mutant.	83
Figure 35: Treatment with ARTD inhibitors cannot rescue the defect of the CHIKV V33E macrodomain mutant.	84
Figure 36: The proteolytically inactive CASA mutant of the CHIKV replicon can partially be rescued by addition of exogenous protease domain.	85
Figure 37: Addition of the exogenous CHIKV macrodomain or full-length nsP3 cannot rescue the CHIKV V33E mutant.	86
Figure 38: Co-transfection of the proteolytically inactive CASA replicon can partially rescue the replication and processing defect of the macrodomain inactive V33E replicon. ...	87
Figure 39: Representative gating strategy of control cells for the flow cytometry analysis of GFP-tagged CHIKV replicons.	88
Figure 40: Representative scatter plots for gating GFP positive cells of ² EGFP and ³ EGFP variants and co-transfection of the CASA replicon.	89
Figure 41: GFP-nanobody-mediated targeting of exogenous macrodomain to the ³ EGFP V33E replicon can partially rescue its defect.	90
Figure 42: Representative scatter plots for gating GFP positive cells of ³ EGFP V33E replicon complementation with the GFP-nanobody-nsP3 macro.	91
Figure 43: Co-expression of plasmids reduces expression of viral proteins and replication from replicon constructs.	92
Figure 44: Representative scatter plots for gating EGFP, mCherry and double positive cells of co-expression experiment with plasmids and replicons.	93
Figure 45: Schematic representation of CHIKV replicon GAA constructs used in the following experiments.	94
Figure 46: Introduction of the V33E macrodomain mutant into the GAA replicon construct further decreases the amount of processed nsP3.	95
Figure 47: NsP2 is a substrate of ARTD10-mediated MARYlation in vitro that can be reversed by the nsP3 macrodomain.	96
Figure 48: Interferon-inducible mono-ARTDs MARYlate nsP2 in vitro.	97
Figure 49: NsP2 is a substrate of MARYlation in cells.	98
Figure 50: ARTD10 partially co-localizes with replicon derived nsP2 in cells.	100

Figure 51: Establishment of the nsP2 protease assay in vitro.	101
Figure 52: ARTD10-mediated MARylation inhibits nsP2 protease activity in a dose-dependent manner.	102
Figure 53: The inhibitory effect of MARylation on nsP2 protease activity can be reversed by the viral nsP3 macrodomain.	103
Figure 54: Investigation of the replication ability of the CHIKV replicon Y114V macrodomain mutant.	105
Figure 55: Influence of MARylation on replication of the CHIKV Y114V replicon.	106
Figure 56: Full-length ARTD10 reversibly MARylates CHIKV nsP1, nsP2 and nsP3 in vitro.	107
Figure 57: Interferon-inducible mono-ARTDs modify CHIKV nsP1, nsP2 and nsP3 in vitro.	108
Figure 58: ARTD1 does not PARylate CHIKV nsP1, nsP2 or nsP3 in vitro.	109
Figure 59: Schematic representation of the mass spectrometry analysis approaches used to identify potentially MAR-dependent interactors of the nsP3 macrodomain.	111
Figure 60: Analysis of potentially macrodomain-dependent interactors of nsP3 identified by MS.	112
Figure 61: Characterization of the ARTD10-BirA*-HA construct and its interactors.	116
Figure 62: Investigation of ARTD10 binding partners dependent on interferon α and catalytic activity via GFP-Trap and MS.	118
Figure 63: Identification of common interactors of ARTD10 and CHIKV nsP3 in four independent MS approaches.	122
Figure 64: G3BP1 is a substrate of ARTD10-mediated MARylation in vitro reversed by nsP3.	126
Figure S65: Expression and treatment controls for the MS experiments.	CCVI
Figure S66: Biotinylation and streptavidin-enrichment of the nsP3- and nsP3-macro-BirA*-HA constructs.	CCVII
Figure S67: Biotinylation and streptavidin-enrichment of the ARTD10- and ARTD10-GW-BirA*-HA constructs.	CCVII

6.4 List of tables

Table 1: Overview of nsP3 interacting proteins identified in at least three MS approaches (TAP or BioID as indicated)	114
Table 2: Overview of the top 10 proteins enriched for ARTD10-BirA*-HA wt compared to the inactive GW mutant	117
Table 3: Overview of the interferon-enriched binding partners of GFP-ARTD10 that were identified by MS in the presence and absence of IFNα.	119
Table 4: Overview of the wt-enriched binding partners of GFP-ARTD10 that were identified by MS in the presence and absence of IFNα.	120
Table 5: Overview of selected, common interactors of CHIKV nsP3 and ARTD10 identified by MS analysis.	123

6.5 Curriculum Vitae

Personal Information

Sarah Krieg
 Vaalser Straße 432
 D-52074 Aachen
 Born October 16th, 1990 in Cologne
 Nationality: German

Education

Doctoral Studies 2016 – dato	RWTH Aachen University & University Hospital Aachen Ph.D. thesis: “Identification and functional characterization of binding partners and substrates of viral macrodomains with a focus on Chikungunya virus” (Prof. Dr. B. Lüscher/ Dr. P. Korn, née Verheugd – Institute of Biochemistry and Molecular Biology)
M.Sc. Molecular and Applied Biotechnology 2013 - 2015	RWTH Aachen University Focus: Red Biotechnology Master thesis: “Functional characterization of the cyclin Y/CDK16 kinase complex with regard to autophagy” (Prof. Dr. B. Lüscher/ Dr. J. Vervoorts – Institute of Biochemistry and Molecular Biology) <i>grade for master thesis: 0.9; final grade: 1.1</i>
B.Sc. Molecular and Applied Biotechnology 2010 - 2013	RWTH Aachen University Bachelor thesis: „Characterisation of the β -1,4- Endoglucanase Cell-1 from <i>Reticulitermes flavipes</i> , expressed in two different expression systems“ (Prof. Dr. R. Fischer/ Dr. U. Commandeur – Institute for Molecular Biology) <i>grade for bachelor thesis: 1.0; final grade: 2.1</i>
general qualification for university entrance 2001 - 2010	Dreikönigsgymnasium, Cologne <i>grade: 1.3</i>
primary school 1997 - 2001	Marienschule, Cologne

6.6 Scientific Contributions

6.6.1 Publications in scientific journals

Eckeï L*, **Krieg S***, Bütepage M, Lehmann A, Gross A, Lippok B, Grimm AR, Kümmerer BM, Rossetti G, Lüscher B, Verheugd P (2017) The conserved macrodomains of the non-structural proteins of Chikungunya virus and other pathogenic positive strand RNA viruses function as mono-ADP-ribosylhydrolases. *Scientific Reports* 7:41746. doi:10.1038/srep41746

**these authors contributed equally to this work*

Lüscher B, Bütepage M, Eckeï L, **Krieg S**, Verheugd P, Shilton BH (2018) ADP-Ribosylation, a Multifaceted Posttranslational Modification Involved in the Control of Cell Physiology in Health and Disease. *Chem Rev* 118 (3):1092-1136. doi:10.1021/acs.chemrev.7b00122

Krieg S, Lüscher B, Vervoorts J, Dohmen M (2018) Studying the Role of AMPK in Autophagy. *Methods in molecular biology (Clifton, NJ)* 1732:373-391. doi:10.1007/978-1-4939-7598-3_24

Bütepage M, **Krieg S**, Eckeï L, Li J, Rossetti G, Verheugd P, Lüscher B (2018) Assessment of Intracellular Auto-Modification Levels of ARTD10 Using Mono-ADP-Ribose-Specific Macrodomains 2 and 3 of Murine Artd8. *Methods in molecular biology (Clifton, NJ)* 1813:41-63. doi:10.1007/978-1-4939-8588-3_4

Bütepage M, Preisinger C, von Kriegsheim A, Scheufen A, Lausberg E, Li J, Kappes F, Feederle R, Ernst S, Eckeï L, **Krieg S**, Müller-Newen G, Rossetti G, Feijs KLH, Verheugd P, Lüscher B (2018) Nucleolar-nucleoplasmic shuttling of TARG1 and its control by DNA damage-induced poly-ADP-ribosylation and by nucleolar transcription. *Sci Rep* 8 (1):6748. doi:10.1038/s41598-018-25137-w

Krieg S, Pott F, Eckeï L, Verheirstraeten M, Bütepage M, Lippok B, Goffinet C, Lüscher B, Verheugd P (2020) Mono-ADP-ribosylation by ARTD10 restricts Chikungunya virus replication by interfering with the proteolytic activity of nsP2. *bioRxiv:2020.2001.2007.896977*. doi:10.1101/2020.01.07.896977

Dohmen M*, **Krieg S***, Agalaridis G, Zhu X, Shehata SN, Pfeiffenberger E, Amelang J, Bütepage M, Buerova E, Pfaff CM, Chanda D, Geley S, Preisinger C, Sakamoto K, Lüscher B, Neumann D, Vervoorts J (2020) AMPK-dependent activation of the Cyclin Y/CDK16 complex controls autophagy. *Nat Commun* 11 (1):1032. doi:10.1038/s41467-020-14812-0

**these authors contributed equally to this work*

Lüscher B, Verheirstraeten M, **Krieg S**, Korn P (2022) Intracellular mono-ADP-ribosyltransferases at the host-virus interphase. *Cellular and molecular life sciences : CMLS* 79 (6):288. doi:10.1007/s00018-022-04290-6

6.6.2 Presentations at scientific meetings

Poster presentation: “Mono-ARTDs - potential host factors targeted by viral macrodomains”; *EMBO Meeting, ADP-ribosylation in signaling events, Mannheim, Germany (2016)*

Poster presentation: “Mono-ADP-ribosylation as a modulator of Chikungunya virus infection”; *28th Annual Virology Meeting GfV2018, Wurzburg, Germany (2018)*

Oral presentation: “Chikungunya virus infection is modulated by mono-ADP-ribosylation”; *CSHL Meeting: PARP Family and ADP-Ribosylation, Cold Spring Harbor, New York, USA (2018)*

Poster presentation: “CHIKV replication is regulated by ARTD10-mediated mono-ADP-ribosylation”; *29th Annual Virology Meeting GfV2019, Düsseldorf, Germany (2019)*

Poster presentation: “The proteolytic activity of Chikungunya virus nsP2 is restricted by PARP10-mediated mono-ADP-ribosylation”; *30th Annual Virology Meeting GfV2021, Hannover, Germany (2021)*

6.7 Eidesstattliche Erklärung

Ich, Sarah Krieg,

erklärt hiermit, dass diese Dissertation und die darin dargelegten Inhalte die eigenen sind und selbstständig, als Ergebnis der eigenen originären Forschung, generiert wurden.

Hiermit erkläre ich an Eides statt

1. Diese Arbeit wurde vollständig oder größtenteils in der Phase als Doktorand dieser Fakultät und Universität angefertigt;
2. Sofern irgendein Bestandteil dieser Dissertation zuvor für einen akademischen Abschluss oder eine andere Qualifikation an dieser oder einer anderen Institution verwendet wurde, wurde dies klar angezeigt;
3. Wenn immer andere eigene- oder Veröffentlichungen Dritter herangezogen wurden, wurden diese klar benannt;
4. Wenn aus anderen eigenen- oder Veröffentlichungen Dritter zitiert wurde, wurde stets die Quelle hierfür angegeben. Diese Dissertation ist vollständig meine eigene Arbeit, mit der Ausnahme solcher Zitate;
5. Alle wesentlichen Quellen von Unterstützung wurden benannt;
6. Wenn immer ein Teil dieser Dissertation auf der Zusammenarbeit mit anderen basiert, wurde von mir klar gekennzeichnet, was von anderen und was von mir selbst erarbeitet wurde;
7. Teile dieser Arbeit wurden zuvor veröffentlicht und zwar in:

Ecke L*, **Krieg S***, Bütepage M, Lehmann A, Gross A, Lippok B, Grimm AR, Kümmerer BM, Rossetti G, Lüscher B, Verheugd P (2017) The conserved macrodomains of the non-structural proteins of Chikungunya virus and other pathogenic positive strand RNA viruses function as mono-ADP-ribosylhydrolases. *Scientific Reports* 7:41746. doi:10.1038/srep41746

**these authors contributed equally to this work*

Krieg S, Pott F, Ecke L, Verheirstraeten M, Bütepage M, Lippok B, Goffinet C, Lüscher B, Verheugd P (2020) Mono-ADP-ribosylation by ARTD10 restricts Chikungunya virus replication by interfering with the proteolytic activity of nsP2. *bioRxiv:2020.2001.2007.896977*. doi:10.1101/2020.01.07.896977

Datum

Unterschrift

6.8 Danksagung

Danke an alle die zu der Entstehung dieser Thesis direkt oder indirekt beigetragen haben!

Als Erstes möchte ich meiner Betreuerin Dr. Patricia Korn danken: Danke, dass du mir die wichtige Aufgabe anvertraut hast deine erste PhD zu sein! Und danke, dass du mich immer unterstützt hast, mir viel Freiraum gegeben hast und mich aber auch angetrieben hast, als ich es brauchte – besonders bei der Entstehung dieser Arbeit.

Dann möchte ich meinem Doktorvater Prof. Dr. Bernhard Lüscher danken – für viel Input und wissenschaftliche Diskussion und dafür, dass du immer ein offenes Ohr hattest. Außerdem dafür, dass du die Dinge oft positiver gesehen hast als ich und mich immer unterstützt hast. Ich danke Prof. Dr. Michael Huber für die Betreuung dieser Arbeit als Zweitgutachter.

Thanks to Giulia Rosetti for the *in silico* analyses of the macrodomains. Danke an Alexander R. Grimm für den Support bei den CD Analysen. Danke, Juliane Lüscher-Firzlaff, für die Einweisung zu den Sequenziergelen. Thanks to Agnieszka Bochyńska, Joël Guillaume and Fabian Peisker for the help with the analyses of the flow cytometry data. Danke an die IZKF Confocal Core Facility oder genauer gesagt Prof. Dr. Gerhard Müller-Newen und Dr. Sabrina Ernst bei der Unterstützung bei der Aufnahme der Mikroskopiebilder. Außerdem danke ich Dr. Marc Dohmen, der mich für die Nutzung des Confocals unterwiesen hat. Danke an Ferdinand Kappes und Malte Prell für den Input bei der Etablierung des BioID Systems. Stefanie Gostek für die Vorbereitung der Proben und Christian Preisinger danke ich für die Massenspektrometrie-Messungen und die initiale Auswertung der Daten.

Danke an alle unsere ehemaligen Studenten, die uns auf dem CHIKV Projekt unterstützt haben: Anka Güldenpfennig, Jonas Fechner, Laura Krutt, Laura Wontroba und Franziska Kaesler. Danke an Laura Eckei-Potthoff, die viele der initialen Daten auf dem Projekt generiert hat und an Mareike Bütepage, die viele der Tools zur Detektion von MARYlierung etabliert hat. And thank you to Maud Verheirstraeten, it was great to have a fellow PhD student and a friend on the project! Außerdem danke an Barbara Lippok, die das Projekt immer mit allem Möglichen unterstützt, zum Beispiel mit der Generierung von stabilen Zelllinien. Danke Alexandra Golzmann für die vielen Versuche *ARTD10* in der qPCR zu messen.

Weiterhin möchte ich allen Mitstreitern auf dem ADP-Ribosylierungsthema danken für Diskussion und Input, gemeinsame Nutzung von Reagenzien und rekombinanten Proteinen und manchmal gemeinsamer Verzweiflung bei der Detektion von MARYlierung in Zellen.

Alles in allem möchte ich einfach der gesamten Biochemie danken, 3. und 5. Stock, und alle die damit assoziiert sind und waren: ich hatte nicht nur tolle Kollegen, sondern habe auch viele fantastische Freunde gefunden, die meine Jahre in der Biochemie sehr bereichert haben! Ich hatte bei der Arbeit und außerhalb der Arbeit eine geniale Zeit, die ich nicht missen möchte! Auch wenn die Wissenschaft (oder auch das Privatleben) manchmal anstrengend und frustrierend war(en) habt ihr mich immer aufgemuntert und motiviert und ich bin jeden Tag gerne zur Arbeit gekommen.

Als letztes möchte ich meiner Familie danken, die mich mein ganzes Leben immer unterstützt hat und ohne die ich sicherlich nicht da wäre wo ich heute bin! Danke, Fabian! Du hast mich immer unterstützt und mich sowohl ertragen wenn ich schlecht gelaunt war als auch wenn ich aufgedreht war, weil ich alleine zu Hause am Schreibtisch den ganzen Tag noch mit niemandem geredet hatte. Danke, dass du immer versuchst zu verstehen, was ich da eigentlich mache und mit mir darüber zu diskutieren! Ohne dich hätte ich das nicht geschafft!